

Contaminant diffusion and sorption  
of an artificial leachate in selected geologic barriers  
of Frankonia, Bavaria, Germany

Dissertation  
presented to the  
Department of Geology  
at the  
Julius-Maximilians-University, Würzburg  
Germany

by  
Uwe R. Kackstaetter, M.Sc. GEOL  
2003



### Abstract

The geologic barrier represents the final contact between a landfill and the environment. Ideally suited are clays and mudstones because of sufficient vertical and lateral extent, low hydraulic conductivities and high sorptive characteristics. Since hydraulic conductivity is no longer the single criteria to determine transport and retardation of contaminants in geologic landfill barrier materials, diffusive and sorptive characteristics of 4 different clay and mudstone lithologies in Northern Bavaria, were investigated. Cored samples from various depths were used in this study and subjected to evaluations of geochemistry, mineralogy, physical parameters, sorption and diffusion. A transient double reservoir with decreasing source concentration was designed and constructed using clear polycarbonate cylinders for undisturbed clay plugs of 2 to 4cm thickness. Samples were also fitted with internal electrical conductivity probes to determine the migration of the diffusive front. A multi chemical species synthetic landfill leachate was contrived to simulate and evaluate natural pollutant conditions. A computational method for determining mineralogy from geochemical data was also developed. It was found that sorptive processes are mostly controlled by the quality and type of fine grained phyllosilicates and the individual chemical species involved exhibited linear, Freundlich, as well as Langmuir sorption properties. Effective diffusion and sorption coefficients were also determined using POLLUTEv6 (GAEA, 1997) software and receptor reservoir concentrations for K, Na, Ca, Cu, NH<sub>4</sub>, Cl, NO<sub>3</sub>, SO<sub>4</sub> and concentration totals at predetermined time intervals. Anion exclusion proved to be a major factor in the diffusion process and seemed to explain many observed anomalies. Furthermore, diffusion coefficients were found to vary during the course of the experiment using a multi chemical species leachate. Strong indications point toward the major role of pore space quality, shape, and form as control of diffusive properties of a geologic barrier. A correlation of CEC<sub>Na</sub> of the samples with D<sub>e</sub> may point to a possible deduction of diffusive properties for multi species leachates without extensive and time consuming laboratory tests.

### Abstract

Die geologische Barriere stellt die letzte Verbindung zwischen Mülldeponie und Umwelt dar. Ideal geeignet sind Tone und Tonsteine, da diese ausgedehnte horizontale und vertikale Mächtigkeiten, niedrige hydraulische Koeffizienten, und hohe Sorptionskapazitäten aufweisen. Da hydraulische Konduktivitäten nicht länger alleine maßgebend sind, um Transport und Rückhaltevermögen verschiedener Kontaminanten in geologischen Deponiebarrieren zu beurteilen, wurden 4 verschiedenen Tonsteine des Nordbayerischen Raumes auf ihre Sorptions- und Diffusionseigenschaften hin untersucht. Dazu wurde ein zeitabhängiges Diffusionssystem aus zwei Kammern für abnehmende Anfangskonzentrationen aus durchsichtigem Polykarbonat für 2 bis 4 cm dicke ungestörte Tonproben entwickelt. Jede Probe wurde auch mit internen Sensoren zur elektrischen Leitfähigkeitsmessung bestückt, um das Fortschreiten der Diffusionsfront zu ergründen. Ein synthetisches Deponiesickerwasser wurde entworfen, das in seiner Zusammensetzung den natürlichen Inhaltsstoffen und Konzentration authentischer Sickerwässer ähnelt. Auch wurde eine Methode zur Berechnung der Mineralogie der Tonsteine anhand geochemischer Analysen entwickelt. Es zeigte sich, dass Sorptionsprozesse hauptsächlich durch die Eigenschaften der vorhandenen, feinkörnigen Phyllosilikate beeinflusst werden. Die gegebenen chemischen Inhaltsstoffe des Sickerwassers zeigen dabei lineare, Freundlich- und Langmuir-Sorptionseigenschaften. Effektive Diffusions- und Sorptionskoeffizienten wurden mit Hilfe des Computerprogramms POLLUTEv6 (GAEA, 1997) und der Konzentrationsstärken von K, Na, Ca, Cu, NH<sub>4</sub>, Cl, NO<sub>3</sub>, SO<sub>4</sub>, sowie Konzentrationssummen in bestimmten Zeiteinheiten ermittelt. Anionausschluss stellte sich als grundlegend für die Diffusion heraus und viele beobachtete Anomalien ließen sich dadurch erklären. Auch liefen die Diffusionsprozesse mit einem Gemisch chemischer Inhaltsstoffe keineswegs statisch ab, sondern variierten während des Versuchsdurchlaufs. Vieles weist auf den starken Einfluss der Porenraumeigenschaften und Charaktere hin, welche die Diffusionseigenschaften der geologischen Barrieren zu beeinflussen scheinen. Eine Verbindung von KAK<sub>Na</sub> und D<sub>e</sub> könnte sich als mögliche zeitsparende Methode zur Ermittlung von Diffusionskoeffizienten herausstellen, ohne auf langwierige und ausgedehnte Laborversuche angewiesen zu sein.

## Acknowledgments

This dissertation is part of the continuation of the BayFORREST (Bavarian Network for Waste Research and Residual Re-Use) research study F22(F) “*Hydraulic conductivity and sorption behavior of organic and inorganic contaminants within selected geologic barriers.*” Research for this work was conducted from 1994 to 1998 at the Department of Hydrogeology and Environment, Institute for Geology, University of Würzburg, Germany. Continuation of data analysis and sorption batch experiments were carried out by the Author at the facilities of The People’s Lab LLC, Berthoud, Colorado, USA from 2000 to 2002.

The author would like to extend his special thanks first and foremost to Dr. Peter Udluft for his support, frank discussion, training, encouragement, and supervision of the dissertation. Further appreciation is given to the faculty and staff at the Institute for Geology:

- For help with the analytical work: Adolf Heilos, Dipl.-Geol. Eleni Zagana, Dr. Holger Mainardy and especially Mrs. Zhi Zhi Li who spent countless overtime hours analyzing samples.
- For assistance with literature, the petrographic microscope and thin section analysis: Dr. Wolfgang Trapp
- For aid with financial management and bureaucratic paperwork: Dipl.-Geol. Parviz Mansourie and Mr. Peter Sorg at the University Financial Department.
- To my colleagues at the institute, working with the same geologic barrier materials: Dr. Dieter Pötzl, who started the initial project in hydraulic conductivity. Dipl.-Geol. Peter Jost, my office mate and co-worker, researching physical and geochemical characteristics of the geologic barrier materials.

A special recognition for financing the project in its entirety is given to the Bavarian Network for Waste Research and Residual Re-Use (BayFORREST). Further appreciation goes to the Biozentrum of the Universität Würzburg, for their friendly support and use of the Scanning Electron Microscope facilities. Additional thanks goes to Mr. Stan Pond (PE<sup>1</sup>) and his company Pond Engineering, Colorado, USA, for his help, development and manufacturing of the diffusion cell apparatus and to ACME Analytical Laboratories LTD, Vancouver, Canada, for their assistance and prompt analysis of sample materials.

A heart warming thank you to my close co-workers at the Institute, Dipl.-Geol. Frank Bärle, Dr. Claudia Bärle, Dr. Gerold Heinrichs, and especially my good friend Dr. Günter Kus for many hours of stimulating discussion, critical analysis, and physical help with the project. Furthermore, my deepest gratitude for their involvement in the project is extended to

- my close friend Mr. Matthias Hasselblatt, a non-geologist, and my son Ruben Kackstaetter, sacrificing their private time to help with the assembly of the diffusion cell apparatus and clean up of the research facilities.
- my daughters Heidi and Ruth Kackstaetter, acting as science interns and helping with the analytical work of the sorption batch experiments.
- Paul & Audra Felt, who sacrificed their time and talents in proof reading and editing the manuscript.

And finally, my deepest and most heartfelt thanks goes to my children Christy, Jon, Katrina, and Rachel for their patience and courage moving to a foreign country, learning a new language, while missing out on “daddy”; and at last to my dear wife and eternal companion, Laura, for her emotional support, countless hours of proofreading and encouragement, besides being a full time mother to our seven children, and following me halfway around the world for the sake of this project.

---

<sup>1</sup> Registered Professional Engineer



*All nature is but art, unknown to thee;  
All chance, direction, which thou canst not see;  
All discord, harmony not understood;  
All partial evil, universal good;  
And spite of pride, in erring reason's spite,  
One truth is clear, Whatever is, is right.*

- Alexander Pope

*And behold, all things have their likeness,  
and all things are created and made to bear record of me,  
both things which are temporal, and things which are spiritual;  
things which are in the heavens above, and things which are on the earth,  
and things which are in the earth, and things which are under the earth,  
both above and beneath:  
all things bear record of me.*

- Joseph Smith

## Contents

1	Introduction	14
1.1	The geologic barrier	14
1.2	Purpose of Study & Selection of Geologic Barrier Material	15
1.3	General Procedures	16
1.3.1	Engineering and construction of diffusion apparatus.	16
1.3.2	Development of artificial leachate	18
1.3.3	Geochemical, petrographic, & mineralogical analysis of sample materials	18
1.3.4	Identification of relevant physical parameters of the samples	19
1.3.5	Computer analysis and modeling of the data	19
2	Selected Clay barriers and their Geology	20
2.1	Regional Geography and Geology	20
2.2	Stratigraphic overview	22
2.3	Description of selected barrier units	27
2.3.1	Lower Jurassic Amaltheen Clay (Kalchreuth)	27
2.3.2	Upper Triassic Feuerletten (Creußen)	28
2.3.3	Triassic Lehrberg Layers (Langenzenn)	29
2.3.4	Lower Triassic Röttone (Marktheidenfeld)	30
3	Geochemistry	32
3.1	Major Element Geochemistry	32
3.2	Minor Element Geochemistry	36
3.3	Organic Carbon Content and LOI (Loss-On-Ignition)	40
3.4	Cation Exchange Capacity	43
4	Mineralogy	46
4.1	General Mineralogy of Clays	46
4.2	Determination of Mineralogy	51
4.2.1	X-ray determinative techniques	51
4.2.2	Scanning Electron Microscopy (SEM)	54
4.2.3	Optical microscopy	58
4.2.4	Mineralogical calculations	64
4.3	The Mineralogy of the Selected Geologic Barriers	77
5	Physical Properties	80
5.1	Grains size analysis	80
5.1.1	Lithological classification according to size fractions	80
5.1.2	Moment Statistics	81
5.1.3	Grain Size Analysis Results	82
5.3	Hydraulic Data	86
5.3.1	Hydraulic Conductivity ( $k_f$ )	86
5.3.2	Discharge Velocity ( $v_p$ )	88
5.3.3	Seepage Velocity ( $v_s$ )	88
5.3.4	Effective Porosity	90
5.4	Discussion of Hydraulic Data	90

---

6	Contaminants	93
6.1	Landfill Leachates	93
6.2	Synthetic Landfill Leachate (SLL)	94
7	Sorption	98
7.1	Sorption and Sorbent Properties	98
7.2	Sorption and Sorbate Properties	101
7.3	Sorption Isotherms	104
7.3.1	Freundlich Sorption Isotherm	104
7.3.2	Langmuir Sorption Isotherm	104
7.3.3	Graphical Sorption Isotherm Representation	105
7.3.4	Sorption Isotherms for Organic Sorbates	106
7.4	Sorption Batch Experiments	107
7.5	Results of Sorption Analysis	109
7.5.1	Calcium	111
7.5.2	Copper	112
7.5.3	Potassium	113
7.5.4	Sodium	114
7.5.5	Ammonium	115
7.5.6	Chloride	115
7.5.7	Sulfate	117
7.5.8	Nitrate	118
7.5.9	2-Chlorophenol	119
7.5.10	Total Sorbent Components	122
7.6	Retardation	123
8	Diffusive Transport through Clays	125
8.1	Diffusion principles	125
8.2	Laboratory Diffusion Experiments	127
8.2.1	Diffusion Apparatus	128
8.3	Data evaluation and modeling using POLLUTEv6	131
8.3.1	POLLUTEv6 input parameters	132
8.4	Diffusion Results - Comparison and Discussion	133
8.4.1	Calcium Diffusion	137
8.4.2	Copper Diffusion	139
8.4.3	Potassium Diffusion	140
8.4.4	Sodium Diffusion	141
8.4.5	Ammonium Diffusion	142
8.4.6	Chloride Diffusion	143
8.4.7	Sulfate Diffusion	144
8.4.8	Nitrate Diffusion	145
8.4.9	2-Chlorophenol Diffusion	146
8.4.10	Total Diffusion of SLL	147
9	Conclusions	151
9.1	Geochemistry	151
9.2	Mineralogy	151
9.3	Physical Properties	151
9.4	Sorption	151
9.5	Diffusion	152

9.5.1 Modeling	152
9.5.2 Ion exclusion	152
9.5.3 Diffusion processes	152
9.6 Possible Future Applications	153
9.6.1 Pore spaces	153
9.6.2 CEC <sub>Na</sub>	153
References	154
Appendix A	165
Appendix A.1- Drill Profiles of Cored Samples	165
Appendix B	166
Appendix B.1- Major Rock Forming Elements	166
Appendix B.2- Minor Geochemical Elements	168
Appendix B.3 - Carbon and LOI constituent content	169
Appendix B.4 - Pearson Correlation Matrices of geochemical constituents	171
B.5 - Results of CEC analysis	177
Appendix C	178
Appendix C.1- Talled results of mineral calculations	178
Appendix C.2 - Summary of step by step mineral calculating procedures	184
Appendix C.3 - Analytical results for Total S, Sulfide S and SO <sub>3</sub>	185
Appendix C.4 - Pearson's correlation analysis between mineral calculations and measured mineral data	186
Appendix D	188
Appendix D.1: Results of Batch Sorption Experiments	188
Appendix D.2: Results of Sorption Isotherm Calculations	189
Appendix D.3: Development of sorption isotherm equation for 2-chlorophenol	191
Appendix D.4: Significant correlation of cation exchange capacities vs. sorption coefficients (K <sub>d</sub> )	193
Appendix D.5: Table of sorption coefficients (K <sub>d</sub> ), retardation factors (R), and transient times for individual pollutant species and geologic barrier samples	193
Appendix E	195
Appendix E.1 -Overview of grain size nomenclature as given by POPPE <i>et al.</i> (2003)	195
Appendix E.2 -Tabulated and graphical results of grain size analysis	196
Appendix E.3 -Results of water absorption, moisture content, grain density.	198
Appendix E.4 - Hydraulic Data for B = Feuerletten, K = Amaltheen Clay, L = Lehrberg Layers, M = Lower Rötton samples	199
Appendix E.5 -Equations for calculating hydraulic conductivity from permanent and falling head experiment	200
Appendix F	201
Appendix F.1 - Results of chemical characteristic computations using SRC (2000) software	201
Appendix F.2 - Summary of results of activity coefficient calculations for SLL at varying temperatures using PHREEQC <sub>i</sub> (2002)	204
Appendix G	208
Appendix G.1 - Diffusion Experiment Data with Lithium Bromide	208
Appendix G.2 - Diffusion Experiment Data with SLL	210

---

Appendix G.3 - Diffusion Coefficients calculated with Pollute6.3 according to receptor reservoir. . . . .	217
Appendix G.4 - Graphical representation of diffusion modeling outcome for source reservoir. . . . .	217
Appendix H . . . . .	220
Appendix H.1 - Significant correlations of Soil pH, Mineralogy, Kd and $D_e$ values vs. $D_e$ . . . . .	220
Appendix H.2 - Significant correlations of barrier physical properties vs. $D_e$ . . . . .	221
Appendix H.3 - Significant correlations of Geochemistry and CEC vs. $D_e$ . . . . .	222

## Illustrations

Figure 1.1 - Map of Bavaria . . . . .	15
Figure 1.2 - Through diffusion non-steady state apparatus . . . . .	17
Figure 1.3 - Interchangeable front and end systems . . . . .	17
Figure 2.1 - Sample core locations within Franconia . . . . .	20
Figure 2.4 (Part B) - 3 D illustration showing surface geology, topography, and stratigraphic cross section . . . . .	24
Figure 2.5 - Stratigraphic section of Triassic Middle & Upper Keuper and Jurassic Lias & Dogger . . . . .	25
Figure 2.6 - Stratigraphic Section of Lower Triassic Lower Muschelkalk and Upper Buntsandstein . . . . .	26
Figure 2.7 - Coring Profile of Amaltheen Clay at sample location . . . . .	27
Figure 2.8 - Coring Profile of Feuerletten Clay at sample location . . . . .	28
Figure 2.9 - Coring Profile of Lehrberg Layers at sample location . . . . .	29
Figure 2.10 - Coring Profile of Lower Röttone at sample location . . . . .	30
Figure 3.1 - Major element concentration . . . . .	32
Figure 3.3 - Distribution plot of natural geologic barriers samples in a MgO-Fe <sub>2</sub> O <sub>3</sub> -K <sub>2</sub> O ternary diagram . . . . .	33
Figure 3.2 - MgO-Al <sub>2</sub> O <sub>3</sub> -K <sub>2</sub> O ternary diagram . . . . .	33
Figure 3.4 - A barycentric stereo plot of the MgO-Fe <sub>2</sub> O <sub>3</sub> -K <sub>2</sub> O-CaO system . . . . .	34
Figure 3.5 - Plot of Max/Min values for rock forming oxides compared to threshold and anomalies . . . . .	34
Figure 3.6 - Arithmetic mean of minor element composition compared with average shale . . . . .	36
Figure 3.7 - Stratigraphic core section of the Amaltheen Clay with concentration profiles . . . . .	38
Figure 3.8 - Stratigraphic core section of the Feuerletten Clay with concentration profiles . . . . .	38
Figure 3.10 - Stratigraphic core section of the Lower Röttone with concentration profiles . . . . .	39
Figure 3.9 - Stratigraphic core section of the Lehrberg Layers with concentration profiles . . . . .	39
Figure 3.11 - Plot of investigated samples related to shale colors . . . . .	41
Figure 3.12 - Schematic of the ion exchange reaction using a CEC measurement with BaCl <sub>2</sub> . . . . .	43
Figure 3.13 - Plot of base CEC, $\sum$ cations, Ca <sup>2+</sup> , Mg <sup>2+</sup> , K <sup>+</sup> , and Na <sup>+</sup> in order of sample pH . . . . .	44
Figure 4.1 - Schematics of silica tetrahedra . . . . .	47
Figure 4.2 - Schematics of octahedra and associated sheet structure . . . . .	47
Figure 4.3 - X-ray pattern of untreated Feuerletten clay . . . . .	51
Figure 4.5 - SEM micrograph of Amaltheen clay sample . . . . .	54
Figure 4.6 - SEM micrograph showing hexagonal kaolinite . . . . .	54
Figure 4.7 - SEM micrograph of Feuerletten specimen . . . . .	56
Figure 4.8 - Lower Rötton sample . . . . .	57
Figure 4.9 - Photomicrograph and digital enhanced relief image of Amaltheen sample . . . . .	60
Figure 4.10 - Feuerletten sample photomicrograph (plain light, above) and digital enhanced relief image . . . . .	61
Figure 4.11 - Photomicrograph and digital enhanced relief image of Lehrberg layers . . . . .	62
Figure 4.12 - Lower Rötton photomicrograph (plain light, above) and digital enhanced relief image . . . . .	63
Figure 4.13 - Scatterplot of TiO <sub>2</sub> vs. Kaolinite concentrations . . . . .	66
Figure 4.15 - Relationship of K <sub>2</sub> O and MgO concentrations to whole rock illite . . . . .	70
Figure 4.16 - Sum of calculated minerals . . . . .	75
Figure 4.17 - Stratigraphic core section of the Feuerletten Clay with mineral concentration profiles . . . . .	77
Figure 4.18 - Stratigraphic core section of the Amaltheen Clay with mineral concentration profiles . . . . .	78
Figure 4.19 - Stratigraphic core section of the Lehrberg Layers with mineral concentration profiles . . . . .	78
Figure 4.20 - Stratigraphic core section of the Lower Röttone with mineral concentration profiles . . . . .	79
Figure 5.1 - Ternary plot of sand, silt and clay fractions . . . . .	81
Figure 5.2 - Depth profile of sand, silt, and clay grain sizes within the Feuerletten stratigraphy . . . . .	82
Figure 5.3 - Depth profile of sand, silt, and clay grain sizes within the Amaltheen clay . . . . .	83
Figure 5.4 - Lehrberg Layer depth profile of sand, silt, and clay grain sizes . . . . .	84
Figure 5.5 - Depth profile of sand, silt, and clay grain sizes in the Lower Rötton section . . . . .	84

Figure 5.6 - Comparison of calculated gypsum and swelling clay (montmorillonite/smectite) concentrations with water absorption capacities	85
Figure 5.7 - Diffusion cell set-up for sample saturation and hydraulic conductivity testing	87
Figure 5.8 - Depth profile of hydraulic data ( $k_p$ , $v_p$ , $v_s$ ) for Feuerletten	90
Figure 5.9 - Depth profile showing hydraulic data ( $k_p$ , $v_p$ , $v_s$ ) for Amaltheen clay	90
Figure 5.10 - Lehrberg Layers presented with depth profile of hydraulic data ( $k_p$ , $v_p$ , $v_s$ )	92
Figure 5.11 - Depth profile of Lower Röttone with hydraulic data ( $k_p$ , $v_p$ , $v_s$ )	92
Figure 7.1 - Adsorption vs. Absorption	98
Figure 7.2 - CEC vs surface areas of clays	100
Figure 7.3 - Schematic view of ionic sorption characteristics	101
Figure 7.4 - Graphical representation of sorption isotherms	105
Figure 7.5 - Plot of results of sorption experiments	111
Figure 7.6 - Relationship of linear Ca $K_d$ and calculated montmorillonite./ smectite.	111
Figure 7.7 - Plot of linear Cu $K_d$ vs. calculated clay concentrations	112
Figure 7.8 - Relation of Na $K_d$ to calculated montmorillonite./ smectite.	113
Figure 7.9 - Correlation of linear $NH_4$ $K_d$ with calculated montmorillonite./ smectite.	115
Figure 7.10 - Linear Cl $K_d$ vs. calculated hematite and gypsum.	116
Figure 7.12 - Coordination phenomenon of surface hydroxyls being replaced by anions	117
Figure 7.11 - $K_d$ - $SO_4$ plot against calculated montmorillonite-smectite concentrations.	117
Figure 7.14 - Schematic of Stern and Gouy layers with corresponding cation-anion concentration	117
Figure 7.13 - Linear $SO_4$ $K_d$ vs. selected cationic $K_d$ scatterplot	118
Figure 7.15 - $K_d$ - $NO_3$ plotted against sum of measured carbon & MnO	119
Figure 7.16 -Total Carbon vs. $K_d$ - Chlorophenol plot	120
Figure 7.17 -Graph of $K_d$ 2-Chlorophenol vs. soil pH	120
Figure 7.18 -Total calculated clay minerals plotted against linear $K_d$ - Chlorophenol	121
Figure 7.19 -Comparison of soil pH, % total carbon, % calculated clay and $K_d$ - Chlorophenol	122
Figure 7.20 - Plot of $K_d$ - Total against difference of CEC cation sum & CEC $Ba^{2+}$	122
Figure 8.1 - Sequential illustration of diffusion process in a homogenous media	125
Figure 8.2 - Graphical representation of tortuosity	126
Figure 8.3 - Engineering detail of sample plug holder for diffusion apparatus	128
Figure 8.4 - Various interchangeable attachments to be mounted to sample plug	129
Figure 8.5 - Sample cell set-up during diffusion experiment	130
Figure 8.6 - Cumulative concentration of Li and Br versus time in receptor and source reservoirs	133
Figure 8.7 - Cumulative concentrations of chemical species versus time in receptor reservoir	136
Figure 8.7 - Total $D_e$ of samples investigated	147
Figure 8.8 - Apparent internal clay plug conductivities for indicated distances from the source	150

## Tables

Table 1.1 - German example of geologic barrier requirement for various landfill sites	14
Table 1.2 - Selected geologic barrier units	15
Table 3.1 - Relative aqueous mobilities of selected elements in waters of the secondary environment	37
Table 3.2 - Averages for $C_{org}$ , $M_{org}$ , $CO_2$ by LECO™ & BALL (1964), DEAN (1974), GOLDIN (1987) - methods	41
Table 3.3 - Summary of selected CEC results	44
Table 3.4 - Selected CEC base saturation and pH	44
Table 4.1 - Classification of major phyllosilicate groups	48
Table 4.2 - Classification of mixed layered phyllosilicates	50
Table 4.3 - Results of the X-ray diffraction, IR-spectroscopic and mineral specific chemical investigations	53
Table 4.4 - Results of point-count analysis of representative samples from selected locations	58
Table 4.5 - Idealized chemical compositions used in calculating mineral components	65
Table 4.6 - Comparison of calculated vs. standard molecular weight of clays	66
Table 4.7 - Mole ratio comparison of $Al_2O_3$ and $K_2O$ in Sericite and Kspar.	71
Table 4.8 - Results of mineral calculations of representative samples from selected locations	72
Table 5.1 - Verbal description FOLK (1980) of Moment statistics and Ternary analysis after SHEPARD (1954)	82
Table 6.1 - Comparison of various summarized landfill data	93
Table 6.2 - Comparison of artificial leachate conc. of selected ions with leachate conc. of the Raindorf landfill	94
Table 6.3 - Chemicals used in the construction of a Synthetic Landfill Leachate.	95
Table 6.4 - Concentrations of ions in SLL and computed ionic strength, ion activity coefficients, and $a_i$ 's.	97
Table 7.1 - Valence / Coordination number ratios	100
Table 7.2 - Solubility, polarity, $K_{oc}$ & $\log K_{ow}$ data for common organic contaminants	103
Table 7.3 - Characteristics of physical and chemisorptive properties	106
Table 7.4 - Artificial Leachate Concentrations for Batch Sorption Experiment	108
Table 7.5 - Analytic Schedule of Ions & Compounds for Batch Sorption Experiment	108
Table 7.6 - Calcium Sorption Coefficients for artificial leachate	112
Table 7.7 - Copper Sorption Coefficients for artificial leachate	113
Table 7.8 - Potassium Sorption Coefficients for artificial leachate	114
Table 7.9 - Sodium Sorption Coefficients for artificial leachate	114
Table 7.10 - Ammonium Sorption Coefficients for artificial leachate	115
Table 7.11 - Chloride Sorption Coefficients for artificial leachate	116
Table 7.12 - Sulfate Sorption Coefficients for artificial leachate	117
Table 7.13 - Nitrate Sorption Coefficients for artificial leachate	119
Table 7.14 - 2-Chlorophenol Sorption Coefficients for artificial leachate	120
Table 7.15 - 2-Chlorophenol Sorption Coefficients for experimental ( $K_d$ , $K_d$ linear) and calculated data	121
Table 7.16 - Sorption Coefficients for total artificial leachate	123
Table 8.1 - Summary of various diffusion testing methods	127
Table 8.2 - Results of diffusion experiments in sample L6 & L11.5 using LiBr	133
Table 8.3 - Effective Calcium Diffusion Coefficients for artificial leachate	138
Table 8.4 - Effective Copper Diffusion Coefficients for artificial leachate	140
Table 8.5 - Effective Potassium Diffusion Coefficients for SLL	141
Table 8.6 - Effective Sodium Diffusion Coefficients for artificial leachate	142
Table 8.7 - Effective Ammonium Diffusion Coefficients for SLL	143
Table 8.8 - Effective Chloride Diffusion Coefficients for artificial leachate	144
Table 8.9 - Effective Sulfate Diffusion Coefficients for artificial leachate	145
Table 8.10 - Effective Nitrate Diffusion Coefficients for SLL	146
Table 8.11 - Effective 2-Chlorophenol Diffusion Coefficients for artificial leachate	147
Table 8.12 - Effective Diffusion Coefficients for Total artificial leachate	148



## Abbreviations

~	approximately, about
$\gamma$	activity coefficient of an ion
$\tau$	tortuosity factor expressed as the ratio of shortest distance to actual length squared $(x/x_a)^2$
2-CPL	2-chlorophenol
AEC	Anion Exchange Capacity
$a_i$	ionic activity (mol/L)
b.s.	below surface
C	aqueous concentration (usually in mg/ml or g/L)
CEC	Cation Exchange Capacity
cf.	<i>confer</i> or compare; synonymous to "as quoted in"
cm	centimeter
D	diffusion coefficient (usually expressed in $\text{cm}^2/\text{s}$ )
$D_a$	apparent diffusion coefficient
$D_e$	effective diffusion coefficient for soils, includes porosity and the tortuosity factor
DIN	Deutsches Institut für Normung = German Standards Institute
$D_s$	effective diffusion coefficient of the reactive solute
$e$	void ratio
e.g.	<i>exempli gratia</i> , for example
EDTA	<u>E</u> thlened <u>i</u> aminet <u>e</u> tetra <u>a</u> cetic <u>a</u> cid; $\text{C}_{10}\text{H}_{16}\text{N}_2\text{O}_8$ ; Molecular weight = 292.25
EDX	Energy Dispersive X-ray. Usually coupled with the SEM.
EPA	Environmental Protection Agency (United States Regulatory Department for Contaminants)
f	flux; referred to contaminant flux by diffusion
$f_{oc}$	Weight fraction of organic carbon in sorbent material
g	grams
Ger.	German
h/l	hydraulic gradient
HIOC	hydrophobic ionizable organic compound
I	ionic strength (mol/L)
I/S	Illite - Smectite interstratified clays
i.e.	<i>id est</i> , that is
IAP	Ion Activity Product; activity coefficient of a solute times molality
ICP-AES	Inductively Coupled Plasma - Atomic Emission Spectrometry

---

ID	in-diffusion
IEP	Isoelectric Point
IR	infrared
$K_{aq}$	Aqueous mobility coefficient for elements in waters of the secondary environment
$K_d$	Sorption or distribution coefficient
$k_f$	Hydraulic conductivity (SI units: $m\ s^{-1}$ )
$K_{oc}$	Sorption or distribution coefficient for organic carbon
$K_{ow}$	Octanol Water Partition Coefficient (SI units: unit less)
$K_p$	Partition coefficient; analogous to $K_d$ for non-linear sorption
$K_{so}$	Solubility coefficient
L	liter
LECO™	Trademark: Synonymous for C, S, N, & O detection systems developed by LECO Corp.
LOI	loss-on-ignition
m	meter
M	Langmuir sorption isotherm constant; equivalent to sorption maxima isotherm
mg	milligrams
mont./smec.	Montmorillonite -Smectite; referred to as swelling clays.
MW	Molecular Weight
n	Freundlich sorption isotherm constant
$n_e$	effective porosity
PCP	Pentachlorophenol
R	retardation factor or retardation coefficient (unitless)
$R^2$	Goodness-of-fit measure or coefficient of determination ranging in value from 0 to 1.
RE or REE	rare earth elements
S	Freundlich sorption isotherm constant
sec. or s	seconds
SEM	Scanning Electron Microscope
sig.	Observed significance level; values with sig. of $\leq 0.05$ are usually deemed significant
$S_L$	Langmuir isotherm constant; equivalent to $K_d$ for given sorption maxima (M)
SLL	Synthetic Landfill Leachate
t	time
TD	through-diffusion
$t_e$	lag-time, intercept on time axis of cumulative flux vs. time plot for steady state diffusion
$v_f$	discharge velocity

$v_s$	seepage velocity
$w_b$	water “binding” or absorption capacity of a soil in percent
$x/m$	weight sorbate divided by weight sorbent (usually $\mu\text{g/g}$ , $\text{mg/g}$ or $\text{g/kg}$ )
XRD	X-ray diffraction

## 1 Introduction

### 1.1 The geologic barrier

Surface and subsurface geology as a natural restraint for contaminant transport is of primary importance when selecting landfill and waste disposal sites. While most landfills are developed as multi barrier systems, the geologic barrier represents the final contact between the landfill and the environment. A geologic barrier should in its broadest sense seal the landfill and impede the transport of pollutants. The general requirements for effective barriers are: (a) low permeabilities, (b) high retardation capacities regarding mobile contaminants, and (c) sufficient vertical and lateral extent. In order to meet these demands, several western countries drafted legal requirements for geologic barriers in the development of various landfill sites (see Table 1.1).

**Table 1.1** - German example of geologic barrier requirement for various landfill sites

Legal source and Landfill type code	Typical waste material	Minimal required thickness m	Hydraulic conductivity (K) m/s
TA-Si DK I	construction debris	no requirements	no requirements
TA-Si DK II	Household waste	$\geq 20$	$\leq 10^{-5}$
TA-A	Industrial waste	$\geq 20$	$\leq 10^{-5}$

Only very limited numbers of natural geologic units tend to fall within these requirements. Clays and mudstones are generally selected because they appear to be ideally suited as waste disposal barriers. They naturally occur with a sufficient vertical and lateral extent. Further favorable characteristics are relatively low hydraulic conductivities often coupled with high plasticity, which leads to self healing of fractures. Undesired secondary flow along fissures within rock units may also be inhibited by the self healing properties. Furthermore, clays generally exhibit high sorption capabilities, thus retarding the transport of a variety of pollutants.

However, while the indicated physical requirements seem to be adequate in describing an effective geologic barrier, current observations indicate possible barrier failures under certain circumstances. SCHNEIDER & GÖTTNER, (1991) conclude that landfills may contaminate the groundwater even with optimal natural and engineered barriers. They further explain that quantitative predictions of contamination as a function of space and time appears to be extremely difficult, because interfering physical, chemical and biological processes exhibit very complex subsurface transport conditions of contaminants. Geotechnical experiences over the last few years have shown that physical criteria of soils and rocks are inadequate to evaluate landfill barriers. Today, geochemical investigations of chemical reactions in clay units in conjunction with various test substances are the preferred approach [ USTRICH (1991); SCHNEIDER & GÖTTNER (1991)]. Therefore, estimation of long term retardation stabilities of clays depends highly on sorption and structural properties of the clay mineralogy. For example, clay samples containing high amounts of illite-kaolinite exhibit poor sorption capabilities but are chemically resistant. Samples with higher proportions of smectites display good sorption characteristics but are chemically unstable in the presence of certain contaminants [ USTRICH (1991), HASSENPATH (1988)]. Hydraulic conductivity is no longer the single criteria to determine transport and retardation of contaminants within such geologic units. SHACKELFORD (1991) argues that diffusion could be a significant, if not dominant transport process in many waste disposal situations. His findings strongly indicate that in the absence of coupled flow processes, the best contaminant barrier that can be built is one in which diffusion controls the transport of the contaminant [DANIEL & SHACKELFORD (1988); SHACKELFORD (1988)]. Processes of sorption and diffusion do play an important part. While recognized by science, there is currently no acknowledged standardized procedure for geotechnical investigations using diffusion and absorption as evaluation for subsurface contaminant transport. A

promising attempt was made by ROWE *et al.* (1999), but the suggested assessment limits itself to geosynthetic clay liners. Testing approaches for lithologic samples from natural geologic barriers are limited.

Considerable research in diffusive contaminant transport has focused on clay and clay minerals. However, the majority of studies dealt with disturbed samples, e.g. compacted or artificially engineered clay liners in waste disposal sites. Only a limited number of researchers tackled studies with undisturbed samples, for example CZURDA and WAGNER (1986), COOK (1988), KLOTZ (1988), BARONE *et al.* (1989, 1990, 1992), ALLARD *et al.* (1991), and SCHNEIDER and GÖTTNER (1991).

In addition, analyses of pollutant diffusion through clays often focus on single ionic components or organic compounds in unrealistically elevated concentrations (BARONE *et al.*, 1992). Very few investigations (SHACKELFORD *et al.*, 1989; SHACKELFORD & DANIEL, 1991a) attempted the use of artificial leachates in representative concentration, incorporating the probable interactions of various chemical components in true leachates.

## 1.2 Purpose of Study & Selection of Geologic Barrier Material

The purpose of this study is to examine sorptive and diffusive pollutant transport behaviors within selected geologic barriers using an artificial leachate. Transport characteristics are then related to geochemical, mineralogical and physical parameters. By comparing the data, possible simplified indicators for sorptive and diffusive pollutant transport in the subsurface were investigated. Because of high expenses associated with core drilling to obtain undisturbed samples, excess drill cores from a previous study on flow characteristics of various organic and inorganic pollutants in natural geologic barriers were utilized. Research was limited by the availability and quality of cored material. Available samples were taken from various depths of four different clays and mudstones in Northern Bavaria, Germany. These lithologies are commonly considered excellent natural barriers for waste disposal sites. A short description of units sampled is summarized in table 1.2. Locations of the drill sites are also shown in figure 1.1.

**Table 1.2** - Selected geologic barrier units

Relative age	Stratigraphic Name	Short description	Location	Sample Abbreviation
Jurassic	Amaltheen Clay	mudshale to siltshale	Kalchreuth	K
Triassic	Feuerletten	mudstone to siltstone	Creußen	B
Triassic	Lehrberg Layers	siltstone to siltshales	Langenzenn	L
Triassic	Lower Röttonsteine	Siltstone to Siltshale	Marktheidenfeld	M

All selected samples fulfill the requirements for natural geologic barriers, namely (a) 3m minimal thickness, (b) high adsorption capacity, (c) clay mineral content, and (d) wide lateral spread. Chapter 2 contains an individual discussion on each of the localities and their parameters.



**Figure 1.1** - Map of Bavaria indicating sample coring locations. K = Kalkreuth; Amaltheen clay; B = Birkenschlag; Feuerletten clay; L = Langenzenn, Lehrberg Layers; M = Marktheidenfeld, Lower Röttone.

### 1.3 General Procedures

To attain the primary and secondary objectives of the study the following steps were utilized: (1) engineering and construction of diffusion apparatus; (2) development of artificial leachate; (3) geochemical, petrographic, & mineralogical analysis of sample materials; (4) identification of relevant physical parameters of the samples; and (5) computer analysis and modeling of the data.

#### 1.3.1 Engineering and construction of diffusion apparatus.

A number of laboratory methods were developed to measure diffusion coefficients in porous media. Two common basic types of diffusion testing are (a) in-diffusion (ID) and (b) through-diffusion (TD) techniques [CHO *et al.* (1993)]. The in-diffusion method uses one leachate reservoir adjacent to a sample chamber. During the experiment, the concentration of the leachate diminishes in the source, while concentration in the sample increases. After conclusion of the ID-test, the sample is usually sectioned and a concentration profile within the specimen is established.

The through-diffusion technique requires a sample to be sandwiched between a source and a collection chamber. The source reservoir is maintained at a constant leachate concentration, while the collection chamber commonly contains distilled water. The latter is monitored regularly to establish the arrival of various leachate ions or chemical compounds. When the activity of the leachate chemicals in the collection reservoir becomes constant with time, a steady state condition of diffusion is reached and the experiment is terminated. Again the sample is dissected and concentrations are profiled.

Possible adaptations for the above mentioned methods could result in significant improvements in determining diffusion coefficients. ROWE *et al.* (1988) for example introduces a non steady state TD system that allows independent evaluation of sorption coefficients as well. This is especially advantageous when trying to evaluate retardation of pollutants in geologic barriers below waste disposal sites.

For this study a diffusion cell system with the following characteristics was developed: (1) A totally translucent system that allows visual monitoring of the complete system including the sample chamber with clay plug (figure 1.2). This is advantageous when studying diffusion of dyes. (2) Interchangeable end equipment to diffusion apparatus allowing pre-saturation of clay plugs (figure 1.3). (3) sample holder with implanted electrodes for electric conductivity measurements within the clay plug. (4) Reusable leachate and collection chamber attachments, as well as sample cell holders. (E) Easy accessible leachate and collection reservoirs. The consequent equipment can be seen in figure 1.2.

Samples used in the experiment consist of 2 cm to 4 cm thick drill core slices. The outside of each sample core is fitted with three equally spaced electrodes. Each of these small devices consists of two 3mm long gold coated spikes spaced 2.5 mm apart and attached to color coded wires. Thus prepared, the sample is then mounted in a clear polycarbonate cylinder using translucent, specially

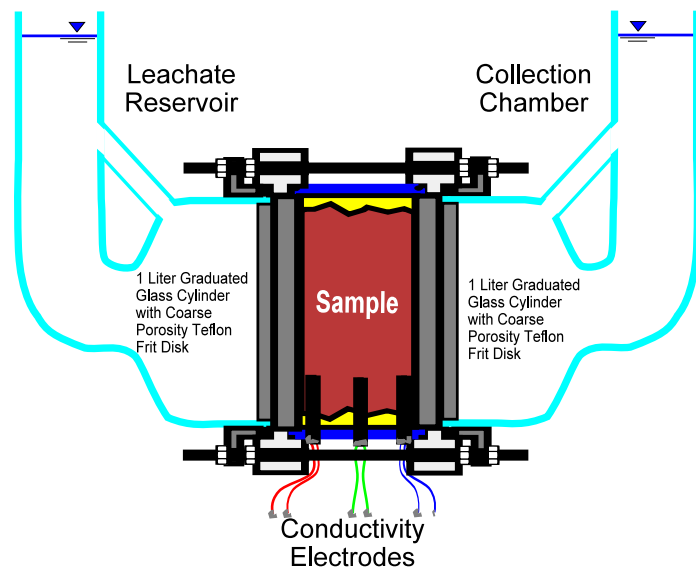


**Figure 1.2** - Through diffusion non-steady state apparatus. Clay sample core, approximately 2 to 4cm in thickness is mounted with clear epoxy into a polycarbonate sleeve. Endplates are composed of coarse Teflon frit disks.

(3) sample holder with implanted electrodes for electric conductivity measurements within the clay plug. (4) Reusable leachate and collection chamber attachments, as well as sample cell holders. (E) Easy accessible leachate and collection reservoirs. The consequent equipment can be seen in figure 1.2.

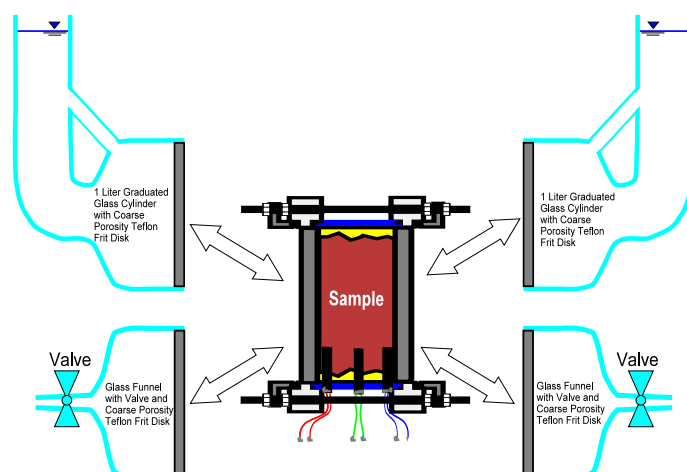


**Figure 1.3** - Interchangeable front and end systems to be mounted to samples in sample holder. This design allows for a variety of different tests.

formulated epoxy resin<sup>2</sup>. Prepared samples were placed in distilled water for several months before being mounted into the sample holder.

Before the actual diffusion test phase, several different interchangeable systems (Figure 1.3) were attached to the sample in the sample holders to further saturate the mounted cores or to instigate hydraulic conductivity experiments, as needed.

After the saturation phase was completed, the diffusion experiments were conducted in climate chambers at 10°C. The temperature is according to DIN 18 130 (1989) for evaluation of hydraulic conductivities and represents conditions to be expected in subsurface lithologies a few tens of meters from the surface. In reference to KOHLER and HARSTRÖM (1994), who suggest that active landfills can reach internal temperatures of up to 90°C, a few diffusion experiments were either conducted or concluded at elevated temperatures of 30°C.

### 1.3.2 Development of artificial leachate

In order to evaluate diffusion and sorption parameters in said samples, an artificial leachate was developed. One of common objections in modern diffusion research is the use of highly concentrated test solutions. BARONE *et al.* (1992) indicates that such elevated chemical concentration either never occur in nature or only exist under rare and extreme circumstances. Another concern is the common use of only a single test parameter, neglecting the interaction of the various substances in a leachate. Development of an artificial average landfill leachate was therefore of major importance.

The requirements for the artificial leachate were as follows:

- Concentration and variety of ions and chemical compounds in the leachate approximates conditions of genuine landfill leachates.
- To simplify the analysis of leachate contents, concentrations needed to be high enough to allow easy detection. Therefore, only constituents found in original landfill waters with concentration of 10 mg/L or more were simulated.
- The leachate should exhibit enough chemical stability over an extended time period without adjusting the solution to artificial pH levels contrary to authentic landfill percolates.

### 1.3.3 Geochemical, petrographic, & mineralogical analysis of sample materials

To establish a geochemical profile, each sample was analyzed by various digestive methods and ICP-AES technologies for a total of 33 chemical elements or their oxides. Further analysis included graphite and organic carbon, CO<sub>2</sub>, as well as sulfide and SO<sub>4</sub> sulfur with the LECO<sup>®</sup> method. LOI techniques at varying temperatures were also employed to estimate water, organic C, and CO<sub>2</sub> contents in the samples [ DEAN (1974)].

Mineralogy of the samples was established by XRD and IR-spectrometry, especially helpful in determining clays. The research was substantiated by thin section and point count analysis, as well as SEM applications. The use of SEM-EDX was also considered but yielded only very limited results. By using geochemical and mineralogical data, attempts were made to establish a definite mineral composition of each of the samples.

---

<sup>2</sup>Research with epoxy materials showed resin EP 116 (Höchst GmbH) and hardener VEH 2628 (Höchst GmbH) in a mixture of 100 g to 41.3 g respectively as best suited for this study. The material can be used around wet materials and sets within 60 minutes. The cured product is virtually transparent, has an outstanding chemical resistance and most important, is inert to ion exchanges, as established by the author through batch experiments.



The chemical behavior of the sampled units was also attained by virtue of the following analytical methods. The Mehlich-Method [KRETZSCHMAR (1991)] was employed to establish the CEC (Cation Exchange Capacity) of the rocks. According to procedures given in DIN 19 684 TEIL 1 (1977), pH measurements were made by combining a sample slurry with a 0.01M CaCl<sub>2</sub> solution. Further sorption characteristics were determined by using a batch method, similar to USEPA OPPTS 835.1220 (1998) and GUADALIX and PARDO (1995).

#### 1.3.4 Identification of relevant physical parameters of the samples

One of the most useful analysis of sedimentary rocks is the grain size distribution FOLK (1980), aiding in petrologic interpretation. The small grain sizes of the clay and mudstones samples called for grain size analytical procedures according to DIN 18 123 (1983), comprising sieve and elutriation analysis. In addition, grain density was evaluated. An important parameter in establishing void ratio  $e$  and effective porosity  $n_e$ , measurements were done according to DIN 18 124 (1997) using a 25 ml pycnometer or calculated from available hydraulic data..

Testing for a whole suite of physical soil parameters appears to be out of place in a diffusion study. However, a great variety of these tests are quickly administered. The idea was to look for a correlation between the diffusion and sorption data and physical soil characteristics. The examinations were limited to those relating to the influence of moisture in the rock samples. Selected tests include consistency limits, such as ductility, plasticity, and contraction limit evaluation, consistency index, moisture-holding capacity, and natural moisture equivalent. However, many of these soil parameters, while conducted in previous studies of the sample materials could not be correlated with the samples used in the diffusion experiment.

A previous investigation (PÖTZL, 1998) of same sample materials determining the hydraulic conductivities of the samples subjected to various contaminant solutions yielded a wealth of hydraulic information. Available data often matched core depths for this sorption and diffusion investigation precisely, thus were directly incorporated into this study. Where depth variances existed, enough circumstantial data was available to extrapolate closely matching averages for the necessary coring depth.

#### 1.3.5 Computer analysis and modeling of the data

Evaluation of the sorptive character of the various chemical species of the artificial leachate within each specific lithologic sample was accomplished by using the regression and graphical function in the SSPS statistical and analytical software (SSPS, 1999)

Interpreting the diffusion data needed a more specific analytical approach. Here the software POLLUTEv6 (GAEA, 1997) developed by ROWE *et al.* (1994) and distributed by GAEA Ltd, Canada, was most qualified. The program solves one dimensional dispersion-advection equations for a layered deposit of finite or even infinite extent. As indicated by ROWE *et al.* (1994), PolluteV6 does not require "time-marching" procedures, unlike other finite element and finite difference formulations. The concentration of a contaminant can therefore be directly determined at any specified time without calculating the concentrations at earlier times. The software is hence very well suited for modeling approaches of diffusion in laboratory sample plugs.

## 2 Selected Clay barriers and their Geology

### 2.1 Regional Geography and Geology

Frankonia in the Northern part of Bavaria, Germany, contains several lithologic clay units suitable for geologic barriers. For this study coring samples from a Jurassic and three Triassic rock units were available. Figure 2.1 shows coring locations.

The region of Franconia approximates the Northern 1/3 of the German state of Bavaria, comprising approximately

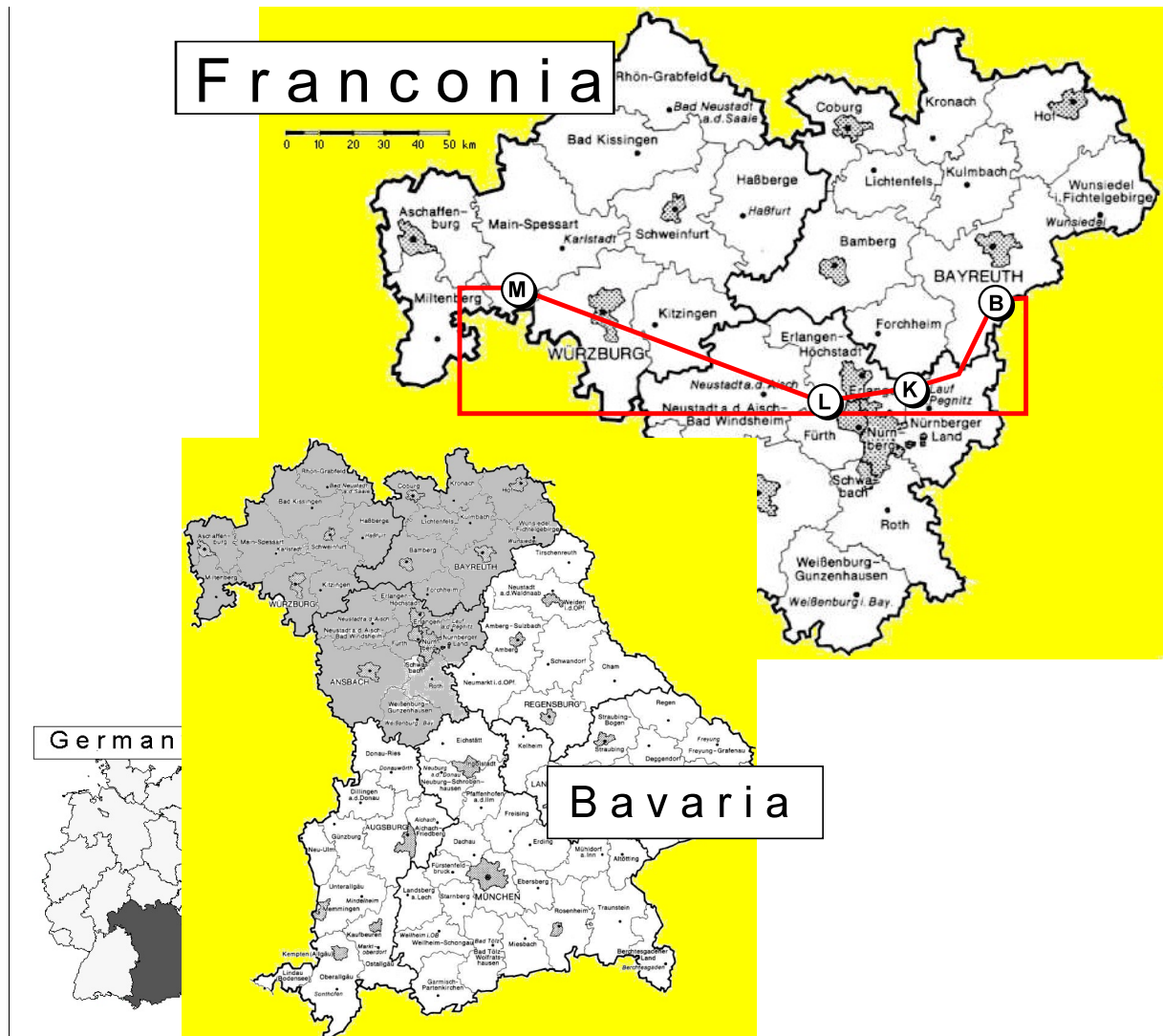


**Figure 2.1** - Sample core locations within Franconia, Bavaria, Germany. Outlined area shows geographic extent of geologic map and stratigraphic section shown in figure 2.4. Key: K = Kalchreuth; Jurassic Amaltheen clay; B = Birkenschlag; Triassic Feuerletten clay; L = Langenzenn, Triassic Lehrberg Layers; M = Marktheidenfeld, Triassic Lower Rötone.

24,000 km<sup>2</sup>. The area is divided into three subregions, Lower Franconia (Ger. Unterfranken), Middle Franconia (Ger. Mittelfranken), and Upper Franconia (Ger. Oberfranken). For the following brief discussion on physical geography and simplified geology of the regions, please refer to figures 2.2 and 2.3 respectively.

With 8,487 km<sup>2</sup> in size, Lower Franconia is the largest region of Franconia and the Northwestern most part of Bavaria. It is traversed centrally by the Main River. Agriculture is widely pursued, and industry is centered at Würzburg (the region's capital), Schweinfurt, and Aschaffenburg to the West. Bad Kissingen in North Central Lower Franconia is a noted resort. The area is framed to the Northwest by hilly regions of the Rhön and Spessart Mountains with elevations in the 900 meters and 500 meters respectively. The basalt and phonolite peaks of the Rhön appeared

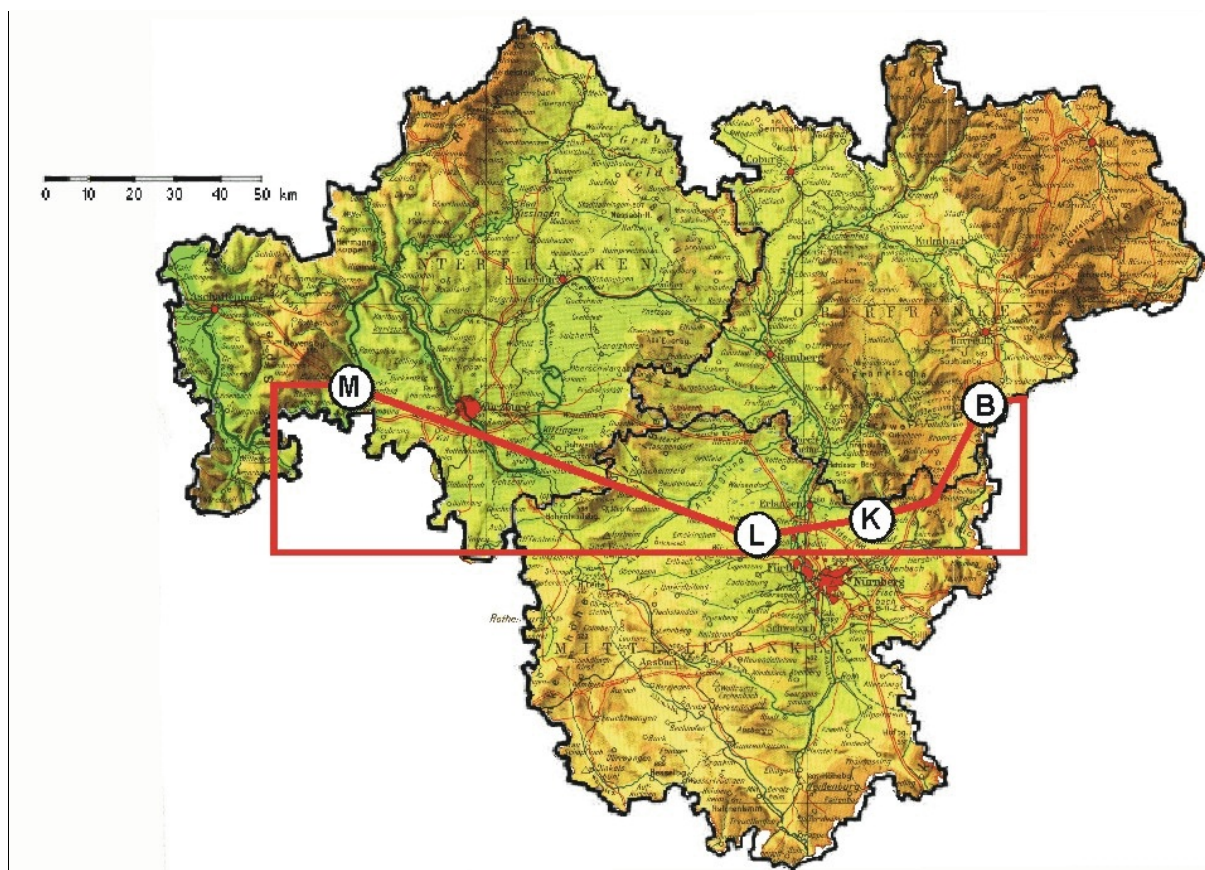


**Figure 2.2** - Physiographic map of Franconia. (Source: HARMS ATLAS, 1977) Outlined area shows extent of geologic map and stratigraphic section shown in figure 2.4. Key: K = Kalchreuth; Jurassic Amaltheen clay; B = Birkenschlag; Triassic Feuerletten clay; L = Langenzenn, Triassic Lehrberg Layers; M = Marktheidenfeld, Triassic Lower Röttone.

in the Tertiary, during a time of intense volcanic activity. The Spessart is part of the central German crystalline zone, consisting in Lower Franconia predominantly of Lower Paleozoic schists and gneiss. These metamorphic mountains were also subjected to fracturing, indicated by sets of Northwest to Southeast trending fault systems. The Eastern edge of the Spessart is covered by Lower Triassic Sandstones. The only Permian lithologies in Franconia can be found in small slivers toward the Western borders of the Spessart and at the edge of the region. Triassic sedimentary rocks are indicative from the Spessart to the Eastern borders, where Lower Franconia is flanked by the gentle hills of the Steigerwald and Haßberge with elevations in the upper 400 to lower 500 meters. This hilly region with their Southern extension Frankenhöhe in Middle Franconia, form a watershed divide. Drainage to the East will merge into the Main River and continues from the Rhine River to the West into the Northern sea, while flow pattern to the East will travel Southward to the Danube River, therefore streaming into the Black Sea. (RUTTE, 1957; RUTTE, 1981; NESTMEYER, 1996; BAYERISCHES GEOLOGISCHES LANDESAMT, 1981a + b). Sample location M (Marktheidenfeld) for this study in the Lower Triassic Röttone lithologies is located in the Mid-Southern outskirts of Lower Franconia.

Middle Franconia, comprising about 7,617 km<sup>2</sup>, identifies the Southern part of Franconia and the North central section of Bavaria. Centrally located is Ansbach, the capital, while the conglomerations of the large cities Nuernberg, Fürth, and Erlangen to the Northeast are distinguish industrial and cultural centers. Except for the region of indicated cities, most of Middle Franconia is hilly and fertile. The area is flanked to the West by the gentle rises of the Frankenhöhe with elevations in the lower 500 meters. The Franconian Jura Mountains with altitudes around 600 meters are comprised of Jurassic Sedimentary rocks and flank Middle Franconia to the South and East. The remaining regions of Middle Franconia exhibit mainly Triassic sedimentary rocks. The three major rivers of this area, Altmühl, Rednitz, and Pegnitz, drain to the South and Southeast. (RUTTE, 1957; RUTTE, 1981; NESTMEYER, 1996; BAYERISCHES GEOLOGISCHES LANDESAMT, 1981). Two of the sample locations for this research, L (Langenzenn), Triassic Lehrberg Layers, and K (Kalchreuth), Jurassic Amaltheen Clay, are located in the North and Northeastern

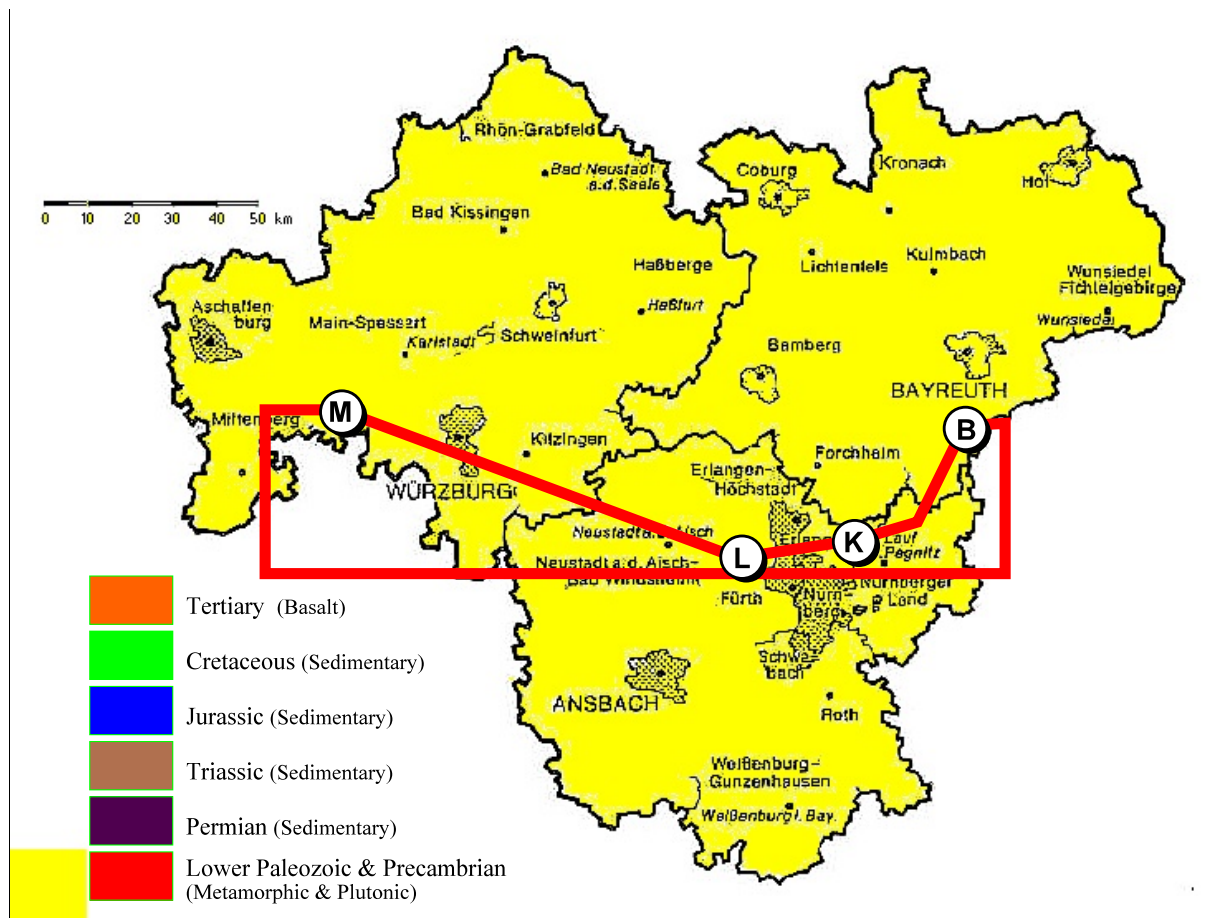


**Figure 2.3** - Simplified regional geologic overview of Franconia. (after BAYERISCHES GEOLOGISCHES LANDESAMT, 1981) Outlined area shows extent of geologic map and stratigraphic section shown in figure 2.4. Key: K = Kalchreuth; Jurassic Amaltheen clay; B = Birkenschlag; Triassic Feuerletten clay; L = Langenzenn, Triassic Lehrberg Layers; M = Marktheidenfeld, Triassic Lower Röttone.

boundaries of Middle Franconia.

Upper Franconia, about 7,501 km<sup>2</sup> in size, is located to the Northeast of the Franconian region. The capital Bayreuth to the Southeast, as well as Bamberg, Coburg, and Hof are the chief cities and industrial centers. The far Northeastern section of the area touches the Czech border. Except for a narrow strip on it's Western border, where the Main and Regnitz rivers have leveled the topography, Upper Franconia is likely the most mountainous of the three Franconian regions. Centrally located, stretching to the South into the Fränkische Alb are the hills of the Fränkische Schweiz. Dominated by characteristic steep Jurassic limestone cliffs and canyons, the area exhibits elevations in the upper 500 meter range. Except to the South, the Fränkische Schweiz is surrounded sides by topographically more subdued Triassic lithologies, thus forming the center of a North-northwest trending synclinal structure. The large mountain ranges of Fichtelgebirge and Frankenwald, comprised mostly of Paleozoic and Precambrian metamorphic and plutonic rocks, cover the Northeastern 1/3 of Upper Franconia. Elevation is in the 800 to upper 900 meter range, with Franconia's highest point, the Ochsenkopf Mountain (1024 m), being located in Southeastern part. Some Northwest trending faulting is exhibited in the crystalline rocks of these mountains. Between Fränkische Schweiz and Fichtelgebirge is a small strip of block faulting. Here small strips of sedimentary Mesozoic rocks were laterally displaced against each other during strong tectonic events in the Tertiary. The region is drained by the Main and Pegnitz rivers. The Main follows an Easterly course, and Pegnitz exhibits a Southward flow. (RUTTE, 1957; RUTTE, 1981; NESTMEYER, 1996; BAYERISCHES GEOLOGISCHES LANDESAMT, 1981a+b). Sample site B (Birkenschlag), Triassic Feuerletten clay, is situated in the central South eastern border of Upper Franconia.

## 2.2 Stratigraphic overview

Geologically older lithologies are found to the West of the area of interest decreasing in age toward the East. Following this pattern, sample sites for the clay cores used in this study follow this trend. Figure 2.4B shows the



stratigraphy, surface geomorphology and surface geology in a longitudinal cross section along mentioned sample side. For the following discussion, reference should be made to the above mentioned figure in addition to more detailed stratigraphic sections summarized in figure 2.5 and 2.6.

The geologically youngest samples for this study were drilled in a clay pit near Kalchreuth, consisting of the Early Jurassic Amaltheen Clay or Lias δ (Jlδ) unit. This dark shale with an average thickness of 35 m is part of 85 m of the clays and marls of the Lias lithologies, including a Triassic-Jurassic transition zone composed of sandstone and clay lenses. This Rhaet-Lias transition zone and the before mentioned Lias stratigraphies are commonly mapped as Tku + Jl. The Lias units are overlain by the Jurassic Dogger units consisting of sandstones, clays, marls and oolitic limestones (see figure 2.5).

Just below the Rhaet-Lias transitional unit lies the red mudstones and shales with dolomite and sandstone beds of the Feuerletten (Trkmf), the next sample of interest. The Feuerletten lithologies exhibit an average thickness of 60 m and were cored near Birkenschlag, furthest to the East in the cross section shown in figure 2.4. The unit is preceded at the base by the Triassic Sandstone Keuper with alternating layers of claystone and sandstone, interbedded with dolomite (see figure 2.5).

Quaternary	Q <sub>s</sub>	Sand cover, drift sand	
	Q <sub>l</sub>	Loess, loess loam, loam cover	
Cretaceous	Ku	Upper Cretaceous Layers Sandstones, Clays, Marls, Limestones	
Jurassic	Jm	Malm (White Jura) Marls, Limestones & Dolomite (layered & reef structures)	
	Jd	Dogger (brown Jura) sandstones with iron oxide seams, clays, marls, & oolitic limestones	
	Jl+ Tku	Lias (Black Jura) Clays, marls, & limestones partly bituminous, base sandstones Upper Keuper (Rhaet) Sandstones & Clays	
	Trkmf	Feuerletten (Nodular Marl) red claystones with dolomite and sandstone beds	
	Trkms	Sandstone Keuper alternating layers of Claystone & Sandstone with interbedded Dolomite	
	Trkmg	Gypsum Keuper predominantly claystones interbedded with Marl and Gypsum, some Sandstone	
	Trkl	Lower Keuper Clay & Marl with Sandstone, Dolomite, & Limestone	
	Triassic	Trmu	Upper Muschelkalk Limestone, Marl, & Claystones
		Trmm	Middle Muschelkalk Marl, Claystone, Limestone & Dolomite, Gypsum, Anhydrite, some Halite
		Trml	Lower Muschelkalk Limestone & calcareous Marl
Trsu		Upper Buntsandstein Claystones & finegrained Sandstones	
Trsm		Middle Buntsandstein predominantly medium to coarse grained Sandstones, occasionally pebbly	
Permian	Trsl	Lower Buntsandstein predominantly finegrained Sandstones with some Claystones	
	Pz	Zechstein Dolomite & Claystones with Anhydrite & Halite	
	Pr	Rotliegendes Sandstones, fan conglomerate	

Figure 2.4 (Part A) - Legend for 3 D Map showing surface geology, topography, and stratigraphic cross section for area of interest.

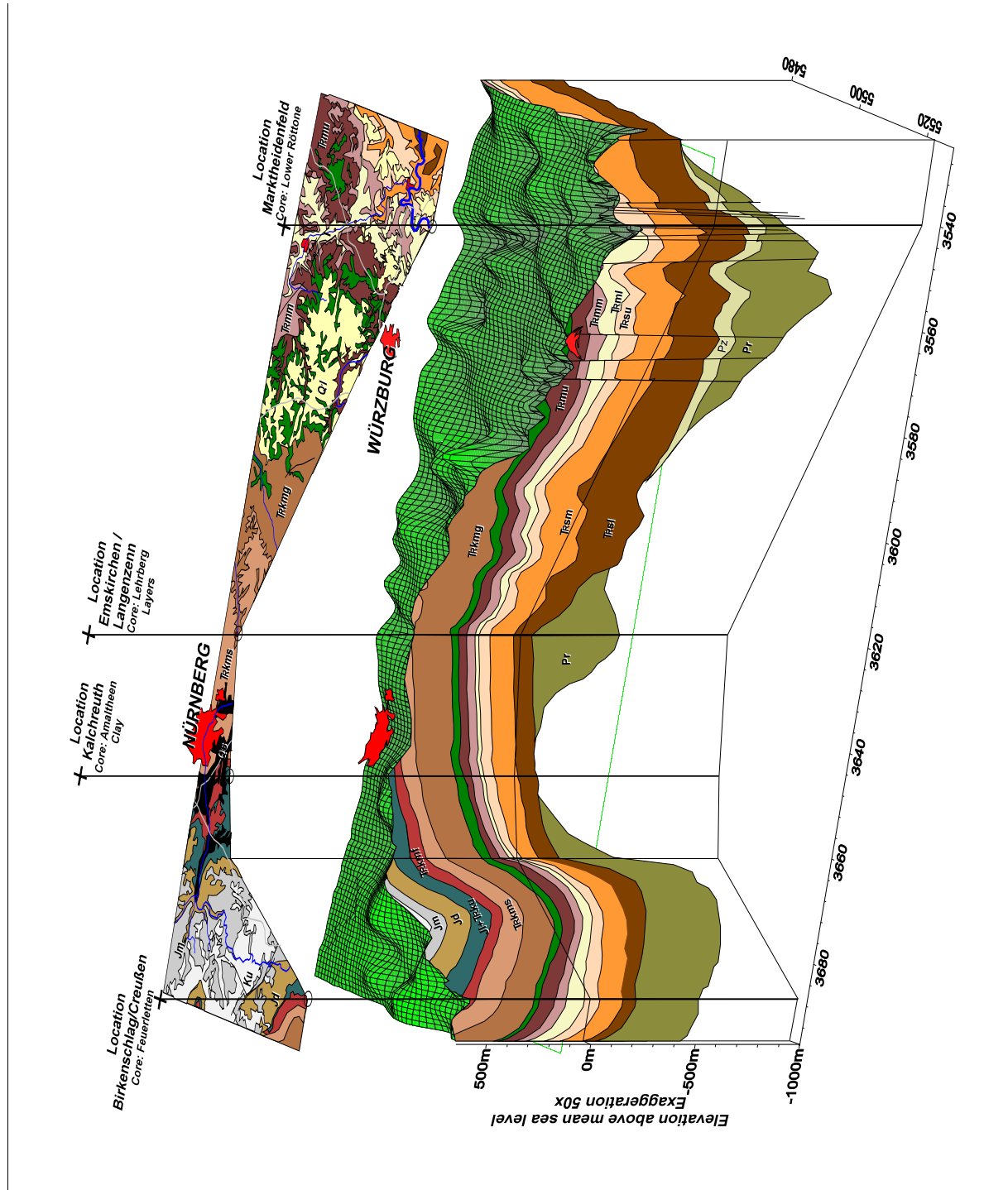


**Figure 2.4 (Part B)** - 3 D illustration showing surface geology, topography, and stratigraphic cross section for area of interest. Values along the x-axis plane correspond with the first for digits of the Gauß-Krüger coordinate system. Information for illustration extracted from (RUTTE, 1957; RUTTE, 1981; BAYERISCHES GEOLOGISCHES LANDESAMT, 1981a+b).

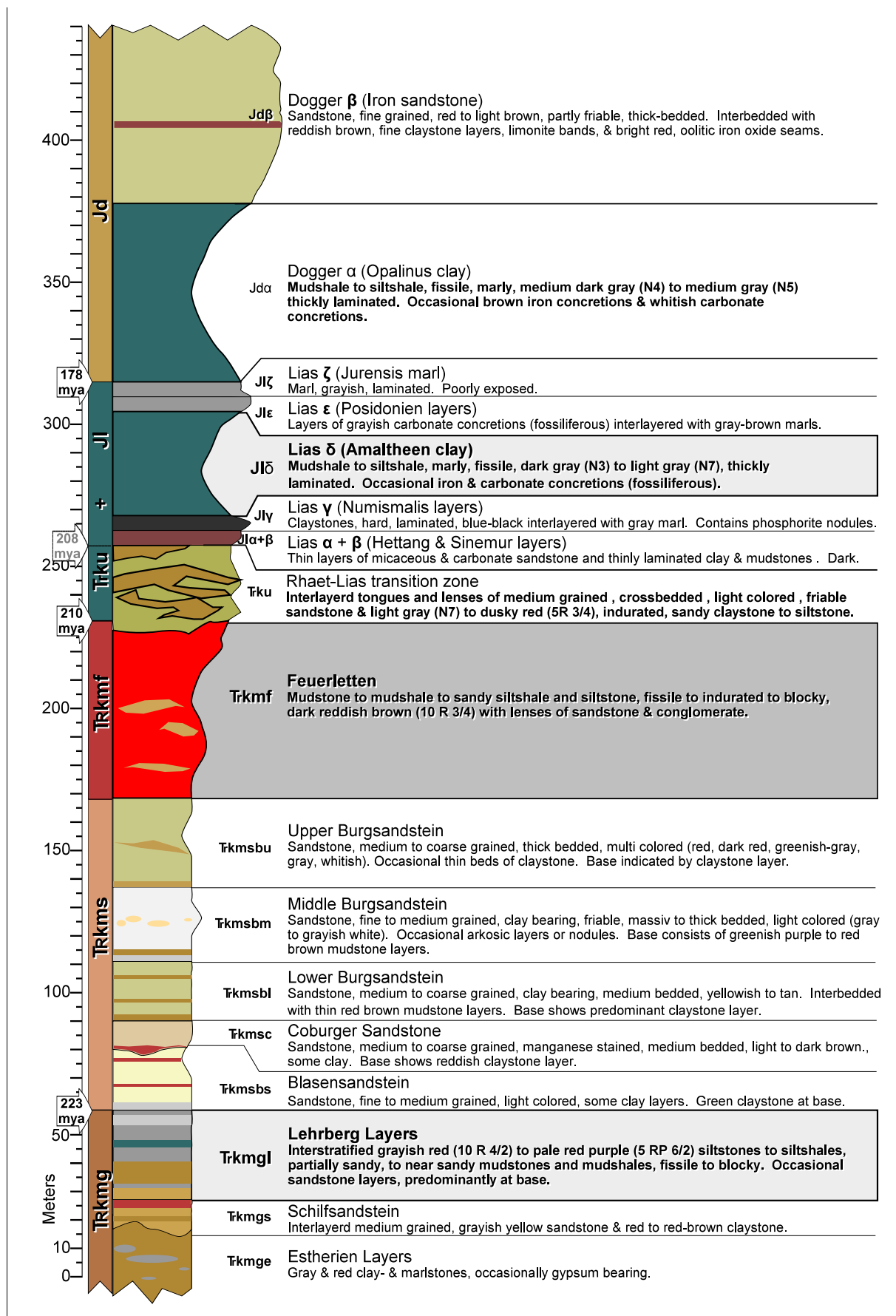
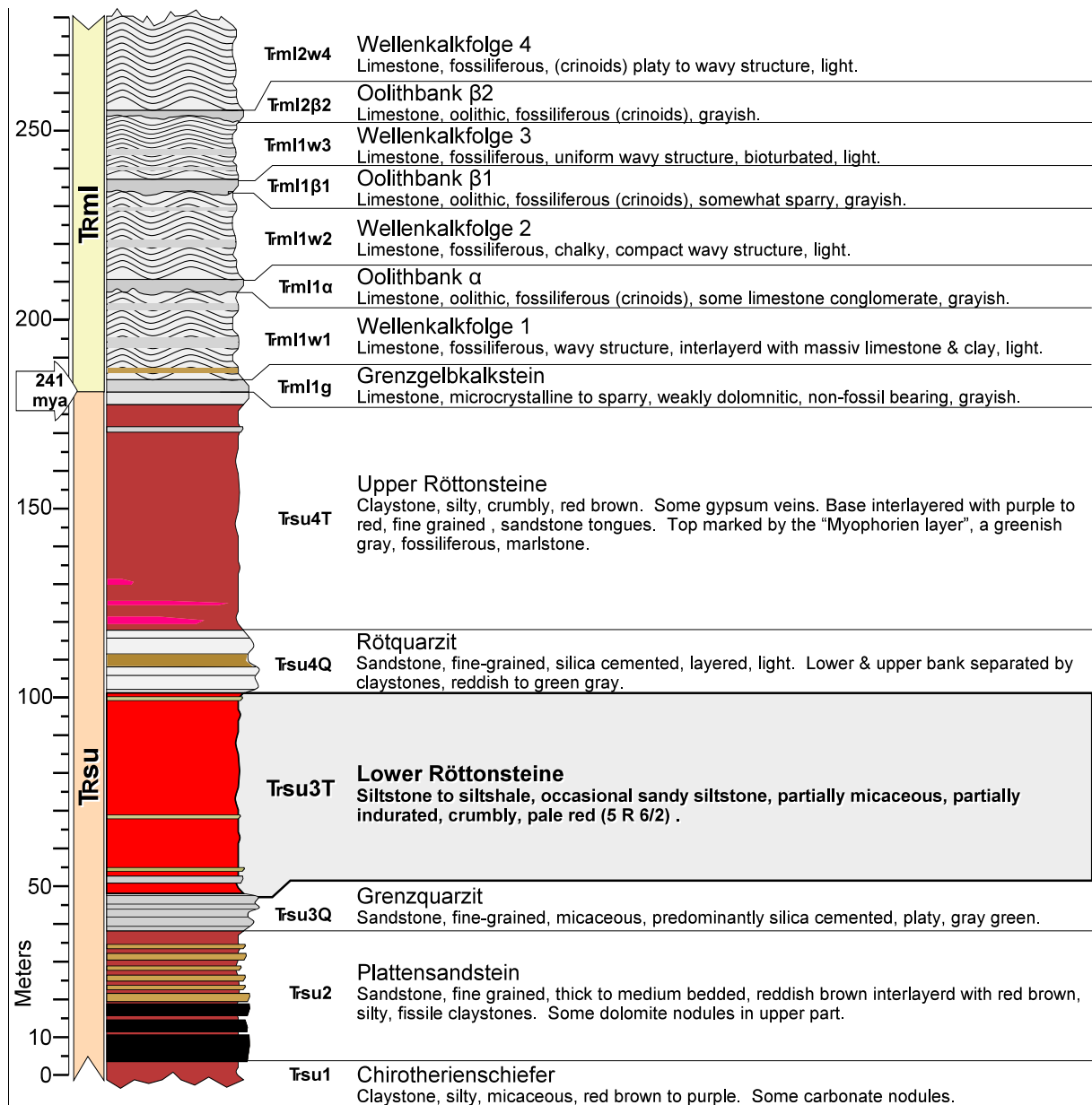


Figure 2.5 - Stratigraphic section of Triassic Middle & Upper Keuper and Jurassic Lias & Dogger lithologies. Units of interest highlighted. Compiled from RUTTE, 1957; RUTTE, 1981; BAYERISCHES GEOLOGISCHES LANDESAMT, 1981a+b; SCHWARZMEIER, 1979.



**Figure 2.6** - Stratigraphic Section of Lower Triassic Lower Muschelkalk and Upper Buntsandstein. Lithology of interest highlighted. Compiled from RUTTE, 1957; RUTTE, 1981; BAYERISCHES GEOLOGISCHES LANDESAMT, 1981a+b; SCHWARZMEIER, 1979.

Below the Sandstone Keuper starts the Triassic Gypsum Keuper (Trkmg) with predominant claystones interbedded with marl, gypsum and occasional sandstone. The youngest unit of Trkmg are the Lehrberg Layers, interstratified siltstones and siltshales which were cored in a clay pit mine near Langenzenn for this study. The average thickness of this unit approximates 30 m. The stratigraphy is shown in figure 2.5

The oldest samples used are Triassic Lower Röttone (Tsu3T) cored at exposed surface location Marktheidenfeld. They are one of the highest members of the Early Triassic Upper Buntsandstein Formation (so3T) and consist of slightly sandy, micaceous, weakly laminated, pale reddish brown (10 R 5/4) clay- and siltstones. In the area of Marktheidenfeld thicknesses of 17m to 21m are reached. Interbedding with up to 0.20m fine grained siliceous sandstones and gypsiferous banks of a few centimeters, occasionally replaced by calcite and dolomite crystals, can be found near the base (Schwarzmeier, 1979). The member is sandwiched between the predominantly silty and occasionally gypsiferous Upper Rötton Member (so4T) and the medium to coarsely laminated, very fine grained Plattensandstein Member (so2T) below. The prominent 0.25m to 3m thick marker of the Frankonian Chirotherienquarzit, a fine to medium grained, primarily silica cemented, platy, ledge-forming sandstone, separates the Upper and Lower Röttone (Rutte, 1957). While thickness of the Upper Röttone decreases toward the North



(Amorbach: 14m; Wertheim & Kronach: 8m; Bad Kissingen: 0.50m; Mellrichstadt: 0m), an increase is observed in the Lower Röttone (Amorbach: 5m; Schweinfurt: 25m; Mellrichstadt: 70m) (Rutte, 1981).

The depositional environment of the Lower Röttone appears to be terrestrial indicated by root horizons and reptile tracks in interlayered sand tongues. Toward the Southeast of Kulmbach, at the edge of the depositional basin, overall thickness of the Upper Buntsandstein decreases and coarsegrained, arkosic material becomes increasingly dominant (Schwarzmeier, 1981). For a detailed stratigraphic illustration of the location of the Lower Röttone within a stratigraphic section see figure 2.6.

## 2.3 Description of selected barrier units

### 2.3.1 Lower Jurassic Amaltheen Clay (Kalchreuth)

The Amaltheen clay or Lias  $\delta$  (Jl $\delta$ ) is the mightiest of the Lias units measuring approximately 40 m at the sample coring vicinity (HAARLÄNDER, 1966). The unit consists of uniform, marine sediments, mostly dark gray (N3) to light gray (N7) fissile, marly mudshales to siltshales. Weathering decalcifies the Amaltheen lithologies often resulting in unctuous clays (HAARLÄNDER, 1966). *Amaltheus costatus* REIN and *Amaltheus margeritatus* MONTF. fossils are often found within the Amaltheen Clay. Iron concretions of up to 15 cm diameter are common in the middle and upper third of the unit.

The center of these argillaceous ironstones frequently consist of one or more gray calcite nodules, often surrounded by limonite. On occasion dark cored, gray pebble phosphate, about 10 cm in diameter, is found. The mineralogical composition of muscovite/illite (~60%), kaolinite (~13%), quartz (~11%), and carbonates (~5%) suggest a marine depositional environment (DOBNER, 1984).

The exact location of the Amaltheen Clay sample core used in this study is R<sup>44</sup> 37 640 / H<sup>54</sup> 90 090 in the Gauß-Krüger coordinate system, a point near the village of Kalchreuth, about 10.5 km SE from the city of Erlangen. The coring log is summarized in appendix A.1. The

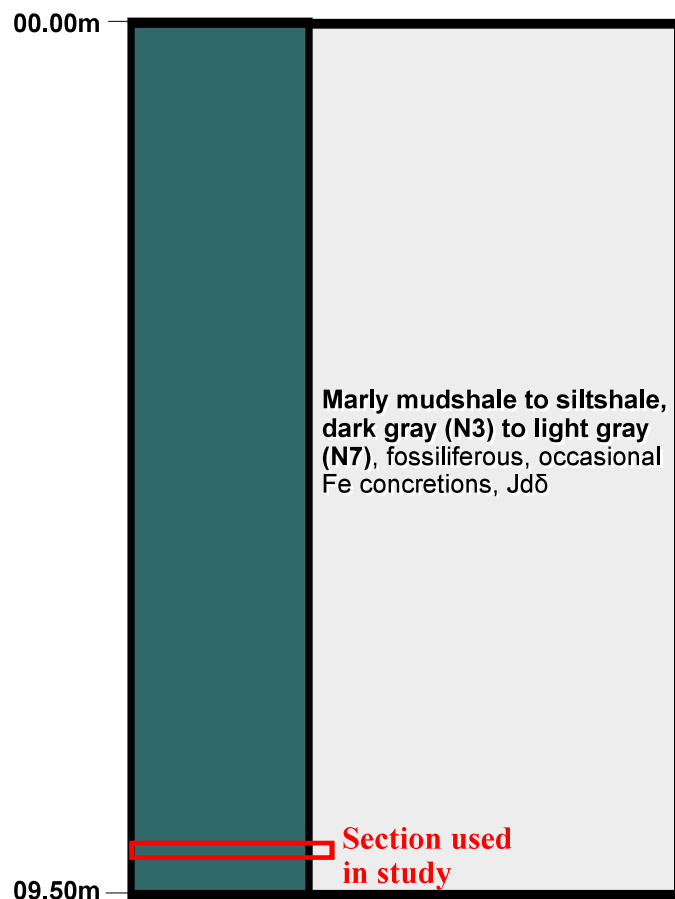


**Figure 2.7** - Coring Profile of Amaltheen Clay at sample location. Area of core used in study indicated. Descriptive log summarized in appendix A.1.

core shows very uniform lithology and is graphically represented in figure 2.7. As indicated in the figure, the core sample used in this study was taken from a depth of 9 m<sup>3</sup>.

### 2.3.2 Upper Triassic Feuerletten (Creußen)

The Feuerletten clay (Trkmf) can exhibit thicknesses of 50 to 60 meters (FÜRST, 1956; PASCHE, 1993a). Composition is predominantly dark reddish brown to purplish-red, partly greyish-green, mudstones to mudshales and sandy siltshales to siltstones. The unit vacillates from fissile to indurated to blocky in its appearance. Occasional calcareous marl nodules with diameters of up to 5cm were described by PASCHE (1993b). Except for areas of caliche and in the vicinity of calcite conglomerations, the Feuerletten unit is carbonate free. Occasional minor lenticular layers of fine sand are also observed.

The depositional environment of the Feuerletten clays was most likely on the fringe of a basin, dominated by an oscillating deltaic environment (RUTTE, 1957). Because of 9 - 11% linear drying shrinkage in Feuerletten materials, DOBNER (1984) suggests a high fraction of expansive clays. He also lists the average mineralogical analysis as illite / muscovite (~27%), montmorillonite and mixed-layer clays (~20%), quartz and feldspars (~27%), carbonates (~5%), and kaolinite (~10%). The Heavy mineral analysis of the unit shows 82% zircon, 5% monazite, 5% tourmaline, 7% rutile, and 1% staurolite (HÄNEL, 1974).

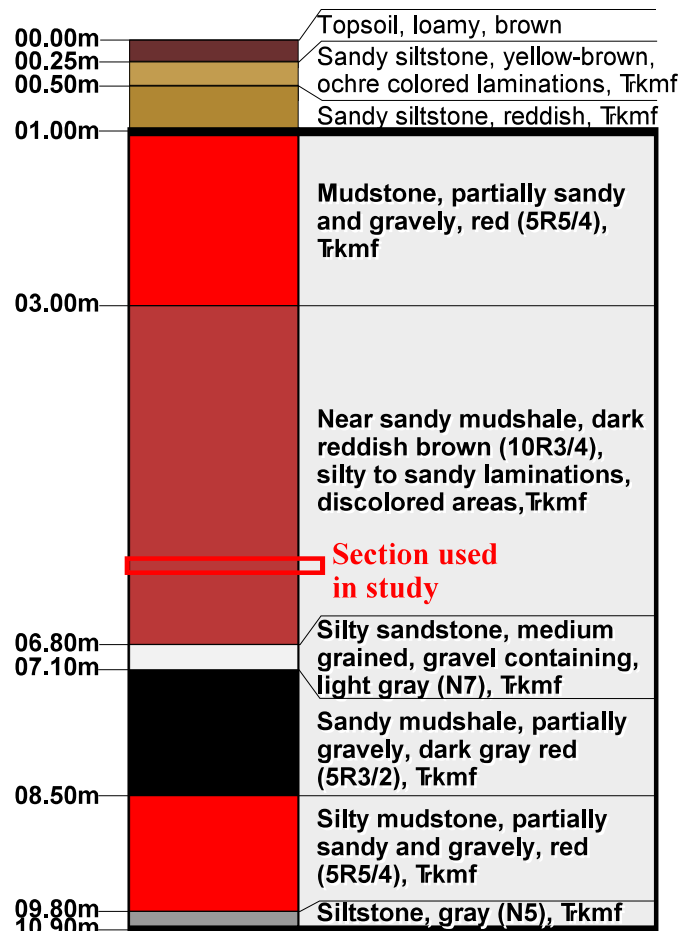


**Figure 2.8** - Coring Profile of Feuerletten Clay at sample location. Area of core used in study indicated. Descriptive log summarized in appendix A1.

The Feuerletten core was drilled in a forested area about 4.2 km NW of the city of Creußen at R<sup>44</sup> 71 260 / H<sup>55</sup> 26 860 (Gauß-Krüger coordinates) to a total depth of 10 m. The drilling profile is shown in figure 2.8 and a detailed written log is found in appendix A.1. The upper 0.75 m of the core consist of sandy siltstones, followed below by 2m of red, partly sandy to gravelly mudstone. Continuing downward, the next 3.8 m consist of dark reddish brown near sandy mudshales with discolored areas and silty to sandy laminations. This section is underlain by 30 cm of light grey, medium grained, partially gravelly, silty sandstone, pursuit by 1.4 m of dark grey red sandy mudshales. The

<sup>3</sup> Decision of core samples used in this research was dependent upon availability and experimental sustainability of the sample. While experiments were conducted with many more samples, only those mentioned in this research survived the diffusion tests and were useful at the end in procuring useable data.

lower 1.5 m exhibit red silty mudstones with a 20 cm grey siltstone layer at the base. The sample for this study was taken from a coring depth of 6 m as indicated in figure 2.8.

### 2.3.3 Triassic Lehrberg Layers (Langenzenn)

The exact location of the coring point for the Lehrberg Layer samples is R<sup>44</sup> 12 630 / H<sup>54</sup> 85 540 (Gauß-Krüger coordinates) in an old clay pit near the city of Langenzenn. The total drill depth was 14 m. Detailed profiles are given in figure 2.9 and appendix A.1.

The Lehrberg Layers (Trkmgl) consist of thin layered interstratified grayish red to pale red purple, partially sandy, weakly dolomitic siltstones to siltshales to near sandy mudstones and mudshales. The appearance of the layers is often blocky to fissile. Thin bands of fine, grey, micaceous sandstone are often traversing the Lehrberg lithologies. Sandstones are predominantly observed about 1.5 to 4 m above the base of the unit. The Lehrberg stratigraphy is sandwiched between the capping Blasensandstein (Trkmsbs) and the subjacent Schilfsandstein (Trkmgs), both medium grained sandstones. The transition to the overlying Blasensandstein is indicated by light-grey, 10 to 15 cm thin, marly beds (BERGER, 1966 & 1975). Thickness of the Lehrberg Layers averages West of the Frankenalb 25 to 30 m and in the area of Kulmbach - Bayreuth 35 to 45m (DOBNER, 1984).

The depositional environment was predominantly fluviomarine with gypsiferous, fossil-poor sediments and occasional sand illuviations, indicative

of dry periods (RUTTE, 1957). Mineralogical averages are given by DOBNER (1984) as illite / muscovite (52 - 72 weight %), quartz (10 - 30 weight %), and feldspars (6 - 12 weight %). Kaolinite occurs in traces. Dolomites dominate the carbonate fraction and are concentrated in clay-silt layers with a variation of 2 to 10 weight %.

The core taken at the sampling site consists of colorful fine sandstone and sandy siltstone layers of varying thickness in the upper 2.5 m section, followed by another 2.5 m of fairly uniform pale red purple siltshale with greyish red discolorations at the base. The next 5.4 m are comprised of an undifferentiated pale red purple siltstone. One of the research samples was extracted at 6 m coring depth from top of this unit. Below are two small layers of marly

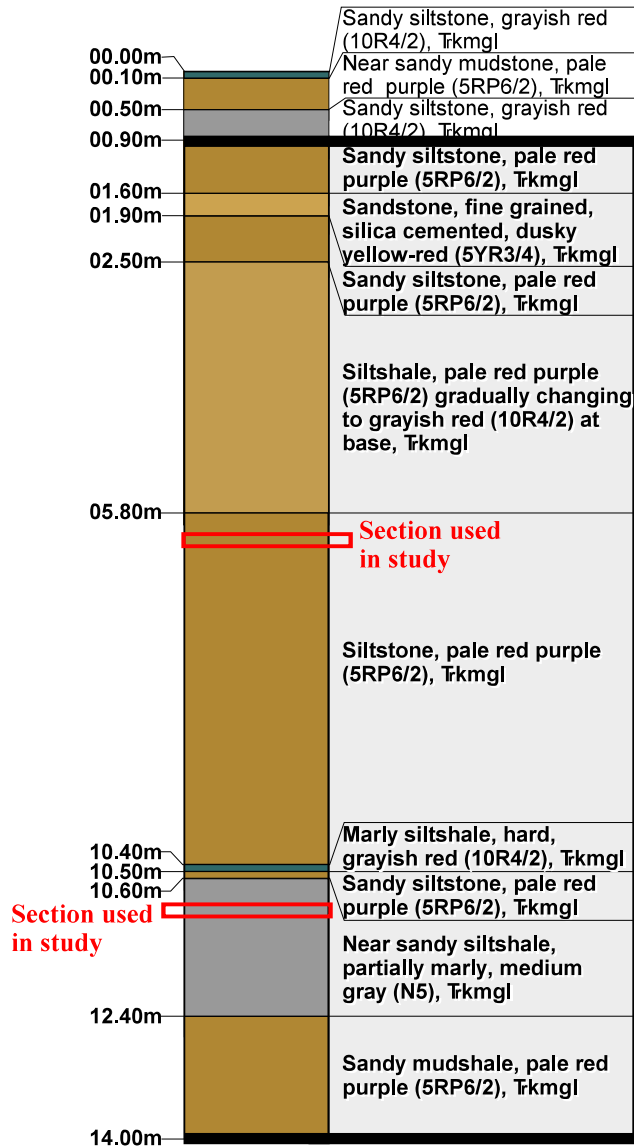


**Figure 2.9** - Coring Profile of Lehrberg Layers at sample location. Area of cores used in study indicated. Descriptive log summarized in appendix A1.

siltshale and sandy siltstone of 10 cm each, underlain 1.8 m of medium grey, partially marly, near sandy siltshale, where another research sample was taken at 11 m coring depth. The base of the core is formed by 1.6 m of pale red purple sandy mudshale.

### 2.3.4 Lower Triassic Röttone (Marktheidenfeld)

DOBNER (1984) describes the Lower Röttone (Tsu3T) as slightly sandy, micaceous, poorly stratified clay- and siltstones. Closer investigation reveals not true clays, but partially indurated, crumbly, pale red siltstones with elevated amount of clay sized particles. The average mineralogy of the clay fraction is illite (~ 90 weight %), chlorite (~ 4 weight %), and corrensite (~ 6 weight %). The Röttone probably formed in a limnic - terrestrial environment. The terrestrial influence is substantiated by the total mineralogy, which shows approximately 45 weight percent quartz (SALGER & SCHWARZMEIER, 1985), the highest of all samples used. The thickness of the unit can approximate 50 m, with 17 to 21 m in the core drilling vicinity.

The unit is capped by 10 to 15 m of fine-grained, silica cemented sandstones, called the Rötquarzit (Tsu4Q). The Trsu3T is truncated at the base by a few meters of Grenzquarzit (Trsu3Q), a fine-grained, micaceous, predominantly silica cemented, platy sandstone. Just above the Grenzquarzit with the Lower Rötton lithologies, pale purple to greyish green reduction horizons of up to 20 cm were observed. Other common stratigraphic observation in Trsu3T are fine-grained sandstone lenses, gypsum bearing strings, and silica cemented strata displaying ripple marks (SCHWARZMEIER, 1979). The range of the Rötton formation stretches from the Southwest to the Northeast through Lower Franconia. Extensive sediments of the unit in Upper Franconia are only found North of the city of Kronach. Toward the Southeast the clay- and siltstone lithologies are gradually replaced by sandstones (DOBNER, 1984).

The exact coring location for the Löwer Röttone is R <sup>35</sup> 41 540 / H <sup>55</sup> 22 580 (Gauß-Krüger coordinates), approximately 2.5 km Southwest of the city of Marktheidenfeld.. The detailed drill profile is shown in figure 2.10 and appendix A.1. Total coring depth was 13 m. The upper 2 m of the core consist of interstratified silt-, sand-, and claystones of varying thicknesses. Below are 1 m of

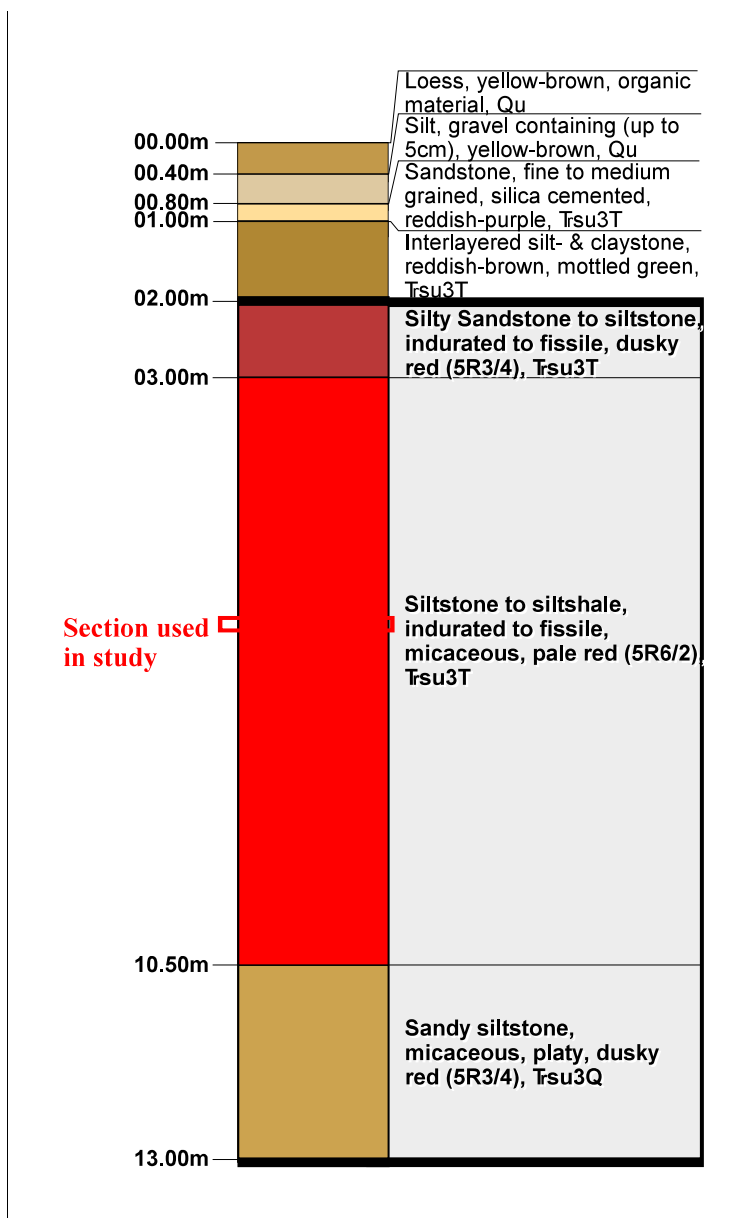


**Figure 2.10** - Coring Profile of Lower Röttone at sample location. Area of core used in study indicated. Descriptive log summarized in appendix A1.

dusky red, indurated to fissile silty sandstone to siltstone, followed by 7.5 m of pale red, micaceous, indurated to fissile siltstone to siltshale. The sample used for this study was taken from the later at a coring depth of 6 m. The base of the core exposes 2.5 m of dusky red, platy, micaceous, sandy siltstone.

### 3 Geochemistry

In order to understand composition and character of the investigated clay as natural geologic barriers, a complete geochemical analysis for major and minor elements was attempted. In addition, exchangeable ions within the samples were also surveyed. Results not only helped to decipher composition, origin, and history of the various lithologic units, but more important, aided in the understanding of transport and sorption characteristics. For this purpose various analytical systems were employed. Main analytical tools for the investigation of solids were ICP-AES (Inductively Coupled Plasma Atomic Emission Spectrometry) analysis using two different digestive techniques:

(A) Whole rock analysis for major rock forming elements: Core cuttings are pulverized to Mesh 60 (grain size: 0.15mm). A 200 mg sample split is fused with 1.2 g of  $\text{LiBO}_2$  (lithium borate) at approximately  $925^\circ\text{C}$  for about 45 minutes. Loss on ignition (LOI) is also recorded. Resulting material is then dissolved in 100 ml 5%  $\text{HNO}_3$  (nitric acid) and analyzed by ICP-AES for  $\text{SiO}_2$ ,  $\text{Al}_2\text{O}_3$ ,  $\text{Fe}_2\text{O}_3$ ,  $\text{MgO}$ ,  $\text{CaO}$ ,  $\text{Na}_2\text{O}$ ,  $\text{K}_2\text{O}$ ,  $\text{TiO}_2$ ,  $\text{P}_2\text{O}_5$ ,  $\text{MnO}$ ,  $\text{Cr}_2\text{O}_3$ , and  $\text{BaSO}_4$ , as well as oxides of Ni, Sr, Zr, Y, Nb, and Sc. Results are summarized in appendix B.1.

(B) Total digestion for minor element composition: A 250 mg sample pulp (Mesh 60, grain size: 0.15mm) is digested with 10mL  $\text{HClO}_4$ (perchloric acid)- $\text{HNO}_3$ (nitric acid)- $\text{HCl}$ (hydrochloric acid)- $\text{HF}$ (hydrofluoric acid) at  $200^\circ\text{C}$  to fuming and stretched to 10mL with diluted aqua regia. The solution is then analyzed by ICP-AES for As, Ba, Be, Bi, Cd, Co, Cr, Cu, La, Mo, Nb, Ni, Pb, Sb, Sn, Th, U, V, Y, and Zn. This leach is partial for magnetite, chromite, barite, oxides of aluminum (Al), manganese (Mn) and zirconium (Zr), and also massive sulfides. Chromium (Cr), antimony (Sb), arsenic (As) are subject to some loss due to volatilization during  $\text{HClO}_4$  fuming (see appendix B.2 for complete test results)

In addition, carbon and sulphur content was also examined in most samples. By using the LECO™ method, graphite, organic carbon, and  $\text{CO}_2$ , as well as sulfide and sulfate sulphur were distinguished. The complete tabulated results of the geochemical investigation are compiled in appendix B.3.

#### 3.1 Major Element Geochemistry

By studying the major or rock forming elements, certain compositional characteristics can be established. Figure 3.1 depicts analytical results from a pulp composite of each locality versus an average shale composition given by KRAUSKOPF (1979) and LEVINSON (1980). Most units fall closely within the average concentration ranges. Obvious visual exceptions are the Lehrberg Layer samples showing an increase in Ca and Mg with a simultaneous depletion in Si and Al, indicating the presence of major carbonate concentrations. Units with larger Ca than Mg content, such as the Amaltheen lithologies, denote calcite as main carbonate. Lithologies with approximately equal amounts of the two elements (e.g. Lehrberg layers, Feuerletten) tend to contain dolomite as

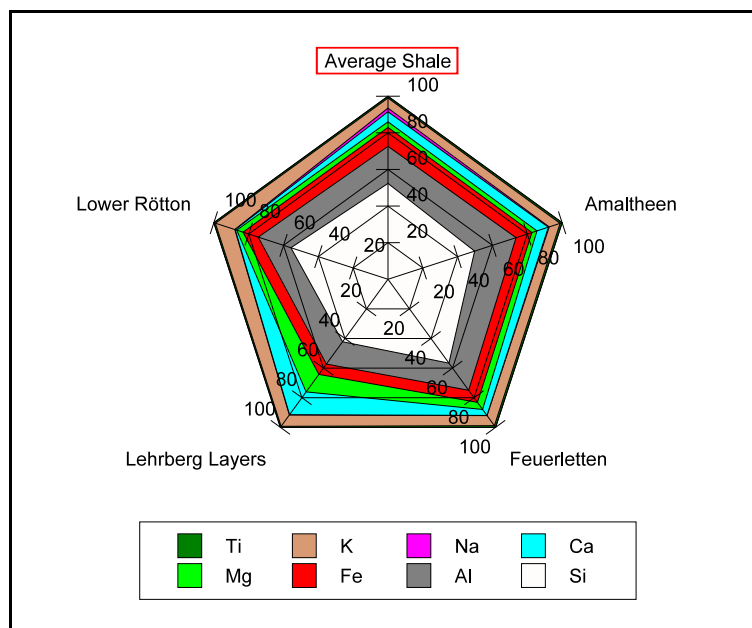


**Figure 3.1** - Major element concentration from pulp composite of the geologic barrier units investigated vs. average shale composition. Stacked radar graph. Values recalculated to 100%. (average composition data after KRAUSKOPF (1979) and LEVINSON (1980)).

carbonate mineral. The presence of K can be proportionally correlated with the amount of common potassium containing minerals in clay bearing samples. Illite, sericite and occasionally K-feldspar are most likely candidates. Mineralogical investigations described in chapter 4 point toward illite as the main K containing mineral in the samples investigated. The presence of titanium was correlated to the kaolinite content in the samples (see chapter 4). Si concentrations above the average, as seen in Feuerletten and Lower Rötton samples are indicative of elevated quartz concentrations.

Another helpful approach in deciphering the geochemistry of the various units is the use of ternary diagrams. When using  $\text{SiO}_2$  as one of the end-members, the least variation among the different lithologies is observed. Clustering according to environment of deposition is most pronounced when  $\text{MgO-Al}_2\text{O}_3\text{-K}_2\text{O}$  are used as geochemical end-members. In figure 3.2 samples from a marine Amaltheen Clay plot as one distinguished cluster in the center of the I/S (illite-smectite mixed layer) compositional field. The position is described by the illite-smectite mineralogy of the sample. Terrestrial units (Feuerletten, Lower Rötton) tend to exhibit a slightly elongated cluster on the lower border of the I/S field. The mineralogy varies slightly in illite, smectite and I/S mixed layer content. Still part of the terrestrial groupings yet exceptional because of their strongly elongated, linear cluster are the Lehrberg layers. High dolomite concentrations tend to stretch the group toward the MgO end-member.

The greatest spread of data points can be observed when  $\text{MgO-Fe}_2\text{O}_3\text{-K}_2\text{O}$  are used as geochemical end-members in a ternary plot. This appears to be obvious when compositional fields of the various clay minerals are also shown, filling large areas of the diagram. However, distinct groupings according to environment of deposition can still be observed. Closest clustering and therefore least geochemical variation is observed in marine samples. As a single unit the terrestrial Feuerletten lithologies show the closest grouping of data points. The Lehrberg Layers exhibit the greatest

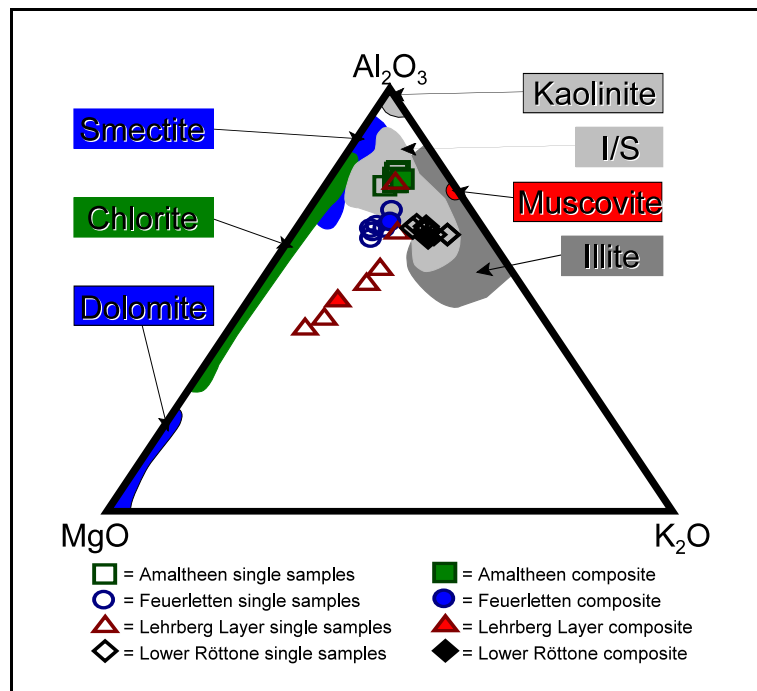


**Figure 3.2** -  $\text{MgO-Al}_2\text{O}_3\text{-K}_2\text{O}$  ternary diagram showing distribution of natural geologic barriers sampled and corresponding compositional fields of representative clay minerals and dolomite (compositional field data after PETTJOHN (1975), FOLK (1980), WEAVER (1989), and JASMUND & LAGALY (1993)).

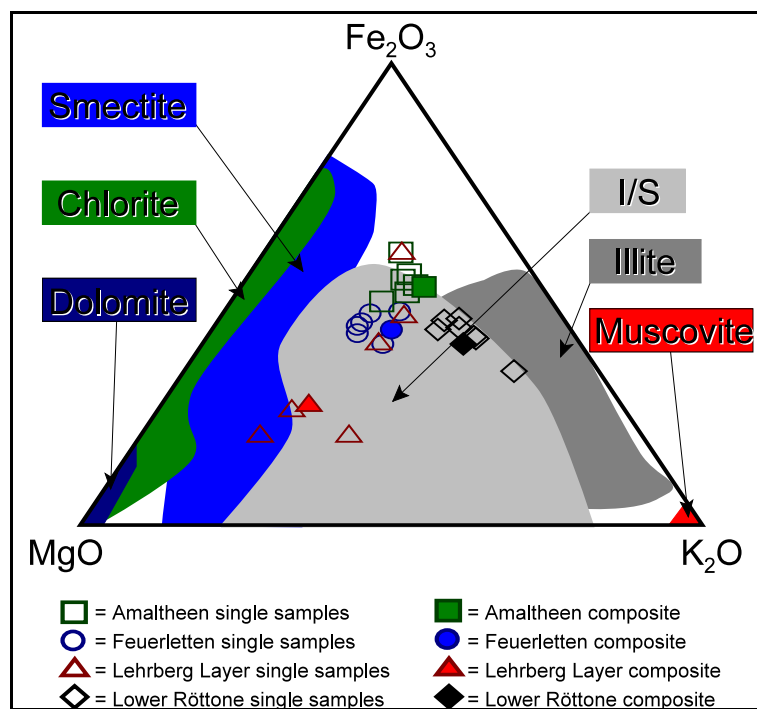


**Figure 3.3** - Distribution plot of natural geologic barriers samples in a  $\text{MgO-Fe}_2\text{O}_3\text{-K}_2\text{O}$  ternary diagram. Corresponding compositional fields of representative clay minerals and dolomite after data from PETTJOHN (1975), FOLK (1980), WEAVER (1989), and JASMUND & LAGALY (1993).



spread and variation. By individually observing each unit investigated in context with their depositional environments, the following general geochemical observations are made (see figure 3.3).

Individual clustering and 3-dimensional distribution of data becomes obvious when plotted in a barycentric pyramid (see figure 3.4). Next to the previously drawn ternary MgO-Fe<sub>2</sub>O<sub>3</sub>-K<sub>2</sub>O assemblage, the CaO endmember was added. Resulting figure 3.4 was computed with CSpace 1.0 (TORRES-ROLDÁN *et al.*, 1999) showing the spacial arrangement of geochemical data derived from the 4 lithologies. Figure can be effectively viewed with a pair of stereo glasses to perceive the 3 dimensional distribution effect. The Lower Röttone show the tightest clustering furthest removed from the CaO-MgO endmembers. With an increase in carbonates, the Amaltheen Clay samples plot approximately in the center of the pyramid. The tight constellation of data points suggests very little geochemical variation in both cases. The Feuerletten data trends toward the CaO endmember, suggesting an influx in calcite mineralogy. The Lehrberg Layers, exhibiting the widest data spread and a linear elongation toward the center of the MgO-CaO, are indicative of a more dolomitic (marly) mineralogy. Both the Lehrberg Layers and Feuerletten Clays show the greatest variation of major element geochemistry along their respective coring profiles.

Another approach for deciphering the geochemistry of the various geologic barriers investigated is to establish geochemical threshold and anomalous values and compare the various elements in a geochemical profile with these values. KACKSTAETTER (1990) defines the threshold value as the mean plus/minus one standard deviation and the anomalous value as the mean plus/minus two standard deviations. The

geochemical background is given as any value between the upper and lower threshold limits. These definitions for background, threshold and anomalies will work adequately well, as long as no complex ore bodies are involved (PETERS, 1978). The graphical representation can be viewed in figure 3.5.

The Feuerletten lithologies show little variation for the most part. The high and low values lie predominantly between the threshold and anomalous limits. The greatest spread is seen for CaO and MnO. Both high values come from the same coring depth at 7.5 m. The peak for calcium oxide slightly surpassing the anomalous line, coupled with normal MgO values is indicative of calcite. This is also substantiated by the highest LOI within the Feuerletten core, suggesting the release of CO<sub>2</sub> upon LOI heating. While Mn is commonly associated with Fe, there appears to be no correlation between the two metals in all samples. CaO and MnO show a significant 82% correlation in a 2-tailed Pearson analysis for all lithologies (see appendix B.4). The manganese peak is most likely associated with calcite, being also confirmed by maximum values for both Ca and Mn from the same sampling depth in the Feuerletten

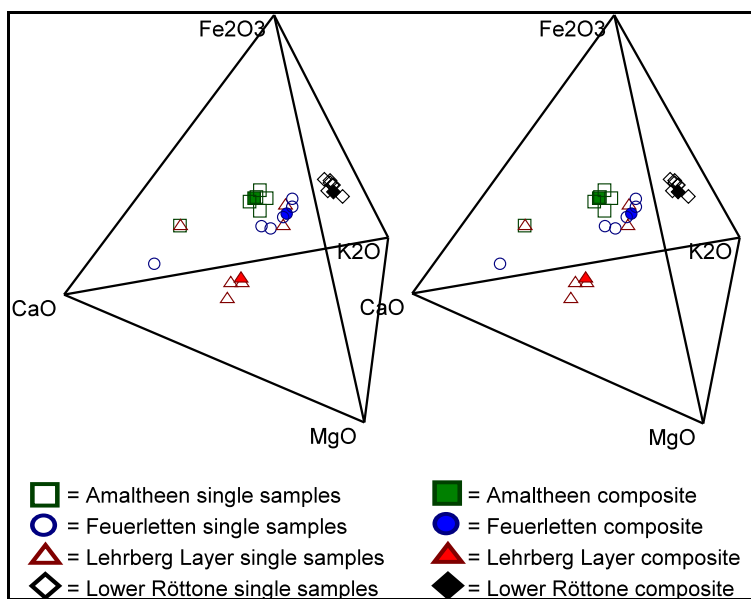


**Figure 3.4** - A barycentric stereo plot of the MgO-Fe<sub>2</sub>O<sub>3</sub>-K<sub>2</sub>O-CaO system. To view figure in 3D use stereo goggles or focus each of your eyes independently on each half of the figure respectively. Created with CSpace 1.0 (TORRES-ROLDÁN *et al.*, 1999).



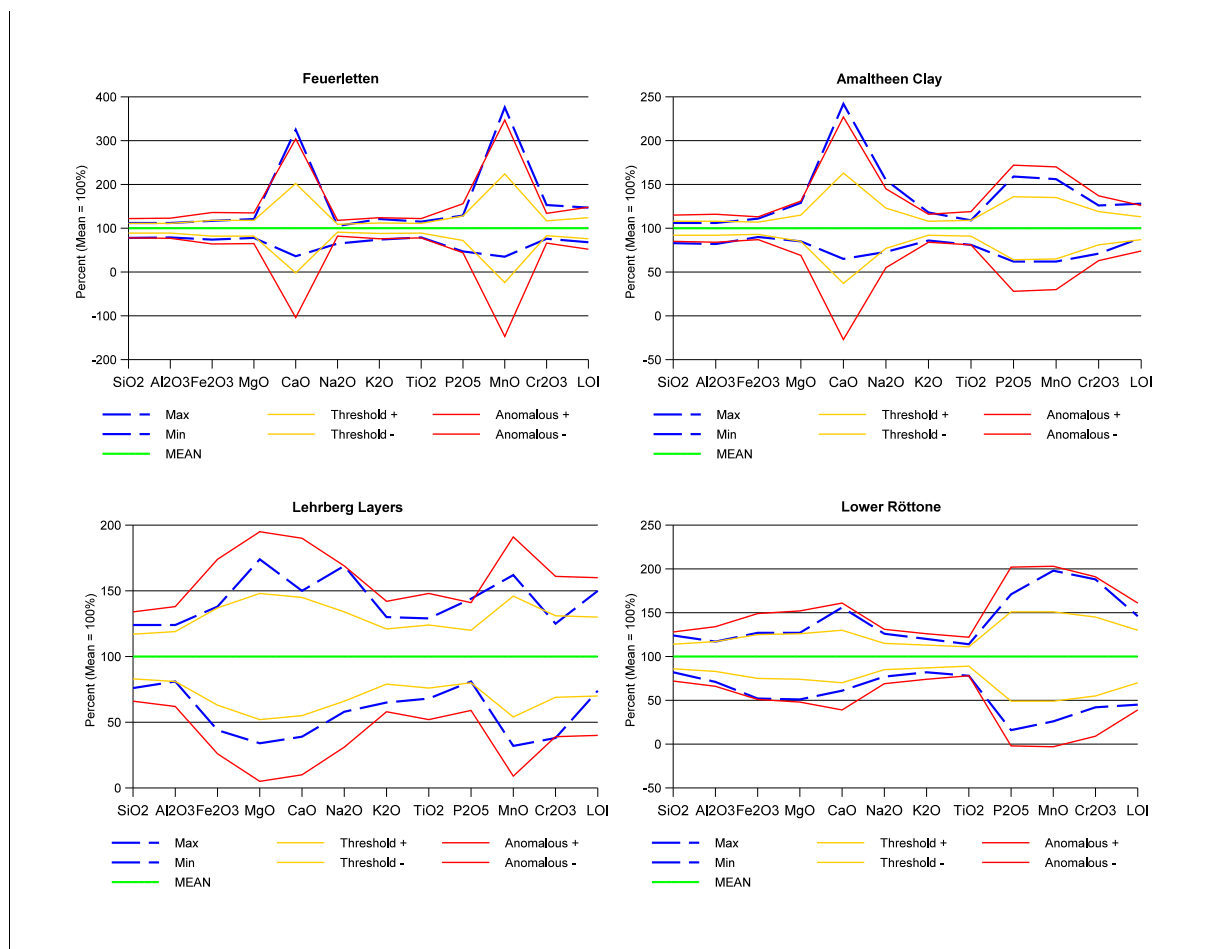


**Figure 3.5** - Plot of Max/Min values for rock forming oxides compared to threshold and anomalies for Feuerletten, Amaltheen Clay, Lehrberg Layers, and Lower Röttone coring sections. Value for Mean set at 100% and data recalculated accordingly. Threshold values estimated as mean  $\pm$  1 standard deviation and anomalies as mean  $\pm$  2 standard deviations (KACKSTAETTER, 1990).

lithology. KRAUSKOPF (1979) explains that the precipitation of manganese after the iron has separated out can be effected by a reducing conditions, where Mn will form carbonates or silicates. The highest Fe concentrations are found at 3 to 6 m, thus leaving the possibility of a later Mn precipitation at 7.5 m, most likely at such a reducing environment.

As seen in figure 3.5, the Amaltheen Clay appears also fairly uniform in its geochemical make-up of major rockforming elements. Exceptions are an anomalous CaO peak, this time coupled with increased MgO. However, the Ca and Mg maxima do not occur at the same depth level. Calcium is concentrated at the core base where also the highest LOI value is found, again suggesting calcite. Magnesium may be indicative of some dolomite at a depth of 3.5 m, where Mg and Ca measurements are almost equivalent. Values slightly above anomalous are also found for Na<sub>2</sub>O and K<sub>2</sub>O. While sodium may point toward the marine origin of the Amaltheen Clay, potassium might be indicative of the clay minerals. All other geochemical concentrations of rock forming oxides are situated mainly between the established threshold and anomaly boundaries.

The greatest variations of oxide geochemistry is found in the Lehrberg Layers (figure 3.5). While values stay between threshold and anomalous limits, a great spread from maximum to minimum is evident. Mg and Ca indicate carbonate minerals, but the sizable range suggests that some sections of the Lehrberg lithologies are almost devoid of carbonates while others are saturated. Even the SiO<sub>2</sub> and Al<sub>2</sub>O<sub>3</sub> show the most sizeable scatter of all investigated lithologies, suggesting an advanced internal diversity of sedimentary minerals.

The Lower Röttone are fairly uniform, displaying no anomalous tendencies. The widest distribution can be observed in the P<sub>2</sub>O<sub>5</sub>, MnO, Cr<sub>2</sub>O<sub>3</sub>, and LOI section of the graph (see figure 3.5). Intriguing is the elevated concentrations in

Cr with a significant 73.3% correlation in 2-tailed Pearson evaluation (appendix B.4) to  $Al_2O_3$ . LEVINSON (1980) indicates a chromium substitution in micas possibly explaining the correlation with Al. He further explains that Cr mobility is limited to detrital materials because of its high environmental stability and therefore tends to concentrate in the heavy fractions of soils and sediments. The later possibility is substantiated by a significant 84% correlation in 2-tailed Pearson test (appendix B.4) of  $Cr_2O_3$  to the "Other" category in point count analysis.

The marine lithologies: The Amaltheen lithologies exhibit little geochemical variation throughout the 9.5 m of stratigraphic drill core.  $SiO_2$  contents tend to decrease slightly with depth. The Mg/Ca Ratio in the samples are indicative of calcite as predominant carbonate mineral. An exception is represented by a 12.8% CaO concentration at 9.5m coring depth indicating an influx in carbonate minerals.

The terrestrial lithologies: The Feuerletten unit shows some geochemical variations over the entire 10m of coring section. The relation of  $SiO_2$  to  $Al_2O_3$  coupled with a constant  $K_2O$  value suggests a predominantly illite-smectite mineralogical composition. This was validated by XRD analysis described in chapter 4. Greatest variation in geochemical composition is found in the samples of the Lehrberg Layers. The  $SiO_2$  content ranges from 24% to 54%. The  $Al_2O_3$  concentration stays below 20% but varies between 6.5% to 16.9%. Similarly,  $K_2O$  extends from 2.5% to 5.5%. The greatest diversity, however, is found in the CaO and MgO concentrations, most likely due to the dolomite interlayering of the unit. The upper 10m of the Lower Röttone show for the most part very little variation in their geochemical composition. However, the lithologic change in the lower 3m of the section from a siltshale to a sandy siltstone is also reflected in its geochemistry. Here, the  $SiO_2$  content rises from about 55% to 70.5% and  $Al_2O_3$  concentration drops from ca. 17% to 12%. Lack of carbonate minerals is explained by low CaO (<0.8%) and MgO (<0.3%) values.

### 3.2 Minor Element Geochemistry

Minor element geochemistry was established by whole rock analysis and total digestion coupled with ICP-AES detection for 35 elements, namely Ag, Al, As, Au, Ba, Be, Bi, Ca, Cd, Co, Cr, Cu, Fe (total), K, La, Mg, Mn, Mo, Na, Nb, Ni, P, Pb, Sc, Sb, Sn, Sr, Th, Ti, U, V, W, Y, Zn, and Zr. Data for Ag, Au, Be, Bi, Cd, Mo, Sb, Sn, W and U were eliminated from the results because of high detection limits or insignificant elemental variations near the detection limit. The analytical results for Al, Ca, K, Mg, Mn, Na, P, and Zr were compared with and incorporated into the analytical results of the major element geochemistry (see appendix A.1). The remaining 17 elements were subjected to statistical correlations to investigate geochemical relationships. Results are summarized in appendix B.2. The measurements were also compared with average concentrations of the various elements in common shales and claystones given by KRAUSKOPF (1979), LEVINSON (1980), DIETRICH *et al.* (1982) and DEGENS (1965). Most minor elements are within the range of common shale or claystone composition (Figure 3.6). However, all lithologies of interest are depleted in Cu, Sr, and Y. While Feuerletten and Lower Röttone

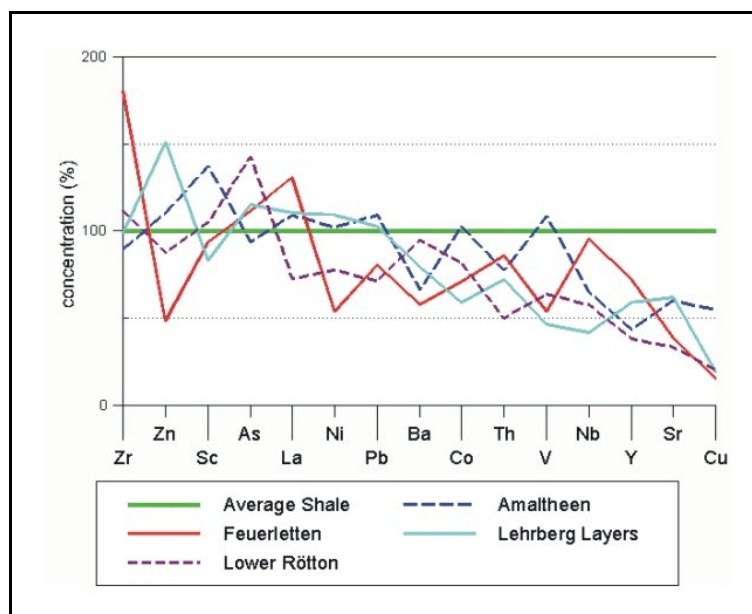


**Figure 3.6** - Arithmetic mean of minor element composition compared with average shale. Shale values set at 100% and lithologies of interest recalculated accordingly. Average shale data compiled from DIETRICH *et al.* (1982).

samples are normalized for most of the remaining elements, the Amaltheen Clay and Lehrberg Layer samples show further low values for Nb, V, and Th as indicated in figure 3.6. Only two elements evaluated lie above the values for a common shale, Zr and Zn for Feuerletten and Lehrberg Layers respectively.

In investigating the distribution of minor geochemical elements within the stratigraphic profiles of researched lithologies, it might be helpful to consult relative aqueous mobilities of elements in waters of the secondary environment. Soviet geochemists have qualified such mobility rates of an element in water by the following equation (PEREL'MAN, 1977):

$$\text{Eq. 3.1} \quad K_{aq.} = \frac{m * 100}{a * n}$$

where  $K_{aq.}$  = coefficient of aqueous migration  
 $m$  = concentration of an element in surface or ground water which drains an area (g/L)  
 $n$  = content of element in lithology over or through which the water flows (%)  
 $a$  = total dissolved solids in water (g/L)

The greater the  $K_{aq.}$  the greater the mobility of the element. PEREL'MAN (1977) gives the following examples: For Ca and Mg in the majority of landscapes the  $K_{aq.}$  ranges from 2 to 20, whereas K lies within 0.2 to 2.  $Fe^{3+}$  with a  $K_{aq.}$  of less than 0.1 is immobile in the weathering zone. U and Mo have an  $K_{aq.}$  of greater than 1 in the oxidizing environment and are therefore considered mobile in this realm. Table 3.1 summarizes the relative mobilities of selected elements.

**Table 3.1** - Relative aqueous mobilities of selected elements in waters of the secondary environment (after PEREL'MAN, 1977: Tables 4 and 10)

Relative Mobilities	Environmental Conditions	
	Oxidizing (pH > 4)	Reducing Gley (without hydrogen sulfide)
Very Mobile $K_{aq.} = 10$ to 100	S, Cl, Br, I, B, He, Rn	Cl, Br, I, B, He, Rn
Mobile $K_{aq.} = 1$ to 10	Ca, Na, Mg, F, Sr, Zn, U, Mo, V, Se, Te, Re	Ca, Na, Mg, F, Sr, $Mn^{2+}$ , Zn, Cu, Ni, Pb, Cd
Slightly Mobile $K_{aq.} = 0.1$ to 1.0	Si, K, Mn, P, Ba, Li, Rb, Cs, Pb, Ni, Cu, Co, As, Cd, Tl, Ra, Hg, Ag	$Fe^{2+}$ , Co, Hg, Ag, Si, K, P, Ba, Li, Rb, Cs, As, Tl, Ra
Immobile $K_{aq.} = < 0.1$	Fe; see note 3 below	U, Mo, V, Se, Te, Re

Notes:

- (a) Zn, Cu, Ni, Pb and Cd are mobile or slightly mobile if pH < 7; these elements precipitate in an alkaline environment )  
 (b) Hg and Ag are slightly mobile in both acid and alkaline environments
- Most elements listed are assumed to travel as ions, however some (e.g. Mo, U, V, Se, Re) travel as complexes (e.g.  $MoO_4^{2-}$ )
- Elements chemically immobile in all common aqueous environments: Al, Ga, Cr, Ti, Zr, Hf, Y, RE, Nb, Ta, Be, Th, Sn, Pt, Au.

The marine lithologies of the Amaltheen section show the least amount of variation in minor element concentration. Tracing the element concentrations along the stratigraphic depth profile as indicated in figure 3.7, the following observations can be made. With one exception at 9 m coring depth, the concentration of V follows the amount of  $Cr_2O_3$  in the sediment. Cr and Zr are very stable in the environment and act as an indicator of heavy detrital minerals. While zirconium can also be authigenic (FOLK, 1980; BUTTERFIELD, 1936), it is chiefly a very common heavy detrital mineral. V on the other hand is mobile in oxidizing acid-alkaline waters (table 3.1), but immobile in reducing environments (LEVINSON, 1980; PEREL'MAN, 1977). Vanadium at the mentioned depth is probably a good indicator

of the change from oxidizing to reducing conditions. At 9 m Zn is also prominently elevated (168 ppm) while Pb declines. This could indicate an introduction of H<sub>2</sub>S at the indicated depth, presumably through organic decay, making Zn and Pb immobile, congruent with observed concentration profiles. Elemental enrichments in line with Cr and Zr may be prescribed to the heavy mineral fractions of the detrital materials as seen at coring depth 2.8 m and 5.8 m. Thus the elevated zinc at depth 2.8 m (138 ppm) might be attributed to sphalerite grains. According to table 3.1, Ni is more mobile in the reducing than the oxidizing environments. The observed nickel concentrations with depths are also in favor of an reducing environment beginning at approximately 8.5 m profile depths.

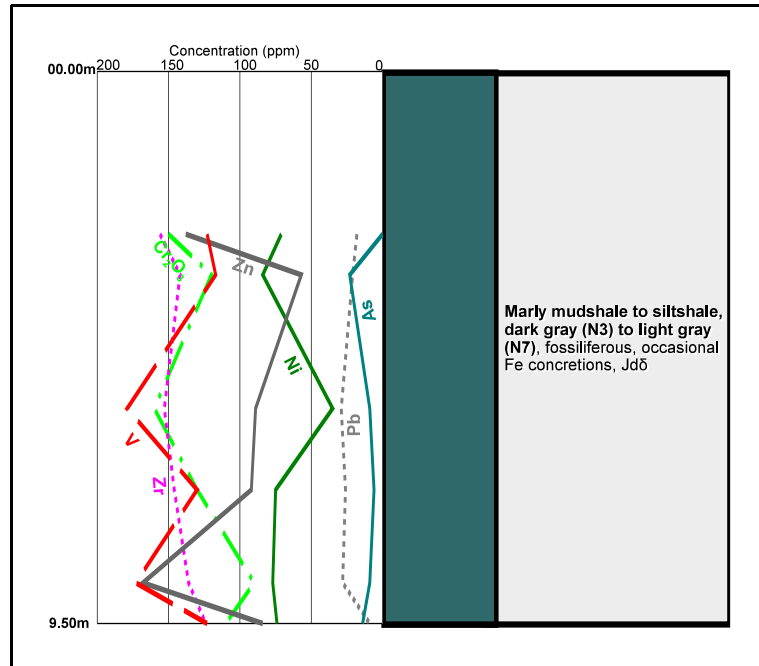


Figure 3.7 - Stratigraphic core section of the Amaltheen Clay with concentration profiles of V, Zr, Cr<sub>2</sub>O<sub>3</sub>, Zn, Ni, As, and Pb.

For the most part, however, the marine sample minor element concentrations lie well within the local background and stay also below the common averages.

Most of terrestrial lithologies show distinct variations in their minor element geochemistry. The Feuerletten unit is an exception with a rather uniform elemental distribution. Only zirconium is elevated, especially in the lower section (509 ppm). Reasons are most likely mineralogical, such as (a) selective concentration of Zr minerals or (b) change in source material of the paleoenvironment. This is especially evident in said lower section where the lithology changes to a grey siltstone. La, Pb, Ni, and to some extent Zn follow the concentration profile of vanadium (figure 3.8). While no oxidizing reduction profile is evident as shown in the previous Amaltheen Clay, some core sections may be selectively adsorptive to those minerals. This is supported by a significant positive correlation in the 90 percentiles of V and Cu to carbon and sulfur concentrations established with the LECO™ method (see appendix B.4). An increase in organic materials may be responsible for slight elevations in V, Pb, La, Zn, and Ni values at coring depth of 1.7 m, 4.6 m, and 7.5 m (figure 3.8).

The Lehrberg Layers have a rather divers geochemical profile of minor elements. Nevertheless, areas of high and low concentrations are easily correlated to the various lithologies in the section (as seen in fig. 3.9). Ni and Zn show an anomalous high in the upper 1.5 m but decrease to average content at lower depths. Geochemical associations are also visible within the profile. While

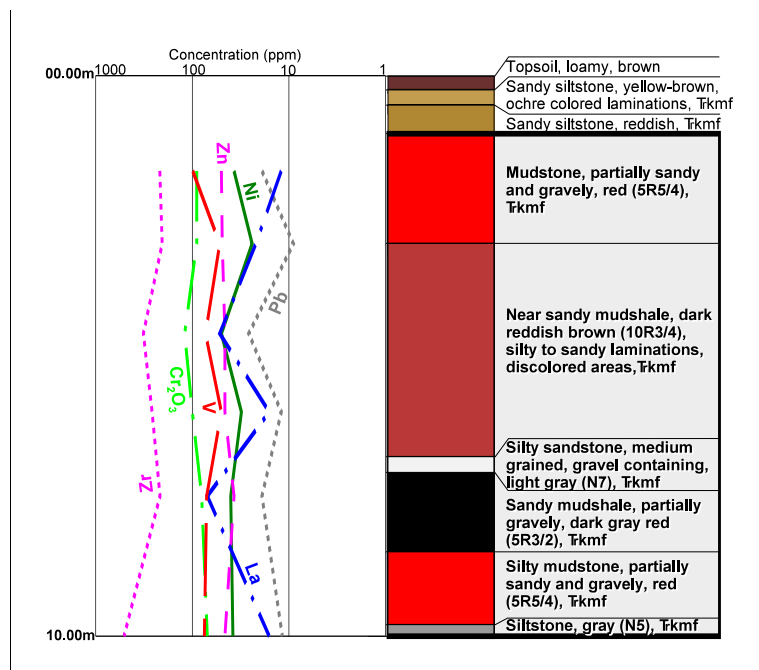


Figure 3.8 - Stratigraphic core section of the Feuerletten Clay with concentration profiles of Zr, V, Cr<sub>2</sub>O<sub>3</sub>, Zn, La, Ni, and Pb. Concentration scale is logarithmic.

Zn, As, Co, and Cu show a common concentration pattern almost in opposition to the distribution profile of Pb and Ni. Only common factor is an elevated concentration in the upper part of the section. The distribution may be partially controlled by the dolomitization of the host rock material or selective scavenging by Fe and Mn bearing minerals. NOWLAN (1976) showed a strong affinity of As to iron oxides and of Ba, Cd, Co, Ni, Tl, and Zn to manganese oxides. The Lehrberg Layers contain up to 9.5% Fe<sub>2</sub>O<sub>3</sub> and 0.36% MnO, the highest amounts of all sampled units. Sorption characteristics may thus be influenced and may vary throughout the unit. The plot of Zr is indicative of detrital heavy minerals within the section. While mostly uniform, changes occur in the lower section congruent with changes in lithologies.

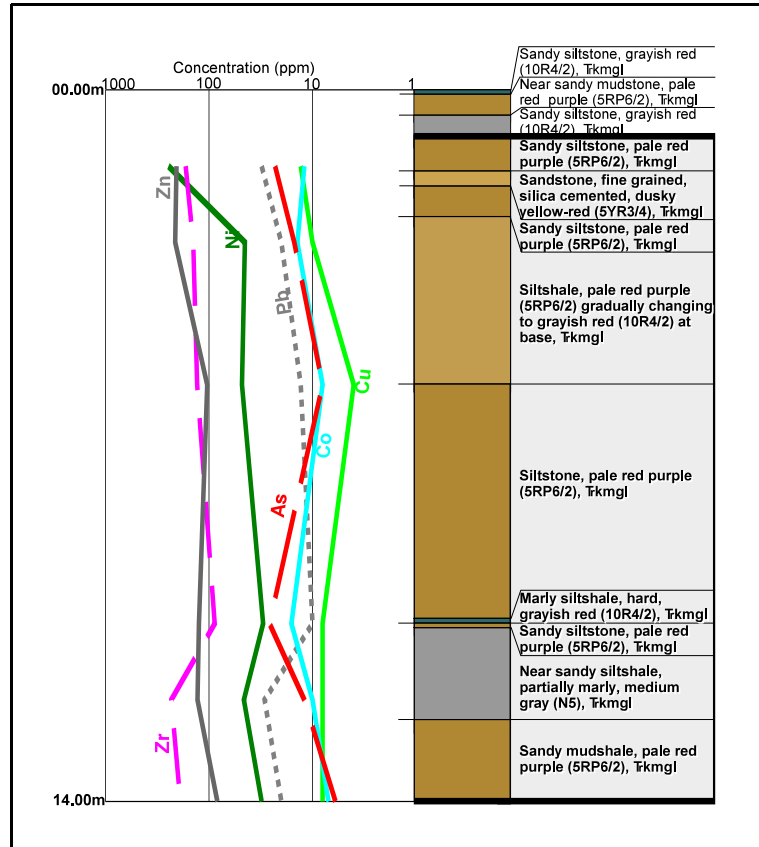


Figure 3.9 - Stratigraphic core section of the Lehrberg Layers with concentration profiles of Zr, Zn, Ni, As, Co, Cu, and Pb. Concentration scale is logarithmic.

The concentration profile of the Lower Röttone shows two distinct geochemical horizons (fig. 3.10). Enrichment in chemical elements is particular at 3.3 m coring depth. A second zone at 6.2 m shows a depleted section of 0.3 m followed by an enriched horizon of 1 m to 1.5 m. Only the Pb and Zr profile is in direct opposition to the concentrations of Cr<sub>2</sub>O<sub>3</sub>, Zn, V, Ni, and Co. Zirconium is indicative of the detrital heavy mineral fractions in the Röttone sediments, such indicating that the geochemical profile is most likely secondary in nature. Several factors may be responsible for the element assemblages present, such as changes in sorption characteristics, variations in joint patterns and permeabilities, or transitions in geochemical environments. Nevertheless, it can be assumed that all of the traits mentioned will influence the contaminant transport through the geologic barrier.

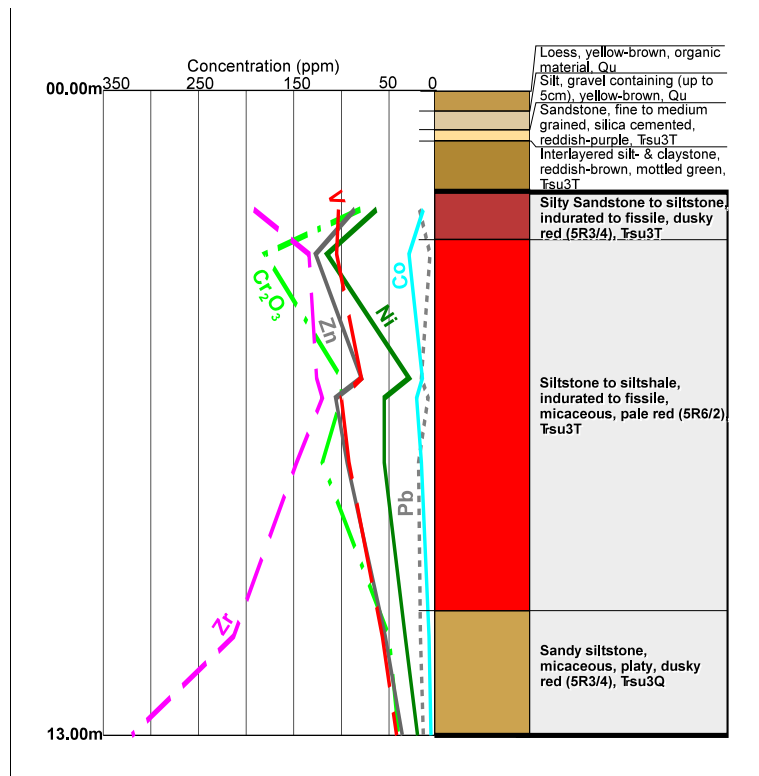


Figure 3.10 - Stratigraphic core section of the Lower Röttone with concentration profiles of Zr, V, Cr<sub>2</sub>O<sub>3</sub>, Zn, Ni, Co, and Pb.

### 3.3 Organic Carbon Content and LOI (Loss-On-Ignition)

Organic carbon significantly influences the sorption characteristics of any material. In order to estimate sorption coefficients ( $K_d$ -values), a basic knowledge of the  $C_{org}$  (organic carbon) concentrations in the materials to be investigated is essential. A detailed discussion about sorption processes and their relation to geologic barrier materials is given in chapter 7. One of the fastest and easiest methods in determining  $C_{org}$  and other heat sensitive components, is the use of LOI (loss-on-ignition) methods.

When fusing and decomposing sample pulps during whole rock analysis, loss-on-ignition (LOI) is experienced and recorded. Controlling factors of this phenomenon may include the outgassing of volatile elements, carbon or sulphur species being “burned”, carbonate minerals liberating  $CO_2$  upon decomposition, or connate or crystal lattice water in the sample being discharged. Because of the high temperatures involved, LOI is usually a combination of several of the factors mentioned. However, using this phenomenon, BALL (1964), DEAN (1974) and GOLDIN (1987) suggested and evaluated methods to quickly estimate organic carbon content, as well as soil moisture and  $CO_2$  in most geological sample pulps. Samples are first dried at  $105^\circ C$  for 24 h. Changes in weight are recorded as water content. Secondly, assuming that organic substances decompose at  $200^\circ C$  to  $550^\circ C$ , the sample is subjected to the later temperature for an equal time period. Weight changes are listed as organic matter content. Conversion to organic carbon concentrations can be accomplished using conversion factors. TRAPP AND MATTHIES (1996), for example, attained an average relationship for soils as  $M_{org}$  (total organic matter) =  $1.724 C_{org}$  (total organic carbon). However, own calculations show conversion factors for samples investigated to be much higher, ranging from 5.8 to 113 (see table 3.2). Finally, carbon dioxide ( $CO_2$ ) will be released from dolomite at  $700^\circ C$  and  $750^\circ C$  and from  $CaCO_3$  at  $800^\circ C$  to  $850^\circ C$ . Therefore, the sample pulp is heated to  $1000^\circ C$  for 24 h and the results are tabulated as amount of  $CO_2$ . This method is certainly a great asset for rapid and inexpensive evaluation for a variety of rocks. Regardless, the disadvantages for clay containing samples need to be discussed. According to DEAN (1974) samples without carbonate and organic materials will give erroneous values at the  $1000^\circ C$  temperature. Secondly, clay minerals contain a significant amount of crystal water, resulting in a weight decrease of 5% at the highest temperature. The LECO™ method is much more expensive and time consuming, yet yields far more accurate results.

First, total carbon content ( $C_{tot}$ ) is measured by combusting a 100 mg sample split in the LECO™ Carbon Analyzer. Acid insoluble carbon ( $C_{ins}$ ) is determined next by leaching 100 mg of the material in 15% HCl at  $70^\circ C$  for 1 hour. The residue is washed, dried at  $140^\circ C$  for 2 hours and subjected to LECO™ carbon analysis. In a third run, graphite carbon ( $C_{gra}$ ) is investigated by igniting 100 mg material at  $600^\circ C$  for 1 hour, followed by the same type of leaching and analytical procedures as described for  $C_{ins}$ . In case of erroneous results, the following  $C_{gra}$  determination method is applied. The sample material (100 mg) is combined in a teflon beaker with 5ml  $HNO_3$  and 5ml 50% HF and subjected to a hot bath for 1 hour. Contents are then emptied in a filtering crucible. After washing and drying the residue, carbon content is measured with the LECO™ apparatus. Results from the investigations above are used to calculate organic carbon ( $C_{org}$ ), carbon dioxide carbon ( $C_{co2}$ ), and carbon dioxide ( $CO_2$ ) according to equation 3.2, 3.3, and 3.4.

$$\text{Eq. 3.2} \quad C_{org} = C_{ins} - C_{gra}$$

$$\text{Eq. 3.3} \quad C_{co2} = C_{tot} - C_{ins}$$

$$\text{Eq. 3.4} \quad CO_2 = C_{co2} * 3.67$$

where  $C_{org}$  = organic carbon  
 $C_{ins}$  = insoluble carbon  
 $C_{gra}$  = graphite carbon  
 $C_{co2}$  = carbon dioxide carbon  
 $C_{tot}$  = total carbon

Both soil and plant samples can be processed, after appropriate calibrations are made. Although the LECO™ instrument is sensitive to within 0.001%, natural concentration variability in samples/standards usually limits measurements to within 0.01%. Table 3.2 shows the values of organic C, organic matter, and CO<sub>2</sub> content established by the LECO™ and other methods, as well as M<sub>org</sub> to C<sub>org</sub> conversion factors estimated from the LECO™ results. Included is the CO<sub>2</sub> content established through mineral calculation procedures as described in chapter 4.

**Table 3.2** - Averages for C<sub>org</sub>, M<sub>org</sub>, and CO<sub>2</sub> determined by LECO™ analyzer and BALL (1964), DEAN (1974), GOLDIN (1987) - methods. M<sub>org</sub> to C<sub>org</sub> conversion factors attained by comparing M<sub>org</sub> (@ 550°C) with C<sub>org</sub> LECO™ values. Additional CO<sub>2</sub> estimation through mineral calculations (see chapter 4 & appendix C)

	C <sub>org</sub> (LECO) %	M <sub>org</sub> (550°C) %	C <sub>org</sub> =X M <sub>org</sub> X (Conversion factor)	CO <sub>2</sub> (LECO) %	CO <sub>2</sub> (1000°C) %	CO <sub>2</sub> (Min. calc) %
Amaltheen Clay	1.2	7.02	5.9	4.1	4.3	5.6
Feuerletten	0.03	3.40	113.0	6.2(3.3)	2.8(3.2)	5.7
Lehrberg Layers	0.08	2.88	37.1	9.8	8.8	11.1
Lower Röttone	0.07	2.73	42.3	<1	2.0	1.0

Best correspondence of values is observed in the estimation of CO<sub>2</sub>. Values in brackets are averages with sample B7.5 (Feuerletten) removed, which shows a high CO<sub>2</sub> (14.87%) due to increased carbonates. Poor correspondence is found within the C<sub>org</sub> and M<sub>org</sub> values estimated by the two methods. However, a general trend suggests that all LECO™ measured C<sub>org</sub> concentrations below 0.0825% relate to heat estimated M<sub>org</sub> values of under 3.5%. Respectively, samples with LECO™ values over 0.825% appear to exceed the 7% M<sub>org</sub> margin in 550°C measurements. Complete results are summarized in appendix B.3.

In conjunction with XRD investigations, organic carbon contents of sample fractions smaller 2µm were investigated by the dichromatic acid method. Resulting Cr<sup>3+</sup> ions were determined photometrically. Recovery rate for C<sub>org</sub> is roughly 60% to 90% (WALKLEY and BLACK (1934); ALLISON (1960)). Dichromatic acid opening produces sufficient results among the active forms of organic C. SCHULTE (1995) concludes that carbonates and elemental C do not introduce any significant error. However, he also describes three main flaws of the method: (1) inorganic constituent interference, (2) differences in digestion conditions and reagent composition, and (3) composition of the organic matter itself. Results of the dichromatic acid investigation are shown in table 4.3. The C<sub>org</sub> contents established with this method in the smaller 2µm fraction are significantly higher than values obtained with LECO™ analysis from total samples. Aside from possible errors introduced by the dichromatic acid method as described above, results illustrate a most likely association of C<sub>org</sub> with the clay fraction of the material.



Color of the lithologic sample can be used as a quick estimate of organic carbon concentration. PETTJOHN (1975) and POTTER *et al.* (1980) demonstrated that shale colors are significantly related to the  $C_{org}$  content and  $Fe^{2+}/Fe^{3+}$  mole ratio of the material. Figure 3.11 shows the approximate plot<sup>4</sup> of the Frankonian geologic barrier samples in a shale color graph-chart proposed by POTTER *et al.* (1980). Oxidizing environments with a high  $Fe^{3+}/Fe^{2+}$  ratio are low in organics and show a red coloration. On the other hand, samples from a reducing environment, such as marine shales, will display a high  $C_{org}$  concentration and a low  $Fe^{3+}$  content, lacking in red iron oxide minerals. However, overall

organic matter concentrations in sediments is usually low. TRASK and HAMMER (1934) concluded in their research of 25 000 samples that only a few formations exceed 4%  $M_{org}$ . The general average ranges around 1.5%  $M_{org}$  or the equivalent of about 1%  $C_{org}$ . Organic carbon content of near shore marine sediments may be up to 1.5% (PETTJOHN, 1975). It can be safely concluded that of the various methods employed for the estimation of  $C_{org}$ , data obtained through the LECO™ method is plausibly the most reliable. Therefore, calculations and modeling involving organic carbon concentrations will be based on the LECO™ results. Appendix B.4 includes a curve fitting model to convert LOI values for  $CO_2$  (100°C) and  $C_{org}$  (550°C) to more desired LECO™ parameters. Thus results can be quickly approximated within the realm of this study when LECO™ data is lacking. Calculated values (in italics) are also included in the appendix.

Interesting are significant Pearson correlation relationships for carbons, sulfur, and gases with major rock forming oxides as summarized in appendix B.4.  $C_{org}$ -LECO™ agrees with  $Al_2O_3$  and  $Na_2O$  at 81.3% and 86.3% respectively. While the Al value would point toward a connection of C with clay minerals in general, the  $Na_2O$  results point toward a more specific correlation with smectite/montmorillonite, clay minerals with high Na values. A correspondence between  $C_{org}$ -LECO™ and  $C_{org}$ -550°C exists in the 80<sup>th</sup> percentile. However, instead of also correlating with Na,  $C_{org}$ -550°C correlates with  $TiO_2$  and  $Cr_2O_3$  at the 0.01 significance level and with  $Al_2O_3$  (77.5%) at the 0.05 level. This change in significance level and discrepancies with the other oxides reiterates the problems of the BALL (1964), DEAN (1974) and GOLDIN (1987) in determining C with LOI-approaches in clay rich samples. The interference of lattice or crystal water impedes accurate results.

Intriguing are 91.6% and 87.6% correlations of  $S_{total}$  and  $SO_4$  with  $Na_2O$  respectively at the 0.01 significance level and of correspondence in the 70<sup>th</sup> percentiles of lesser significance with  $Al_2O_3$ . This relationship points toward a correlation of S with clay minerals, especially black shales, which is a common occurrence (KRAUSKOPF, 1979). The lack of correlation between S and Fe suggests an absence of a common pyrite to shale relationship. Instead a significant correlation in the 90<sup>th</sup> percentile of S and  $SO_4$  with  $C_{org}$ -LECO™ is observed, indicative of a secondary affinity of S to C.

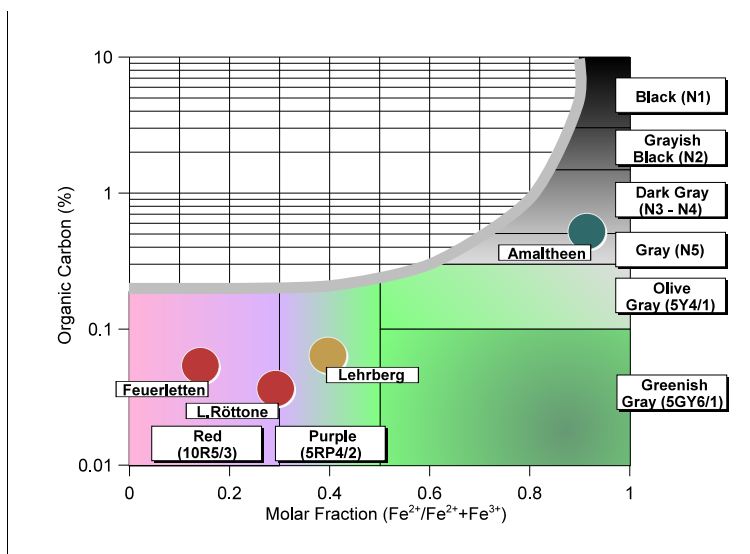


**Figure 3.11** - Plot of investigated samples related to shale colors. Chart shows  $C_{org}$  concentration vs. oxidation state of iron as mole fraction. From POTTER *et al.* (1980). (see also footnote)

<sup>4</sup>Exact plot was not possible since only total Fe (as  $Fe_2O_3$ ) was measured.



### 3.4 Cation Exchange Capacity

The cation exchange capacity (CEC) of a material is simply a measure of the quantity of sites on the material surface that can retain cations by electrostatic forces. Cation exchange sites are found primarily on clay and organic matter ( $M_{org}$ ) surfaces. In clays, two causes of negative surface charges can be distinguished. First a permanent negative charge produced by isomorphous substitution, commonly in crystal structures of 2:1 clays (e.g. exchange of  $Mg^{2+}$  for  $Al^{3+}$ ). Secondly, a pH dependent exchange capacity imposed by unsatisfied bonds on broken crystal edges and -OH groups. Cations retained by negative charges are easily exchanged with other positively charged ions, for example from contaminant solutions. The CEC is therefore an important parameter in the study of sorption processes within clay bearing geologic barriers (see chapter 7).

A variety of methods were developed to estimate the CEC. For a precise measurement, ROSS (1995) suggests a  $BaCl_2$ -compulsive exchange procedure. KRAUSE *et al.* (1993) also indicates a high precision when extracting ions by means of a barium chloride solution.

Such Ba based techniques can be found in MEHLICH (1938 and 1948), DIN 19 684 Teil 8 (1977), GILLMAN (1979), GILLMAN AND SUMPSTER (1986), RHOADES (1982), and KRETZSCHMAR (1991), just to name the most commonly used. For this study an adapted MEHLICH (1948)-method was applied, allowing the pH to be regulated at 8.1. The schematics of the exchange reaction is illustrated in figure 3.12.

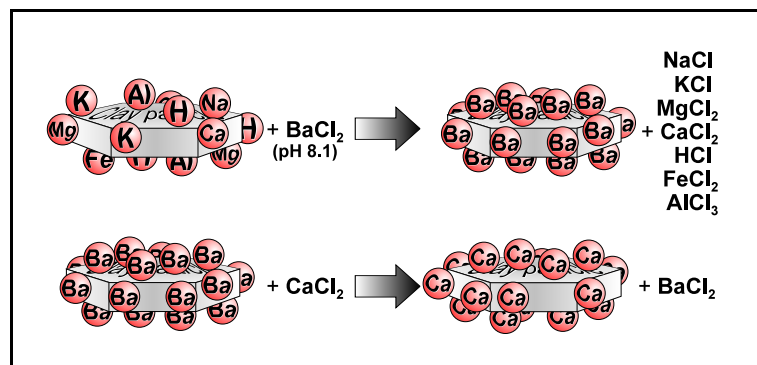


**Figure 3.12** - Schematic of the ion exchange reaction using a CEC measurement with  $BaCl_2$  (modified after KRETZSCHMAR (1991)).

CEC measurement with adapted MEHLICH (1948)  $BaCl_2$  - method:

- a. A 5g sample (grain size: < 0.125mm) is mixed with 25 ml  $BaCl_2$  solution (25g  $BaCl_2 \cdot 2H_2O$  is added to 22.5ml triethanolamine; mixture is diluted to nearly 1000ml with aqua dest.; pH 8.1 adjusted with conc. HCl; solution then filled to exactly 1000ml.)
- b. Mixture is agitated vigorously to complete dispersion
- c. Suspension is then centrifuged at 4000rpm for 15 min and clear extractant is decanted and collected
- d. Agitating and centrifuging process (b & c) is repeated three times.
- e. 25ml  $BaCl_2$  solution (25g  $BaCl_2 \cdot 2H_2O$  in 1000ml aqua dest.) are added to sample and steps b and c are repeated (extractant is added to previous collection)
- f. Sample is now washed by repeatedly adding 25ml aqua dest., agitating, centrifuging and decanting (extractant is discarded), until all non-sorbed Ba is removed ( $H_2SO_4$  test of discarded solution: Ba will form white precipitate).
- g. Extractant from steps c and d is diluted to 250ml with aqua dest. and analyzed for  $Na^+$ ,  $K^+$ ,  $Mg^{2+}$ , and  $Ca^{2+}$ .
- h. Washed sample from step f is combined with 25ml  $CaCl_2$  solution (50g  $CaCl_2 \cdot 2H_2O$  in 1000ml aqua dest.)
- i. Mixture is agitated and centrifuged as in steps b and c, repeated 4 times. Extractant is collected.
- j. Extractant is stretched to 100ml with aqua dest. and analyzed for  $Ba^{2+}$ .

Since CEC is normally expressed in units of charge per weight of material investigated, results have to be converted. Two different, but numerically equivalent sets of units are conventionally used: meq/100 g (milliequivalents of charge per 100 g of dry sample) or  $cmol_c/kg$  (centimoles of charge per kilogram of dry sample)<sup>5</sup>.

<sup>5</sup>Other equivalents: meq/100g = mval/100g;  $cmol_c/kg$  = mmol<sub>c</sub>/100g

$$\text{Eq. 3.5} \quad \frac{x * \frac{100}{W_s}}{W_{\text{mol}x} \div VAL_x} = \frac{\text{meq}}{100 \text{ g}} = \frac{\text{cmol}_c}{\text{kg}}$$

where  $x$  = measured concentration of a specific cation in mg/L  
 $W_s$  = weight of the sample in grams  
 $W_{\text{mol}x}$  = molecular weight of specific cation  
 $VAL_x$  = valence of the specific cation

Conversion of analytical results to conventional CEC units can be accomplished by applying equation 3.5. The table 3.3 summarizes the results of the CEC investigation.

**Table 3.3** - Summary of selected CEC results. Proper values are bolded. For complete results see appendix B.5.

Sample	BaCl <sub>2</sub> - exchange				CaCl <sub>2</sub> - exchange	
	Na <sup>+</sup> (cmol/kg)	K <sup>+</sup> (cmol/kg)	Ca <sup>2+</sup> (cmol/kg)	Mg <sup>2+</sup> (cmol/kg)	Σ cation (cmol/kg)	CEC (Ba <sup>2+</sup> ) (cmol/kg)
Amaltheen K9	3.7	10.7	37.9	15.0	67.3	<b>48.1</b>
Feuerletten B6	3.6	6.7	86.6	52.6	149.5	<b>137.2</b>
Lehrberg L6	3.4	6.7	26.9	22.0	59.0	<b>46.0</b>
Lehrberg L11	3.1	7.3	22.9	26.6	59.9	<b>59.4</b>
L. Röttone M6	6.4	5.2	42.2	12.0	65.8	<b>62.3</b>

In order to check for validity of the results and to gain more detailed information about the cations involved in the exchange process, percent base saturation is calculated using equation 3.6 (SUMNER and MILLER, 1996).

$$\text{Eq. 3.6} \quad \frac{\sum X_{\text{Na,K,Mg,Ca}}}{\text{CEC}} * 100$$

where  $\sum X_{\text{Na,K,Mg,Ca}}$  = sum of basic cations  
CEC = cation exchange capacity

The sum of the basic cations (e.g. Na<sup>+</sup>, K<sup>+</sup>, Mg<sup>2+</sup>, Ca<sup>2+</sup>) is divided by the CEC and multiplied by 100. Results are summarized in table 3.4.

**Table 3.4** - Selected CEC base saturation and pH. For complete results see appendix B.5.

Sample	pH	% base saturation	Sample	pH	% base saturation	Sample	pH	% base saturation
K9.0	7.71	139.9	L6.0	7.86	128.3	M6.0	6.70	105.6
B6.0	7.92	109.0	L12.0	7.83	100.8			

The percent base saturation indicates the amount of the exchange sites being occupied by the basic cations. The remaining sites, if any, are commonly filled with acidic cations, most likely H<sup>+</sup> and Al<sup>3+</sup>. The ratio of basic to acidic exchangeable cations determines soil pH. Lower soil pH concentrations should yield lower base saturation percentages unless other influencing factors are present.

Most samples with well occupied exchange sites and a soil pH of around 7.5 will show base saturation values of about 90% to 100%. Samples over 100% are influenced by other chemically processes skewing the exchange results. When calculating base saturation according to the data in table 3.4, it is obvious that some saturation values appear erroneously high with percentages of over 100 (see appendix B.5). Allowing an error margin of 10% will still leave 6 out of 9 samples with an unacceptable base saturation. By recalculating base values for the exchangeable cations as well as cation sum, setting the CEC values equal to 100% and plotting this data in order of

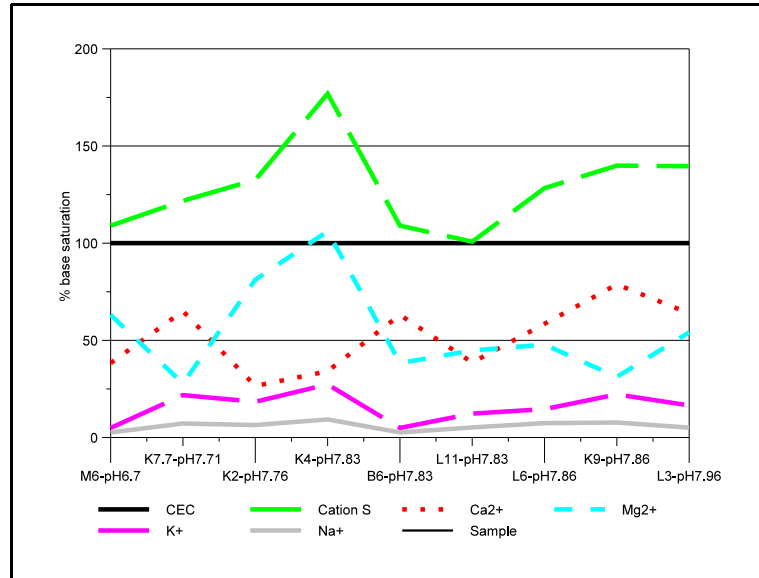


**Figure 3.13** - Plot of base CEC, cations, Ca<sup>2+</sup>, Mg<sup>2+</sup>, K<sup>+</sup>, and Na<sup>+</sup> in order of sample pH (measured in CaCl<sub>2</sub>). CEC = 100%; all other values recalculated accordingly.

sample pH (fig. 3.13), the interfering base cation is easily identified as Ca<sup>2+</sup> and even Mg<sup>2+</sup>. Where calcium values are high, as seen in the K-samples (Amaltheen Clay), the sum of cations is pushed above the CEC data, resulting in false base saturations. In sample K4 calcium ions exceed even the CEC base, suggestive of a massive desorption factor when sample is inundated with high concentrations of foreign cations. For K7.7 and K9 the intervening ion is Mg<sup>2+</sup>. The interfering ion is most likely supplied by sulfates or carbonates in the material. While a linear correlation is not observed, most CEC parameters show a slight cubic curve relationship with common carbonate or sulfate building blocks. It is important to realize, however, that the CEC value obtained from the second exchange (Ba<sup>2+</sup>) is the crucial parameter, giving the actual cation exchange capacity of the material. In conclusion, the CEC investigation suggests that desorption processes in the geologic barrier samples outweighs the exchange capacities.

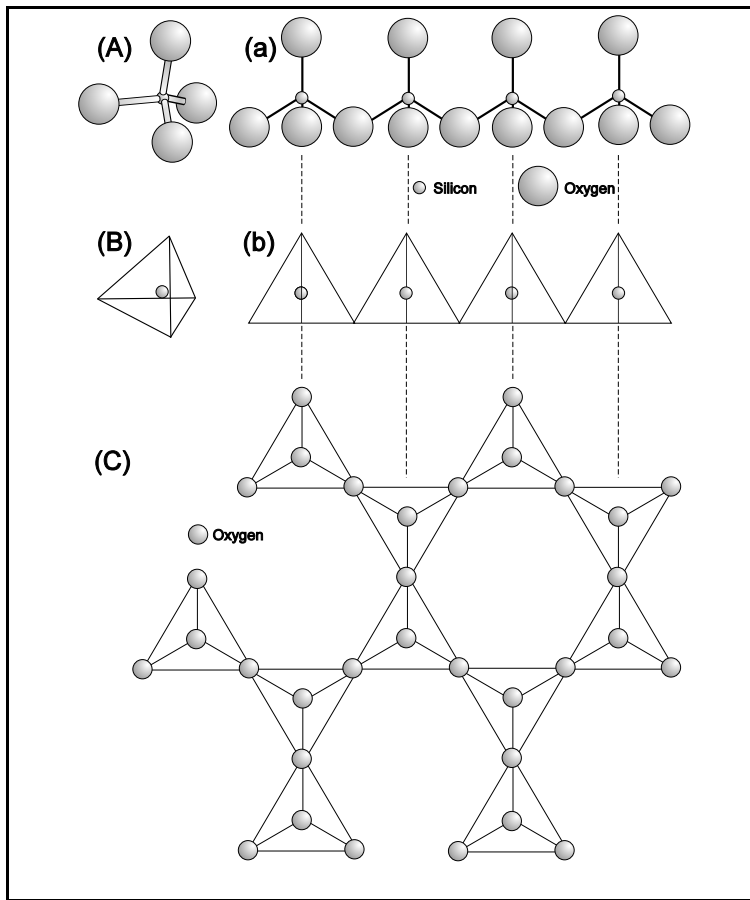
## 4 Mineralogy

### 4.1 General Mineralogy of Clays

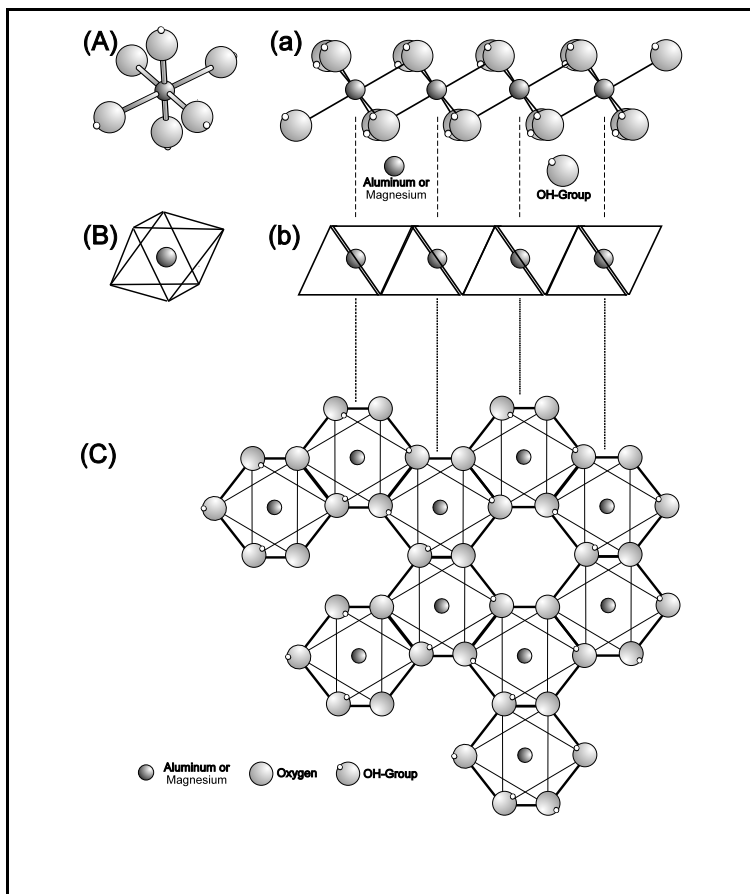
Clays are silicate minerals and belong to the family of phyllosilicates or sheet silicates. Their basic structural building blocks are linked silica tetrahedra ( $\text{SiO}_4$ ) forming a sheet by sharing oxygen atoms (see Fig. 4.1). This layer or sheet is combined with another layer grouping of cations, usually Al, Mg, or Fe in six-coordination with oxygen or hydroxyl anions, forming an octahedral pattern around the cation. A sheet is formed by sharing of the oxygen or the hydroxyl anions with neighboring octahedra (see Fig. 4.2). These octahedral sheets are usually named after two common, layered hydroxide minerals, gibbsite ( $\text{Al}(\text{OH})_3$ ) and brucite ( $\text{Mg}(\text{OH})_2$ ), forming dioctahedral and trioctahedral layers, respectively (LAMBE and WHITMAN, 1979). The silica tetrahedra, gibbsite, and brucite layers are stacked on top of each other and combined by sharing of oxygen and hydroxyl ions. A two-layer mineral or 1:1 layer results when only one surface of an octahedral sheet is shared with a tetrahedral layer (e.g. kaolinite). In this case, the unshared octahedral surface consists of hydroxyl ions (OH). A 2:1 or three-layered sheet is formed by sandwiching an octahedral sheet between two tetrahedral layers, sharing both octahedral surfaces with adjacent tetrahedral layers (see Tab. 4.1).

Those individual 1:1 or 2:1 layers may combine to form a specific mineral. If the tetrahedral cations consist exclusively of Si and all octahedral cations are either Al (dioctahedral) or Mg (trioctahedral) without any substitution, then the resulting layers are electrostatically neutral. Individual 2:1 sheets are held together by van-der-Waals bonds (e.g. talc, pyrophyllite). However, isomorphous substitution of lower charged for higher charge cations results in an overall negative layer charge. This unequal charge is balanced by positively charged interlayer material, combining the separate 1:1 or 2:1 layers. The material between the layers can be individual cations (micas), hydrated cations (expanded clays), hydroxide groups (chlorite-like clays) and whole additional octahedral hydroxide sheets (chlorites) (WEAVER, 1989). Thus, chlorite consists of an additional sheet as interlayer material and is therefore referred to as 2:2 or 2:1:1 layer unit.

Stacking of composite octahedral-tetrahedral layers occurs always in the crystallographic c-axis direction. Most phyllosilicates exhibit a monoclinic or triclinic crystal structure and display a pseudo-hexagonal nature in the a-b plane of the crystal. All sheet-silicates show perfect basal cleavage between the individual layers (BERRY AND MASON, 1959). The various phyllosilicate types can be generally classified according to their structural unit (e.g. 1:1, 2:1, 2:2), their dioctahedral (gibbsite) and trioctahedral (brucite) characteristics, and their unit spacing (see Tab. 4.1). Five major groupings of sheet silicate minerals are thus established: (1) the kaolinite-serpentine group, (2) the talc-pyrophyllite group, (3) the micas and brittle micas, (4) the smectite-vermiculite group, and (5) the chlorites (BAILEY, 1980). CHAMLEY (1989) and WEAVER (1989) identify a sixth type, the 2:1 layer palygorskite-sepiolite group of fibrous clays and inverted ribbons. They do not represent sheet silicates in a strict sense but rather exhibit a needle-like morphology. Their growth along the c axis is limited, however, the tetrahedral sheets extend for considerable distances in the a and b directions. These sheets invert at periodic intervals along the b axis, forming a checkerboard pattern with water molecules filling the empty spaces (WEAVER, 1989).

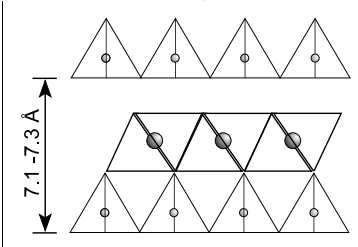
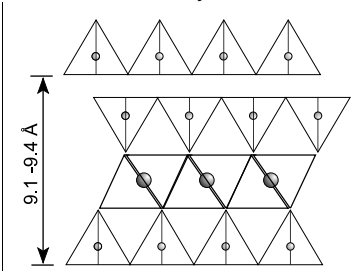
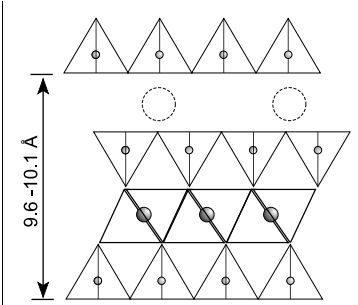
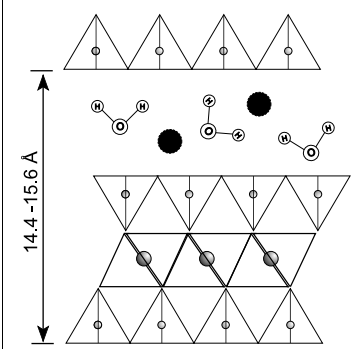


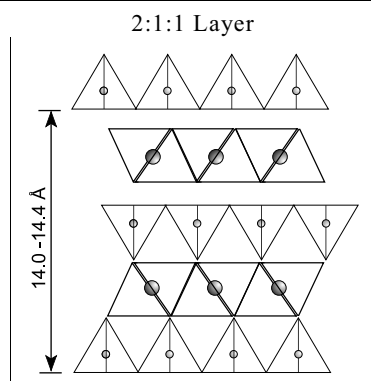
**Figure 4.1** - Schematics of silica tetrahedra and associated sheet structure. 3D representation of single tetrahedra: (A) ball-and-stick model, (B) diagrammatic with center cation. 2D linked sheet structure: (a) ball-and-stick, (b) diagrammatic. (C) Projected ab-plane diagrammatic view of sheet.



**Figure 4.2** - Schematics of octahedra and associated sheet structure. 3D representation of single octahedra: (A) ball-and-stick model, (B) diagrammatic with center cation. 2D linked sheet structure: (a) ball-and-stick, (b) diagrammatic. (C) Projected ab-plane diagrammatic view of sheet.

**Table 4.1** - Classification of major phyllosilicate groups after WEAVER (1989), LAGALY & KÖSTER (1993), CHAMLEY (1989), and BERRY & MASON (1959).

Layer type	Dioctahedral (Gibbsite-Type Layers)	Trioctahedral (Brucite-Type Layers)
<p>1:1 Layer</p> 	<p><u>Kaolinites</u></p> <p>Basic Chemistry <math>\text{Al}_4\text{Si}_4\text{O}_{10}(\text{OH})_8</math></p> <p>Examples Kaolinite, Nacrite, Dickite</p>	<p><u>Serpentines</u></p> <p>Basic Chemistry <math>\text{Mg}_6\text{Si}_4\text{O}_{10}(\text{OH})_8</math></p> <p>Examples Chrysolite, Antigorite</p>
<p>2:1 Layers</p> 	<p><u>Pyrophyllites (fire-clays)</u></p> <p>Basic Chemistry <math>\text{Al}_2\text{Si}_4\text{O}_{10}(\text{OH})_2</math></p> <p>Examples Pyrophyllite</p>	<p><u>Talcs</u></p> <p>Basic Chemistry <math>\text{Mg}_3\text{Si}_4\text{O}_{10}(\text{OH})_2</math></p> <p>Examples Talc</p>
	<p><u>① Micas ② Brittle Micas</u></p> <p>Basic Chemistry ① <math>\text{KAl}_2(\text{AlSi}_3\text{O}_{10})(\text{OH})_2</math> ② <math>\text{CaAl}_2(\text{AlSi}_3\text{O}_{10})(\text{OH})_2</math></p> <p>Examples ① Illite, Muscovite, Glauconite ② Margarite</p>	<p><u>① Micas ② Brittle Micas</u></p> <p>Basic Chemistry ① <math>\text{KMg}_3(\text{AlSi}_3\text{O}_{10})(\text{OH})_2</math> ② <math>\text{CaMg}_3(\text{AlSi}_3\text{O}_{10})(\text{OH})_2</math></p> <p>Examples ① Phlogopite, Biotite (Fe for Mg) ② Anandite, Clintonite</p>
	<p><u>① Smectites (② Vermiculites)</u></p> <p>Basic Chemistry <math>\text{R}_x\text{AlSi}_4\text{O}_{10}(\text{OH})_2 \cdot n\text{H}_2\text{O}</math></p> <p>Examples ① Montmorillonite, Nontronite (② Vermiculite (di))</p>	<p><u>① Smectites ② Vermiculites</u></p> <p>Basic Chemistry <math>\text{R}_x\text{MgSi}_4\text{O}_{10}(\text{OH})_2 \cdot n\text{H}_2\text{O}</math></p> <p>Examples ① Saponite, Hectorite, Stevensite ② Vermiculite (tri)</p>



Chlorites

Basic Chemistry  
 $Al_2(AlSi_3O_{10})(OH)_8$

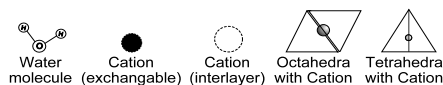
Examples  
 Donbassite (di)  
 Cookeite, Sudoite (di,tri)

Chlorites

Basic Chemistry  
 $Mg_3Al(AlSi_3O_{10})(OH)_8$

Examples  
 Chlorite, Clinocllore (tri)

Legend:



Basic Chemistry

Substitutions in formula possible  
 e.g. Fe

R = exchangeable cation

Another major group of phyllosilicates is known as mixed layered minerals. Here, a single clay crystal is made up of a composite of different basic structures in the layer planes (VELDE, 1995). Smectite, for example, might have some of the layers exchanged by a layer of mica, resulting in a new mineral with characteristic properties. Major classifications of mixed layer minerals are shown in Table 4.2. Phyllosilicates with regular mixed layering are relatively limited and usually associated with high temperature environments, such as hydrothermal alterations. Their mineral layers exhibit a regular, repeated pattern with equal proportions of the two component structures stacked in sequence, as illustrated in Table 4.2. Most common regularly stacked clays are alternating layers of illite/smectite and chlorite/smectite. Randomly layered minerals can be described according to type and proportion of the two or more types of layers (see Tab. 4.2). These phyllosilicates are by far the most common and are probably the second most abundant clay minerals next to illite. The most frequently encountered representatives of this group consist of randomly alternating illite/smectite stacks and are generally referred to as I/S physils (WEAVER, 1989). However, certain regularities may exist in the layer sequences of I/S physils, leading to a classification by Reichweite numbers, where R0 = random I/S layering, R1 = I:S, R2 = I:I:S, and R3 = I:S:I:I (JAGODZINSKI, 1949).

**Table 4.2 -** Classification of mixed layered phyllosilicates with examples of most common minerals (modified after VELDE (1995) and REYNOLDS (1980))

<b>Regular Mixed Layering</b>			
Structure A	<u>Mica : Smectite</u>		
Structure B	<table border="0" style="width: 100%;"> <tr> <td style="text-align: center; vertical-align: top;"> <u>Dioctahedral</u> illite/smectite <i>rectorite</i> (Na mica) <i>allevardite</i> (K mica) </td> <td style="text-align: center; vertical-align: top;"> <u>Trioctahedral</u> biotite/smectite <i>hydrobiotite</i> </td> </tr> </table>	<u>Dioctahedral</u> illite/smectite <i>rectorite</i> (Na mica) <i>allevardite</i> (K mica)	<u>Trioctahedral</u> biotite/smectite <i>hydrobiotite</i>
<u>Dioctahedral</u> illite/smectite <i>rectorite</i> (Na mica) <i>allevardite</i> (K mica)	<u>Trioctahedral</u> biotite/smectite <i>hydrobiotite</i>		
Structure A			
Structure B			
Structure A	<u>Chlorite : Smectite</u>		
Structure B			
Structure A	<table border="0" style="width: 100%;"> <tr> <td style="text-align: center; vertical-align: top;"> <u>Dioctahedral</u> <i>sudoite</i> </td> <td style="text-align: center; vertical-align: top;"> <u>Trioctahedral</u> <i>correnite</i> </td> </tr> </table>	<u>Dioctahedral</u> <i>sudoite</i>	<u>Trioctahedral</u> <i>correnite</i>
<u>Dioctahedral</u> <i>sudoite</i>	<u>Trioctahedral</u> <i>correnite</i>		
Structure B			
Structure A	<u>Dioctahedral - Trioctahedral</u> tosudite		
<hr/>			
<b>Random Mixed Layering</b>			
Structure A	<u>Mica : Smectite</u>		
Structure A	illite/smectite biotite/smectite		
Structure B	celadonite/smectite glauconite/smectite		
Structure B			
Structure B			
Structure A	<u>Chlorite : Smectite</u>		
Structure A	<u>Kaolinite : Smectite</u>		
Structure B			
Structure A	<u>Mica : Chlorite</u>		



## 4.2 Determination of Mineralogy

The usual approach in studying the mineralogy of fine grained sedimentary rocks are x-ray determinative techniques and electron microscope investigations, especially when clay minerals are involved. Because of variable clay compositions and crystal structures only reasonable precise estimates ( $\pm 5\%$ ) are frequently possible. Analyzing the chemical composition of sedimentary rocks can yield additional mineralogical information. As with fine grained igneous rocks, it is possible to calculate mineral compositions in fine grained sediments using geochemical data. However, because of a broad range in mineral composition and association, establishing routine calculations using sedimentary chemistries are usually time consuming and have received little attention. A few successful attempts were made by IMBRIE and POLDERVAART (1959), MIETSCH (1962), PEARSON (1978) and WIEGMANN *et al.* (1982), as discussed below.

In order to determine the mineralogy of the clays investigated, four methods were employed. The first and most common method in the routine mineralogical analysis of clay bearing sediments are X-ray determinative methods. Secondly, a SEM (scanning electron microscope) was used as a qualitative approach to minerals and fine grained structures. Thirdly, a much less common approach to the study of fine grained sediments was examined, using rock thin sections for optical investigations and point counting procedures. And fourth, the rarely employed method of establishing routine mineralogical calculations from geochemical data was attempted.

### 4.2.1 X-ray determinative techniques

The most common routine approach for mineral identification of fine-grained sediments are X-ray diffractive (XRD) methods. Two representative samples from each unit were subjected to XRD studies by first carefully drying the material. This was accomplished by either using an desiccator with calcium chloride or ammonium nitrate as drying agents, or heating the sample to 60°C in a drying cabinet for several hours. In order to identify the clay minerals, cementing agents and iron oxides were removed. A 10% H<sub>2</sub>O<sub>2</sub> (hydrogen peroxide) solution was used to eliminate organic components. Calcareous cement was extracted through a 0.1 m EDTA (ethylenediaminetetraacetic acid) or an acetate buffer solution (KOHLENER *et al.*, 1994). To control x-ray interferences through iron and iron oxides, they too were removed by applying the MEHRA and JACKSON (1960) method. A first sample run gave a qualitative overview of the material.

For a quantitative work the material was segregated into a grain size fraction of smaller 2 $\mu$ m. Further investigation involved oriented sample mounts by (1) preparing a clay-water suspension (50mg material/5ml dest. H<sub>2</sub>O), (2) pipetting several drops of the suspension onto a glass slide and (3) allowing this clay slurry to dry. Clay flakes tend to align themselves parallel to their basal or 001 planes. A typical X-ray pattern and major identified peaks of such an oriented slide is seen in figure 4.3 (Feuerletten mudstone). Quartz is definitely present despite the particle size of smaller 2 $\mu$ m, indicating the silty character of the material. Clay peaks are

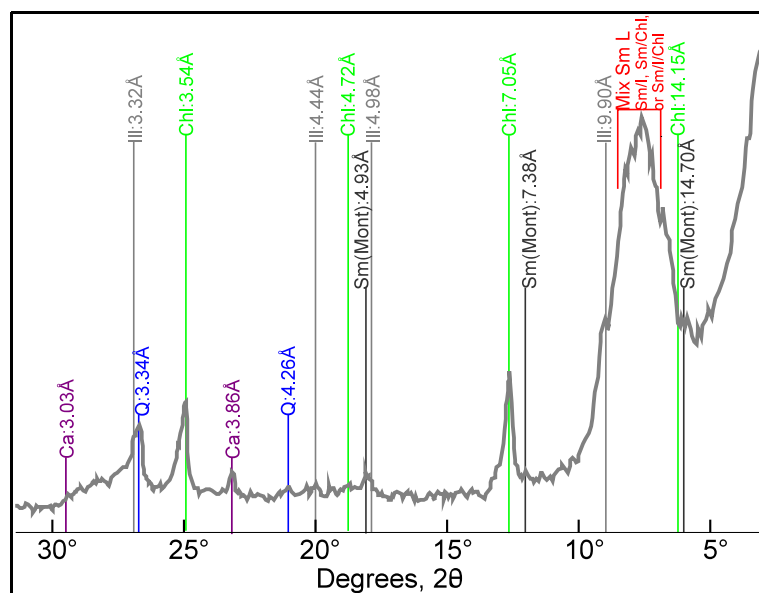


**Figure 4.3** - X-ray pattern of untreated Feuerletten clay sample B 3.0, <2 $\mu$ m. Identification of major peaks: Ill=Illite, Chl=Chlorite, Sm=Smectite, Mont=Montmorillonite, Q=Quartz, Ca=Calcite

well defined, indicating the presence of various clay species. In order to unambiguously differentiate between the various clays in a sample additional testing as described below was performed. Further tests revealed the absence of kaolinite and dolomite, as well as the presence of mixed layered smectite:illite:chlorite clays in this particular sample

Expanding clays (e.g. smectites) were identified by the ethylene glycol solvation method and XRD. A prepared sample mount was placed for one week into a desiccator next to a dish of ethylene glycol (WILSON, 1987; TRIBUTH, 1991). Especially smectites show a rather uniform response to this treatment, yielding a XRD detectable basal spacing of  $\sim 17 \text{ \AA}$ . Vermiculite clays are also susceptible to this procedure but with different resulting spacings of 14.3 to 16.3  $\text{\AA}$  (WILSON, 1987). Mixed-layered clays can also be distinguished and quantified by a combination of various solvation methods, heat treatment and mathematical approximations (KOHLENER *et al.*, 1994).

Identification of kaolinite in a mixture with other clay minerals was accomplished by heat treating the sample at 550-600°C for 1 hour. This method destroys the crystallinity through dehydroxylation in nearly all kaolinites. Comparing XRD patterns before and after heating indicates a missing basal reflection at 7  $\text{\AA}$  for kaolinite clays after the treatment (WILSON, 1987). Problems only arise in the presence of chlorite with 002 reflection at 7  $\text{\AA}$ , which is not effected by heat.

Additional information was obtained by applying IR-spectrometry to the identification of mixed clay samples. The material was combined with KBr (potassium bromide), pressed into pellets and subjected to IR investigation. Quantitative differentiation between kaolinite, chlorite, and illite is made according to IR absorption patterns (WILSON, 1987; KÖSTER AND SCHWERTMANN, 1993). Figure 4.4 shows various IR-absorption spectra for indicated clay minerals. Kaolinite displays indicative absorption bands at 3695-3700  $\text{cm}^{-1}$  and 3620-3625  $\text{cm}^{-1}$ . Illite is somewhat variable but has a characteristic maxima at 3625  $\text{cm}^{-1}$ . Greatest variations are found in the IR-spectra of chlorite.

In order to compliment the XRD and IR mineralogical analysis, additional chemical testing was performed. Sample splits were treated with dichromic acid to determine the organic content by photometric measurement of the resulting Cr(III)-organo complex in the solution. Results are shown in Table 4.3. Corresponding tests were performed during the geochemical survey involving the LECO™ process and the DEAN (1974) LOI (loss-on-ignition) method (see also chapter 3). Total carbonate content was determined according to DIN 18 129 (1990) using a 10% HCl solution to liberate and measure  $\text{CO}_2$ . Individual calcite and dolomite was quantified by XRD. As cross reference Ca and Mg ions in a sample leachate were measured and corresponding dolomite and calcite contents were calculated. Illite content was calculated by multiplying the  $\text{K}_2\text{O}$  values from the geochemical analysis with an empirical factor of 12.6 determined by KOHLER *et*

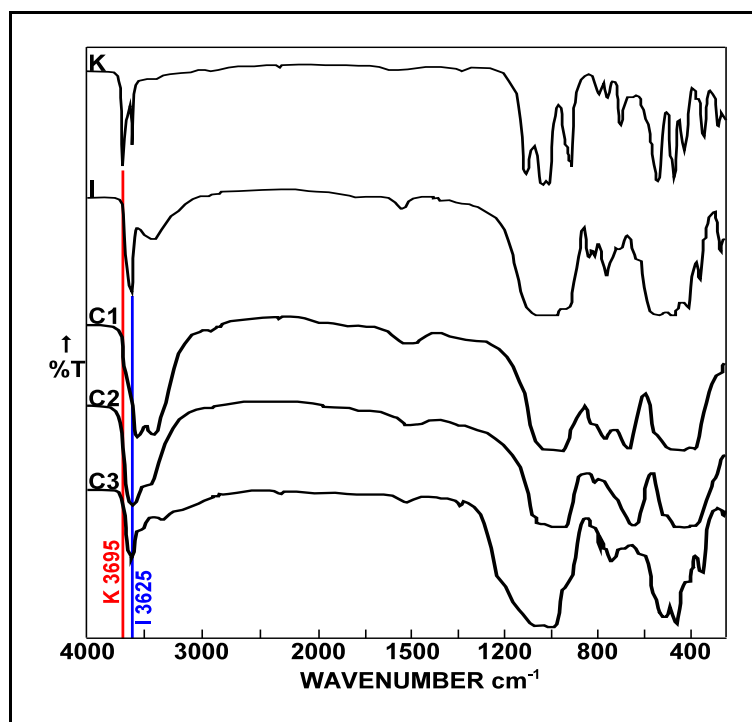


**Figure 4.4** - General IR spectra of kaolinite (K), illite (I), and chlorite species brunswigite (C1), penninite (C2) and sudoite (C3). Distinguished IR sorption bands of K 3695 and I 3625. (After WILSON, 1987).

al. (1994). His basic assumptions conclude that sample particle size below  $2\mu\text{m}$  should have geochemical K exclusively attributed to illites. This, however, may not be accurate, since the very similar mineral sericite was necessary to account for  $\text{K}_2\text{O}$  and  $\text{Al}_2\text{O}_3$  discrepancies during mineral calculations as discussed below. KOHLER *et al.* (1994) also gives the following formula (eq. 4.1) to estimate illite content from a mixture of illite, kaolinite, chlorite and montmorillonite in percent using XRD patterns:

$$\text{Eq. 4.1} \quad \text{Illite}(\%) = 100 * \frac{10A_{\text{Illite}}}{1.0A_{\text{Illite}} * 0.24A_{\text{Kaol}} * 1.07A_{\text{Chlorite}} * 0.22A_{\text{Mont}}}$$

where A = planimetric intensity

A good approximation of A is accomplished by multiplying the peak height (intensity) with half of the peak width. The numerics given in equation 4.1 are peak correction factors of intensities established by TRIBUTH (1991) and LAVES and JÄHN (1972).

**Table 4.3** - Results of the X-ray diffraction (XRD), IR-spectroscopic and mineral specific chemical investigations of representative samples ( $2\mu\text{m}$  fraction) from selected geologic barrier units. Sample number corresponds with depth of sample core (m) from surface. Organic content by dichromatic acid method (see chap. 3).

Sample Sample Depth	Quartz	Carbonate Calcite Dolomite	Organic	Kaolinite	Illite (calculated)	Swell.Clay (calculated)	Chlorite
Marktheidenfeld							
Lower Röttone (Trsu3T)							
4.8	~45 %	-	1.5 %	-	~39 %	~11 %	max. 5 %
8.5	~45 %	-	1.3 %	-	~40 %	~10 %	max. 5 %
Langenzenn							
Lehrberglayers (Trkmgl)							
3.0	~20 %	(D) 7.3 %	1.3 %	-	~39 %	~21 %	5-10 %
10.5	~5-10 %	(D) 48.5 %	2.1 %	-	~10 %	~20 %	5-10 %
Birkenschlag							
Feuerletten (Trkmf)							
3.0	~30 %	(C) 5.0 %	1.4 %	-	~22 %	~38 %	5-10 %
8.5-10.0	~35 %	(D) 4.5 %	1.3 %	-	~20 %	~30 %	5-10 %
Kalchreuth							
Amaltheenshale (Jl8)							
2.8-3.5	~30 %	(C) 10.0 %	1.8 %	22 %	~15 %	~15 %	~5-10 %
7.0-7.8	~30 %	(C) 6.4 %	0.8 %	16 %	~18 %	~22 %	~5-10 %

Mixed layer clay species composition (such as I/S) can be estimated by associating the geochemically derived illite content with the value calculated from planimetric intensities. Results of the various XRD investigations, calculations and specific additional tests are summarized in table 4.3.

Kaolinite is absent from all Triassic “continental” clay-bearing units (Feuerletten, Lehrberg layers, Lower Röttone). Marine shales of Jurassic age (Amaltheen Clay) show moderate 16% to 22% of the mineral. The lowest amount of swelling clays is found in the Lower Röttone (10% to 11%). Most of this mineral species is present in the Upper Triassic Feuerletten unit. Chlorite is recognized in all units with concentration ranges from maximal 5% to maximal 10%. Illite is also found in all of the samples. The oldest investigated lithologies (Lower Röttone, Lehrberg layers) contain most of the illite (up to 40%), while the layers of the Jurassic lithology (Amaltheen Clay) exhibits only 15% to 18% of the mineral. According to XRD studies, carbonate minerals are absent from the oldest unit (Lower Röttone). The Lehrberg Layers contain dolomite in significant amounts (L10.5 = 48.5%). The Feuerletten lithologies show a mix of dolomite (4.5%) lower in the section, while calcite (5.0%) predominates the upper part. The Amaltheen Clays exhibit 6.4% to 10% calcite. Quartz is present in all the samples with an average concentration of 30% due to fine silty character of most of the material. The highest organic amount is found in the lower section of the Lehrberg Layers. This, however, might be a skewed result due to the very high carbonate content. If organics in the Lower

Lehrberg Layers a treated as an anomalous value, then organic material measured by the dichromatic acid method show highest concentration in the darker units (Amaltheen shale, up to 1.8%) as expected by POTTER *et al.* (1980) who relates color of the rock to organic carbon content and Fe concentrations (see also chapter 3).

Concentrations evaluated by XRD studies only investigated the grain fraction smaller  $2\mu\text{m}$ . This allowed for an unambiguous identification of clay minerals and concentration relationships among the phyllosilicates. In order to consider the mineralogy of the whole sample additional investigations are necessary.

#### 4.2.2 Scanning Electron Microscopy (SEM)

The SEM can be an invaluable tool in studying fine grained materials. A small sample chip, not larger than  $1\text{cm}^3$  is placed into a high vacuum environment and subjected to a focused high potential electron beam (up to 50kV), scanning the sample surface in a raster fashion. The primary beam striking the specimen liberates low-energy secondary electrons which accelerate toward and are detected by a collector. The amplified secondary electron signal is then processed by a cathode ray tube with an electron beam traverse synchronous to the primary beam raster sweep (MCHARDY and BIRNIE, 1987). The result is a virtual 3D image of the specimen surface on the tube. Magnification is controlled by electronically adjusting the relative sizes of the two rasters.

A side effect of this method is the generation of X-rays during the high potential electron impact on the sample surface. Each chemical element in the specimen will produce X-rays of characteristic energies and wavelength. An additional energy dispersive X-ray (EDX) detector unit attached to the SEM is able to process the various energies and translate them into qualitative and semi-quantitative elemental composition read-outs. Only elements with atomic number greater than 11 (Na) and with concentrations above approximately 1% are displayed (WELTON, 1984).

Samples prepared for SEM analysis must be able to discharge the extensive electron bombardment in order to avoid accumulation of electrical charges. This is accomplished by mounting the material with a conductive cement on an aluminum or graphite sample holder. Additional coating of this assembly with a  $200\text{ \AA}$  thin layer of graphite, gold or palladium is necessary to obtain a clear image of an insulating material, such as rock (WELTON, 1984). Samples are now ready for SEM and EDX studies.

Because samples must be completely dry before they can be subjected to metal coatings and SEM investigations, clay specimens pose a special problem. The material tends to shrink during the drying process, distorting surface textures. In order to effectively protect the original structures in most cases, several alternate drying methods are discussed by MCHARDY and BIRNIE (1987) such as freeze-drying and critical-point drying. TOVEY AND WONG (1978) argue that many of these alternate drying methods might avoid shrinkage distortion but can create other disturbances on the sample surface. MCHARDY and BIRNIE (1987) and TOVEY and WONG (1978), however, deal predominantly with unconsolidated materials, such as soils and clay slurries. In contrast, this study involves consolidated fine grained sedimentary rock units, such as mudstones, siltstones and shales.

For the purpose of this investigation, several representative samples of approximately  $1\text{ cm}^3$  size were taken from the drilling cores of the various locations. The material was oven dried, followed by vacuum dessication, mounted on graphite sample holders and Au sputter coated. According to TOVEY and WONG (1978), oven drying is superior to air drying in many clay samples. HENNING and STÖRR (1986) show no special drying technique for consolidated clay materials prior to metal coating but deem the untreated specimens as sufficient. Nevertheless, possible surface distortion during sample preparation is taken into consideration.

SEM investigations of the Amaltheen lithologies reveal the typical shale structure of the material (see fig. 4.5). The clay minerals resemble platy aggregates oriented in a more or less parallel fashion, consisting mostly of illite/smectite and occasional kaolinite (see fig. 4.6). Silt grains are usually rounded, less than 30 $\mu\text{m}$  in size, show very little

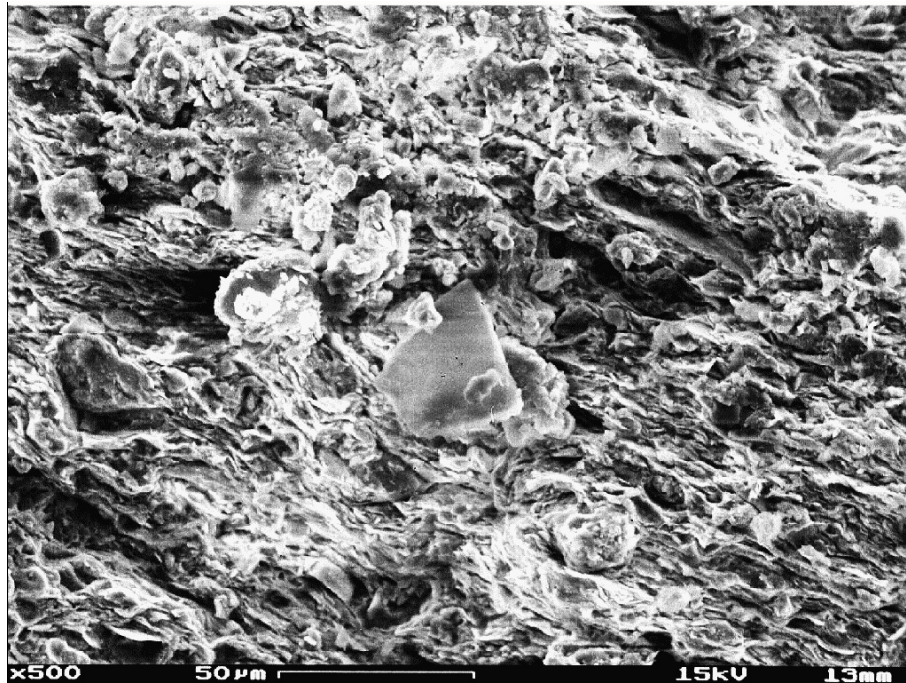


**Figure 4.5** - SEM micrograph of Amaltheen clay sample (core depth 7.5m). Typical shale structure containing parallel oriented illite-smectite with quartz-grain (silt) inclusions. Smectite distortion through drying prevalent.

overgrowth, and are embedded into the surrounding clay flakes. Disturbance of the material through drying and the vacuum sample preparations is obvious. Overall dry shrinkage is usually parallel to the clay orientation. In addition, swelling clay minerals tend to curl during the drying process giving the surface a disordered appearance. Additional disarray might have been caused by bioturbation, common in marine shales and clays (BENNETT *et al.*, 1990). On

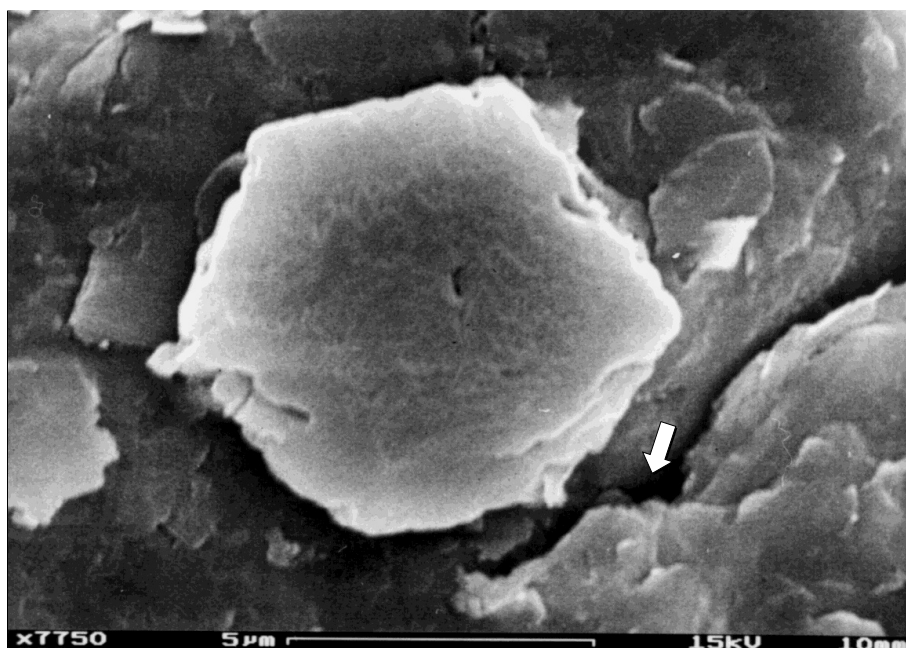


**Figure 4.6** - SEM micrograph showing hexagonal kaolinite (center) and microfracture (arrow) in Amaltheen clay (core depth 7.5 m)



occasion, small iron concretions ( $<10\mu\text{m}$ ) with a calcitic center are found. Calcareous fossil fragments in form of unidentified shell fragments are also infrequently present. Attempted examination of voids in the Amaltheen samples failed. Fractures are interpreted as shrinkage features rather than authigenic pore space (see fig. 4.6).

Samples of the Feuerletten unit present a rather disordered array of particles under the SEM (fig. 4.7). The predominant minerals are quartz, illites, and smectites. Quartz grains tend to be rather angular in appearance with

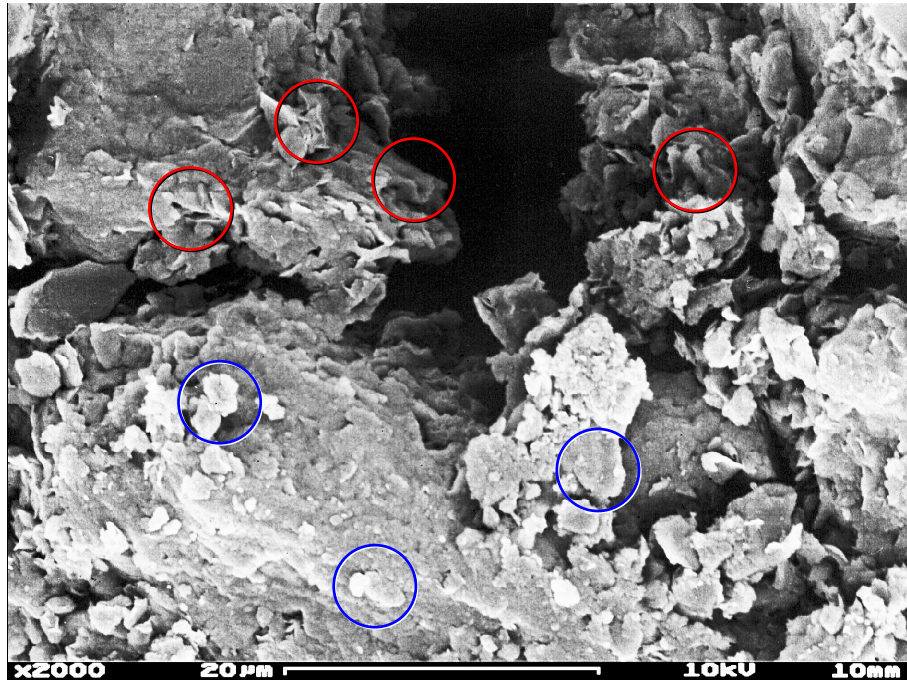


**Figure 4.7** - SEM micrograph of Feuerletten specimen (core depth 4.5 m). Quartz grains:○, clay particles (probably I/S):○; representative mineral samples in center of circle. Pore spaces and fractures apparently secondary.

sizes rarely exceeding  $10\mu\text{m}$ . Arrangements of clay flakes varies. Platy aggregates with folds and parallel alignment are commonly observed. Surface distortion through the drying process is prevalent. As seen in figure 4.7 micropores may be rather large, but are most likely shrinkage features related to sample preparation. This is supported by loosening of grains or grain aggregates with small fractures along the grain perimeter. Similar properties were observed in the samples of the Lehrberg layers. Because of strong surface distortions, diagenetic relationships between the different mineral grains could not be observed in both of the units.

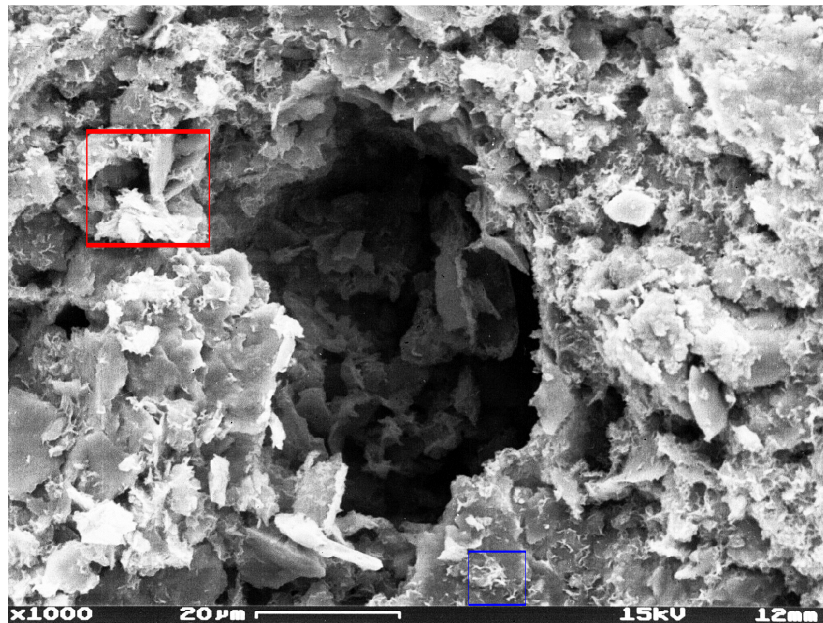


**Figure 4.8** - Lower Röttton sample (core depth 6.0 m). Large original micropore. Examples of a) well-developed “card-house” structure framed by □; b) small (~1 $\mu$ m) diagenetic illite growth framed by □.

Lower Röttone show very little surface distortion under the SEM (fig. 4.8). The main minerals are illite and quartz with occasional smectite. Quartz grains are angular to subangular with sizes up to 10 $\mu$ m. Detrital illite flakes tend to be large (about 10 $\mu$ m). While some parallel arrangement occurs, the “card-house” structure dominates (see fig. 4.8). Well developed authigenic illite overgrowth forms clusters on the surfaces of detrital illite flakes. This secondary mineral consists of small (1 $\mu$ m or less) flakes forming an edge-to-face arrangement. Original pore spaces tend to be rather large (>20 $\mu$ m) and voids exhibit typical “non-stress” characteristics. Secondary pore spaces is usually evident as elongated fractures, commonly parallel to occasional bedding planes.

## 4.2.3 Optical microscopy

One of the most common procedures in investigating sedimentary rocks is the use of thin-sections and the optical microscope. However, fine grained sediments have received little attention. Common notion of most researchers can be summarized by a statement from ADAMS *et al.* (1984):

*“Clays and shales are too fine-grained for study using the petrographic microscope and must be examined by electron microscopy or X-ray diffraction.”*

While generally true, nevertheless, much additional information can be contrived from optical microscope studies of fine-grained materials. As discussed by POTTER *et al.* (1980) many features such as detrital and authigenic minerals, cements, pellets, grain sizes, lineations can be examined. CARROZI (1960) also made attempts to provide descriptions of common shales and claystones for optical work. FOLK (1980) suggests that the best technique is to examine thin-sections for genetic relationships and associations of the minerals armed with the information gained from XRD and related studies. Results of the investigations of thin-sections of the various samples are therefore supplemental in nature.

**Table 4.4** - Results of point-count analysis of representative samples from selected locations. Material too fine for positive identification (<0.03mm) attributed to clay (undifferentiated). Sericite refers to coarse illite/mica. Samples: K=Amaltheen Clay; B=Feuerletten; L=Lehrberg Layers; M=Lower Rötton. Abbreviations: w/ incl.=with inclusions; authig.=authigenetic growth; metam.=metamorphic; heavy=total heavy minerals.

	K7.2	K9.0	B6.0	L6.0	L7.6	L11.0	M3.3	M6.0	M7.5
<b>Quartz</b>	<b>12.0%</b>	<b>19.0%</b>	<b>6.7%</b>	<b>6.0%</b>	<b>21.6%</b>	<b>17.7%</b>	<b>10.4%</b>	<b>24.9%</b>	<b>25.5%</b>
w/ incl.	--	--	--	--	3.9%	8.3%	--	--	--
authig.	--	1.4%	1.1%	--	--	--	3.2%	15.9%	9.0%
<b>Clay</b>	<b>68.8%</b>	<b>70.4%</b>	<b>73.9%</b>	<b>10.3%</b>	<b>65.0%</b>	<b>60.3%</b>	<b>68.8%</b>	<b>66.0%</b>	<b>67.8%</b>
Sericite	5.6%	2.1%	--	10.3%	8.5%	27.0%	0.8%	0.7%	2.5%
Fe-stain	--	--	11.8%	--	15.1%	9.4%	--	1.4%	2.5%
<b>Carb.</b>	<b>4.0%</b>	<b>4.9%</b>	<b>2.8%</b>	<b>83.7%</b>	---	---	---	---	---
Dol	--	--	--	80.3%	--	--	--	--	--
Cal	4.0%	4.9%	2.8%	3.4%	--	--	--	--	--
<b>Rock-F.</b>	---	---	<b>5.0%</b>	---	---	<b>1.6%</b>	---	---	---
chert	--	--	4.5%	--	--	1.6%	--	--	--
clay	--	--	0.5%	--	--	--	--	--	--
metam.	--	--	--	--	--	--	--	--	--
<b>K-spar</b>	---	---	---	---	---	---	<b>0.8%</b>	<b>2.0%</b>	<b>1.6%</b>
<b>Other</b>	<b>0.8%</b>	<b>0.7%</b>	---	---	<b>0.7%</b>	<b>1.0%</b>	<b>16.8%</b>	---	---
isotropic	--	--	--	--	0.7%	--	16.8%	--	--
heavy	0.8%	0.7%	--	--	--	1.0%	--	--	--
<b>Opac</b>	<b>4.8%</b>	<b>4.9%</b>	<b>4.5%</b>	---	<b>1.3%</b>	<b>19.3%</b>	<b>3.2%</b>	<b>2.1%</b>	<b>0.8%</b>
<b>Void</b>	<b>9.6%</b>	<b>tr.</b>	<b>6.7%</b>	---	<b>11.2%</b>	---	---	<b>4.9%</b>	<b>4.1%</b>

Visual representation of the results in form of photomicrographs can be challenging. Because of lack in detail, WEAVER (1989) indicates that black and white photomicrographs are usually not worth publishing. However, digital manipulation of the photographs can significantly aid in the interpretation. Using a relief enhancing algorithm, microfabric textures become more visible. Light colors result in a high relief while dark colors appear as indentations (see figures 4.9 to 4.13).

About three representative samples from each drill core were selected. The material was vacuum impregnated with blue resin to contrast pore spaces and voids. Specimens were then cut parallel to the coring direction using oil to avoid dissolution and leaching. Thin sections were trimmed to standard thickness of 0.02 mm. Results of an attempted point counting analysis are summarized in table 4.4. All materials too small to be distinguished (usually all particles



less than 0.03 mm in size) were allotted to the clay section. Fine grained material showing a reddish, brown or dark-brown to black coloration were further subdivided into Fe-stained clay. Sericite describes all identifiable phyllosilicates resembling mica grains.

According to point-count analysis of the Amaltheen samples approximately 70% fine grained materials are observed. The fine-grained structure consisting of very small (<0.02mm) grains and flakes in a parallel arrangement making an individual distinction of grains very challenging (fig. 4.9). Visibility of weak lineations is enhanced through a digital relief image of the original micrograph (fig. 4.9). Fine parallel fractures tend to cut the layer orientation of the material at approximately 30°. Distance between lineations range from 0.05 mm to 2.5 mm. Voids or pore spaces as indicated by the colored resin are present where fractures are widening. Point count analysis discloses void contents from traces to 9.6%. Identifiable quartz ranges from 12% at coring depths of 7.2 m with an increase to about 20% closer to the base of the stratigraphic section. Authigenic quartz overgrowth and cement is also observed. Opaque minerals average about 3% to 5% and occur as spheroidal clusters or elongated grains arranged in bands. Identifiable carbonate minerals consist of calcite nodules or shell fragments averaging about 4% of total grain count.

The Feuerletten material consists of basically randomly oriented grains. Visible quartz content is about 6.7%. Grains are commonly moderately well rounded with occasional quartz overgrowth. Diagenetic chert was also observed and comprises 1.1% of the rock. The fine grained material (~74%) represents an undifferentiated mixture of clay flakes, small quartz grains, and some carbonates (fig. 4.11). A carbonaceous clay with high birefringent material in its interstices was identified in 1.1% of all grains counted. About 11% of the rock contains very dark brown to almost black Fe-stained clay mineral flakes. Calcite (~2.8%) may occur as 0.01mm small distinctly rhombohedral grains covering other detrital material or as 0.1mm to 0.3mm large, high birefringent particles. Pore space is incorporated into a well developed, seemingly random fracture network comprising roughly 7% of the sample (fig 4.10). Occasional parallel lineation is more clearly seen in an digital enhanced photomicrograph (fig 4.10) and relief image. Lineations may follow fracture zones but can also extend through the whole sample without indication of pore space.

The Lehrberg layers may contain bands of fine grained, micritic dolomite (~80%) with about 3.5% of diagenetic calcite. Clay flakes within these carbonate layers resemble mica and comprise roughly 10%. Quartz content is about 6%. The majority of the Lehrberg lithology, however, consists of approximately 60% to 65% fine grained materials with about 8% to 27% of the whole rock resembling larger sericite flakes. Fe-staining of the flakes is common and comprises 10% to 15% of total grains counted. Opaque material consists mainly of up to 19% black to deep red brown bands, especially in lower stratigraphic samples (see fig. 4.11). Grains are usually arranged in a "card-house" structure. Visible pore space (11.2%) was only found in sample L7.6 resembling open spaces within the microfabric. Fractures are indicated but less prominent

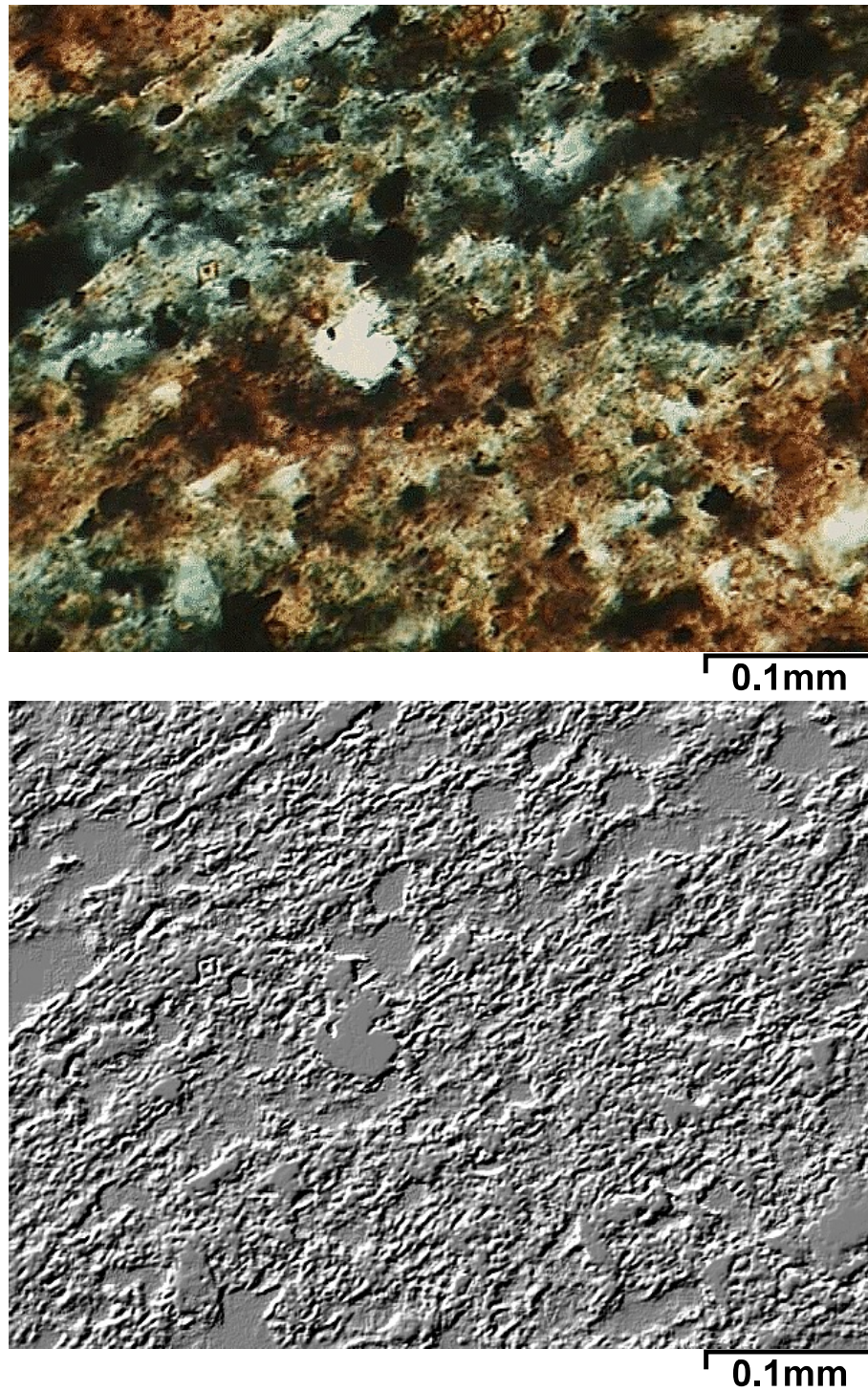


**Figure 4.9** - Photomicrograph (plain light, above) and digital enhanced relief image (below) of Amalthean sample (coring depth 7.5m). Parallel layering of fine grained material prominent (e.g. bands of opaque material). Some weak parallel lineation at approx.  $30^\circ$  to mineral layering visible in relief image (e.g. left center to upper right).



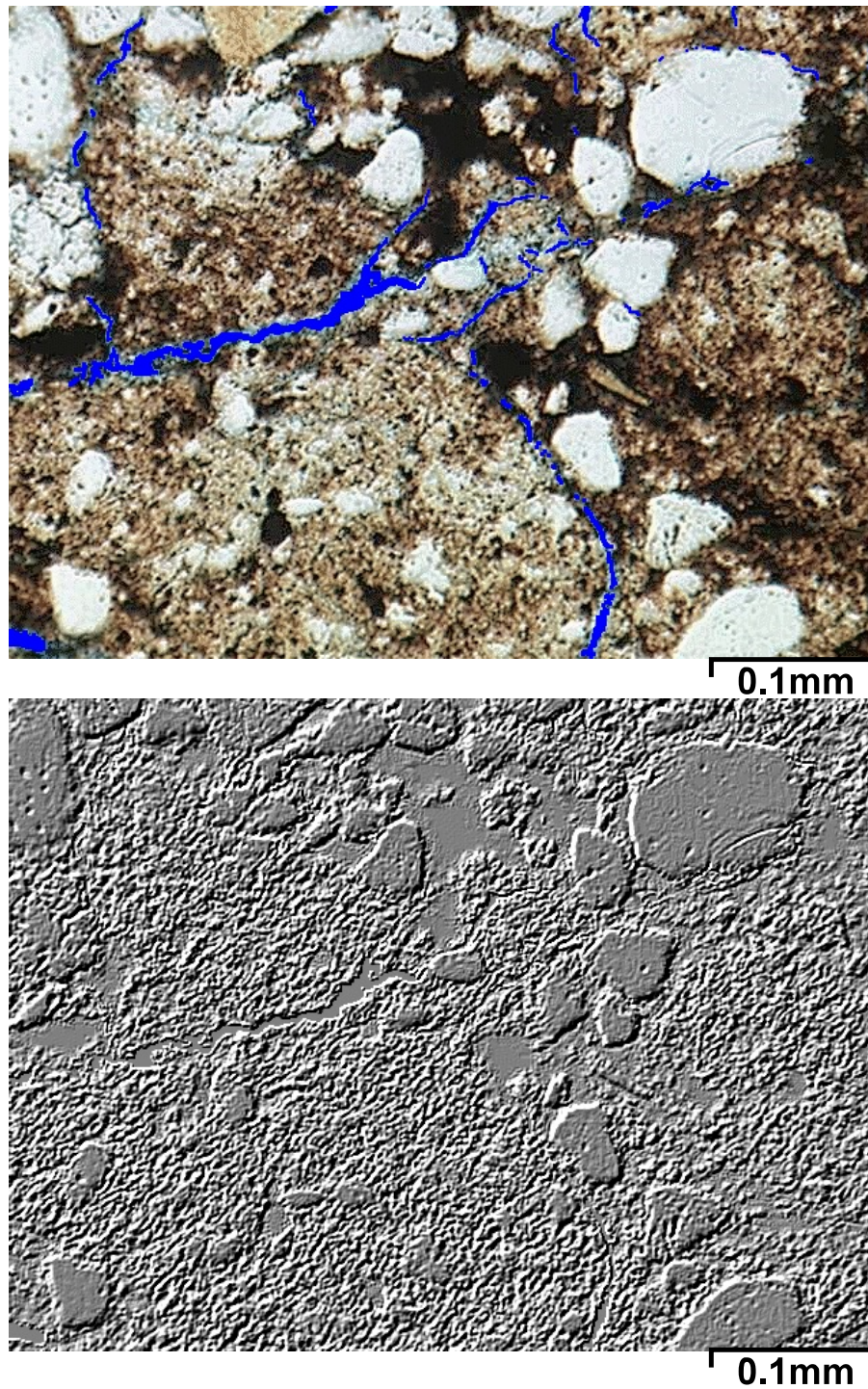


**Figure 4.10** - Feuerletten sample photomicrograph (plain light, above) and digital enhanced relief image (below); coring depth 6m. Pore space in form of fractures prominent (above, enhanced by blue coloration). Fine grained "card house" structure barely identifiable. Occasional parallel lineation (e.g. left center to upper center).



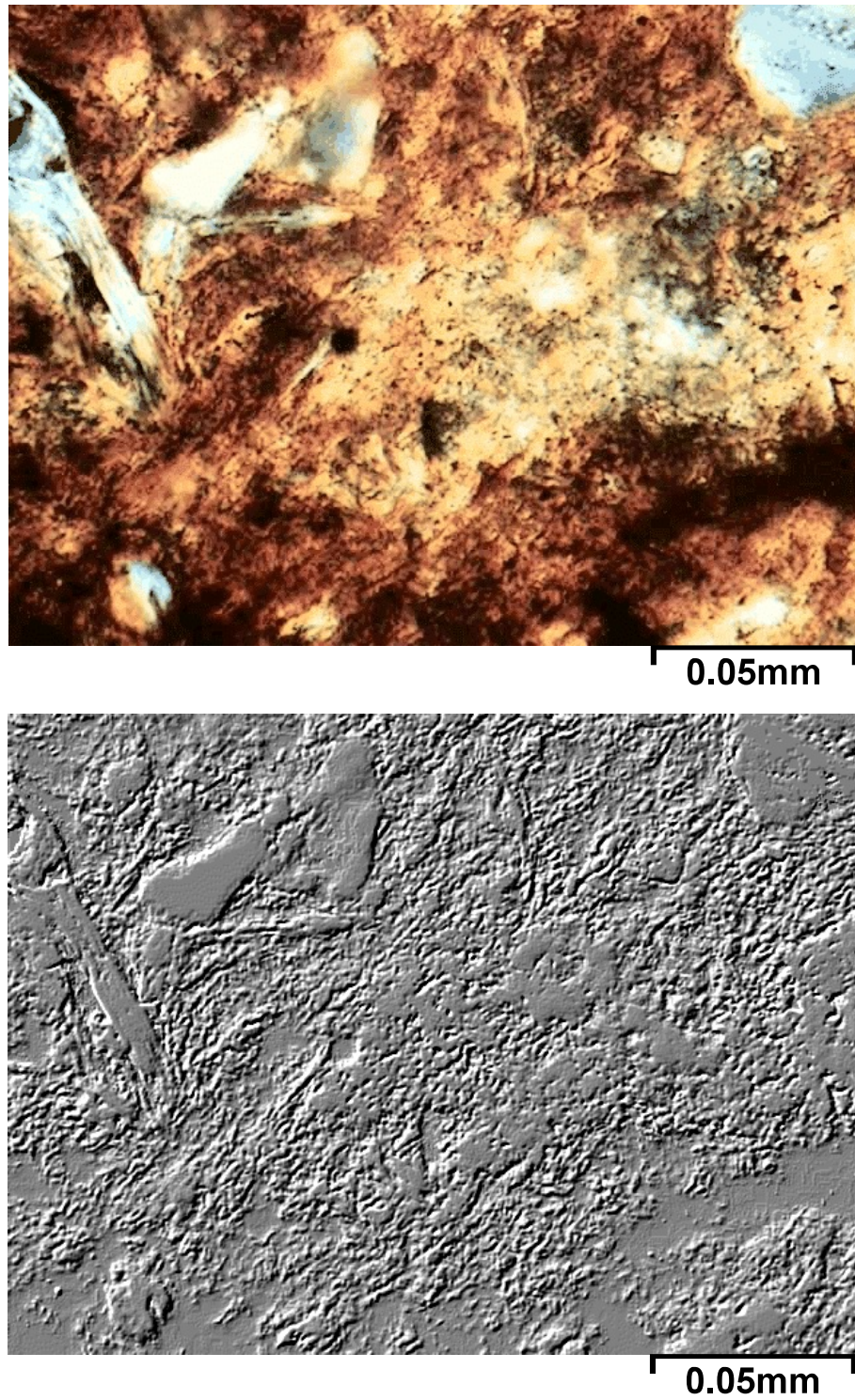


**Figure 4.11** - Photomicrograph (crossed nicols, above) and digital enhanced relief image (below) of Lehrberg layers (coring depth 12m). "Card House" structure evident. Prominent mica particle at left center. Fine material often Fe-stained (dark to very dark to opaque; lower edge and lower right corner).



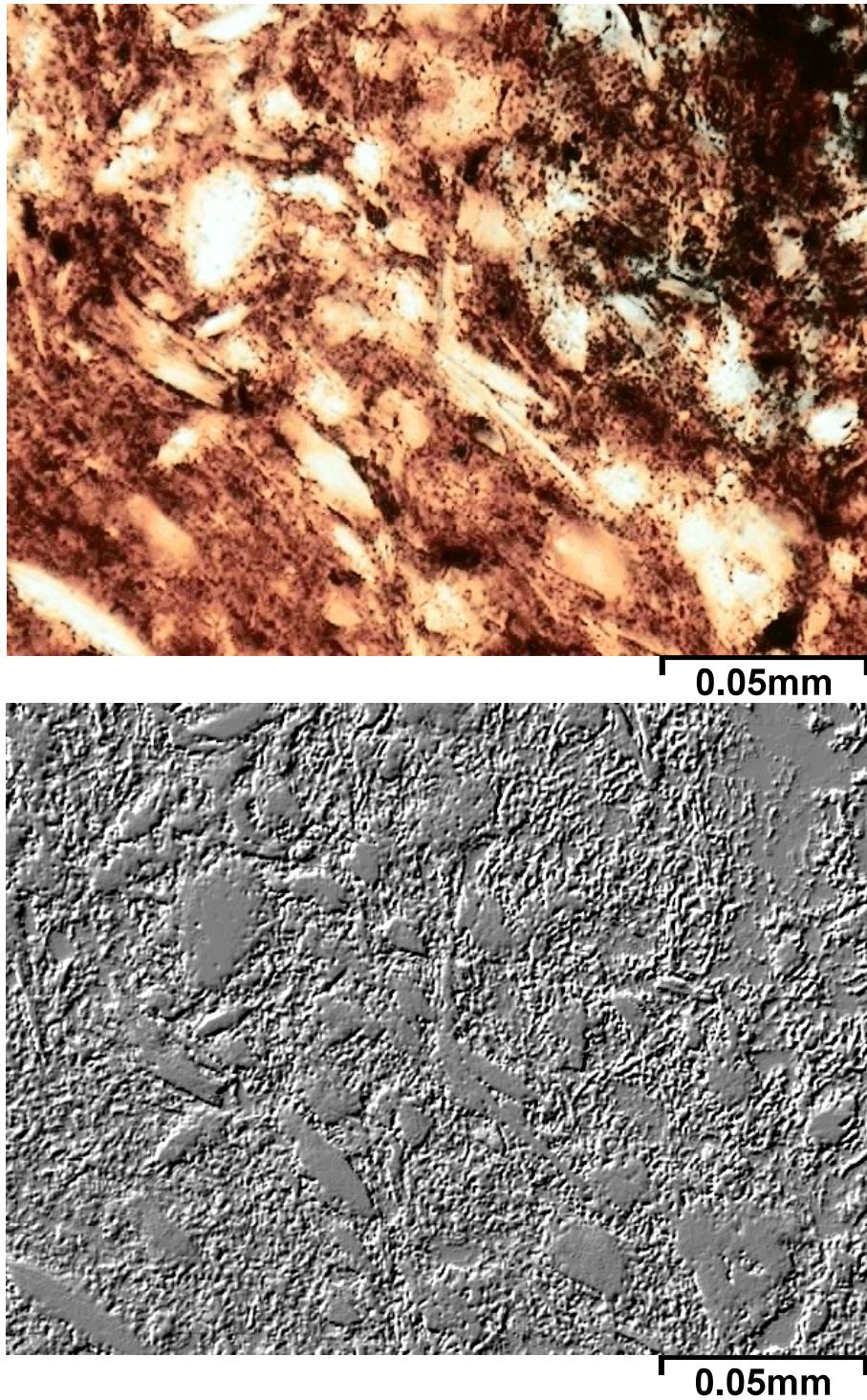


**Figure 4.12** - Lower Rötton photomicrograph (plain light, above) and digital enhanced relief image (below), coring depth 6m. Prominently parallel particle arrangement with occasional "card house" structures. Material often Fe-stained ( very dark to opaque; upper right corner).

Samples of the Lower Rötton show between 65% and 70% in fine materials. The non-differentiable clay particles display a characteristic platy texture in a mixed microstructure of “card house” and parallel alignment (fig. 4.12). Heavy Fe-staining is common resulting in a dark brown to almost opaque appearance of the clay in thin-sections. Detrital quartz (9% to 15%) consists of fine, rounded plutonic grains with inclusions and undulose extinction. Intriguing is the presence of secondary silica. Diagenetic quartz growth (9% to 16%) is observed on detrital grains or interstitially between clay flakes in the lower stratigraphic section. Samples from the upper stratigraphy, however show approximately 17% of an isotropic, vein and pore space filling isotropic material resembling opal. Here, authigenic quartz growth, predominantly on detrital grains, is only 3%. Slightly altered potassium feldspar is also present comprising between 0.8% and 2% of the total grain count. Opaque minerals (0.8% to 3.2%) consist of either heavy Fe-staining or spheroidal hematite displaying a dark to brick red rim. Pore space is commonly absent in upper stratigraphic samples, probably being completely filled by opal. In other stratigraphic areas fractures and voids around the margins of larger grains are the predominant pore space and comprise about 4% to 5% of the total count. Lineations are also frequently present (fig 4.12), but are rarely developed into fractures.

#### 4.2.4 Mineralogical calculations

Using the above mentioned methods of x-ray analysis, SEM studies, and thin section investigations in establishing the mineralogy of selected geologic barriers, several drawbacks are encountered. SEM methods can only look at very small sample sizes and are therefore limited for bulk compositional studies. The unambiguously valuable x-ray determinative techniques for clay identification are confined in their approach of whole rock analysis since they only consider the < 2 $\mu$ m fraction. Yet when estimating the interactive sorption and diffusion properties of a geologic barrier, the whole rock sample with a complete mineral suite will be involved, not just sedimentary particles of a certain grain size. Point counting techniques have merit in sedimentary rock studies but subsume problems of small sample sizes and inherent difficulties of positively distinguishing or identifying small grains.

In order to compensate for these drawbacks and for a better understanding of geochemical associations within the sediments, a calculation of the mineralogy from geochemical data was attempted. While an established routine for fine grained igneous and metamorphic rocks, sedimentary mineralogies have rarely been subject to such computational analysis. IMBRIE and POLDERVAART (1959) were among the first to establish a workable routine calculation for mineral compositions from bulk chemical analysis for a limited range of sedimentary rocks. NICHOLLS (1962) approached the problem by combining normative calculations of known phases into meaningful minerals by comparing a great variety of sediments. MIETSCH (1962) used simultaneous graphical equations for known or estimated geochemical and mineralogical data in order to narrow a compositional probability field. Both approaches, however, are far to time consuming for routine sedimentary work.

PEARSON (1978) showed how a similar graphical method may be used to justify computer solving of a series simultaneous equations set up to represent realistic clay phases in a carboniferous mudstone sequence. His procedure, however, is only applicable for samples containing little or no smectite or swelling clay. Other methods using a variety of matrix calculations and similar mathematical methods were introduced by URBAN (1978), TSCHERNJAK *et al.* (1979), and WIEGMANN *et al.* (1981). All of the researchers mentioned above concluded that satisfactory calculations can only be performed when the qualitative mineralogy has been established by additional methods, such as optical microscopy or x-ray techniques and appropriate adjustments are made in the computations. Irregardless, all of the calculations are still influenced by the assumptions of the author and the analytical data available. While most of the assumptions made are commonly applicable, many of them are not case specific enough to allow for a generalization. A major reason is the great diversity in mineral composition of fine grained sediments and a variable geochemistry within minerals, especially clays. In addition, diagenetic processes may further alter the mineralogy and geochemistry of the rock.

It was therefore necessary to develop a routine calculation for mineral composition specific for the material investigated and for the mineralogical and geochemical data available. The first step in this process is to establish a suite of observed minerals. Secondly, additional minerals can be ascertained because of geochemical characteristics (e.g. high Ti contents are probably associated with rutile). Thirdly, statistical methods were used to investigate geochemical and mineralogical association, allotting certain chemical elements unambiguously to certain minerals.

The suite of minerals to be used in the calculation can be summarized as follows. Minerals definitively recognized through x-ray and optical determinative methods were quartz, kaolinite, chlorite, illite, swelling clays (smectites), dolomite and calcite. Additionally, minor minerals identified through thin-sections and optical microscopy are fine grained muscovite or sericite, hematite, K-feldspar, and apatite. Muscovite/sericite are also shown by DOBNER (1984) to be present in the Lower Röttone, Lehrberg Layers and Amaltheen Clay samples. Other minerals may be assumed because of their very common nature in sedimentary rocks as well as through geochemical associations and their mentioning in supporting literature. IMBRIE AND POLDERVAART (1959) in their mineral calculations list pyrite, gypsum, rutile, albite and ferro-dolomite as candidates. Pyrite and gypsum are most likely present in some of the samples investigated because total sulfur and sulphide sulfur was indicated during geochemical analysis. Furthermore, both minerals are mentioned to be contained in the Lower Röttone and Amaltheen Clay by DOBNER (1984). Rutile and albite can be presumed because of geochemical association with measured  $TiO_2$  and  $Na_2O$  respectively. Ferrodolomite is very likely when carbonate minerals and  $Fe_2O_3$  coexist in sufficient quantities as was indicated in a few of the samples studied.

Certain assumptions and simplifications needed to be made in order to calculate mineralogy from elemental oxide contents. Simplified ideal compositions for each mineral listed as oxides was established. Care was taken to find relationships between minerals to be calculated and minor oxides. The results are summarized in table 4.5:

**Table 4.5 -** Idealized chemical compositions used in calculating mineral components.

Quartz	$SiO_2$	Calcite	$CaO - CO_2$
Gypsum	$CaO - SO_3 - 2H_2O$	Dolomite	$CaO - MgO - 2CO_2$
Pyrite	$FeS_2$ ( $Fe_2O_3 \cdot 0.6994=Fe$ )	Ferrodolomite	$CaO - 0.5 Fe_2O_3 - 2CO_2$
Apatite	$3CaO - P_2O_5$	Illite	$3.7SiO_2 - 0.7Al_2O_3 - 0.1Fe_2O_3 - 0.3MgO - 0.3K_2O - 2.7H_2O$
Albite	$Na_2O - Al_2O_3 - 6SiO_2$	Sericite	$3SiO_2 - 1.5Al_2O_3 - 0.5K_2O - 1H_2O$
K-spar	$3SiO_2 - 0.5Al_2O_3 - 0.5K_2O$	Chlorite	$3SiO_2 - 1Al_2O_3 - 0.6Fe_2O_3 - 3.7MgO - 3.9H_2O$
Rutile	$TiO_2$	Mont. / Smectite	$4SiO_2 - 1Al_2O_3 - 0.1Na_2O - 0.1CaO - 10.9H_2O$
Hematite	$Fe_2O_3$	Kaolinite	$2SiO_2 - 1Al_2O_3 - 0.05TiO_2 - 2H_2O$

While most of the idealized compositions are straight forward and can be derived directly from the respective chemical formulas of the minerals, clay mineralogy is often far more complex. In order to accomplish the most truthful compositional representation, oxide allotments are comprised in such a manner that the summative molecular weight from the respective mole fractions of individual oxides corresponds closely with the true average molecular weight of the mineral. Table 4.6 compares calculated versus true molecular weights of the 5 assessed clays.

**Table 4.6** - Comparison of calculated vs. standard molecular weight of clays used in calculating mineral components.

Clay	Idealized composition	Calculated molecular weight	Standard Molecular weight
Illite	3.7SiO <sub>2</sub> - 0.7Al <sub>2</sub> O <sub>3</sub> - 0.1Fe <sub>2</sub> O <sub>3</sub> - 0.3MgO - 0.3K <sub>2</sub> O - 2.7H <sub>2</sub> O	398.64	389.34 <sup>1</sup>
Sericite	3SiO <sub>2</sub> - 1.5Al <sub>2</sub> O <sub>3</sub> - 0.5K <sub>2</sub> O - 1H <sub>2</sub> O	398.30	398.71 <sup>2</sup>
Chlorite	3SiO <sub>2</sub> - 1Al <sub>2</sub> O <sub>3</sub> - 0.6Fe <sub>2</sub> O <sub>3</sub> - 3.7MgO - 3.9H <sub>2</sub> O	597.41	595.22 <sup>3</sup>
Mont. / Smectite	4SiO <sub>2</sub> - 1Al <sub>2</sub> O <sub>3</sub> - 0.1Na <sub>2</sub> O - 0.1CaO - 10.9H <sub>2</sub> O	550.46	549.07 <sup>3</sup>
Kaolinite	2SiO <sub>2</sub> - 1Al <sub>2</sub> O <sub>3</sub> - 0.05TiO <sub>2</sub> - 2H <sub>2</sub> O	262.15	258.16 <sup>3</sup>

Sources: <sup>1</sup> GAINES *et al.* (1997); <sup>2</sup> O'DONOGHUE (1990); <sup>3</sup> DUDA & REJL (1990), used Clinochlore for Chlorite & Montmorillonite for Mont. / Smectite;

Greater details of deriving the idealized composition of the above clays shall be given in the following discussion of mineral calculation procedures. A step by step outline of procedures is summarized in appendix C.2. The usual approach requires to find a rock forming oxide with a unique association to a certain mineral. For example, P<sub>2</sub>O<sub>5</sub> can be clearly identified with the mineral apatite (3CaO - P<sub>2</sub>O<sub>5</sub>), since no other mineral is affiliated with the same phosphorus oxide. Oxides shared in a great variety of minerals, such as SiO<sub>2</sub> or Al<sub>2</sub>O<sub>3</sub> are commonly less helpful in determining mineral assemblages. In general equation 4.2 is used to compute the percentage of a certain mineral from rock forming oxide analysis data.

$$\text{Eq. 4.2} \quad \% \text{min} = \frac{\% \text{xO}}{MW_{\text{xO}} * MW_{\text{min}} * \text{mf xO}_{\text{min}}}$$

where %min =percentage of calculated mineral  
 %xO =percentage of rock forming oxide associated with mineral of interest  
 MW<sub>xO</sub> =molecular weight of rock forming oxide  
 MW<sub>min</sub> =molecular weight of mineral of interest  
 mf xO<sub>min</sub> =mole fraction of rock forming oxide in idealized mineral formula

#### Step 1: Calculating percent Kaolinite using TiO<sub>2</sub>

Strangely enough, TiO<sub>2</sub> correlates significantly high with Al<sub>2</sub>O<sub>3</sub> using Pearson statistics (see appendix B.4.1) and in scatter plots with 2µm kaolinite concentrations (figure 4.13). As stated by CORRENS AND TILLMANN (1978), some kaolinite exhibits significant TiO<sub>2</sub> contents. WEAVER AND POLLARD (1973) give a TiO<sub>2</sub> range for kaolinites of 0.41% to 2.48% with an average content of 1.43%. Thus kaolinite may contain one of the highest titanium concentrations of the sheet silicates. Leaching experiments by DOLCATER *et al.* (1970) indicate that the Ti content in the kaolinite structure averages about 15%. WEAVER (1989) states that most of the TiO<sub>2</sub> in kaolinite is in the form of 0.1µm anatase pellets. Additional impurities such as Fe<sub>2</sub>O<sub>3</sub> and MgO may also be present. RENGASAMY (1976) gives the structural formula of a Georgia type commercial kaolinite after removal of all impurities as Si<sub>4.04</sub>Al<sub>3.78</sub>Fe<sub>0.08</sub>Ti<sub>0.10</sub>O<sub>10</sub>(OH)<sub>8</sub>. Thus using TiO<sub>2</sub> for calculating percentages of kaolinite appears to be a valid approach. The indicated idealized kaolinite formula of 2SiO<sub>2</sub> - 1Al<sub>2</sub>O<sub>3</sub> - 0.05TiO<sub>2</sub> - 2H<sub>2</sub>O appears appropriate and coincides with the data given by RENGASAMY (1976). For simplification the trace of iron oxide occasional present in the kaolinite structure was not considered because of the small quantities involved.



By using a scatterplot of TiO<sub>2</sub> versus kaolinite for the sample suite smaller than 2µm, certain relationships are evident (see figure 4.13). Samples containing no kaolinite consist of up to 0.63% TiO<sub>2</sub>. Titanium oxide concentrations of 0.64% or more show a second order polynomial relationship with kaolinite. Regression analysis and curve fitting give an intersection of calculated and observed graphs at 0.639 % TiO<sub>2</sub>. This values serves as an estimated cut-off point between samples containing kaolinite and those lacking the silicate in mineral calculations. Inferring the 0.639% TiO<sub>2</sub> cut-off to the whole rock assemblage, using percent clay data, a 0.82% cut-off was computed. Thus the differentiation of kaolinite versus rutile was determined by the 0.82% TiO<sub>2</sub> cut-off. Hence the following rule was applied for calculation of kaolinite in the samples:

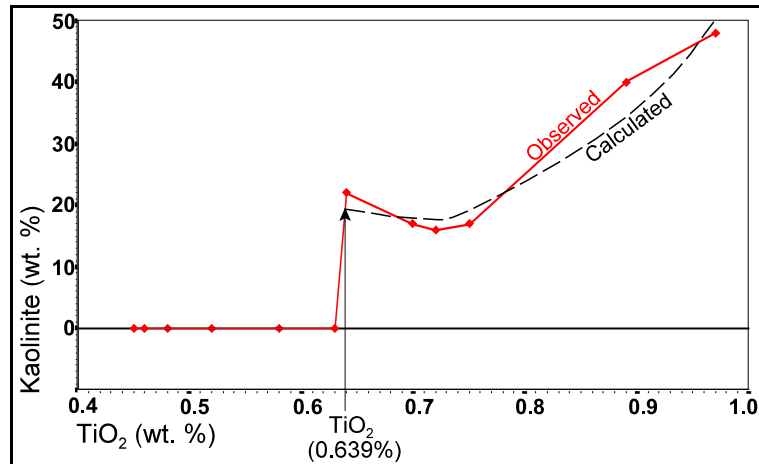


**Figure 4.13** - Scatterplot of TiO<sub>2</sub> vs. Kaolinite concentrations in samples <2µm. Second order polynomial curve for TiO<sub>2</sub> concentrations of 0.64% or greater calculated as: [Kaol] = 233.5 + (-617.9)\*[TiO<sub>2</sub>] + 442.9\*[TiO<sub>2</sub>]<sup>2</sup>.

From TiO<sub>2</sub> concentrations of whole rock analysis 0.82% (cut-off for presence of kaolinite) are subtracted. If the result is less than zero, no Kaolinite is believed to be present and all TiO<sub>2</sub> is allotted to rutile. In case the result is greater than zero, 0.82% TiO<sub>2</sub> is allotted to rutile and the remainder is calculated as kaolinite according to equation 4.2. The amount of other oxides used in the calculation of kaolinite, such as SiO<sub>2</sub>, Al<sub>2</sub>O<sub>3</sub>, and H<sub>2</sub>O are computed as generalized by equation 4.3. These other oxide quantities are tracked in a tally sheet as seen in appendix C.1. Water is commonly believed to be lost during the geochemical analytical process and is therefore tallied under LOI.

**Eq. 4.3** 
$$\%xO = mf \ xO_{min} * \%min * MW_{xO} * MW_{min}$$

- where %min =percentage of calculated mineral
- %xO =percentage of rock forming oxide associated with mineral of interest
- MW<sub>xO</sub> =molecular weight of rock forming oxide
- MW<sub>min</sub> =molecular weight of mineral of interest
- mf xO<sub>min</sub> =mole fraction of rock forming oxide in idealized mineral formula

**Step 2: Establishing percent Rutile using TiO<sub>2</sub>**

Since no other mineral of interest contains TiO<sub>2</sub>, remaining titanium oxide values determined during step 1 are now calculated as rutile using the above equation. The oxide is now completely allotted.

**Step 3: Calculating percent Apatite from P<sub>2</sub>O<sub>5</sub>**

Since no other mineral is considered as to containing P<sub>2</sub>O<sub>5</sub>, all of the oxide is allotted to apatite. The remaining CaO is tracked according to equation 4.3 and the procedure described above.

**Step 4: Computing Gypsum from S if data is available**

Sulfur analysis by LECO™ was performed for several samples of Feuerletten, Amaltheen, Rötton and Lehrberg Layer clays. Results were given as total S, sulfide S and SO<sub>3</sub>. Complete analytical results and procedures are summarized in appendix C.3. Gypsum is calculated using SO<sub>3</sub> according to equation 4.2 and idealized formula CaO - SO<sub>3</sub> - 2H<sub>2</sub>O, completely allotting SO<sub>3</sub>. CaO and H<sub>2</sub>O are tracked as described above.

Step 5: Calculating Pyrite from S if data is available

As described in step 4, LECO™ for sulfur are applied to the calculation of pyrite. Equation 4.2 is used and S is now entirely distributed. Since Fe<sub>2</sub>O<sub>3</sub> is not used in the idealized chemical formula for pyrite, Fe in the iron sulfide is converted to Fe<sub>2</sub>O<sub>3</sub> by  $Fe_{\text{pyrite}} / 0.6994$  for tracking purposes.

Step 6: Figuring Smectite Clay from Na<sub>2</sub>O

Only two minerals of interest show Na<sub>2</sub>O in their idealized chemical formula, smectite (4SiO<sub>2</sub> - 1Al<sub>2</sub>O<sub>3</sub> - 0.1Na<sub>2</sub>O - 0.1CaO - 10.9H<sub>2</sub>O) and albite (Na<sub>2</sub>O - Al<sub>2</sub>O<sub>3</sub> - 6SiO<sub>2</sub>). The sodium oxide concentrations and relationships among the two minerals needed to be established. A regression analysis between the oxide of interest (geochemical data) and the amount of mineral present (x-ray data) will usually yield a satisfactory numerical or curve fitting association to be used in establishing mineral concentrations. In the case of clay minerals, the 2µm fraction was used in a first approach to avoid interfering mineralogies of larger grain sizes. Once successful, the whole rock relationship for oxide and clay mineral was extrapolated from total clay percentages in the complete sample. While this approach was found to be very successful in calculating mineral concentrations from geochemical data, it proved to be fruitless in the case of smectite and Na<sub>2</sub>O. During the 2µm separation process, the dispersing agent sodium pyrophosphate (Na<sub>2</sub>P<sub>2</sub>O<sub>7</sub> x 10 H<sub>2</sub>O) was used, severely falsifying the geochemical analytical results for Na<sub>2</sub>O and P<sub>2</sub>O<sub>5</sub> in the clay size fraction. Hence a varying approach for establishing the sodium oxide / mineral relationship had to be employed.

Some basic generalizations and assumptions aided in the process. It is assumed that all smectite resides in the <2µm fraction while albite probably exists in the larger grain sizes. By knowing the percent of clay in the total sample and the amount of smectite within this clay fraction (see table 4.3), the amount of Na<sub>2</sub>O needed to satisfy the smectite mineralogy can be estimated for selected samples. The remaining sodium oxide should therefore reside in albite. In this manner probable Na<sub>2</sub>O distributions for albite and smectite can be estimated and used in the before mentioned regression analysis. Figure 4.14 summarizes the association of sodium oxide in smectite to whole rock smectite concentrations. The observed

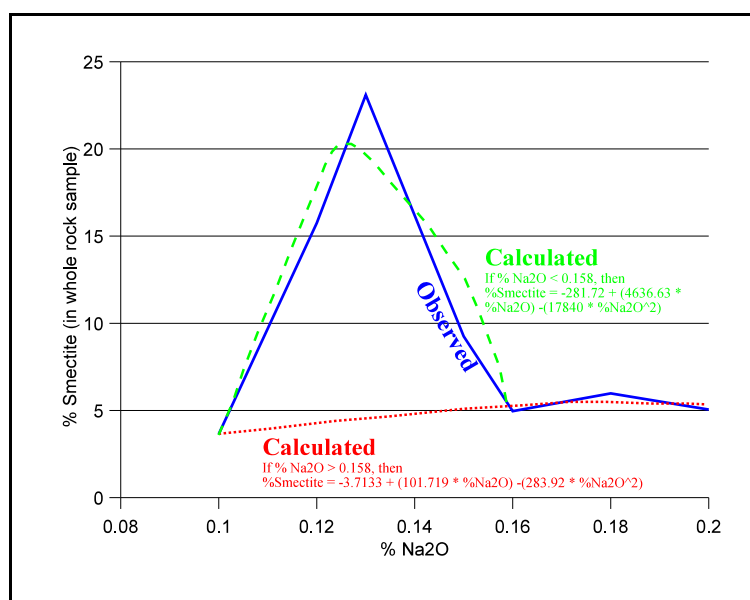


Figure 4.14 - Relationship of Na<sub>2</sub>O vs. Smectite concentrations with calculated curves and associating formulas for mineral concentration modeling..

correlation shows two distinctly different curve relationships for Na<sub>2</sub>O concentrations above and below 0.158%. Two distinct equations were therefore established to determine smectite concentrations from Na<sub>2</sub>O amounts.

$$\text{Eq. 4.4} \quad \% \text{Smectite} = -3.7133 + (101.719 * \% \text{Na}_2\text{O}) - (283.92 * \% \text{Na}_2\text{O}^2)$$

If  $\% \text{Na}_2\text{O} > 0.158\%$

$$\text{Eq. 4.5} \quad \% \text{Smectite} = -281.72 + (4636.63 * \% \text{Na}_2\text{O}) - (17840 * \% \text{Na}_2\text{O}^2)$$

If  $\% \text{Na}_2\text{O} < 0.158\%$

After calculating smectite, individual oxide concentrations used in the smectite mineralogy are computed according to equation 4.3 and tracked. Remaining  $\text{Na}_2\text{O}$  is assigned to albite.

Step 7: Calculating Albite from remaining  $\text{Na}_2\text{O}$

The persisting  $\text{Na}_2\text{O}$  from step 6 is now used to solve for percent albite according to equation 4.2. If no  $\text{Na}_2\text{O}$  is remaining or has a negative number than albite is equal to zero. After completing step 7, sodium oxide will be now wholly allotted.

Step 8: Computing Calcite using  $\text{CaO}$  and  $\text{CO}_2$

The relationship of  $\text{CaO}$ ,  $\text{MgO}$ , and  $\text{CO}_2$  for specific carbonate mineral concentration and computing details in sedimentary rocks are well established by IMBRIE & POLDERVAART (1959). Their advice for the calculating procedures was adopted as follows:

From the molecular proportion of  $\text{CO}_2$  the proportion of calcium oxide remaining after allowing for  $\text{CaO}$  used in gypsum, apatite, and smectite is subtracted. The balance represents the amount of dolomite necessary to use up all of the  $\text{CO}_2$ . By subtracting this balance from the available calcium oxide, the molecular proportion of calcite is determined. When total  $\text{MgO}$  and  $\text{CaO}$  are insufficient to use up  $\text{CO}_2$ , ferrodolomite is calculated by subtracting the  $\text{MgO}$  molecular weight ratio from the above mentioned balance and multiplying the answer by the molecular weight of ferrodolomite.

The key for precise calculation of carbonates, such as calcite, lies in the accurate determination of the  $\text{CO}_2$  concentration. Herein lay the greatest challenge since the carbon dioxide determination by LECO™ and LOI methods were insufficiently accurate to yield meaningful results in several samples, especially those of greater carbonate latitudes, such as Lehrberg Layer clays. While greatest agreement was found in most cases when LECO™ data was used, mineral calculation results were often still erroneous. Therefore a somewhat different approach was employed.

Since the amount of  $\text{CO}_2$  used was tallied in the mineral calculations, the difference between total carbon dioxide available and allotted gave a measure of computational reliability. The greater the difference, the more erroneous the results. If, however, tallied  $\text{CO}_2$  would zero out available  $\text{CO}_2$ , the computational results were most believable. To achieve the state of accuracy despite variations in  $\text{CO}_2$  measurements, the complete mineral calculations package must be established first. Calculations were started using measured carbon dioxide values at first. If discrepancies between measured and tallied  $\text{CO}_2$  were observed, the measured or input data was adjusted until the resulting calculations yielded the smallest possible difference between input and tallied values. The results of this approach can be found in appendix C.1 under the column "Remain" or as summaries in table 3.2 of the previous chapter. In most cases the

difference shows zero or at least very small discrepancies. Carbon dioxide concentrations established through the mineral calculation appear to be the most reliable for particular sample suites.

#### Step 9: Calculating Dolomite and Ferrodolomite from MgO

First the MgO mole fraction is determined by dividing the molecular weight of magnesium oxide into percent MgO. The magnesium oxide carbonate value allotted for dolomite in the calcite calculations of step 8 are now subtracted from the MgO mole fraction. If the difference is smaller than zero, ferrodolomite is calculated as indicated above. Percent dolomite is now computed by using the remaining CaO, dividing it by the molecular weight for calcium oxide and multiplying the answer by the molecular weight of dolomite. Any remaining MgO is assigned to chlorite and illite calculations. Both CO<sub>2</sub> and CaO are now completely allotted!

#### Step 10: Calculation of percent Illite from K<sub>2</sub>O and MgO data

IMBRIE & POLDERVAART (1959) use a potassium / magnesium mole ratio to establish relationships between illite and sericite clay minerals. They suggested that two first order alternatives are possible, depending on the relative proportions of K<sub>2</sub>O and MgO. First the molecular ratio for potassium oxide (MR<sub>K<sub>2</sub>O</sub>) is established by taking percent K<sub>2</sub>O and dividing it by the molecular weight of the same oxide. Secondly, the mol ratio MgO (MR<sub>MgO</sub>) is determined by applying the equivalent computation to percent MgO remaining after carbonate computations. From the results, a ratio is established as:

$$3 * MR_{K_2O} / 2 * MR_{MgO}$$

If this ratio equals or exceeds 1, IMBRIE & POLDERVAART (1959) would calculate all of the MgO as illite and the balance of K<sub>2</sub>O as sericite. While appropriate for their investigation of the Permian Florena Shale, it yielded only partial satisfactory results for the geologic barriers used in this investigation. However, using this ratio approach but combining it with a regression analysis and curve fitting correlation of MgO and K<sub>2</sub>O with whole rock illite concentrations (see figure 4.15), a different system was established.

If the before mentioned ratio is smaller than 1, percent illite can be satisfactorily calculated using percent MgO as demonstrated with equation 4.6. Otherwise equation 4.7 and percent K<sub>2</sub>O is to be used.

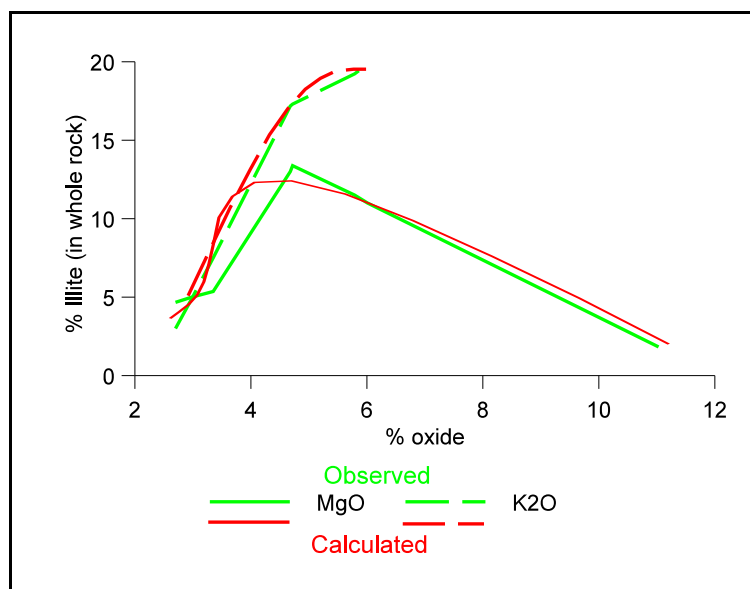


**Figure 4.15** - Relationship of K<sub>2</sub>O and MgO concentrations to whole rock illite content showing observed and calculated values. MgO curve to be used if  $3 * MR_{K_2O} / 2 * MR_{MgO} < 1$ ; otherwise K<sub>2</sub>O computed as illite.

$$\text{Eq. 4.6} \quad \% \text{Illite} = -18.095 + (10.0391 * \% \text{MgO}) - (0.7462 * \text{MgO}^2)$$

$$\text{If } 3 * \text{MR}_{\text{K}_2\text{O}} / 2 * \text{MR}_{\text{MgO}} < 1$$

$$\text{Eq. 4.7} \quad \% \text{Illite} = -40.777 + (20.5364 * \% \text{K}_2\text{O}) - (1.7464 * \text{K}_2\text{O}^2)$$

$$\text{If } 3 * \text{MR}_{\text{K}_2\text{O}} / 2 * \text{MR}_{\text{MgO}} \geq 1$$

Step 11: Compute chlorite from remaining MgO

Any remaining MgO from previous calculations is now allotted to the clay mineral chlorite, idealized formula  $3\text{SiO}_2 - 1\text{Al}_2\text{O}_3 - 0.6\text{Fe}_2\text{O}_3 - 3.7\text{MgO} - 3.9\text{H}_2\text{O}$ , according to equation 4.2. If tallied magnesium oxide is less than zero, no chlorite is computed. MgO is now completely assigned.

Step 12: Estimating percent Sericite and Potassium Feldspar from remaining  $\text{K}_2\text{O}$  and  $\text{Al}_2\text{O}_3$

Oxides of aluminum and potassium are very common constituents in many minerals. While most of the oxides were allotted to this point,  $\text{Al}_2\text{O}_3$  and  $\text{K}_2\text{O}$  are major building blocks in sericite and potassium feldspar, the last remaining minerals to be calculated. Both minerals were observed during thin-section and point count analysis at various degrees in certain samples and must therefore be considered in the calculation. In order to see which of the two minerals is predominant and what oxide quantity is to be assigned to each mineral, the following approach was used.

**Table 4.7 -** Mole ratio comparison of  $\text{Al}_2\text{O}_3$  and  $\text{K}_2\text{O}$  in Sericite and Kspar. (MW = Molecular Weight).

Mineral	Idealized Formula	MW $\text{Al}_2\text{O}_3$	MW $\text{K}_2\text{O}$	MW $\text{Al}_2\text{O}_3$ in mineral	MW $\text{K}_2\text{O}$ in mineral	MW $\text{Al}_2\text{O}_3$ <sub>(mineral)</sub> / MW $\text{K}_2\text{O}$ <sub>(mineral)</sub>
Sericite	$3\text{SiO}_2 - 1.5\text{Al}_2\text{O}_3 - 0.5\text{K}_2\text{O} - 1\text{H}_2\text{O}$	101.9600	94.1956	152.9400	47.0978	3.2473
K-Feldspar	$3\text{SiO}_2 - 0.5\text{Al}_2\text{O}_3 - 0.5\text{K}_2\text{O}$	50.9800	47.0978	50.9800	47.0978	1.0824

According to their idealized chemical make-up, sericite and K-spar exhibit different molecular ratios of  $\text{Al}_2\text{O}_3$  to  $\text{K}_2\text{O}$ . For sericite this ratio equals 3.247, while K-feldspar is equivalent to 1.082 as seen in table 4.7. Remaining  $\text{Al}_2\text{O}_3$  from the previous mineral calculations can be divided by remaining  $\text{K}_2\text{O}$ . When comparing the resulting ratios to the results for sericite and potassium feldspar, the following observation can be made. Values close to 3.2 or higher are most likely associated with predominating sericite with little or no Kspar present. Ratios of 1.1 or smaller would point to potassium feldspar as the main mineral. A sliding scale of allotment of oxides can be established for values between 1.1 and 3.2 as represented by equation 4.8 and 4.9.

$$\text{Eq. 4.8} \quad \% \text{K}_2\text{O}_{\text{Sericite}} = \frac{\% \text{K}_2\text{O} * (46.1926 * \text{Ratio}^{\text{Al}_2\text{O}_3/\text{K}_2\text{O}} - 50)}{100}$$

$\text{K}_2\text{O}$  to be used in Sericite calculations.

$$\text{Eq. 4.9} \quad \% \text{K}_2\text{O}_{\text{Kspar}} = \frac{\% \text{K}_2\text{O} * (-46.1926 * \text{Ratio}^{\text{Al}_2\text{O}_3/\text{K}_2\text{O}} + 150)}{100}$$

$\text{K}_2\text{O}$  to be used in Potassium Feldspar calculations.

If the  $Al_2O_3/K_2O$  ratio for remaining oxides is greater than 3.247, 100%  $K_2O$  is calculated as sericite. Should the same ratio be at 1.082 or below,  $Al_2O_3$  is completely assigned to Kspar. For values between 3.247 and 1.082, percent remaining potassium oxide is basically split between sericite and Kspar according to equation 4.8 and 4.9. The amount of both minerals is then calculated according to equation 4.2. All  $K_2O$  should now be allotted except where the ratio is smaller than 1.082.

Step 13: Remaining  $Fe_2O_3$  assigned to Hematite

In the last and final step, the remaining iron (III) oxide is assigned to hematite. Since the idealized formula is the same as the oxide formula, no special calculation is necessary. All oxides analyzed during whole rock geochemical investigation were utilized during mineral computations with the following exceptions:

Two of the rock forming oxides analyzed during the geochemical investigation,  $Cr_2O_3$  and  $MnO$  were not assigned to any particular minerals. Their total amounts were rather minor and they did not fit in any idealized formula for the mineral suite observed. Manganese oxide may be most likely present as wad or similar common mineral stain not easily distinguished from iron oxides during optical mineralogy. Chromium, on the other hand could occur in small amounts as very stable detrital chromite in the heavy mineral fraction of the geologic barrier material. LEVINSON (1980) also reports Cr as possible substitution in micas or clay minerals.

Results of mineral calculations are summarized in table 4.8. Talled results of the computations are represented in appendix C.1.

**Table 4.8** - Results of mineral calculations of representative samples from selected locations. Samples: K=Amaltheen Clay; B=Feuerletten; L=Lehrberg Layers; M=Lower Rötton.

<b>Sample B3.0</b>				<b>Sample B6.0</b>			
% Clay	60.8	<b>Results</b>		% Clay	49	<b>Results</b>	
SiO <sub>2</sub>	52.07	Quartz	24.19	SiO <sub>2</sub>	51.88	Quartz	25.84
Al <sub>2</sub> O <sub>3</sub>	15.71	<b>Minor constituents</b>		Al <sub>2</sub> O <sub>3</sub>	14.45	<b>Minor constituents</b>	
Fe <sub>2</sub> O <sub>3</sub>	6.26	MgO	4.72	Fe <sub>2</sub> O <sub>3</sub>	6	MgO	4.72
		Gypsum	0.21			Gypsum	0.32
		CaO	2.96			Pyrite	0.00
		Na <sub>2</sub> O	0.13			Na <sub>2</sub> O	0.13
		Apatite	0.20			Apatite	0.22
		K <sub>2</sub> O	3.41			Albite	0.00
		Albite	0.00			K <sub>2</sub> O	3.31
		K-spar	0.00			TiO <sub>2</sub>	0.79
		Rutile	0.82			P <sub>2</sub> O <sub>5</sub>	0.1
		Hematite	4.33			MnO	0.04
		SUM	5.57			Hematite	4.85
Cr <sub>2</sub> O <sub>3</sub>	0.009	<b>Carbonates</b>		Cr <sub>2</sub> O <sub>3</sub>	0.01	<b>Carbonates</b>	
LOI	13.9	Calcite	0.00	LOI	14	Calcite	0.00
CO <sub>2</sub>	4.65	Dolomite	9.73	CO <sub>2</sub>	7.28	Dolomite	15.26
C-Graphite	0.01	Ferrodolomite	0.00	C-Graphite	0.03	Ferrodolomite	0.00
C/ORG	0.03	SUM	9.73	C/ORG	0	SUM	15.26
C/TOT	0.67	<b>Clay Minerals</b>		C/TOT	1.71	<b>Clay Minerals</b>	
S/TOT	0.04	Illite	12.67	S/TOT	0.06	Illite	12.67
S-/S	0	Sericite	21.25	S-/S	0	Sericite	20.40
SO <sub>3</sub> (calc.)	0.100	Chlorite	8.85	SO <sub>3</sub> (calc.)	0.150	Chlorite	4.01
CO <sub>2</sub> (calc.)	2.309	Mont. / Smec.	19.55	CO <sub>2</sub> (calc.)	6.156	Mont. / Smec.	19.55
		Kaolinite	0.00			Kaolinite	0.00
		SUM	62.30			SUM	56.62

Table 4.8 - continued

<b>Sample B10.0</b>		<b>Results</b>	
% Clay	26.8	Quartz	35.53
SiO2	58.4		
Al2O3	13.17		
Fe2O3	4.12	<b>Minor constituents</b>	
MgO	3.35	Gypsum	0.00
CaO	3.21	Pyrite	0.00
Na2O	0.12	Apatite	0.15
K2O	3.15	Albite	0.00
TiO2	0.76	K-spar	1.50
P2O5	0.07	Rutile	0.76
MnO	0.04	Hematite	3.30
Cr2O3	0.01	SUM	5.72
LOI	11.7		
CO2	5.04	<b>Carbonates</b>	
C-Graphite	0	Calcite	0.00
C/ORG	0	Dolomite	10.56
C/TOT	1.37329	Ferrodolomite	0.00
	700272		
	48	SUM	10.56
S/TOT			
S-/S		<b>Clay Minerals</b>	
SO3 (calc.)	0.000	Illite	7.16
CO2 (calc.)	5.032	Sericite	20.20
		Chlorite	3.31
		Mont. / Smec.	17.78
		Kaolinite	0.00
		SUM	48.45

<b>Sample K7.2</b>		<b>Results</b>	
% Clay	27.2	Quartz	31.40
SiO2	49.29		
Al2O3	20.56		
Fe2O3	6.18	<b>Minor constituents</b>	
MgO	2.53	Gypsum	0.00
CaO	3.91	Pyrite	0.00
Na2O	0.18	Apatite	0.39
K2O	2.98	Albite	1.01
TiO2	0.91	K-spar	0.00
P2O5	0.18	Rutile	0.82
MnO	0.11	Hematite	5.91
Cr2O3	0.01	SUM	8.13
LOI	12.5		
CO2	5.8	<b>Carbonates</b>	
C-Graphite	0	Calcite	0.00
C/ORG	0.85	Dolomite	12.86
C/TOT	2.43	Ferrodolomite	0.49
S/TOT		SUM	13.34
S-/S			
SO3 (calc.)	0.000	<b>Clay Minerals</b>	
CO2 (calc.)	5.791	Illite	2.53
		Sericite	23.69
		Chlorite	0.00
		Mont. / Smec.	5.40
		Kaolinite	5.91
		SUM	37.52

<b>Sample K 3.0</b>		<b>Results</b>	
% Clay	31.1	Quartz	30.83
SiO2	49.31		
Al2O3	20.9		
Fe2O3	5.63	<b>Minor constituents</b>	
MgO	2.7	Gypsum	0.00
CaO	4.03	Pyrite	0.00
Na2O	0.2	Apatite	0.31
K2O	2.96	Albite	1.19
TiO2	0.92	K-spar	0.00
P2O5	0.14	Rutile	0.82
MnO	0.14	Hematite	5.41
Cr2O3	0.02	SUM	7.72
LOI	12.6		
CO2	6.1	<b>Carbonates</b>	
C-Graphite	0	Calcite	0.00
C/ORG	1.38	Dolomite	13.25
C/TOT	3.04212	Ferrodolomite	0.22
	5340599		
	46	SUM	13.47
S/TOT			
S-/S		<b>Clay Minerals</b>	
SO3 (calc.)	0.000	Illite	3.57
CO2 (calc.)	6.091	Sericite	22.89
		Chlorite	0.00
		Mont. / Smec.	5.27
		Kaolinite	6.56
		SUM	38.30

<b>Sample K9.0</b>		<b>Results</b>	
% Clay	25.1	Quartz	31.76
SiO2	51		
Al2O3	21.36		
Fe2O3	6.34	<b>Minor constituents</b>	
MgO	2.29	Gypsum	1.77
CaO	3.58	Pyrite	2.02
Na2O	0.3	Apatite	0.00
K2O	3.04	Albite	2.42
TiO2	0.99	K-spar	0.00
P2O5	0	Rutile	0.82
MnO	0.1	Hematite	4.92
Cr2O3	0.009	SUM	11.95
LOI	11.6		
CO2	4.9	<b>Carbonates</b>	
C-Graphite	0	Calcite	0.00
C/ORG	0.89	Dolomite	11.77
C/TOT	1.68	Ferrodolomite	0.10
S/TOT	1.41	SUM	11.88
S-/S	1.08		
SO3 (calc.)	0.824	<b>Clay Minerals</b>	
CO2 (calc.)	2.895	Illite	0.98
		Sericite	25.12
		Chlorite	0.00
		Mont. / Smec.	1.25
		Kaolinite	11.16
		SUM	38.51

Table 4.8 - continued

<b>Sample L3.0</b>			
% Clay	44.05	<b>Results</b>	
SiO <sub>2</sub>	49.17	Quartz	21.22
Al <sub>2</sub> O <sub>3</sub>	16.9		
Fe <sub>2</sub> O <sub>3</sub>	7.12	<b>Minor constituents</b>	
MgO	4.03	Gypsum	0.27
CaO	3.29	Pyrite	0.00
Na <sub>2</sub> O	0.15	Apatite	0.35
K <sub>2</sub> O	4.68	Albite	0.09
TiO <sub>2</sub>	0.72	K-spar	2.75
P <sub>2</sub> O <sub>5</sub>	0.16	Rutile	0.72
MnO	0.07	Hematite	5.84
Cr <sub>2</sub> O <sub>3</sub>	0.01	SUM	10.02
LOI	12.1		
CO <sub>2</sub>	5.16	<b>Carbonates</b>	
C-Graphite	0.025	Calcite	0.00
C/ORG	0.095	Dolomite	10.82
C/TOT	1.815	Ferrodolomite	0.00
S/TOT	0.05	SUM	10.82
S-/S	0		
SO <sub>3</sub> (calc.)	0.125	<b>Clay Minerals</b>	
CO <sub>2</sub> (calc.)	6.211	Illite	10.24
		Sericite	29.50
		Chlorite	5.43
		Mont. / Smec.	12.37
		Kaolinite	0.00
		SUM	57.54

<b>Sample L11.0</b>			
% Clay	18.25	<b>Results</b>	
SiO <sub>2</sub>	33.23	Quartz	15.16
Al <sub>2</sub> O <sub>3</sub>	11.06		
Fe <sub>2</sub> O <sub>3</sub>	3.46	<b>Minor constituents</b>	
MgO	11.03	Gypsum	0.21
CaO	12.37	Pyrite	0.00
Na <sub>2</sub> O	0.1	Apatite	0.31
K <sub>2</sub> O	3.43	Albite	0.51
TiO <sub>2</sub>	0.43	K-spar	5.90
P <sub>2</sub> O <sub>5</sub>	0.14	Rutile	0.43
MnO	0.33	Hematite	2.05
Cr <sub>2</sub> O <sub>3</sub>	0.01	SUM	9.41
LOI	24.6		
CO <sub>2</sub>	19.4	<b>Carbonates</b>	
C-Graphite	0.01	Calcite	0.00
C/ORG	0.06	Dolomite	40.68
C/TOT	3.08	Ferrodolomite	0.00
S/TOT	0.04	SUM	40.68
S-/S	0		
SO <sub>3</sub> (calc.)	0.100	<b>Clay Minerals</b>	
CO <sub>2</sub> (calc.)	11.030	Illite	1.85
		Sericite	19.45
		Chlorite	8.35
		Mont. / Smec.	3.54
		Kaolinite	0.00
		SUM	33.19

<b>Sample L6.0</b>			
% Clay	10.5	<b>Results</b>	
SiO <sub>2</sub>	37.26	Quartz	12.44
Al <sub>2</sub> O <sub>3</sub>	11.12		
Fe <sub>2</sub> O <sub>3</sub>	4.38	<b>Minor constituents</b>	
MgO	9.43	Gypsum	0.38
CaO	11.2	Pyrite	0.00
Na <sub>2</sub> O	0.15	Apatite	0.35
K <sub>2</sub> O	3.76	Albite	0.09
TiO <sub>2</sub>	0.51	K-spar	4.07
P <sub>2</sub> O <sub>5</sub>	0.16	Rutile	0.51
MnO	0.36	Hematite	0.00
Cr <sub>2</sub> O <sub>3</sub>	0.007	SUM	5.40
LOI	21.7		
CO <sub>2</sub>	8.62	<b>Carbonates</b>	
C-Graphite	0.03	Calcite	19.58
C/ORG	0.07	Dolomite	0.00
C/TOT	1.46	Ferrodolomite	0.00
S/TOT	0.07	SUM	19.58
S-/S	0		
SO <sub>3</sub> (calc.)	0.175	<b>Clay Minerals</b>	
CO <sub>2</sub> (calc.)	4.984	Illite	10.22
		Sericite	0.00
		Chlorite	36.54
		Mont. / Smec.	12.37
		Kaolinite	0.00
		SUM	59.13

<b>Sample M4.8</b>			
% Clay	49.3	<b>Results</b>	
SiO <sub>2</sub>	54.79	Quartz	21.60
Al <sub>2</sub> O <sub>3</sub>	18.01		
Fe <sub>2</sub> O <sub>3</sub>	6.77	<b>Minor constituents</b>	
MgO	3	Gypsum	0.00
CaO	0.7	Pyrite	0.00
Na <sub>2</sub> O	0.2	Apatite	0.22
K <sub>2</sub> O	5.79	Albite	1.19
TiO <sub>2</sub>	0.72	K-spar	6.28
P <sub>2</sub> O <sub>5</sub>	0.1	Rutile	0.72
MnO	0.1	Hematite	4.76
Cr <sub>2</sub> O <sub>3</sub>	0.02	SUM	13.17
LOI	7.4		
CO <sub>2</sub>	1.3	<b>Carbonates</b>	
C-Graphite	0	Calcite	0.40
C/ORG	0.06	Dolomite	2.30
C/TOT	0.05	Ferrodolomite	0.00
S/TOT	0	SUM	2.70
S-/S	0		
SO <sub>3</sub> (calc.)	0.000	<b>Clay Minerals</b>	
CO <sub>2</sub> (calc.)	-0.037	Illite	19.58
		Sericite	28.24
		Chlorite	7.62
		Mont. / Smec.	5.27
		Kaolinite	0.00
		SUM	60.72



Table 4.8 - continued

Sample M6.0				Sample M8.5			
% Clay	29.9	<b>Results</b>		% Clay	49.6	<b>Results</b>	
SiO <sub>2</sub>	54.04	Quartz	19.90	SiO <sub>2</sub>	60.52	Quartz	27.44
Al <sub>2</sub> O <sub>3</sub>	17.79			Al <sub>2</sub> O <sub>3</sub>	15.89		
Fe <sub>2</sub> O <sub>3</sub>	6.67	<b>Minor constituents</b>		Fe <sub>2</sub> O <sub>3</sub>	5.68	<b>Minor constituents</b>	
MgO	2.75	Gypsum	0.00	MgO	2.25	Gypsum	0.00
CaO	0.56	Pyrite	0.00	CaO	0.48	Pyrite	0.00
Na <sub>2</sub> O	0.18	Apatite	0.39	Na <sub>2</sub> O	0.16	Apatite	0.44
K <sub>2</sub> O	6.11	Albite	1.01	K <sub>2</sub> O	6.01	Albite	0.85
TiO <sub>2</sub>	0.69	K-spar	9.42	TiO <sub>2</sub>	0.68	K-spar	12.74
P <sub>2</sub> O <sub>5</sub>	0.18	Rutile	0.69	P <sub>2</sub> O <sub>5</sub>	0.2	Rutile	0.68
MnO	0.1	Hematite	4.76	MnO	0.07	Hematite	4.05
Cr <sub>2</sub> O <sub>3</sub>	0.01	<b>SUM</b>	16.27	Cr <sub>2</sub> O <sub>3</sub>	0.01	<b>SUM</b>	18.76
LOI	6.9			LOI	5.6		
CO <sub>2</sub>	0.99	<b>Carbonates</b>		CO <sub>2</sub>	0.85	<b>Carbonates</b>	
C-Graphite	0	Calcite	0.26	C-Graphite	0	Calcite	0.22
C/ORG	0.05	Dolomite	1.84	C/ORG	0.04	Dolomite	1.58
C/TOT	0.06	Ferrodolomite	0.00	C/TOT	0.05	Ferrodolomite	0.00
S/TOT	0	<b>SUM</b>	2.10	S/TOT	0	<b>SUM</b>	1.79
S-/S	0			S-/S	0		
SO <sub>3</sub> (calc.)	0.000	<b>Clay Minerals</b>		SO <sub>3</sub> (calc.)	0.000	<b>Clay Minerals</b>	
CO <sub>2</sub> (calc.)	0.037	Illite	19.50	CO <sub>2</sub> (calc.)	0.037	Illite	19.57
		Sericite	26.50			Sericite	20.86
		Chlorite	7.03			Chlorite	5.25
		Mont. / Smec.	5.40			Mont. / Smec.	5.29
		Kaolinite	0.00			Kaolinite	0.00
		<b>SUM</b>	58.44			<b>SUM</b>	50.98

In order to validate the results of the mineral calculations, several procedures were employed. A simple and rapid validation method is the summation of minerals calculated in each sample. Values should equal 100 percent if the calculation error is zero. Results are summarized in figure 4.16. The Lower Röttton, Lehrberg Layer, and Feuerletten samples fall within ±5% of the anticipated total.

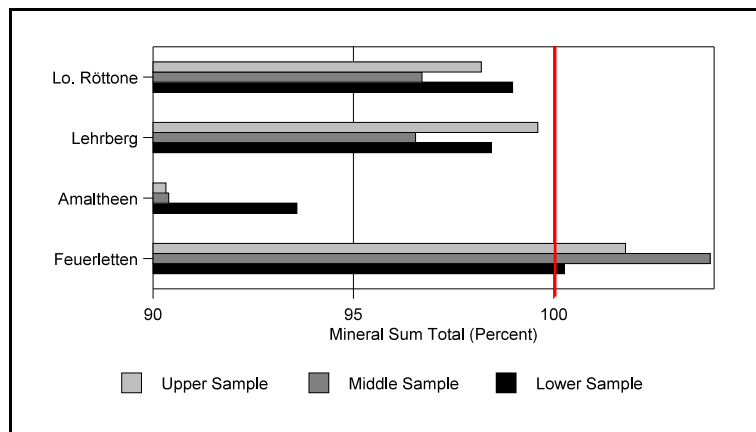


Figure 4.16 - Sum of calculated minerals in upper, central, and lower samples of each stratigraphic unit.

The Amaltheen clay, however, is an exception and falls almost 10 % short in at least two of the samples investigated. The reason for the error becomes obvious when the tally sheets in appendix C.1 are summoned. All of the K-samples in question show a remainder of Al<sub>2</sub>O<sub>3</sub> between 6.5% and 7.5% after calculation and allotment of the various oxides. The possibility therefore exists that (a) either some of the clay minerals may have a slightly different structural formula, containing more Al<sub>2</sub>O<sub>3</sub> than indicated, or (b) an additional

unidentified mineral consisting predominantly of aluminum oxide, such as diaspor, might be present. However, adjusting calculating parameters to satisfy Al<sub>2</sub>O<sub>3</sub> allotment gives erroneous results in other areas. Since the error is only marginal within a 10% margin and general mineralogical results are deemed plausible, no further attempt was made to correct this discrepancy in the calculation procedures.

To show significant matches between minerals identified and minerals calculated, a bivariate Pearson's Correlation analysis was performed using point count and XRD data. The results of the most significant correlations are summarized in appendix C.4. Most clay minerals demonstrate a substantial correlation in their calculation when compared to the XRD analysis, even though the x-ray determinative techniques were performed on particle sizes

smaller than  $2\mu\text{m}$ . Kaolinite shows 99.2% significant correlation followed by swelling clays (montmorillonites / smectites) with 90.5% and illite in the 83.2 percentile. The later, however, deserves special consideration because of its association with sericite, as discussed below. Oddly, the mineral chlorite exhibits no correlation between measured and calculated fractions. This is easily explained when considering that chlorite was estimated as a content range during XRD studies rather than concrete percentage amounts. Most samples investigated will fall well within this range during mineral calculations with only one exceptions, sample L6.0 (Lehrberg Layers) with exorbitant calculated chlorite values of 36.5 %. The problem in this instance lies with an excess of MgO in the sample since no dolomite was extrapolated during carbonate calculation procedures, leaving all of the magnesium oxide for chlorite computations.

The oddity in respect to the clay mineral calculations is evidently the sheet silicate sericite. FOLK (1980) describes this mineral as fine grained muscovite, somewhat coarser than illite. Both minerals show extreme similarities and are impossible to distinguish by optical methods. He further indicates the ineptness of x-ray diffractive techniques when identifying illite versus sericite, except the later has moderately sharper peaks. While sericite was omitted from the XRD analysis in favor of illite, it became evident from the geochemistry of the geologic barriers that some sericite and potassium feldspar must be present in selected samples. Otherwise high residual amounts of  $\text{Al}_2\text{O}_3$  and  $\text{K}_2\text{O}$  were encountered during the mineral calculations. Also, the coarser grained sericite may have been eliminated in the XRD studies during the preparation of the  $2\mu\text{m}$  fraction. Since both clay minerals have such a tight resemblance, it may be advantageous to view them as a group instead of separate mineral species when considering the calculated results..

In general, the calculated carbonates did not correlate with the carbonates distinguished in the  $2\mu\text{m}$  fraction. This phenomenon follows a logical trend indicating that most of the carbonates are probably not in the fine grained, but other fraction of the sedimentary lithologies. A better correspondence in the carbonate mineralogy can be found in the correlation of calculated results versus point count data. Here, computed calcite corresponds with point counted dolomite at a high significance and 100%. This could be the result of a mistaken identity during point count analysis, allotting dolomite instead of calcite, since no distinguishing staining techniques were employed. However, only one sample, again Lehrberg Layers 6.0 shows dolomite as well as calcite during the thin section count, while mineral calculations indicate solely calcite. Another explanation for the discrepancy would be a change in mineralogy on a small scale. While the sample prepared for the thin section may indeed exhibit dolomite as the main carbonate, the sample processed for geochemical analysis, even though only centimeters away, could indeed contain predominantly calcite.

Other interesting verifying correlations are found in the minor mineral assemblages. Potassium feldspar matches to 79% with illite identified in the XRD investigation. This coincides with the method used by KOHLER *et al.* (1994) to quantify illite from geochemical potassium contents. In addition, point count of positively identified K-feldspar matches to 81.4% with the minor minerals calculated.

All in all the mineral calculation appears to match in general with the established mineralogy identified through various other methods. A few exceptions are indicated, such as sample L6.0. Armed with this knowledge, the impact of complete mineralogy can now be discussed and concluded.

### 4.3 The Mineralogy of the Selected Geologic Barriers

In conclusion the mineralogical calculations are found to be reliable indicators of the true mineralogy encountered in the samples. Drawing on tables 4.8 and the correlations statistics described in appendix C.4, the following mineral compositional summary can be given.

As summarized in figure 4.17, the Feuerletten clay appears to exhibit a fairly consistent mineralogy with variations at depth due to changing stratigraphy. Little variance is seen in the minor mineralogy with a average concentration of about 5.5%. Gypsum, ranging from 0% to 0.32%, tends to be depleted with depth, while potassium feldspar is not found in the upper sample sections. Hematite as the predominant iron oxide appears to stay below 5% in all samples. The predominant carbonate is dolomite ranging in values from 9.73% to 15.26%. Calcite and ferrodolomite seem to be absent. Quartz increases with depth from 24.5% to 35.5%, coinciding nicely with the increased silt content at the bottom of the stratigraphic section. The majority of clay minerals are indeed within the fine grained division of the sample as indicated by the close approximation of the sum percent clay calculated and the fine grained mineral fraction established during grain size analysis.

For example, sum of clay minerals calculated in sample B3.0 equals 62.3 % while the grain size fraction listed under “% clay” in the lefthand column of table 4.8 reads 60.8%. Exception is sample B10.0 where calculated clays exhibit 48.5% while the fine grain size fraction shows only 26.8%, indicating that some of the clay minerals might be larger then 2µm. Sericite / illite group, often coarse grained, may be the most likely candidate. When adding both of these clay minerals together, the calculated results for the sericite / illite assemblage hover right around 25% in the “B” samples. Chlorite appears to dissipate with depth, ranging from 8.85% in the upper section to 3.3% in B10.0. The swelling clays, during calculations identified as montmorillonite / smectite have a very consistent concentration of around 19%. Kaolinite is absent in all of the samples. The Feuerletten samples appear to present a very uniform mineralogy with minor depth variations of selected minerals, except within the lowest part of the section. Sample B6.0 taken at the approximate stratigraphic center and chosen to represent the Feuerletten during the diffusion analysis appears to be adequate.

The mineralogical distribution within the Amaltheen clay unit is shown in figure 4.18. The minor mineralogy increases from 7.7% in the upper sections to 11.95% in the lower stratigraphies. The most common minor mineral appears to be hematite with concentrations around 5%. Gypsum and pyrite are absent except for the lowest sample (K9.0) where they occur as 1.8% and 2% respectively. Potassium feldspar is absent while albite ranges from 1% to 2.4%. Carbonates occur as prevailing dolomite decreasing from 13.25% to 11.7% with depth. Small amounts of ferrodolomite are also present, ranging from 0.1% to 0.5%. Quartz is very consistent with concentration around 31%. In all cases the sum of the calculated clay minerals is slightly higher than the corresponding 2µm grain size fraction, indicating some slightly coarser clay mineralogy overall. The illite / smectite combination is remarkably constant at around 26% in all samples. Chlorite is absent and the swelling clays range from 5.4% to 1.25% with the later found

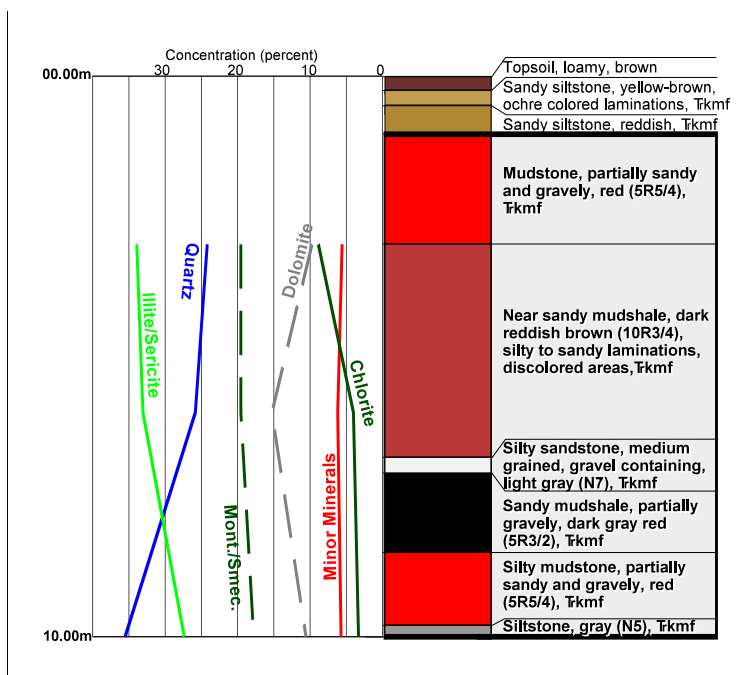
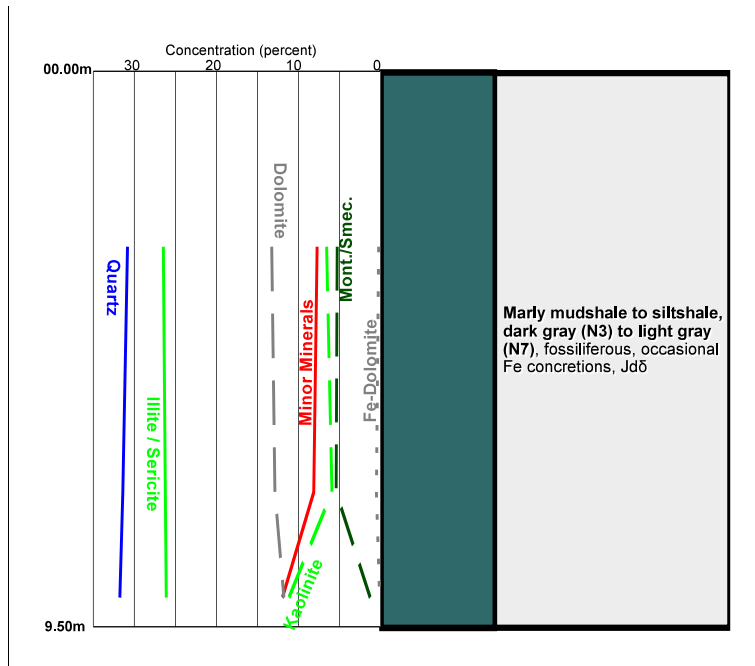


Figure 4.17 - Stratigraphic core section of the Feuerletten Clay with mineral concentration profiles from calculations.



**Figure 4.18** - Stratigraphic core section of the Amaltheen Clay with mineral concentration profiles from calculations.

in the stratigraphically lowest sample. Kaolinite is also present showing the greatest latitude of all minerals with 11.2% in sample K9.0 to 5.9% in sample K7.2. On average the Amaltheen mineralogy is very consistent, especially in the stratigraphic section above 7.2 meters. Largest changes are found in the lowest or K9.0 sample. Incidentally, K9.0 was chosen for the diffusion investigation.

As can be seen in figure 4.19, the Lehrberg Layers exhibit the greatest variation of all geologic barriers investigated. The minor mineralogy ranges from 5.4% to 10% with the lowest concentration in the mid stratigraphic sample L6.0. Gypsum is present in small amounts in all samples

from 0.2% to 0.38%. While pyrite is absent, hematite occurs from 0% in midsection to 5.8%. Potassium feldspar ranges between 4% to 6.3% while albite stays consistently around 0.1% above 7 meters, while the lowest sample exhibits 0.5% of the sodium feldspar. Quartz, a good indicator of uniformity jumps between 12.4% and 21.2%. Carbonates show a great latitude and variety with total concentrations decreasing with depth from 10.8% in sample L3.0 to 40.7% in sample L11.0. The latitude of dolomite is 0% in sample L6.0 to 40.7% in sample 11.0 where it is the only carbonate present. Calcite in contrast, is the only carbonate in sample L6.0 with a concentration of 19.6%. These results coincide with common descriptions in the literature, where the Lehrberg Layers are often described as marly or calcareous. The calculated concentrations of clay minerals also show a great fluctuation at the three indicated depths within the profile. While kaolinite is absent in all samples, both the illite /smectite group and chlorite have ranges from 39.7% to 10.2% and 36.5% to 5.43% respectively. Relative abundance of both clays appear to be inversed very similar to the carbonates described above. Chlorite also follows the approximated trend of calcite within the depth profile of the Lehrberg Layers. The swelling clays, commonly denoted as the montmorillonite/smectite group, exhibit

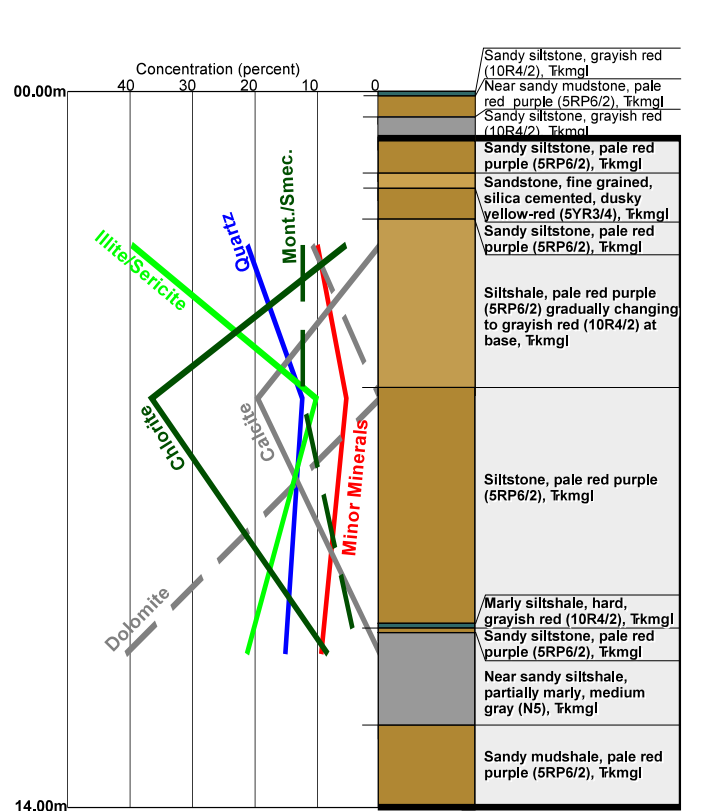


**Figure 4.19** - Stratigraphic core section of the Lehrberg Layers with mineral concentration profiles from calculations.

a more uniform distribution with 3.54% at depth and 12.4% above 6.5 meters. The extreme mineralogical and geochemical variations within the Lehrberg Layers warranted two samples to be investigated during the diffusion experiment. Section depth 6.0 meters and 11.0 meters were therefore selected.

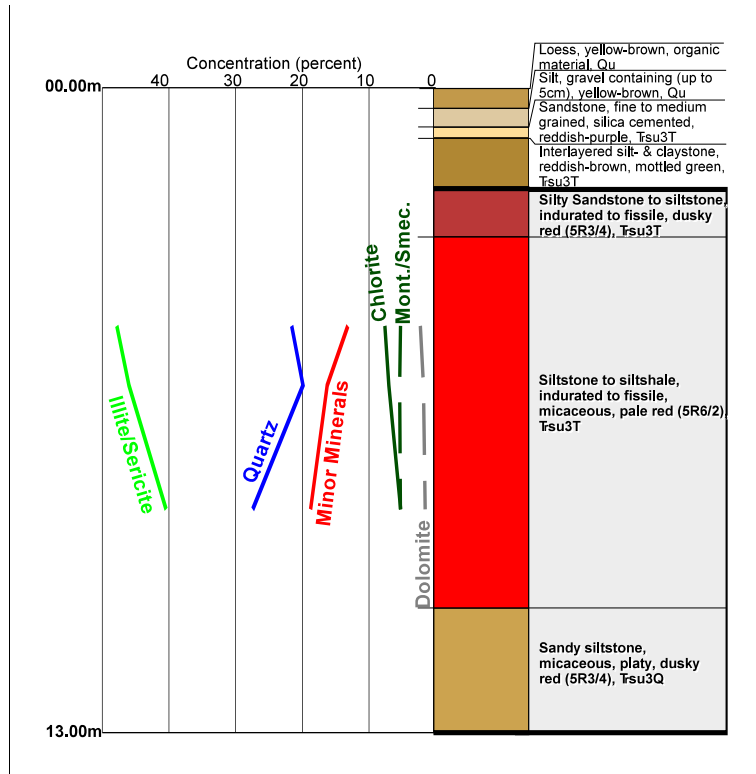


**Figure 4.20** - Stratigraphic core section of the Lower Röttone with mineral concentration profiles from calculations.

The depth distribution of the calculated mineralogy for the center part of the Lower Röttone is represented in figure 4.20. Minor mineral concentrations increase from 13.2% to 18.8% with depth. Potassium feldspar is the predominant mineral within this group with 6.3% in the upper section and 12.7% in the lower areas. Hematite is fairly constant between 4% to 4.8%. Gypsum and pyrite are absent while the sodium feldspar albite shows low concentrations around 1% and little variations. Dolomite ranges from 2.3% to 1.6% and appears to be the only carbonate present. From all of the geologic barriers, the illite/smectite group in the Lower Röttone lithologies has the highest concentrations with values reaching 47.8% in the upper section to 40.4% in the lower parts. This comes as no surprise since the sample is

generally described as “micaceous”, therefore exhibiting an influx of sericite or fine grained muscovite. The montmorillonite/smectite assemblage shows no variations with values around 5.3%, while chlorite is slightly depleted with depth, decreasing from 7.6% to 5.3%. Quartz shows some variations from 19.9% to 27.4%. For the most part, the Lower Röttone can be considered fairly uniform and only the center sample M6.0 was chosen for the diffusion evaluations.

## 5 Physical Properties

### 5.1 Grains size analysis

One of the most common physical parameters to be determined is the grain size distribution of the selected geologic barriers. In order to accomplish this goal, the grain size determination was performed after DIN 18 123 (1983) as a combined sieve and hydrometer analysis. The later uses a method described by BOUYOUCOS (1963) and CASAGRANDE, (1934), where the floatation depth of a hydrometer is measured as a function of time, providing an indication of the solution density. Soil particles with higher densities than the dispersing aqueous solution tend to settle with time and the fraction of particles remaining in suspension at a given measurement depth is estimated from the fluid density. By applying Stokes' law, which states that the terminal velocity of a particle is proportional to the square of particle radius, the particle-size distribution can also be estimated.

The analysis was performed by using a 10 to 14 g untreated sample and disintegrating it with mortar and pestle. The material was then mixed with distilled water, vibrated for 24 hours and was subjected to 45 minutes of ultrasonic dispersion treatment before wet sieving. The sieve fraction smaller than 63 $\mu$ m was further processed with 0.5 g of sodium pyrophosphate ( $\text{Na}_2\text{P}_2\text{O}_7 \times 10 \text{H}_2\text{O}$ ). However, the Amaltheen clay necessitated a much larger amount of the dispersing agent, on average 2 to 2.5 g, before any flocking of particles could be controlled.

Grain sizes were allotted according to an updated Wentworth grain size classification as presented by POPPE *et al.* (2003) and reproduced in appendix E.1. Results of the analysis are summarized in appendix E.2. In order to further classify the geologic barriers in their sedimentological realm further techniques were employed using the results of grain size analysis and distribution as a base.

#### 5.1.1 Lithological classification according to size fractions

Classifying the lithologies according to their approximate relations between size fractions is a common approach, usually by applying a ternary diagram with a plot of indicated sand, silt and clay percentages. However, the majority of the available ternary taxonomies are standardized for the investigation of soils, such as the very common U.S. Soil textural taxonomy presented by STAFF (1993). Since the material investigated are classified as rock and not soil, classification schemes used by sedimentologists are of much more appropriate application.

Most sedimentary rocks are classified according to systems presented by either SHEPARD (1954) or FOLK (1980). SHEPARD (1954) uses a single ternary diagram with sand, silt, and clay to indicate the relative proportions among these three grades within a sample. This scheme, however, is problematic when processing sediments with significant amounts of gravel. A second ternary diagram was added by SCHLEE (1973) to accommodate for the gravel fraction. FOLK's (1980) system is also based on two triangular diagrams with 21 major categories. However, he uses the term mud, defined as silt plus clay. FOLK (1980) uses a classification emphasizing the concentration as a function of the highest current velocity at the time of deposition in connection with the maximum grain size of the detritus available, while SHEPARD (1954) emphasizes sorting and reworking in the ratios of sand, silt, and clay (POPPE and POLLONI, 2000). The later scheme appears to be more appropriate for fine grained sediments as are the geologic barriers investigated. The results are therefore classified according to SHEPARD (1954) and summarized in figure 5.1.

Common to all samples is a very low sand concentration of only 1% to 18%. Exceptions are Feuerletten surface sample (B0.0) and a deep Lower Rötton sample (M11.0) which approximate 40% sand content. Two of the Lehrberg Layer materials investigated also show elevated sand composition in the 24% range. The siltiest sample belongs to the Amaltheen clay lithologies (K7.5) with 90% silt content. Most of the clay size particulates are found in Feuerletten sample B1.7, approaching almost 75%. The Feuerletten samples are spread over the largest area in the

ternary plot and are therefore the least uniform in their grain size distribution. Ranges include “sand-silt-clay” with high sand content, “silty clay” with large clay amounts, and “clayey silt” with in influx in silt. The least variation is found in the marine Amaltheen clay with a spread between the silt and clay fractions but of fairly constant and low sand compositions from 1% to 9%. Small differences are also observed within the silt fraction of the terrestrial Lower Röttone with contents between 28% to 42%. Here, greatest variations are found between sand and clay. Table 5.1 shows a compilation of descriptive terminologies as indicated by the ternary plot shown.

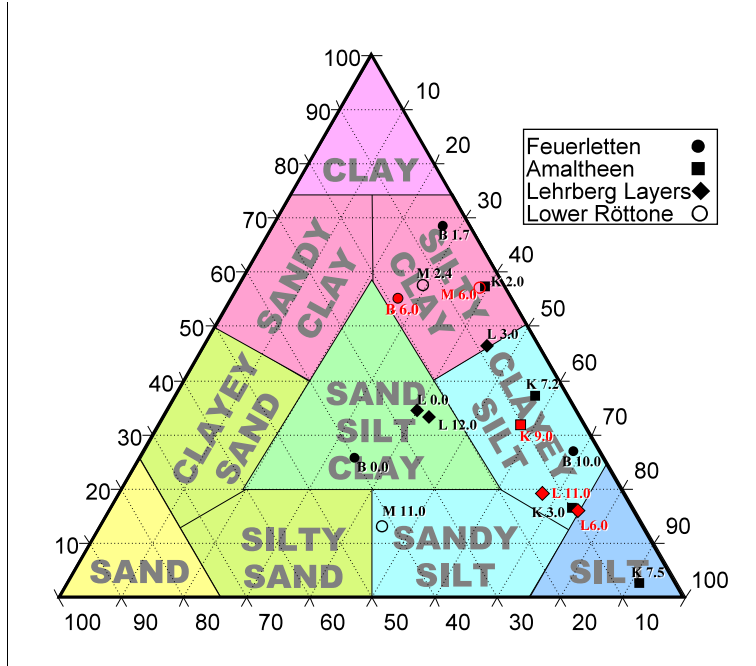


**Figure 5.1** - Ternary plot of sand, silt and clay fractions for geologic barrier samples showing SHEPARD’S (1954) compositional fields. Numbers indicate sampling depth while letters show sampling locations. Samples used in diffusion experiments indicated in red.

5.1.2 Moment Statistics

MCBRIDE (1971) indicates that most grain-size distributions approach a normal (or Gaussian) distribution when f size is plotted on an arithmetic scale, conventional moment statistics can be used to characterize individual samples. The following descriptive statistics are commonly used:

- (A) First Moment Statistic: Indicator of the average grain size or central tendency of the grain size distribution curve - the mean ( $x_\phi$ ).

**Eq. 5.1** 
$$x_\phi = \frac{\sum \%_{gr} \phi}{100}$$

where  $\%_{gr}$  = grain size percentage  
 $\phi$  = midpoint of phi grain-size grade

- (B) Second Moment Statistic: Measure of sorting or uniformity of grains, also indicated as spread around the mean - standard deviation ( $\sigma_\phi$ ).

**Eq. 5.2** 
$$\sigma_\phi = \sqrt{\frac{\sum \%_{gr} (\phi - x_\phi)^2}{100}}$$

- (C) Third Moment Statistic: Evaluation of symmetry or asymmetry of the grain size distribution and grain size excesses or “tails” (FOLK, 1980) - Skewness ( $Sk_\phi$ ).

**Eq. 5.3** 
$$Sk_\phi = \sqrt{\frac{\sum \%_{gr} (\phi - x_\phi)^3}{100 \sigma_\phi^3}}$$

- (D) Fourth Moment Statistic: Kurtosis ( $K_\phi$ ) - A measure with no visual analogy, but which is commonly inappropriately related to peakedness (BAKER, 1968).

Eq. 5.4

$$K_\phi = \sqrt{\frac{\sum \%_x (\phi - x_\phi)^4}{100\sigma_\phi^4}}$$

The results of the moment statistics analysis are summarized in appendix E.2. Using the verbal equivalent to the numerical values calculated a summary description is given in table 5.1 for each sample investigated.

### 5.1.3 Grain Size Analysis Results

**Table 5.1** - Verbal description FOLK (1980) of Moment statistics and Ternary analysis after SHEPARD (1954; fig. 5.1). B= Feuerletten; K= Amaltheen clay; L= Lehrberg Layers; M= Lower Röttone

Sample	Ternary Diagram (Figure 5.1)	Sorting (Moment Statistic)	Skewness (Moment Statistic)	Kurtosis (Moment Statistic)
B0.0	Sand-silt-clay,	very poorly sorted,	strongly coarse skewed,	very leptokurtic.
B1.7	Silty clay,	poorly sorted,	very strongly coarse skewed,	extremely leptokurtic.
B6.0	Silty clay,	very poorly sorted,	very strongly coarse skewed,	extremely leptokurtic.
B10.0	Clayey silt,	poorly sorted,	very strongly coarse skewed,	extremely leptokurtic.
K2.0	Silty clay,	poorly sorted,	very strongly coarse skewed,	extremely leptokurtic.
K3.0	Clayey silt,	very poorly sorted,	very strongly coarse skewed,	extremely leptokurtic.
K7.2	Clayey silt,	very poorly sorted,	very strongly coarse skewed,	extremely leptokurtic.
K7.5	Silt,	poorly sorted,	very strongly coarse skewed,	extremely leptokurtic.
K9.0	Clayey silt,	very poorly sorted,	very strongly coarse skewed,	extremely leptokurtic.
L0.0	Sand-silt-clay,	very poorly sorted,	very strongly coarse skewed,	very leptokurtic.
L3.0	Silty clay,	very poorly sorted,	very strongly coarse skewed,	extremely leptokurtic.
L6.0	Clayey silt to silt,	very poorly sorted,	very strongly coarse skewed,	extremely leptokurtic.
L11.0	Clayey silt,	very poorly sorted,	very strongly coarse skewed,	extremely leptokurtic.
L12.0	Sand-silt-clay,	very poorly sorted,	very strongly coarse skewed,	very leptokurtic.
M2.4	Silty clay,	very poorly sorted,	very strongly coarse skewed,	extremely leptokurtic.
M6.0	Silty clay,	poorly sorted,	very strongly coarse skewed,	extremely leptokurtic.
M11.0	Sandy silt,	very poorly sorted,	strongly coarse skewed,	very leptokurtic.

As expected from mineralogical thin section studies, moment statistics confirm that sorting of the materials is predominantly very poor to poor. All samples show a statistical “tail” or skewness in the coarse grained material. Matter of fact,  $Sk_\phi$  exceeds the 1.00 limit given by FOLK (1980). The bulk of the grains falls therefore into the fine grained section. This narrow variation of the bulk of the grains also identifies all samples investigated as very to extremely leptokurtic. Most fluctuation can be found in the word description for samples subjected to the ternary sand-silt-clay plot as shown in figure 5.1 and described in section 5.1.1.



In order to visually summarize the findings of the grain size analysis, the proven method of depth profile plots as employed in previous chapters was utilized. Results can be viewed in figure 5.2, 5.3, 5.4, and 5.5. The Feuerletten clay is depicted in figure 5.2. The silt concentration appears to be fairly uniform with depth except for the lowest point where a layer of grayish siltstone increases the silt content dramatically. Sand size particles are more common at the top of the section and vary slightly within 20% for the remainder of the section. Clay sizes are the least uniform. They show a dramatic high of nearly 70% at about 3 m depth and diminish to below 30% at the bottom of the stratigraphic unit. For the most part, clay is the paramount particle size. The Feuerletten lithologies show the greatest variations in particle sizes of all units investigated.

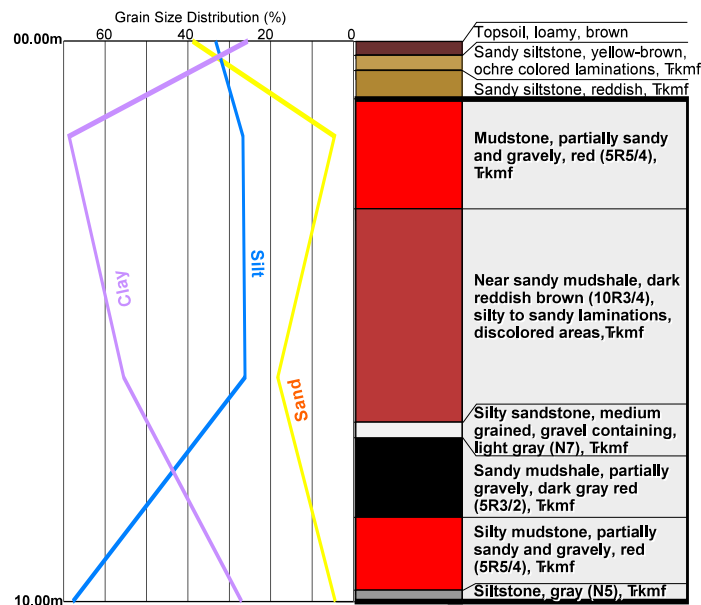


**Figure 5.2** - Depth profile of sand, silt, and clay grain sizes within the Feuerletten stratigraphy. Sand, silt and clay recalculated to 100%. Plot visualizes more or less average compositions since not every depth section was analyzed.

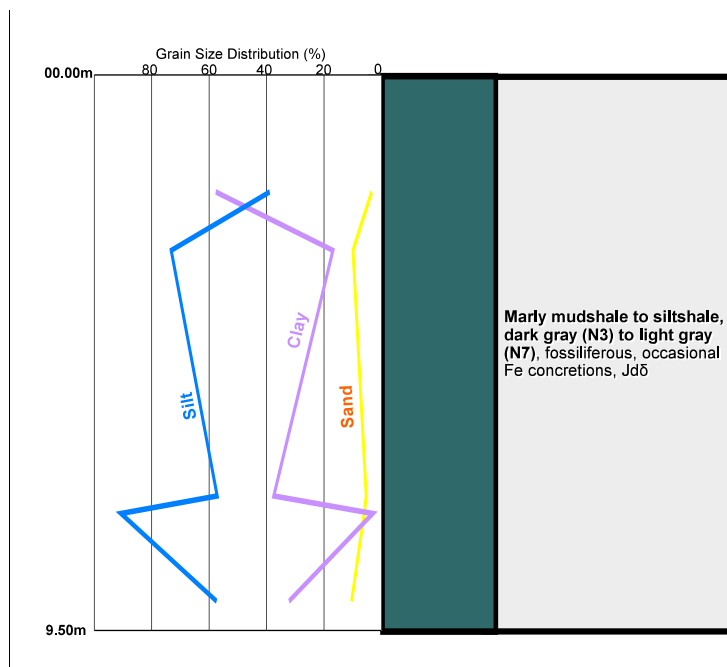


**Figure 5.3** - Depth profile of sand, silt, and clay grain sizes within the Amaltheen clay. Sand, silt and clay recalculated to 100%. Plot visualizes more or less average compositions since not every depth section was analyzed.

The Amaltheen clay stratigraphy and corresponding grain size profiles are portrayed in figure 5.3. The sand concentration is low and very uniform, while silt and clay particles exhibit an inversely proportional relationship. This is surprising since the stratigraphy appears to be fairly uniform in macro-optical investigations. Silt sized particles appear to outnumber clay except for the upper 2 m of the stratigraphic unit. However, as can be seen in appendix E.2, the silt fraction is mainly fine to very fine, therefore approximating a coarse clay size.

The Lehrberg Layers exhibit some grain size variation at the top and bottom of the stratigraphic profile, while the center section remains relatively uniform, as indicated in figure 5.4. Sand sizes stay below 10% but increase to over 20% in the upper and lower section. With approximately 70%, silt is the predominant size and varies little in the lower 2/3 of the stratigraphy. In the upper 1/3 of the Lehrberg Layer drill core, congruent with lithological changes, silt and clay concentrations are about equal in a range from 40% to 45%.

The Lehrberg Layers exhibit some grain size variation at the top and bottom of the stratigraphic profile, while the center section remains relatively uniform, as indicated in figure 5.4. Sand sizes stay below 10% but increase to over 20% in the upper and lower section. With approximately 70%, silt is the predominant size and varies little in the lower 2/3 of the stratigraphy. In the upper 1/3 of the Lehrberg Layer drill core, congruent with lithological changes, silt and clay concentrations are about equal in a range from 40% to 45%.

The grain size distribution along the stratigraphic profile of the Lower Rötone is shown in figure 5.5. Clay with just below 60% commences to be the dominating grain size for the upper central section investigated. The change in lithology at the base of the unit to a sandy siltstone is evident in the particulates. Here sand and silt are above 40% while clay drops strikingly to almost 10%. Silt, in general, is reasonably uniform with a steady increase from about 30% in the upper section to around 45% at the bottom.

5.2 Water Absorption

Water absorption is the ability of dry soil to draw in and retain capillary water. While a common standardized engineering test in countries applying the metric system, analyzing water absorption in the laboratory is somewhat uncommon in the U.S. An accepted procedure in Europe for the determination of said parameter is DIN 18.132 (1993): “Soil-testing Procedures and Testing Equipment for the Determination of Water Absorption”. Here a dried sample is connected with a calibrated glass-tube filled with distilled water. The amount of water absorbed by the soil over a 24 hour period is determined by the volume change observed in the tube and is then related to the weight of the initial sample. Water absorption ( $w_b$ ) is expressed as percent.

Water absorption data can be related to clay mineralogy. GUDEHUS (1981) reports that a silty kaolinite clay, for example has a  $w_b$  of 30%, pure kaolinite demonstrates 80%  $w_b$ , while pure montmorillonitic swelling clays will

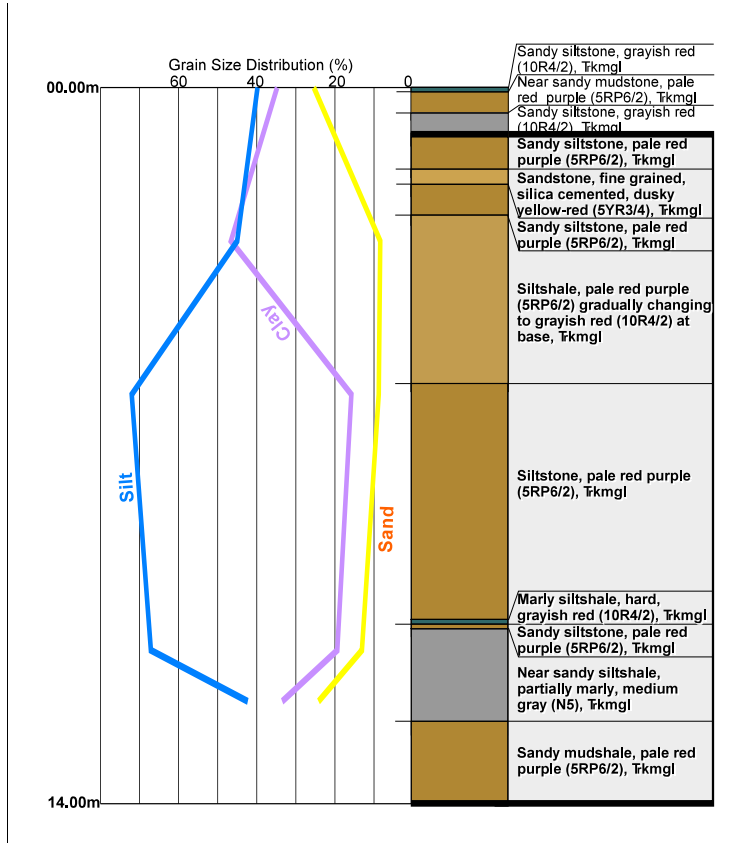


Figure 5.4 - Lehrberg Layer depth profile of sand, silt, and clay grain sizes. Indicated grain sizes recalculated to 100%. Plot visualizes more or less average compositions since not every depth section was analyzed.

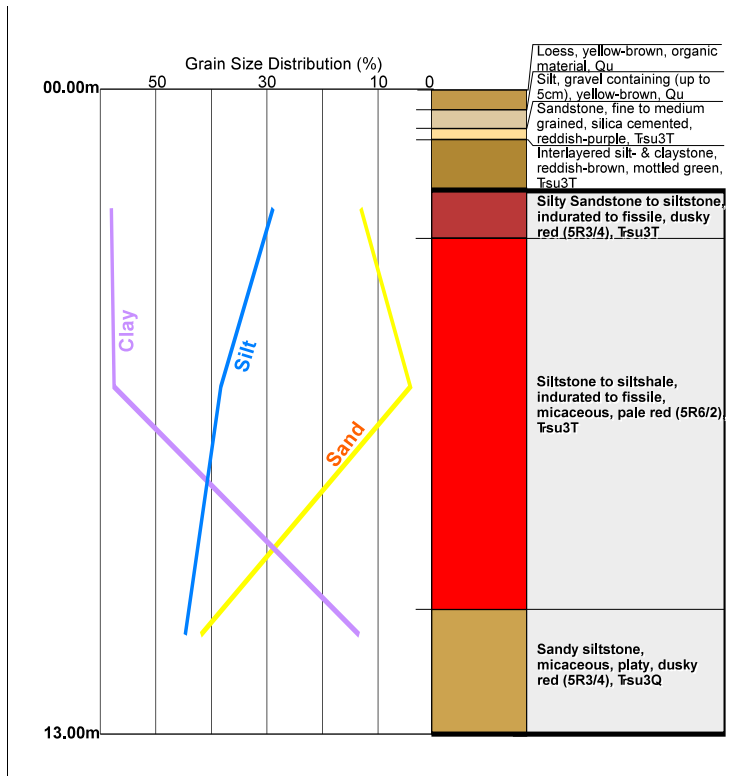
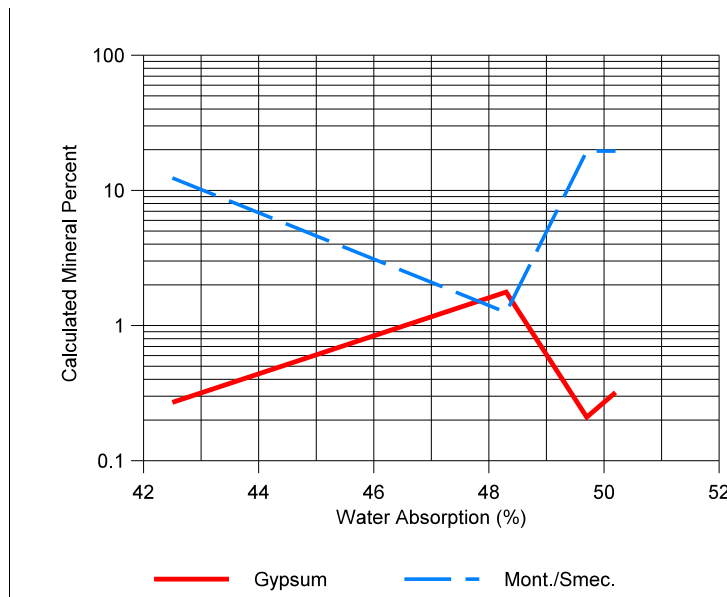


Figure 5.5 - Depth profile of sand, silt, and clay grain sizes in the Lower Rötton section. Sand, silt and clay recalculated to 100%. Plot visualizes more or less average compositions since not every depth section was analyzed.

exhibit incredible water absorption capacities in the range from 300 % (Ca-Montmorillonite) to 700% (Na-Montmorillonite).



**Figure 5.6** - Comparison of calculated gypsum and swelling clay (montmorillonite/smectite) concentrations with water absorption capacities. Samples without available gypsum data were eliminated.

The results of the water absorption analysis of geologic barrier samples is summarized in appendix E.3. When compared with the calculated mineralogy of swelling clays or montmorillonite-smectite group, a puzzling observation is made. The water absorption data correlates very poorly with the calculated swelling clay content and can not be used as a direct indicator of the designated clay. The reason for this behavior is given by AZAM *et al.* (2000), arguing that the swelling potential of clay-calcium sulfate mixtures decreases as the percentage of gypsum in studied samples increases. In order to determine if calcium sulfate might indeed influence the swelling potential and therefore the water

absorption characteristic of the clay in question, both calculated montmorillonite-smectite and gypsum concentrations were compared to water absorption characteristics as indicated in figure 5.6. It can be plainly seen that calcium sulfate mineral concentration is inversely proportional to the swelling clay content in relation to  $w_b$ . If the water absorption data is corrected with the gypsum content of the soil sample according to equation 5.5, a 83% match between montmorillonite-smectite and  $w_b$  can be obtained.

**Eq. 5.5** 
$$\%_{mont./smec.} = 19.8254 - (0.2153 * w_b * \%_{gypsum})$$

Where  $\%_{mont./smec.}$  = percent of montmorillonite-smectite mineral group  
 $w_b$  = water absorption capacity in percent  
 $\%_{gypsum}$  = percent of gypsum mineral in sample

If the averages of the data is compared, Feuerletten clays show the highest water absorption with 51.5%. This correlates nicely with the highest calculated swelling clay content (17.96%) of all geologic barriers investigated. Kaolinite is absent and gypsum concentration is calculated at 0.18%. When using equation 5.5 with these averages, a swelling clay content of 17.83% is computed, demonstrating the influence of gypsum and montmorillonite-smectite concentrations on water absorption in said samples.

The lowest water absorption values of 42.9% are found in the Lower Rötton samples. Here, gypsum and kaolinite are absent, but the montmorillonite-smectite group comprises only 5.32%. However, comparison with results from equation 5.5 shows a poor correlation, indicating other factors of water absorption, such as the mineral illite which is present at about 19% in the Lower Rötton lithologies.

The Lehrberg Layers have an average  $w_b$  of 50.2%, 9.42% swelling clays, 0.29% gypsum and no kaolinite. The water absorption indicated is somewhat skewed because of an anomalously high water absorptive value showing 68% in sample L12.0. When eliminated,  $w_b$  drops to 44.2%. Again, correlation with computed results according to equation 5.5 are poor, pointing to other factors of water absorptive qualities. The clay mineral illite may play an important role, but it varies greatly through the lithologies of the Lehrberg Layers from 1.9% to 10.24%.

The Amaltheen clay water absorptive capacity is 48% on average, with 7.87% kaolinite, 0.59% gypsum and only 3.97% of the swelling clay group. The  $w_b$  properties are in this scenario most likely not connected to the amount of montmorillonite-smectite in the sample. Illite is also significantly low. However, Amaltheen samples appear to be high in calculated sericite (~ 23%) which might be the likely candidate for the water absorptive properties in these marine clays.

While the study of water absorption is often used as a coarse indicator for the presence of swelling clays, the method has to be used with caution. As can be plainly seen, gypsum appears to be a significant inhibitor in the water absorptive properties of a material. Other factors yet unknown will definitively play a further role.

### 5.3 Hydraulic Data

The hydraulic data for the geologic barrier samples of interest was in greater part established by PÖTZL (1998). His work was a precursor to this study, using the same sample materials. General values for hydraulic conductivity, gradients, discharge velocities, seepage velocities and effective porosity were in part taken from PÖTZL (1998), with some verification for samples used in the diffusion research. The hydraulic data is summarized in appendix E.4.

#### 5.3.1 Hydraulic Conductivity ( $k_f$ )

FETTER (1980) defines hydraulic conductivity ( $k_f$ ) as a coefficient of proportionality describing the rate at which water can move through a permeable medium. The density and kinematic viscosity of the water must be considered when establishing the  $k_f$  value. Obvious factors that influence said parameter are porosity and permeability of the transmitting material. Hydraulic conductivity is established according to Darcy's Law (HÖLTING, 1992) which is summarized in equation 5.6.

$$\text{Eq. 5.6} \quad Q = k_f * A * \frac{h}{l}$$

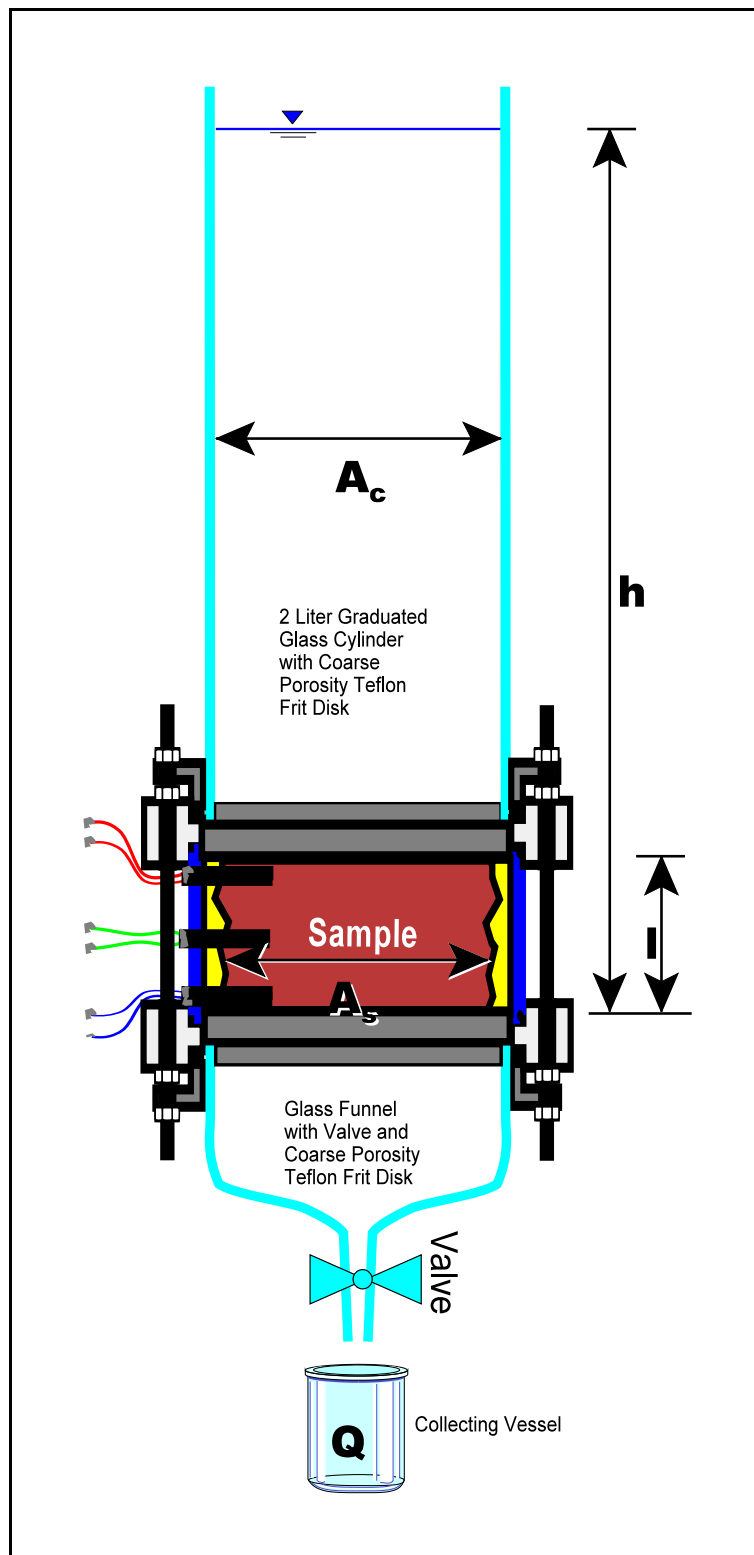
Where	Q	= discharge in volume per time ( $L^3/t$ )
	$k_f$	= hydraulic conductivity in distance per time ( $L/t$ )
	A	= cross sectional area of the flow medium ( $L^2$ )
	$h/l$	= hydraulic gradient ( $L/L$ )
	h	= change in hydraulic head, e.g. head <sub>1</sub> - head <sub>2</sub> (L)
	l	= distance between the two hydraulic heads in h (L)

This equation can be rearranged to show  $k_f$  or the hydraulic conductivity with the dimensions of length per time or velocity (equation 5.7).

$$\text{Eq. 5.7} \quad k_f = \frac{Q}{A * \frac{h}{l}}$$

Laboratory testing for hydraulic conductivity was performed according to DIN 18 130 TEIL 1 (1989). For samples used during the diffusion experiments, the procedure was modified as illustrated below.

A sample core was saturated for several weeks in distilled water and afterwards fixed into the diffusion cell holder with epoxy resin. A 2 liter glass container was mounted at the top of the sample, while a collecting chamber was attached to the bottom as seen figure 5.7.



attached to the bottom as seen figure 5.7.

The top cylinder was then filled with distilled water, covered with a watch glass and the height of the liquid from the bottom of the sample was cautiously measured and recorded. The whole system was placed into a climate chamber at 10°C and the collecting vessel at the underside was sampled as needed, approximately daily. The volume of the water discharged below was carefully established from the weight of the discharge collected in the vessel marked  $Q$  in figure 5.7. The exact volume of water in  $Q$  was calculated from the weight and the correction factor for water volume at temperatures of 10°C. Since only small amounts of water moved through the system at a given time, the change in water level above the sample indicated by " $h$ " was negligible and could not be accurately determined. The system could therefore be treated as a "permanent head" hydraulic conductivity experiment. It was also possible to process the experimental set-up as a "falling head" test, if changes in " $h$ " were deducted from the volume of the discharge collected below. The equations from calculating hydraulic conductivity from the above mentioned experimental lay out are given in appendix E.5. The results correspond well with the values given by PÖTZL (1998) when direct comparisons were possible.

**Figure 5.7** - Diffusion cell set-up for sample saturation and hydraulic conductivity testing.  $Q$  = discharge,  $A_s$  = cross-sectional area of sample,  $A_c$  = cross sectional area of column,  $l$  = length or thickness of sample,  $h$  = height of water column.

### 5.3.2 Discharge Velocity ( $v_f$ )

Even though hydraulic conductivity has the unit of velocity, it does not express the true speed of water movement through a given material. Rather it describes water movement as the movement of a volume of water through a cross-sectional area over a period of time, such as cubic meters per square meter per second ( $\text{m}^3/\text{m}^2/\text{s}$ ). The later can be reduced to length over time (m/s), given the false impression of velocity.

In order to describe a true velocity of water moving through a sample or an aquifer, the rate of discharge of water per unit area measured at right angles to the direction of flow is applied. The result is known as discharge velocity ( $v_f$ ), specific discharge, or Darcy velocity and can be portrayed as the flux per unit area. It is calculated from the hydraulic conductivity and the gradient according to Darcy's Law as described in equation 5.8 below.

$$\text{Eq. 5.8} \quad v_f = \frac{Q}{A} = k_f * \frac{h}{l}$$

Where	$v_f$	= discharge velocity in distance per time (L/t)
	$Q$	= discharge in volume per time ( $\text{L}^3/\text{t}$ )
	$k_f$	= hydraulic conductivity in distance per time (L/t)
	$A$	= cross sectional area of the flow medium ( $\text{L}^2$ )
	$h/l$	= hydraulic gradient (L/L)
	$h$	= change in hydraulic head, e.g. head <sub>1</sub> - head <sub>2</sub> (L)
	$l$	= distance between the two hydraulic heads in h (L)

FETTER (1980) identifies  $v_f$  as an apparent velocity, representing the velocity at which water would move through an aquifer if the aquifer were an open conduit. It is the average velocity for the entire cross-sectional area and can be easily established from data collected during hydraulic conductivity experiments. The results of discharge velocity calculations are recapped in appendix E.4.

### 5.3.3 Seepage Velocity ( $v_s$ )

The Darcy velocity, however, does not represent the true velocity, since water actually passes only through void or pore spaces, often through a variety of twisted passages. Thus borrowing the definition for  $v_f$  and injecting the void spaces where water movement takes place would yield the following: Seepage of water through an unsaturated porous medium, per unit area of void space, perpendicular to the direction of flow. This velocity, called pore or seepage velocity ( $v_s$ ) is the average linear speed at which water actually moves within the pores and approximates the average actual velocity of an unsaturated flow. This true or seepage velocity is greater than the Darcy velocity and is therefore equal to  $v_f$  divided by the effective porosity as seen in equation 5.9.

$$\text{Eq. 5.9} \quad v_s = \frac{Q}{n_e * A} = \frac{k_f * h}{n_e * l} = \frac{v_f}{n_e}$$

Where

- $v_s$  = seepage velocity in distance per time (L/t)
- $v_f$  = discharge velocity in distance per time (L/t)
- $n_e$  = effective porosity, dimensionless
- $Q, A, k_f, h, l,$  = see equation 5.8

In order to calculate  $v_s$  one needs to know the effective porosity. This, however, is often not possible or has a large error margin because of the very fine grained nature of involved samples, which often transmit water through fractures instead of pores. The seepage velocity is therefore established by tracer experiments. A chemical marker is injected into a percolating solution used for hydraulic conductivity testing. Tracer concentrations are measured in regular intervals at the collecting vessels. Results can be analyzed graphically as described by HÖLTING (1992), generating several seepage velocities. The first appearance of the chemical marker is equated with  $v_s \text{ max}$ , or the maximal seepage velocity. Accordingly, the minimal velocity ( $v_s \text{ min}$ ) would correspond with the last sighting of the tracer. SCHWEIZER *et al.* (1985) mentions additional seepage velocities, such as median velocity ( $v_s \text{ med}$ ) at 50% chemical marker recovery, dominating or main velocity ( $v_s \text{ main}$ ) at the maximal concentration peak, or average velocity ( $v_s \text{ avg}$ ) defined as the arithmetic mean of all singular seepage velocities identified. KÄSS (1967) warns that the recovery curve of the chemical tracer does not follow a Gaussian distribution. Thus averages cannot be established by looking at the peak of the tracer curve but rather fall within 2/3 to 1/2 of the descending section of the graph.

PÖTZL (1998) established average seepage velocities for many geologic barrier samples through lithium bromide tracer experiments. To keep samples free from contamination, similar tests were not conducted for samples involved in this study. However, a quadratic regression curve correlation was identified between  $v_s$  established by PÖTZL (1998) and computed  $v_f$  values as indicated in equation 5.10.

$$\text{Eq. 5.10} \quad v_s = 1.6 * 10^{-7} - (1.9614 * v_f) + (4.6 * 10^7 * v_f^2)$$

Where

- $v_s$  = seepage velocity in distance per time (L/t)
- $v_f$  = discharge velocity in distance per time (L/t)

Seepage values were therefore calculated using above equation. Table 5.2 shows the computed versus measured  $v_s$  data.

**Table 5.2** - Calculated  $v_s$  using equation 5.10 and measured  $v_s$  from PÖTZL (1998). Samples used in diffusion experiments marked in red.

	calculated		PÖTZL (1998)			calculated		PÖTZL (1998)	
Feuerletten	$v_s$ (m/s)	$v_s$ (m/s)	$v_s$ (m/s)	$v_s$ (m/s)	Lehrberg	$v_s$ (m/s)	$v_s$ (m/s)	$v_s$ (m/s)	$v_s$ (m/s)
B1.7	1.43E-07	1.60E-07			L3.0	1.43E-07	1.60E-07		
B2.3	1.94E-07	2.70E-07			L5.2	1.41E-07			
<b>B2.7</b>	<b>1.80E-07</b>	<b>1.80E-07</b>			<b>L6.0</b>	<b>3.09E-07</b>			
B3.0	1.39E-07				L7.5	7.23E-07			
<b>B6.0</b>	<b>1.24E-07</b>				L7.6	1.41E-07			
B7.0	1.40E-07	1.30E-07			L10.9	1.94E-07	2.70E-07		
<b>B8.5</b>	<b>1.80E-07</b>	<b>2.00E-07</b>			<b>L11.0</b>	<b>1.92E-07</b>			
Average:	1.59E-07	1.88E-07			Average:	2.35E-07	2.15E-07		



Amaltheen	$v_s$ (m/s)	$v_s$ (m/s)	Lower Röt.	$v_s$ (m/s)	$v_s$ (m/s)
K1.0	3.44E-07	2.50E-07	M3.3	1.50E-07	
K2.5	1.39E-07	1.50E-07	M4.7	1.41E-07	8.60E-08
K2.8	4.39E-07	5.00E-07	M4.8	1.50E-07	1.90E-07
K3.0	3.22E-06		M5.8	1.48E-07	5.70E-08
K3.6	1.39E-07		M5.9	1.50E-07	
K4.0	2.19E-07	3.00E-07	M6.0	1.41E-07	
K7.2	1.39E-07	9.40E-08	M6.1	1.40E-07	8.80E-08
K9.0	6.75E-08		M6.2	1.20E-07	1.30E-07
Average:	5.99E-07	2.59E-07	Average:	1.42E-07	1.10E-07

### 5.3.4 Effective Porosity

The effective porosity or  $n_e$  is defined as the ratio of water permeable pore volume to the total volume of a representative sample. In natural lithologies or soils, where water movement is produced by a combination of capillary, molecular, and gravitational forces,  $n_e$  can be approximated by the specific yield or drainage porosity. This parameter is defined as the ratio of the quantity of water drained by gravity from a saturated material to the total volume of the sample. It should be noted that the definition of effective porosity describes a measurement of pore fluid displacement rather than the volume of water that occupies pore spaces. Hence, effective porosity must be smaller than the total pore space or total porosity.

MAROTZ (1968) attempted to calculate effective pore porosity from hydraulic conductivity data. However, effective clay pore porosity appears to be negligible since most of the effective pore space is concentrated along fractures or fissures. A correlation between  $k_f$  and  $n_e$  as indicated by MAROTZ (1968) was not observed.

Eq. 5.11

$$n_e = \frac{v_f}{v_s}$$

Where

$n_e$	= effective porosity, dimensionless
$v_s$	= seepage velocity in distance per time (L/t)
$v_f$	= discharge velocity in distance per time (L/t)

Once discharge and seepage velocities are known, effective porosity can be easily calculated. When equation 5.9 is solved for  $n_e$ , the effective porosity can be described as the ratio of discharge to seepage velocity as indicated in equation 5.11. Results are summarized in appendix E.4.

### 5.4 Discussion of Hydraulic Data

The hydraulic parameters of hydraulic conductivity, discharge and seepage velocity can be easily visualized when plotted on a logarithmic scale according to sample depth next to the lithologic profile of the indicated geologic barrier (see figure 5.8, 5.9, 5.10, and 5.11). Beginning with the Feuerletten clay, the hydraulic data is fairly uniform through the whole unit for the actual or seepage velocities. Both  $k_f$  and  $v_f$  concur with the uniformity for the midsection but are elevated in the lower and upper part of the unit, as can be seen in figure 5.8. The influx of coarser materials at the top and the bottom might be responsible for the change in hydraulic components, slightly increasing the velocities of migrating water. The sample for the diffusion study is very representative for the indicated unit.

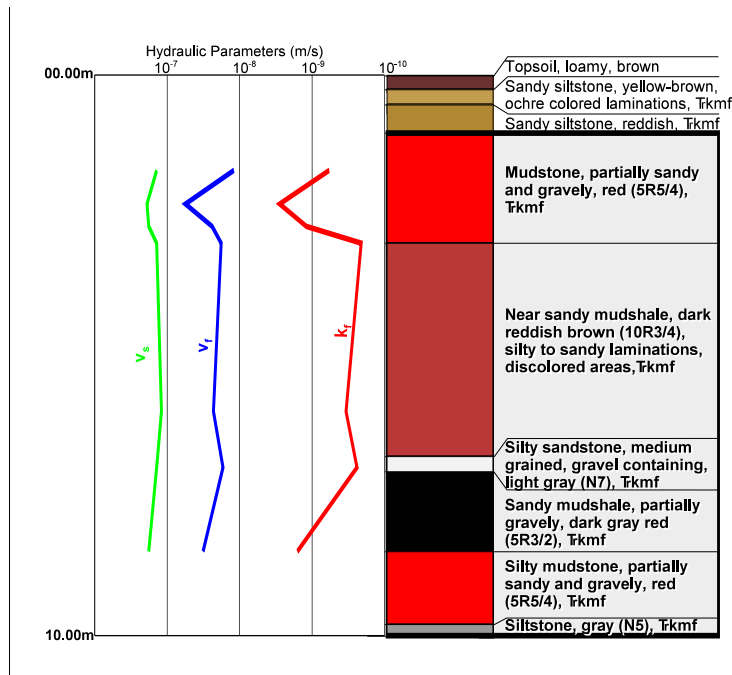


Figure 5.8 - Depth profile of hydraulic data ( $k_f$ ,  $v_s$ ,  $v_f$ ) for Feuerletten lithologies. Logarithmic scale for hydraulic velocities.

The Amaltheen clay has macroscopically a very uniform appearance as discussed previously. However, all hydraulic data decreases more or less uniformly with depth as indicated by figure 5.9. Interesting are abrupt and fluctuating changes in all three velocities, including seepage velocity within the upper lithologies at coring depths from 2.8 to 3.6 meters. The seepage velocity increases from an average value of about  $1.4 \cdot 10^{-7}$  m/s to  $3.2 \cdot 10^{-6}$  m/s at 3 meters profile depth with similar enlargements indicated for  $v_f$  and  $k_f$ . The later, however, show a sharp drop by factor 10 just  $\frac{1}{2}$  meter below this high velocity area. Incidentally, sample K9.0 selected for the diffusion study is taken from the bottom of said unit.

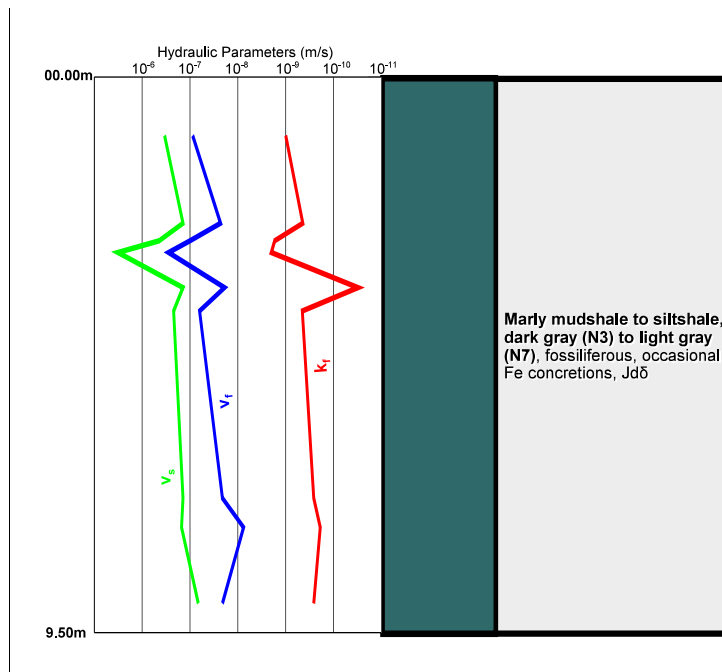


Figure 5.9 - Depth profile showing hydraulic data ( $k_f$ ,  $v_s$ ,  $v_f$ ) for Amaltheen clay. Logarithmic scale for hydraulic parameters.

The decrease of hydraulic velocities with depth is very similar to the observation made by GAUTSCHI (2001) in related Opalinus clays. He further indicates that decompression and weathering near the surface will lead to an increase in hydraulic conductivity in these areas, while higher pressure at depth would instigated a self-healing of fractures, decreasing permeabilities. On the other hand, weathering processes on the surface would lead to accumulation of expansive clays, sealing underlying fractured zones in the unit. These descriptions would definitely fit well with the observations made in the depicted core section of the Amaltheen clay barrier. The zone of fluctuation, however, as described above, may also be due to a change in mineralogy and grain size, indicated by a higher

calculated montmorillonite-smectite and lower kaolinite concentrations than those found at depth of 9 meters.

The Lehrberg Layers have the greatest diversity in their lithological make-up. As expected, the hydraulic data follows the same trend as seen in figure 5.10. At a depth of about 6 meters, both discharge velocity and hydraulic conductivity show an increase, coinciding with a lithological change from siltshale to a siltstone respectively. About 1.5 meters deeper,  $v_s$ ,  $v_f$  and  $k_f$  sharply drop to their lowest values in the upper half of the siltstone section. The overall trend of the later two is a continual increase with depth by a factor of 10, while seepage velocity stays fairly constant at roughly  $1.5 \cdot 10^{-7}$  m/s. At the last depth evaluated, about 11 meters, the lithology changes to a near sandy siltshale with

little change in all 3 hydraulic parameters. While most of the hydrology observed blatantly follows the lithology, the influx in values near the center of the siltstone sequence suggests a fractured area. Diffusion study samples were taken to represent the lithological diversion. Thus, sample L6.0 is from the fluctuation zone, while L11.0 describes the lithologic transition zone into a gray, marly siltshale.

The Lower Rötton was investigated at the area of interest, from about 3 to 6 meters coring depth. Here, the lithology presents itself as somewhat uniform, yet the hydraulic data shows a few surprises as can be seen in figure 5.11. Hydraulic conductivity rises sharply from 3.3 to 4.7 meters only to level out at about  $2.1 \cdot 10^{-10}$  m/s with greater depth. The discharge velocity appears to increase steadily over the 3 meters observed, while the true or seepage velocity exhibits a great uniformity over the sampled area. From 5.9 to 6.2 meters a small band of fluctuation is observed in  $v_f$  and  $k_f$  with the discharge velocity showing the greatest diversion. This variation however is hardly noticeable within  $v_s$ .

The reason for fluctuation lies probably in the nature of the lithology, described as indurated to fissile. In the solidified areas, hydraulic conductivity is expected to be low, while fissile rock types should display an increase in hydraulic parameters, allowing fluid flows along microfractures or the platy fabric of the sample material. From the  $v_f$  data it could be deduced that fissibility increases to a depth of about 6 meters where layers may vacillate into induration. Accordingly, the sample for the diffusion study was taken from this area of variation.

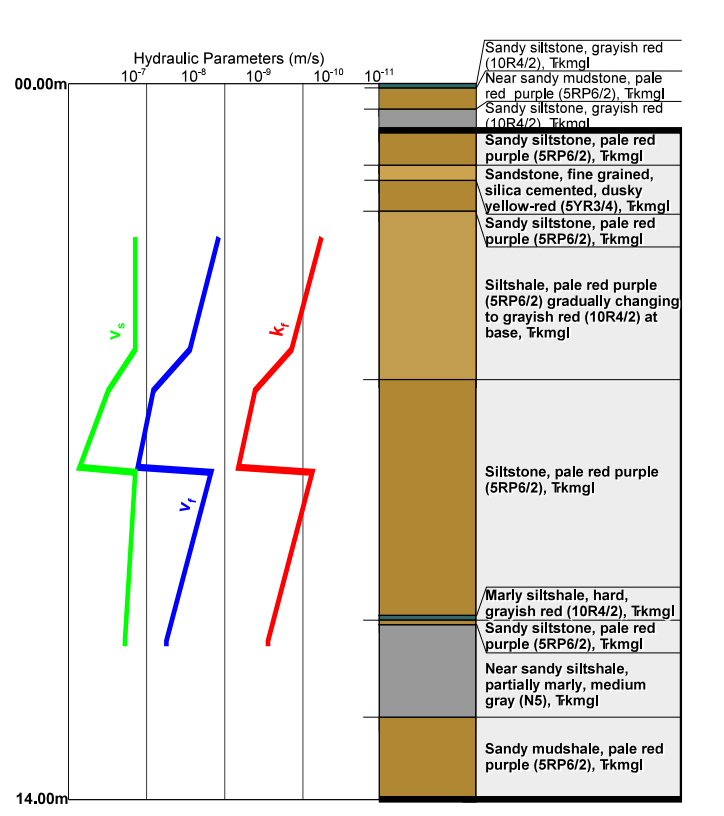


Figure 5.10 - Lehrberg Layers presented with depth profile of hydraulic data ( $k_p$ ,  $v_p$ ,  $v_s$ ). Hydraulic velocities in logarithmic scale.

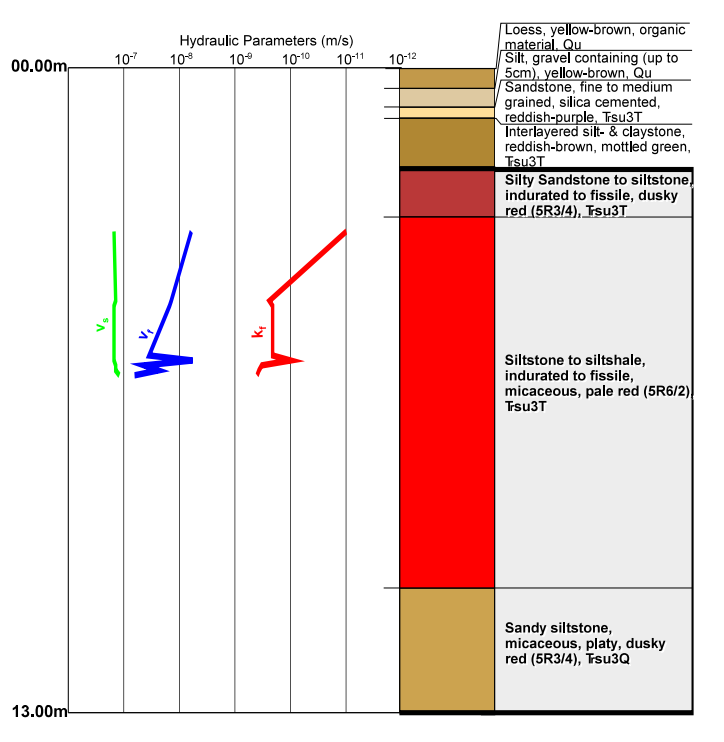


Figure 5.11 - Depth profile of Lower Rötton with hydraulic data ( $k_p$ ,  $v_p$ ,  $v_s$ ). Logarithmic scale for hydraulic parameters.

## 6 Contaminants

Much attention has been given to transport of pollutants through the subsurface. Problems however arise when geologic barrier samples are tested with a variety of modeling substances. One of common objections in modern diffusion research is the use of highly concentrated test solutions. BARONE *et al.* (1992) indicates that such elevated chemical concentrations never occur in nature or only exist under rare and extreme circumstances. Another concern is the common use of only a single test parameter, neglecting the interaction of the various substances in a leachate. SHACKELFORD *et al.* (1989) and SHACKELFORD & DANIEL (1991b) tried to address these problems by employing an artificial leachate consisting of cations Cd, Ca, K, Zn and the anions Br, Cl, I, SO<sub>4</sub> in acceptable concentrations ranges approaching average waste leachates. The choices indicated, however, were based more on convenience to study ions with a great variety of chemical properties, such as size or sorbent attributes, rather than actual components found in landfill contaminants. Other researchers, such as ZIEGLER & LECHNER (1994), attempted to develop simple, but much more realistic synthetic leachates in appropriate concentrations. In order to evaluate diffusion and sorption parameters during this investigation, the development of a synthetic average landfill leachate was of major importance.

**Table 6.1** - Comparison of various summarized landfill data (see sources below). Average or typical values. n.l. = not listed.

	ATV1	ATV2	ATV3	MLL	YMLL	CT1	CT5	CT15
pH	7.5	7.0	7.9	6.3	5.3	n.l.	n.l.	n.l.
conductance (mhos/cm)	10,000	60,298	22,001	6,700	n.l.	n.l.	n.l.	n.l.
Cl <sup>-</sup> (mg/L)	2,000	38,544	6,701	980	800	2,000	1,500	500
SO <sub>4</sub> <sup>-2</sup> (mg/L)	300	2,053	2,572	380	n.l.	n.l.	n.l.	n.l.
NO <sub>3</sub> <sup>-</sup> (mg/L)	3	5.9	720	4	n.l.	n.l.	n.l.	n.l.
Na <sup>+</sup> (mg/L)	n.l.	n.l.	n.l.	700	n.l.	n.l.	n.l.	n.l.
K <sup>+</sup> (mg/L)	n.l.	n.l.	n.l.	n.l.	500	2,000	700	100
Ca <sup>+2</sup> (mg/L)	n.l.	n.l.	n.l.	1,000	n.l.	n.l.	n.l.	n.l.
NH <sub>4</sub> <sup>+</sup> (mg/L)	500	1,438	782	300	300	1,500	350	60
Fe (mg/L)	50	n.l.	17.8	430	500	700	600	100
Heavy Metals (mg/L) ∑Cu,Ni,Zn,Hg,Pb,Cd,As,	0.335	1.079	6.689	23.250	n.l.	n.l.	n.l.	n.l.
Phenols (mg/L)	0.006	n.l.	27.7	n.l.	n.l.	n.l.	n.l.	n.l.

Source: German landfills: ATV1= municipal landfills, ATV2= historic landfills, ATV3= other or remaining landfills, after ATV-ARBEITSGRUPPE (1988). U.S. landfills: MLL = municipal landfills after LEE & JONES-LEE (1993); YMLL = younger municipal landfills after SHAMS-KHORZANI *et al.* (1994); CT1, CT5, CT15 = leachate concentration trends for a 1 year, 5 year, 15 year old landfill respectively after MCBEAN & ROVERS (1999).

## 6.1 Landfill Leachates

Before a synthetic landfill leachate (SLL) could be developed, the composition of various contaminant solutions from several landfills needed to be researched. Unfortunately, leachate compositions show extreme variations, even

seasonally within the same landfill. One factor for the variation is definitely the age of a given site as indicated by USEPA (1995) or McBEAN and ROVERS (1999). The other factors are described by ECKENFELDER and MUSTERMAN (1994) as composition and extend of waste, permeability of the landfill materials, precipitation, and ambient air temperature. In order to develop a representative SLL, a literature search of common leachate compositions was attempted. While preference was to be given to composite summaries analyzing several landfills, the variance in concentrations was significant as can be seen in table 6.1.

The divergence in leachate composition is more than obvious, even when comparing averages of various landfill investigations. It was therefore impossible to conclude a medium leachate makeup representative of all waste disposal sites. In order to develop a SLL, modeling after an existing municipal landfill leachate from the general geographic location of the geologic barriers was undertaken. This differing approach was also compared to average leachate compositions collected from various waste disposal sites in the same geographic region. Data for the above mentioned in comparison with the SLL is represented in table 6.2.

**Table 6.2** - Comparison of artificial leachate concentration of selected ions with leachate concentrations of the Raindorf landfill (LGA, 1996 (unpublished data)) and average landfill leachate concentrations according to ATV (1988) report.

Selected ions	SLL (Artificial Leachate)	Landfill Raindorf leachate conc.	Landfill leachate averages & ranges (ATV, 1988)	
			Avg.	Range
Cl <sup>-</sup>	7052 mg/l	6575 mg/l	6701 mg/l	36 - 36146 mg/l
SO <sub>4</sub> <sup>2-</sup>	2502 mg/l	6250 mg/l	2572 mg/l	18 - 14968 mg/l
NO <sub>3</sub> <sup>-</sup>	823 mg/l	643 mg/l	720 mg/l	<0.1 - 14775 mg/l
Na <sup>+</sup>	4327 mg/l	5945 mg/l	not measured	
K <sup>+</sup>	629 mg/l	600 mg/l	not measured	
Ca <sup>2+</sup>	409 mg/l	464 mg/l	not measured	
NH <sub>4</sub> <sup>+</sup>	710 mg/l	314 mg/l	782 mg/l	<5 - 6036 mg/l
* Cu <sup>2+</sup> (∑ Pb, Cd, Cu, Ni, Hg, Zn, Cr)	11 mg/l	12.26 mg/l	10.14 mg/l	0.05 - 102.3 mg/l
CPL (2-Chlorophenol)	35 mg/l	0.014 mg/l	27.7 mg/l	<0.01 - 350 mg/l

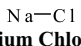
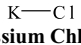
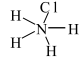
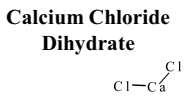
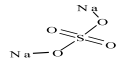
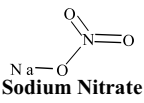
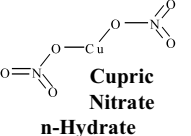
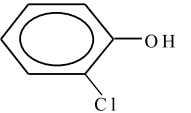
\* Copper concentration representative for sum of Pb, Cd, Cu, Ni, Hg, Zn, & Cr

## 6.2 Synthetic Landfill Leachate (SLL)

Several requirements were imposed on the artificial leachate or SLL. First, the concentration and variety of ions and chemical compounds in the leachate approximates conditions of genuine landfill leachates. As compiled in table 6.2, compositions of recent landfills were used. No historic landfill was included because of frequently extreme concentrations which were hard to stabilize in an SLL. Secondly, individual ionic concentrations needed to be high enough to allow easy detection and thus simplify the analysis of leachate contents. Therefore, only constituents found in original landfill waters with concentration of 10 mg/L or more were simulated. Third, the leachate should exhibit enough chemical stability over an extended time period without adjusting the solution to artificial pH levels contrary to authentic landfill percolates. In order to accomplish the later requirement, iron, even though present in genuine leachates at levels exceeding 10 mg/L (see table 6.1), needed to be excluded because of induced instabilities to the

SLL. Table 6.3 gives a list of chemicals used in aqueous solution, their general properties, and mixing concentrations in creating the synthetic landfill leachate.

**Table 6.3** - Chemicals used in the construction of a Synthetic Landfill Leachate. Indicated are chemical structure, name, formula, quantities used for SLL, molecular weight, Log  $K_{ow}$ , and calculated & measured solubilities.

Structure & Name	Formula	SLL concentration	Mol. Weight	<sup>1</sup> Log $K_{ow}$	<sup>1</sup> calc. solubility mg/L @ 25°C	Solubility mg/L
 <b>Sodium Chloride</b>	NaCl	7,200 mg/L	58.44	-0.46	339,500	<sup>2</sup> 357,000 @ 25°C
 <b>Potassium Chloride</b>	KCl	1,200 mg/L	74.55	-0.46	330,600	<sup>6</sup> 342,400 @ 20°C
 <b>Ammonium Chloride</b>	NH <sub>4</sub> Cl	2,100 mg/L	53.49	-4.37	1,000,000	<sup>3</sup> 372,000 @ 20°C
 <b>Calcium Chloride Dihydrate</b>	CaCl <sub>2</sub> * 2H <sub>2</sub> O	1,500 mg/L	147.0	0.05	97,970	<sup>6</sup> 1,281,000 @ 40°C
 <b>Sodium Sulfate</b>	Na <sub>2</sub> SO <sub>4</sub>	3,700 mg/L	142.04	-4.38	1,000,000	<sup>6</sup> 481,000 @ 40°C
 <b>Sodium Nitrate</b>	NaNO <sub>3</sub>	1,100 mg/L	84.99	-0.79	605,500	<sup>6</sup> 882,700 @ 20°C
 <b>Cupric Nitrate n-Hydrate</b>	Cu(NO <sub>3</sub> ) <sub>2</sub> * 3H <sub>2</sub> O	40 mg/L	187.56	-0.61	168,100	<sup>6</sup> 1,252,500 @ 20°C
 <b>2-Chlorophenol</b>	C <sub>6</sub> H <sub>5</sub> OCl	35 mg/L	128.56	2.16 ( <sup>4</sup> 2.15)	5165	<sup>5</sup> 11,300 @ 25°C

References: <sup>1</sup>calculated using SRC (2000). For references on  $K_{ow}$  calculations and uses see appendix F.1. <sup>2</sup>MERCK INDEX (1989). <sup>3</sup>DEAN (1985). <sup>4</sup>HANSCH *et al.* (1995). <sup>5</sup>BANERJEE *et al.* (1980). <sup>6</sup>KALTOFEN *et al.* (1972).

Included in table 6.3 is the  $K_{ow}$  or octanol-water partition coefficient. Commonly used to determine the solubility and sorbent behaviors of organic molecules, it can also be employed to estimate behaviors of inorganic compounds. Since the SRC (2000) software package used by the U.S. EPA to determine the impact of various contaminants in the environment allows the calculation of a multitude of chemical characteristics, including  $K_{ow}$ , important computational results are included in the before mentioned table. Complete data compiled with the SRC (2000) program is summarized in appendix F.1.

In order to establish the chemical behavior of the characteristic ions in the SLL, knowledge of the ionic strength and ionic activity would be advantageous. Ions in solution tend to be encapsulated by water molecules with additional H<sub>2</sub>O molecules as spacer keeping the ions far apart. As salt concentrations increase, the anions and cations in solution

are forced to move closer, are more likely to come in contact with each other and will exert Coulombic<sup>6</sup> forces. According to LANGMUIR (1997) these forces are proportional to the charge of the ions involved and the Coulombic effects are embodied in the definition of ionic strength (I). Equation 6.1 summarizes the calculation of I.

$$\text{Eq. 6.1} \quad I = 0.5 (c_1 z_1^2 + c_2 z_2^2 + c_3 z_3^2 \dots \dots c_n z_n^2)$$

where I = Ionic Strength in mol/L  
 c = Concentration of ion species in mol/L  
 z = Valence of ion species

The ionic strength is therefore a measure of the charge and concentration of ions in solution. LANGMUIR (1997) points out the ionic strength of a solution affects the solubility of ionic species, most often increasing the solubility. This phenomenon is also known as "salting in". The net effect of this observation for the diffusion and sorption research could mean that in the geologic barrier material, minerals or exchangeable ions might be more soluble when subjected to a leachate than a ground water environment. Table 6.4 recaps the ionic strength of individual aqueous species and their sum within the SLL.

The limitations of I for ionic interaction assessments spawns from the fact that ionic strength only considers valance, but not the interaction of differing ions. For this purpose a correction factor in essence was introduced by the Debye-Hückel Theory (cf. DREVER, 1982), accounting for the apparent decrease of concentration because of this interaction. The resulting activity coefficient ( $\gamma$ ) is a function of the hydrated radius of the ion, the respective charge or valance (z), and the ionic strength of the solution (I). Calculation of the activity coefficient for individual ions is given in the Debye-Hückel equation, summarized below as equation 6.2.

$$\text{Eq. 6.2} \quad \log \gamma_i = \frac{-A z_i^2 \sqrt{I}}{1 + B a_i \sqrt{I}}$$

where  $\gamma_i$  = activity coefficient of specific ion  
 A =  $1,824,928 * \rho_w^{0.5} * (\epsilon T)^{-1.5}$   
 $\rho_w$  = density of water at a given temperature  
 $\epsilon$  = dielectric constant of water at a given temperature<sup>7</sup>  
 T = temperature in Kelvin  
 z = valence of ion species  
 I = Ionic Strength in mol/L  
 B =  $50.3 * (\epsilon T)^{-0.5}$   
 $a_i$  = ionic size of ion species (size parameter look-up from Debye-Hückel ion size table)

When charged ions are dispersed in an aqueous solution, the electrostatic forces acting on the ions decrease inversely with the square of the distance from each other. Since Coulombs equation (see footnote) is designed for charged particles in a vacuum, adjustments for ions in water are made by multiplying the square of the radius with the appropriate dielectric constant (LANGMUIR, 1997). The Coulombic forces must therefore increase as the ion density or ion concentration increases. Thus the activity coefficient is bound to decrease as the ionic strength increases. The activity coefficient is therefore a measure of the effective ionic strength. According to LANGMUIR (1997), several assumptions incorporated in the Debye-Hückel equation become invalid and lead to its failure at high ionic strength

6

Coulomb's law: Force between charges - If two charges ( $q_1$  and  $q_2$ ) are at a distance (r) in a vacuum, the force between them is described as  $F = \frac{q_1 q_2}{r^2}$  (CRC, 1985)

7

The dielectric constant for various temperatures can be obtained by the following equation (LANGMUIR, 1997):  
 $\epsilon = 2727.586 + 0.6224107 T + 466.9151 \ln T - 52000.87/T$



where ion activity coefficients increase. Modifications for activity coefficient models for ions at varying ranges of ionic strengths were made based on the original equation. The model most appropriate for the ionic strength of 0.3 mol/L for the SLL is the empirical Davis expression given in equation 6.3 (LANGMUIR, 1997).

$$\text{Eq. 6.3} \quad \log \gamma = -A z^2 \left( \frac{\sqrt{I}}{1 + \sqrt{I}} - 0.3I \right)$$

where  $\gamma$  = activity coefficient  
 $A = 1,824,928 * \rho_w^{0.5} * (\epsilon T)^{-1.5}$   
 $\rho_w$  = density of water at a given temperature  
 $\epsilon$  = dielectric constant of water at a given temperature  
 $T$  = temperature in Kelvin  
 $z$  = valence  
 $I$  = Ionic Strength in mol/L

The Davis equation is used in the aqueous solution modeling software PHREEQCi (2002), where activity coefficients are also calculated. The software was therefore employed to solve the respective  $\gamma$ 's for the SLL. Complete listing of computational results is given in appendix F.2. Activity coefficients for ions present in the synthetic leachate are summarized in table 6.4.

Once the concentration of an ion in solution and the activity coefficient is known, the ion activity or short "activity" ( $a_i$ ) can be derived. HÖLTING (1992) describes the activity as a measure of interaction of ions in solution in terms of their analytically determined concentration. In summary, the higher the ion concentration, the greater the interference among the individual ions. Thus the  $a_i$  is modeling the chemical activity of an ion in solution and is portrayed in equation 6.4.

$$\text{Eq. 6.4} \quad a_i = \gamma * c$$

where  $a_i$  = ionic activity  
 $\gamma$  = activity coefficient  
 $c$  = ion concentration in mol/L

**Table 6.4** - Concentrations of ions present in SLL and computed ionic strength, ion activity coefficients, and  $a_i$ 's.

Ion	Conc. mg/L	Conc. mol/L	Conc. (eq.)mol/L	Ionic Str. mol/L	Ion Activity coefficients		$a_i$	
					10°C	30°C	10°C	30°C
Cl <sup>-</sup>	7052.2	0.1989	0.1989	0.0995	0.1362	0.1347	0.0271	0.0268
SO <sub>4</sub> <sup>-2</sup>	2502.3	0.0260	0.0521	0.0521	0.0045	0.0043	0.0001	0.0001
NO <sub>3</sub> <sup>-</sup>	823.2	0.0133	0.0133	0.0066	0.0389	0.0385	0.0005	0.0005
Na <sup>+</sup>	4327.4	0.1882	0.1882	0.0941	0.1345	0.1330	0.0253	0.0250
K <sup>+</sup>	629.4	0.0161	0.0161	0.0080	0.0108	0.0106	0.0002	0.0002
Ca <sup>+2</sup>	409.0	0.0102	0.0204	0.0204	0.0025	0.0024	2.5E-05	2.4E-05
NH <sub>4</sub> <sup>+</sup>	709.7	0.0392	0.0392	0.0196	0.0311	0.0307	0.0012	0.0012
Cu <sup>+2</sup>	10.5	0.0002	0.0003	0.0003	3.9E-05	2.6E-05	6.5E-09	4.3E-09
C <sub>6</sub> H <sub>5</sub> OCl	35.0	0.0003						
SUM:	16498.7	0.4924	0.5286	0.3007	0.3585	0.3541	0.0545	0.0538

The  $a_i$  for the various ionic species in the SLL are presented in table 6.4. As indicated, the most active species in the SLL are Na<sup>+</sup> and Cl<sup>-</sup>, while the least active ions are calcium and copper. The activities at the two temperatures shown, which correspond to the temperatures of the diffusion experiment, do not significantly vary.

## 7 Sorption

Sorption is the interaction of a contaminant with a solid. ALLEY (1993) more specifically defines it as the attraction of an aqueous species to the surface of a solid. The sorbing species, in this case the dissolved pollutant is called the sorbate. The attracting solid, usually the soil or rock with which the sorbate interacts is known as the sorbent. The process of sorption can be further differentiated into adsorption and absorption (see figure 7.1).

Adsorption occurs on the surface of the sorbent particles. A major control of adsorption is the surface area of the solid. Because of small particle size and therefore large surface areas, clays exhibit natural adsorption properties. The process is more or less temporary. The sorbate can sometimes be removed by changing physical or chemical conditions. Absorption refers to the penetration or incorporation of the sorbate into the physical structure of the sorbent. Here, the process appears to be more permanent.

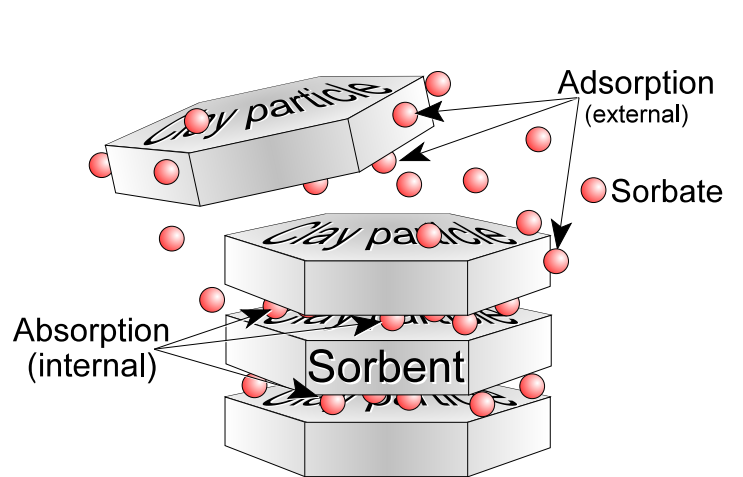


Figure 7.1 - Adsorption vs. Absorption

However, when investigating pollutant and soil interactions, this distinction serves little purpose because there is seldom information concerning the specific nature of the interaction. The term sorption is a generic expression to encompass both phenomena.

Several factors control the interaction of contaminants with subsurface or aquifer materials. Chemical and physical properties of the sorbate, size, texture and composition of the sorbent surface and physical structure, as well as characteristics of the media fluid involved are all contributing factors. These key properties can be used to effectively describe the sorption properties of the contaminant and soil interactions.

### 7.1 Sorption and Sorbent Properties

Sorption is influenced by certain characteristics of the soil (sorbent), the pollutant (sorbate) and sorbate solvent, usually an aqueous solution. Sorbent key factors are (a) organic carbon content, (b) texture (surface area) of the soil particles, and (c) surface charge of the particles. For ionic contaminant sorption, soil pH resembles another important controlling factor. The contaminant solution must also migrate fairly slow to insure that sorption occurs at equilibrium (ALLEY, 1993). Such slow movement of pollutant materials is unequivocally assured in clay barriers.

Generally the relationship of sorption to sorbent properties involves porosity and density, and independently the organic carbon content of the material. This finds expression in the retardation equation as follows:

$$\text{Eq. 7.1} \quad R = 1 + \frac{\rho_b}{n_e} K_p$$

where R = Retardation factor or Distribution Ratio  
 $\rho_b$  = dry (bulk) density of material  
 $n_e$  = Effective Porosity  
 $K_p$  = Partition Coefficient (non-linear sorption) or Distribution Coefficient  $K_d$  (linear sorption)

The partition ( $K_p$ ) or distribution ( $K_d$ ) values represents the sorption coefficient. According to LOEHR (1993), chemicals that do not interact with the sorbent, such as chlorides and nitrates<sup>8</sup>, have a sorption coefficient of zero and the retardation factor equals one. The sorption of dissolved molecular organic substances by soils and sediments has been found to be proportional to the amount of solid organic matter present and relatively independent of the weight of associated inorganic materials (LANGMUIR, 1997). Therefore, the sorption or distribution coefficient for organic contaminants on organic carbon is defined as:

$$\text{Eq. 7.2} \quad K_{oc} = \frac{\mu\text{g adsorbed} / \text{g organic carbon}}{\mu\text{g} / \text{mL solution}}$$

In short  $K_{oc}$  is the ratio of the amount of chemical adsorbed per unit weight of organic carbon (oc) in the soil or sediment to the concentration of the chemical in solution at equilibrium (LYMAN, 1990). In order to place  $K_{oc}$  in relation to the total sorbent amount and establish an actual sorption parameter regarding organic pollutants for the materials tested, equation 7.3 is employed.

$$\text{Eq. 7.3} \quad K_d = K_{oc} f_{oc}$$

where  $K_d$  = Sorption Coefficient  
 $K_{oc}$  = Adsorption or Distribution Coefficient for Organic Carbon  
 $f_{oc}$  = Weight fraction of organic carbon in sorbent material

While organic pollutant sorption is principally influenced by the carbon content of the sorbent, inorganic ionic sorption processes are much more complex. MCBRIDE (2000) states that the properties of the mineral surface, i.e. the nature of metal constituting the sorption site, dictates to some extent the tendency of the sorbate for chemisorption.

Certain clay minerals, such as montmorillonite, vermiculite and illite, contain exchangeable cation sites, which invite absorption of positively charged ions within the structure of the mineral itself (see table 4.1). This phenomenon enhances the sorption characteristics of certain clays.

The silica tetrahedrons and aluminum and magnesium octahedrons in clay minerals terminate in hydroxyl (OH) groups on the clay surface. Here, adsorption takes place and can be predicted using a simple ratio of the valence of the tetrahedral or octahedral metals to their coordination number as listed in table 7.1. Silica, for example, has a valence of +4 and coordinates this charge with 4 oxygen in the tetrahedral structure, resulting in a ratio or valence charge of  $+4 / 4 = +1$  exhibited on the surface of the tetrahedron. Magnesium with a charge of +2 and a coordination number of 6 exhibits a octahedral surface charge of only  $+2 / 6 = +0.33$ . Therefore, metal cations are much more likely to adsorb onto surfaces with reduced positive charges. Thus, groups at the bottom of table 7.1 will favor cationic chemisorption, while those at the top will exhibit a greater affinity for anionic sorption processes. LANGMUIR (1997) gives three further important causes for generally negative surface charges in clay particles. These are: (a) Isomorphous substitutions, the main cause of negative surface charges in smectites and vermiculites; (b) Lattice imperfections / defects, yields permanent surface charges and is important in smectites and somewhat in illites; and

---

<sup>8</sup> KOWALENKO and YU (1996) as well as this study show that nitrate adsorption does indeed occur contrary to the current notion that  $\text{NO}_3^-$  is a non-sorbing species. Details are discussed below under "7.6.8 Nitrate".

(c) Broken or unsatisfied bonds, is pH dependent, chief source of surface charge for kaolinite and importance increases with decreasing particle size in other clays.

**Table 7.1** - Valence / Coordination number ratios for various mineral building blocks

Group	Valence of Center Metal	Co-ordination number	Ratio Valence/Coordination Number (Group Surface Charge)
Si - tetrahedrons	+4	4	+1.00
Ti - octahedrons	+4	6	+0.67
Fe - octahedrons	+3	6	+0.50
Al - octahedrons (Gibbsite layers)	+3	6	+0.50
Mg - octahedrons (Brucite layers)	+2	6	+0.33

Another critical factor is the total surface area of the sorbate. Surface area increases exponentially with decrease in grain size. Fine grained clays with particles sizes of 2  $\mu\text{m}$  or smaller are therefore excellent sorbent materials. This is indicated by the correlation of the cation exchange capacities with total surface area. BRUNAUER *et al.* (1938) introduced the BET-method for differentiating between adsorptive or outer surfaces and absorptive surfaces or inner surfaces. This differentiation has merit when establishing exchangeable versus fixed cation sorption.

HEIMERL (1995) shows a definite relationship of cation exchange capacities (CEC) to surface area of clay minerals, illustrated by figure 7.2. The trend is obvious for clay mineral surface investigations using the Methylene Blue Method and calculations according to HEIMERL (1995). Data established with the BET Method does not correlate well using only the four units of interest. BET - CEC interrelations are slightly better with additional samples included.

The cation exchange capacity is an important measure of sorptive capabilities of the sorbent. Preferred sorption sites in clay molecules are often occupied by naturally occurring cations. When high concentrations of leachate cations enter the geologic barrier, cation exchange processes must innately take place. Thus, desorption processes within the sorbent develop in order to vacate sorption sites for leachate cations. This process is governed by hierarchy of ionic affinities in relation to the sorbent. Those ions with greater bonding affinities will displace already sorbed ions of lesser affinity. HÖLTING (1992) presents a general hierarchy of bonding intensities for ion exchanges on minerals as follows:

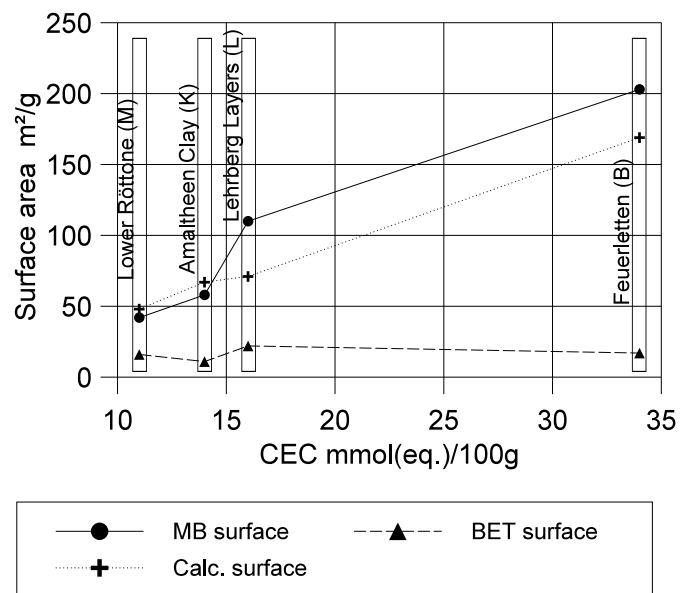
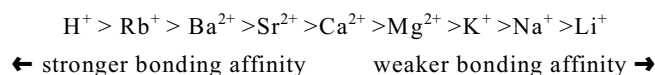
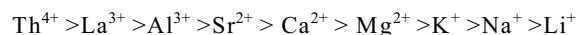


**Figure 7.2** - CEC vs surface areas of clays for Lower Röttone (M), Amaltheen Clay (K), Lehrberg Layers (L), and Feuerletten (B). MB = Methylene Blue Method; BET = Brunauer, Emmett & Teller Method (BRUNAUER *et al.*, 1938). Data adapted from HEIMERL (1995).

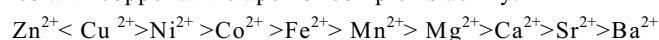


SCHACHTSCHABEL *et al.* (1989) gives a similar hierarchy specifically for smectite clays as shown below

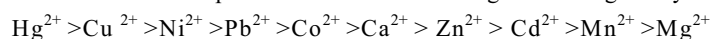


The apparent regularity in this hierarchy can be interrupted by the presence of certain minerals, especially clays. Potassium, for example, will not be attracted to kaolinite, but has a much greater affinity toward mica or montmorillonite (HÖLTING, 1992). The presence of organic matter in the geologic barriers will further influence the sorption / desorption sequence. MCBRIDE (2000) lists two slightly different affinity series for soil organic matter sorption:

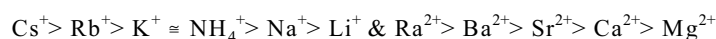
(a) the Irving-Williams series with copper at the apex of complex stability:



(b) approximate order of divalent metal sorption in relation to Pauling electronegativity:



BØRRETZEN and SALBU (1999) concur with TURNER (1995), that adsorption occurs as an ion exchange processes on clays rather than bonding to a charged -OH surface site. They describe yet another sequence of bonding strength attributed to clay minerals:



Selectivity for various sorbate ions may also be affected by the presence of diverse oxides. In the presence of manganese oxides, sorption is highly selective for copper, nickel, cobalt and lead, while Fe, Al, and Si oxides preferably adsorb  $\text{Pb}^{2+}$  and  $\text{Cu}^{2+}$  (MCBRIDE, 2000). Thus sorbate constituents have a definite influence on the sorptive characteristics of the geologic barrier.

## 7.2 Sorption and Sorbate Properties

Key contaminant (sorbate) properties effecting sorption are (a) water solubility, (b) ionic size and valence, (c) sorbate concentration and in addition for organic pollutants (d) polarity of the contaminant, as well as (e)  $K_{ow}$  (Octanol Water Partition Coefficient). While sorbate properties for organic contaminants can be determined with very few parameters, inorganic ion species are much more complex in their interaction. MCBRIDE (2000) proposes a simplified approach to sorbate interactions with the sorbent surface expressed as the ratio between the Ionic Activity Product (IAP)<sup>9</sup> and the solubility coefficient ( $K_{so}$ ).

<sup>9</sup> To derive IAP: (1) calculate ionic strength (I) of sorbate; (2) compute ion activity coefficient ( $\gamma$ ) for each constituent using Debye-Hückel equation for  $I < 0.1\text{m}$  (DREVER, 1982) or Davis equation for  $I < 0.5\text{m}$  (DAVIS, 1962); (3) assess activity (a) by multiplying  $\gamma$  with molar concentration; (4) estimate IAP by multiplying “ $a_i$ ” values for each possible compound combination.

Solubility is defined as the maximum amount of a substance that will dissolve in a given amount of solvent at a certain temperature. In sorption processes, however, this condition is no longer static but rather becomes a dynamic interactive process since new ions are continually introduced while others are removed from the sorbate. Thus, solubility implies nothing about the activities of highly charged ions, since activity depends also on ion concentration (activity = activity coefficient  $\times$  molality). Activity can therefore be thought of as the “effective” concentration. Accordingly the resulting IAP becomes an expression of the “as-is” ionic solubility condition.

Figure 7.3 schematically describes the progression of sorption with change in IAP. Chemisorption is the most stable form of surface retention and commonly occurs in acidic pH conditions, a surplus of available sorbent sites, and/or limited total concentration of ions in solution. Given these circumstances, solubility far outweighs the specific ion activities. Thus metals or oxyanions spread across freely available discrete sorption sites on the sorbent.

Clustering occurs by polymerization of sorbate molecules at same discrete chemisorptive retention sites of sorbent particles. This process is commonly observed with strongly hydrolyzed metal cations. SCHEIDEGGER *et al.* (1996)

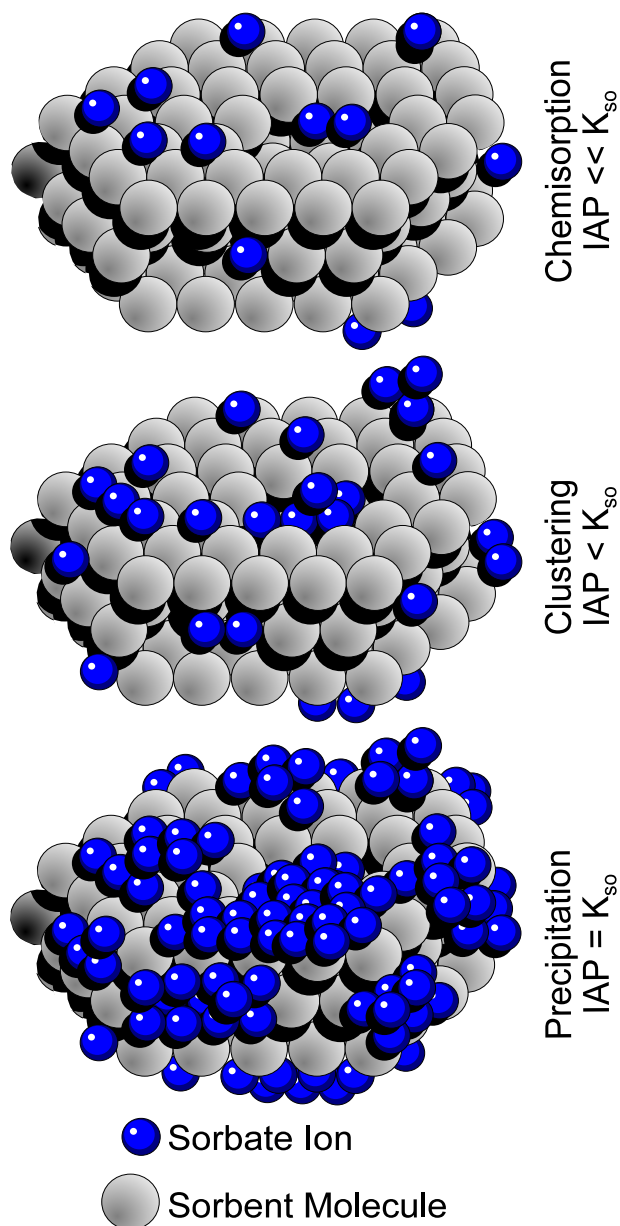


Figure 7.3 - Schematic view of ionic sorption characteristics according to IAP /  $K_{so}$  ratios. Chemisorption for IAP  $\ll$   $K_{so}$ , Clustering for IAP  $<$   $K_{so}$ , Surface precipitation for IAP =  $K_{so}$ . (According to MCBRIDE, 2000)

on silicate clays, especially at high pH. Cation exchanges, however, may be the predominant sorption. Interpretation of sorption characteristics of inorganic sorbate species is discussed further in “7.4 Sorption Isotherms”.

An important factor controlling the solubility and mobility of an organic contaminant is the polarity of that contaminant compound. Polar substances display a higher solubility and lower sorption capability than non-polar substances. Solubility is therefore inversely proportional to the amount of sorption that the contaminant can undergo.

In order to quantitatively qualify solubility and sorption in organic contaminants of interest the  $K_{ow}$  (Octanol Water Partition Coefficient) can be used. The  $K_{ow}$  defines the ratio of the solute concentration in an octanol phase to the solute concentration in the water phase of an octanol-water mixture. The value expresses the water repelling characteristic or hydrophobicity of a contaminant. Octanol is chosen as a reference solvent since it closely models

the chemical characteristics of lipids found in living organisms. It therefore is an easy measure of bio concentration effects for potential contaminants. Because of a wide spread in  $K_{ow}$  values among various compounds, this unit-less ratio is often expressed as a logarithm. A  $\text{Log } K_{ow}$  of 2.00 would mean that the contaminant is 100 times more soluble in octanol than in water. Compounds with greater  $K_{ow}$  values are therefore less soluble in water and more likely to adsorb to soil particles (BEDIENT *et al.*, 1994).

Table 7.2 summarizes solubility,  $K_{oc}$  and  $\text{Log } K_{ow}$  data for some selected organic contaminants. For comparison two inorganic pollutants are included. Aromatic hydrocarbons of the benzene or toluene group dissolve reasonably well in water. However, they are non-polar therefore showing fair sorption characteristics. Many polar organic contaminants are derivatives of phenols, herbicides, and pesticides. Greater solubility in water also results in lowered sorptive abilities. In contrast, solubility of ionic contaminants, such as most inorganic compounds, is controlled mainly by soil pH.

**Table 7.2** - Solubility, polarity,  $K_{oc}$  &  $\text{Log } K_{ow}$  data for common organic contaminants. Inorganic pollutant data given for comparison

Contaminant	Water Solubility @ 298 K (mg/L)	$\text{Log } K_{ow}$	Soil Sorption $K_{oc}$ (L/kg)
Benzene	1,760 <sup>1</sup>	2.13 <sup>1</sup>	38 <sup>1</sup>
Toluene	515 <sup>1</sup>	2.69 <sup>1</sup>	90 <sup>1</sup>
Phenol	82,000 <sup>1</sup>	1.46 <sup>2</sup>	110 <sup>1</sup>
Naphthalene	31.7 <sup>1</sup>	3.3 <sup>1</sup>	690 <sup>1</sup>
Atrazine	33 <sup>3</sup>	2.61 <sup>2</sup>	163 <sup>3</sup>
DDT	0.004 <sup>3</sup>	6.91 <sup>2</sup>	24,000 <sup>3</sup>
2-Chlorophenol	28,500 <sup>2</sup>	2.16 <sup>2</sup>	443.1 <sup>2</sup>
Sodium Chloride	357,000 <sup>2</sup>	-0.46 <sup>2</sup>	14.3 <sup>2</sup>
Ammonium Nitrate	1,000,000 <sup>2</sup>	-4.39 <sup>2</sup>	14.3 <sup>2</sup>

References: 1- USACE, 1995    2- SRC, 2000    3- HERNER *et al.*, 1996



### 7.3 Sorption Isotherms

The sorptive characteristics of a soil for a given pollutant can be expressed by a sorption isotherm, which is a graphic representation of the amount of contaminant sorbed versus its concentration in solution. The shape of the resulting isotherm graph is indicative of the type of sorbate - sorbent interaction (Figure 7.4). In order to model sorptive behavior of various soils and contaminants and to calculate sorption coefficients, isotherm equations are employed.

#### 7.3.1 Freundlich Sorption Isotherm

The Freundlich isotherm is one of the simplest and most frequently used mathematical sorption models. It finds expression in the equation:

$$\text{Eq. 7.4} \quad \frac{x}{m} = SC^n \quad \text{"or"} \quad \frac{x}{m} = SC^{\frac{1}{n}}$$

where  $x/m$  = weight sorbate divided by weight sorbent (usually  $\mu\text{g/g}$ ,  $\text{mg/g}$  or  $\text{g/kg}$ )  
 $S$  = a constant  
 $C$  = sorbate aqueous concentration (usually in  $\text{mg/ml}$  or  $\text{g/L}$ )  
 $n$  = a constant

$S$  is often referred to the capacity or affinity of the sorbent, while  $n$  is an indicator of the sorption intensity (SUFFET and MCGUIRE, 1980). The range of the  $n$  values is approximately 0.6 to 3.3 with a usual spread from 0.9 to 1.4 (LANGMUIR, 1997; LYMAN *et al.*, 1982). The Freundlich sorption isotherm is linear when  $n = 1$  (Figure 7.4). In this case the sorption coefficient  $K_d$  can be calculated directly by solving equation 7.4 for  $S$ .

$$\text{Eq. 7.5} \quad S = \frac{x/m}{C} = K_d$$

If  $n$  is smaller than 1, a concave or favorable Freundlich isotherm results. The opposite is true for  $n$  values greater than 1, consequently showing convex, unfavorable or negative Freundlich isotherms (Figure 7.4). Establishing  $K_d$  coefficients for these later cases involves a logarithmic plot of expression 7.4, which yields:

$$\text{Eq. 7.5} \quad \log \frac{x}{m} = \log S + n \log C$$

If a Freundlich isotherm is obeyed, the data will now plot on a straight line.  $\log S$  is the Y intercept and  $n$  is the slope of the line. Solving for  $S$  will now yield the desired  $K_d$  value. LANGMUIR (1997) asserts that nonreactive sorbates exhibit  $K_d = 0$ , while a reactive contaminant  $K_d$  may exceed 100. The Freundlich isotherm is empirical and assumes an infinite number of available sorption sites on the sorbent. While it describes adequately the sorption processes in dilute solutions, limitations for elevated contaminant concentrations are often encountered.

#### 7.3.2 Langmuir Sorption Isotherm

The Langmuir isotherm avoids this criticism by presuming a dynamic equilibrium at higher solute concentrations where the rate of sorption equals the rate of desorption. It is usually generalized as follows:

$$\text{Eq. 7.6} \quad \frac{x}{m} = \frac{S_L M C}{1 + S_L C}$$

where  $x/m$  = weight sorbate divided by weight sorbent (usually  $\mu\text{g/g}$ ,  $\text{mg/g}$  or  $\text{g/kg}$ )  
 $S_L$  = a constant  
 $C$  = sorbate aqueous concentration (usually in  $\text{mg/ml}$  or  $\text{g/L}$ )  
 $M$  = a constant

The finite supply of sorption sites are expressed by  $M$ , indicating the maximum possible sorption by the sorbent. LANGMUIR (1997) states that the maximum sorption is usually assumed to represent monolayer surface coverage and

approaches the value of  $x/m$  where the isotherm curve flattens (Figure 7.4). ROY *et al.* (1992) expresses that according to the conclusions of some investigators, the Langmuir constant ( $S_L$ ) is somehow related to the bonding energy between the sorbed ion and the sorbent, but a specific functional relationship was uncertain. The constant  $S_L$  also represents the sorption coefficient ( $K_d$ ) for a given sorption maxima represented by  $M$  within the Langmuir sorption model.

Solving form  $M$  and  $S_L$  requires a linear expression of the Langmuir isotherm. This is accomplished by taking the inverse of the expression, yielding:

$$\text{Eq. 7.7} \quad \frac{1}{x/m} = \frac{1}{S_L M C} + \frac{1}{M}$$

If the data plot for  $1/x/m$  versus  $1/C$  renders a straight line, the Langmuir isotherm is observed. The inverse of the Y intercept ( $1/M$ ) represents the sorption maxima  $M$  and the slope of the graph is equal to  $1/S_L M$ . While the Langmuir equation satisfies the requirement for a more realistic sorption model with finite sorption capacities, in many cases sorption maximas will never be realized because of low solute concentration. The Freundlich isotherm model will usually fit Langmuir isotherms within the first 1/3 to 2/3 of the  $x/m$  versus  $C$  data plot, thus making it the preferred equation for most sorption batch modeling applications.

### 7.3.3 Graphical Sorption Isotherm Representation

In addition to the above common mathematical isotherm equations, MCBRIDE (2000) gives 4 graphical types of isotherm classifications and similar interpretations were attempted by DOMENICO and SCHWARTZ (1990), MELNYK (1985), SHACKELFORD and DANIEL (1991a), and WEBER and SMITH (1987). A generalized graphical representation for different sorption isotherms taken from the above sources is summarized in Figure 7.4. With the exception of the convex Freundlich, C-type and S-type isotherms, it is generally observed that higher fractions of sorbate species are sorbed at lower sorbate concentrations.

The relationship between the shape of plotted sorption curves and sorbate-sorbent interaction are adequately described by MCBRIDE (2000). His classification is quoted here in its entirety:

*“The **L-type (Langmuir) isotherm** reflects a relatively high affinity between the adsorbate and adsorbent, and is usually indicative of chemisorption.*

*The **S-type isotherm** suggests cooperative adsorption, which operates if adsorbate-adsorbate is stronger than the adsorbate-adsorbent interaction.*

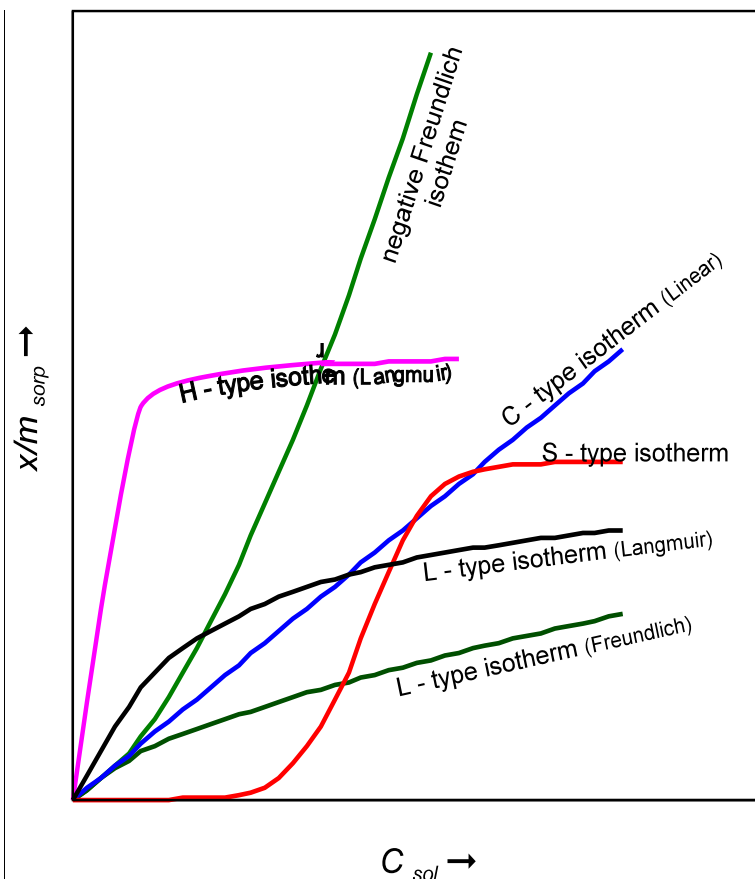


**Figure 7.4** - Graphical representation of sorption isotherms according to MCBRIDE (2000), DOMENICO AND SCHWARTZ (1990), MELNYK (1985), SHACKELFORD AND DANIEL (1991a), and WEBER AND SMITH (1987).

*This condition favors the clustering of adsorbate molecules at the surface because they bond more strongly with one another than with the surface.*

*The **C-type (constant partitioning) isotherm**, which suggests a constant relative affinity of the adsorbate molecules for the adsorbent, is usually observed only at the low range of adsorption. Deviation from the linear isotherm is likely at high adsorption levels. Nevertheless, because many nonpolar organic compounds of interest in soils are adsorbed at quite low concentrations, the linear C-type isotherm is often a reasonable description of reality.*

*The **H-type isotherm**, indicative of very strong adsorbate-adsorbent interaction (e.g. chemisorption), is really an extreme case of the L-type. This isotherm is not often encountered with organic molecules because few of them form strong ionic or covalent bonds with soil colloids.”*

- MCBRIDE (2000)

Comparing these statements with figure 7.3 and 7.4, it can be generalized that H- and L-type isotherms point to a chemisorptive interaction between sorbate and sorbent, while S- and C- types suggest more likely physical sorption parameters. A summary of physical and chemisorptive properties for sorbate and sorbent attributes is given in Table 7.3.

**Table 7.3** - Characteristics of physical and chemisorptive properties after MCBRIDE (2000)

Property	Physical Sorption	Chemical Sorption
Sorption isotherm	S-type, C-type, or Freundlich with $N > 1.0$	Freundlich with $N < 1.0$ or Langmuir (L- & H-type)
Slope of Isotherm	Greater at higher adsorbate concentration	Smaller at higher adsorbate concentration
Sorbate properties	usually organic	usually inorganic
Dependence on Sorbent properties	Relatively little (predominantly carbon content)	Great
Dependence on Sorbate properties	Great	Great
Number of layers of Sorbed molecules	Multiple	Single

#### 7.3.4 Sorption Isotherms for Organic Sorbates

Since the influence of sorbent attributes changes drastically for organic sorbates, sorption isotherms for organic sorbates can be estimated by a different approach. The  $K_d$  value for organic pollutants indicates the binding tendency of that compound to organic matter in the soil when dissolved in water. It therefore represents the likelihood of the compound moving from the water phase to organic carbon particles. As also indicated in the beginning of the chapter, organic sorbate sorption can be calculated using only limited characteristics of the sorbent, such as organic carbon content. Regardless of the soil,  $K_d$  values for organic pollutants are often calculated using equation 7.3. While the amount of organic carbon in the sediment ( $f_{oc}$ ) is easily determined, the sorption coefficient for the organic fraction of the soil ( $K_{oc}$ ) is not always readily available. However,  $K_{oc}$ , also called the partitioning coefficient between organic carbon and water, is very closely related to  $K_{ow}$  or the octanol-water partitioning coefficient. The later is much easier

estimated, either by direct measurement or mathematical from solubility data. In order to estimate  $K_{oc}$  from  $K_{ow}$  data and solving for the sorption coefficient, KARICKHOFF (1981) uses the following equation:

$$\text{Eq. 7.8} \quad K_d = f_{oc} K_{oc} = f_{oc} (0.411 K_{ow})$$

where  $K_d$  = Sorption Coefficient  
 $K_{oc}$  = Adsorption or Distribution Coefficient for Organic Carbon  
 $K_{ow}$  = Octanol-Water Partitioning Coefficient  
 $f_{oc}$  = Weight fraction of organic carbon in sorbent material

A similar estimation approach was used by SCHWARZENBACH AND WESTALL (1981) yielding the formula:

$$\text{Eq. 7.9} \quad K_d = f_{oc} K_{oc} = f_{oc} 10^{(0.72 \log K_{ow} + 0.49)}$$

While these organic sorption isotherm models work well in soils because of accumulated organic carbon particles, difficulties may arise in subsurface lithologies. Here, organic carbon is often diminished and other vehicles of sorption should be considered. LENZ (1991) tried to devise a mathematical sorption model not limited by organic carbon alone (Equation 7.10). While predominantly devised for forest soils, it may also be considered useful for evaluating other sorbent materials. As a desirable side-effect, the equation derived by LENZ (1991) negates any sorbate parameters and focuses solely on sorbent characteristics, thus describing the total sorption capacity of the soil. The formula implements organic carbon content, clay and silt fractions, and soil pH as follows:

$$\text{Eq. 7.10} \quad \text{SORP} \left( \frac{\text{mmol}(\text{eq})}{100\text{g}} \right) = cf (2 C_{org} (\%) + 0.5 \text{CLAY} (\%) + 0.15 \text{SILT} (\%))$$

$0.25$  if  $\text{pH} < 3$   
 $0.3$  if  $3 < \text{pH} < 4$   
 $0.5$  if  $4 < \text{pH} < 5$   
 $0.7$  if  $5 < \text{pH} < 6$   
 $0.9$  if  $6 < \text{pH} < 7$   
 $1.0$  if  $\text{pH} > 7$

$C_{org}$ ,  $\text{CLAY}$  and  $\text{SILT}$  are stated in percent and refer to the ratio of the weight in grams of the respective material per given grams of soil times 100. The  $cf$  factor relates to the soil pH. The resulting sorption capacity ( $\text{SORP}$ ) is expressed in common cation exchange capacity (CEC) units of  $\text{mmol}(\text{eq})/100\text{g}$  and can also be regarded as the effective CEC of the material. The resulting value is therefore an expression of total possible sorption capacity and is comparable to  $M$  in the Langmuir equation (Eq. 7.6 & Eq. 7.7). While sorbent specific  $K_d$  values can not be estimated with equation 7.10,  $\text{SORP}$  gives a reasonable estimation of the sorbate quantity a specific lithologic sample may hold.

#### 7.4 Sorption Batch Experiments

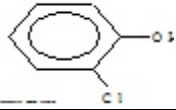
The sorption coefficient ( $K_d$ ) of lithologic materials can be established by laboratory batch experiments. Several approaches are cited in the literature, for example ROY *et al.* (1992), GUADALIX AND PARDO (1995), LANGMUIR (1997), USEPA OPPTS 835.1110 (1998), and USEPA OPPTS 835.1220 (1998). In general, set amounts of sorbent solids are subjected to varying concentrations of an aqueous species sorbate and agitated over a period of time. After centrifugation the remaining concentration of the sorbate species in solution is measured. The difference between

initial and final concentrations constitutes the amount of the species sorbed. A graphical and mathematical analysis of final concentrations versus amounts sorbed will generate the sorption isotherm for the specific sorbate and sorbent. Most standardized sorption test procedures, such as USEPA OPPTS 835.1110 (1998) and USEPA OPPTS 835.1220 (1998), will use the Freundlich isotherm in their sorption analysis, since it approximates the Langmuir isotherm in most commonly encountered lower concentration ranges.

In order to determine sorption isotherms and coefficients for Amaltheen clay, Feuerletten, Lehrberg Layers, and Lower Röttonsteine, the following batch procedure was employed:

- (1) Approximately 50g of a representative sample from each unit, corresponding with sample depths used in the diffusion experiments, was carefully manually disintegrated using a mortar and pestle.
- (2) Pulverized 10g fractions for each sample were transferred to four 125ml polypropylene bottles and each of the sample bottles were filled with artificial leachate concentration according to table 7.4

**Table 7.4** - Artificial Leachate Concentrations for Batch Sorption Experiment.

Ions & Compounds	Dilution			
	1/1 mg/L	1/10 mg/L	1/100 mg/L	1/1000 mg/L
Cl <sup>-</sup>	7052	705.2	70.5	7.05
SO <sub>4</sub> <sup>-2</sup>	2502	250.2	25.0	2.5
NO <sub>3</sub> <sup>-</sup>	823.2	82.3	8.23	0.82
Na <sup>+</sup>	4327	432.7	43.3	4.3
K <sup>+</sup>	629.4	62.9	6.3	0.6
Ca <sup>+2</sup>	409	40.9	4.1	0.4
NH <sub>4</sub> <sup>+</sup>	709.7	70.9	7.1	0.7
Cu <sup>+2</sup>	10.5	1.05	0.11	0.01
C <sub>6</sub> H <sub>5</sub> OCl 	35	3.5	0.35	0.04

- (3) In addition, blind samples for each concentrations without sorbent were prepared.
- (4) All samples were agitated in a rotational shaker at 20°C for 24 hours.
- (5) After completion, samples were centrifuged at approximately 3000 rpm for 20 minutes and the clean aqueous sorbate was decanted through Whatman® #42 ashless filterpaper into a clean polypropylene collection bottle.
- (6) Samples were analyzed according to the following schedule shown in table 7.5:

**Table 7.5** - Analytic Schedule of Ions & Compounds for Batch Sorption Experiment.

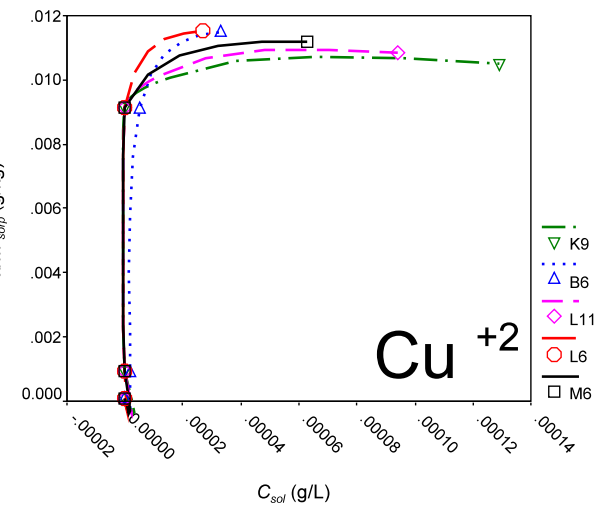
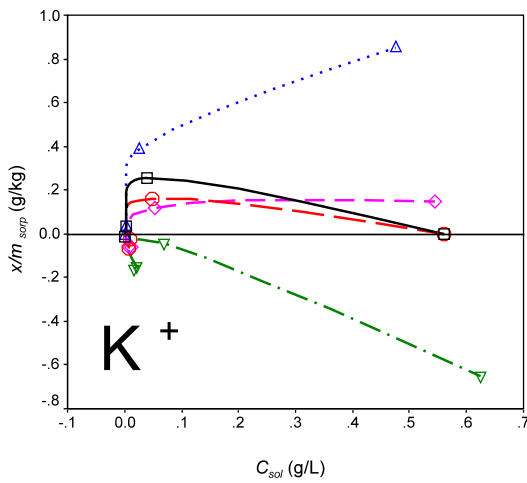
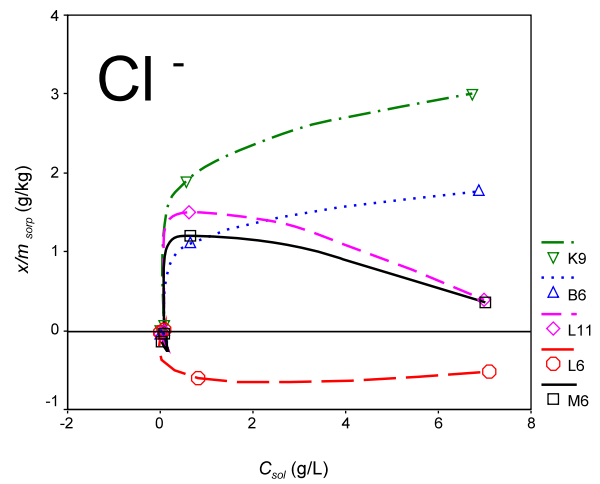
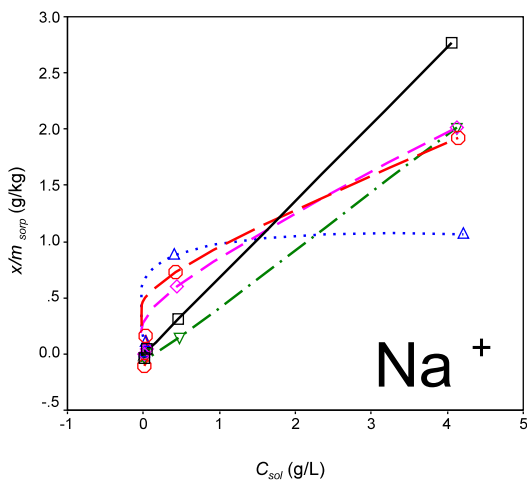
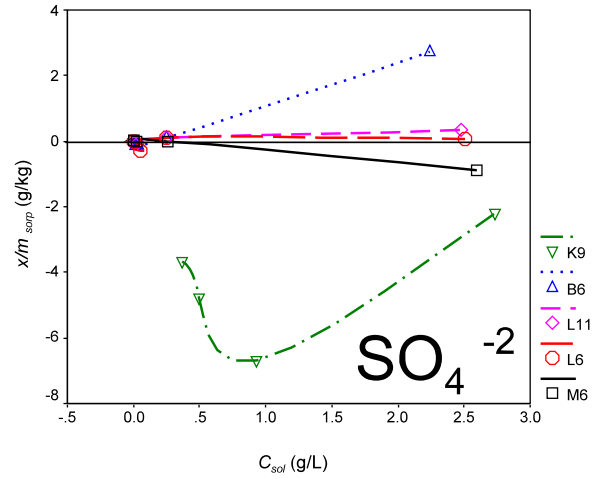
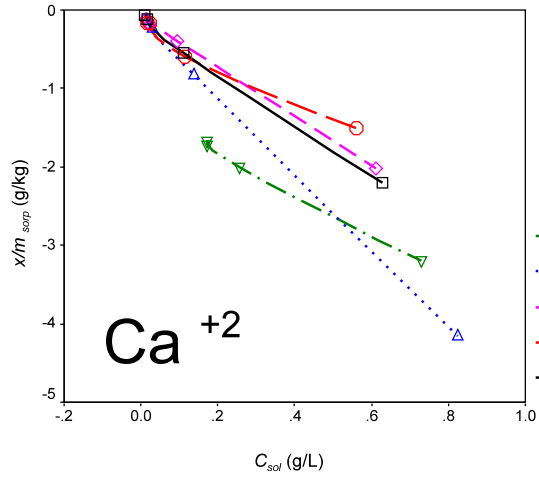
Ions & Compounds	Method
K <sup>+</sup> , Na <sup>+</sup> , Ca <sup>+2</sup> , Cu <sup>+2</sup>	ICP-AES; Group 2C Method ACME Analytical Laboratories, Canada
SO <sub>4</sub> <sup>-2</sup>	HACH DR/2000 Spectrophotometer; Method 8051, HACH (1996)
NO <sub>3</sub> <sup>-</sup>	HACH DR/2000 Spectrophotometer; Method 8039, HACH (1996)
Cl <sup>-</sup>	HACH DR/2000 Spectrophotometer; Method 8113, HACH (1996)
NH <sub>4</sub> <sup>+</sup>	HACH DR/2000 Spectrophotometer; Method 8038, HACH (1996)
C <sub>6</sub> H <sub>5</sub> OCl	HACH DR/2000 Spectrophotometer CHEMetrics® Inc., Phenol Vacu-vial Method K-8003

Results of the analysis are tabulated in appendix D.1.

- (7) Results of amount sorbed versus final amount in solution were plotted and interpreted for sorption mechanisms and common isotherms.
- (8) Interpretation was finalized by completing regression analysis of selected isotherms using SPSS Software (SPS, 1999) to evaluate best isotherm fit.  $K_d$  values were then calculated, compared, and the most likely  $K_d$  value indicated for each given sorbate - sorbent interaction.

### 7.5 Results of Sorption Analysis

When adding a highly concentrated ionic solution to samples of geologic barrier material, not all species in the solution will be equally sorbed. As can be easily ascertained, some species will evidently desorb, causing ionic sorption sites to be vacated for other competing ions. In contrast to CEC evaluations, this sorption test was not only concerned with cationic exchange systems, but with anionic interactions as well. The isotherms presented must thus always be viewed as part of a total complex system as would occur under realistic natural conditions and not as individual parameters. Liberal use of superscript or other indicators denoting total summative amounts of species in the artificial leachate indicate the complex nature of the system. In order to assess sorption isotherms, a graphical plot of the amount sorbed for a given sorbate species versus the final aqueous concentration of that species is necessary. The various resulting graphs are displayed in figure 7.5. A complete summary of all  $K_d$  values and their calculation procedures is given in appendix D.2. The *weighted average* reported below acts as an aid in the interpretation of sorption isotherms. The *average* represents the slope of a tangent to the isotherm at the origin and thus approximates the linear distribution coefficient  $K_d$ . The following will discuss individual ions & compounds of the artificial leachate and their individual sorption characteristics within specific geologic barriers.





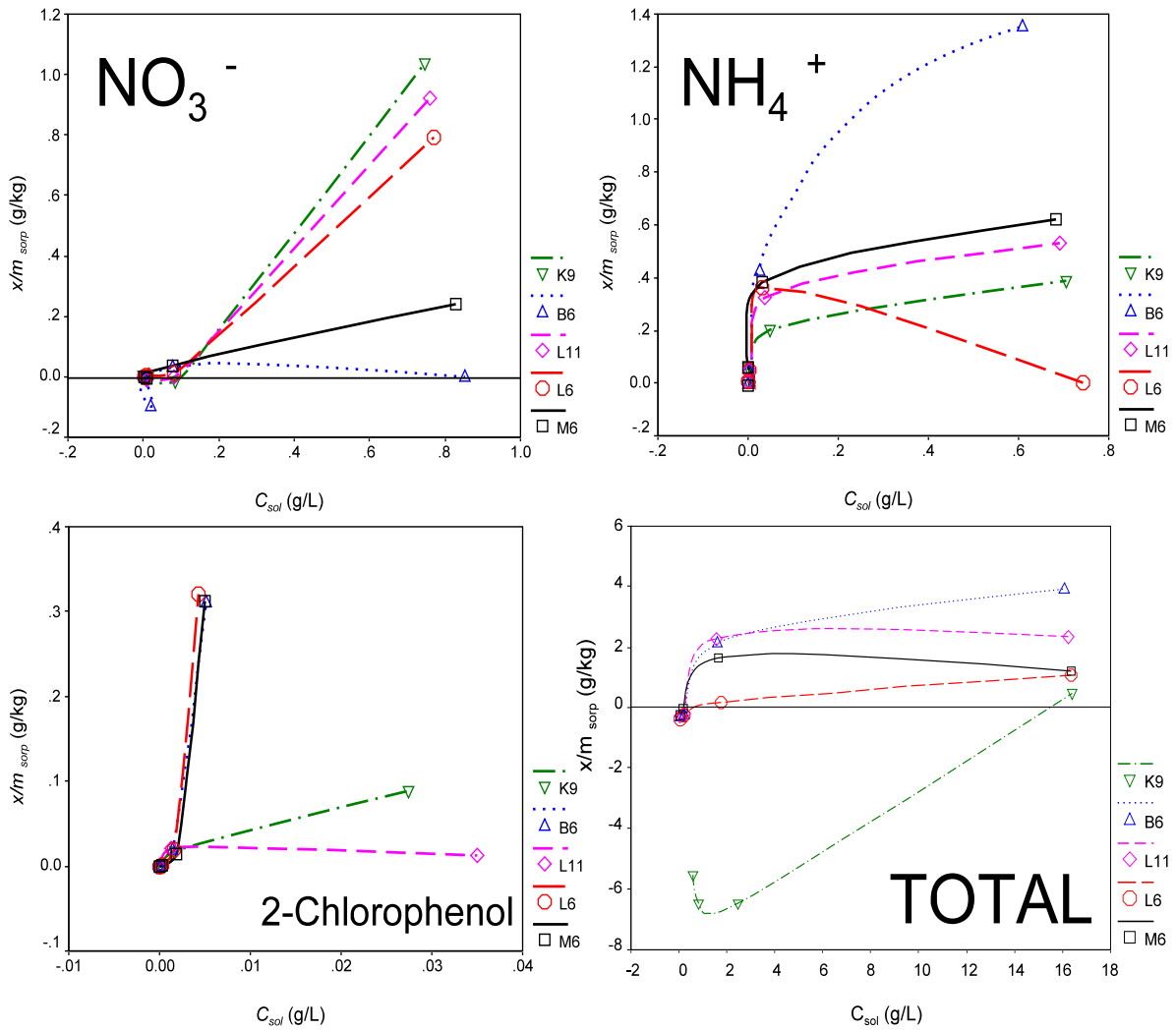


**Figure 7.5** - Plot of results of sorption experiments. Amount sorbed ( $x/m_{sorp}$ ) vs final concentration ( $C_{sol}$ ) of sorbate solution (Appendix D.1). Samples: M6 - Lower Röttone (6 m b.s.); L6 - Lehrberg Layers (6 m b.s.); L11 - Lehrberg Layers (11 m b.s.); B6 - Feuerletten (6 m b.s.); K9 - Amaltheen Clay (9 m b.s.).

### 7.5.1 Calcium

During the sorption experiments, dissolution of calcium from the sample material was observed in all cases. The greatest desorption of Ca with -4.9 L/kg occurred in the Feuerletten sample (B6) while the Lehrberg Layers show the lowest desorptive values ranging from -3.16 L/kg to -2.42 L/kg. With the exception of sample L6, calcium ions are most likely desorbed from montmorillonite-smectite clays in the sample. The concentration of Ca<sup>+2</sup> ions was 409 mg/L out of 16498.7 mg/L total

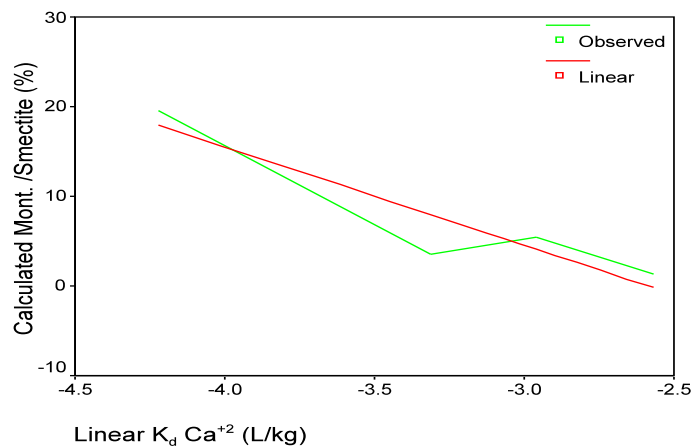


**Figure 7.6** - Relationship of linear Ca  $K_d$  and calculated montmorillonite./ smectite.

ions, while the ionic strength equates to 20.4 mmol/L out of a total I of 300.7 mmol/L for the artificial leachate. When the amount of this particular clay species from the mineral calculations is plotted against linear  $K_d$  values, exclusive sample L6, a discriminate linear correlation is observed as demonstrated in figure 7.6. As indicated by LANGMUIR (1997), both vermiculites and smectites have about 0.7 moles exchangeable interlayer cations. The amount of divalent cations, however, is greater in montmorillonites or vermiculites than in other smectites, where monovalent cations predominate. A summary of Ca- $K_d$  values is given in table 7.6.

**Table 7.6** - Calcium Sorption Coefficients for artificial leachate. Superscripts in header denote summative totals in undiluted artificial leachate.  $K_d$  superscript n = Freundlich constant.

Sample	Sorption Type	$K_d$	Weighted Average (linear $K_d$ )
M6	Freundlich desorption	- 3.18 <sup>n0.80</sup> L/kg	- 2.96 L/kg
L6	Linear desorption	- 2.42 L/kg	- 2.20 L/kg
L11	Linear desorption	- 3.16 L/kg	- 3.31 L/kg
B6	Linear desorption	- 4.93 L/kg	- 4.22 L/kg
K9	Freundlich desorption	- 3.67 <sup>n0.44</sup> L/kg	- 2.57 L/kg

### 7.5.2 Copper

The SLL concentration for  $\text{Cu}^{+2}$  was 10.52mg/L or 0.331 mmol/L for a total leachate concentration of 300.7 mmol/L. Copper ions exhibit the H-type or extreme Langmuir sorptive characteristics with very high values, indicating a very strong sorbate-sorbent relationship. Similar observations of high retardation in clays for Cu and other heavy metals were made by ALLARD *et al.* (1991). As discussed by MCBRIDE (2000), extreme chemisorption is the most likely scenario for the isotherms observed. Thus Cu sorption is very stable and shows a low adsorbate in relation to the amount of available sorbent material.

When correlating the representative  $K_d$  values with calculated mineralogy it is ascertained that copper sorption is clay dependent as indicated in figure 7.7. While DREVER (1982) ascertains that manganese oxides in soil show an aggravated affinity for heavy metals, the observation could not be confirmed since measured MgO did not correlate well with  $K_d$ -Cu values. On the other hand, montmorillonite-smectite and chlorite appear to favor heavy metal sorption while the illite-sericite group shows an adverse effect. It should be noted, however, that separating illite and sericite (muscovite) produces a slight positive and poorly defined correlation of illite to  $K_d$ -Cu while sericite displays

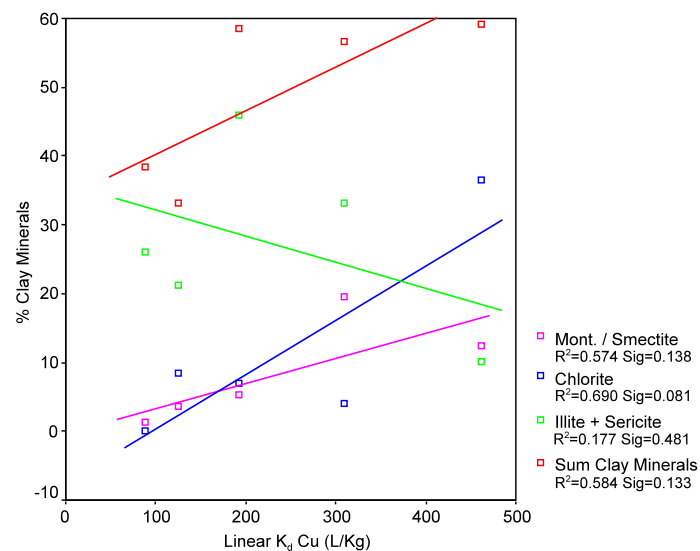


**Figure 7.7** - Plot of linear Cu  $K_d$  vs. calculated clay concentrations for samples used in the diffusion experiments. Linear correlations of regression analysis are indicated by lines of respective coloration.

a definite negative correlation. Hence for the results exhibited in figure 7.7, the contrary correlation in sericite overwhelmingly subdues the feeble positive correlation found in illite. The reason for this behavior is unclear. A likely explanation could be a larger grain size for illite and definitely sericite, decreasing the surface area of the clay particles and therefore being less favorable to pollutant sorption than the finer grained mineral relatives. The Feuerletten clay sample (B6) exhibits the greatest Cu-sorption affinity. The respective  $K_d$  values are exhibited in table 7.7.

**Table 7.7** - Copper Sorption Coefficients for artificial leachate. Superscripts in header donate summative totals in undiluted artificial leachate.  $K_d$  superscript M = Langmuir constant (max. sorption capacity)

Cu <sup>+2</sup> MW: 63.55g C <sub>leachate</sub> : 10.52 <sup>16499</sup> mg/L I <sub>leachate</sub> : 0.331 <sup>300.7</sup> mmol/L			
Sample	Sorption Type	$K_d$	Weighted Average (linear $K_d$ )
M6	H-type (Langmuir)	$9.7 \cdot 10^7 M^{0.010}$ L/kg	191.96 L/kg
L6	H-type (Langmuir)	$9.1 \cdot 10^7 M^{0.011}$ L/kg	461.24 L/kg
L11	H-type (Langmuir)	$9.9 \cdot 10^7 M^{0.010}$ L/kg	125.36 L/kg
B6	H-type (Langmuir)	$1.0 \cdot 10^{48} M^{0.010}$ L/kg	309.71 L/kg
K9	H-type (Langmuir)	$1.0 \cdot 10^8 M^{0.010}$ L/kg	88.63 L/kg

### 7.5.3 Potassium

The SLL has a concentration of 629.4 mg/L or I of 8.05 mmol/L for potassium out of a total 16499 mg/L total dissolved ionic pollutants. The sorption parameters are varied. A definite Langmuir or L type sorptive characteristic is observed in the Feuerletten clay (B6) and as H-type in one of the Lehrberg Layer samples (L11). The other lithologies exhibit either sorption and desorption characteristics as indicated in figure 7.5. Mineralogical correlations are very poor and were not displayed. A sketchy correspondence, however, was found between  $K^+$  and the montmorillonite-smectite group. The perceived distributions could be indicative of the competitive nature of the ions involved in the sorption process rather than characteristic mineralogy. While concentrations are low, adequate free exchange sites are available on the minerals involved. With increased ionic quantities, potassium may be replaced in favor of divalent cations. This, however, appears to be only a partial explanation, since Na, which has even weaker bonding affinities than K, demonstrates true sorption values and is unaffected by desorption. The original amount of exchangeable  $K^+$  present in the geologic barrier material and the ionic composition and concentration of the leachate must clearly play an important roll. Thus it is noteworthy, that during CEC evaluations, exchangeable potassium in the investigated samples

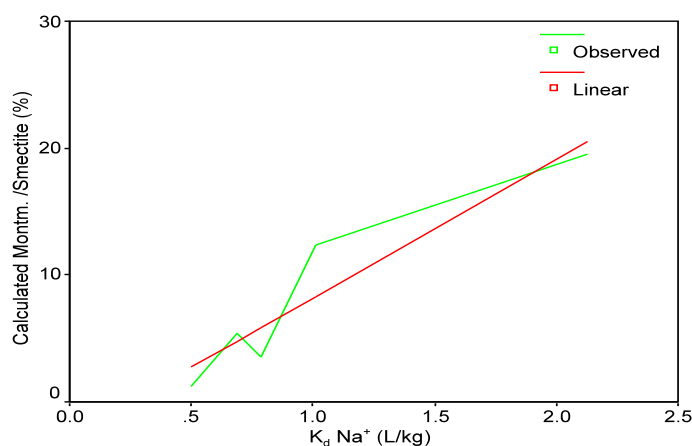


**Figure 7.8** - Relation of Na  $K_d$  to calculated montmorillonite./ smectite.

was two to three times more prevalent than exchangeable Na, excepted in the Lower Rötton sample (M6), where sodium prevailed. Notwithstanding, the exact processes are unclear since retardation is evaluated for the whole rock instead of discriminate values for individual mineral species.  $K_d$  values and sorption types are displayed in table 7.8.

**Table 7.8** - Potassium Sorption Coefficients for artificial leachate. Superscripts in header donate summative totals in undiluted artificial leachate.  $K_d$  superscript M = Langmuir constant (max. sorption capacity)

<b>K<sup>+</sup></b> MW: 39.102g $C_{\text{leachate}}$ : 629.4 <sup>16499</sup> mg/L $I_{\text{leachate}}$ : 8.048 <sup>300.7</sup> mmol/L			
Sample	Sorption Type	$K_d$	Weighted Average (linear $K_d$ )
M6	Sorption / Desorption	N/A	0.04 L/kg
L6	Sorption / Desorption	N/A	0.03 L/kg
L11	H-type (Langmuir)	38.02 <sup>M 0.140</sup> L/kg	0.26 L/kg
B6	L-type (Langmuir)	0.97 <sup>M 9.960</sup> L/kg	1.76 L/kg
K9	linear desorption	-0.88 L/kg	0 L/kg

#### 7.5.4 Sodium

Table 7.9 shows the Na<sup>+</sup>  $K_d$  values for the SLL and representative geologic barriers. A graphic rendition of the results is also shown in figure 7.5. The sodium concentration in a total leachate of 16400 mg/l equals 4327 mg/l or an ionic strength of 94.1 mmol/L. C-type or linear sorption is observed in Lower Rötton and Amaltheen clay samples indicating constant relative affinities of the sorbate for the sorbent and is usually observed at the low range of sorption (MCBRIDE, 2000). Chemisorption of the L-type is described in both samples of the Lehrberg Layers. The Feuerletten sample displays extreme Na chemisorption indicated by the H-type isotherm. Sodium correlates very nicely ( $R^2$ : 0.886; sig: 0.017) with calculated montmorillonite-smectite concentrations as displayed in figure 7.8. Because sodium in the artificial leachate has one of the highest ion activities, interactions at the exchange sites of the smectite mineral should predominate, leading to the retardations observed.

**Table 7.9** - Sodium Sorption Coefficients for artificial leachate. Superscripts in header donate summative totals in undiluted artificial leachate.  $K_d$  superscript n = Freundlich constant, M = Langmuir constant (max. sorption capacity)

<b>Na<sup>+</sup></b> MW: 22.98g $C_{\text{leachate}}$ : 4327 <sup>16499</sup> mg/L $I_{\text{leachate}}$ : 94.114 <sup>300.7</sup> mmol/L			
Sample	Sorption Type	$K_d$	Weighted Average (linear $K_d$ )
M6	C-type (Linear)	0.69 L/kg	0.61 L/kg
L6	L-type (Freundlich)	1.01 <sup>n 0.49</sup> L/kg	0.43 L/kg
L11	L-type (Freundlich)	0.79 <sup>n 0.81</sup> L/kg	0.49 L/kg
B6	H-type (Langmuir)	2.13 <sup>M 1.565</sup> L/kg	0.25 L/kg
K9	C-type (Linear)	0.50 L/kg	0.44 L/kg

7.5.5 Ammonium

The polyatomic ammonium cation has an ionic strength of 19.6 mmol/L out of 300.7 mmol/L total in the undiluted synthetic landfill leachate. Three of the samples, the Lower Röttone, the lower Lehrberg Layers, and the Amaltheen Clay, show extreme chemisorption marked by the H-type isotherm, with the later possessing the greatest sorption coefficient of 211 L/kg. The Freundlich L-type found in the Feuerletten sample is indicative of an abundance of still unoccupied sorption sites. Only sample

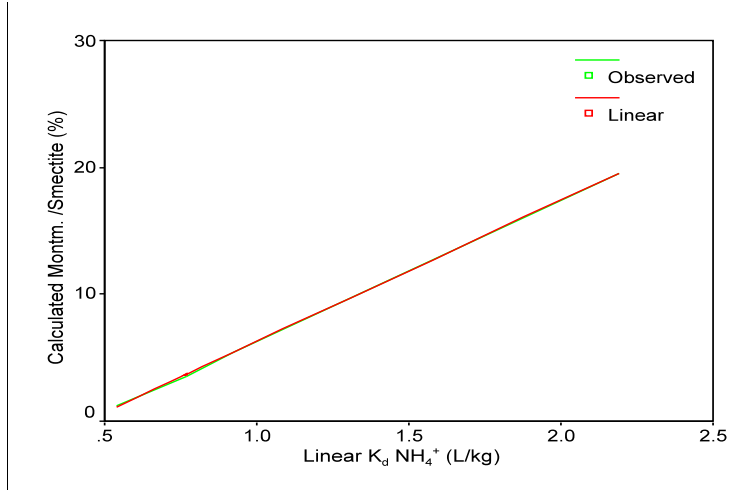


Figure 7.9 - Correlation of linear NH<sub>4</sub> K<sub>d</sub> with calculated montmorillonite./ smectite.

L6 displays sorption characteristics at low concentrations and desorption of already sorbed NH<sub>4</sub> ions at higher ionic strengths. When Ammonium-K<sub>d</sub> values are correlated with calculated mineral concentrations, the results are rather ambiguous. However, when removing sample L6 and then plotting linear K<sub>d</sub> versus montmorillonite-smectite a perfect match (R<sup>2</sup>: 1.000; sig: 0.000) is obtained as shown in figure 7.9. It is therefore postulated that NH<sub>4</sub> sorption is predominantly smectite clay controlled. A similar linear near perfect match was observed for organic carbon and calculated albite versus ammonium K<sub>d</sub> values. As discussed by LANGMUIR (1997), albite may show a pH-dependent surface charge, while carbon has a high affinity for ammonium. The complete results of sorption coefficients for ammonium are presented in figure 7.5 and table 7.10.

Table 7.10 - Ammonium Sorption Coefficients for artificial leachate. Superscripts in header donate summative totals in undiluted artificial leachate. K<sub>d</sub> superscript n = Freundlich constant, M = Langmuir constant (max. sorption capacity)

NH <sub>4</sub> <sup>+</sup> MW: 18.099g C <sub>leachate</sub> : 709.7 <sup>16499</sup> mg/L I <sub>leachate</sub> : 19.607 <sup>300.7</sup> mmol/L			
Sample	Sorption Type	K <sub>d</sub>	Weighted Average (linear Kd)
M6	H-type (Langmuir)	94.28 <sup>M0.561</sup> L/kg	0.92 L/kg
L6	Sorption / Desorption	N/A	0.05 L/kg
L11	H-type (Langmuir)	52.28 <sup>M0.517</sup> L/kg	0.77 L/kg
B6	L-type (Freundlich)	2.14 <sup>n 0.52</sup> L/kg	2.19 L/kg
K9	H-type (Langmuir)	211.14 <sup>M0.282</sup> L/kg	0.54 L/kg

7.5.6 Chloride

Chloride is the simplest anion present in the SLL and it's sorptive interaction can be seen in table 7.11 and figure 7.5. The concentration in the full strength leachate of 16499 mg/L is 7052 mg/L corresponding to an I of 99 mmol/L. The anion has therefore the highest ionic strength of all pollutants investigated. Most samples show sorption / desorption relationships with the chloride species, while Feuerletten and Amaltheen clay samples exhibit L-type or Freundlich isotherms. Lehrberg Layer sample L6 contributes additional Cl ions. It can be ascertained that this particular unit may contain additional chloride minerals such as halite or sylvite.

**Table 7.11** - Chloride Sorption Coefficients for artificial leachate. Superscripts in header donate summative totals in undiluted artificial leachate.  $K_d$  superscript n = Freundlich constant.

Sample	Sorption Type	$K_d$	Weighted Average (linear $K_d$ )
$Cl^-$ MW: 35.453g $C_{leachate}: 7052^{16499} mg/L$ $I_{leachate}: 99.458^{300.7} mmol/L$			
M6	Sorption / Desorption	N/A	0.06 L/kg
L6	Desorption/ Sorption	N/A	-0.07 L/kg
L11	Sorption / Desorption	N/A	0.06 L/kg
B6	L-type (Freundlich)	$1.19^{n0.20}$ L/kg	0.25 L/kg
K9	L-type (Freundlich)	$1.29^{n0.81}$ L/kg	0.43 L/kg

Anionic sorption depends on attraction toward oxide mineral or other positively charged surfaces, rather than clays which are negatively charged. According to DREVER (1982) the surfaces of said oxides and some other minerals are often terminated with hydroxyl (OH) groups. Thus in acidic environments the OH endings will accept a proton and become  $OH_2^+$ . A positively charged surface prevails, resulting in small CEC and a finite anion exchange capacity (AEC). Ion exchanges involving non-clay minerals are thus pH dependent. The isoelectric point (IEP) denotes the pH condition where the surface charges are balanced, usually identified as the level where CEC and AEC are zero (LANGMUIR, 1997). At the indicated pH level for the SLL of 6.16, LANGMUIR (1997) and DREVER (1982) list various positively charged minerals capable of anionic sorption, such as periclase ( $MgO$ ), gibbsite, rutile or anatase ( $TiO_2$ ), iron oxide species like hematite, goethite, and limonite, even sodium feldspar (albite). Potassium feldspar is probably at the isoelectric point at pH 6.16, therefore being most likely inactive in the ion exchange and sorption processes.

Nice correlations can be obtained between  $Cl-K_d$  and calculated hematite and gypsum concentrations as seen in figure 7.10. While chloride sorption on hematite is easily explained when considering the aforementioned, gypsum has its very own dynamic and can actually dissolve under a variety of conditions. However, as explained by KRAUSKOPF (1979), solubility of  $CaSO_4$  will decrease at the presence of its own ions in solution or when presented with a solution of  $CaCl_2$ . A solution-precipitation relationship of the sulfate mineral in the presence of the SLL appears to be an unlikely vehicle for the removal of leachate ions. It is expected that gypsum likewise exhibits positively charged surfaces.

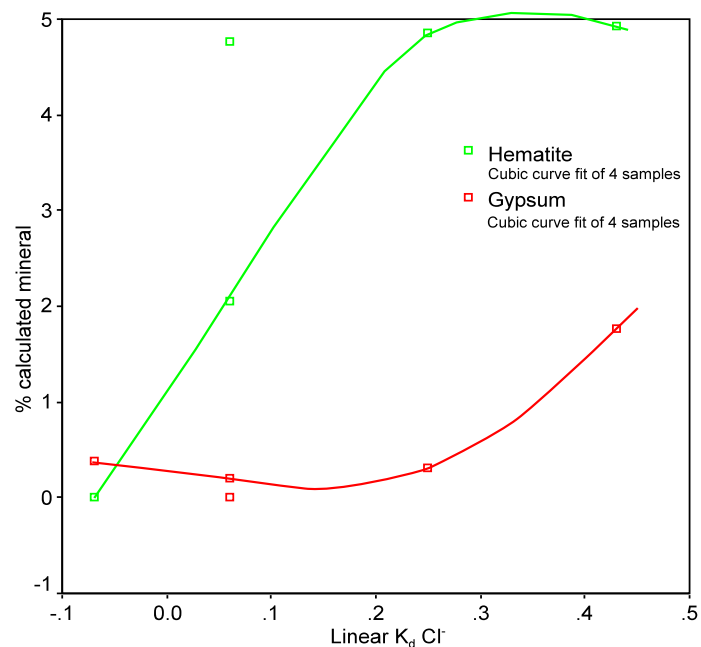


**Figure 7.10** - Linear  $Cl K_d$  vs. calculated hematite and gypsum. Curves indicate cubic fit for 4 selected samples.

7.5.7 Sulfate

The polyatomic sulfate ion ( $\text{SO}_4^{-2}$ ) has a concentration of 2502 mg/L out of 16,499 mg/L total dissolved ions in the SLL resulting in an  $I$  of 52.1 mmol/L. The results of the sorption batch experiment is summarized in table 7.12, as well as figure 7.5. Definite linear sorptive behavior was found only in the Feuerletten clay (B6). The Lehrberg Layer samples show an insignificantly small sorption, while the Lower Rötton and Amaltheen Clays are endowed with desorptive behaviors. The best correlation of  $K_d$ - $\text{SO}_4$  was found with calculated amount montmorillonite-smectite in the samples as indicated in figure 7.11. A possible explanation can be seen in figure 7.12 describing the replacement of double or neighboring surface hydroxyls on clay or oxide surfaces with preferred divalent sulfate ions from the solution. This explains the observed clay-anion correlation only for  $\text{SO}_4^{-2}$  but lacking in the other anions.

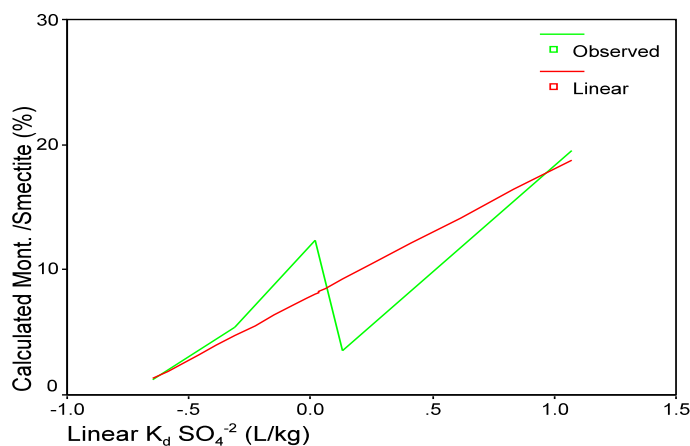


Figure 7.11 -  $K_d$ - $\text{SO}_4$  plot against calculated montmorillonite-smectite concentrations. Linear graph estimated from regression analysis.

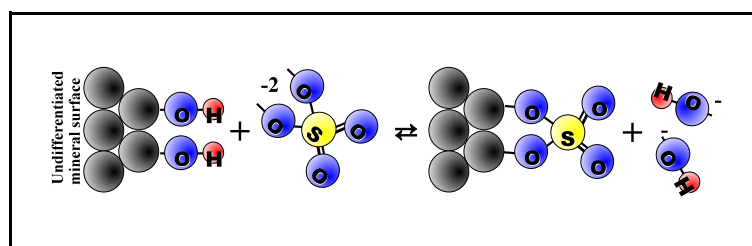
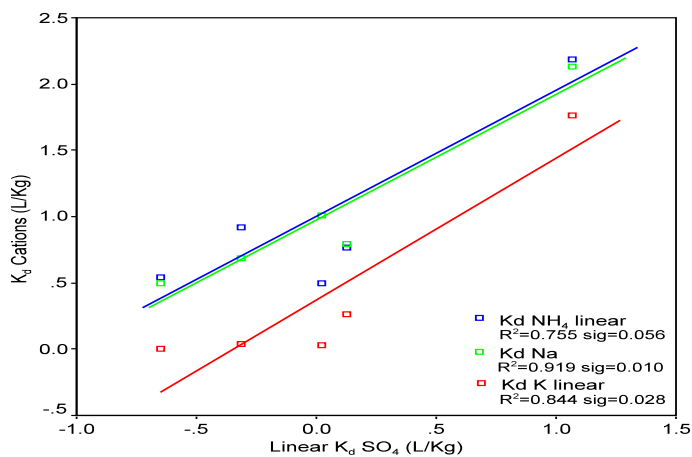


Figure 7.12 - Coordination phenomenon of surface hydroxyls being replaced by anions at the mineral & water interface according to SCHINDLER (1980) as shown in DREVER (1982).

Table 7.12 - Sulfate Sorption Coefficients for artificial leachate. Superscripts in header donate summative totals in undiluted artificial leachate.

$\text{SO}_4^{-2}$ MW: 96.057g $C_{\text{leachate}}$ : 2502 <sup>16499</sup> mg/L $I_{\text{leachate}}$ : 52.099 <sup>300.7</sup> mmol/L			
Sample	Sorption Type	$K_d$	Weighted Average (linear $K_d$ )
M6	very weak linear desorption	-0.35 L/kg	-0.31 L/kg
L6	no significant sorption	N/A	0.02 L/kg
L11	no significant sorption	N/A	0.13 L/kg
B6	C-type (Linear)	1.28 L/kg	1.07 L/kg
K9	Desorption/ Sorption	N/A	-0.65 L/kg





**Figure 7.13** - Linear  $SO_4$   $K_d$  vs. selected cationic  $K_d$  scatterplot with linear correlations indicated by lines of respective coloration.

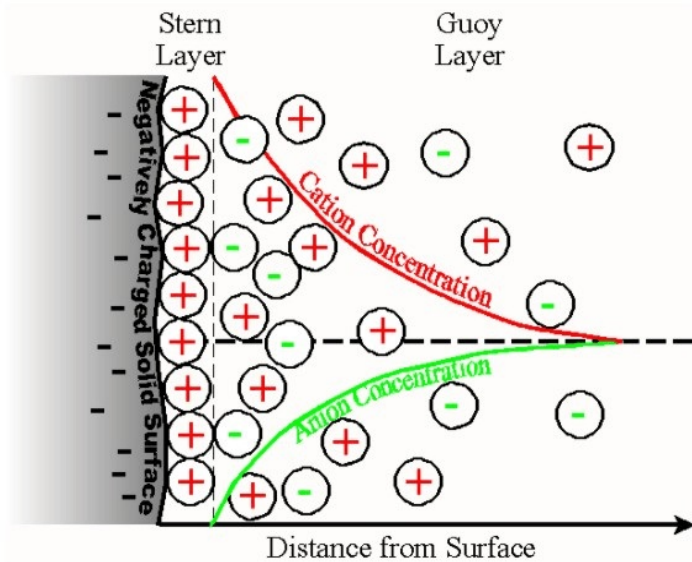


**Figure 7.14** - Schematic of Stern and Gouy layers with corresponding cation-anion concentration in the diffusive (Gouy) double layer. (after DREVER, 1982)

Another intriguing correlation is found when plotting  $K_d$ - $SO_4$  to  $K_d$  values of cations as displayed in figure 7.13. Here, the sorptive forces are indicative of electrical double layering resulting in *Stern* and *Gouy* layers. As described by Drever (1982), the solid surface of the negatively charged clay mineral is inundated by a layer of fixed cations, the so called *Stern* layer. With distance from the mineral surface, the electric potential decreases, leading to a diffusive or *Gouy* layer, where the concentration of unbalanced ions diminishes exponentially. DREVER (1982) indicates furthermore, that the stability and thickness of the Gouy layer depends approximately on the ionic strength of the solution. A weak  $I$  will result in electrostatic repulsion of similarly charged ions in the Gouy layer, while an increase in ionic strength will compress the diffuse layer, overcoming electrostatic repulsion in the molecules through the much greater van-der-Waals forces. This would explain the desorption / sorption phenomenon of  $SO_4$  indicated in the Amaltheen Clay sample and to a lesser extent the  $Cl^-$  behavior in sample L6. Interestingly enough, however, a similar correlation is not found for the monovalent anions. A graphical summary of the process can be viewed in figure 7.14.

#### 7.5.8 Nitrate

Results for sorption of nitrates ( $NO_3^-$ ) in the SLL are compiled in table 7.13 and graphically represented in figure 7.5. The polyatomic anion has an ionic strength of 6.6 mmol/L out of 300.7 mmol/L for the total artificial leachate, corresponding to 823.2 mg/L  $NO_3^-$ . All samples show linear sorption characteristics except the Feuerletten clay which indicates a very weak and almost negligible sorption / desorption characteristic. RYAN *et al.* (2001) indicates in his research that soils with significant nitrate adsorption showed an Al-rich allophane clay content compared with negligible  $NO_3^-$  adsorption in a more weathered, Si-rich allophane and halloysite clays. However, a similar observation relating to clay mineralogy in the samples investigated could not be made. Neither  $Al_2O_3$  concentrations as halloysite indicators nor their remainder after mineral calculations showed any correlation with  $NO_3^-$  sorption.

**Table 7.13** - Nitrate Sorption Coefficients for artificial leachate. Superscripts in header denote summative totals in undiluted artificial leachate.  $K_d$  superscript n = Freundlich constant, M = Langmuir constant (max. sorption capacity)

$\text{NO}_3^-$ MW: 62.065g $C_{\text{leachate}}: 823.2^{16499}$ mg/L $I_{\text{leachate}}: 6.632^{300.7}$ mmol/L			
Sample	Sorption Type	$K_d$	Weighted Average (linear $K_d$ )
M6	C-type (Linear)	0.29 L/kg	0.27 L/kg
L6	C-type (Linear)	1.05 L/kg	0.92 L/kg
L11	C-type (Linear)	1.25 L/kg	1.21 L/kg
B6	Weak sorption/ desorption	N/A	0.00 L/kg
K9	C-type (Linear)	1.44 L/kg	1.24 L/kg

KOWALENKO and YU (1996) suggest two types of anion adsorption, one where the process is not specific to the type of anion and the other where there is a particular affinity for a specific anion of group of anions. They conclude that nitrate adsorption occurs by the non-specific process and will cause nitrate to move slower than water in soil. Thus, nitrate sorption correlates poorly with calculated mineral as well as measured carbon and manganese oxide content individually. Hematite as a primary oxide with assumed positive surface charges did not correlate significantly with the sorption coefficient of interest. In the end, the best correlation for  $K_d\text{-NO}_3$  was obtained when the sum of MnO plus carbon is plotted against sorption as indicated in figure 7.15.

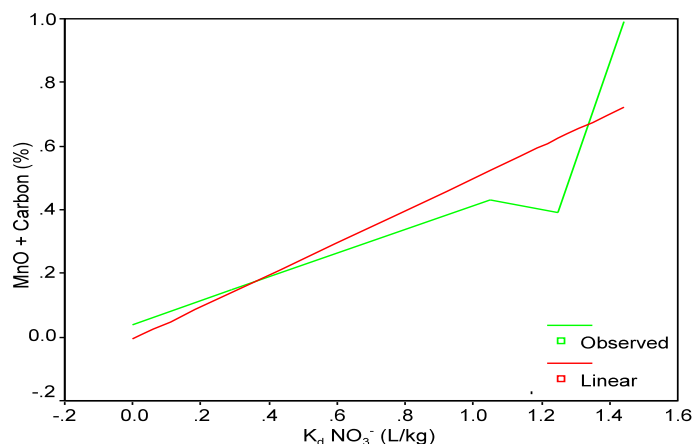


**Figure 7.15** -  $K_d\text{-NO}_3$  plotted against sum of measured carbon & MnO concentrations. Linear graph shown based on regression analysis.

These sorption observations are significant and correspond with findings of KOWALENKO and YU (1996). Their research on selected Canadian soils indicates that nitrate adsorption does occur contrary to the current notion that  $\text{NO}_3^-$  is not considered as a sorbing species, but is assumed to move freely with soil water.

#### 7.5.9 2-Chlorophenol

Chlorophenol is the organic representative in the SLL since phenols are the organic pollutants with the highest concentration in landfill leachates. It is represented with 35 mg/L out of 16499 mg/L total constituents in the artificial leachate. The sorptive characteristic in the Feuerletten, the Lower Rötton, and one of the Lehrberg Layer samples can be classified as a negative freundlich sorption isotherm. However, the “negative” effect on the graph is very subtle, leaving the impression of a linear correspondence (figure 7.5). Sorptive/ desorptive properties are found in sample L11, while the Amaltheen Clay is the only unit with a true L-type isotherm.

**Table 7.14** - 2-Chlorophenol Sorption Coefficients for artificial leachate. Superscripts in header denote summative totals in undiluted artificial leachate.  $K_d$  superscript n = Freundlich constant, M = Langmuir constant (max. sorption capacity)

<b>C<sub>6</sub>H<sub>5</sub>OCl</b>		MW: 128.56g	$C_{\text{leachate}}: 35^{16499}$ mg/L	$I_{\text{leachate}}: \text{N/A}$
Sample	Sorption Type	$K_d$	Weighted Average (linear $K_d$ )	
M6	Negative Freundlich	14115.62 <sup>n2.10</sup> L/kg	43.50 L/kg	
L6	Negative Freundlich	918.33 <sup>n1.59</sup> L/kg	52.68 L/kg	
L11	Sorption/ Desorption	N/A	0.37 L/kg	
B6	Negative Freundlich	619.01 <sup>n1.52</sup> L/kg	45.22 L/kg	
K9	L-type (Langmuir)	77.27 <sup>M0.09</sup> L/kg	3.10 L/kg	

Chlorophenols are observed to adsorb on organic matter, with the result that adsorption is strong in organic soils, but low in mineral soils (WHO, 1998). Hence estimating  $K_d$  values for organic contaminants from the soil organic fraction, which often ranges up to 10%, is a popular and verified approach. Problems are encountered, however, for subsurface lithologies as indicated in this study, where organic C concentrations are less than 1%. The correlation is much better when total carbon concentrations are used. As can be seen in figure 7.16, a quadratic correspondence is observed.

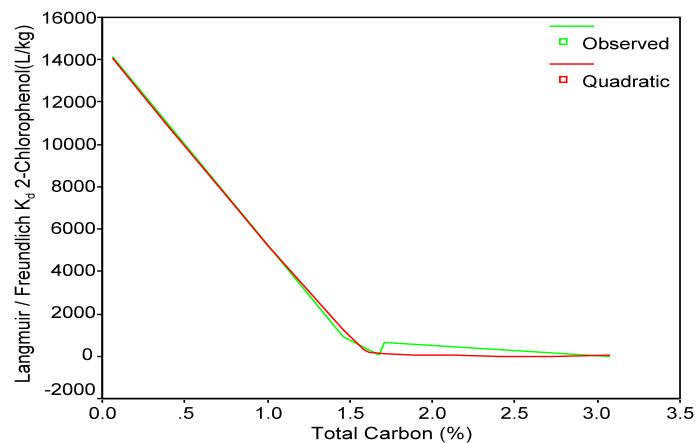


**Figure 7.16** -Total Carbon vs.  $K_d$  - Chlorophenol plot. Quadratic graph indicated by  $R^2 = 0.997$ , sig. = 0.003, and  $K_d\text{-Chlorophenol} = 14880.0 - (13391 * C\text{-total}) + (2782.52 * C\text{-total}^2)$ .

DiVINCENZO and SPARKS (2001) studied sorption mechanisms of parachlorophenol (PCP) on various soils and made an astonishing discovery. At soil/sorbate pH 4.0, PCP displays the characteristics of a hydrophobic ionizable organic compound (HIOC) and has a linear sorption isotherm. Increasing the pH level to 8.0 changes the organic compound to a neutral or protonated form resulting in a Langmuir sorption characteristic. Taking into consideration that 2-chlorophenol acts similarly, the popular  $K_d$  calculations for organic compounds using carbon concentrations were adjusted to include the pH value of the sample. The development of such a sorption isotherm equation for 2-chlorophenol is summarized in appendix D.3. The resulting equation is given as equation 7.11.

$$\text{Eq. 7.11} \quad K_d = \frac{K_{tc}}{f_{tc}} (-9934.9 + (2714.59 \text{ pH}) + (-183.82 \text{ pH}^2))$$

where  $K_d$  = Sorption Coefficient for 2-Chlorophenol  
 $K_{tc}$  = Sorption or Distribution Coefficient for Total Carbon  
 pH = Sorbent material pH  
 $f_{tc}$  = Weight percent of total carbon in sorbent material

Calculating  $K_d$  for chlorophenol according to equation 7.8, 7.9 and 7.11 yields the results summarized in table 7.15. When compared with experimentally determined  $K_d$  values it is more than obvious that the sample pH dependent equation 7.11 produces by far the best results, stressing in this case the inadequacy of calculations developed for soil parameters as applicable for rock lithologies. Hence carbon content alone does not account for the total 2-chlorophenol sorption observed.

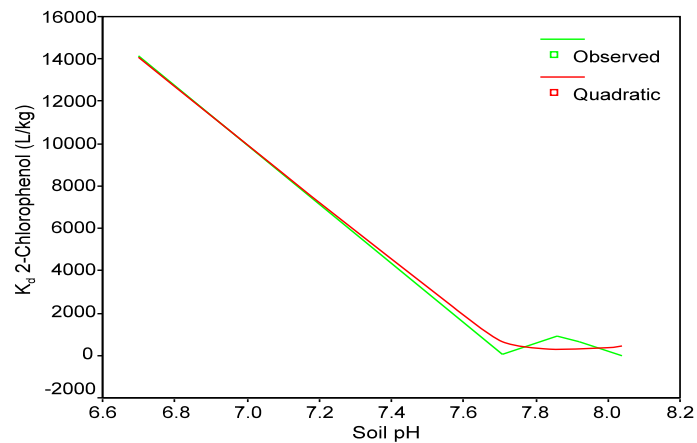


**Figure 7.17** -Graph of  $K_d$  2-Chlorophenol vs. soil pH. Quadratic curve fit shown by  $R^2 = 0.993$ , sig. = 0.007,  $K_d$  2-chlorophenol =  $597119 + (-151046 * \text{Soil pH}) + (9556.42 * \text{Soil pH}^2)$ .

**Table 7.15** - 2-Chlorophenol Sorption Coefficients for experimentally determined ( $K_d$ ,  $K_d$  linear) and calculated data according to equations 7.11, 7.8, and 7.9.

Sample	$K_d$	$K_d$ linear	Eq. 7.11	Eq. 7.8	Eq. 7.9
B 6.0	619.0	45.2	530.3	101.6	189.8
K 9.0	77.3	3.1	74.0	99.8	186.4
L 6.0	918.3	52.7	1123.2	86.7	162.0
L 11.0	0.0	0.4	0.3	183.0	341.8
M 6.0	14115.6	43.5	14175.8	3.6	6.7

Chlorophenol sorption depending on mineralogy should be far more prevalent since of the greater concentration of minerals in comparison with available soil carbon. Apparently soil pH again plays an important role in this process (see figure 7.17). The WHO (1998) indicates a variable absorption rate for 2-chlorophenol with acidic soils strongly binding the compound, while sorption is described as minimal under alkaline conditions. Further indication is given by ALY and FAUST (1964) that large amounts of clay were necessary to adsorb small quantities of 2,4-DCP in aqueous suspensions, even with pH 3.6-4.8. The soil pH relationship to the experimentally determined 2-chlorophenol sorption coefficient in this study becomes evident in figure 7.17. Here, minimal sorption is observed for soil pH values greater than 7.6, while a lower soil pH leads to a linearly increasing sorption coefficient.

DIVINCENZO and SPARKS (2001) ascertain an undeniable influence of clay minerals in the sorption of parachlorophenol. A similar pattern is observed when linear chlorophenol  $K_d$  values are plotted against the sum of calculated clay minerals as seen in figure 7.18. BØRRETZEN and SALBU (1999) concluded that sorption of neutral phenol species might predominated for carbon, while the ionized phenol species may be preferred by clay minerals and/or iron oxide, the later being pH dependent. Combining the previous observations and summarizing the results in figure 7.19, the results appear to be inconclusive. A

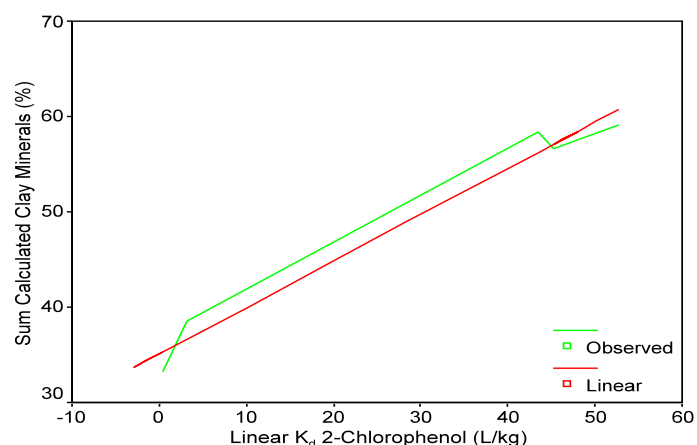


**Figure 7.18** -Total calculated clay minerals plotted against linear  $K_d$  - Chlorophenol. Linear correlation indicated by  $R^2 = 0.975$ , sig. = 0.002.

definite dependence on soil pH for the sorption of chlorophenol is indicated in the Lower Röttone sample (M 6.0). The  $K_d$  values also follow the total clay content very nicely. Total carbon content agrees with the elevated sorption in samples B 6.0 (Feuerletten), K 9.0 (Amaltheen Clay), and L 6.0 (Lehrberg Layers). Puzzling is the indicated slump for the Lehrberg Layer sample L 11.0, where total carbon is at its highest, but the sorption isotherm shows the lowest value. The reason for the pattern may be explained by SEIP *et al.* (1986) as quoted in WHO (1998) who concluded that chlorophenols bound to soils are continually turned over, and that binding sites may be saturated under the appropriate conditions, leading to increased mobility and a decreased residence time of chlorophenols in the sample. It should also be specified that chlorophenol is unlikely to act independent during the sorption processes, but will probably interact with the various constituents of the SLL.

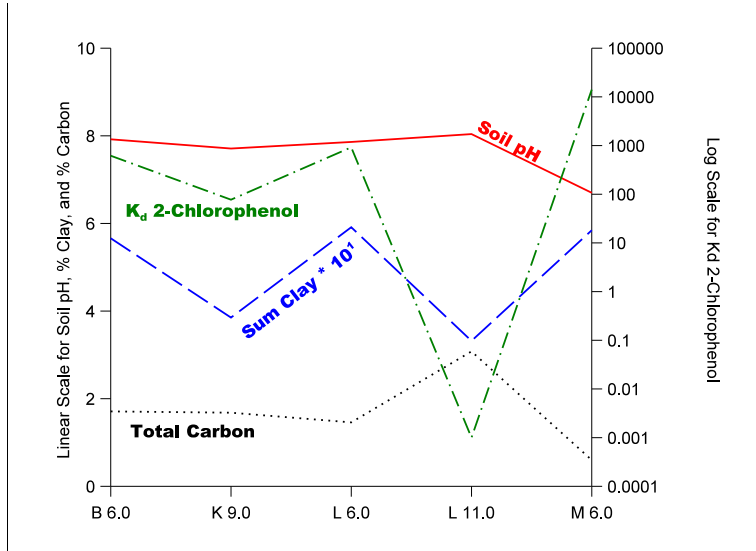


Figure 7.19 -Comparison of soil pH, % total carbon, % calculated clay and  $K_d$  - Chlorophenol for geologic barrier samples indicated.

7.5.10 Total Sorbent Components

The results of the sorption coefficients for the total SLL are exhibited in table 7.16. Here, the sum total of the  $K_d$  of all leachate species is represented. Because of the great variety of sorptive mechanisms, the presented data reveals the predominate form of sorption in a geologic barrier sample. Thus the Lower Röttone (M6) and one of the Lehrberg Layer samples exhibits an H-type Langmuir sorption isotherm, suggestive of a very strong adsorbate-adsorbent interaction (e.g. chemisorption). The L-Type Langmuir isotherm is displayed by the Feuerletten clay (B6), reflecting a relatively high affinity between the adsorbate and adsorbent, and is usually indicative of chemisorption according to MCBRIDE (2000). A linear or C-type isotherm belongs to the L6 sample suggesting a constant relative affinity of the adsorbate molecules for the adsorbent, is usually observed only at the low range of adsorption. It is also more common in physical sorption rather than chemical attributes (MCBRIDE, 2000). The Amaltheen Clay is the only geologic barrier unit with desorption characteristics at lower leachate concentration and sorptive behavior at higher sorbate amounts. It is therefore possible that the K9 sample has the greatest concentration of exchangeable ions as a possible sorptive mechanism. When compared to CEC parameters no correlation is evident unless the difference of the CEC sum of cations and CEC  $Ba^{2+}$  exchange is taken and compared to total  $K_d$  values as shown in

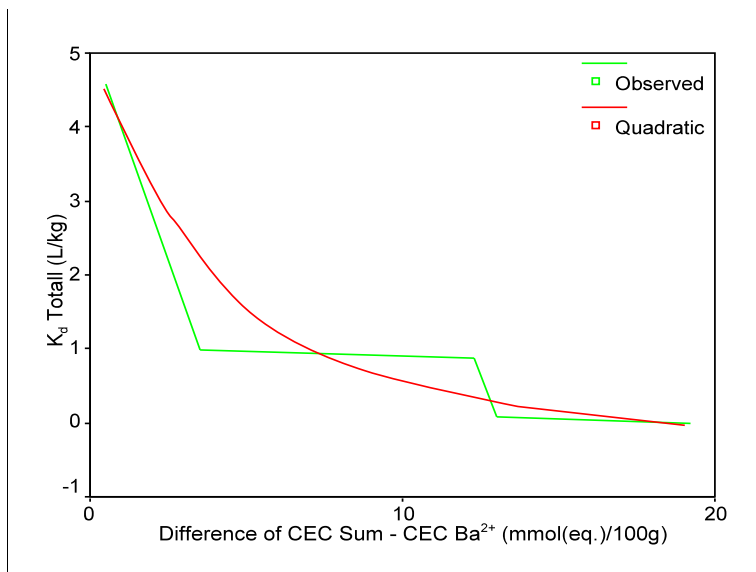


Figure 7.20 - Plot of  $K_d$  - Total against difference of CEC cation sum & CEC  $Ba^{2+}$ . Graph indicates Logarithmic correlation of  $R^2 = 0.912$ , sig. = 0.011,  $K_d$ -Total =  $3.3705 + (-1.2042 * \ln(\text{CEC difference}))$

figure 7.20. It can be assumed that the greater the difference in the two cation exchange capacities, the greater the ionic exchange of the geologic barrier and hence, the smaller the actual overall sorptive parameter. Bivariate Pearson's correlation of  $K_d$  values with cation exchange capacities are summarized in appendix D.4. A limited number of sorption isotherms can indeed be correlated directly with either the CEC  $Ba^{2+}$  or CEC cation sum. Among those are  $Cu^{2+}$ ,  $K^+$ ,  $Na^+$  and  $NH_4^+$ . Sulfate and calcium will only correlate with CEC  $Ba^{2+}$ , not with CEC sum. It is therefore believed that the ionic species mentioned will sorb with an ionic exchange mechanism, while all others are more likely to be subject to different sorptive parameters.

**Table 7.16** - Sorption Coefficients for total artificial leachate.  $K_d$  superscript M = Langmuir constant (max. sorption capacity)

<b>Total</b> MW: 505.956g $C_{leachate}$ : 16498.7 mg/L $I_{leachate}$ : 300.7 mmol/L			
Sample	Sorption Type	$K_d$	Weighted Average (linear $K_d$ )
M6	H-Type (Langmuir)	0.99 <sup>M 2.261</sup> L/kg	0.08 L/kg
L6	C-Type (Linear)	0.08 L/kg	0.06 L/kg
L11	H-Type (Langmuir)	4.57 <sup>M 1.407</sup> L/kg	0.14 L/kg
B6	L-Type (Langmuir)	0.87 <sup>M 3.954</sup> L/kg	0.23 L/kg
K9	Desorption / Sorption	N/A	-0.01 L/kg

## 7.6 Retardation

Armed with knowledge about sorption coefficients, the retardation factor (R) can now be calculated according to the previously introduced equation 7.1. According to DREVER (1982), R can be used to estimate approximately how rapidly an introduced pollutant may migrate. LANGMUIR (1997) explains that for  $K_d = 0$  and  $R = 1$ , no retardation is observed; for  $K_d = 1$  and  $R = 5$  to 11, a contaminant would move 9 to 20 % as far as the groundwater; for  $K_d = 10$  and  $R = 41$  to 101, the contaminant moves only 1% to 2.4% of the distance traveled by ground water during the same time. This observation can be mathematically summarized and results in transit time (t) based solely on advective transport of a pollutant species according to equation 7.12 given by SHACKELFORD (1993).

Eq. 7.12

$$t = \frac{L R}{v_s}$$

where

t	=	transit time
L	=	distance traveled
R	=	retardation factor
$v_s$	=	seepage velocity

The retardation and transit time data for the individual pollutant species in the SLL is displayed in appendix D.5. Overall, the heavy metal species  $Cu^{2+}$  experiences the greatest retardation in all geologic barrier samples and can be classified as immobile. The organic representative, 2-chlorophenol, exhibits similar retardation properties, with a drastic exception in Lehrberg Layer sample L 11. Ammonium is the third less mobile species in most geologic barriers, excluding samples L 6 (Lehrber Layers) and the Feuerletten clay where  $NH_4^+$  appears to be relatively mobile. The remaining chemical species show reasonable mobilities within the sample materials with sulfate being an oddity only in L 11. The geologic barriers with the least amount of retardation for specific pollutants with transient times of

2 days/cm or less are the Lower Rötton clays for K, Cl, SO<sub>4</sub>, and NO<sub>3</sub>; the L6 Lehrberg Layers for K, NH<sub>4</sub>, Cl, SO<sub>4</sub>, and total species; the L11 Lehrberg samples for Cl and SO<sub>4</sub>; the Feuerletten clay barrier for NO<sub>3</sub>; and the Amaltheen clay only for total pollutant species. The sodium retardation corresponds well with the values calculated by PÖTZL (1998) on same geologic barrier materials. However, discrepancies are found in his R estimations for phenol, which is almost classifiable as a non-sorbing species by PÖTZL (1998). The reason for this disagreement may be due to several factors:

- (A) differing compounds where PÖTZL (1998) uses phenol, while this study used 2-chlorophenol;
- (B) PÖTZL (1998) estimates R from column spiking experiments looking at recovering concentration, while this study calculated R values from experimentally determined sorption coefficients and physical parameters of the samples;
- (C) As a result of the various approaches in estimating retardation by both parties, PÖTZL (1998) most likely described a linear sorption isotherm, while this study exposed a negative Freundlich and Langmuir mechanism
- (D) PÖTZL (1998) worked with 0.01 and 0.05 mol/L phenol as a single pollutant, while this study experimented with much lower concentrations of 0.0003 mol/L 2-chlorophenol in a matrix of other chemical species.



8 Diffusive Transport through Clays

The movement of contaminant concentrations through various media is referred to as flux and usually entails fluid flow or migration through the subsurface as indicated by ZHANG and BENNETT (1995). While most contaminant transport models in coarser grained materials will favor hydraulic parameters and coupled flow processes, the situation changes drastically when finer grained materials with low hydraulic conductivities and Darcian velocities are considered. ROWE (1987) indicates that mechanical dispersion is insignificant to diffusive processes when the fluid flow is smaller or equal to  $3.17 \cdot 10^{-9}$  m/s. GILLHAM *et al.* (1984) as quoted in SHACKELFORD (1991) concludes that diffusion is dominant when the seepage velocity is around  $1.59 \cdot 10^{-10}$  m/s. Since this study is related to geologic barrier materials with physical properties that significantly retard fluid flow, the investigation of diffusive transport of contaminants through barrier clay samples was of predominant importance.

8.1 Diffusion principles

Diffusion is defined as the slow intermixing of two or more contacting substances without the influence of outside forces, but through the inherent individual motion of atoms, ions, molecules or colloids (NEUMÜLLER, 1977). Thus, two substances will slowly intermix on their own accord as illustrated in figure 8.1. The underlying premiss of diffusion is Fick's first law which is summarized as one directional flow or flux of the concentration of a substance as displayed by equation 8.1 (CRC, 1985):

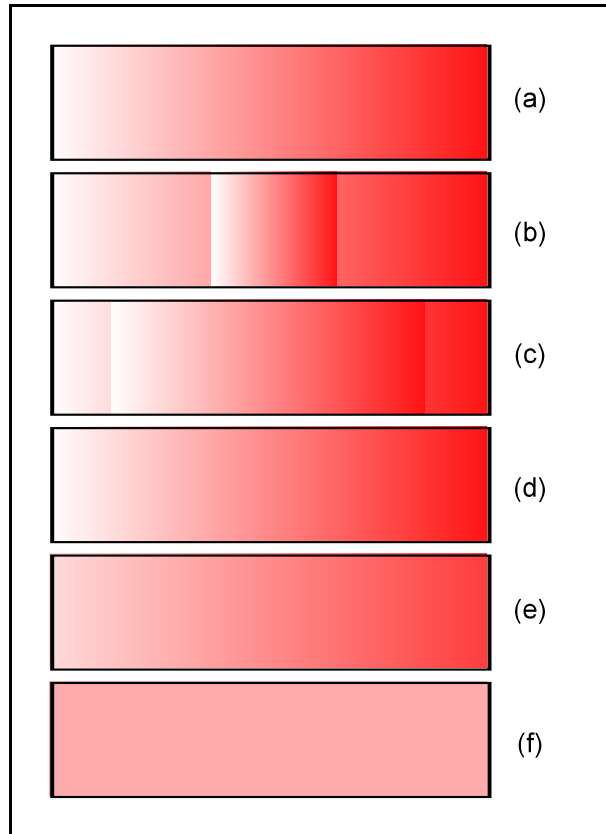


Figure 8.1 - Sequential illustration of diffusion process in a homogenous media from (a) through (f), where (f) is complete mixing.

Eq. 8.1

$$f = -D \frac{\delta C}{\delta x}$$

- where f = flux across a unit area perpendicular to flow direction x
- D = diffusion coefficient
- $\delta C$  = change in concentration
- $\delta x$  = change in distance

While the diffusion coefficient described above works well for homogenous materials, such as mixing of gases or solutions, it does not adequately delineate diffusion in soils. Here, porosity and transport path length play an important role to depict  $D_e$  or the effective diffusion coefficient.

Eq. 8.2

$$\tau = \left( \frac{x}{x_a} \right)^2$$

- where  $\tau$  = tortuosity factor
- x = straight line distance between two points in the soil
- $x_a$  = actual distance through tortuous pathways around grains between two points in the soil

The transport pathway of the contaminant through the sample is expressed by the tortuosity factor ( $\tau$ ) as described by equation 8.2 (SHACKELFORD, 1991). A graphical representation of  $\tau$  is given in figure 8.2. SHACKELFORD and DANIEL (1991a) report  $\tau$  values for saturated soils anywhere from 0.025 to 0.57. The tortuosity factor, however, is very difficult to establish. Indeed, SHACKELFORD (1991) writes that there are currently no satisfactory methods to determine  $\tau$  independently. An effective diffusion coefficient ( $D_e$ ) for saturated soils is therefore defined, as can be seen in equation 8.3, which includes the effects of tortuosity.

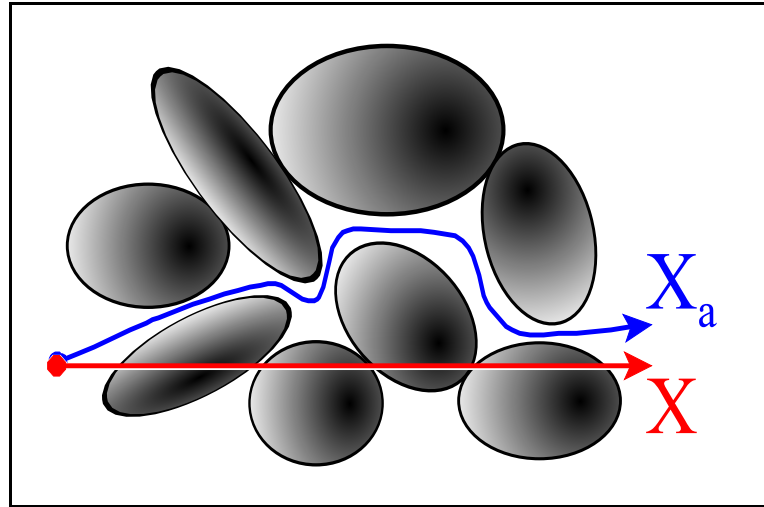


**Figure 8.2** - Graphical representation of tortuosity for contaminant transport around soil particles. See also equation 8.2, where  $x$  is the straight line distance between two points in the soil matrix and  $x_a$  is the actual length of the tortuous pathways around grains between same two points.

$$\text{Eq. 8.3} \quad D_e = D\tau$$

where  $D_e$  = effective or observed diffusion coefficient  
 $\tau$  = tortuosity factor  
 $D$  = diffusion coefficient for free-solutions or aqueous diffusion coefficient

In order to apply Fick's first law of diffusion toward saturated soils, the porosity of the medium through which a contaminant might diffuse needs to be also included. Hence equation 8.1 can be rewritten as follows:

$$\text{Eq. 8.4} \quad f_d = -D_e n \frac{\delta C}{\delta x}$$

where  $f_d$  = diffusive flux across a unit area perpendicular to flow direction  $x$   
 $D_e$  = effective diffusion coefficient  
 $n$  = porosity  
 $\delta C$  = change in concentration  
 $\delta x$  = change in distance

While equation 8.4 now adequately describes the diffusion of a non-sorbent chemical species through a non-reactive medium, it must be considered that sorption plays a major role in subsurface contaminant transport processes. QUIGLEY *et al.* (1987) as quoted by SHACKELFORD (1991) describes the  $D_a$  or  $D_s$  diffusion factors as follows:

$$\text{Eq. 8.5} \quad D_s = D_a = \frac{D_e}{R}$$

where  $D_a$  = apparent diffusion coefficient  
 $D_s$  = effective diffusion coefficient of the reactive solute  
 $D_e$  = effective diffusion coefficient  
 $R$  = retardation coefficient

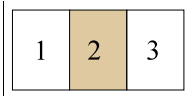
It should be noted that the influencing sorption characteristics in equation 8.5 will vary according to the type of geologic barrier tested. As reported by SHACKELFORD and DANIELS (1991 a+b) it is therefore necessary to always report associated  $R$  values when presenting  $D_a$  or  $D_s$  coefficients.

8.2 Laboratory Diffusion Experiments

Several laboratory methods were developed to measure diffusion coefficients in porous media. Most diffusion experiments can be divided into two common basic types which are (a) in-diffusion (ID) and (b) through-diffusion (TD) techniques (CHO et al., 1993). During ID testing, a sample is placed adjacent to the source leachate reservoir. While the experiment progresses, the concentration of the leachate diminishes in the source, while concentration in the sample increases. After conclusion of the ID-test, the sample is often sectioned and a concentration profile within the specimen is established, if no collection or receptacle reservoir was used adjacent to the lower end of the sample. If a receptor reservoir is part of the experiment, it may be sampled concurrent with the source reservoir at regular time intervals to establish a leachate species concentration profile over time.

In the TD experiment the sample is sandwiched between a source and a collection chamber. The source reservoir is maintained at a constant high leachate concentration. In turn, the collection chamber commonly contains distilled water and is monitored at regular intervals to establish the arrival of the various leachate ions or chemical compounds. When the activity of the leachate chemicals in the collection reservoir becomes constant with time, a steady state condition of diffusion is reached and the experiment is terminated. Again the sample might be dissected and concentrations are profiled.

**Table 8.1** - Summary of various diffusion testing methods and their advantages and disadvantages according to SHACKELFORD (1991). The method used in this study is highlighted.

Method	Description 1 = source, 2 = sample 3 = collection, C = chemical concentration			Advantage	Disadvantage
Steady-State	TD method where $C_1 > C_2$ . Experiment continues until $\delta C_1/t = \delta C_2/t$			No need to know R. Samples can be presaturated with contaminant	Contaminant C in 1 to be constant. Excessive time required.
Time-lag	TD method where $C_1 = \text{high}, C_2 = 0, \text{soil } C = 0$ . Evaluated as plot of Q vs. t.			Less control of test conditions than steady state.	R must be known. Very long testing periods.
Transient Column	Constant source concentrations. 3 = porous plate. Constant flow from 1 to 3 established. Then constant C in 1 injected.  Decreasing source concentration. 3 = porous plate. Source allowed to percolate through sample to 3. $C_1$ not replenished			Widely used, lots of previous experience. POLLUTEv6 used to evaluate data.	$D_e$ must be separated from dispersion caused by flow or $v_s$ must be very low. " $n_e$ " must be known. Very long test durations
Transient half cell	ID method. 1 = soil mixed with leachate, 2 = sample soil, 3 = absent. $C_1$ decreases, $C_2$ increases. Samples dissected & profiled.			Preferred method. Easy to administer. Lots of data available.	Not appropriate for undisturbed or very large samples. Plugs must be dissected.
Transient double reservoir	Constant source concentration. ID method. 1 = source, 2 = sample, 3 = collector. $C_1$ kept constant, 3 regularly sampled.			$D_e$ = hydrodynamic distribution coefficient since $v_s = 0$ . No need to dissect samples. TD conditions not necessary, easier to perform & shorter test durations than TD. POLLUTEv6 used to evaluate data.	Samples presaturated with $H_2O$ = long test prep. Labor intensive & time consuming to keep $C_1$ constant.
	Decreasing source concentration. ID method. 1 = source, 2 = sample, 3 = collector. 1 initially stocked with leachate C, 1 & 3 regularly sampled.				Samples presaturated with $H_2O$ = long test prep.
Transient single reservoir	Constant source concentration. Same as double but with 3 removed.			$D_e$ = hydrodynamic distribution coefficient since $v_s = 0$ . TD conditions not necessary, easier to perform & shorter test durations than TD. POLLUTEv6 used to evaluate data.	Samples presaturated with $H_2O$ = long test prep. Dissection needed. Labor intensive & time consuming to keep $C_1$ constant.
	Decreasing source concentration. Same as double but with 3 removed.				Samples presaturated with $H_2O$ = long test prep. Dissection needed.

Possible adaptations for the above mentioned methods could result in significant improvements for determining diffusion coefficients. ROWE *et al.* (1988) for example introduces a non steady state TD system that allows

independent evaluation of sorption coefficients as well. This is especially advantageous when trying to evaluate retardation of pollutants in geologic barriers below waste disposal sites. SHACKELFORD (1991) gives a detailed description of various adaptations, methods, and experimental set-ups currently used in diffusion testing to the two systems described above, as well as their advantages and disadvantages. Table 8.1 summarizes his findings and the various applicable diffusion testing methods.

The method of choice for this study was the transient double reservoir ID method with decreasing source concentration. From the numerous advantages given in table 8.1, two were of primary importance. First, it was not necessary to dissect the sample plugs after the experiment, which is applicable for soft disturbed clay samples, but rather difficult with the undisturbed solid lithologies of the geologic barriers. Besides, the risk of contamination for low concentrations of involved leachate species during the dissection process is rather high. Secondly the software POLLUTEv6 (GAEA, 1997) could be utilized for rapid evaluation of collected diffusion data. The only drawback was an extensive sample preparation of up to one year in order to presaturate the plugs for the diffusion experiment.

### 8.2.1 Diffusion Apparatus

Paramount for this study was the development and engineering of a diffusion test chamber to accommodate the decreasing source transient double reservoir ID method discussed earlier. The required characteristics can be summarized as follows:

(A) A totally translucent system that allows visual monitoring of the complete system including the sample chamber with clay plug. This is advantageous for future studies when diffusion of dyes might be required. It also may help to identify any discoloration in the sample caused by the reaction of the synthetic landfill leachate (SLL) with the sample material

(B) The cell and reservoir attachment to the diffusion cell should be interchangeable. This would allow adding specialized equipment for the pre-saturation of clay plugs.

(C) Since samples were not to be dissected after the experiment because of contamination problems and material consistency, another system was devised to approximate the advancing diffusion front through the clay plug. Each plug was to be implanted with 3 small electrodes for electric conductivity measurements along the length of the sample.

(D) All systems except the clay plug itself should be reusable, especially the source and receptor reservoirs, as well as sample cell holders.

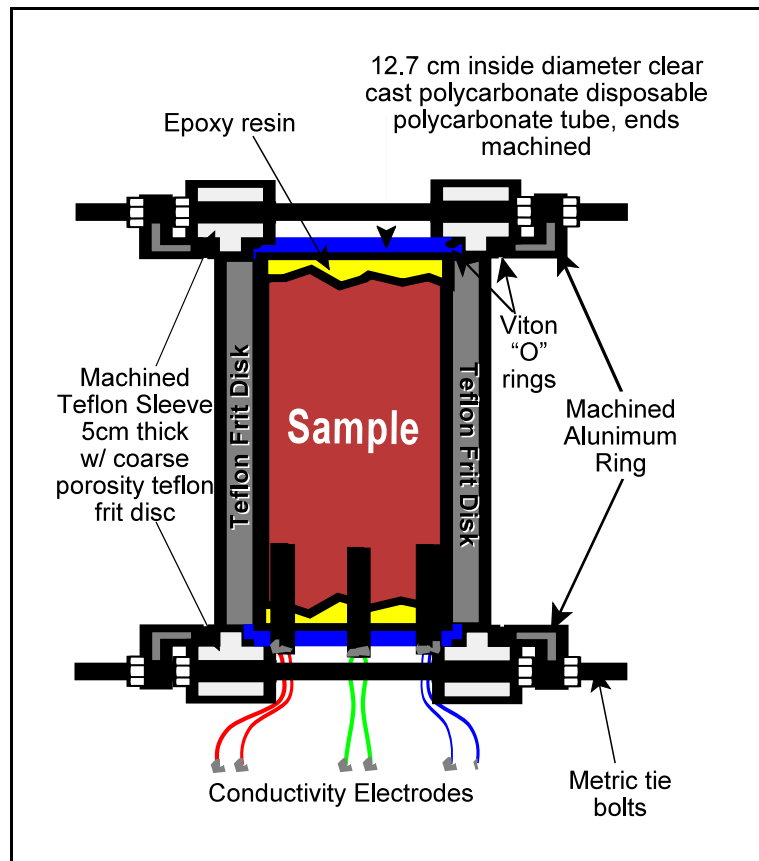


Figure 8.3 - Engineering detail of sample plug holder for diffusion apparatus.

(E)The reservoirs were to be easily accessible in order to maintain fluid levels and/or collect samples without disturbing the clay plugs themselves.

In order to meet the above requirements, a sample holder was constructed out of two machined aluminum rings. These rings would clamp down on a 5.0 cm long, 12.7 cm inside diameter disposable sample chamber made of clear cast polycarbonate tubing. The chamber was mounted via two 5 cm thick, circular Teflon sleeves with coarse porosity 2.5 cm Teflon frit disks fitted snugly and sealed hermetically to any interchangeable equipment by viton "O" ring seals. Samples are attach to the polycarbonate sleeves by epoxy resin as described below. A detailed drawing of the sample holder is given in figure 8.3.

Several interchangeable attachments were engineered and can be mounted to the sample holder either vertically or horizontally. A summary of these attachments is shown in figure 8.4. Attachment marked (a) in the drawing is a vertical 2 L cylinder, which can be used for saturation, falling head hydraulic conductivity testing and presaturation of the plugs. It may also be employed for other diffusion tests as described in table 8.1. Figure 8.4 (b) are the actual diffusion testing attachments adopted for this experiment. Mounted on both sides of the horizontally aligned sample chamber, one became the source reservoir, the other the receptor vessel. Both attachment can hold 1 liter of liquid respectively. Attachment labeled (c) in the figure is a glass funnel with a Teflon valve to be mounted either in the vertical or horizontal position. Originally designed to allow high gradient pressures, it failed in it's intended application, by either popping out during the pressurized phase or shattering from being mounted to tightly. It was used as a funnel during presaturation testing and hydraulic conductivity evaluations.

#### 8.2.2 Sample Preparation , Procedures, and Data Collection

Most of the geologic barrier cores available had slowly dried during the 4 years in a temperate storage chamber and deemed unusable for the intended study. A few coring sections however appeared to have adequate moisture contents to be utilized. From these limited sections about 35 initial sample plugs were selected for the experiments according to the following two criteria: (A) The samples should have no fractures or show visible shrinkage

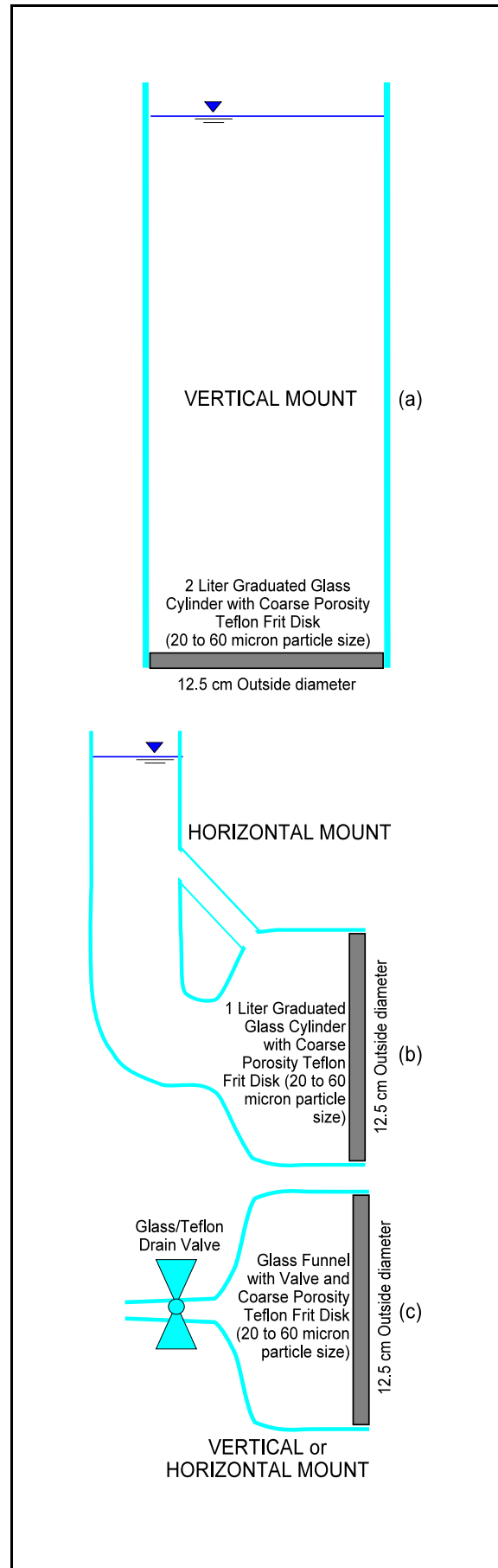


**Figure 8.4** - Various interchangeable attachments to be mounted to sample plug holder depicted in figure 8.3.

distortions and (B) core plugs should be in the depth vicinity of those used for previous hydrologic experiments (PÖTZL, 1998) for easy data comparison and utilization.

After the initial selection, core samples were sliced with a large flat blade chisel into 2 to 5 cm thick plugs. Sample chips above and below the created plugs were collected for destructive x-ray, SEM and thin-section studies as well as geochemical analysis and sorption experiments. Approximately half of the plug material was mounted into clear polycarbonate sleeves by epoxy resin as follows, while the other half was left in an unmounted state.

In order to affix the samples, each plug is first fitted with three separate electrodes at about equal distances along its thickness. These probes are made from 3mm long gold coated double pins with a gap of 2.54 mm and attached to color coded wires. Some geologic barrier materials were too hard for the needle-like spikes to be inserted by simply pushing them into the sample. In this case, small holes were pre-drilled using a diamond bit prior to inserting the probes. Thus prepared, the sample is then fastened in a clear cylinder by pouring resin EP 116 (Höchst GmbH) and hardener VEH 2628 (Höchst GmbH) in a mixture of 100 g to 41.3 g respectively in the space between the disposable polycarbonate sleeve and the sample. The resin was excellently suited for the intended application, setting within 60 minutes and will cure in wet environments. The hardened product is virtually transparent, has an outstanding chemical resistance and most important, is inert to ion exchanges, as established during this study through batch experiments. described below.

Both mounted and unmounted samples were then placed for 6 to 9 months in sealed basins filled with distilled water for saturation. It was noted that several of the plugs were destroyed during this process by crumbling or disintegrating. Since only a limited amount of material was available, destroyed samples could not be replaced. Surviving unmounted samples were now also prepared by affixing them into the clear sample holders as described above.

Usable samples were placed in a vertical position with the 2 L graduated cylinder attachment (figure 8.4[a]) on top. The bottom of the sample holder received the glass funnel as seen in figure 8.4[c]. The graduated cylinder was filled with distilled water and the sample was placed into a climate chamber at 10°C. The flow of the water was monitored and it was established if saturated conditions were achieved. Another set of clay plugs was destroyed during this phase of the experiment. Samples remained for another 1 to 2 months in this hydraulic flow set-up before switching the system to the diffusion attachments as depicted in figure 8.5.

During the diffusion phase, the sample holder is mounted in a horizontal position, and the diffusion reservoirs depicted by figure 8.4[b] are attached to each end of the sample. A visual representation of the set-up is given in figure 8.5. One of the reservoirs acts as a source and is filled with 1 L of SLL or LiBr solution, the other reservoir serves as the collector and contains 1 L of distilled water. A small amount of 10 mL is removed from each chamber at predetermined time intervals of a few days and kept in cold storage until analyzed for chemical species. Diffusion testing was performed in climate chambers at 10°C. The temperature is according to DIN 18 130 TEIL 1 (1989)

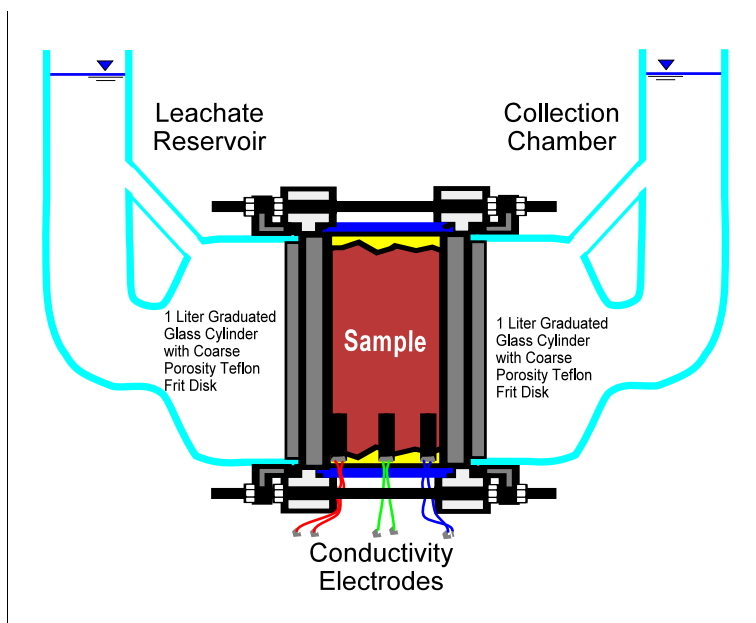


Figure 8.5 - Sample cell set-up during diffusion experiment.

for evaluation of hydraulic conductivities and represents conditions to be expected in subsurface lithologies a few tens of meters from the surface. In reference to KOHLER and HARSTRÖM (1994), who suggest that active landfills can reach internal temperatures of up to 90°C, a few diffusion experiments were either conducted or concluded at elevated temperatures of 30°C.

As indicated earlier 10 mL samples were taken from the source and receptor reservoirs at time interval  $t$ . The collected fluid samples were analyzed as follows:

1. Li, Br, Cl, SO<sub>4</sub>, NO<sub>3</sub>, NH<sub>4</sub>, CPL (Chlorphenol) by UV/Vis spectrometer
2. Anion concentration also occasional confirmed by HPLC
3. Na, K, Ca by flame photometer
4. Cu by AAS

All concentrations are recorded in mg/L and results are summarized in appendix G.1 and G.2. Of the original 35 samples, only 7 survived and their diffusion results formed the basis for the end product of this research.

### 8.3 Data evaluation and modeling using POLLUTEv6

One of the biggest problems in determining diffusion in lithologic samples is the effect of  $K_d$  on  $D$ . While the determined coefficient  $K_d$  from batch experiments gives a good indication of the sorptive behavior for involved sorbate species and sorbent materials, it often has a poor resemblance to sorptive behaviors within the limiting porosities of solid samples. Using these established sorption coefficients in diffusion modeling yields very often results that will not match the test data. The influence of varying porosities, anion exclusions, osmotic pressures, and/or ion exchanges in the sample plugs will often result in very dissimilar  $K_d$  values. To resolve this caveat it would be preferable to model  $K_d$  and  $D$  simultaneously from only the diffusion test data. As described by ROWE *et al.* (1988 & 1994) this can be successfully accomplished by using the software POLLUTEv6. Here,  $D$  and  $K_d$  are adjusted until a match with sample data is observed. This approach permits very accurate calculation of concentration in only a few seconds on a computer and hence is well suited for use in interpretation of the results of column tests (ROWE *et al.*, 1988).

POLLUTEv6 uses the algorithms described in section 8.1 for the computation. Additional mathematical considerations are explained below. The first step in using the program is to consider the type of input parameters required. The following segment describes the input data used for the computations.



### 8.3.1 POLLUTEv6 input parameters

Number of layers and sublayers. Layers are utilized to input variations in hydraulic parameters within a sample. Since the clay plugs were considered to be uniform, no further action is required. An input of the number of sublayers is used in the output of calculated concentration profile through the sample plug and are not necessary if only the concentrations on top and below the sample are considered. Sublayers were initially modeled to approximate the approaching diffusion front with the change in conductivity of the imbedded electrodes in the samples. Because of the high degree of inaccuracy in identifying the arrival of individual chemical species at the electrode interfaces, sublayers were not recorded in data summaries.

Thickness of the sample. Sample thickness is inputted in centimeters.

Dry density. Dry density was entered as  $\text{g/cm}^3$  according to data given in appendix D.5.

Porosity. The input parameter of porosity into the software model can be either total porosity ( $n$ ) or effective porosity ( $n_e$ ), the former being relatively easily established by experimental means. Both parameters were successfully used in diffusion models by ROWE *et al.* (1999). Yet he warns that care should be taken in using total porosity for deducing diffusion coefficients, especially in thicker samples and it may be necessary to establish the effective porosity for certain ionic species (e.g chloride). Because  $n_e$  was established for the geologic barrier samples during this research, it was commonly used as the porosity parameter of choice for diffusion modeling (appendix E.4). Porosity is entered as a unitless value from 0 (=0%) to 1 (=100%)

Coefficient of hydrodynamic dispersion / diffusion. Hence dispersion by flow is not considered in this study, but only pure diffusion is being evaluated, parameters for mechanical dispersion are set to zero. Thus the input for the coefficient of hydrodynamic dispersion becomes the effective diffusion coefficient ( $D_e$ ). This input quantity in conjunction with the distribution coefficient was repeatedly changed until the model match the observed data. The unit for the parameter is  $\text{cm}^2/\text{s}$ .

Distribution coefficient. This input parameter describes a linear  $K_d$  in the unit of  $\text{cm}^3/\text{g}$  which is the numerical equivalent of L/kg recorded and expressed in appendix D.2 of this study. The modeling approach used linear  $K_d$  wherever possible. However, Freundlich and Langmuir sorptive algorithms were also tried. Their input will override the linear distribution coefficient described here.

Fractures. No fractures were modeled and value was set to zero.

Top and bottom boundary conditions. The boundary condition between the source reservoir and the sample plug can be described as a "Finite Mass Boundary". Here, the initial concentration ( $c_i$ ) in the source decreases with time as the contaminant migrates into the sample. According to ROWE *et al.* (1988 & 1994) this boundary condition can be mathematically described as:

$$\text{Eq. 8.6} \quad C(t) = C_i - \frac{1}{h_r} \int_0^t f(t) dt$$

where  $C(t)$  = concentration at top boundary at time  $t$   
 $C_i$  = initial concentration in source reservoir  
 $h_r$  = reference height of source reservoir leachate (volume of source fluid per unit area)  
 $f(t)$  = mass flux of contaminant into sample at time  $t$

While the software is capable of modeling many more parameters in this type of boundary, such as flow or seepage into the sample, concentration increases through addition of landfill materials or removal of leachate through collection systems, only pure diffusion was considered. All other source reservoir parameters were set to zero.

A similar model is adopted for the boundary between the sample and the receptor vessel. In the POLLUTEv6 model (ROWE *et al.*, 1994) it is termed as “Fixed Outflow Velocity”. The terminology is somewhat misleading, since only pure diffusion is considered without any flow or seepage. However, the software was designed for real world application as in modeling leachate flow and contaminant transport into an underlying aquifer. In order to change the aquifer into a static receptor or collection chamber filled with distilled water, the flow parameters were set to zero and the porosity factor of the “aquifer” to 1 (= 100%). The following equation 8.7 describes these lower boundary conditions mathematically.

$$\text{Eq. 8.7} \quad C(t) = \frac{1}{h_{rc}} \int_0^t f_c(t) dt$$

where  $C(t)$  = concentration at receptor boundary at time  $t$   
 $h_{rc}$  = reference height of collector vessel (volume of source fluid per unit area)  
 $f_c(t)$  = mass flux of contaminant from sample into receptor at time  $t$

**Initial concentration profile.** This option allows the user to define initial concentrations of the diffusing species at specified depth within the sample plug. It was used for chemical species that appeared immediately in the collection reservoir without lag time, thus indicating initial concentrations in the barrier materials. The setting was used for diffusion modeling of Na, K, and Ca where the first measured concentration at time 2 days was assumed to be the approximate background concentration of the material. Another application for initial concentration profile was employed in almost all samples when evaluating changes in diffusion mechanisms during the course of the experiment. Here, the calculated end-concentration profile within the sample for one phase of the model became the starting concentration profile for a subsequent modeling approach. Some samples, such as Lower Röttone M6 showed at least three distinct chronological diffusive changes and characteristics are discussed below.

#### 8.4 Diffusion Results - Comparison and Discussion

In order to test the diffusion system, two selected samples with a good track record of stability during the presaturation phase were chosen in a first trial using lithium bromide as a tracer species. The results of the LiBr diffusion test is shown in table 8.2 and later figure 8.6.

**Table 8.2** - Results of diffusion experiments in sample L6 & L11.5 using LiBr.  $D_e$  established by Pollute software,  $D_a$  by  $t_e$  method, and  $D_e$  by  $t_e$ - $K_d$  correction algorithm.

Sample	Species	$D_e$ (cm <sup>2</sup> /s) POLLUTEv6 (GAEA, 1997)	$K_d$ (cm <sup>3</sup> /g) POLLUTEv6 (GAEA, 1997)	$D_a$ (cm <sup>2</sup> /s) $t_e$ -method	$\sqrt{-K_d}$	$D_e$ (cm <sup>2</sup> /s) $t_e$ -method * $\sqrt{-K_d}$
L6 @ 10°C	Br	2.27E-06	14.00 <sup>0.5</sup> Freundlich	5.58E-07	3.74	2.09E-06
	Li	2.19E-06	8.00 <sup>0.5</sup> Freundlich	5.02E-07	2.83	1.42E-06
L11.5 @ 10°C	Br	5.10E-06	12.00 <sup>0.5</sup> Freundlich	1.34E-06	3.46	4.65E-06
	Li	1.16E-06	1.00 <sup>0.5</sup> Freundlich	1.10E-06	1.00	1.10E-06

Calculations for the effective diffusion coefficients ( $D_e$ ) were accomplished by POLLUTEv6 (GAEA, 1997) software using the receptor reservoir data.  $D_e$  for the anion are in the magnitude range of studies performed by SHACKELFORD and DANIEL (1991b) and SHACKELFORD *et al.* (1989), reporting Br-  $D_e$  values from  $3.9 \cdot 10^{-6} \text{ cm}^2/\text{s}$  to  $10.6 \cdot 10^{-6} \text{ cm}^2/\text{s}$  in disturbed kaolinite clays. Overall diffusive values for bromide in compacted clay soils are given by SHACKELFORD (1991) in a summary of researched values as  $1.0 \cdot 10^{-6}$  to  $18 \cdot 10^{-6} \text{ cm}^2/\text{s}$ . No comparative study was found for lithium. To further check the validity of the  $D_e$  values, the time-lag method described by OSCARSON (1994) was employed.

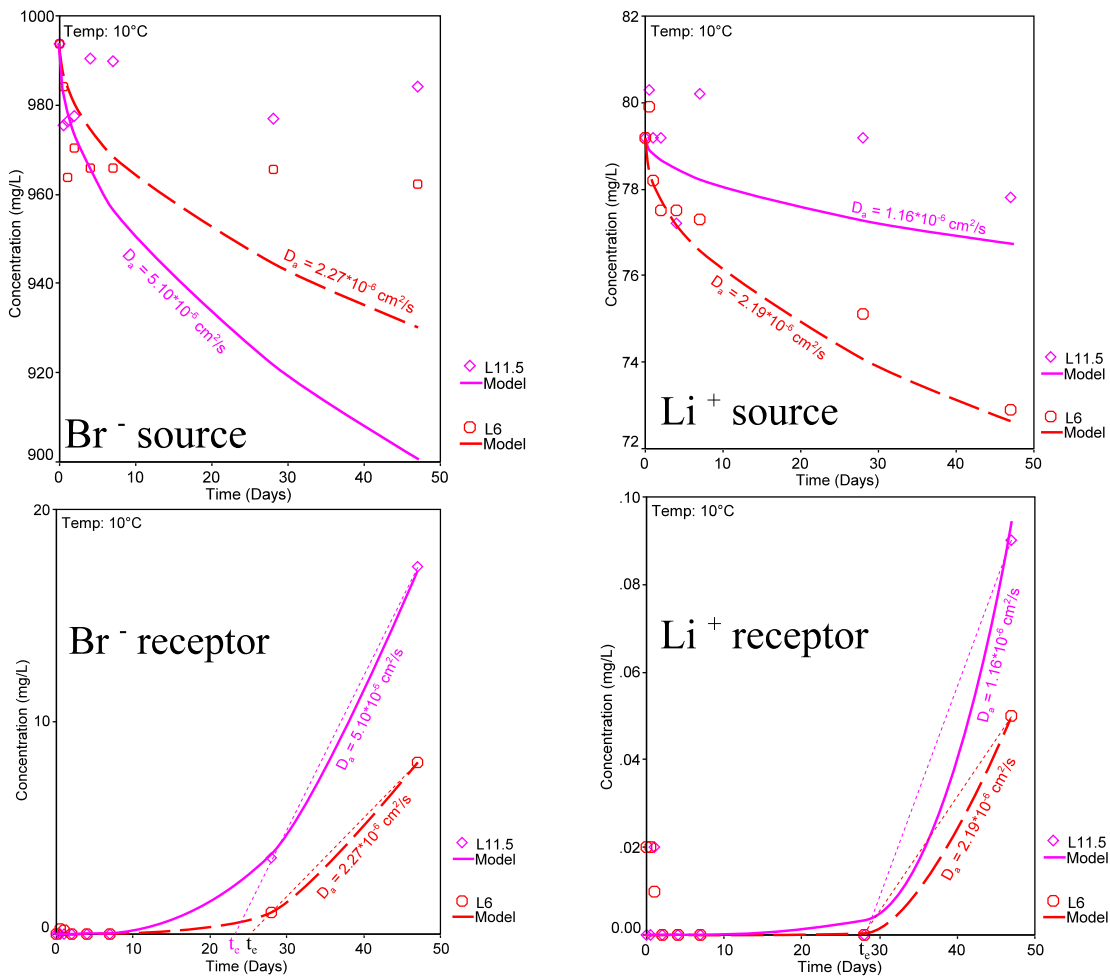


**Figure 8.6** - Cumulative concentration of Li and Br versus time in receptor and source reservoirs of the diffusion apparatus for samples L6 and L11.5. Observed data represented as points, theoretical model from POLLUTEv6 (GAEA, 1997) computations indicated as curves. Lag-time ( $t_e$ ) approximated by assuming steady state conditions for last two data points.

He argues that diffusion systems in clays will eventually approach a steady state condition where the cumulative species concentration versus time will become linear. Thus, the linear part of the curve can be extended to the x-intercept, which defines the lag time ( $t_e$ ). Using equation 8.8 given by OSCARSON (1994), the apparent diffusion coefficient ( $D_a$ ) can be calculated.

**Eq. 8.8** 
$$D_a = \frac{L^2}{6t_e}$$

- where  $D_a$  = apparent diffusion coefficient  
 $L$  = length of the clay plug  
 $t_e$  = time-lag established from steady state section of cumulative concentration vs. time graph

A direct comparison of the diffusive values thus obtained with POLLUTEv6 (GAEA, 1997) calculations is not possible since  $D_a$  is related to  $D_e$  as shown in equation 8.5. While  $D_a$  is a function of the sorptive characteristics of the geologic barrier material, the effective diffusion coefficient ( $D_e$ ) is not (SHACKELFORD, 1991), differing from  $D_a$  often by a magnitude of  $10^{-1}$ . Therefore,  $D_a$  established by the time-lag method must be multiplied by the corresponding retardation factor (R) for the specific soil and chemical species in order to obtain comparable results with those given by the POLLUTEv6 (GAEA, 1997)  $D_e$  values. However, R was not attained for Li and Br, but non-linear Freundlich sorption coefficients ( $K_d$ ) were instituted during POLLUTEv6 (GAEA, 1997) modeling. When resolving the Freundlich exponent, 0.5, into the given  $K_d$  value, the square-root of  $K_d$  is delineated, as can be seen in table 8.2, column  $\sqrt{K_d}$ . Multiplying the values in the column indicated with corresponding time-lag  $D_a$  coefficients,  $D_e$  is the resultant. As shown in table 8.2,  $D_e$  from time-lag is in very close agreement with  $D_e$  established by the software calculations.

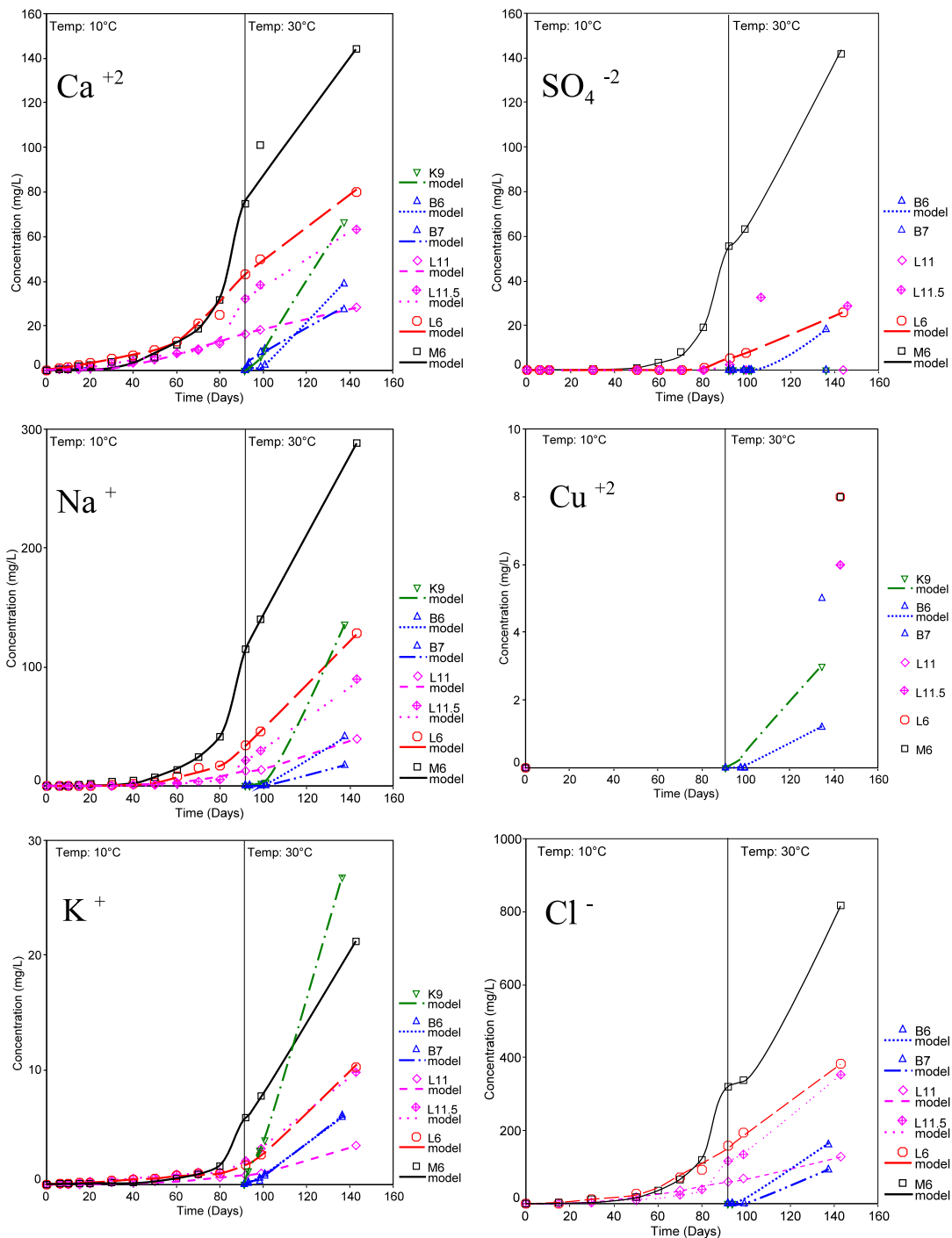
Even though LiBr is used in many experiments as an apparent non-sorbing tracer, surveying the results for Li and Br diffusion in table 8.2 indicates some sorption which is evidently greater for the anion than for the cation. This observation is congruent with those made by ROWE *et al.* (1999) stating that anions are often subject to exclusions. Double layers of Gouy and Stern (see figure 7.14) may overlap at closely adjacent clay particles, thus inhibiting the migration of negatively charged ions. This phenomenon is referred to as anion exclusion. While it can be modeled as a pseudo sorptive parameter, according to ROWE *et al.* (1999) anion exclusion reduces the effective porosity for specific pollutants well below the total porosity of the sample. The experimental data and resolving computations indicate that bromide exclusion as described is a plausible explanation for the calculated sorption values. Similar observations are made for the various anions present in the SLL as discussed below.

Scanning figure 8.6 it is observed that a good fit between data and model is shown for the chemical species in the receptor reservoir. However, poor correspondence is shown for corresponding data in the source vessel. A slightly better fit is indicated for lithium, while Br describes the poorest relationship to the model. While discouraging, these differences in source and receptor vessels are not uncommon. ROWE *et al.* (1999) investigated possibilities for chemical concentration anomalies in the source. Anion exclusion as described above may change the effective porosity in the clay plug close to the source faster, where anionic concentrations are highest, while porosities close to the receptor did not yet deviate. Another possibility is counter-osmotic flow from the clay plug into the source reservoir. As indicated by ROWE *et al.* (1999), receptor concentration might increase while the source experiences ionic deviations through osmosis and anion exclusions, negating the "best fit" of the diffusion coefficient.

The following will discuss the diffusive properties of individual species of the SLL for the selected geologic barrier samples. For the reasons given above, only the receptor was used to establish the diffusion parameters during all experiments. A summary of the diffusion coefficients and corresponding sorptive parameters can be found in appendix G.3. Graphical representation of the source is compiled in appendix G.4.

Graphic results of the diffusion coefficient modeling shown in figure 8.7 are based on the receptor reservoir data and a modeling approach using POLLUTEv6 (GAEA, 1997) software. For samples M6 (Lower Röttone), L6, L11, and L11.5 (Lehrberg Layers) no single software model would satisfy the data points. Since these samples were subjected to a temperature change during the total experiment duration of 144 days, it was assumed that the diffusion coefficient would also change with the higher temperature. Splitting the model into two at the 10°C-30°C interface yielded satisfactory match of data with the theoretical curve. For  $D_e^{30^\circ\text{C}}$  a tapered presaturation of chemical species along the length of the clay plugs is naturally indicated and was therefore included into the elevated temperature model. Thus an obvious change in the effective diffusion coefficients was observed with change in temperature and is listed as such in tables below. For the M6, L6, and L11.5 samples a change of the

diffusion coefficient at the temperature change was not satisfactory in describing the theoretical data fit in most cases. As can be seen in figure 8.7 a drastic increase in receptor concentrations for some chemical species suddenly appears in the indicated geologic barrier plugs after an experimental duration of about 50 to 80 days. This increased data slope is identified by OSCARSON (1994) as the steady-state diffusive condition of the sample, which is often assigned it's own ubiquitous diffusion coefficient. Hence different  $D_e$  values were modeled for the assumed steady state condition of the data within the selected clay plugs. When treated in this fashion, a satisfactory correspondence between measured and modeled data was observed.



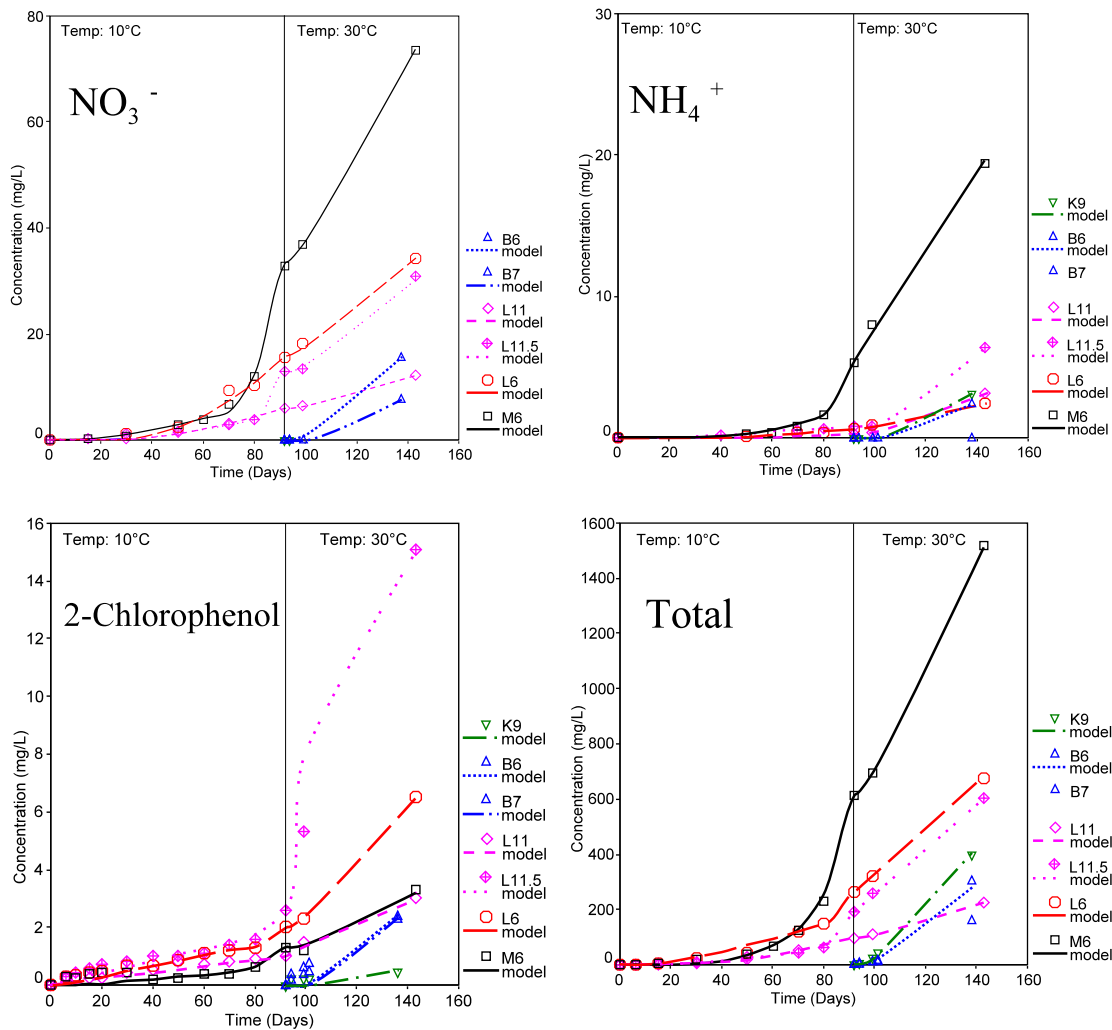


**Figure 8.7** - Cumulative concentrations of chemical species versus time in receptor reservoir. Observed data represented by symbol points. Curves describe theoretical model from POLLUTEV6 (GAEA, 1997) calculations. Letter indicates location, number corresponds with sampling core depth in meters. K = Amaltheen Clay; B = Feuerletten; L = Lehrberg Layers; M = Lower Röttone.

In most cases this additional steady-state  $D_e$  coefficient for samples M6, L6 and L11.5 appears irrationally high. One has to keep in mind, however, that this value does not necessarily reflect the steady state condition but the change from the previous  $D_e$  value to the steady state coefficient within a very short time period. It is therefore proposed that these transitional diffusion coefficients will be treated as a temporary occurrence, rather than a representative average.

#### 8.4.1 Calcium Diffusion

SHACKELFORD and DANIEL (1991a) list the diffusion coefficient for  $\text{Ca}^{2+}$  in an aqueous solution at 25°C and infinite dilution as  $7.92 \cdot 10^{-15} \text{ cm}^2/\text{s}$ . As indicated in table 8.3 the determined  $D_e$  values for calcium in the saturated barrier samples of limiting porosities are well below the diffusion of the species in water. ROWE *et al.* (1988) established  $D_{\text{Ca}^{2+}}$  in an undisturbed clay till to be around  $3.8 \cdot 10^{-6} \text{ cm}^2/\text{s}$ .

**Table 8.3** - Effective Calcium Diffusion Coefficients for artificial leachate modeled with POLLUTEv6 (GAEA, 1997). Superscripts in header denote summative totals in undiluted artificial leachate.  $K_d$  superscript n = Freundlich constant. Temporary transitional model in *italics* as explained above.

$\text{Ca}^{+2}$		MW: 40.08g	$C_{\text{leachate}}: 409^{16499}$ mg/L	$I_{\text{leachate}}: 20.410^{300.7}$ mmol/L	
Sample	Temp.	Duration (days)	$D_e$ (cm <sup>2</sup> /s) POLLUTEv6 (GAEA, 1997)	$K_d$ (L/kg) POLLUTEv6 (GAEA, 1997)	$K_d$ (L/kg) batch-exp.
M6	10°C	0 to 70	$9.84 * 10^{-6}$	$50^{n0.5}$	
	10°C	70 to 92	$88.0 * 10^{-6}$	$1000^{n0.2}$	- 3.18 <sup>n 0.80</sup>
	30°C	92 to 143	$11.4 * 10^{-6}$	-0.17 <sup>n1</sup>	
L6	10°C	0 to 50	$1.80 * 10^{-6}$	0	
	10°C	50 to 92	$33.6 * 10^{-6}$	$450^{n0.5}$	- 2.42
	30°C	92 to 143	$6.10 * 10^{-6}$	-0.13 <sup>n1</sup>	
L11	10°C	0 to 92	$5.30 * 10^{-6}$	1.5	
	30°C	92 to 143	$2.40 * 10^{-6}$	-0.12 <sup>n1</sup>	- 3.16
L11.5	10°C	0 to 70	$2.00 * 10^{-6}$	0	
	10°C	70 to 92	$350.0 * 10^{-6}$	$> 5000^{n0.3}$	
	30°C	92 to 143	$7.50 * 10^{-6}$	-0.15 <sup>n1</sup>	
B6	30°C	0 to 44	$16.9 * 10^{-6}$	$14^{n0.5}$	- 4.93
B7	30°C	0 to 44	$11.0 * 10^{-6}$	-0.80 <sup>n1</sup>	
K9	30°C	0 to 44	$15.7 * 10^{-6}$	$10^{n0.5}$	- 3.67 <sup>n 0.44</sup>

Excluding the temporary diffusion condition indicated in table 8.3, Feuerletten and Amaltheen clay lithologies exhibit the highest calcium diffusion, while the lowest values are observed in the Lehrberg Layers. Nevertheless, diffusive parameters for  $\text{Ca}^{2+}$  during this research are around  $10^{-1}$  cm<sup>2</sup>/s greater than those indicated by ROWE *et al.* (1988). It is obvious, that desorption of calcium as established during sorption experiments is paramount for the data divergence. Hence, the concentrations observed in the receptor, which form the base for the diffusion calculations are actually a mixture of exchangeable as well as induced Ca. When comparing significant correlations,  $D_e^{\text{Ca}^{2+}}$  has a negative mineralogical correspondence with MnO (see appendix H.1). Since a greater concentration of manganese oxide retards the diffusion coefficient of  $\text{SO}_4$  in a proportional manner, a selective calcium sulfate retardation by presence of MnO is suspected. The best Pearson correlation of  $D_e^{\text{Ca}^{2+}}$  is with  $\text{TiO}_2$  as shown in appendix H.3. Furthermore, a corresponding correlation is found for  $D_e^{\text{SO}_4}$  and titanium oxide, suggesting an involvement of calcium sulfate diffusion with  $\text{TiO}_2$  as a whole. Titanium oxide concentrations were also used as one of the attributes in the mineralogical calculation of kaolinite. Since the diffusion coefficient does not equally relate to the mentioned clay mineral, it can be safely assumed that the interaction of calcium sulfate diffusion with  $\text{TiO}_2$  must be outside of the clay mineralogy. The explanation for the relationship of the  $\text{TiO}_2$  -  $D_e^{\text{Ca}^{2+}}/D_e^{\text{SO}_4}$  relationship is unclear.

The correlation table in appendix H.3 also exhibits a correspondence of the effective sulfate and calcium diffusion coefficients with  $\text{Fe}_2\text{O}_3$ . Since iron oxide exhibits strong sorptive characteristics, it may well interact with the diffusion process. Oxides may scavenge selected ions removing them from solutions and freeing the available pore space for the diffusive flux of calcium or calcium sulfate. The fact that a diffusing cation will travel in the company of a complementary anion was also observed by LAKE and ROWE (1999). They showed in a sodium chloride diffusion experiment that  $\text{Na}^+$  slows down the rate of movement of the counter ion  $\text{Cl}^-$  across the sample, resulting in a lower but corresponding chloride diffusion coefficient. Hence  $\text{Ca}^{2+}$  is most likely to diffuse with  $\text{SO}_4^{2-}$  even in the presence of a variety of chemical species. Another plausible explanation would be the desorption of calcium present on the oxide surfaces by the onslaught of massive ion concentrations. This may be also supported by observing the desorptive



characteristics shown in figure 7.5 with the diffusion values presented in table 8.3. Thus, a proportional correspondence between  $D_e^{Ca^{2+}}$  and  $K_d^{Ca^{2+}}$  is observed. The elevated diffusion coefficient perceived during this study is most likely a result of an influx in exchangeable Ca during the forward migration of the diffusive front.

#### 8.4.2 Copper Diffusion

The diffusion coefficient for  $Cu^{2+}$  in an aqueous solution at 25°C and infinite dilution is given as  $7.13 \cdot 10^{15} \text{ cm}^2/\text{s}$  (SHACKELFORD and DANIEL, 1991a). As previously defined, this diffusion coefficient will drastically reduce when  $Cu^{2+}$  ions are subjected to the confining pore space and tortuosity of a soil medium. However, heavy metal cations are notoriously sorptive in a clay environment. Copper showed some of the highest  $K_d$  values of all chemical species during this research. It is therefore expected that diffusion, if observed at all, must be elevated to overcome the opposing sorptive forces. While most of the samples used showed copper in the receptor only after an experimental duration of 144 days, two samples K9 and B6 experienced a shorter duration. This extended time limited a valid modeling approach with POLLUTEv6 (GAEA, 1997) and match could not be obtained. As summarized in table 8.4, the time lag method ( $t_e$ ) was employed according to equation 8.5 and 8.8. The two  $D_e$  coefficient obtained through software modeling for samples K9 and B6 were used to calibrate the  $t_e$  computations. The necessary retardation factor for estimating the effective from the apparent diffusion coefficient was obtained by using the M value of the experimentally determined Langmuir sorption coefficient as an exponent and multiplying the resultants by 10 as illustrated in equation 8.9. (See also table 8.4).

Eq. 8.9

$$R = \text{Langmuir } K_d^M * 10$$

where R = Retardation factor

$\text{Langmuir } K_d$  = sorption coefficient according to Langmuir

M = a constant referring to the maximum sorptive capacity of the sorbent

Diffusive rates are observed to be highest in the Amaltheen Clay (K9) and Feuerletten (B6) samples. When comparing the  $Cu_e$ - $D_e$  using a bivariate two-tailed Pearson correlation with other geologic barrier properties, the following is observed with a 90<sup>th</sup> percentile correspondence: At the 0.01 significance level, apatite, linear Cl sorption coefficient, and effective porosity; and at 0.05 significance level, kaolinite, gypsum, grain sorting and grain kurtosis (see appendix H.1 & H.2). Porosity shows a negative trend of declining  $D_e$  with increasing  $n_e$ . A greater porosity may allow a larger number of  $Cu^{2+}$  ions to be sorbed, hence decreasing the diffusion coefficient. The correlation with the mineral gypsum may point to a link with the findings of AZAM *et al.* (2000), who states that the swelling potential of clay-calcium sulfate mixtures decreases with increase in calcium sulfate concentration. It is observed in this study that as the amount of gypsum increases so does the effective diffusion coefficient of Cu. If the swelling potential of clay is decreased, a decrease of the sorptive characteristic properties of the phyllosilicate mineral may be argued, therefore an increase in  $D_e$ . Copper and chloride ions may diffusive as a corresponding cation/anion pair. This would explain the  $D_e^{Cu^{2+}}$  positive affinity with  $K_d^{Cl^{linear}}$ . The other correlations are unclear, because they appear to only effect the Cu ions and none of the other diffusing chemical species. It can be safely attested, however, that the incredible sorptive properties of heavy metals are probably the underlying cause for the observations.

**Table 8.4** - Effective Copper Diffusion Coefficients for artificial leachate modeled with POLLUTEv6 (GAEA, 1997) and  $t_c$  method. Superscripts in header denote summative totals in undiluted artificial leachate.  $K_d$  superscript n = Freundlich constant, M = Langmuir constant (max. sorption capacity).

$\text{Cu}^{+2}$		MW: 63.55g	$C_{\text{leachate}}: 10.52^{16499} \text{mg/L}$		$I_{\text{leachate}}: 0.331^{300.7} \text{mmol/L}$		
Sample	Temp.	Duration (days)	$D_e$ ( $\text{cm}^2/\text{s}$ ) POLLUTEv6 (GAEA, 1997)	$K_d$ (L/kg) POLLUTEv6 (GAEA, 1997)	$D_e$ ( $\text{cm}^2/\text{s}$ ) $t_c$ -method	R ( $10 * K_d$ - Langmuir <sup>M</sup> )	$K_d$ (L/kg) batch-exp.
M6	10°C	0 to 92	0				
	30°C	92 to 143	no data match		$2.25*10^{-6}$	12.02	$9.7*10^7 M^{0.010}$
L6	10°C	0 to 92	0				
	30°C	92 to 143	no data match		$1.74*10^{-6}$	12.23	$9.1*10^7 M^{0.011}$
L11	10°C	0 to 92	0				
	30°C	92 to 143	no data match		$3.21*10^{-6}$	12.02	$9.9*10^7 M^{0.010}$
L11.5	10°C	0 to 92	0				
	30°C	92 to 143	no data match				
B6	30°C	0 to 44	$17.8*10^{-6}$	$3^{n0.01}$	$20.2*10^{-6}$	12.02	$1.0*10^{48} M^{0.010}$
B7	30°C	0 to 44	no data match				
K9	30°C	0 to 44	$38.4*10^{-6}$	$8^{n0.01}$	$40.5*10^{-6}$	30.20	$1.0*10^8 M^{0.010}$

#### 8.4.3 Potassium Diffusion

In an aqueous solution at 25°C and infinite dilution the diffusion coefficient for  $\text{K}^+$  is  $19.6*10^{15} \text{cm}^2/\text{s}$  as indicated by SHACKELFORD and DANIEL (1991a). In the investigated clay sample plugs, a decrease in  $D_e$  is of course expected given the increase in tortuosity. SHACKELFORD and DANIEL (1991b) show an effective potassium diffusion coefficient in disturbed clay plugs in the range from  $11.1*10^{-6}$  to  $20.2*10^{-6} \text{cm}^2/\text{s}$  for commercial kaolinite clays and around  $19.5*10^{-6} \text{cm}^2/\text{s}$  for natural clays. In undisturbed clay samples tested at 10°C by BARONE *et al.* (1989) using a multi-species leachate,  $D_{\text{K}^+}$  is indicated as  $6.0*10^{-6} \text{cm}^2/\text{s}$  with a  $K_d$  of 1.7 L/kg. ROWE *et al.* (1988) gives effective K diffusion coefficients in a clay till of  $6.3*10^{-6}$  to  $7.0*10^{-6} \text{cm}^2/\text{s}$ . During this study  $D_e$  was somewhat lower and ranged from a high of  $3.17*10^{-6} \text{cm}^2/\text{s}$  for the Amaltheen clay sample to a low of  $0.58*10^{-6} \text{cm}^2/\text{s}$  for sample L11 of the Lehrberg Layers. Results are summarized in table 8.5.

During bivariate two-tailed Pearson correlation as shown in appendix H.1 through H.3,  $D_e^{\text{K}^+}$  shows little correspondence with other geologic barrier attributes. At a 0.05 significance level a positive 80<sup>th</sup> percentile correlation is shown with the effective sodium diffusion coefficient. Because Na and K are compatible ions, a match between there diffusive properties should not be surprising.

**Table 8.5** - Effective Potassium Diffusion Coefficients for SLL modeled with POLLUTEv6 (GAEA, 1997). Header superscripts denote summative totals in undiluted artificial leachate.  $K_d$  superscript n = Freundlich constant, M = Langmuir constant (max. sorption capacity). Temporary transitional model in *italics* as explained above.

$K^+$					
MW: 39.102g		$C_{\text{leachate}}: 629.4^{16499}$ mg/L		$I_{\text{leachate}}: 8.048^{300.7}$ mmol/L	
Sample	Temp.	Duration (days)	$D_e$ (cm <sup>2</sup> /s) POLLUTEv6 (GAEA, 1997)	$K_d$ (L/kg) POLLUTEv6 (GAEA, 1997)	$K_d$ (L/kg) batch-exp.
M6	10°C	0 to 70	$0.42 * 10^{-6}$	$2^{n0.5}$	
	10°C	70 to 92	$5.14 * 10^{-6}$	$70^{n0.3}$	0
	30°C	92 to 143	$2.49 * 10^{-6}$	-0.1 <sup>n1</sup>	
L6	10°C	0 to 50	$0.08 * 10^{-6}$	-0.13 <sup>n1</sup>	
	10°C	50 to 92	$0.58 * 10^{-6}$	$5^{n0.5}$	0
	30°C	92 to 143	$1.30 * 10^{-6}$	0	
L11	10°C	0 to 92	$0.20 * 10^{-6}$	-0.07 <sup>n1</sup>	38.02 <sup>M 0.140</sup>
	30°C	92 to 143	$0.58 * 10^{-6}$	0	
L11.5	10°C	0 to 70	$0.11 * 10^{-6}$	-0.15 <sup>n1</sup>	
	10°C	70 to 92	$2.14 * 10^{-6}$	$20^{n0.5}$	
	30°C	92 to 143	$1.33 * 10^{-6}$	-0.15 <sup>n1</sup>	
B6	30°C	0 to 44	$1.11 * 10^{-6}$	-0.09 <sup>n1</sup>	0.97 <sup>M 9.960</sup>
B7	30°C	0 to 44	$1.53 * 10^{-6}$	-0.07 <sup>n1</sup>	
K9	30°C	0 to 44	$3.17 * 10^{-6}$	0.05	-0.88

#### 8.4.4 Sodium Diffusion

SHACKELFORD and DANIEL (1991a) give the diffusion coefficient for  $Na^+$  in an aqueous solution at 25°C and infinite dilution as  $13.3 * 10^{15}$  cm<sup>2</sup>/s. Again, a strong reduction of this coefficient is expected in the confining pore spaces of a lithologic sample. Effective sodium diffusion coefficients given by ROWE *et al.* (1999) for experiments on disturbed bentonite clays with single salt solutions range from  $0.6 * 10^{-6}$  to  $3.5 * 10^{-6}$  cm<sup>2</sup>/s. BARONE *et al.* (1989) shows an effective diffusion coefficient for sodium as  $4.6 * 10^{-6}$  cm<sup>2</sup>/s and a corresponding  $K_d$  of 0.25 L/kg in undisturbed clay samples tested at 10°C with a leachate containing several chemical species. For a clay till,  $D_{Na^+}$  is around  $4.8 * 10^{-6}$  to  $5.7 * 10^{-6}$  cm<sup>2</sup>/s (ROWE *et al.*, 1988), while CROOKS and QUIGLEY (1984) report effective Na diffusion coefficients between  $2.5 * 10^{-6}$  to  $3.5 * 10^{-6}$  cm<sup>2</sup>/s using a saline leachate in a silty clay.

Depending on temperature a similar range of  $D_e$  distribution for sodium is observed during this experiment. During both temperature settings, Lower Röttone (M6) exhibit the highest diffusion coefficients while the Lehrberg Layers are in the lower groupings as indicated in table 8.6. A near 100% correspondence was observed for  $D_e^{Na^+}$  with  $D_e^{Cl^-}$  during bivariate two-tailed Pearson computations as indicated in appendix H.1. Because of the large concentration in the SLL and sodium's obvious affinity for the Cl anion, the observation is in agreement with findings by SHACKELFORD and DANIEL (1991a). They mention the influence of the electrical potential gradient created by diffusing oppositely charged ions in solution as quoted by ROBINSON and STOKES (1959). Here, the slower moving ion speeds up while the faster moving ion slows down, with a net result of both ions migrating at similar speeds.

**Table 8.6** - Effective Sodium Diffusion Coefficients for artificial leachate modeled with POLLUTEv6 (GAEA, 1997). Superscripts in header denote summative totals in undiluted artificial leachate.  $K_d$  superscript n = Freundlich constant, M = Langmuir constant (max. sorption capacity). Temporary transitional model in *italics* as explained above.

$\text{Na}^+$		MW: 22.98g	$C_{\text{leachate}}: 4327^{16499} \text{mg/L}$	$I_{\text{leachate}}: 94.114^{300.7} \text{mmol/L}$	
Sample	Temp.	Duration (days)	$D_e$ ( $\text{cm}^2/\text{s}$ ) POLLUTEv6 (GAEA, 1997)	$K_d$ (L/kg) POLLUTEv6 (GAEA, 1997)	$K_d$ (L/kg) batch-exp.
M6	10°C	0 to 70	$1.17 \cdot 10^{-6}$	$20^{n0.5}$	
	10°C	70 to 92	$12.3 \cdot 10^{-6}$	$700^{n0.3}$	0.69
	30°C	92 to 143	$4.10 \cdot 10^{-6}$	$-0.15^{n1}$	
L6	10°C	0 to 70	$0.65 \cdot 10^{-6}$	$12^{n0.5}$	
	10°C	70 to 92	$2.28 \cdot 10^{-6}$	$30^{n0.5}$	$1.01^{n0.49}$
	30°C	92 to 143	$1.80 \cdot 10^{-6}$	$-0.1^{n1}$	
L11	10°C	0 to 92	$0.86 \cdot 10^{-6}$	0.4	$0.79^{n0.81}$
	30°C	92 to 143	$1.43 \cdot 10^{-6}$	0.7	
L11.5	10°C	0 to 70	$0.99 \cdot 10^{-6}$	0.5	
	10°C	70 to 92	$4.87 \cdot 10^{-6}$	$30^{n0.5}$	
	30°C	92 to 143	$1.60 \cdot 10^{-6}$	$-0.15^{n1}$	
B6	30°C	0 to 44	$1.85 \cdot 10^{-6}$	0.15	$2.13^M 1.565$
B7	30°C	0 to 44	$1.08 \cdot 10^{-6}$	0	
K9	30°C	0 to 44	$3.41 \cdot 10^{-6}$	0.5	0.50

#### 8.4.5 Ammonium Diffusion

Ammonium is a very uncommon ion to be used in single species diffusion testing and no comparative studies were found. However, it should be noted that it is an integral part of landfill leachates and should be included in applicable modeling attempts. While exhibiting rather large  $K_d$  values as indicated in appendix D.2, the sorptive properties of  $\text{NH}_4^+$  follow the Langmuir model with limited sorption sites to occupy. Since the concentration of Ammonium in the SLL is rather large, sorption sites should be filled rather quickly and diffusive flux ought to continue uninterrupted. However,  $\text{NH}_4^+$  is a rather large ion, which might experience porosity interference. It is therefore expected that ammonium might diffuse slower than other ions. Indeed, one of the lowest diffusive rates of all chemical species, measuring only  $0.09 \cdot 10^{-6} \text{cm}^2/\text{s}$ , was observed in sample L11.5 at 10°C. At 30°C  $D_e$  ranges from  $0.29 \cdot 10^{-6}$  (L6) to  $3.18 \cdot 10^{-6} \text{cm}^2/\text{s}$  (L11.5). The Amaltheen clay (K9) is on the low end with  $0.95 \cdot 10^{-6} \text{cm}^2/\text{s}$  followed by the Feuerletten clay (B6) at  $1.09 \cdot 10^{-6} \text{cm}^2/\text{s}$  and the Lower Röttone (M6) showing a  $D_e$  of  $1.90 \cdot 10^{-6} \text{cm}^2/\text{s}$ .  $D_e^{\text{NH}_4^+}$  had no significant correlation with other lithological or geochemical parameters when evaluated with a bivariate two-tailed Pearson analysis.

**Table 8.7** - Effective Ammonium Diffusion Coefficients for SLL modeled with POLLUTEv6 (GAEA, 1997). Header superscripts denote summative totals in undiluted artificial leachate.  $K_d$  superscript n = Freundlich constant, M = Langmuir constant (max. sorption capacity). Temporary transitional model in *italics* as explained above.

$\text{NH}_4^+$		MW: 18.099g	$C_{\text{leachate}}: 709.7^{16499}$ mg/L	$I_{\text{leachate}}: 19.607^{300.7}$ mmol/L	
Sample	Temp.	Duration (days)	$D_e$ (cm <sup>2</sup> /s) POLLUTEv6 (GAEA, 1997)	$K_d$ (L/kg) POLLUTEv6 (GAEA, 1997)	$K_d$ (L/kg) batch-exp.
M6	10°C	0 to 80	$0.73 \cdot 10^{-6}$	$94.28^{n0.517}$	
	10°C	80 to 92	$2.69 \cdot 10^{-6}$	0	$94.28^M 0.561$
	30°C	92 to 143	$1.90 \cdot 10^{-6}$	$-0.175^{n1}$	
L6	10°C	0 to 92	$0.15 \cdot 10^{-6}$	0	0
	30°C	92 to 143	$0.29 \cdot 10^{-6}$	0	
L11	10°C	0 to 92	$0.58 \cdot 10^{-6}$	$52.28^{M0.517}$	$52.28^M 0.517$
	30°C	92 to 143	$1.34 \cdot 10^{-6}$	$52.28^{M0.517}$	
L11.5	10°C	0 to 92	$0.09 \cdot 10^{-6}$	$-0.41^{n1}$	
	30°C	92 to 143	$3.18 \cdot 10^{-6}$	$52.28^{n0.52}$	
B6	30°C	0 to 44	$1.09 \cdot 10^{-6}$	$2.14^{n0.52}$	$2.14^n 0.52$
B7	30°C	0 to 44	0		
K9	30°C	0 to 44	$0.95 \cdot 10^{-6}$	$211.14^M 0.282$	$211.14^M 0.282$

#### 8.4.6 Chloride Diffusion

ROWE *et al.* (1999) lists chloride diffusion coefficients in experiments on disturbed bentonite clays with single salt solutions in the range of  $0.36 \cdot 10^{-6}$  to  $2.1 \cdot 10^{-6}$  cm<sup>2</sup>/s. Diffusion values given by SHACKELFORD and DANIEL (1991b) during laboratory tests on disturbed clay plugs are between  $4.5 \cdot 10^{-6}$  to  $16.4 \cdot 10^{-6}$  cm<sup>2</sup>/s for commercial kaolinites and  $4.7 \cdot 10^{-6}$  cm<sup>2</sup>/s for natural clays. For undisturbed clay samples evaluated at 10°C with a multi-species leachate,  $D_{\text{Cl}}$  is reported as  $7.5 \cdot 10^{-6}$  cm<sup>2</sup>/s with a  $K_d$  value of 0 L/kg. (BARONE *et al.*, 1989). Other work by BARONE *et al.* (1990) on natural clays yielded a effective chloride diffusion coefficient of  $1.4 \cdot 10^{-6}$  to  $1.6 \cdot 10^{-6}$  cm<sup>2</sup>/s. Overall diffusive values for chloride in compacted clay soils are summarized by SHACKELFORD (1991) in the magnitude of  $1.5 \cdot 10^{-6}$  to  $4.7 \cdot 10^{-6}$  cm<sup>2</sup>/s. At infinite dilution in an aqueous solution at 25°C, SHACKELFORD and DANIEL (1991a) mention an diffusion coefficient for Cl<sup>-</sup> of  $20.3 \cdot 10^{15}$  cm<sup>2</sup>/s.

The greatest chloride diffusion coefficient was observed for the Lower Rötton sample, with  $3.4 \cdot 10^{-6}$  cm<sup>2</sup>/s at 10°C and  $31.2 \cdot 10^{-6}$  cm<sup>2</sup>/s at 30°C. This fast diffusive behavior may suggest the transport along micro-fractures instead of pores in the M6 sample. Further suggestive evidence for a fracture based diffusive flux is given by elevated diffusion rates in the Lower Rötton barrier material for sodium, nitrates, and 2-chlorophenol as well. At lower temperatures,  $D_e$  for the Lehrberg Layer material ranges from  $0.34 \cdot 10^{-6}$  to  $0.85 \cdot 10^{-6}$  cm<sup>2</sup>/s, increasing at higher temperatures from  $1.15 \cdot 10^{-6}$  to  $4.18 \cdot 10^{-6}$  cm<sup>2</sup>/s. Similar values were obtained for the Feuerletten lithologies.

Interesting results were obtained when comparing  $D_e^{\text{Cl}^-}$  with other geologic barrier parameters using bivariate two-tailed Pearson calculations as displayed in appendix H. A 100% match was obtained when compared with sorption coefficient of chlorophenol. Significant correspondence at the 0.01 level and 90<sup>th</sup> percentiles is shown for CEC<sup>Na+</sup> and negatively with soil pH. At the 0.05 significance level,  $D_e^{\text{Cl}^-}$  agrees with Ba and K<sub>2</sub>O concentration in the sample, and negatively with sorting and skewness of the grain size analysis.

The agreement of  $D_e^{Cl^-}$  with the chlorophenol sorption coefficient and soil pH is explained when considering the chemical and sorptive characteristics of 2-chlorophenol. Validated by DIVINCENZO and SPARKS (2001), 2-chlorophenol may exist either as a neutral species or in the ionic form liberating a chlorine ion depending on pH. In addition, the pH dependent sorptive characteristic of the organic chemical species is discussed by BØRRETZEN and SALBU (1999). As described in section 7.6.9, minimal sorption for 2-chlorophenol is observed for soil pH values greater than 7.6, while a lower soil pH leads to a linearly increasing sorption coefficient. Hence the Cl diffusion coefficient would increase with increased introduction of Cl<sup>-</sup> from chlorophenol. Raising the pH would cause a decrease in  $D_e^{Cl^-}$  because less chloride cations would be created from the organic phenol in the SLL. The close correspondence with  $CEC^{Na^+}$  listed above is obviously the resultant of the partnering preferred cation with the Cl anion in the diffusion process. Unclear is the relationship of  $D_e^{Cl^-}$  with Ba and K<sub>2</sub>O. Possible is the occupation of Ba and K at preferred Na sorption sites. Thus, high amounts of Ba and K in the sample would reduce the sorption of Na and result in a faster diffusive rate. Results of the experiment are compiled in table 8.8.

**Table 8.8** - Effective Chloride Diffusion Coefficients for artificial leachate modeled with POLLUTEv6 (GAEA, 1997). Superscripts in header denote summative totals in undiluted artificial leachate.  $K_d$  superscript n = Freundlich constant. Temporary transitional model in *italics* as explained above.

Cl <sup>-</sup>	MW: 35.453g	$C_{leachate}$ : 7052 <sup>16499</sup> mg/L	$I_{leachate}$ : 99.458 <sup>300.7</sup> mmol/L		
Sample	Temp.	Duration (days)	$D_e$ (cm <sup>2</sup> /s) POLLUTEv6 (GAEA, 1997)	$K_d$ (L/kg) POLLUTEv6 (GAEA, 1997)	$K_d$ (L/kg) batch-exp.
M6	10°C	0 to 70	$3.40 * 10^{-6}$	$50^{n0.6}$	
	10°C	70 to 92	<i>1540 * 10<sup>-6</sup></i>	<i>&gt; 5000<sup>n0.5</sup></i>	0
	30°C	92 to 143	$31.2 * 10^{-6}$	$800^{n0.5}$	
L6	10°C	0 to 50	$0.34 * 10^{-6}$	$-0.1^{n1}$	
	10°C	50 to 92	<i>1.90 * 10<sup>-6</sup></i>	<i>200<sup>n0.1</sup></i>	0
	30°C	92 to 143	$2.60 * 10^{-6}$	$-0.13^{n1}$	
L11	10°C	0 to 92	$0.85 * 10^{-6}$	0.08	0
	30°C	92 to 143	$1.15 * 10^{-6}$	0.08	
L11.5	10°C	0 to 70	$0.62 * 10^{-6}$	0	
	10°C	70 to 92	<i>20.3 * 10<sup>-6</sup></i>	<i>285<sup>n0.6</sup></i>	
	30°C	92 to 143	$4.18 * 10^{-6}$	0.1	
B6	30°C	0 to 44	$3.03 * 10^{-6}$	$1.19^{n0.2}$	$1.19^{n0.20}$
B7	30°C	0 to 44	$4.58 * 10^{-6}$	0.5	
K9	30°C	0 to 44	no data		$1.29^{n0.81}$

#### 8.4.7 Sulfate Diffusion

The diffusion coefficient for SO<sub>4</sub><sup>2-</sup> at 25°C and infinite dilution in an aqueous solution is  $10.6 * 10^{15}$  cm<sup>2</sup>/s (SHACKELFORD and DANIEL, 1991a). As a large polyatomic cation, sulfate should be an excellent candidate for anion exclusion in small pore spaces. Therefore, very low  $D_e^{SO_4^{2-}}$  values were expected unless fracturing in the geologic barrier materials would be present. Diffusive restriction through the exclusion process is nicely observed in sample L6. Here,  $D_e^{SO_4^{2-}}$  at 10°C and for the duration of 0 to 92 days is  $4.20 * 10^{-6}$  cm<sup>2</sup>/s while dropping to  $0.63 * 10^{-6}$  cm<sup>2</sup>/s at 30°C during the later duration of the experiment. It is indicated that the large SO<sub>4</sub> ions will migrate well during low concentration profiles of the diffusive phase. When more and more ions from various chemical species at higher

concentrations are involved, anion exclusion appears to take effect. Sample L6 also shows corresponding changes in diffusion values for  $\text{NO}_3^-$ , another large cation.

The diffusion of sulfate exhibits matches with many lithological parameters when subjected to a bivariate two-tailed Pearson correlation and results are summarized in appendix H. The most significant (0.01 level) correspondence showing a negative trend is found for  $K_d\text{NO}_3^-$  and dry bulk density. Nitrate sorption may influence sulfate migration by occupying limited pore space, contributing to an anion exclusion effect. The negative association of  $D_e^{\text{SO}_4^{2-}}$  the dry bulk density may be a reference to the pore space of the lithologic sample. Other matches correspond with those found for  $D_e^{\text{Ca}^{+2}}$  and indicate the association of the  $\text{SO}_4$  anion with Ca cation.

**Table 8.9** - Effective Sulfate Diffusion Coefficients for artificial leachate modeled with POLLUTEv6 (GAEA, 1997). Superscripts in header denote summative totals in undiluted artificial leachate.  $K_d$  superscript n = Freundlich constant. Temporary transitional model in *italics* as explained above.

$\text{SO}_4^{2-}$	MW: 96.057g	$C_{\text{leachate}}: 2502^{16499}$ mg/L	$I_{\text{leachate}}: 52.099^{300.7}$ mmol/L		
Sample	Temp.	Duration (days)	$D_e$ ( $\text{cm}^2/\text{s}$ ) POLLUTEv6 (GAEA, 1997)	$K_d$ (L/kg) POLLUTEv6 (GAEA, 1997)	$K_d$ (L/kg) batch-exp.
M6	10°C	0 to 70	$1.05 * 10^{-6}$	$10^{n0.6}$	
	10°C	70 to 92	$6.30 * 10^{-6}$	$80^{n0.3}$	-0.35
	30°C	92 to 143	$3.50 * 10^{-6}$	$10^{n0.5}$	
L6	10°C	0 to 92	$4.20 * 10^{-6}$	$160^{n0.5}$	0
	30°C	92 to 143	$0.63 * 10^{-6}$	$-0.14^{n1}$	
L11	10°C	0 to 92	0		0
	30°C	92 to 143	0		
L11.5	10°C	0 to 92	$4.30 * 10^{-6}$	$150^{n0.4}$	
	30°C	92 to 143	error		
B6	30°C	0 to 44	$4.05 * 10^{-6}$	1.28	1.28
B7	30°C	0 to 44	$11.0 * 10^{-6}$	0	
K9	30°C	0 to 44	no data		0

#### 8.4.8 Nitrate Diffusion

According to LI and GREGORY (1974), the diffusion coefficient for  $\text{NO}_3^-$  in an aqueous solution at 25°C and infinite dilution is  $19.0 * 10^{15}$   $\text{cm}^2/\text{s}$ . As described under 8.4.7, sulfate diffusion, anion exclusion phenomena should prevail in the case of  $\text{NO}_3^-$ , a large polyatomic anion. This observation is again sustained by sample L6, where  $D_e$  is reduced with advancing experiment time because of increased anion exclusions at higher SLL concentrations.

The best correspondence of  $D_e^{\text{NO}_3^-}$  is shown with the mineral gypsum at -99.8% at a significance level of 0.002 during bivariate two-tailed Pearson statistical analysis. As explained in 8.4.2, copper diffusion, the presence of calcium sulfate will decrease the swelling potential of clay and most likely alter the sorptive properties of the material (AZAM *et al.*, 2000). However, the presence of  $\text{CaSO}_4$  may well interact with the  $\text{NO}_3^-$  ions and retard their flux. High concentrations of the sulfide mineral should their fore be counterproductive to the diffusive process of nitrate. LANGMUIR (1997) gives an inverse relationship of  $\text{SO}_4$  and  $\text{NO}_3^-$  in the natural waters of the Berkshire aquifer, United Kingdom. Here nitrate values are high when sulfate is low and vice versa.

**Table 8.10** - Effective Nitrate Diffusion Coefficients for SLL modeled with POLLUTEv6 (GAEA, 1997). Header superscripts denote summative totals in undiluted artificial leachate.  $K_d$  superscript n = Freundlich constant, M = Langmuir constant (max. sorption capacity). Temporary transitional model in *italics* as explained above.

$\text{NO}_3^-$		MW: 62.065g	$C_{\text{leachate}}: 823.2^{16499} \text{mg/L}$	$I_{\text{leachate}}: 6.632^{300.7} \text{mmol/L}$	
Sample	Temp.	Duration (days)	$D_e$ ( $\text{cm}^2/\text{s}$ ) POLLUTEv6 (GAEA, 1997)	$K_d$ (L/kg) POLLUTEv6 (GAEA, 1997)	$K_d$ (L/kg) batch-exp.
M6	10°C	0 to 70	$0.58 * 10^{-6}$	0	
	10°C	70 to 92	$21.0 * 10^{-6}$	$149^{n0.6}$	0.29
	30°C	92 to 143	$5.24 * 10^{-6}$	0.29	
L6	10°C	0 to 92	$4.10 * 10^{-6}$	3.8	1.05
	30°C	92 to 143	$2.20 * 10^{-6}$	0	
L11	10°C	0 to 92	$1.02 * 10^{-6}$	0.25	1.25
	30°C	92 to 143	$1.15 * 10^{-6}$	0.25	
L11.5	10°C	0 to 80	$0.85 * 10^{-6}$	0.1	
	10°C	80 to 92	$5.90 * 10^{-6}$	0	
	30°C	92 to 143	$3.70 * 10^{-6}$	1.25	
B6	30°C	0 to 44	$2.63 * 10^{-6}$	$-52.74^{M0.036}$	0
B7	30°C	0 to 44	$1.87 * 10^{-6}$	0	
K9	30°C	0 to 44	no data		1.44

#### 8.4.9 2-Chlorophenol Diffusion

At 30°C 2-chlorophenol (2-CPL) diffusion ranges from  $1.41 * 10^{-6}$  to  $190 * 10^{-6} \text{cm}^2/\text{s}$ . While sorption plays a definite role in the diffusive flux of 2-CPL, the extreme variation of  $D_e$  may be indicative of pore size. High  $D_e^{2\text{-CPL}}$  values may point toward transport through fractures and micro-fractures in the sample. During bivariate two-tailed Pearson statistical evaluation significant correspondence was observed for all parameters which also matched with  $D_e^{\text{Cl}^-}$ , as explained above. Experimental results are indicated in table 8.11.



Table 8.11 - Effective 2-Chlorophenol Diffusion Coefficients for artificial leachate modeled with POLLUTEv6 (GAEA, 1997). Superscripts in header denote summative totals in undiluted artificial leachate.  $K_d$  superscript n = Freundlich constant, M = Langmuir constant (max. sorption capacity). Temporary transitional model in *italics* as explained above.

$C_6H_5OCl$		MW: 128.56g	$C_{leachate}: 35^{16499}$ mg/L	$I_{leachate}: N/A$	
Sample	Temp.	Duration (days)	$D_e$ (cm <sup>2</sup> /s) POLLUTEv6 (GAEA, 1997)	$K_d$ (L/kg) POLLUTEv6 (GAEA, 1997)	$K_d$ (L/kg) batch-exp.
M6	10°C	0 to 70	$0.71 * 10^{-6}$	-0.1 <sup>n1</sup>	
	10°C	70 to 92	$11.0 * 10^{-6}$	$25^{n0.3}$	14115.62 <sup>n2.10</sup>
	30°C	92 to 143	$130 * 10^{-6}$	$1000^{n0.3}$	
L6	10°C	0 to 70	$2.06 * 10^{-6}$	0	
	10°C	70 to 92	$26.0 * 10^{-6}$	$200^{n0.2}$	918.33 <sup>n1.59</sup>
	30°C	92 to 143	$18.3 * 10^{-6}$	$10^{n0.5}$	
L11	10°C	0 to 92	$1.43 * 10^{-6}$	-0.15 <sup>n1</sup>	0
	30°C	92 to 143	$5.60 * 10^{-6}$	-0.15 <sup>n1</sup>	
L11.5	10°C	0 to 70	$3.00 * 10^{-6}$	-0.15 <sup>n1</sup>	
	10°C	70 to 92	$39.0 * 10^{-6}$	$100^{n0.3}$	
	30°C	92 to 143	$190 * 10^{-6}$	-0.15 <sup>n1</sup>	
B6	30°C	0 to 44	$12.0 * 10^{-6}$	$3^{n0.5}$	619.01 <sup>n1.52</sup>
B7	30°C	0 to 44	$80.0 * 10^{-6}$	$5^{n1.5}$	
K9	30°C	0 to 44	$1.41 * 10^{-6}$	$77.27^{M0.09}$	$77.27^{M0.09}$

#### 8.4.10 Total Diffusion of SLL

In order to compare overall diffusion coefficients with those of individual chemical species, the weighted averages from individual  $D_e$  values were computed according to source concentrations. The results are given in appendix G.3 as well as table 8.12. In general good matches were obtained for diffusion coefficients at 30°C. One has to consider, however, that missing diffusion values for individual species in some cases, especially for the 10°C sections in L6 and L11.5, will skew the weighted average values.

The calculated diffusion coefficients for 30°C range from  $0.94 * 10^{-6}$  to  $5.56 * 10^{-6}$  cm<sup>2</sup>/s as indicated in figure 8.7. The Feuerletten samples (B) exhibit uniform  $D_e$  values while the Lehrberg Layer lithologies (L) display the greatest variations even within ½ meter when comparing samples L11 and L11.5. High values may be suggestive of fracture transport, as seen in the Lower Rötton sample (M6). Lehrberg Layer L6 is the only sample that demonstrates a reduction of diffusive flux from 10°C to 30°C, a possible progressive anion exclusion with influx in chemical species concentration.

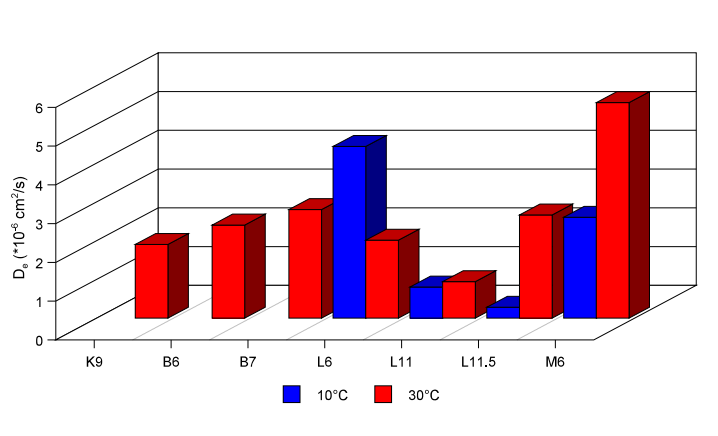


Figure 8.7 - Total  $D_e$  of samples investigated for 10°C and 30°C

**Table 8.12** - Effective Diffusion Coefficients for Total artificial leachate modeled with POLLUTEv6 (GAEA, 1997). Header superscripts denote summative totals in undiluted artificial leachate.  $K_d$  superscript n = Freundlich constant, M = Langmuir constant (max. sorption capacity). Temporary transitional model in *italics* as explained above.

<b>Total</b> MW: 505.956g $C_{\text{leachate}}$ : 16498.7 mg/L $I_{\text{leachate}}$ : 300.7mmol/L						
Sample	Temp.	Duration (days)	$D_e$ (cm <sup>2</sup> /s) POLLUTEv6 (GAEA, 1997)	$K_d$ (L/kg) POLLUTEv6 (GAEA, 1997)	$D_e$ (cm <sup>2</sup> /s) weighted average	$K_d$ (L/kg) batch-exp.
M6	10°C	0 to 70	2.60*10 <sup>-6</sup>	23 <sup>n0.7</sup>	2.24*10 <sup>-6</sup>	
	10°C	70 to 92	53.2*10 <sup>-6</sup>	600 <sup>n0.7</sup>	666*10 <sup>-6</sup>	0.99 <sup>M 2.261</sup>
	30°C	92 to 143	5.56*10 <sup>-6</sup>	0.1	15.9*10 <sup>-6</sup>	
L6	10°C	0 to 70	4.43*10 <sup>-6</sup>	-4.5 <sup>n1</sup>	1.22*10 <sup>-6</sup>	
	10°C	70 to 92	4.81*10 <sup>-6</sup>	82 <sup>n0.7</sup>	2.32*10 <sup>-6</sup>	0.08
	30°C	92 to 143	2.01*10 <sup>-6</sup>	-0.14 <sup>n1</sup>	2.04*10 <sup>-6</sup>	
L11	10°C	0 to 92	0.80*10 <sup>-6</sup>	3 <sup>M0.2</sup>	0.81*10 <sup>-6</sup>	4.57 <sup>M 1.407</sup>
	30°C	92 to 143	0.94*10 <sup>-6</sup>	1 <sup>n0.5</sup>	1.08*10 <sup>-6</sup>	
L11.5	10°C	0 to 70	0.28*10 <sup>-6</sup>	-0.02 <sup>n1.2</sup>	1.28*10 <sup>-6</sup>	
	10°C	70 to 92	9.50*10 <sup>-6</sup>	100 <sup>n0.7</sup>	19.1*10 <sup>-6</sup>	
	30°C	92 to 143	2.66*10 <sup>-6</sup>	-0.152 <sup>n1</sup>	3.17*10 <sup>-6</sup>	
B6	30°C	0 to 44	2.40*10 <sup>-6</sup>	3 <sup>n0.5</sup>	3.07*10 <sup>-6</sup>	0.87 <sup>M 3.954</sup>
B7	30°C	0 to 44	2.80*10 <sup>-6</sup>	-1.1 <sup>n1</sup>	2.84*10 <sup>-6</sup>	
K9	30°C	0 to 44	1.90*10 <sup>-6</sup>	0	1.40*10 <sup>-6</sup>	0

A bivariate two-tailed Pearson statistic reveals 98.1% positive match with a significance of 0.003 between  $D_e^{\text{Total}}$  and  $CEC^{\text{Na}}$ . A similar strong correspondence is observed with  $D_e^{\text{CPL}}$  and  $K_d^{\text{CPL}}$ . Carbon reveals a negative correlation at the 90<sup>th</sup> percentile with a significance of 0.023 and a similar positive indication is observed for  $D_e^{\text{Cl}}$ . At the upper 80<sup>th</sup> percentile with a significance of 0.039,  $K_2O$  is in agreement with the total diffusion coefficient. Since carbon is known to be an effective sorbent, it is not surprising that C influences  $D_e$  if averaged across all the chemical species. The more carbon in a sample, the greater the sorption and the less effective diffusion should become. Because NaCl was the major constituent of the SLL, correlations between  $D_e^{\text{Total}}$  and Cl or Na parameters should also come as no surprise. Unclear is the relationship of the total diffusion coefficient with potassium. It may be indicative of a sorbing interaction with K bearing minerals or certain clays, hence no significant match for specific clay minerals was observed.

Because of lithological constraints it was not possible to section the sample plugs after the completion of the diffusion experiment and evaluate the concentrations of the various mineral species with depth. However, as described above, conductivity probes were inserted into the samples at certain intervals. While it is impossible to determine individual pollutants and their depth profile in this manner, a fairly good overview of the progression of the diffusive front, steady state condition and even counter osmotic flows can be estimated on the total clay plug concentrations in relation to the concentrations in the receptor reservoir. The results are shown in figure 8.8. Because it was not possible to determine the actual electric conductivity within the sample in this manner, because of uncertainties in the interference of porosities, clay pore fluids and insertion depth of the electrodes, a percentile change in conductivity can be deduced. For this purpose was the initial measurement before induration with the SLL set to 100. All other measurements were then normalized to this percentile datum. True conductivities were used for the receptor, however at maximum depth from the source. It is important to realize that the receptor data is therefore not to scale with the

internal clay plug conductivities. Even though three electrodes were inserted into each sample, some of the probes failed. Hence their data was omitted from figure 8.8.

Several processes can be indicated from the graphs. Steady state conditions are reached, when the curve for the conductivities in the interior of the sample plug describe a line without a slope, parallel to the x-axis. This can be seen in sample Feuerletten sample B6, for example. Here, at 10 days experimental duration and at depth of 0.7 cm, the graph shows steady state condition while this status has not yet been reached for the greater depths of 1.5 and 2.2 cm. For the longer duration experiments with temperature changes, additional observations can be made. Lehrberg Layer sample L11.5 exhibits a counter osmotic flow process, where a slight decrease in conductivities is observed during the first 20 days, most evident in the sample close to the receptor. L6 is a good example of changes in concentrations congruent with the tri-fold  $D_e$  modeling approach as used with samples L6, M6, L11.5 with during POLLUTEv6 (GAEA, 1997) computation. An abrupt change in the concentration patterns at depth 0.2 cm from the source is observed at 50 to 60 days. While sorption sites are probably being occupied before, at that point in time, available sorbent properties are saturated and greater amounts of chemical species are breaking through. The slight drop at the temperature change from 10°C to 30°C at 92 days has been previously interpreted as an increase in anion exclusion, reducing the amount of chemical species, and can be nicely verified with the conductivity probe data. Anion exclusion is also visible in the Lower Rötton sample M6 during the 30°C phase where the conductivity curve at depth 1.9 cm is slowly declining. When looking at these graphs carefully, the interpretations of the indicated diffusive process can be verified. Inserting these conductivity samplers into the clay plug therefor has proven to be an invaluable tool in diffusion data interpretation.

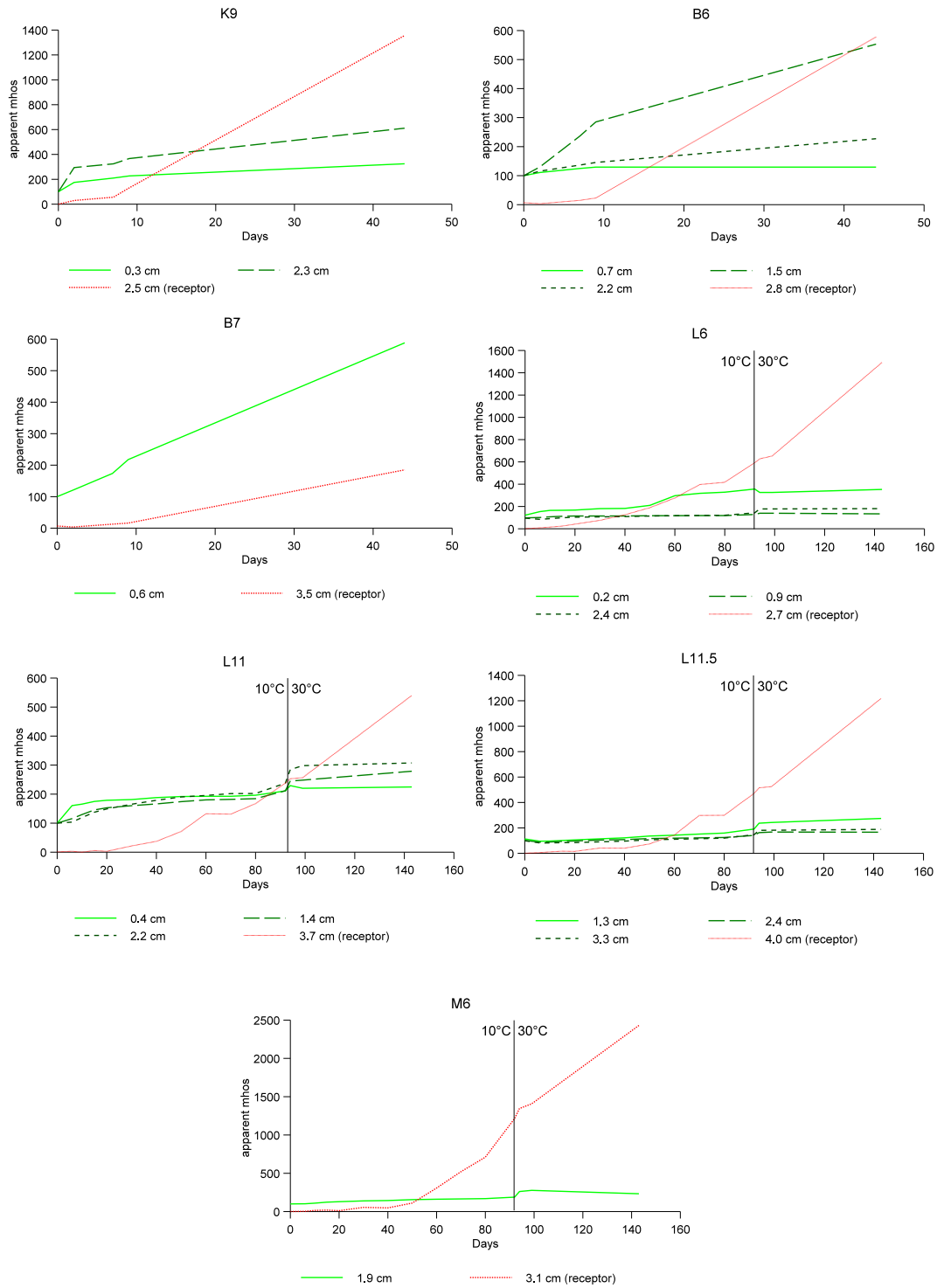


**Figure 8.8** - Apparent internal clay plug conductivities for indicated distances from the source reservoir in comparison with the receptor vessel conductivities.

## 9 Conclusions

While modeling diffusion coefficients of individual chemical species in a high concentration mixture of a synthetic landfill leachate can help in understanding certain underlying premises of such a massive chemical migration by diffusion, the net result for future use is however the understanding of the flux of the total system or the total diffusion coefficient. As indicated by HÖLTING (1992), clay materials will often act as a chromatographic system through ion exclusions, causing a sieve-effect in geologic barriers, allowing some ions to apparently move faster through the system than others. It must be understood that all chemical species will follow a cation-anion balance. For example in a diffusion test with KCl, the anion Cl may appear to migrate faster than the cation K, the anion will partner with another cation through exchange processes or other mechanisms to satisfy the total ionic balance. This can be verified by the close relationship of  $D_e^{\text{Total}}$ , acquired by concentration profiles in the receptor and modeling with POLLUTEv6 (GAEA, 1997) and the  $D_e^{\text{Total}}$  derived from the weighted average of diffusion coefficients for individual chemical species. Discrepancies between those two values may occur if one or more additional ions are introduced through exchange processes which were not determined during the analysis of the receptor and source fluids. The following overall conclusion can be derived from this research:

### 9.1 Geochemistry

Determining the geochemistry of the geologic barrier material had most value for mineralogical calculations. Certain sorptive characteristics and properties can be deduced from the presence of manganese and iron oxides, often neglected when working with more prominent sorptive processes in clay materials. Some diffusive processes are indicated to be influenced by  $K_2O$  and Ba concentrations in the geologic barriers. The reasons are not understood and further research is recommended.

### 9.2 Mineralogy

Knowledge of sample mineralogy is most helpful in determining sorptive processes. Still, mineral composition of fine grained lithologies are not easily ascertained. XRD evaluations are most useful, but are limited for certain mineralogies. Mineral calculations from geochemical data for fine grained igneous rock are a proven approach, but are difficult for suites of sedimentary samples. Indeed, each sample set will require the development of own unique computational approaches. However, it was found that some commonalities in the calculations among a variety of sedimentary lithologies exists and are proven useful for minor mineral and carbonate calculations. Clay mineralogy is the most difficult to determine through mathematical approaches using whole rock geochemical data. Yet some relationships were indicated during this study. The possibility of an universally applicable computation of kaolinite from the presence of  $TiO_2$  should be further investigated.

### 9.3 Physical Properties

The physical parameters of the geologic barrier lithologies in light of diffusive processes are mostly important if relating to porosity or pore space. Thus bulk density, dry density, grain sorting and kurtosis are often found to show correspondence with  $D_e$  values of chemical species. Flow parameters, such as hydraulic conductivity, would be important if mechanical flux would be modeled in combination with diffusive transport processes. Because this was not the case during this research, the usefulness of physical properties is limited to the afore mentioned.

### 9.4 Sorption

Sorptive processes in clay barriers are mostly controlled by the quality and type of fine grained phyllosilicates. Other indicators appear to be oxides of manganese and iron. Carbon, which plays a major role in the sorptive processes of surface soils, is limited for deep lithologic barrier materials.  $K_d$  values determined through batch experiments often coincide with those defined through POLLUTEv6 (GAEA, 1997) modeling, nonetheless, only if steady state diffusive conditions are approached. The use of a multi chemical species synthetic leachate was of importance since certain ionic exchange characteristics did take effect, which correlated slightly with CEC values of the geologic barrier.

## 9.5 Diffusion

Diffusion experiments are lengthy and difficult, especially for undisturbed samples. Preparation, experiment and evaluation times may exceed one year and are not very cost effective. Barrier material with the quality necessary to conduct this diffusion study was limited. From the 35 initially selected samples, only 7 survived the diffusion experiments and delivered useful data. Under these circumstances diffusion testing does not lend itself to be a routine, standardized laboratory procedure for the evaluation of geologic barriers, as may be approached for disturbed, compacted materials. It would be advantageous to find a less involved parameter from which diffusive behaviors can be deduced. While the sample and data density were low for statistical purposes, the following general conclusions can be drawn.

### 9.5.1 Modeling

POLLUTEv6 (GAEA, 1997) has proven to be an invaluable tool in the determination of diffusion coefficients, as well as  $K_d$  and  $K_p$  values congruently. Modeling was much more sensitive and also time consuming than anticipated. Since the sample plugs could not be dissected and concentration profiles established, data from the receptor reservoir was sufficient to establish diffusion data.

### 9.5.2 Ion exclusion

Anion exclusion proved to be a major important factor in diffusion modeling and can be used to explain many observed anomalies. Since diffusion is influenced by sorption and effective porosity, anion exclusion may exhibit pseudo-sorptive characteristics not manifest during batch experiments. More likely, large anions will effectively reduce the effective porosity by plugging pore spaces when excluded through Guoy and Stern layer overlaps. This is much more evident when a synthetic landfill leachate is used, where many ionic species are interacting.

### 9.5.3 Diffusion processes

Diffusion through undisturbed clay plugs is more interactive than previously anticipated. Diffusion coefficients are not static, but actually vary during the course of the experiment, until a quasi steady-state condition is reached. Even then, sorptive ion exchange and ion exclusion processes may continue to act on  $D_e$  over time. Verification of such modeled and observed behavior was made easily by conductivity probes inserted at various depth intervals into the clay sample plugs.

## 9.6 Possible Future Applications

The following could not be satisfactorily answered during this research. Below are strong indicators that warrant possible future applications and research studies.

### 9.6.1 Pore spaces

As indicated by ROWE *et al.* (1999), porosity is of major importance in diffusion research. However, this study indicates that the quality of the pore spaces may be even of greater importance than the quantity, especially in fine grained, non fractured materials. While the parameter for effective porosity includes a qualitative approach to the evaluation of pore spaces, it is overall deficient. When comparing materials with the same  $n_e$ , one may have an array of many small passages while the other may exhibit a few but larger diameter openings. The former would cause a much greater anion exclusion effect than the later. Hence a study of the quality of the porosity of a sample in relation to the diffusive properties may give new indications for the evaluation of ionic chromatographic effects, filtering properties, changes in chemical fluxes and sorptive behaviors. This research strongly indicates that the quality of the pore spaces plays indeed a major role in the diffusive-sorptive process of migrating pollutants through the subsurface.

### 9.6.2 $CEC_{Na}$

The cation exchange capacity of Na correlates nicely with the total effective diffusion coefficient of the SLL for various geologic barrier materials. A linear and quadratic relationship could be established and is represented as equation 9.1 and 9.2 respectively.

$$\text{Eq. 9.1} \quad D_e^{Total} = -2.6483 + (CEC_{Na} * 1.2897)$$

$$\text{Eq. 9.2} \quad D_e^{Total} = -7.7903 + (3.6084 * CEC_{Na}) + (-0.238 * CEC_{Na}^2)$$

where  $D_e^{Total}$  = effective diffusion coefficient for total of species in a SLL in  $cm^2/s$   
 $CEC_{Na}$  = Sodium cation exchange capacity in  $mmol(eq)/100g$

While the number of samples used for deducing these equations was only 5 and therefore on the low end to arrive at such bold conclusions, it was possible to test these formulas against other experimental data presented in the literature. SHACKELFORD *et al.* (1989) reported CEC values as well as  $D_e$  coefficients using a multi species artificial leachate with disturbed kaolinite and natural clay sample plugs. Employing his data and the deduced equations above, the correspondence with equation 10.2 showed an error margin of only 7.5% for the kaolinite samples. Natural clays used by SHACKELFORD *et al.* (1989), however, did not fare as well, displaying an error of 106% when evaluated with the above quadratic equation. Nevertheless, it was encouraging that the  $D_e$  approximations based on  $CEC_{Na}$  data as indicated during this research were applicable at least in part for outside data. While not yet conclusive, the exchange capacity of sodium may hold an important clue for evaluating diffusion coefficients in geologic barrier samples and multi species leachates without expensive and cumbersome diffusion laboratory tests.

## References

- Adams, A.E., MacKenzie, W.S., and Guilford, C., 1984, Atlas of sedimentary rocks under the microscope. Longman publishers.
- Allard, B., Håkansson, K., Karlsson, S., and Sigas, E., 1991, A field study of diffusion controlled migration of copper, zinc and cadmium in a clay formation. *Water, Air, and Soil Pollution* 57-58, p. 259-268.
- Alley, W., 1993, Regional Groundwater Quality. Van Nostrand Reinhold, N.Y., N.Y.
- Allison, L.E., 1960, Wet combustion apparatus and procedure for organic and inorganic carbon in soil. *Soil Sci. Soc. Am. Proc.*, vol. 24, p.36-40.
- Aly, O. M., and Faust, S.D., 1964, Studies on the fate of 2,4-D and ester derivatives in natural surface waters. *Agric. Food Chem.*, vol. 12, no. 6, p. 541-546.
- ATV-Arbeitsgruppe, 1988, Die Zusammensetzung von Deponiesickerwässern. *Müll & Abfall*, vol. 2, p. 67-71
- Azam, S., Abduljawad, S.N., Al-Shayea, N.A., and Baghabra Al-Amoudi, O.S., 2000, Effects of Calcium Sulfate on Swelling Potential of an Expansive Clay. *Geotechnical Testing Journal*, vol. 23, No. 4, p. 389-403
- Bailey, S.W., 1980, Structures of layer silicates. In: Brindley G.W., Brown, G. (Eds.), *Crystal Structures of clay minerals and their X-ray identification*. Mineral. Soc., London, p. 123.
- Baker, R.A., 1968, Kurtosis and Peakedness. *J. Sed. Pet.*, Vol. 38, p. 679 - 680.
- Ball, D.F., 1964, Loss-on-ignition as an estimate of organic matter and organic carbon in non-calcareous soils. *J. Soil Sci.*, Vol. 15, p. 84-92.
- Banerjee, S., Yalkowsky, S.H., and Valvani, S.C., 1980, Water Solubility and Octanol/water Partition Coefficients of Organic Limitations of the Solubility Partition Coefficient Correlation. *Environ. Sci. Technol.*, Vol. 14, p. 1227-1229.
- Barone, F.S., Rowe, R.K., and Quigley, R.M., 1992, A laboratory estimation of diffusion and adsorption coefficients for several volatile organics in a natural clayey soil. *Journal of Contaminant Hydrology* 10 (3), p. 225-250.
- Barone, F.S., Rowe, R.K., and Quigley, R.M., 1990, Laboratory determination of chloride diffusion coefficient in an intact shale. *Can. Geotech. J.* 27, p. 177-184.
- Barone, F.S., Yanful, E.K., Quigley, R.M., and Rowe, R.K., 1989, Effect of multiple contaminant migration on diffusion and adsorption of some domestic waste contaminants in a natural clayey soil. *Can. Geotech. J.* 26 (2), p. 189-198.
- Bayerisches Geologisches Landesamt, 1981a, Erläuterungen zur Geologischen Karte von Bayern 1:500,000. GLA, Munich, Germany.
- Bayerisches Geologisches Landesamt, 1981b, Geologische Karte von Bayern 1:500,000. GLA, Munich, Germany.
- Bedient, P.H., Rifai, H.S., and C.J. Newell, *Ground Water Contamination: Transport and Remediation*. Prentice Hall, Englewood Cliffs, NJ.
- Bennett, R.H., O'Brien, N.R., and Hulbert, M.H., 1990, Determinants of Clay and Shale Microfabric Signatures: Processes and Mechanisms. In: Bennett, R.H., Bryant, W.R., and Hulbert, M.H. (Eds.), *Microstructure of Fine-Grained Sediments: From Mud to Shale; Frontiers in Sedimentary Geology Series*, Springer, New York, p. 5-32.
- Berger, K., 1966, Erläuterungen zur Geologischen Karte von Bayern, 1:25000, Blatt 6530, Langenzenn. GLA, Munich, Germany.



- Berger, K., 1975, Erläuterungen zur Geologischen Karte von Bayern, 1:25000, Blatt 6430, Langenzenn. GLA, Munich, Germany.
- Berry, L.G., and Mason, B., 1959, Mineralogy - Concepts, Descriptions, Determinations. W.H. Freeman, San Francisco.
- Børretzen, P., and Salbu, B., 1999, Geochemical Models for Sediment-Seawater Interactions. Laboratory for Analytical Chemistry, Institute for Chemistry and Biotechnology, Agricultural University of Norway, 1432 Ås, Norway, p. 1-28.
- Bouyoucos, G.J., 1963, Hydrometer method improved for making particle size analysis of soil. Agron. J., Vol. 54, p. 464-465.
- Brunauer, S., Emmett, P.H. and Teller, E., 1938, Adsorption of gases in multimolecular layers. J. Am. Chem. Soc., Vol. 60, p. 309-319.
- Butterfield, J.A., 1936, Outgrowths on zircon. Vol. 73, Geol. Mag., p. 511-516.
- Carozzi, A.V., 1960, Microscopic Sedimentary Petrography. John Wiley and Sons, New York.
- Casagrande, A., 1934, Die Aräometer-methode zur Bestimmung der Kornverteilung von Böden und anderen Materialien. Berlin: Julius Springer.
- Chamley, H., 1989, Clay Sedimentology. Springer, Heidelberg.
- Cho, W.J., Oscarson, D.W., and Hahn, P.S., 1993, The measurement of apparent diffusion coefficients in compacted clays: an assessment of methods. Applied Clay Sci., Vol. 8, No. 4, p. 283 - 294.
- Cook, A. J., 1988, A desk study of surface diffusion and mass transport in clay. British Geological Survey Technical Report WE/88/34.
- Correns, C.W., and Tillmanns, 1978, Titanium: Handbook of Geochemistry, Vol. II/2, Ti(22), Springer.
- CRC, 1985, CRC Handbook of Chemistry and Physics. Weast, R.C., Astle, M.J., and Beyer, W.H. (Eds.), 65<sup>th</sup> edition, CRC Press Inc., Boca Raton, Florida.
- Crooks, V.E., and Quigley, R.M., 1984, Saline leachate migration through clay: A comparative laboratory and field investigation. Can. Geotech. J., Vol. 21, p. 349-362.
- Czurda, K., and Wagner, J.F., 1986, Diffusion und Sorption von Schwermetallen in tonigen Barrieregesteinen. In: Rentz, O., Steirth, J., Zillox, L (Eds.). Premiere colloque scientifique des Universities du Rhin superieur; Recherches sur l'environnement dans la region. P. 785-793.
- Daniel, D.E. and Shackelford, C.D., 1988, Disposal barriers that release contaminants only by molecular diffusion. Nucl. Chem. Waste Manage., 8, p. 299-305.
- Davis, C.W., 1962, Ion Association. Butterworth, Washington D.C.
- Dean, J.A., 1985, Lange's Handbook of Chemistry. 13th Ed, McGraw-hill Book Co., N.Y., N.Y.
- Dean, W.E., 1974, Determination of carbonate and organic matter in calcareous sediments and sedimentary rocks by loss on ignition: comparison with other methods. J.Sed.Pet., 44, No. 1, p. 242-248.
- Degens, E.T., 1965, Geochemistry of Sediments - A brief summary. Prentice-Hall, N.J.
- Dietrich, R.V, Dutro, J.T., and Foose, R.M. (Editors), 1982, AGI Data Sheets for the Geologist in the Field, Laboratory and Office. 2<sup>nd</sup> edition, American Geological Institute, Alexandria, Virginia.
- DIN.18.123, 1983, Baugrund, Untersuchung von Bodenproben, Bestimmung der Korngrößenverteilung. Beuth, Berlin.

- DIN.18.124, 1997, Baugrund, Untersuchung von Bodenproben - Bestimmung der Korndichte - Kapillarpyknometer, Weithalspyknometer. Beuth, Berlin.
- DIN.18.129, 1990, Baugrund, Versuche und Versuchsgeräte: Kalkgehaltsbestimmung. Beuth, Berlin.
- DIN.18.130 Teil 1, 1989, Baugrund, Versuche und Versuchsgeräte: Bestimmung des Wasserdurchlässigkeitsbeiwertes, Laborversuch. Beuth, Berlin.
- DIN.18.132, 1993, Baugrund, Versuche und Versuchsgeräte Bestimmung des Wasseraufnahmevermögens. Entwurf Juli 1993, Beuth, Berlin.
- DIN.19.684 Teil 1, 1977, Bodenuntersuchungsverfahren im Landwirtschaftlichen Wasserbau, chemische Laboruntersuchungen, Bestimmung des pH -Wertes des Bodens und Ermittlung des Kalkbedarfs. Berlin, Beuth.
- DIN.19.684 Teil 8, 1977, Bodenuntersuchungsverfahren im Landwirtschaftlichen Wasserbau, chemische Laboruntersuchungen: Bestimmung der Austauschkapazität des Bodens und der austauschbaren Kationen. Beuth, Berlin.
- DiVincenzo, J.P., and Sparks, D.L., 2001, Sorption of the Neutral and Charged Forms of Pentachlorophenol on Soil: Evidence for Different Mechanisms. *Arch. Environ. Contam. Toxicol.*, vol. 40, p. 445-450
- Dobner, A, 1984, Tone, Mergel, Lehme. In: *Oberflächennahe mineralische Rohstoffe von Bayern*. Geol. Bavarica, GLA, Munich, Germany, Vol. 86, p. 441 - 494.
- Dolcater, D.L., Syers, J.K., and Jackson, M.L., 1970, Titanium as free oxide and substituted forms in kaolinite and other soil minerals. *Clays & Clay Minerals*, 18, p.71-79.
- Domenico, P.A., and Schwartz, F.W., 1990, *Physical and chemical hydrogeology*. New York: John Wiley & Sons.
- Drever, J.I., 1982, *The Geochemistry of Natural Waters*. Prentice-Hall, New Jersey.
- Duda, R., and Rejl, L., 1990: *Minerals of the World*. Arch Cape Press, New York.
- Eckenfelder, W.W., and Musterman, J.L., 1994, *Leachate treatment technologies to meet alternative discharge requirements*. Eckenfelder, Inc. Nashville, TN.
- Fetter, C.W.Jr., 1980, *Applied Hydrology*. Merrill Publishing, Columbus, Ohio.
- Folk, R.L., 1980, *Petrology of Sedimentary Rocks*. Hemphill Publishing Company, Austin.
- Fürst, M., 1956, *Erläuterungen zur Geologischen Karte von Bayern, 1:25000, Blatt 6135, Creußen*. GLA, Munich, Germany
- GAEA, 1997, *POLLUTE V6 - Professional Version 6.3.2*. DOS-Software, GAEA Environmental Engineering Ltd., 1575 Lyons Ave., Windsor, Ontario, Canada N9J 3K4.
- Gaines, R.V., Skinner, H. C.W., Foord, E.E., and Rosenzweig, A., 1997, *Dana's New Mineralogy*. 8<sup>th</sup> Edition, John Wiley & Sons, New York.
- Gautschi, A., 2001, Hydrogeology of a fractured shale (Opalinus Clay): Implications for deep geological disposal of radioactive wastes. *Hydrogeology Journal*, vol. 9, p. 97-107.
- Gillham, R.W., Robin, M.L.J., Dytynshyn, D.J., and Johnston, H.M., 1984, Diffusion of nonreactive and reactive solutes through fine grained barrier materials. *Can. Geotech. Journ.*, vol. 21, p. 541 - 550.
- Gillman, G.P, and Sumpter, E.A., 1986, Modification to the compulsive exchange method for measuring exchange characteristics of soils. *Aust. J. Soil Res.*, vol. 24, p. 61-66.

- Gillman, G.P., 1979, A proposed method for the measurement of exchange properties of highly weathered soils. *Aust. J. Soil. Res.*, vol. 17, p. 129-139.
- Goldin, A., 1987, Reassessing the use of loss-on-ignition for estimating organic matter content in non-calcareous soils. *Commun. Soil Sci. Plant Anal.*, Vol. 18, p. 1111-1116.
- Guadalix, M.E., and Pardo, M.T., 1995, Zinc sorption by acid tropical soils as affected by cultivation. *Eur. J. Soil Sci.* 46, p. 317 - 321.
- Gudehus, G., 1981, *Bodenmechanik*. Ferdinand Enke Verlag, Stuttgart.
- Haarländer, W., 1966, *Geologische Karte von Bayern 1:25000, Erläuterungen zum Blatt 6432 Erlangen-Süd*. GLA, Munich, Germany.
- HACH, 1996, *DR/2000 Spectrophotometer Procedures Manual*. 11<sup>th</sup> edition, Hach Company, Loveland, CO.
- Hänel, R., 1974, *Geologische Karte von Bayern 1:25000, Erläuterungen zum Blatt 6433, Lauf a.d. Pegnitz*. GLA, Munich, Germany.
- Hansch, C., Leo, A. and Hoekman, D., 1995, *Exploring QSAR. Hydrophobic, Electronic, and Steric Constants*. ACS Professional Reference Book. Washington, DC: American Chemical Society.
- Harms Atlas, 1977, *Deutschland und die Welt. Ausgabe Bayern*. List Verlag, Munich, Germany.
- Hassenpath, R., 1988, *Bodenmechanische Veränderungen reiner Tone durch Adsorption chemischer Verbindungen (Batch- und Diffusionsversuche)*. *Mitteil. Inst. Grundbau & Bodenmechanik*, Nr. 134, ETH Zürich.
- Heimerl, H., 1995, *Methodenoptimierung zur Analyse der Schadstoffmobilität in tonigen Deponiedichtungsmaterialien*. Dissertation, University of Regensburg, Germany.
- Henning, K.H., and Störr, M., 1986, *Electron micrographs (TEM, SEM) of clays and clay minerals*. Series in Geological Science, Akademie Verlag, Berlin, No. 25.
- Herner, A.E., A.G. Hornsby, R.D. Wauchope, 1996, *Pesticide Properties in the Environment*. Springer Publishers, New York.
- Hölting, B., 1992, *Hydrogeologie: Einführung in die allgemeine und angewandte Hydrogeologie*. 4<sup>th</sup> edition, Enke Verlag.
- Howard, P.H., Boethling, R.S., Stiteler, W.M., Meylan, W.M., Hueber, A.E., Beauman, J.A., and Larosche, M.E., 1992, Predictive model for aerobic biodegradability developed from a file of evaluated biodegradation data. *Environ. Toxicol. Chem.* Vol. 11, p. 593-603.
- Imbrie, J., and Poldervaart, A., 1959, Mineral Compositions Calculated from Chemical Analyses of Sedimentary Rocks. *J. Sediment. Petrol.*, 29, No. 4, p. 588-595
- Jagodzinski, H., 1949, Eindimensionale Fehlordnung in Kristallen und ihr Einfluß auf die Röntgeninterferenzen. In: *Berechnung des Fehlordnungsgrades aus den Röntgenintensitäten*, *Acta Crystallogr.*, Z, p. 201-207.
- Jasmund, K., and Lagaly, G., 1993, *Tonminerale und Tone: Struktur, Eigenschaften, Anwendungen und Einsatz in Industrie und Umwelt*. Jasmund, K. and Lagaly, G. (Eds.), Steinkopff, Darmstadt.
- Joback, K.G., 1982, *A Unified Approach to Physical Property Estimation Using Multivariate Statistical Techniques*. Stevens Institute of Technology, submitted to the Dept. of Chem. Eng. for M.S. Degree at the Massachusetts Institute of Technology in June 1984.

- Kackstaetter, U.K., 1990, Stratigraphy, Petrology, Geochemistry, and Diagenesis of the Early Jurassic Springdale Sandstone, Shivwits, Washington County, Utah. Master's Thesis, Brigham Young University, Provo, Utah.
- Kaltofen, R., Opitz, R., Schumann, K., and Ziemann, J., 1972, Tabellenbuch Chemie. 6<sup>th</sup> edition, VEB Deutscher Verlag für Grundstoffindustrie, Leipzig, German Democratic Republic.
- Karickhoff, S.W., 1981, Semi-Empirical Estimation of Sorption of Hydrophobic Pollutants on Natural Sediments and Soils. *Chemosphere* 10, Pergamon, Oxford, UK, p. 833-846.
- Käss, W., 1967, Erfahrungen mit Uranin bei Färbeversuchen. *Steir. Beitr. Hydrogeol., N.F.*, Graz, Jg. 1966/67, p. 123-132.
- Klotz, D., 1988, Bestimmung von Diffusionskoeffizienten in bindigen und sandigen Sedimenten aus der Gegend von Gorleben. *Institut für Hydrologie, GSF-Bericht/Hy 38/88*, p. 16-20
- Kohler, E.E., and Harström, J., 1994, Langzeitverhalten und deponierelevante Grenzflächenreaktionen von HDPE-Ton-Kombinationsdichtungen. *BayForrest 2 Statusseminar, Berichtsheft 2*, TU München, p. 245 - 251.
- Kohler, E.E., Heimerl, H., and Czurda, K., 1994, Quantitative Mineralanalyse, Sonderdruck. In: *Methodenhandbuch für tonmineralogische Untersuchungen*, Bundesanstalt f. Geowiss. u. Rohstoffe, Hannover (in preparation).
- Köster, H.M., and Schwertmann, U., 1993, Beschreibung einzelner Tonminerale. In: *Jasmund, K. and Lagaly, G. (Eds.), Tonminerale und Tone: Struktur, Eigenschaften, Anwendungen und Einsatz in Industrie und Umwelt*. Steinkopff, Darmstadt, p. 33-88.
- Kowalenko, C.G., and Yu, S., 1996, Assessment of nitrate adsorption in soils by extraction, equilibration and column-leaching methods. *Can. J. Soil Sci.*, vol. 76, p. 49 -57.
- Krause, C., Fisch, E., and Rohrbach, J., 1993, Kationenaustauschkapazität - Ein Beitrag zur Methoden-Standardisierung für die Bewertung mineralischer Deponiebasisabdichtungen. *Keram. Zeitschr.*, vol. 45, no. 7, p. 385-389.
- Krauskopf, K.B., 1979, *Introduction to geochemistry*. McGraw-Hill Book Co.
- Kretzschmar, R., 1991, *Kulturtechnisch - Bodenkundliches Praktikum. Ausgewählte Labormethoden - Eine Anleitung zum selbständigen Arbeiten an Böden*. 7. Aufl., Eigenverlag, Kiel.
- Lagaly, G., and Köster, H.M., 1993, *Tone und Tonminerale*. In: *Jasmund, K. and Lagaly, G. (Eds.), Tonminerale und Tone: Struktur, Eigenschaften, Anwendungen und Einsatz in Industrie und Umwelt*. Steinkopff, Darmstadt, p. 1-29.
- Lake, C.B., and Rowe, R.K., 1999, *Diffusion of sodium and chloride through geosynthetic clay liners*. Geotechnical Research Report GEOT-5-99, Geotechnical Research Centre, Univ. Of Western Ontario, London, Ontario, Canada.
- Lambe, T.W., and Whitman, R.V., 1979, *Soil Mechanics*, SI Version. Wiley & Sons, New York.
- Langmuir, D., 1997, *Aqueous environmental geochemistry*. Prentice Hall.
- Laves, D. u. Jähn, G., 1972, Zur quantitativen röntgenographischen Bodenton-Mineralanalyse. *Arch. Acker- u. Pflanzenbau u. Bodenkde.*, 16, H. 10, p. 735-739.
- Lee, G.F., and Jones-Lee, A., 1993, Groundwater pollution by municipal landfills: Leachate composition, detection and water quality significance. *Proc. Sardinia '93 IV International Landfill Symposium*, Sardinia, Italy, Oct. 1993, p. 1093 - 1102.

- Lenz, R., 1991, Charakteristika und Belastungen von Waldökosystemen NO-Bayerns - eine landschaftsökologische Bewertung auf stoffhaushaltlicher Grundlage. Forschungszentrums Waldökosysteme, Reihe A, vol. 80.
- Levinson, A.A., 1980, Introduction to exploration geochemistry. 2<sup>nd</sup> ed., Applied Publishing Ltd..
- LGA, 1996, Sickerwasseranalysen der Deponie Raindorf - unpublished data.
- Li, Y.H, and Gregory, S., 1974, Diffusion of ions in sea water and deep sea sediments. *Geochimica et Cosmochimica Acta*, Vol. 35, No. 5, p. 703 - 714.
- Loehr, R.C., 1993, Bioremediation of soils. In: Daniel, D.E. (Ed.), *Geotechnical Practice for Waste Disposal*, Chapman & Hall, p. 520 - 550.
- Lyman, W.J. 1990. Adsorption coefficient for soils and sediments. In: Lyman, W.J. et al. (Eds.), *Handbook of Chemical Property Estimation Methods*. Washington, DC: American Chemical Society. Chapter 4.
- Lyman, W.J., Rheel, W.F., and Rosenblatt, D.H., 1982, *Handbook of chemical property estimation methods. Environmental behavior of organic compounds*. New York, McGraw-Hill.
- MacKay, D., 1991, SOIL fugacity model. *Multimedia Environmental Models*. Lewis Publishers, Chelsea, MI
- Marotz, G., 1968, Technische Grundlagen einer Wasserspeicherung im natürlichen Untergrund. *Schriftenreihe KWK*, Vol. 18, Hamburg.
- McBean, E.A., and Rovers, F.A., 1999, Landfill Leachate Characteristics as Inputs for the Design of Wetlands used as Treatment Systems. In: Mulamootil, G., McBean, E.A, and Rovers, F.A., (Eds.), *Constructed Wetlands in the Treatment of Landfill Leachate*. CRC Press, LLC, Boca Ralton, FL, p. 1-16.
- McBride, E.F, 1971, Mathematical Treatment of Size Distribution Data. In: Carver, R.E. (Ed.), *Procedures in sedimentary petrology*, Wiley-Interscience, A division of John Wiley and Sons, New York, chapter 6, p. 109 - 127.
- McBride, M.B, 2000, Chemisorption and precipitation reactions. In: Sumner, M.E. (Ed.), *Handbook of soil science*, CRC Press, p. B-265 - B-302.
- McHardy, W.J., and Birnie, A.C., 1987, Scanning electron microscopy. In: Wilson, M.J. (Ed.), *A handbook of determinative methods in clay mineralogy*, Blackie, Chapman & Hall, p. 174-208.
- Mehlich, A., 1938, Use of triethanolamine acetate-barium hydroxide buffer for the determination of some base exchange properties and lime requirement of soil. *Soil Sci. Soc. Am. Proc.*, vol. 29, p. 374-378.
- Mehlich, A., 1948, Determination of cation- and anion-exchange properties of soils. *Soil Sci.*, vol. 66, p. 429-445.
- Mehra, O.P., and Jackson, M.L., 1960, Iron oxide removal from soils and clays by a dithionite-citrate system buffered with sodium bicarbonate. *Clays & Clay Minerals*, 7, p. 317-327.
- Melnyk, T.W., 1985, Effects of sorption behavior on contaminant migration. Atomic Energy of Canada Limited (AECL-8390), Whiteshell Nuclear Research Establishment, Pinawa, Manitoba R0E 1L0.
- Merck Index, 1989, *An Encyclopedia of Chemicals and Drugs*. Budavari, S. *et.al.*(Eds), Rahway, N.J., 11th Ed., Merck & Co., Inc.
- Meylan, W.M. and Howard, P.H., 1991, Bond contribution method for estimating Henry's Law Constants. *Environ. Toxicol. Chem.* Vol. 10, p. 1283-1293. (HENRYWIN Software available from Syracuse Research Corp, Environmental Science Center, Syracuse, NY 13210).
- Meylan, W.M. and Howard, P.H., 1993, Computer estimation of the atmospheric gas-phase reaction rate of organic compounds with hydroxyl radicals and ozone. *Chemosphere* Vol. 26, p. 2293-2299.

- Meylan, W.M. and Howard, P.H., 1994a, Upgrade of PCGEMS Water Solubility Estimation Method (May 1994 Draft). Prepared for Boethling, R.S.: U.S. Environmental Protection Agency, Office of Pollution Prevention and Toxics, Washington, DC; prepared by Syracuse Research Corporation, Environmental Science Center, Syracuse, NY 13210.
- Meylan, W.M. and Howard, P.H., 1994b, Validation of Water Solubility Estimation Methods Using Log  $K_{ow}$  for Application in PCGEMS & EPI (Sept 1994, Final Report). Prepared for Boethling, R.S., U.S. Environmental Protection Agency, Office of Pollution Prevention and Toxics, Washington, DC; prepared by Syracuse Research Corporation, Environmental Science Center, Syracuse, NY 13210.
- Meylan, W.M. and Howard, P.H., 1995, Atom/fragment contribution method for estimating octanol-water partition coefficients. *J. Pharm. Sci.* Vol. 84, p. 83-92.
- Meylan, W.M., Howard, P.H., Aronson, D., Printup, H., and Gouchie, S., 1997, Improved Method for Estimating Bioconcentration Factor (BCF) from Octanol-Water Partition Coefficient. SRC TR-97-006 (2nd Update), prepared for: Robert S. Boethling, EPA-OPPT, Washington, DC; Contract No. 68-D5-0012; Syracuse Research Corp., Environmental Science Center, 6225 Running Ridge Road, North Syracuse, NY 13212.
- Mietsch, A.T., 1962, Computing Mineral Compositions of Sedimentary Rocks from Chemical Analyses. *J. Sediment. Petrol.*, 32, No. 2, pp. 217-225
- Mill, T., Haag, W., Penwell, P., Pettit, T. and Johnson, H., 1987, Environmental Fate and Exposure Studies Development of a PC-SAR for Hydrolysis: Esters, Alkyl Halides and Epoxides. EPA Contract No. 68-02-4254. Menlo Park, CA, SRI International.
- Nestmeyer, R., 1996, Franken. Michael Müller Publishers, Erlangen, Germany.
- Neumüller, O.A., 1977, Basis-Römpf: Taschen-Lexikon der Chemie, ihrer Randgebiete und Hilfswissenschaften. Band 1, Franckh'sche Verlagshandlung Stuttgart.
- Nicholls, G.D., 1962, A scheme for recalculating the chemical analyses of argillaceous rocks for comparative purposes. *Am. Mineral.* 47, p. 34-36.
- Nowlan, G.A., 1976, Concretionary manganese-iron oxides in streams and their usefulness as a sample medium for geochemical prospecting. *J. Geochem. Explor.*, vol. 6, p. 193-210.
- O'Donoghue, M., 1990; American Nature Guides - Rocks and Minerals. Gallery Books, New York.
- Oscarson, D.W., 1994, Surface Diffusion: Is it an important Transport Mechanism in Compacted Clays? *Clays & Clay Minerals*, Vol. 42, No. 5, p. 534-543.
- Pasche, E., 1993a, Erläuterungen zu einer Geologischen Karte - Detail-Kartierung des Nord-Ost-Bereichs Blatt Creußen (6135). Part I, Dipl. Arb. Geol. Inst. Univ. Würzburg (unpublished)
- Pasche, E., 1993b, Wasserdruckversuche und Bohrung im Nord-Ost Bereich von Blatt Creußen (6135). Part II, Dipl. Arb. Geol. Inst. Univ. Würzburg (unpublished)
- Pearson, M.J., 1978, Quantitative Clay Mineralogical Analyses from the Bulk Chemistry of Sedimentary Rocks. *Clays & Clay Minerals*, 26, No. 6, p. 423-433
- Perel'man, A.I., 1977, Geochemistry of Elements in the Supergene Zone. Israel Program for Scientific Translations, Keter Publishing, Jerusalem. John Wiley.
- Peters, W.C., 1978, Exploration and mining geology: John Wiley & Sons, New York.
- Pettijohn, F.J., 1975, Sedimentary Rocks. 3<sup>rd</sup> ed., Harper & Row.

- PHREEQCi, 2002, Windows computer program for simulating chemical reactions and transport processes in natural or contaminated water. Version 2.6.0.1, Release May 30, 2002, by Charlton, S.R. and Parkhurst, D.L., U.S. Geological Survey, Denver, CO 80225-0286.
- Poppe, L.J., and Polloni, C.F. (eds.), 2000, USGS East-Coast Sediment Analysis: Procedures, Database, and Georeferenced Displays, U.S. Geological Survey Open-File Report 00-358, CD-ROM. (online)
- Poppe, L.J., Paskevich, V.F., Williams, S.J., Hastings, M.E., Kelly, J.T., Belknap, D.F., Ward, L.G., FitzGerald, D.M., and Larsen, P.F., 2003, Surficial Sediment Data from the Gulf of Maine, Georges Bank, and Vicinity: A GIS Compilation. U.S. Geological Survey Open-File Report 03-001.
- Potter, P.E., Maynard, J.B., and Pryor, W.A., 1980, *Sedimentology of Shale*. Springer Verlag, Heidelberg.
- Pötzl, D., 1998, Durchfluß- und Sorptionsverhalten ausgewählter geologischer Einheiten gegenüber organischen und anorganischen Modellsubstanzen - Untersuchung an ungestörten Proben. *Hydrogeologie & Umwelt*, Vol. 15.
- Quigley, R.M., Yanful, E.K., and Fernandex, F., 1987, Ion transfer by diffusion through clayey barriers. In: Woods, R.D. (Ed.), *Geotechnical Practice for Waste Disposal*. Am. Soc. Civ. Eng., Special Publication 13, p. 137 - 158.
- Rengasamy, P., 1976, Substitution of iron and titanium in kaolinite. *Clays & Clay Minerals*, Vol. 24, p. 265-266.
- Reynolds, R.C., 1980, Interstratified clay minerals. In: Brindley G.W., Brown, G. (Eds.), *Crystal Structures of clay minerals and their X-ray identification*. Mineral. Soc., London, p. 249-303.
- Rhoades, J.D., 1982, Cation exchange capacity. In: A.L. Page (Ed.) *Methods of soil analysis, Part 2 Chemical and microbiological properties*, 2nd ed., *Agronomy* 9, p. 149-157.
- Robinson, R.A., and Stokes, R.H., 1959, *Electrolyte solutions*. 2<sup>nd</sup> Edition, Butterworth Scientific Publications, London, England
- Ross, D.S., 1995, Recommended Methods for determining Soil Cation Exchange Capacity. In: *Recommended Soil Testing Procedures for the Northeastern United States*, 2<sup>nd</sup> ed., Northeastern Regional Pub. No. 493.
- Rowe, K.R., Cears, C.J., and Barone, F., 1988, Laboratory determination of diffusion and distribution coefficients of contaminants using undisturbed clayey soil. *Can. Geotech. J.*, Vol. 25, p. 108 -118.
- Rowe, K.R., Lake, C.B., and Petrov, R.J., 1999, Apparatus and procedures for assessing inorganic diffusion coefficients for geosynthetic clay liners. *Geotechnical Research Centre Report, GEOT-2-99*.
- Rowe, R.K., Booker, J.R, and Fraser, M.J, 1994, *PolluteV6 User's Guide*. GAEA Env. Engineering Ltd, Windsor, Ontario, Canada.
- Rowe, R.K., 1987, Pollutant transport through barriers. In: Woods, R.D. (Ed.), *Geotechnical Practice for Waste Disposal*. Am. Soc. Civ. Eng., Special Publication 13, p. 159 - 181.
- Roy, W.R., Krapac, I.G., Chou, S.F.J., and Griffin, R.A., 1992, Batch-Type Procedures for Estimating Soil Adsorption of Chemicals. EPA Technical Resource Document 530/SW-87/006-F, Office of Solid Waste and Emergency Response, USEPA, Washington, D.C.
- Rutte, E., 1957, *Einführung in die Geologie von Unterfranken*. Würzburg.
- Rutte, E., 1981, *Bayerns Erdgeschichte. Der geologische Führer durch Bayern*. 1. Ed., Ehrenwirth Munich.
- Ryan, M.C., Graham, G.R., and Rudolph, D.L., 2001, Contrasting Nitrate Adsorption in Andisols of Two Coffee Plantations in Costa Rica. *Journal of Environmental Quality*, Vol. 30, p. 1848-1852.

- Salger, M., and Schwarzmeier, J., 1985, Tonmineralogische Untersuchungen im Buntsandstein des Ostspessarts. Vol. 87, Geol. Bavarica, GLA, Munich, Germany, p. 91-96.
- Schachtschabel, P., Blume, H.P., Brümmer, G., Hartge, K.H., and Schwertmann, U., 1989, Lehrbuch der Bodenkunde. 12<sup>th</sup> edition, Enke Verlag.
- Scheidegger, A.M., Lamble, G.M., and Sparks, D.L., 1996, Mechanisms of Nickel Sorption on Pyrophyllite: Macroscopic and Microscopic Approaches. Soil Sci. Soc. Am. J., vol. 60, p. 1763 - 1772.
- Schindler, P.W., 1980, Surface complexes at oxide water interfaces. In Adsorption at the Solid-Liquid Interface, Anderson, M.A., and Rubin, A.J. (Eds.), Ann Arbor Science Publishers, Ann Arbor, MI, p. 1 - 76.
- Schlee, John, 1973, Atlantic Continental Shelf and Slope of the United States sediment texture of the Northeastern part. U.S. Geological Survey Professional Paper 529-L.
- Schneider, W. & Göttner, J.J., 1991, Schadstofftransport in mineralischen Deponieabdichtungen und natürlichen Tonschichten. Geol. Jb., C 58, Hannover Schweizbart.
- Schulte, E.E., 1995, Recommended Soil Organic Matter Tests. In: Recommended Soil Testing Procedures for the Northeastern United States, 2<sup>nd</sup> ed., Northeastern Regional Pub. No. 493.
- Schwarzenbach, R., and Westall, J., 1981, Transport of Nonpolar Organic Compounds from Surface Water to Groundwater. Laboratory Sorption Studies, Environ. Sci. Technol. 15, p. 1360-1367.
- Schwarzmeier, J., 1979, Geologische Karte von Bayer, Erläuterungen zum Blatt Nr. 6123 Marktheidenfeld, Bayerisches Geologisches Landesamt.
- Schwarzmeier, J., 1981, Geologische Karte von Bayer 1:500 000, Bayerisches Geologisches Landesamt.
- Schweizer, R., Stober, I., and Strayle, G., 1985, Auswertungsmöglichkeiten von Tracerversuchen im Grundwasser. Abhandlungen Geologisches Landesamt B.-Württ., vol. 11, p. 93-139.
- Seip, H.M., Alstad, J., Carlberg, G.E., Martinsen, K., and Skaane, R., 1986, Measurement of mobility of organic compounds in soils. Sci. total Environ., vol. 50, p. 87-101.
- Selvakumar, A. and Hsieh, H.N., 1987, Adsorption of Organic Compounds by Microbial Biomass. Int J Environ Stud, Vol. 30, p. 313-319.
- Shackelford, C.D., 1988, Diffusion as transport process in fine grained barrier materials. Geotech. News, 6(2), p. 24-27.
- Shackelford, C.D., 1991, Laboratory diffusion testing for waste disposal - A review. J. Contam. Hydrol., 7, p. 177-217.
- Shackelford, C.D., 1993, Contaminant Transport. In: Daniel, D.E. (Ed.), Geotechnical Practice for Waste Disposal, Chapman & Hall, p. 31 - 65.
- Shackelford, C.D., and Daniel, D.E., 1991a, Diffusion in saturated soils: I. Background. ASCE J. Geotech. Eng., Vol. 117(3), p. 467-484.
- Shackelford, C.D., and Daniel, D.E., 1991b, Diffusion in saturated soils: II. Results for Compacted Clays. ASCE J. Geotech. Eng., Vol. 117(3), p. 485-506.
- Shackelford, C.D., Daniel, D.E., and Liljestrand, H.M., 1989, Diffusion of inorganic chemical species in compacted clay soils. Journal of Contaminant Hydrology, Vol. 4, No. 3, p.241-273.
- Shams-Khorzani, R., Knox, T.D., and Brockway, R.C., 1994, Sanitary Landfill Leachate Treatment and Disposal. Public Works, June, p. 46-49.



- Shepard, F.P., 1954, Nomenclature based on sand-silt-clay ratios: *Journal Sedimentary Petrology*, vol. 24, p. 151-158.
- SPSS, 1999, SPSS Software for Windows, Rel. 9.0.1. Chicago: SPSS Inc.
- SRC, 2000, EPIWIN - EPA Estimations Suite PC-Programs for Windows, EPIWIN Version 3.10. Syracuse Research Corporation, Environmental Chemistry Center, 6225 Running Ridge Road, North Syracuse, NY 13212. (For complete software overview and reference listing see appendix F.1)
- Staff, S. S. D., 1993, Soil survey manual. United States Department of Agriculture, Washington, DC.
- Stein, S.E. and Brown, R.L., 1994, Estimation of normal boiling points from group contributions. *J. Chem. Inf. Comput. Sci.* Vol. 34, p. 581-587.
- Suffet, I.H., and McGuire, M.J., Editors, 1980, Activated Carbon Adsorption of Organics from the Aqueous Phase. Vol. 1, Ann Arbor Science Publishers, Michigan.
- Sumner, M. E., and Miller, W.P., 1996, Cation exchange capacity, and exchange coefficients. In: D. L. Sparks (Ed.) *Methods of soil analysis. Part 2: Chemical properties*, (3rd ed.) ASA, SSSA, CSSA. Madison, WI.
- Tchernjak, L.P., Nesterenko, I.P., and Soroka, A.C., 1979, Determination of the mineralogical composition of clay raw materials using computer techniques. *Steklo i ceramica*, Moscow, 3, p. 17-19.
- Torres-Roldán, R.L., García-Casco, A. & García-Sánchez, P.A., 1999, CSpace: An integrated workplace for the graphical and algebraic analysis of phase assemblages on 32-bit Wintel platforms. *Computers and Geosciences*. CSpace Version 1.0.1.26, Djinn Works, Departamento de Mineralogía y Petrología, Universidad de Granada. Facultad de Ciencias, Fuentenueva s/n, 18002-Granada, Spain.
- Tovey, N.K., and Wong, K.Y., 1978, Preparation, selection and interpretation problems in scanning electron microscope studies of sediments. In: Whalley, W.B. (Ed.), *Scanning Electron Microscopy in the Study of Sediments - a symposium*, Geo Abstracts Limited, Norwich, England, p. 181-200.
- Trapp, S., and Matthies, M., 1996, *Dynamik von Schadstoffen - Umweltmodellierung mit Cemos*. Springer, Berlin.
- Trask, P.D., and Hammar, H.E., 1934, Organic content of sediments. *Amer. Petrol. Inst.*, 15<sup>th</sup> Ann. Mtg., Dallas, reprint.
- Tributh, H., 1991, Qualitative und "quantitative" Bestimmung der Tonminerale in Bodentonen. In: Tributh, H., and Lagaly, G. (Eds.), *Identifizierung und Charakterisierung von Tonmineralen. - Berichte der Deutschen Ton- u. Tonmineralgruppe e.V., DTTG-Convention, Gießen, May, 10.-12., 1989*.
- Turner, D.R., 1995, Problems in trace metal speciation modeling. In *Metal Speciation and Bioavailability in Aquatic Systems*, Tessier, A., and Turner, D.R. (Eds.). Wiley, Chichester, p. 149-203.
- Urban, H., 1978, Eine Methode zur rechnerischen Bestimmung von Illit und Kaolinit in Tonen und keramischen Massen. *Sprechsaal 111*, p. 373-378.
- USACE (Army Corps of Engineers), CEMP-RT, 1995, *Engineering and Design - Soil Vapor Extraction and Bioventing*. CE Publication EM 1110-1-4001.
- USEPA, 1995, *Groundwater and Leachate Treatment Systems*. EPA Publication EPA 625-R-94-005.
- USEPA OPPTS 835.1110, 1998, *Activated sludge isotherm. Fate, Transport, and Transformation Test Guidelines*. EPA Publication EPA 712-C-98-298.
- USEPA OPPTS 835.1220, 1998, *Sediment and soil adsorption/desorption isotherm. Fate, Transport, and Transformation Test Guidelines*. EPA Publication EPA 712-C-98-048.

- Ustrich, E., 1991, Geochemische Untersuchungen zur Bewertung der Dauerbeständigkeit mineralischer Abdichtungen in Altlasten und Deponien. Geol. Jb., C 57, Hannover Schweizbart.
- Velde, B., 1995, Composition and Mineralogy of Clays. In: Velde, B. (Ed.), Origin and Mineralogy of Clays. Springer, New York, p. 8-41.
- Walkley, A., and Black., I.A., 1934, An examination of Degtjareff method for determining soil organic matter and a proposed modification of the chromic acid titration method. Soil Sci., vol. 37, p.29-37.
- Weaver, C.E., 1989, Clays, Muds, and Shales. Elsevier.
- Weaver, C.E., and Pollard, L.D., 1973, The Chemistry of Clay Minerals. Elsevier.
- Weber, W.J., Jr., and Smith, E.H., 1987, Simulation and design models for adsorption processes. Environ. Sc. and Tech., Vol 21(11), p. 1040-1050.
- Welton, J.E., 1984, SEM Petrology Atlas. Methods in Exploration Series, AAPG, No. 4.
- Wentworth, C.K., 1922, A scale of grade and class terms for clastic sediments: Journal of Geology, v. 30, p. 377-392.
- WHO, 1989, Environmental Health Criteria 93: Chlorophenols other than Pentachlorophenol. International Programme on Chemical Safety, World Health Organization, Geneva.
- Wiegmann, J., Horte, C.H., and Kranz, G., 1982, Determination of the complete mineral composition of clays. International Clay Conference 1981, Elsevier, p. 365-372.
- Wilson, M.J., 1987, X-ray powder diffraction methods. In: Wilson, M.J. (Ed.), A handbook of determinative, methods in clay mineralogy, Blackie, Chapman & Hall, p. 26-98.
- Zhang, C., and Bennett, G.D., 1995, Applied Contaminant Transport Modeling: Theory and Practice. Van Nostrand Reinhold, New York, New York.
- Ziegler, C., and Lechner, P., 1994, Stofftransport durch vertikale Dichtungselemente. Österreichische Wasser- und Abfallwirtschaft, vol. 46, No. 7/8, p. 149- 153.

## Appendix A

## Appendix A.1- Drill Profiles of Cored Samples

---

Title: Kalchreuth - Amaltheen Clay (Sample designation K)

Location (Gauß-Krüger Coordinate System): R<sup>44</sup>37640/H<sup>54</sup>90090      Head Elevation /Datum: 410 m

---

Stratigraphy / Lithology: Lias  $\delta$

- 9.50 m Claystone, grey, marly, fossil bearing, occasional iron concretions - **Final Depth**

---

Title: Birkenschlag - Feuerletten (Sample designation B)

Location (Gauß-Krüger Coordinate System): R<sup>44</sup>71260/H<sup>55</sup>26860      Head Elevation /Datum: 420 m

---

Stratigraphy / Lithology: kmF

- 0.25 m Topsoil, brown, clayey
  - 0.50 m Claystone, yellow-brown, silty, ochre interstratification
  - 1.00 m Claystone, red, silty, fine-sandy
  - 3.00 m Claystone, red, fine-sandy, sandy, occasionally fine to medium gravelly
  - 6.80 m Claystone, red, greyish-green areas, fine-sandy interstratification
  - 7.10 m Sandstone, whitish-grey, medium sandy, very silty, fine to medium gravelly
  - 8.50 m Claystone, greyish-red, fine to medium sandy, fine to medium gravelly
  - 9.80 m Claystone, red, fine-sandy, fine to coarsely gravelly
  - 10.00 m Claystone, grey, silty to fine-sandy - **Final Depth**
- 

Title: Langenzenn - Lehrberg Layers (Sample designation L)

Location (Gauß-Krüger Coordinate System): R<sup>44</sup>12630/H<sup>54</sup>85540      Head Elevation /Datum: 340 m

---

Stratigraphy / Lithology: kmL

- 0.10 m Claystone, greyish-green
  - 0.50 m Claystone, red
  - 0.90 m Claystone, greenish yellow to purple
  - 1.60 m Claystone, red
  - 1.90 m Sandstone, yellow, silica cemented
  - 2.50 m Claystone, red
  - 5.00 m Claystone, red, yellow discolorations
  - 5.80 m Claystone, greyish-green
  - 10.40 m Claystone, red
  - 10.50 m Clayey marl, greyish-green, very hard
  - 10.60 m Claystone, red
  - 12.40 m Claystone, partly marly, grey
  - 14.00 m Claystone, red - **Final Depth**
- 

Title: Marktheidenfeld - Lower Röttone (Sample designation M)

Location (Gauß-Krüger Coordinate System): R<sup>35</sup>41540/H<sup>55</sup>22580      Head Elevation /Datum: 265 m

---

Stratigraphy / Lithology: Quaternary / so3T / so2

- 0.40 m Loess, yellow- brown, organic
  - 0.80 m Silt, yellow-brown, rocky (up to 5cm diameter)
  - Boundary Quarternary / so3T
  - 1.00 m Sandstone, reddish-purple, fine to medium grained, silica cemented
  - 2.00 m Siltstone - Clay interlayering, reddish-brown, green discolorations, stony (up to 3cm diameter)
  - 10.50 m Claystone, reddish-purple, silty, micaceous
  - Boundary so3T / so2
  - 13.00 m Sandstone, reddish-brown, very fine grained, silty, micaceous, platy - **Final Depth**
-

## Appendix B

## Appendix B.1- Major Rock Forming Elements

0.200 gram samples are fused with 1.2 grams of LiBO<sub>2</sub> and are dissolved in 100 ml of 5% HNO<sub>3</sub>. Analysis by ICP-AES. Number next to sample letter donates coring depth for sample in meters. Anomalous value estimated as MEAN + 2 STANDARD DEVIATIONS (KACKSTAETTER, 1990).

Feuerletten												
ELEMENT	SiO2	Al2O3	Fe2O3	MgO	CaO	Na2O	K2O	TiO2	P2O5	MnO	Cr2O3	LOI
SAMPLES	%	%	%	%	%	%	%	%	%	%	%	%
B1.7	53.29	15.77	5.50	3.03	1.95	0.10	3.41	0.80	0.11	0.03	0.009	13.3
B3.0	52.07	15.71	6.26	4.72	2.96	0.13	3.41	0.82	0.09	0.04	0.009	13.9
B4.6	57.78	15.77	6.27	4.20	2.15	0.13	3.32	0.90	0.10	0.04	0.012	9.3
<b>B6.0</b>	<b>51.88</b>	<b>14.45</b>	<b>6.00</b>	<b>4.72</b>	<b>4.64</b>	<b>0.13</b>	<b>3.31</b>	<b>0.79</b>	<b>0.10</b>	<b>0.04</b>	<b>0.010</b>	<b>14.0</b>
B7.5	40.67	11.37	3.99	3.33	17.59	0.13	2.34	0.62	0.04	0.32	0.008	20.1
B10.0	58.40	13.17	4.12	3.35	3.21	0.12	3.15	0.76	0.07	0.04	0.007	11.7
B-Composite	56.47	16.12	5.43	3.72	2.63	0.08	3.81	0.88	0.10	0.05	0.014	10.2
Mean	52.35	14.37	5.36	3.89	5.42	0.12	3.16	0.78	0.09	0.09	0.009	13.7
Std-Dev	5.83	1.64	0.96	0.69	5.51	0.01	0.38	0.08	0.02	0.11	0.002	3.3
Anomalous +	64.00	17.66	7.27	5.26	16.44	0.15	3.91	0.95	0.13	0.30	0.012	20.3
Anomalous -	40.70	11.09	3.44	2.52	-5.61	0.10	2.41	0.61	0.04	-0.13	0.006	7.2

Amaltheen Clay												
ELEMENT	SiO2	Al2O3	Fe2O3	MgO	CaO	Na2O	K2O	TiO2	P2O5	MnO	Cr2O3	LOI
SAMPLES	%	%	%	%	%	%	%	%	%	%	%	%
K2.8	49.35	21.04	5.51	2.14	4.20	0.19	3.00	0.92	0.12	0.10	0.015	12.7
K3.5	49.27	20.76	5.74	3.25	3.85	0.20	2.92	0.92	0.17	0.18	0.012	12.5
K5.8	51.19	21.11	6.07	2.69	3.42	0.22	3.34	1.00		0.08	0.016	11.5
K7.2	49.29	20.56	6.18	2.53	3.91	0.18	2.98	0.91	0.18	0.11	0.013	12.5
<b>K9.0</b>	<b>51.00</b>	<b>21.36</b>	<b>6.34</b>	<b>2.29</b>	<b>3.58</b>	<b>0.30</b>	<b>3.04</b>	<b>0.99</b>		<b>0.10</b>	<b>0.009</b>	<b>11.6</b>
K9.5	40.41	16.64	6.76	2.17	12.78	0.15	2.55	0.74	0.31	0.20	0.011	16.5
K-Composite	49.61	20.94	6.07	2.22	4.28	0.32	3.51	0.89	0.17	0.18	0.016	11.5
Mean	48.42	20.25	6.10	2.51	5.29	0.21	2.97	0.91	0.20	0.13	0.013	12.9
Std-Dev	3.67	1.63	0.40	0.38	3.36	0.05	0.23	0.09	0.07	0.04	0.002	1.7
Anomalous +	55.76	23.51	6.91	3.28	12.01	0.30	3.43	1.08	0.34	0.22	0.017	16.2
Anomalous -	41.08	16.98	5.29	1.75	-1.43	0.11	2.51	0.74	0.05	0.04	0.008	9.5

Lehrberg Layers												
ELEMENT	SiO2	Al2O3	Fe2O3	MgO	CaO	Na2O	K2O	TiO2	P2O5	MnO	Cr2O3	LOI
SAMPLES	%	%	%	%	%	%	%	%	%	%	%	%
L1.5	40.41	16.64	6.76	2.17	12.78	0.15	2.55	0.74	0.16	0.18	0.010	13.2
L3.0	49.17	16.90	7.12	4.03	3.29	0.15	4.68	0.72	0.16	0.07	0.009	12.1
<b>L6.0</b>	<b>37.26</b>	<b>11.12</b>	<b>4.38</b>	<b>9.43</b>	<b>11.20</b>	<b>0.15</b>	<b>3.76</b>	<b>0.51</b>	<b>0.16</b>	<b>0.36</b>	<b>0.007</b>	<b>21.7</b>
<b>L11.0</b>	<b>33.23</b>	<b>11.06</b>	<b>3.46</b>	<b>11.03</b>	<b>12.37</b>	<b>0.10</b>	<b>3.43</b>	<b>0.43</b>	<b>0.14</b>	<b>0.33</b>	<b>0.010</b>	<b>24.6</b>
L12.0	48.29	14.81	7.15	5.90	4.24	0.19	5.10	0.64	0.17	0.15	0.009	12.9
L14	54.46	11.13	2.29	5.57	7.10	0.29	3.93	0.39	0.25	0.24	0.003	13.8
L-Composite	40.19	12.66	4.44	8.70	9.58	0.13	4.10	0.52	0.19	0.32	0.008	18.9
Mean	43.80	13.61	5.19	6.36	8.50	0.17	3.91	0.57	0.17	0.22	0.008	16.4
Std-Dev	7.40	2.59	1.92	3.03	3.83	0.06	0.83	0.14	0.04	0.10	0.002	4.9
Anomalous +	58.60	18.79	9.03	12.41	16.15	0.29	5.56	0.84	0.24	0.42	0.013	26.1
Anomalous -	29.00	8.43	1.36	0.30	0.84	0.05	2.25	0.30	0.10	0.02	0.003	6.6

Lower Röttone												
ELEMENT SAMPLES	SiO2 %	Al2O3 %	Fe2O3 %	MgO %	CaO %	Na2O %	K2O %	TiO2 %	P2O5 %	MnO %	Cr2O3 %	LOI %
M2.4	58.94	18.14	6.81	2.97	0.38	0.21	5.53	0.79	0.02	0.08	0.008	6.9
M3.3	49.67	18.93	7.38	2.79	0.79	0.16	6.33	0.75	0.12	0.15	0.018	8.7
M5.8	59.91	17.08	6.15	3.12	0.60	0.23	5.25	0.69	0.08	0.05	0.010	6.1
<b>M6.0</b>	<b>54.04</b>	<b>17.79</b>	<b>6.67</b>	<b>2.75</b>	<b>0.56</b>	<b>0.18</b>	<b>6.11</b>	<b>0.69</b>	<b>0.18</b>	<b>0.10</b>	<b>0.010</b>	<b>6.9</b>
M7.5	55.53	17.67	6.32	2.50	0.54	0.17	6.73	0.75	0.21	0.08	0.012	6.3
M11	70.50	12.34	4.41	1.76	0.37	0.14	4.58	0.54	0.17	0.05	0.005	4.2
M13	75.11	11.49	3.01	1.24	0.31	0.19	4.80	0.66	0.08	0.02	0.004	2.7
M-Composite	58.89	17.52	6.18	2.93	0.59	0.20	6.61	0.74	0.17	0.15	0.014	5.6
Mean	60.53	16.21	5.82	2.45	0.51	0.18	5.62	0.70	0.12	0.08	0.010	6.0
Std-Dev	8.45	2.77	1.43	0.64	0.15	0.03	0.74	0.08	0.06	0.04	0.004	1.8
Anomalous +	77.43	21.75	8.69	3.73	0.82	0.24	7.11	0.85	0.25	0.15	0.018	9.6
Anomalous -	43.63	10.66	2.95	1.17	0.20	0.13	4.13	0.54	-0.00	-0.00	0.001	2.3

Feuerletten							
ELEMENT SAMPLES	Ba ppm	Ni ppm	Sr ppm	Zr ppm	Y ppm	Nb ppm	Sc ppm
B1.7	518	37	65	217	6	10	11
B3.0	334	24	101	205	10	13	14
B4.6	292	50	110	321	27	10	14
<b>B6.0</b>	<b>265</b>	<b>31</b>	<b>119</b>	<b>261</b>	<b>9</b>	<b>12</b>	<b>12</b>
B7.5	251	40	207	216	53	8	
B10.0	345	38	98	509	8	10	10
B-Composite	440		112	281	33	17	14
Mean	334	37	117	288	19	11	12
Std-Dev	89	8	44	106	17	2	2
Anomalous +	512	53	204	501	52	14	15
Anomalous -	156	21	29	76	-15	7	9

Amaltheen Clay							
ELEMENT SAMPLES	Ba ppm	Ni ppm	Sr ppm	Zr ppm	Y ppm	Nb ppm	Sc ppm
K2.8	367	71	162	156	8	8	17
K3.5	406	84	169	142	13	4	17
K5.8	503	35	167	153	15	7	19
K7.2	388	75	171	146	9	8	17
<b>K9.0</b>	<b>343</b>	<b>77</b>	<b>175</b>	<b>136</b>	<b>14</b>	<b>9</b>	<b>19</b>
K9.5	299	74	237	124	9	7	18
K-Composite	351		187	110	23	22	19
Mean	384	69	180	143	11	7	18
Std-Dev	63	16	26	11	3	2	1
Anomalous +	510	101	232	164	17	10	20
Anomalous -	258	38	129	121	6	4	16

Lehrberg Layers							
ELEMENT SAMPLES	Ba ppm	Ni ppm	Sr ppm	Zr ppm	Y ppm	Nb ppm	Sc ppm
L1.5	476	246	187	168	20	6	13
L3.0	550	45	45	142	9	4	14
<b>L6.0</b>	<b>275</b>	<b>48</b>	<b>146</b>	<b>130</b>	<b>14</b>		<b>6</b>
<b>L11.0</b>	<b>326</b>	<b>30</b>	<b>244</b>	<b>88</b>	<b>13</b>	<b>4</b>	<b>9</b>
L12.0	511	46	163	231	11	6	12
L14	628	31	333	189	25	3	
L-Composite	434		223	105	25	15	12
Mean	461	74	186	158	15	5	11
Std-Dev	123	77	88	45	5	1	3
Anomalous +	708	229	363	249	26	7	17
Anomalous -	214	-80	9	67	4	2	5

Lower Röttone							
ELEMENT SAMPLES	Ba ppm	Ni ppm	Sr ppm	Zr ppm	Y ppm	Nb ppm	Sc ppm
M2.4	534	63	108	192	24	8	16
M3.3	626	115	95	134	5	7	15
M5.8	494	29	92	126	15	8	14
<b>M6.0</b>	<b>593</b>	<b>55</b>	<b>96</b>	<b>120</b>	<b>4</b>	<b>3</b>	<b>14</b>
M7.5	595	55	103	147	4	8	14
M11	508	33	97	213	5		9
M13	508	20	111	320	12	4	
M-Composite	591		113	134	33	17	15
Mean	551	53	100	179	10	6	14
Std-Dev	49	29	7	66	7	2	2
Anomalous +	648	111	114	311	24	10	18
Anomalous -	454	-6	87	47	-4	2	9

## Appendix B.2- Minor Geochemical Elements

0.250 gram sample was digested with 10 mL HClO<sub>4</sub>-HNO<sub>3</sub>-HCl-HF at 200°C to fuming and then diluted to 10 mL with dilute aqua regia. Analysis by ICP-AES. Leach is partial for magnetite, chromite, barite, oxides of Al, Zr & Mn as well as massive sulfide samples. As, Cr, Sb, Au subject to loss by volatilization during HClO<sub>4</sub> fuming. Number next to sample letter donates coring depth for sample in meters. Anomalous value estimated as MEAN + 2 STANDARD DEVIATIONS (KACKSTAETTER, 1990).

Feuerletten															
ELEMENT	Ba	Ni	Sr	Zr	Y	Nb	Sc	Pb	Cu	Zn	Co	As	Th	La	V
SAMPLES	ppm	ppm	ppm	ppm	ppm	ppm	ppm	ppm	ppm	ppm	ppm	ppm	ppm	ppm	ppm
B1.7	518	37	65	217	6	10	11	19	8	50	13		6	12	99
B3.0	334	24	101	205	10	13	14	9	6	49	13		9	22	52
B4.6	292	50	110	321	27	10	14	26		46	14		20	52	73
<b>B6.0</b>	265	31	119	261	9	12	12	12	5	46	13		7	16	50
B7.5	251	40	207	216	53	8		19	10	37	10	8	12	70	71
B10.0	345	38	98	509	8	10	10	12	6	46	18	21	8	16	75
Mean	334	37	117	288	19	11	12	16	7	46	14	15	10	31	70
Std-Dev	89	8	44	106	17	2	2	6	2	4	2	7	5	22	16
Anomalous +	512	53	204	501	52	14	15	28	11	54	18	28	20	75	103
Anomalous -	156	21	29	76	-15	7	9	5	3	37	9	2	1	-12	37
Amaltheen Clay															
ELEMENT	Ba	Ni	Sr	Zr	Y	Nb	Sc	Pb	Cu	Zn	Co	As	Th	La	V
SAMPLES	ppm	ppm	ppm	ppm	ppm	ppm	ppm	ppm	ppm	ppm	ppm	ppm	ppm	ppm	ppm
K2.8	367	71	162	156	8	8	17	18	27	138	23		6	20	123
K3.5	406	84	169	142	13	4	17	21	19	57	16	23	8	28	117
K5.8	303	35	167	153	15	7	19	29	25	89	18	9	13	33	179
K7.2	388	75	171	146	9	8	17	26	24	92	19	6	7	21	130
<b>K9.0</b>	343	77	175	136	14	9	19	28	30	168	22	9	13	32	173
K9.5	299	74	237	124	9	7	18	9	23	84	19	14	9	23	123
Mean	384	69	180	143	11	7	18	22	25	105	20	12	9	26	141
Std-Dev	63	16	26	11	3	2	1	7	3	37	2	6	3	5	25
Anomalous +	510	101	232	164	17	10	20	36	31	179	24	24	15	36	191
Anomalous -	258	38	129	121	6	4	16	8	18	31	15	0	4	16	90
Lehrberg Layers															
ELEMENT	Ba	Ni	Sr	Zr	Y	Nb	Sc	Pb	Cu	Zn	Co	As	Th	La	V
SAMPLES	ppm	ppm	ppm	ppm	ppm	ppm	ppm	ppm	ppm	ppm	ppm	ppm	ppm	ppm	ppm
L1.5	476	246	187	168	20	6	13	31	13	206	12	23	12	37	86
L3.0	550	45	45	142	9	4	14	20	10	212	14	15	7	17	76
<b>L6.0</b>	275	48	146	130	14		6	13	4	104	8	8	9	27	28
<b>L11.0</b>	326	30	244	88	13	4	9	10	8	125	16	26	6	26	43
L12.0	511	46	163	231	11	6	12	29	8	129	10	12	8	22	53
L14	628	31	333	189	25	3		20	8	83	7	6	10	30	74
Mean	461	74	186	158	15	5	11	21	9	143	11	15	9	27	60
Std-Dev	123	77	88	45	5	1	3	8	3	49	3	7	2	6	20
Anomalous +	708	229	363	249	26	7	17	36	14	241	18	30	13	39	101
Anomalous -	214	-80	9	67	4	2	5	5	3	45	5	0	5	14	19
Lower Röttone															
ELEMENT	Ba	Ni	Sr	Zr	Y	Nb	Sc	Pb	Cu	Zn	Co	As	Th	La	V
SAMPLES	ppm	ppm	ppm	ppm	ppm	ppm	ppm	ppm	ppm	ppm	ppm	ppm	ppm	ppm	ppm
M2.4	534	63	108	192	24	8	16	18	13	86	14	23	13	39	103
M3.3	626	115	95	134	5	7	15	7	10	127	29	14	3	4	105
M5.8	494	29	92	126	15	8	14	16	8	79	15	18	9	25	79
<b>M6.0</b>	593	55	96	120	4	3	14	9	10	106	21	20	2	3	100
M7.5	595	55	103	147	4	8	14	19	10	94	16	21	2	5	92
M11	508	33	97	213	5		9	17	7	54	8	13	3	9	57
M13	508	20	111	320	12	4		14	6	36	6	21	10	37	42
Mean	551	53	100	179	10	6	14	14	9	83	16	19	6	17	83
Std-Dev	49	29	7	66	7	2	2	4	2	28	7	3	4	15	23
Anomalous +	648	111	114	311	24	10	18	23	13	140	30	26	14	47	128
Anomalous -	454	-6	87	47	-4	2	9	6	5	26	1	12	-2	-12	37

## Appendix B.3 - Carbon and LOI constituent content

BALL (1964), DEAN (1974) and GOLDIN (1987) LOI method - three step process:

1. Sample water content (H<sub>2</sub>O-105°C) - dried at 105°C for 24 h; weight differences used to estimate H<sub>2</sub>O content.
2. Sample organic content (Org.-550°C) -heated to 550°C for 24 h; weight changes used to estimate organic matter content.
3. Sample CO<sub>2</sub> content (CO<sub>2</sub>-1000°C)- to 1000°C for 24 h; weight changes used to estimate CO<sub>2</sub>.

## LECO™ Carbon Analyzer

Total carbons estimated by combusting 100 mg sample in analyzer. Acid insoluble carbon determined by leaching 100 mg of sample in 15% HCl at 70°C for 1 hr. Residue is washed, dried at 140°C for 2 hrs and subjected to LECO™ carbon analysis. Graphite carbon measured by igniting 100 mg material at 600°C for 1 hour, followed by leaching 100 mg of sample in 15% HCl at 70°C for 1 hr. Residue is washed, dried at 140°C for 2 hrs and subjected to LECO™ carbon analysis. Erroneous results negated by combining sample material (100 mg) in a teflon beaker with 5ml HNO<sub>3</sub> and 5ml 50% HF, placed in hot bath for 1 hour. Contents are filtered (crucible), washed, and dried. Carbon content is measured with the LECO™ apparatus. Results used to calculate organic carbon (C<sub>org</sub>), carbon dioxide carbon (C<sub>co2</sub>), and carbon dioxide (CO<sub>2</sub>) according to equation 3.2, 3.3, and 3.4.

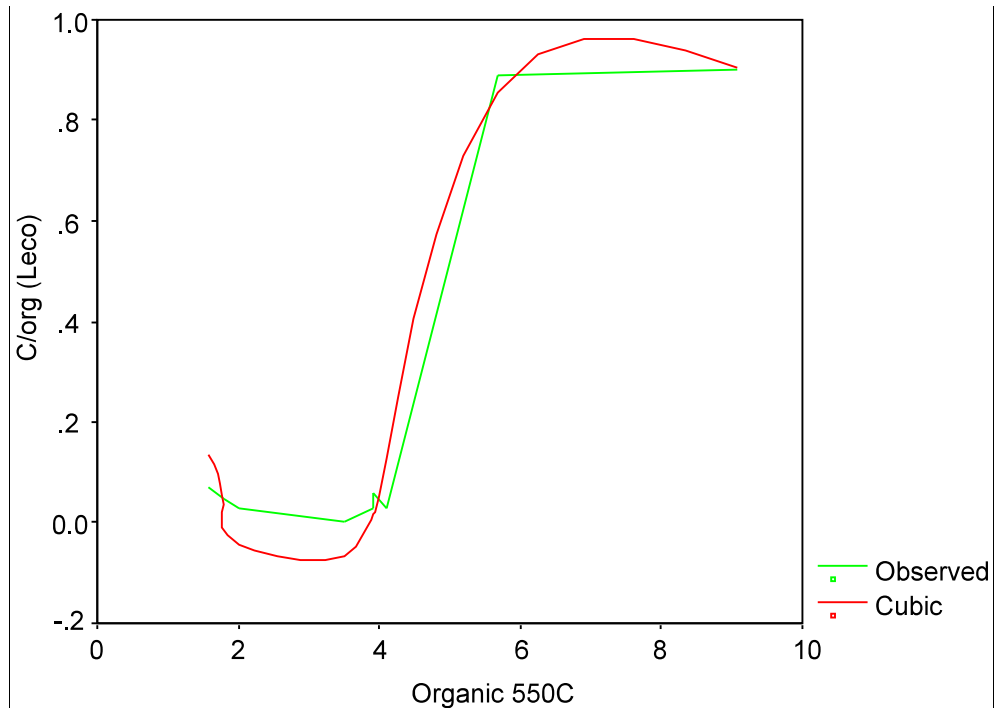
LOI - Loss on Ignition: from Rock forming oxide analysis

Xl water - crystalline water calculated: LOI - $\sum$ LECO-CO<sub>2</sub>, LECO-C-graphite, LECO-C/ORG

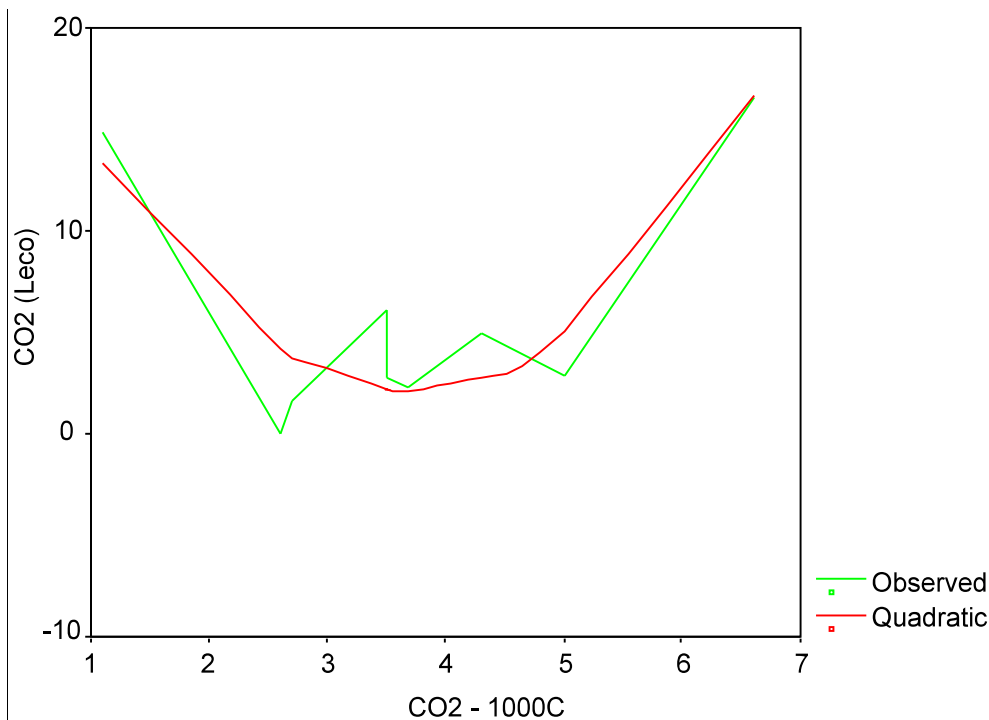
ELEMENT SAMPLES	Xl water %	LOI %	LECO™ carbon analyzer			105°C	550°C	1000°C
			CO <sub>2</sub> %	C-Graphite %	C/ORG %	H <sub>2</sub> O %	Org. %	CO <sub>2</sub> %
B3.0	11.55	13.9	2.31	0.01	0.03	20.5	3.9	3.7
B4.6	7.67	9.3	1.57	0.03	0.03	16.9	4.1	2.7
B6.0	7.85	14	6.12	0.03	0	20	3.5	3.5
B7.5	5.2	20.1	14.87	0	0.03	10.6	2	1.1
K5.8	7.79	11.5	2.79	0.02	0.9	21.3	9.1	3.5
K9.0	7.84	11.6	2.87	0	0.89	17.4	5.7	5
L1.5	5.61	13.2	7.45	0.02	0.12	18.5	3.2	7.4
L6.0	16.62	21.7	4.98	0.03	0.07	15.6	1.6	4.3
L11.0	-3.72	12.9	16.55	0.01	0.06	15.1	3.9	6.6
M2.4	6.82	6.9	0	0	0.08	20.8	2.4	2.4
M6.0	6.05	6.1	0	0	0.05	14.6	3.2	1.7

CO<sub>2</sub> and C<sub>org</sub> estimation where LECO data is unavailable using curve modeling below. Calculated values in *italics*.

ELEMENT SAMPLES	LOI %	<i>Calculated Values</i>		105°C	550°C	1000°C
		CO <sub>2</sub> %	C/ORG %	H <sub>2</sub> O %	Org. %	CO <sub>2</sub> %
B1.7	13.3	<i>2.89</i>	<i>0.02</i>	28.6	3.8	3
B10.0	11.7	<i>3.41</i>	<i>-0.14</i>	14.4	3.1	2.8
K2.8	12.7	<i>2.24</i>	<i>1.38</i>	14.4	7.9	3.4
K7.2	12.5	<i>5.09</i>	<i>0.85</i>	17.4	5.7	5
L3.0	12.1	<i>25.62(?)</i>	<i>-0.13</i>	18.5	3.2	7.4
L10.5	24.6	<i>298.31(?)</i>	<i>-0.16</i>	11	2.8	16.9
M3.3	8.7	<i>4.87</i>	<i>-0.14</i>	20.8	2.4	2.4
M6.2	6.9	<i>4.07</i>	<i>0.04</i>	14.7	1.8	2.6
M7.5	6.3	<i>12.48(?)</i>	<i>-0.07</i>	13.8	3.5	1.2



Correlation of Organic constituents for LOI 550°C vs. C/org. LECO™.  
 Correlation data: Math: Cubic; Rsq: 0.978; d.f.: 5; Sigf: 0.000  
 Equation: %C/org(Leco) = 1.8711-(1.6793\*C<sub>org550</sub>)+(0.4148\*C<sub>org550</sub><sup>2</sup>)-(0.0266\*C<sub>org550</sub><sup>3</sup>)



Correlation of CO<sub>2</sub> for LOI 1000°C vs. CO<sub>2</sub>- LECO™.  
 Correlation data: Math: Quadratic; Rsq: 0.824; d.f.: 6; Sigf: 0.005  
 Equation: %CO<sub>2</sub>(Leco) = 24.9795-(12.445\*CO<sub>2</sub>1000)+(1.6934\*CO<sub>2</sub>1000<sup>2</sup>)



Appendix B.4 - Pearson Correlation Matrices of geochemical constituents

Correlation significance flagged as follows:

	90 <sup>th</sup> %tile	80 <sup>th</sup> %tile	70 <sup>th</sup> %tile
Correlation is significant at the 0.05 level (2-tailed)			
Correlation is significant at the 0.01 level (2-tailed)			

B.4.1 - Geochemical Correlation of minor elements and rock forming oxides (Part 1 - Minor elements)

		Ba	Ni	Sr	Zr	Y	Nb	Sc	Pb	Cu	Zn	Co	As	Th	La	V
Ni	Pearson Correla	0.102	1													
	Sig. (2-tailed)	0.626	.													
	N	25	25													
Sr	Pearson Correla	-0.2	0.13	1												
	Sig. (2-tailed)	0.349	0.53	.												
	N	25	25	25												
Zr	Pearson Correla	-0.19	-0.2	-0.2	1											
	Sig. (2-tailed)	0.352	0.28	0.23	.											
	N	25	25	25	25											
Y	Pearson Correla	-0.31	0.03	0.41	0.1	1										
	Sig. (2-tailed)	0.128	0.9	0.04	0.64	.										
	N	25	25	25	25	25										
Nb	Pearson Correla	-0.52	-0.1	-0.4	0.37	-0.01	1									
	Sig. (2-tailed)	0.012	0.55	0.09	0.08	0.982	.									
	N	23	23	23	23	23	23									
Sc	Pearson Correla	0.122	0.2	0.22	-0.3	0.131	-0.1	1								
	Sig. (2-tailed)	0.588	0.37	0.34	0.2	0.56	0.78	.								
	N	22	22	22	22	22	20	22								
Pb	Pearson Correla	0.079	0.34	0.17	-0.0	0.285	-0.1	0.32	1							
	Sig. (2-tailed)	0.709	0.09	0.41	0.94	0.161	0.81	0.14	.							
	N	25	25	25	25	25	23	22	25							
Cu	Pearson Correla	-0.15	0.29	0.29	-0.4	-0.02	-0.0	0.83	0.46	1						
	Sig. (2-tailed)	0.475	0.17	0.16	0.08	0.934	0.95	0	0.02	.						
	N	24	24	24	24	24	22	21	24	24						
Zn	Pearson Correla	0.252	0.58	0.07	-0.5	-0.18	-0.4	0.16	0.33	0.32	1					
	Sig. (2-tailed)	0.224	0.00	0.74	0.01	0.397	0.08	0.48	0.11	0.13	.					
	N	25	25	25	25	25	23	22	25	24	25					
Co	Pearson Correla	0.05	0.27	-0.1	-0.3	-0.36	0.11	0.61	-0.2	0.56	0.31	1				
	Sig. (2-tailed)	0.814	0.2	0.54	0.2	0.076	0.61	0.00	0.44	0.00	0.13	.				
	N	25	25	25	25	25	23	22	25	24	25	25				
As	Pearson Correla	0.142	0.21	-0.3	0.13	-0.25	-0.2	-0.2	-0.3	-0.3	0.03	0.08	1			
	Sig. (2-tailed)	0.55	0.38	0.19	0.59	0.283	0.47	0.5	0.2	0.23	0.91	0.73	.			
	N	20	20	20	20	20	18	17	20	20	20	20	20			
Th	Pearson Correla	-0.4	0.09	0.23	0.27	0.655	0.22	0.27	0.5	0.29	-0.1	-0.2	-0.21	1		
	Sig. (2-tailed)	0.05	0.69	0.27	0.2	0	0.33	0.23	0.01	0.17	0.68	0.24	0.373	.		
	N	25	25	25	25	25	23	22	25	24	25	25	20	25		
La	Pearson Correla	-0.45	0.05	0.38	0.16	0.91	0.03	0.22	0.4	0.14	-0.2	-0.4	-0.18	0.83	1	
	Sig. (2-tailed)	0.024	0.82	0.06	0.45	0	0.9	0.33	0.05	0.51	0.43	0.07	0.451	0	.	
	N	25	25	25	25	25	23	22	25	24	25	25	20	25	25	
V	Pearson Correla	0.131	0.26	0.11	-0.3	-0.09	0.01	0.86	0.4	0.89	0.24	0.66	-0.23	0.13	-0.0	1
	Sig. (2-tailed)	0.531	0.2	0.59	0.14	0.681	0.96	0	0.05	0	0.24	0	0.331	0.53	0.9	.
	N	25	25	25	25	25	23	22	25	24	25	25	20	25	25	25



B.4.2 - Geochemical Correlation of rock forming oxides with LECO™ and LOI results

		SiO2	Al2O3	Fe2O3	MgO	CaO	Na2O	K2O	TiO2	P2O5	MnO	Cr2O3	LOI
LOI	Pearson Correlation	-0.92	-0.733	-0.848	0.628	0.883	-0.33	-0.5	-0.6	-0.03	0.82	-0.558	1
	Sig. (2-tailed)	0	0.025	0.004	0.07	0.002	0.386	0.166	0.087	0.934	0.007	0.118	.
	N	9	9	9	9	9	9	9	9	9	9	9	9
CO <sub>2</sub> (Leco)	Pearson Correlation	-0.53	-0.524	-0.238	0.22	0.609	-0.16	-0.11	-0.51	0.099	0.493	-0.372	0.503
	Sig. (2-tailed)	0.143	0.148	0.537	0.569	0.082	0.69	0.785	0.16	0.8	0.177	0.325	0.167
	N	9	9	9	9	9	9	9	9	9	9	9	9
C/graphite (Leco)	Pearson Correlation	0.028	-0.269	-0.112	0.562	-0.08	-0.43	-0.19	0.004	0.172	-0.08	0.248	0.172
	Sig. (2-tailed)	0.944	0.484	0.774	0.116	0.834	0.25	0.619	0.993	0.658	0.833	0.52	0.658
	N	9	9	9	9	9	9	9	9	9	9	9	9
C/org (Leco)	Pearson Correlation	0.128	0.813	0.162	-0.48	-0.22	0.863	-0.25	0.708	-0.74	-0.19	0.526	-0.23
	Sig. (2-tailed)	0.742	0.008	0.677	0.195	0.577	0.003	0.52	0.033	0.022	0.626	0.146	0.553
	N	9	9	9	9	9	9	9	9	9	9	9	9
C/total (Leco)	Pearson Correlation	-0.61	-0.381	-0.435	0.045	0.747	0.012	-0.39	-0.32	-0.26	0.554	-0.258	0.593
	Sig. (2-tailed)	0.081	0.311	0.242	0.908	0.021	0.976	0.305	0.397	0.503	0.122	0.502	0.092
	N	9	9	9	9	9	9	9	9	9	9	9	9
S/total	Pearson Correlation	0.108	0.738	0.163	-0.44	-0.19	0.916	-0.29	0.649	-0.7	-0.17	0.202	-0.18
	Sig. (2-tailed)	0.782	0.023	0.675	0.232	0.634	0.001	0.451	0.059	0.038	0.668	0.603	0.638
	N	9	9	9	9	9	9	9	9	9	9	9	9
SO <sub>4</sub> (calc)	Pearson Correlation	0.03	0.723	0.113	-0.35	-0.16	0.876	-0.32	0.642	-0.72	-0.14	0.318	-0.09
	Sig. (2-tailed)	0.938	0.028	0.771	0.352	0.691	0.002	0.396	0.062	0.028	0.723	0.404	0.81
	N	9	9	9	9	9	9	9	9	9	9	9	9
H <sub>2</sub> O 105°C	Pearson Correlation	0.505	0.535	0.45	-0.09	-0.64	0.152	-0.11	0.66	-0.28	-0.7	0.567	-0.34
	Sig. (2-tailed)	0.166	0.138	0.224	0.821	0.066	0.697	0.773	0.053	0.462	0.035	0.112	0.374
	N	9	9	9	9	9	9	9	9	9	9	9	9
Organic 550°C	Pearson Correlation	0.393	0.775	0.372	-0.46	-0.4	0.557	-0.26	0.83	-0.69	-0.5	0.818	-0.37
	Sig. (2-tailed)	0.295	0.014	0.325	0.214	0.284	0.119	0.497	0.006	0.041	0.174	0.007	0.334
	N	9	9	9	9	9	9	9	9	9	9	9	9
CO <sub>2</sub> 1000°C	Pearson Correlation	-0.00	0.222	0.539	0.352	-0.37	0.482	0.325	0.024	0.226	-0.12	-0.121	-0.08
	Sig. (2-tailed)	0.998	0.566	0.135	0.353	0.328	0.189	0.393	0.95	0.559	0.755	0.756	0.84
	N	9	9	9	9	9	9	9	9	9	9	9	9
		CO2 (Leco)	C/graphite (Leco)	C/org (Leco)	C/total (Leco)	S/total	SO4 (calc)	H2O 105°C	Organic 550°C				
LOI	Pearson Correlation												
	Sig. (2-tailed)												
	N												
CO <sub>2</sub> (Leco)	Pearson Correlation	1											
	Sig. (2-tailed)	.											
	N	9											
C/graphite (Leco)	Pearson Correlation	-0.202	1										
	Sig. (2-tailed)	0.602	.										
	N	9	9										
C/org (Leco)	Pearson Correlation	-0.276	-0.195	1									
	Sig. (2-tailed)	0.472	0.616	.									
	N	9	9	9									
C/total (Leco)	Pearson Correlation	0.917	-0.256	0.01	1								
	Sig. (2-tailed)	0.001	0.505	0.98	.								
	N	9	9	9	9								
S/total	Pearson Correlation	-0.246	-0.304	0.908	0.02	1							
	Sig. (2-tailed)	0.524	0.426	0.001	0.959	.							
	N	9	9	9	9	9							
SO <sub>4</sub> (calc)	Pearson Correlation	-0.227	-0.166	0.957	0.057	0.964	1						
	Sig. (2-tailed)	0.558	0.669	0	0.884	0	.						
	N	9	9	9	9	9	9						
H <sub>2</sub> O 105°C	Pearson Correlation	-0.555	0.443	0.392	-0.507	0.272	0.402	1					
	Sig. (2-tailed)	0.121	0.232	0.297	0.163	0.479	0.283	.					
	N	9	9	9	9	9	9	9					
Organic 550°C	Pearson Correlation	-0.226	0.087	0.827	-0.039	0.612	0.726	0.665	1				
	Sig. (2-tailed)	0.558	0.823	0.006	0.92	0.08	0.027	0.051	.				
	N	9	9	9	9	9	9	9	9				
CO <sub>2</sub> 1000°C	Pearson Correlation	0.195	0.068	0.233	0.038	0.315	0.347	0.283	0.242	1			
	Sig. (2-tailed)	0.614	0.862	0.547	0.924	0.41	0.361	0.461	0.531	.			
	N	9	9	9	9	9	9	9	9	9			







## B.4.5 - Geochemical Correlation of minor elements with mineralogical point count analysis

		Ba	Ni	Sr	Zr	Y	Nb	Sc	Pb	Cu	Zn	Co	As	Th	La	V
Quartz	Pearson Correlativ	0.644	-0.02	-0.204	-0.302	-0.463	-0.021	0.433	0.237	0.245	0.338	0.223	0.763	-0.356	-0.373	0.414
	Sig. (2-tailed)	0.085	0.963	0.628	0.467	0.248	0.958	0.283	0.571	0.558	0.412	0.596	0.046	0.387	0.363	0.307
	N	8	8	8	8	8	8	8	8	8	8	8	7	8	8	8
Clay	Pearson Correlativ	0.37	0.238	-0.172	0.256	-0.497	0.805	0.812	-0.156	0.401	-0.021	0.576	0.338	-0.245	-0.373	0.572
	Sig. (2-tailed)	0.368	0.571	0.684	0.54	0.21	0.016	0.014	0.712	0.324	0.953	0.135	0.458	0.559	0.362	0.138
	N	8	8	8	8	8	8	8	8	8	8	8	7	8	8	8
Dolomite	Pearson Correlativ	-0.472	-0.23	0.148	-0.255	0.513	-0.723	-0.792	-0.222	-0.371	-0.046	-0.54	-0.367	0.275	0.389	-0.542
	Sig. (2-tailed)	0.238	0.584	0.727	0.542	0.193	0.043	0.019	0.596	0.361	0.909	0.167	0.419	0.509	0.34	0.165
	N	8	8	8	8	8	8	8	8	8	8	8	7	8	8	8
Calcite	Pearson Correlativ	-0.854	-0.053	0.706	-0.052	0.745	0.177	0.164	0.377	0.584	0.075	-0.128	-0.802	0.805	0.804	0.321
	Sig. (2-tailed)	0.007	0.901	0.05	0.903	0.034	0.674	0.699	0.357	0.128	0.86	0.762	0.03	0.016	0.016	0.438
	N	8	8	8	8	8	8	8	8	8	8	8	7	8	8	8
Rock Fragment	Pearson Correlativ	-0.443	-0.575	-0.059	0.911	0.094	0.562	-0.222	-0.105	-0.391	-0.631	-0.381	-0.065	0.119	0.057	-0.457
	Sig. (2-tailed)	0.271	0.136	0.885	0.001	0.824	0.147	0.598	0.804	0.335	0.092	0.351	0.89	0.778	0.893	0.256
	N	8	8	8	8	8	8	8	8	8	8	8	7	8	8	8
K-Spar	Pearson Correlativ	0.765	0.093	-0.782	-0.446	-0.841	-0.221	0.109	-0.481	-0.211	-0.06	0.372	0.93	-0.828	-0.841	0.107
	Sig. (2-tailed)	0.027	0.827	0.022	0.268	0.005	0.597	0.797	0.227	0.61	0.887	0.364	0.001	0.011	0.005	0.801
	N	8	8	8	8	8	8	8	8	8	8	8	7	8	8	8
Other	Pearson Correlativ	0.476	0.832	-0.4	-0.212	-0.337	0.056	0.176	-0.437	-0.071	0.253	0.69	0.047	-0.318	-0.407	0.145
	Sig. (2-tailed)	0.233	0.01	0.326	0.614	0.414	0.895	0.677	0.279	0.865	0.545	0.058	0.921	0.443	0.317	0.733
	N	8	8	8	8	8	8	8	8	8	8	8	7	8	8	8
Opaque	Pearson Correlativ	0.082	-0.175	0.454	0.599	0.26	0.159	0.056	0.595	0	0.252	-0.281	-0.188	0.281	0.282	-0.139
	Sig. (2-tailed)	0.847	0.679	0.258	0.117	0.534	0.707	0.894	0.12	0.999	0.547	0.5	0.687	0.5	0.499	0.743
	N	8	8	8	8	8	8	8	8	8	8	8	7	8	8	8
Void	Pearson Correlativ	-0.138	-0.242	-0.047	0.154	-0.354	0.387	0.251	0.003	0.149	-0.691	0.011	0.017	-0.284	-0.225	0.119
	Sig. (2-tailed)	0.745	0.564	0.912	0.715	0.39	0.344	0.549	0.994	0.724	0.058	0.979	0.972	0.496	0.592	0.779
	N	8	8	8	8	8	8	8	8	8	8	8	7	8	8	8

## B.5 - Results of CEC analysis

## CEC - Mehlich (1948) - Method

- k. 5g sample (grain size: < 0.125mm) mixed with 25 ml BaCl<sub>2</sub> solution (25g BaCl<sub>2</sub>\*2H<sub>2</sub>O is added to 22.5ml triethanolamine; mixture diluted to nearly 1000ml with aqua dest.; pH 8.1 adjusted with conc. HCl; solution filled to exactly 1000ml.)
- l. Mixture agitated vigorously to complete dispersion
- m. Suspension centrifuged at 4000rpm for 15 min; clear extractant decanted and collected
- n. Agitating and centrifuging process (b & c) repeated three times.
- o. 25ml BaCl<sub>2</sub> solution (25g BaCl<sub>2</sub>\*2H<sub>2</sub>O in 1000ml aqua dest.) added to sample and steps b and c repeated (extractant added to previous collection)
- p. Sample washed by repeatedly adding 25ml aqua dest., agitating, centrifuging and decanting (extractant discarded), until all non-sorbed Ba removed (H<sub>2</sub>SO<sub>4</sub> test of discarded solution: Ba forms white precipitate).
- q. Extractant from steps c and d diluted to 250ml with aqua dest. and analyzed for Na<sup>+</sup>, K<sup>+</sup>, Mg<sup>2+</sup>, and Ca<sup>2+</sup>.
- r. Washed sample from step f combined with 25ml CaCl<sub>2</sub> solution (50g CaCl<sub>2</sub>\*2H<sub>2</sub>O in 1000ml aqua dest.)
- s. Mixture agitated and centrifuged as in steps b and c, repeated 4 times. Extractant collected.
- t. Extractant stretched to 100ml with aqua dest. and analyzed for Ba<sup>2+</sup>.

## pH - DIN 19 684 (1977)

- a. 10g finely pulverized, air dried sample mixed with 25ml of 0.01M CaCl<sub>2</sub> solution.
- b. Mixture is agitated for 5 minutes and left to settle for 1 hr.
- c. pH measured with calibrated pH-meter.
- d. pH-meter calibrated after every 4<sup>th</sup> measurement

Base saturation calculated according to equation 3.6.

SAMPLES	Na <sup>+</sup> mmol/100g	K <sup>+</sup> mmol/100g	Ca <sup>2+</sup> mmol/100g	Mg <sup>+</sup> mmol/100g	Sum Cat mmol/100g	CEC mmol/100g	Base saturation %	Soil pH
B6.0	3.6	6.7	86.6	52.6	149.5	137.2	109.0	7.92
K2.8	3.6	10.3	45.4	14.8	74.1	55.9	132.6	7.76
K3.5	4.0	11.7	45.4	14.6	75.7	42.8	176.9	7.80
K7.2	4.1	12.4	36.9	15.8	69.2	56.8	121.8	7.71
K9.0	3.7	10.7	37.9	15.0	67.3	48.1	139.9	7.77
L6.0	3.4	6.7	26.9	22.0	59.0	46.0	128.3	7.86
L12.0	3.1	7.3	22.9	26.6	59.9	59.4	100.8	7.83
M6.0	6.4	5.2	42.2	12.0	65.8	62.3	105.6	6.70

Appendix C

Appendix C.1- Talled results of mineral calculations

Sample	B3.0	Remain	Quartz	Gypsum	Pyrite	Apatite	Albite	K-spar	Rutile	Hematite	Calcite	Dolomite	FeDol	Illite	Sericite	Chlorite	Mont.	/Smec.	Kaolinite
% Clay	60.8	-1.50												12.67	21.25	8.85		19.55	0.00
SiO2	52.07	0.00	24.19				0.00	0.00						7.06	9.61	2.67		8.53	0.00
Al2O3	15.71	0.15					0.00	0.00						2.27	8.16	1.51		3.62	0.00
Fe2O3	6.26	0.00			0.00					4.33				0.51		1.42			
MgO	4.72	0.00										2.13		0.38		2.21			
CaO	2.96	-0.38									0.00	2.96	0.00					0.20	
Na2O	0.13	-0.09		0.07		0.11	0.00	0.00						0.90	2.51			0.22	
K2O	3.41	0.00																	
TiO2	0.82	0.00							0.82										0.00
P2O5	0.09	0.00				0.09													
MnO	0.04	0.04																	
Cr2O3	0.009	0.01																	
LOI	13.9	-1.31		0.04							0.00	4.65	0.00	1.55	0.96	1.04		6.97	0.00
CO2	4.65	0.00																	
C-Graphite	0.01	0.01																	
C/ORG	0.03	0.03																	
C/TOT	0.67																		
S/TOT	0.04																		
S-S	0	0.00																	
SO3 (calc.)	0.100	0.00		0.10															
% Mineral: 24.19 0.21 0.00 0.20 0.00 0.00 0.82 4.33 0.00 9.73 0.00 12.67 21.25 8.85 19.55 0.00																			
Mineral Sum (%): 101.79																			

Sample	B6.0	Remain	Quartz	Gypsum	Pyrite	Apatite	Albite	K-spar	Rutile	Hematite	Calcite	Dolomite	FeDol	Illite	Sericite	Chlorite	Mont.	/Smec.	Kaolinite
% Clay	49	-7.62												12.67	20.40	4.01		19.55	0.00
SiO2	51.88	0.00	25.84				0.00	0.00						7.06	9.23	1.21		8.53	0.00
Al2O3	14.45	0.04					0.00	0.00						2.27	7.83	0.68		3.62	0.00
Fe2O3	6	0.00			0.00					4.85				0.51		0.64			
MgO	4.72	0.00										3.33		0.38		1.00			
CaO	4.64	-0.42									0.00	4.64	0.00					0.20	
Na2O	0.13	-0.09		0.10		0.12	0.00	0.00						0.90	2.41			0.22	
K2O	3.31	0.00																	
TiO2	0.79	0.00							0.79										0.00
P2O5	0.1	0.00				0.10													
MnO	0.04	0.04																	
Cr2O3	0.01	0.01																	
LOI	14	-3.26																	
CO2	7.28	-0.00									0.00	7.28	0.00	1.55	0.92	0.47		6.97	0.00
C-Graphite	0.03	0.03																	
C/ORG	0	0.00																	
C/TOT	1.71																		
S/TOT	0.06																		
S-S	0	0.00																	
SO3 (calc.)	0.150	0.00		0.15															
% Mineral: 25.84 0.32 0.00 0.22 0.00 0.00 0.79 4.85 0.00 15.26 0.00 12.67 20.40 4.01 19.55 0.00																			
Mineral Sum (%): 103.90																			



Sample	B10.0	Remain	Quartz	Gypsum	Pyrite	Apatite	Albite	K-spar	Rutile	Hematite	Calcite	Dolomite	FeDol	Illite	Sericite	Chlorite	Mont.	/ Smec.	Kaolinite
% Clay	26.8	-21.65												7.16	20.20	3.31		17.78	0.00
SiO2	58.4	0.00	35.53				0.00	0.97						3.99	9.14	1.00		7.76	0.00
Al2O3	13.17	0.00					0.00	0.28						1.28	7.75	0.56		3.29	0.00
Fe2O3	4.12	0.00			0.00					3.30			0.00	0.29		0.53			0.00
MgO	3.35	0.00										2.31		0.22					0.83
CaO	3.21	-0.26					0.08				0.00	3.21	0.00					0.18	
Na2O	0.12	-0.08					0.00	0.25										0.20	
K2O	3.15	0.00							0.76					0.51	2.39				0.00
TiO2	0.76	0.00																	
P2O5	0.07	0.00					0.07												
MnO	0.04	0.04																	
Cr2O3	0.01	0.01																	
LOI	11.7	-1.86												0.87	0.91	0.39		6.34	0.00
CO2	5.04	0.00								0.00	5.04	0.00							
C-Graphite	0	0.00																	
C/ORG	0	0.00																	
C/TOT	1.3733																		
S/TOT	0																		
S- <i>S</i>	0	0.00																	
SO3 (calc.)	0.000	0.00																	
% Mineral: 35.53 0.00 0.00 0.15 0.00 1.50 0.76 3.30 0.00 10.56 0.00 7.16 20.20 3.31 17.78 0.00 Mineral Sum (%): 100.25																			

Sample	K3.0	Remain	Quartz	Gypsum	Pyrite	Apatite	Albite	K-spar	Rutile	Hematite	Calcite	Dolomite	FeDol	Illite	Sericite	Chlorite	Mont.	/ Smec.	Kaolinite
% Clay	31.1	-7.20												3.57	22.89	0.00		5.27	6.56
SiO2	49.31	0.00	30.83				0.82	0.00						1.99	10.36	0.00		2.30	3.01
Al2O3	20.9	7.71					0.23	0.00						0.64	8.79	0.00		0.98	2.55
Fe2O3	5.63	0.00			0.00					5.41			0.08	0.14		0.00			0.00
MgO	2.7	-0.30										2.90		0.11		0.00			0.00
CaO	4.03	-0.27					0.17	0.14			0.00	4.03	0.06					0.05	
Na2O	0.2	0.00																0.06	
K2O	2.96	0.00																	
TiO2	0.92	0.00												0.25	2.71				0.10
P2O5	0.14	0.00					0.14			0.82									
MnO	0.14	0.14																	
Cr2O3	0.02	0.02																	
LOI	12.6	1.93																	
CO2	6.1	-0.31												0.44	1.04	0.00		1.88	0.90
C-Graphite	0	0.00									0.00	6.33	0.09						
C/ORG	1.38	1.38																	
C/TOT	3.0421																		
S/TOT	0																		
S- <i>S</i>	0	0.00																	
SO3 (calc.)	0.000	0.00																	
% Mineral: 30.83 0.00 0.00 0.31 1.19 0.00 0.82 5.41 0.00 13.25 0.22 3.57 22.89 0.00 5.27 6.56 Mineral Sum (%): 90.33																			

Sample	K7.2	Remain	Quartz	Gypsum	Pyrite	Apatite	Albite	K-spar	Rutile	Hematite	Calcite	Dolomite	FeDol	Illite	Sericite	Chlorite	Mont.	Smec.	Kaolinite
% Clay	27.2	-10.32												2.53	23.69	0.00		5.40	5.91
SiO2	49.29	0.00	31.40				0.69	0.00						1.41	10.72	0.00		2.36	2.71
Al2O3	20.56	7.52					0.20	0.00						0.45	9.10	0.00		1.00	2.30
Fe2O3	6.18	0.00			0.00					5.91			0.17	0.10		0.00			
MgO	2.53	-0.36										2.81		0.08		0.00			
CaO	3.91	-0.39									0.00	3.91	0.12					0.05	
Na2O	0.18	0.00					0.12	0.00						0.18	2.80			0.06	0.09
K2O	2.98	0.00																	
TiO2	0.91	0.00							0.82										
P2O5	0.18	0.00					0.18												
MnO	0.11	0.11																	
Cr2O3	0.01	0.01																	
LOI	12.5	2.05			0.00						0.00	6.14	0.19	0.31	1.07	0.00		1.93	0.81
CO2	5.8	-0.53																	
C-Graphite	0	0.00																	
C/ORG	0.85	0.85																	
C/TOT	2.4304																		
S/TOT	0				0.00														
S-S	0	0.00																	
SO3 (calc.)	0.000	0.00																	
% Mineral: 31.40 0.00 0.00 0.39 1.01 0.00 0.82 5.91 0.00 12.86 0.49 2.53 23.69 0.00 5.40 5.91																			
Mineral Sum (%): 90.39																			

Sample	K9.0	Remain	Quartz	Gypsum	Pyrite	Apatite	Albite	K-spar	Rutile	Hematite	Calcite	Dolomite	FeDol	Illite	Sericite	Chlorite	Mont.	Smec.	Kaolinite
% Clay	25.1	-13.41												0.98	25.12	0.00		1.25	11.16
SiO2	51	0.00	31.76				1.66	0.00						0.55	11.37	0.00		0.55	5.11
Al2O3	21.36	6.50					0.47	0.00						0.18	9.65	0.00		0.23	4.34
Fe2O3	6.34	0.00								4.92			0.04	0.04		0.00			
MgO	2.29	-0.31			1.34							2.57		0.03		0.00			
CaO	3.58	-0.62									0.00	3.58	0.03					0.01	
Na2O	0.3	0.00					0.29	0.00										0.01	
K2O	3.04	0.00																0.01	
TiO2	0.99	0.00												0.07	2.97				0.17
P2O5	0	0.00							0.82										
MnO	0.1	0.10																	
Cr2O3	0.009	0.01																	
LOI	11.6	2.33																	
CO2	4.9	-0.76																	
C-Graphite	0	0.00																	
C/ORG	0.89	0.89																	
C/TOT	1.68																		
S/TOT	1.41																		
S-S	1.08	0.00			1.08														
SO3 (calc.)	0.824	0.00																	
% Mineral: 31.76 1.77 2.42 0.00 2.42 0.00 0.82 4.92 0.00 11.77 0.10 0.98 25.12 0.00 1.25 11.16																			
Mineral Sum (%): 94.50																			

Sample	L3.0	Remain	Quartz	Gypsum	Pyrite	Apatite	Albite	K-spar	Rutile	Hematite	Calcite	Dolomite	FeDol	Illite	Sericite	Chlorite	Mont.	/ Smec.	Kaolinite
% Clay	44.05	-13.49												10.24	29.50	5.43		12.37	0.00
SiO2	49.17	0.00	21.22				0.06	1.78						5.71	13.35	1.64		5.40	0.00
Al2O3	16.9	0.00					0.02	0.50						1.83	11.33	0.93		2.29	0.00
Fe2O3	7.12	0.00			0.00					5.84				0.41	0.87				0.00
MgO	4.03	0.00										2.36		0.31	1.35				0.13
CaO	3.29	-0.40																	0.14
Na2O	0.15	0.00			0.09		0.01	0.47											
K2O	4.68	0.00												0.73	3.49				0.00
TiO2	0.72	0.00							0.72										
P2O5	0.16	0.00					0.16												
MnO	0.07	0.07																	
Cr2O3	0.01	0.01																	
LOI	12.1	-0.76			0.06									1.25	1.33	0.64		4.41	0.00
CO2	5.16	-0.00																	
C-Graphite	0.025	0.03																	
C/ORG	0.095	0.10																	
C/TOT	1.815																		
S/TOT	0.05																		
S-S	0	0.00			0.00														
SO3 (calc.)	0.125	0.00			0.12														
% Mineral: 21.22 0.27 0.00 0.35 0.09 2.75 0.72 5.84 0.00 10.82 0.00 10.24 29.50 5.43 Mineral Sum (%): 99.60																			

Sample	L6.0	Remain	Quartz	Gypsum	Pyrite	Apatite	Albite	K-spar	Rutile	Hematite	Calcite	Dolomite	FeDol	Illite	Sericite	Chlorite	Mont.	/ Smec.	Kaolinite
% Clay	10.5	-48.63												10.22	0.00	36.54		12.37	0.00
SiO2	37.26	0.00	12.44				0.06	2.64						5.70	0.00	11.02		5.40	0.00
Al2O3	11.12	0.00					0.02	0.75						1.83	0.00	6.24		2.29	0.00
Fe2O3	4.38	-1.89			0.00					0.00				0.41	5.86				0.00
MgO	9.43	0.00												0.31	9.12				0.13
CaO	11.2	-0.21									10.97								0.14
Na2O	0.15	0.00			0.12		0.01	0.69											
K2O	3.76	2.35												0.72	0.00				0.00
TiO2	0.51	0.00							0.51										
P2O5	0.16	0.00					0.16												
MnO	0.36	0.36																	
Cr2O3	0.007	0.01																	
LOI	21.7	3.05			0.08														
CO2	8.62	0.01																	
C-Graphite	0.03	0.03																	
C/ORG	0.07	0.07																	
C/TOT	1.46																		
S/TOT	0.07																		
S-S	0	0.00			0.00														
SO3 (calc.)	0.175	0.00			0.17														
% Mineral: 12.44 0.38 0.00 0.35 0.09 4.07 0.51 0.00 19.58 0.00 0.00 10.22 36.54 Mineral Sum (%): 96.54																			

Sample	L11.0	Remain	Quartz	Gypsum	Pyrite	Apatite	Albite	K-spar	Rutile	Hematite	Calcite	Dolomite	FeDol	Illite	Sericite	Chlorite	Mont.	Smec.	Kaolinite
% Clay	18.25	-14.94												1.85	19.45	8.35		3.54	0.00
SiO2	33.23	0.00	15.16				0.35	3.82						1.03	8.80	2.52		1.55	0.00
Al2O3	11.06	0.00					0.10	1.08						0.33	7.47	1.42		0.66	0.00
Fe2O3	3.46	0.00			0.00					2.05			0.00	0.07		1.34			0.00
MgO	11.03	0.00										8.89		0.06		2.08			0.00
CaO	12.37	-0.27		0.07		0.17					0.00	12.37	0.00					0.04	0.04
Na2O	0.1	0.00					0.06												
K2O	3.43	0.00						1.00						0.13	2.30				0.00
TiO2	0.43	0.00							0.43										
P2O5	0.14	0.00				0.14													
MnO	0.33	0.33																	
Cr2O3	0.01	0.01																	
LOI	24.6	1.79																	
CO2	19.4	-0.02			0.04						0.00	19.42	0.00			0.88	0.98	1.26	0.00
C-Graphite	0.01	0.01																	
C/ORG	0.06	0.06																	
C/TOT	3.08																		
S/TOT	0.04																		
S-S	0	0.00			0.00														
SO3 (calc.)	0.100	0.00		0.10															
% Mineral: 15.16 0.21 0.00 0.31 0.51 5.90 0.43 2.05 0.00 40.68 0.00 1.85 19.45 8.35 3.54 0.00 Mineral Sum (%): 98.43																			

Sample	M4.8	Remain	Quartz	Gypsum	Pyrite	Apatite	Albite	K-spar	Rutile	Hematite	Calcite	Dolomite	FeDol	Illite	Sericite	Chlorite	Mont.	Smec.	Kaolinite
% Clay	49.3	-11.42												19.58	28.24	7.62		5.27	0.00
SiO2	54.79	0.00	21.60				0.82	4.06						10.92	12.78	2.30		2.30	0.00
Al2O3	18.01	0.00					0.23	1.15						3.51	10.85	1.30		0.98	0.00
Fe2O3	6.77	0.00			0.00					4.76			0.00	0.78		1.22			0.00
MgO	3	0.00										0.50		0.59		1.90			0.00
CaO	0.7	-0.40		0.00		0.12					0.23	0.70	0.00					0.05	0.06
Na2O	0.2	0.00					0.14												
K2O	5.79	0.00						1.06						1.39	3.34				0.00
TiO2	0.72	0.00							0.72										
P2O5	0.1	0.00				0.10													
MnO	0.1	0.10																	
Cr2O3	0.02	0.02																	
LOI	7.4	-0.32			0.00						0.18	1.10	0.00			2.39	1.28	0.90	1.88
CO2	1.3	0.02																	
C-Graphite	0	0.00																	
C/ORG	0.06	0.06																	
C/TOT	0.05																		
S/TOT	0	0.00			0.00														
S-S	0	0.00			0.00														
SO3 (calc.)	0.000	0.00		0.00															
% Mineral: 21.60 0.00 0.00 0.22 1.19 6.28 0.72 4.76 0.40 2.30 0.00 19.58 28.24 7.62 5.27 0.00 Mineral Sum (%): 98.20																			

Sample	M6.0	Remain	Quartz	Gypsum	Pyrite	Apatite	Albite	K-spar	Rutile	Hematite	Calcite	Dolomite	FeDol	Illite	Sericite	Chlorite	Mont.	Smec.	Kaolinite
% Clay	29.9	-28.54												19.50	26.50	7.03		5.40	0.00
SiO2	54.04	0.00	19.90				0.69	6.10						10.88	11.99	2.12		2.36	0.00
Al2O3	17.79	0.00					0.20	1.72						3.49	10.18	1.20		1.00	0.00
Fe2O3	6.67	0.00			0.00					4.76			0.00	0.78		1.13			0.00
MgO	2.75	0.00									0.14		0.40	0.59		1.76			0.05
CaO	0.56	-0.41			0.00		0.21						0.56						0.06
Na2O	0.18	0.00						1.59	0.69					1.38	3.13				0.00
K2O	6.11	0.00																	
TiO2	0.69	0.00																	
P2O5	0.18	0.00				0.18													
MnO	0.1	0.10																	
Cr2O3	0.01	0.01																	
LOI	6.9	-0.42			0.00						0.11		0.88	2.38	1.20	0.83		1.93	0.00
CO2	0.99	-0.00																	
C-Graphite	0	0.00																	
C/ORG	0.05	0.05																	
C/TOT	0.06																		
S/TOT	0																		
S-S	0	0.00			0.00														
SO3 (calc.)	0.000	0.00			0.00		0.39	1.01	9.42	0.69	4.76	0.26	1.84	19.50	26.50	7.03		5.40	0.00
% Mineral: 19.90																			
Mineral Sum (%): 96.71																			

Sample	M8.5	Remain	Quartz	Gypsum	Pyrite	Apatite	Albite	K-spar	Rutile	Hematite	Calcite	Dolomite	FeDol	Illite	Sericite	Chlorite	Mont.	Smec.	Kaolinite
% Clay	49.6	-1.38												19.57	20.86	5.25		5.29	0.00
SiO2	60.52	0.00	27.44				0.58	8.25						10.91	9.44	1.59		2.31	0.00
Al2O3	15.89	0.00					0.17	2.33						3.50	8.01	0.90		0.98	0.00
Fe2O3	5.68	0.00			0.00					4.05			0.00	0.78		0.84			0.00
MgO	2.25	0.00									0.12		0.34	0.59		1.31			0.05
CaO	0.48	-0.41			0.00		0.24						0.48						0.06
Na2O	0.16	0.00						0.10											
K2O	6.01	0.00							2.16	0.68				1.39	2.47				0.00
TiO2	0.68	0.00																	
P2O5	0.2	0.00				0.20													
MnO	0.07	0.07																	
Cr2O3	0.01	0.01																	
LOI	5.6	-1.09									0.09		0.75	2.39	0.94	0.62		1.89	0.00
CO2	0.85	0.00																	
C-Graphite	0	0.00																	
C/ORG	0.04	0.04																	
C/TOT	0.05																		
S/TOT	0																		
S-S	0	0.00			0.00														
SO3 (calc.)	0.000	0.00			0.00		0.44	0.85	12.74	0.68	4.05	0.22	1.58	19.57	20.86	5.25		5.29	0.00
% Mineral: 27.44																			
Mineral Sum (%): 98.97																			

## Appendix C.2 - Summary of step by step mineral calculating procedures using whole rock geochemical oxide data

**1 Kaolinite from TiO<sub>2</sub>**

- 1.a From TiO<sub>2</sub> of whole rock analysis subtract 0.82 (cut-off for presence of kaolinite). If < 0, no Kaolinite is present and all TiO<sub>2</sub> allotted to rutile (2). If > 0, 0.82 allotted to rutile, the remainder to Kaolinite.
- 1.b Calculate % Kaolinite by  $((1.a) / \text{MW TiO}_2 * \text{MW Kaolinite}) / \text{mole fraction TiO}_2$  in Kaolinite (which is 0.1)

**2 Rutile from TiO<sub>2</sub>**

- 2.a Calculate whole rock TiO<sub>2</sub> allotted to Rutile by  $\text{TiO}_2 - (1.a)$ .
- 2.b Calculate % Rutile by assigning (2.a) to % Rutile
- 2.c TiO<sub>2</sub> from analysis is now completely allotted

**3 Apatite from P<sub>2</sub>O<sub>5</sub>**

- 3.a Compute % Apatite by  $(\% \text{P}_2\text{O}_5 / \text{MW P}_2\text{O}_5 * \text{MW Apatite}) / \text{mole fraction P}_2\text{O}_5$  in Apatite (which is 1)
- 3.b P<sub>2</sub>O<sub>5</sub> is now completely allotted

**4 Gypsum from SO<sub>3</sub> (if analysis is available)**

- 4.a Calculate % Gypsum by  $(\% \text{SO}_3 / \text{MW SO}_3 * \text{MW Gypsum}) / \text{mole fraction SO}_3$  in Gypsum (which is 1)
- 4.b SO<sub>3</sub> is now completely allotted

**5 Pyrite from S (if analysis is available)**

- 5.a Figure % Pyrite by  $(\% \text{S} / \text{MW S} * \text{MW Pyrite}) / \text{mole fraction S}$  in Pyrite (which is 2)
- 5.b When calculating Fe<sub>2</sub>O<sub>3</sub> for later use, convert Fe to Fe<sub>2</sub>O<sub>3</sub> by  $\text{Fe} / 0.6994$
- 5.c S is now completely allotted

**6 Smectite from Na<sub>2</sub>O**

- 6.a Calculate %smectite according to: If %Na<sub>2</sub>O < 0.158, then %smectite =  $-281.72 + (4636.63 * \% \text{Na}_2\text{O}) - (17840 * \% \text{Na}_2\text{O}_2)$ ; If %Na<sub>2</sub>O > 0.158, then %smectite =  $-3.7133 + (101.719 * \% \text{Na}_2\text{O}) - (283.92 * \% \text{Na}_2\text{O}_2)$
- 6.b Compute Na<sub>2</sub>O used in smectite by  $(\% \text{smectite} * \text{MW Na}_2\text{O} * \text{mole fraction Na}_2\text{O}(0.05)) / \text{MW Smectite}$

**7 Albite from Na<sub>2</sub>O**

- 7.a Subtract (6.b) from %Na<sub>2</sub>O
- 7.b If (7.a) > 0 then use 7.a for calculating albite by  $\% \text{Na}_2\text{O} / \text{MW Na}_2\text{O} * \text{MW Albite}$ , otherwise albite = 0
- 7.c Na<sub>2</sub>O is now completely allotted

**8 Calcite from CaO**

- 8.a Compute amount CaO available for calcite by  $\text{MW fraction CaO} - \text{MW fraction CaO Gypsum} - \text{MW fraction CaO Apatite} - \text{MW fraction Smectite}$
- 8.b Figure the amount MgO used in dolomitic carbonates by  $\text{MW fraction CO}_2 - \text{MgO Illite} - (8.a)$
- 8.c Calculate CaO used for CaCO<sub>3</sub> by allotting equal amount of MW fraction CaO to dolomitic carbonates:  $(8.a) - (8.b)$
- 8.d Compute % Calcite by  $(8.c) * \text{MW Calcite} / \text{mole fraction CaO}$  in Calcite (which is 1)

**9 Dolomite from MgO**

- 9.a Figure MgO mole fraction by  $\% \text{MgO} / \text{MW MgO}$
- 9.b Subtract (8.b), the MgO Carb value allotted for dolomite from the calcite calculations, from (9.a)
- 9.c If (9.b) < 0, compute %Ferrodolomite as  $((8.b) - (9.a)) * \text{MW Ferrodolomite!}$
- 9.d Compute % Dolomite by remaining CaO /  $\text{Mol Weight CaO} * \text{MW Dolomite}$
- 9.e Assign remaining MgO to Chlorite
- 9.f Both CO<sub>2</sub> and CaO should now be completely allotted!

**10 Illite from K<sub>2</sub>O and MgO**

- 10.a Calculate mole ratio between K and Mg by  $(3 * (\% \text{K}_2\text{O} / \text{MW K}_2\text{O})) / (2 * (9.b))$
- 10.b If (10.a) < 1, then calculate illite according to (10.c), otherwise use (10.d)
- 10.c according to (10.b) %Illite =  $-18.095 + (10.0391 * \% \text{MgO}) - (0.7462 * (\% \text{MgO}_2))$
- 10.d according to (10.b) %Illite =  $-40.777 + (20.5364 * \% \text{K}_2\text{O}) - (1.7464 * (\% \text{K}_2\text{O}_2))$

**11 Chlorite from MgO**

- 11.a If 9.e - MgO Illite > 0, then calculated Chlorite using 9.e - MgO Illite. Otherwise Chlorite = 0
- 11.b Calculate Chlorite by  $\% \text{MgO} (9.e) / \text{MW MgO} * \text{MW Chlorite} / \text{mole fraction MgO}$  in Chlorite (which is 3.7)
- 11.c MgO is now completely allotted!

**12 Sericite and Potassium Feldspar from K<sub>2</sub>O and Al<sub>2</sub>O<sub>3</sub>**

- 12.a Divide remaining Al<sub>2</sub>O<sub>3</sub> by remaining K<sub>2</sub>O
- 12.b Compare Al<sub>2</sub>O<sub>3</sub> / K<sub>2</sub>O ratio from 12.a to Sericite and Potassium Feldspar ratios derived from molecular aluminum oxide and potassium oxide masses in their respective chemical formulas; Sericite: 152.94 (Al<sub>2</sub>O<sub>3</sub>) / 47.098 (K<sub>2</sub>O) = 3.247; Kspar: 50.98 (Al<sub>2</sub>O<sub>3</sub>) / 47.098 (K<sub>2</sub>O) = 1.082
- 12.c If 12.a ratio > 3.247, calculate 100% K<sub>2</sub>O as Sericite. If 12.a ratio < 1.082, calculate 100% Al<sub>2</sub>O<sub>3</sub> as Kspar. If 12.a ratio is between 3.247 and 1.082, allot K<sub>2</sub>O for Sericite and Kspar according to: SericiteK<sub>2</sub>O = %K<sub>2</sub>O \* (46.1926 \* 12.a ratio - 50) / 100; KsparK<sub>2</sub>O = %K<sub>2</sub>O \* (-46.193 \* 12.a ratio + 150) / 100.
- 12.d Calculate Sericite as %SericiteK<sub>2</sub>O(12.c) / MW K<sub>2</sub>O \* MW Sericite / mole fraction K<sub>2</sub>O in Sericite
- 12.e Calculate Kspar as %KsparK<sub>2</sub>O(12.c) / MW K<sub>2</sub>O \* MW Kspar / mole fraction K<sub>2</sub>O in Kspar
- 12.f All K<sub>2</sub>O should be allotted except where 12.a ratio < 1.082!

**13 Hematite from Fe<sub>2</sub>O<sub>3</sub>**

- 13.a All remaining Fe<sub>2</sub>O<sub>3</sub> is subscribed to Hematite. Since oxide formula = idealized mineral formula, no special calculations are necessary.
- 13.b All Fe<sub>2</sub>O<sub>3</sub> is now allotted!

Appendix C.3 - Analytical results for Total S, Sulfide S and SO<sub>3</sub> of selected geologic barrier samples

## LECO™ Sulfur Analyzer

Total sulfur and carbon are analyzed together. A 100 mg sample split is subjected 1,370°C in an oxygen atmosphere. The resulting SO<sub>2</sub> gas is the quantitatively determined with an infrared detector and total S content is extrapolated from the data. Another sample split is first heated to 800°C and afterwards analyzed for S in the LECO™ analyzer. The resulting sulphur content is subtracted from the total S previously established. The difference is equated to sulfide S. Amount SO<sub>3</sub> can now be calculated as:

$$\text{Total S} - \text{Sulfide S} = S_{\text{SO}_3} \quad \text{SO}_3 = S_{\text{SO}_3} * 2.4972$$

Sample	TOTAL S %	SO <sub>3</sub> %	Sulfide S %
B3.0	0.04	0.10	< 0.03
B4.6	< 0.02	0.00	< 0.03
B6.0	0.06	0.15	< 0.03
K5.8	0.63	0.60	0.39
K9.0	1.41	0.82	1.08
L1.5	0.03	0.07	< 0.03
L6.0	0.07	0.17	< 0.03
L11	0.04	0.10	< 0.03
M2.4	< 0.02	0.00	< 0.03
M6.0	< 0.02	0.00	< 0.03
M13	< 0.02	0.00	< 0.03

## Appendix C.4 - Pearson's correlation analysis between mineral calculations and measured mineral data.

Appendix C.4.1 - Significant correlations of XRD analysis vs. calculated mineralogy. Note: XRD data only available for sample fractions < 2 $\mu$ m, while calculations were performed from whole rock geochemical data.

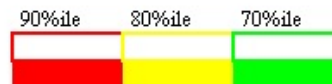
		XRD Analysis					
		Quartz	Calcite	Illite	Smectite	Chlorite	Kaolinite
		<2 $\mu$ m	<2 $\mu$ m	<2 $\mu$ m	/Mont. <2 $\mu$ m	<2 $\mu$ m	<2 $\mu$ m
Illite calculated	Pearson Correlation	0.669	-0.672	0.832	-0.351	-0.864	-0.735
	Sig. (2-tailed)	0.101	0.098	0.02	0.44	0.012	0.06
	N	7	7	7	7	7	7
Mont./ Smectite calculated	Pearson Correlation	-0.376	-0.203	-0.219	0.905	0.518	-0.505
	Sig. (2-tailed)	0.406	0.663	0.637	0.005	0.233	0.248
	N	7	7	7	7	7	7
Chlorite calculated	Pearson Correlation	0.249	-0.575	0.602	0.218	-0.411	-0.844
	Sig. (2-tailed)	0.59	0.177	0.153	0.639	0.359	0.017
	N	7	7	7	7	7	7
Kaolinite calculated	Pearson Correlation	-0.271	0.872	-0.678	-0.179	0.399	0.992
	Sig. (2-tailed)	0.557	0.01	0.094	0.701	0.375	0
	N	7	7	7	7	7	7
Clay calculated	Pearson Correlation	0.131	-0.616	0.633	0.217	-0.339	-0.853
	Sig. (2-tailed)	0.779	0.141	0.127	0.64	0.457	0.015
	N	7	7	7	7	7	7
Calcite calculated	Pearson Correlation	0.821	-0.483	0.679	-0.654	-0.946	-0.372
	Sig. (2-tailed)	0.024	0.273	0.093	0.111	0.001	0.411
	N	7	7	7	7	7	7
Dolomite calculated	Pearson Correlation	-0.83	0.649	-0.786	0.52	0.965	0.609
	Sig. (2-tailed)	0.021	0.115	0.036	0.232	0	0.147
	N	7	7	7	7	7	7
Ferro- dolomite calculated	Pearson Correlation	-0.247	0.679	-0.584	-0.071	0.365	0.821
	Sig. (2-tailed)	0.593	0.094	0.169	0.879	0.421	0.024
	N	7	7	7	7	7	7
Carbonates calculated	Pearson Correlation	-0.819	0.665	-0.793	0.499	0.965	0.633
	Sig. (2-tailed)	0.024	0.103	0.034	0.254	0.001	0.127
	N	7	7	7	7	7	7
Kspar calculated	Pearson Correlation	0.714	-0.612	0.787	-0.653	-0.893	-0.472
	Sig. (2-tailed)	0.072	0.144	0.036	0.112	0.007	0.285
	N	7	7	7	7	7	7
Minor Minerals calculated	Pearson Correlation	0.631	-0.468	0.785	-0.795	-0.883	-0.282
	Sig. (2-tailed)	0.129	0.29	0.036	0.033	0.008	0.541
	N	7	7	7	7	7	7
					90%ile	80%ile	70%ile
Correlation is significant at the 0.05 level (2-tailed).							
Correlation is significant at the 0.01 level (2-tailed).							



Appendix C 4.2 - Significant correlations of point count thin section analysis vs. calculated mineralogy.

		Geochem.			Point Count				
		LOI	Clay	Dolomite	Calcite	Sericite	Opaque	K-Spar	Other
Dolomite	Pearson Correlation	-0.128	0.351	-0.461	-0.368	0.762	0.981	-0.4	0.731
calculated	Sig. (2-tailed)	0.809	0.495	0.357	0.473	0.078	0.001	0.432	0.099
	N	6	6	6	6	6	6	6	6
Calcite	Pearson Correlation	0.852	-0.982	1	0.202	0.124	-0.431	-0.187	-0.444
calculated	Sig. (2-tailed)	0.031	0	0	0.701	0.814	0.394	0.722	0.377
	N	6	6	6	6	6	6	6	6
Carbonates	Pearson Correlation	0.38	-0.206	0.093	-0.284	0.936	0.841	-0.571	0.559
calculated	Sig. (2-tailed)	0.457	0.695	0.861	0.585	0.006	0.036	0.236	0.249
	N	6	6	6	6	6	6	6	6
Chlorite	Pearson Correlation	0.795	-0.982	0.968	-0.037	0.256	-0.293	-0.081	-0.465
calculated	Sig. (2-tailed)	0.059	0	0.002	0.944	0.624	0.573	0.878	0.352
	N	6	6	6	6	6	6	6	6
Illite	Pearson Correlation	-0.184	-0.112	0.149	-0.456	-0.47	-0.523	0.761	-0.885
calculated	Sig. (2-tailed)	0.727	0.832	0.778	0.364	0.347	0.287	0.079	0.019
	N	6	6	6	6	6	6	6	6
Sericite	Pearson Correlation	-0.939	0.952	-0.961	-0.147	-0.296	0.229	0.366	0.351
calculated	Sig. (2-tailed)	0.006	0.003	0.002	0.782	0.569	0.663	0.476	0.496
	N	6	6	6	6	6	6	6	6
Clay	Pearson Correlation	0.218	-0.399	0.485	-0.12	-0.523	-0.718	0.457	-0.996
calculated	Sig. (2-tailed)	0.678	0.434	0.33	0.821	0.287	0.108	0.363	0
	N	6	6	6	6	6	6	6	6
Hematite	Pearson Correlation	-0.745	0.886	-0.818	0.203	-0.602	-0.125	0.221	0.162
calculated	Sig. (2-tailed)	0.089	0.019	0.047	0.699	0.206	0.814	0.674	0.758
	N	6	6	6	6	6	6	6	6
Kspar	Pearson Correlation	-0.294	-0.235	0.104	-0.859	0.299	0.139	0.77	-0.237
calculated	Sig. (2-tailed)	0.572	0.654	0.844	0.029	0.565	0.794	0.073	0.651
	N	6	6	6	6	6	6	6	6
Minor Minerals	Pearson Correlation	-0.856	0.439	-0.504	-0.42	-0.218	0.007	0.814	0.041
calculated	Sig. (2-tailed)	0.03	0.384	0.308	0.406	0.678	0.99	0.048	0.938
	N	6	6	6	6	6	6	6	6

Correlation is significant at the 0.05 level (2-tailed).  
 Correlation is significant at the 0.01 level (2-tailed).



## Appendix D.1

Results of Batch Sorption Experiments, listing amounts sorbed (x/m) and final concentration in solution (C)

SAMPLES	Sorbed Ca (x/m) g/kg	Solution Ca (C) g/L	Sorbed Cu (x/m) g/kg	Solution Cu (C) g/L	Sorbed K (x/m) g/kg	Solution K (C) g/L	Sorbed Na (x/m) g/kg	Solution Na (C) g/L	Sorbed NH <sub>4</sub> (x/m) g/kg	Solution NH <sub>4</sub> (C) g/L
M6-1000	-0.070	0.008	0.0001	0	-0.011	0.002	-0.034	0.008	-0.007	0.001
M6-100	-0.114	0.017	0.0009	0	0.032	0.003	0.039	0.040	0.057	0.001
M6-10	-0.553	0.110	0.0091	0	0.254	0.040	0.307	0.463	0.383	0.030
M6-1	-2.200	0.629	0.0112	6.3E-05	0.000	0.560	2.770	4.050	0.620	0.682
L6-1000	-0.171	0.018	0.0001	0	-0.066	0.007	-0.103	0.015	0.007	0
L6-100	-0.170	0.023	0.0009	0	-0.025	0.009	0.163	0.027	0.051	0.002
L6-10	-0.595	0.114	0.0091	0	0.161	0.049	0.726	0.421	0.360	0.033
L6-1	-1.510	0.560	0.0115	2.7E-05	0	0.560	1.920	4.135	0	0.744
L11-1000	-0.113	0.012	0.0001	0	-0.062	0.007	-0.006	0.005	0.007	0
L11-100	-0.179	0.023	0.0009	0	-0.059	0.012	0.048	0.039	0.049	0.002
L11-10	-0.394	0.094	0.0091	0	0.119	0.053	0.598	0.434	0.326	0.036
L11-1	-2.020	0.611	0.0109	9.4E-05	0.150	0.545	2.020	4.125	0.530	0.691
B6-1000	-0.139	0.015	0.0001	0	-0.009	0.002	0.005	0.004	-0.003	0.001
B6-100	-0.238	0.029	0.0009	2.0E-06	0.032	0.003	0.103	0.033	0.056	0.001
B6-10	-0.827	0.137	0.0091	5.0E-06	0.385	0.026	0.881	0.405	0.427	0.026
B6-1	-4.160	0.825	0.0115	3.3E-05	0.850	0.475	1.070	4.220	1.350	0.609
K9-1000	-1.720	0.173	0.0001	0	-0.163	0.017	-0.029	0.007	0.007	0
K9-100	-1.677	0.173	0.0009	0	-0.149	0.021	0.006	0.043	0.057	0.001
K9-10	-2.008	0.255	0.0091	0	-0.046	0.070	0.151	0.478	0.203	0.048
K9-1	-3.200	0.729	0.0105	1.3E-04	-0.650	0.625	2.020	4.125	0.390	0.705

SAMPLES	Sorbed Cl (x/m) g/kg	Solution Cl (C) g/L	Sorbed SO <sub>4</sub> (x/m) g/kg	Solution SO <sub>4</sub> (C) g/L	Sorbed NO <sub>3</sub> (x/m) g/kg	Solution NO <sub>3</sub> (C) g/L	Sorbed CPL (x/m) g/kg	Solution CPL (C) g/L	Sorbed TOTAL (x/m) g/L sum	Solution TOTAL (C) g/L sum
M6-1000	-0.141	0.021	0.017	0	0.001	0.001	0	4.0E-05	-0.245	0.041
M6-100	-0.038	0.082	-0.020	0.024	-0.006	0.009	0.001	0.0003	-0.048	0.176
M6-10	1.200	0.640	0.000	0.263	0.038	0.078	0.015	0.0019	1.653	1.625
M6-1	0.350	7.003	-0.890	2.598	0.240	0.827	0.313	0.0050	1.214	16.354
L6-1000	-0.025	0.009	-0.025	0.0042	-0.001	0.001	1.0E-04	3.0E-05	-0.384	0.054
L6-100	0.013	0.077	-0.290	0.051	0.003	0.008	0.001	0.0003	-0.253	0.197
L6-10	-0.600	0.820	0.090	0.254	0.014	0.081	0.019	0.0015	0.184	1.772
L6-1	-0.520	7.090	0.050	2.504	0.790	0.772	0.320	0.0043	1.062	16.369
L11-1000	-0.045	0.011	-0.058	0.0075	0.001	0.001	1.0E-04	3.0E-05	-0.276	0.044
L11-100	-0.012	0.080	-0.060	0.028	-0.009	0.009	0.001	0.0002	-0.219	0.193
L11-10	1.500	0.610	0.090	0.254	0	0.082	0.021	0.0013	2.269	1.564
L11-1	0.390	6.999	0.330	2.476	0.920	0.759	0.013	0.0350	2.344	16.241
B6-1000	-0.049	0.012	-0.116	0.0133	-0.002	0.001	1.0E-04	3.0E-05	-0.313	0.047
B6-100	-0.012	0.080	-0.110	0.033	-0.097	0.018	0.001	0.0002	-0.264	0.198
B6-10	1.100	0.650	0.090	0.254	0.034	0.079	0.019	0.0015	2.118	1.579
B6-1	1.770	6.861	2.710	2.238	0	0.851	0.311	0.0052	3.912	16.084
K9-1000	0.018	0.005	-3.653	0.367	0.003	0.001	0	4.0E-05	-5.537	0.570
K9-100	0.076	0.071	-4.780	0.500	-0.009	0.009	0.001	0.0002	-6.474	0.819
K9-10	1.900	0.570	-6.690	0.932	-0.014	0.083	0.017	0.0017	-6.477	2.438
K9-1	3.010	6.737	-2.210	2.730	1.040	0.747	0.089	0.0274	0.500	16.426

## Explanation:

All data corrected for blank sorption during batch experiment.

Samples: M6 - Lower Röttone (6 m b.s.); L6 - Lehrberg Layers (6 m b.s.); L11 - Lehrberg Layers (11 m b.s.); B6 - Feuerletten (6 m b.s.); K9 - Amaltheen Clay (9 m b.s.)

Dilution factors: -1 = 1/1 (undiluted); -10 = 1/10; -100 = 1/100; -1000 = 1/1000

CPL = 2-Chlorophenol

Appendix D.2: Results of Sorption Isotherm Calculations ( $K_d$  Values)

## Methodology:

- (1) Plot of amount sorbed versus final sorbate concentration (Figure 7.5)
- (2) Regression analysis for linear fit of Freundlich, Langmuir & straight line isotherms using SSPS Software (SSPS, 1999) (see equations 7.5 and 7.7).
- (3) Calculations of  $K_d$  values using general linear expression:

$$y = b + ax$$

Results for  $a$  and  $b$ , as well as correlation coefficients are taken from SSPS (1999) regression analysis output, where:

For Straight Line Isotherm:  $y = x/m$  (amount sorbed)  
 $x = C$  (final sorbent concentration)  
 $a = K_d$  (linear sorption coefficient)

For Freundlich Isotherm (Eq. 7.5):  $y = \log x/m$   
 $x = \log C$   
 $a = n$   
 $b = \log S$  ( $S = K_d$ )

For Langmuir Isotherm (Eq. 7.7):  $y = 1/x/m$   
 $x = 1/C$   
 $a = 1/S_L M$  ( $S_L = K_d$ )  
 $b = 1/M$

- (4) Assigning Sorption Isotherm and best  $K_d$  value:  
 Comparing correlation factors of regression analysis for the 3 isotherms and isotherm graphs represented in figure 7.4. Final decision based on shape of graph in figure 7.5, not solely correlation factors. No  $K_d$  values assigned for mixed (sorption/desorption) systems or where linear  $0.3 > K_d > -0.3$ . Best interpretative  $K_d$  value fit bolded in the following table. Bolded values used for further calculations.

Calcium										
Sample	Sorption Type	Weighted Average Kd (l/kg)	Graphic Linear		Freundlich Isotherm			Langmuir Isotherm		
		Kd (l/kg)	Kd (l/kg)	Correlation	Kd (l/kg)	n	Correlation	Kd (l/kg)	M	Correlation
M6	Freundlich desorption	2.96	-3.38	0.996	<b>-3.18</b>	<b>0.80</b>	0.999	-8.15	-1.110	0.980
L6	linear desorption	2.20	<b>-2.42</b>	0.997	-2.30	0.66	0.994	-6.76	-1.446	0.967
L11	linear desorption	3.31	<b>-3.16</b>	1.000	-2.65	0.73	0.991	-9.78	-1.031	0.978
B6	linear desorption	4.22	<b>-4.93</b>	1.000	-4.72	0.84	0.999	-3.45	-2.800	0.994
K9	Freundlich desorption	2.57	-2.67	0.996	<b>-3.68</b>	<b>0.44</b>	0.999	-3.79	-4.250	0.988
Copper										
Sample	Sorption Type	Weighted Average Kd (l/kg)	Graphic Linear		Freundlich Isotherm			Langmuir Isotherm		
		Kd (l/kg)	Kd (l/kg)	Correlation	Kd (l/kg)	n	Correlation	Kd (l/kg)	M	Correlation
M6	H-type (Langmuir)	191.96	94.27	0.281	0.69	0.38	0.976	<b>9.7E+07</b>	<b>0.010</b>	1.000
L6	H-type (Langmuir)	461.24	304.77	0.423	1.05	0.40	0.989	<b>9.1E+07</b>	<b>0.011</b>	1.000
L11	H-type (Langmuir)	125.36	55.03	0.233	0.58	0.37	0.965	<b>9.9E+07</b>	<b>0.010</b>	1.000
B6	H-type (Langmuir)	309.71	292.59	0.623	0.35	0.36	0.854	<b>1.0E+48</b>	<b>0.010</b>	1.000
K9	H-type (Langmuir)	88.63	32.74	0.172	0.59	0.36	0.921	<b>1.0E+08</b>	<b>0.010</b>	1.000
Potassium										
Sample	Sorption Type	Weighted Average Kd (l/kg)	Graphic Linear		Freundlich Isotherm			Langmuir Isotherm		
		Kd (l/kg)	Kd (l/kg)	Correlation	Kd (l/kg)	n	Correlation	Kd (l/kg)	M	Correlation
M6	Sorption/Desorption	0.04	-0.14	0.094	-2.9E-45	-17.97	0.716	-480.00	2.1E-50	0.304
L6	Sorption/Desorption	0.03	-0.02	0.002	-2.6E-50	-25.17	0.811	-116.00	1.7E-50	0.433
L11	H-Type (Langmuir)	0.26	0.31	0.521	0.19	0.23	0.878	<b>38.02</b>	<b>0.140</b>	0.789
B6	L-Type (Langmuir)	1.76	1.57	0.840	2.48	0.78	0.889	<b>0.97</b>	<b>9.960</b>	0.995
K9	linear desorption	0.00	<b>-0.88</b>	0.926	-0.48	0.39	0.344	-108.89	0.018	0.024

Sodium											
Sample	Sorption Type	Weighted Average Kd (l/kg)	Graphic Linear			Freundlich Isotherm			Langmuir Isotherm		
			Kd (l/kg)	Correlation		Kd (l/kg)	n	Correlation	Kd (l/kg)	M	Correlation
M6	C-Type (Linear)	0.61	<b>0.69</b>	1.000		0.71	0.92	0.997	0.60	1.676	0.999
L6	L-Type (Freundlich)	0.43	0.43	0.909		<b>1.01</b>	<b>0.49</b>	0.995	5.12	1.334	0.992
L11	L-Type (Freundlich)	0.49	0.46	0.962		<b>0.79</b>	<b>0.81</b>	0.968	0.08	16.287	1.000
B6	H-Type (Langmuir)	0.25	0.20	0.561		0.75	0.77	0.879	<b>2.13</b>	<b>1.565</b>	0.998
K9	C-Type (Linear)	0.44	<b>0.50</b>	0.999		0.35	1.28	0.999	0.66	0.207	0.998
Ammonium											
Sample	Sorption Type	Weighted Average Kd (l/kg)	Graphic Linear			Freundlich Isotherm			Langmuir Isotherm		
			Kd (l/kg)	Correlation		Kd (l/kg)	n	Correlation	Kd (l/kg)	M	Correlation
M6	H-Type (Langmuir)	0.92	0.73	0.697		0.91	0.38	0.900	<b>94.28</b>	<b>0.561</b>	0.999
L6	Sorption/Desorption	0.05	-0.17	0.135		6.5E-19	-0.35	0.119	-9.9E+49	3.0E-50	0.111
L11	H-Type (Langmuir)	0.77	0.61	0.714		0.78	0.41	0.892	<b>52.28</b>	<b>0.517</b>	1.000
B6	L-Type (Freundlich)	2.19	2.01	0.928		<b>2.14</b>	<b>0.52</b>	0.971	50.11	0.915	0.998
K9	H-Type (Langmuir)	0.54	0.45	0.817		0.46	0.30	0.992	<b>211.14</b>	<b>0.282</b>	0.984
Chloride											
Sample	Sorption Type	Weighted Average Kd (l/kg)	Graphic Linear			Freundlich Isotherm			Langmuir Isotherm		
			Kd (l/kg)	Correlation		Kd (l/kg)	n	Correlation	Kd (l/kg)	M	Correlation
M6	Sorption/Desorption	0.06	0.02	0.008		0.32	0.32	0.314	39.62	-0.187	0.051
L6	Desorption/Sorption	-0.07	-0.05	0.337		0.22	0.59	0.716	-45.50	0.040	0.320
L11	Sorption/Desorption	0.06	0.003	0.000		0.27	0.52	0.441	325.39	-0.042	0.006
B6	L-Type (Freundlich)	0.25	0.23	0.721		<b>1.19</b>	<b>0.20</b>	0.997	2.46	1.737	0.915
K9	L-Type (Freundlich)	0.43	0.38	0.715		<b>1.29</b>	<b>0.81</b>	0.920	6.94	0.522	0.973
Sulfate											
Sample	Sorption Type	Weighted Average Kd (l/kg)	Graphic Linear			Freundlich Isotherm			Langmuir Isotherm		
			Kd (l/kg)	Correlation		Kd (l/kg)	n	Correlation	Kd (l/kg)	M	Correlation
M6	V. weak lin. desorption	-0.31	<b>0.35</b>	0.990		3.8E-18	-0.31	0.100	-9.9E+49	3.0E-50	0.111
L6	No sig. sorption	0.02	0.06	0.172		0.09	0.07	0.029	-51.41	0.089	0.911
L11	No sig. sorption	0.13	0.15	0.913		0.20	0.30	0.864	-2.00	-1.7E-49	0.992
B6	C-Type (Linear)	1.07	<b>1.28</b>	0.999		0.56	2.34	0.221	1.56	0.008	0.324
K9	Desorption/Sorption	-0.65	1.01	0.343		3.80	-0.28	0.284	-6.34	-2.791	0.199
Nitrate											
Sample	Sorption Type	Weighted Average Kd (l/kg)	Graphic Linear			Freundlich Isotherm			Langmuir Isotherm		
			Kd (l/kg)	Correlation		Kd (l/kg)	n	Correlation	Kd (l/kg)	M	Correlation
M6	C-Type (Linear)	0.27	<b>0.29</b>	0.993		0.28	0.77	1.000	14.95	0.097	1.000
L6	C-Type (Linear)	0.92	<b>1.05</b>	0.993		0.70	1.21	0.934	7.27	0.055	0.985
L11	C-Type (Linear)	1.21	<b>1.25</b>	0.991		1.20	0.98	1.000	122.92	0.011	0.975
B6	Weak Sorp./Desorp.	0.00	0.03	0.056		0.53	0.74	0.678	-52.74	0.036	0.999
K9	C-Type (Linear)	1.24	<b>1.44</b>	0.987		1.31	0.80	1.000	34.02	0.179	0.999
2-Chlorphenol											
Sample	Sorption Type	Weighted Average Kd (l/kg)	Graphic Linear			Freundlich Isotherm			Langmuir Isotherm		
			Kd (l/kg)	Correlation		Kd (l/kg)	n	Correlation	Kd (l/kg)	M	Correlation
M6	Negative Freundlich	43.50	63.85	0.896		<b>14115.62</b>	<b>2.10</b>	0.970	-287.31	-0.007	0.997
L6	Negative Freundlich	52.68	76.79	0.921		<b>918.33</b>	<b>1.59</b>	0.955	-150.74	-0.022	1.000
L11	Sorption/Desorption	0.37	0.18	0.100		0.35	0.69	0.717	-928.94	-0.004	0.994
B6	Negative Freundlich	45.22	61.96	0.955		<b>619.01</b>	<b>1.52</b>	0.987	-921.81	-0.004	0.997
K9	L-Type (Langmuir)	3.10	3.11	0.982		2.17	0.83	0.958	<b>77.27</b>	<b>0.090</b>	0.998
TOTAL											
Sample	Sorption Type	Weighted Average Kd (l/kg)	Graphic Linear			Freundlich Isotherm			Langmuir Isotherm		
			Kd (l/kg)	Correlation		Kd (l/kg)	n	Correlation	Kd (l/kg)	M	Correlation
M6	H-Type (Langmuir)	0.08	0.06	0.239		0.94	0.19	0.321	<b>0.99</b>	<b>2.261</b>	0.800
L6	C-Type (Linear)	0.06	<b>0.08</b>	0.922		0.11	0.83	0.997	0.03	4.122	0.998
L11	H-Type (Langmuir)	0.14	0.12	0.438		0.77	0.60	0.431	<b>4.57</b>	<b>1.407</b>	0.398
B6	L-Type (Langmuir)	0.23	0.23	0.770		1.71	0.31	0.948	<b>0.87</b>	<b>3.954</b>	0.990
K9	Desorption/Sorption	-0.01	0.43	0.954		5.63	-0.78	0.858	1.69	0.965	0.463

Weighted Average calculation as interpretative aid according to:

$$Avg_{weighted} = \frac{\frac{(\% / m)_1}{1} + \frac{(\% / m)_{10}}{10} + \dots + \frac{(\% / m)_{1000}}{1000}}{\sum \frac{\%}{C}}$$

Appendix D.3: Development of sorption isotherm equation for 2-chlorophenol in artificial leachate using selected geologic barriers

- (1) Significant correlations established using two-tailed Pearson bivariate correlation with SSPS (1999) software (see correlation results below). Note:  $K_{ic}$  (equivalent to  $K_{oc}$ ) calculated using weighted averages (see weighted average calculation equation above), where  $m$  = amount of total Carbon in sample.

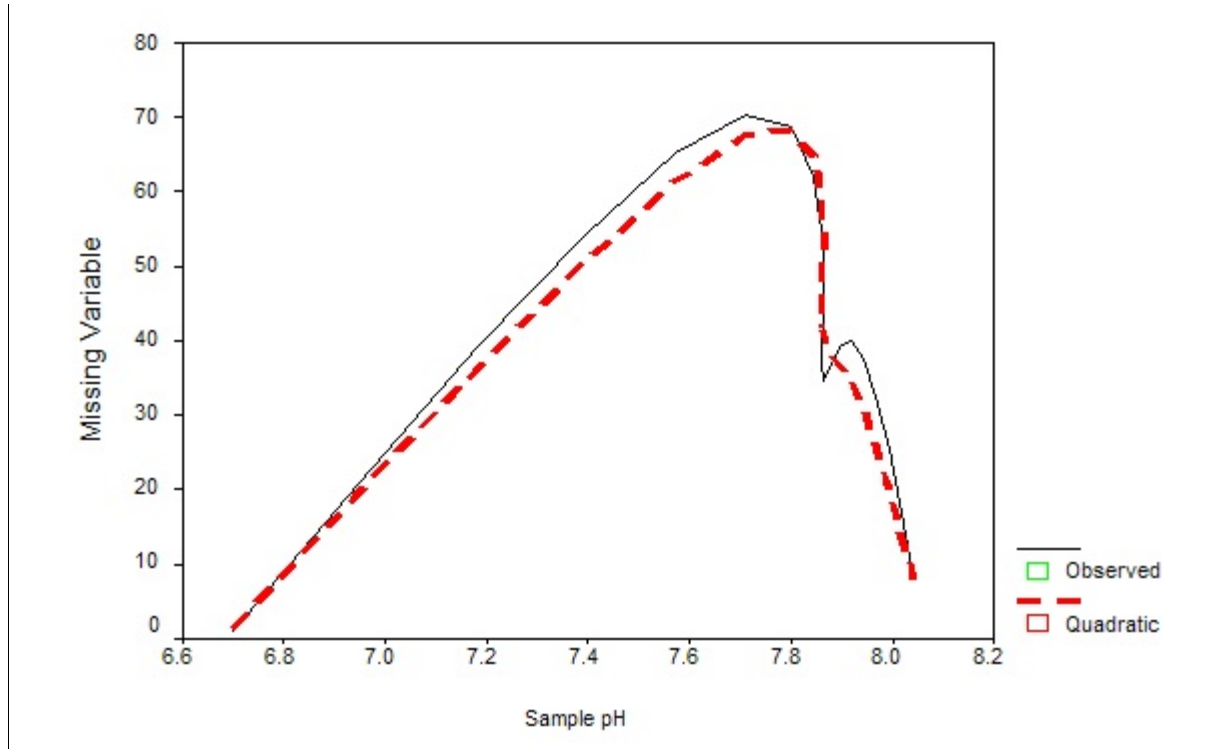
Correlations									
		% org. C	Ktc (weighted averages)	Sample pH	Kd (Experimental)	Kd = Ktc/ftc	1 / ftc	1/pH	Eq. 7.10
% org. C	Pearson Correlation	1.000	-.278	.070	-.283	-.254	-.250	-.095	.011
	Sig. (2-tailed)	.	.650	.912	.645	.680	.685	.879	.988
	N	5	5	5	5	5	5	5	5
Ktc (weighted averages)	Pearson Correlation	-.278	1.000	-.975**	1.000**	.999**	.999**	.981**	-.335
	Sig. (2-tailed)	.650	.	.005	.000	.000	.000	.003	.581
	N	5	5	5	5	5	5	5	5
Sample pH	Pearson Correlation	.070	-.975**	1.000	-.975**	-.978**	-.978**	-1.000**	.380
	Sig. (2-tailed)	.912	.005	.	.005	.005	.004	.000	.552
	N	5	5	5	5	5	5	5	5
Kd (Experimental)	Pearson Correlation	-.283	1.000**	-.975**	1.000	.998**	.999**	.981**	-.341
	Sig. (2-tailed)	.645	.000	.005	.	.000	.000	.003	.575
	N	5	5	5	5	5	5	5	5
Kd = Ktc/ftc	Pearson Correlation	-.254	.999**	-.978**	.998**	1.000	1.000**	.982**	-.328
	Sig. (2-tailed)	.680	.000	.005	.000	.	.000	.003	.590
	N	5	5	5	5	5	5	5	5
1 / ftc	Pearson Correlation	-.250	.999**	-.978**	.999**	1.000**	1.000	.984**	-.332
	Sig. (2-tailed)	.685	.000	.004	.000	.000	.	.002	.585
	N	5	5	5	5	5	5	5	5
1/pH	Pearson Correlation	-.095	.981**	-1.000**	.981**	.982**	.984**	1.000	-.357
	Sig. (2-tailed)	.879	.003	.000	.003	.003	.002	.	.558
	N	5	5	5	5	5	5	5	5
Eq. 7.10	Pearson Correlation	.011	-.335	.380	-.341	-.328	-.332	-.357	1.000
	Sig. (2-tailed)	.988	.581	.552	.575	.590	.585	.558	.
	N	5	5	5	5	5	5	5	5

\*\* . Correlation is significant at the 0.01 level (2-tailed).

- (2) Using  $K_d = K_{oc} * f_{oc}$  yielded non correlating results. Only when total carbon amounts and the inverse of  $f_{ic}$  (total carbon) was used according to  $K_d = K_{ic} * 1/f_{ic}$  were experimental chlorophenol sorption isotherms somewhat approximated. Missing variable for a more precise  $K_d$  match is apparent.



- (3) Influence of sample pH on chlorophenol sorption is evident (Correlation factor .981, sig. .003 for  $K_d$  (experimental) &  $1/pH$ . Missing variable in (2) calculated for each  $K_d = K_{tc} * 1/f_{tc}$  & curve fitted against sample pH yielding quadratic equation (see results below).



Graphical representation of curve fitting statistics for Missing Variable vs. pH for  $K_d$  chlorophenol estimation.

Results of curve fitting statistic using Missing Variable vs. pH for  $K_d$  chlorophenol estimation

Independent: pH									
Dependent	Mth	Rsqr	d.f.	F	Sigf	b0	b1	b2	
Missing Variable	QUA	0.964	2	27.16	.036	-9934.9	2714.59	-183.82	
Quadratic Equation:		Missing Variable = b0 + (b1 * pH) + (b2 * pH <sup>2</sup> )							

- (4) Resulting equation for  $K_d$  estimation for 2-Chlorophenol using artificial leachate in selected geologic barrier sample is:

$$K_d = \frac{K_{tc}}{f_{tc}} (-9934.9 + (2714.59 \text{ pH}) + (-183.82 \text{ pH}^2))$$

where  $K_d$  = Sorption Coefficient for 2-Chlorophenol  
 $K_{tc}$  = Sorption or Distribution Coefficient for Total Carbon  
 pH = Sorbent material pH  
 $f_{tc}$  = Weight percent of total carbon in sorbent material

Appendix D.4: Significant correlation of cation exchange capacities vs. sorption coefficients ( $K_d$ ).

CEC Ba				CEC Sum			
Kd Ca linear	Pearson Correlation	-0.916	-0.842	Kd Cl	Pearson Correlation	0.498	0.621
	Sig. (2-tailed)	0.029	0.074		Sig. (2-tailed)	0.393	0.263
	N	5	5		N	5	5
Kd Cu linear	Pearson Correlation	0.187	0.217	Kd SO4 linear	Pearson Correlation	0.884	0.836
	Sig. (2-tailed)	0.764	0.726		Sig. (2-tailed)	0.046	0.078
	N	5	5		N	5	5
Kd Cu Langmuir	Pearson Correlation	0.983	0.996	Kd NO3	Pearson Correlation	-0.785	-0.726
	Sig. (2-tailed)	0.003	0		Sig. (2-tailed)	0.116	0.165
	N	5	5		N	5	5
Kd K linear	Pearson Correlation	0.987	0.979	Kd Chlorophenol	Pearson Correlation	-0.108	-0.191
	Sig. (2-tailed)	0.002	0.004		Sig. (2-tailed)	0.863	0.758
	N	5	5		N	5	5
Kd Na	Pearson Correlation	0.933	0.93	Kd Chlorophenol linear	Pearson Correlation	0.336	0.34
	Sig. (2-tailed)	0.021	0.022		Sig. (2-tailed)	0.58	0.575
	N	5	5		N	5	5
Kd Na Linear	Pearson Correlation	-0.73	-0.813	Log kd chlorophenol	Pearson Correlation	0.166	0.247
	Sig. (2-tailed)	0.161	0.094		Sig. (2-tailed)	0.79	0.689
	N	5	5		N	5	5
Kd NH4	Pearson Correlation	-0.453	-0.372	Kd Total	Pearson Correlation	-0.012	-0.168
	Sig. (2-tailed)	0.444	0.538		Sig. (2-tailed)	0.985	0.787
	N	5	5		N	5	5
Kd NH4 linear	Pearson Correlation	0.997	0.97	Kd Total Linear	Pearson Correlation	0.865	0.766
	Sig. (2-tailed)	0	0.006		Sig. (2-tailed)	0.058	0.131
	N	5	5		N	5	5
Kd Cl linear	Pearson Correlation	0.254	0.366				
	Sig. (2-tailed)	0.68	0.545				
	N	5	5				

Correlation is significant at the 0.05 level (2-tailed).  
 Correlation is significant at the 0.01 level (2-tailed).



Appendix D.5: Table of sorption coefficients ( $K_d$ ), retardation factors (R), and transient times for individual pollutant species and geologic barrier samples. Calculated according to equation 7.1 and 7.12.

CALCIUM		n	$v_s$ (m/s)	$\rho_s$ (g/cm <sup>3</sup> )	$\rho_l$ (g/cm <sup>3</sup> )	$K_d$ (L/kg)	R	t (days/cm)
M 6	Lower Rötttone	0.34	1.413E-07	2.66	1.76	-3.18	-15.42	-12.6
L 6	Lehrberg Layers	0.33	1.594E-07	2.79	1.87	-2.42	-12.71	-9.2
L 11	Lehrberg Layers	0.325	1.417E-07	2.78	1.88	-3.16	-17.25	-14.1
B 6	Feuerletten	0.31	1.391E-07	2.53	1.75	-4.93	-26.76	-22.3
K 9	Amaltheen Clay	0.21	1.545E-07	2.67	2.11	-3.67	-35.86	-26.9

COPPER		n	$v_s$ (m/s)	$\rho_s$ (g/cm <sup>3</sup> )	$\rho_l$ (g/cm <sup>3</sup> )	$K_d$ (L/kg)	R	t (days/cm)
M 6	Lower Rötttone	0.34	1.413E-07	2.66	1.76	9.70E+07	5.01E+08	4.1E+08
L 6	Lehrberg Layers	0.33	1.594E-07	2.79	1.87	9.10E+07	5.15E+08	3.7E+08
L 11	Lehrberg Layers	0.325	1.417E-07	2.78	1.88	9.90E+07	5.72E+08	4.7E+08
B 6	Feuerletten	0.31	1.391E-07	2.53	1.75	1E+48	5.63E+48	4.7E+48
K 9	Amaltheen Clay	0.21	1.545E-07	2.67	2.11	1.00E+08	1.00E+09	7.5E+08

POTASSIUM		n	$v_s$ (m/s)	$\rho_s$ (g/cm <sup>3</sup> )	$\rho_l$ (g/cm <sup>3</sup> )	$K_d$ (L/kg)	R	t (days/cm)
M 6	Lower Rötttone	0.34	1.413E-07	2.66	1.76	0.04	1.21	1.0
L 6	Lehrberg Layers	0.33	1.594E-07	2.79	1.87	0.03	1.17	0.8
L 11	Lehrberg Layers	0.325	1.417E-07	2.78	1.88	38.02	220.52	180.1
B 6	Feuerletten	0.31	1.391E-07	2.53	1.75	0.97	6.46	5.4
K 9	Amaltheen Clay	0.21	1.545E-07	2.67	2.11	-0.88	-7.84	-5.9

SODIUM		n	$v_s$ (m/s)	$\rho_s$ (g/cm <sup>3</sup> )	$\rho_a$ (g/cm <sup>3</sup> )	$K_d$ (L/kg)	R	t (days/cm)
M 6	Lower Röttone	0.34	1.413E-07	2.66	1.76	0.69	4.56	3.7
L 6	Lehrberg Layers	0.33	1.594E-07	2.79	1.87	1.01	6.72	4.9
L 11	Lehrberg Layers	0.325	1.417E-07	2.78	1.88	0.79	5.56	4.5
B 6	Feuerletten	0.31	1.391E-07	2.53	1.75	2.13	12.99	10.8
K 9	Amaltheen Clay	0.21	1.545E-07	2.67	2.11	0.5	6.02	4.5
AMMONIUM		n	$v_s$ (m/s)	$\rho_s$ (g/cm <sup>3</sup> )	$\rho_a$ (g/cm <sup>3</sup> )	$K_d$ (L/kg)	R	t (days/cm)
M 6	Lower Röttone	0.34	1.413E-07	2.66	1.76	94.28	487.82	399.6
L 6	Lehrberg Layers	0.33	1.594E-07	2.79	1.87	0.05	1.28	0.9
L 11	Lehrberg Layers	0.325	1.417E-07	2.78	1.88	52.28	302.86	247.3
B 6	Feuerletten	0.31	1.391E-07	2.53	1.75	2.14	13.05	10.9
K 9	Amaltheen Clay	0.21	1.545E-07	2.67	2.11	211.14	2121.75	1589.2
CHLORIDE		n	$v_s$ (m/s)	$\rho_s$ (g/cm <sup>3</sup> )	$\rho_a$ (g/cm <sup>3</sup> )	$K_d$ (L/kg)	R	t (days/cm)
M 6	Lower Röttone	0.34	1.413E-07	2.66	1.76	0.06	1.31	1.1
L 6	Lehrberg Layers	0.33	1.594E-07	2.79	1.87	-0.07	0.60	0.4
L 11	Lehrberg Layers	0.325	1.417E-07	2.78	1.88	0.06	1.35	1.1
B 6	Feuerletten	0.31	1.391E-07	2.53	1.75	1.19	7.70	6.4
K 9	Amaltheen Clay	0.21	1.545E-07	2.67	2.11	1.29	13.96	10.5
SULFATE		n	$v_s$ (m/s)	$\rho_s$ (g/cm <sup>3</sup> )	$\rho_a$ (g/cm <sup>3</sup> )	$K_d$ (L/kg)	R	t (days/cm)
M 6	Lower Röttone	0.34	1.413E-07	2.66	1.76	-0.35	-0.81	-0.7
L 6	Lehrberg Layers	0.33	1.594E-07	2.79	1.87	0.02	1.11	0.8
L 11	Lehrberg Layers	0.325	1.417E-07	2.78	1.88	0.13	1.75	1.4
B 6	Feuerletten	0.31	1.391E-07	2.53	1.75	1.28	8.21	6.8
K 9	Amaltheen Clay	0.21	1.545E-07	2.67	2.11	-0.65	-5.53	-4.1
NITRATE		n	$v_s$ (m/s)	$\rho_s$ (g/cm <sup>3</sup> )	$\rho_a$ (g/cm <sup>3</sup> )	$K_d$ (L/kg)	R	t (days/cm)
M 6	Lower Röttone	0.34	1.413E-07	2.66	1.76	0.29	2.50	2.0
L 6	Lehrberg Layers	0.33	1.594E-07	2.79	1.87	1.05	6.95	5.0
L 11	Lehrberg Layers	0.325	1.417E-07	2.78	1.88	1.25	8.22	6.7
B 6	Feuerletten	0.31	1.391E-07	2.53	1.75	0	1.00	0.8
K 9	Amaltheen Clay	0.21	1.545E-07	2.67	2.11	1.44	15.46	11.6
2-CHLOROPHENOL		n	$v_s$ (m/s)	$\rho_s$ (g/cm <sup>3</sup> )	$\rho_a$ (g/cm <sup>3</sup> )	$K_d$ (L/kg)	R	t (days/cm)
M 6	Lower Röttone	0.34	1.413E-07	2.66	1.76	14115.62	72887.42	59705.4
L 6	Lehrberg Layers	0.33	1.594E-07	2.79	1.87	918.33	5202.92	3777.8
L 11	Lehrberg Layers	0.325	1.417E-07	2.78	1.88	0.37	3.14	2.6
B 6	Feuerletten	0.31	1.391E-07	2.53	1.75	619.01	3486.83	2900.7
K 9	Amaltheen Clay	0.21	1.545E-07	2.67	2.11	77.27	777.12	582.1
TOTAL		n	$v_s$ (m/s)	$\rho_s$ (g/cm <sup>3</sup> )	$\rho_a$ (g/cm <sup>3</sup> )	$K_d$ (L/kg)	R	t (days/cm)
M 6	Lower Röttone	0.34	1.413E-07	2.66	1.76	0.99	6.11	5.0
L 6	Lehrberg Layers	0.33	1.594E-07	2.79	1.87	0.08	1.45	1.1
L 11	Lehrberg Layers	0.325	1.417E-07	2.78	1.88	4.57	27.39	22.4
B 6	Feuerletten	0.31	1.391E-07	2.53	1.75	0.87	5.90	4.9
K 9	Amaltheen Clay	0.21	1.545E-07	2.67	2.11	-0.01	0.90	0.7



Appendix E

Appendix E.1 - Overview of grain size nomenclature as given by POPPE *et al.* (2003). Reproduced from USGS Open File Report 03-001.

Φ	PHI - mm CONVERSION $\phi = \log_2 (d \text{ in mm})$ $1 \mu\text{m} = 0.001 \text{mm}$		SIZE TERMS (after Wentworth, 1922)	SIEVE SIZES		Intermediate diameters of natural grains equivalent to sieve size	Number of grains per mg		Settling Velocity (Quartz, 20°C)		Threshold Velocity for traction cm/sec		
	mm	Fractional mm and Decimal inches		ASTM No. (U.S. Standard)	Tyler Mesh No.		Quartz spheres	Natural sand	Spheres (Gibbs, 1971) cm/sec	Crushed	(Nevin, 1946)	(modified from Hjeltrom, 1939)	
-8	256	10.1"	BOULDERS ( $> -8\phi$ )  COBBLES										
-7	128	5.04"											
-6	64.0	2.52"	PEBBLES	2 1/2"									
	53.9			2.12"	2"								
	45.3			1 1/2"	1 1/2"								
	33.1			1 1/4"	1.06"								
	26.9			3/4"	.742"								
	22.6			5/8"	.525"								
	17.0			1/2"	.371"								
	16.0			3/8"	3								
	13.4		Granules	5/16"									
	11.3			4	4								
	9.52		SAND	5	5								
	8.00			6	6								
	6.73			7	7								
	5.66			8	8								
	4.76			10	9								
	4.00			12	10								
	3.36			14	12								
	2.83			16	14								
	2.38			18	16	1.2	.72	.6					
	2.00			20	20	.86	2.0	1.5					
	1.63		25	24									
	1.41		30	28									
	1.19		35	32	.59	5.6	4.5						
	1.00		40	35									
	.840		45	42	.42	15	13						
	.707		50	48									
	.545		60	60	.30	43	35						
	.420		70	65									
	.354		80	80	.215	120	91						
	.297		100	100									
	.250		120	115	.155	350	240						
	.210		140	150									
	.177		170	170	.115	1000	580						
	.149		200	200									
	.125		230	250	.080	2900	1700						
	.105		270	270									
	.088		325	325									
	.074		400	400									
	.062												
	.053												
	.044												
	.037												
	.031												
	.02												
	.016												
	.01												
	.008												
	.005												
	.004												
	.003												
	.002												
	.001												
	.001												

Note: Some sieve openings differ slightly from phi mm scale

Note: Sieve openings differ by as much as 2% from phi mm scale

Note: Applies to subangular to subrounded quartz sand (in mm)

Note: Applies to subangular to subrounded quartz sand

Stokes Law ( $R = 6\pi\eta\gamma V$ )

Note: The relation between the beginning of traction transport and the velocity depends on the height above the bottom that the velocity is measured, and on other factors.

Appendix E.2 - Tabulated and graphical results of grain size analysis. Samples used in Diffusion research indicated

Feuerletten		%			
Phi	mm	B 0.0	B 1.7	B 6.0	B 10.0
Gravel fine	-3	8	0.4	0.0	0.0
Gravel very fine	-2	4	1.9	0.0	0.0
Sand very coarse	-1	2	3.8	0.0	1.3
Sand coarse	0	1	5.3	0.6	0.5
Sand medium	1	0.5	3.6	0.5	1.1
Sand fine	2	0.25	13.3	0.8	6.2
Sand very fine	3	0.125	12.9	2.7	9.2
Silt coarse	4	0.062	8.9	10.3	3.2
Silt medium	5	0.031	8.9	4.7	5.0
Silt fine	6	0.016	6.0	4.7	9.1
Silt very fine	7	0.008	9.5	7.0	8.9
Clay	8	0.004	25.5	68.7	55.5

Amaltheen Clay		%				
Phi	mm	K 7.2	K 7.5	K 2.0	K 3.0	K 9.0
Gravel fine	-3	8	0.0	0.0	0.0	0.0
Gravel very fine	-2	4	0.0	0.3	0.0	0.0
Sand very coarse	-1	2	0.6	0.5	0.2	2.0
Sand coarse	0	1	1.7	1.2	0.2	1.4
Sand medium	1	0.5	0.5	0.9	0.9	1.7
Sand fine	2	0.25	0.5	1.0	0.6	2.2
Sand very fine	3	0.125	2.0	2.4	1.5	2.6
Silt coarse	4	0.062	21.2	13.7	1.5	17.0
Silt medium	5	0.031	6.6	33.9	10.9	10.7
Silt fine	6	0.016	13.0	20.6	21.9	27.6
Silt very fine	7	0.008	16.4	22.5	4.6	17.9
Clay	8	0.004	37.5	3.0	57.7	16.9

Statistical Analysis	B 0.0	B 1.7	B 6.0	B 10.0
Mode	9.00	9.00	9.00	8.93
Mean	5.09	7.86	7.16	6.30
Sorting (Std)	3.11	1.92	2.49	1.98
Skewness	-0.85	-2.34	-1.81	-1.11
Kurtosis	2.11	6.25	4.23	3.48

Statistical Analysis	K 7.2	K 7.5	K 2.0	K 3.0	K 9.0
Mode	9.00	5.50	9.00	6.50	9.00
Mean	6.86	5.90	7.71	6.18	6.49
Sorting (Std)	2.14	1.55	1.73	2.10	2.36
Skewness	-1.64	-2.26	-2.27	-1.76	-1.52
Kurtosis	4.25	8.54	6.87	5.18	3.75

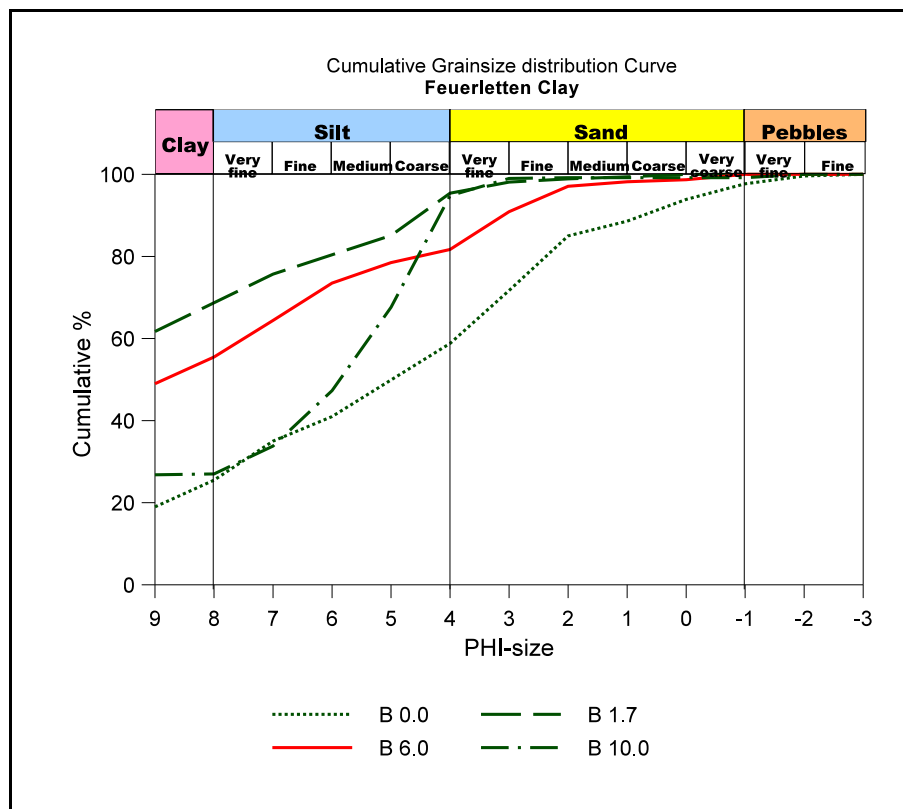
Lehrberg Layers		%				
Phi	mm	L 12.0	L 11.0	L 0.0	L 3.0	L 6.0
Gravel fine	-3	8	0.0	0.0	0.0	0.0
Gravel very fine	-2	4	0.0	0.4	0.0	0.0
Sand very coarse	-1	2	0.4	3.2	0.1	0.6
Sand coarse	0	1	4.5	3.6	1.1	2.1
Sand medium	1	0.5	5.1	1.6	1.7	0.8
Sand fine	2	0.25	7.7	1.2	10.4	1.7
Sand very fine	3	0.125	6.5	3.5	12.1	3.2
Silt coarse	4	0.062	18.7	5.3	6.8	9.6
Silt medium	5	0.031	9.9	21.2	8.6	11.3
Silt fine	6	0.016	3.7	26.5	12.6	22.5
Silt very fine	7	0.008	10.0	14.1	11.8	1.6
Clay	8	0.004	33.5	19.4	34.8	46.6

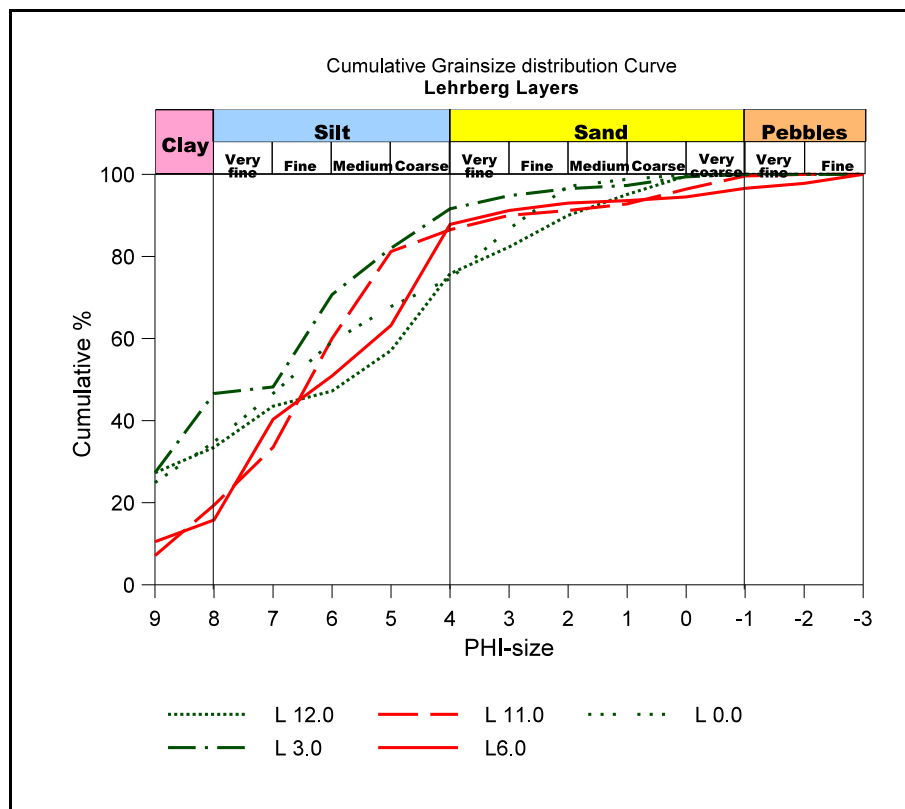
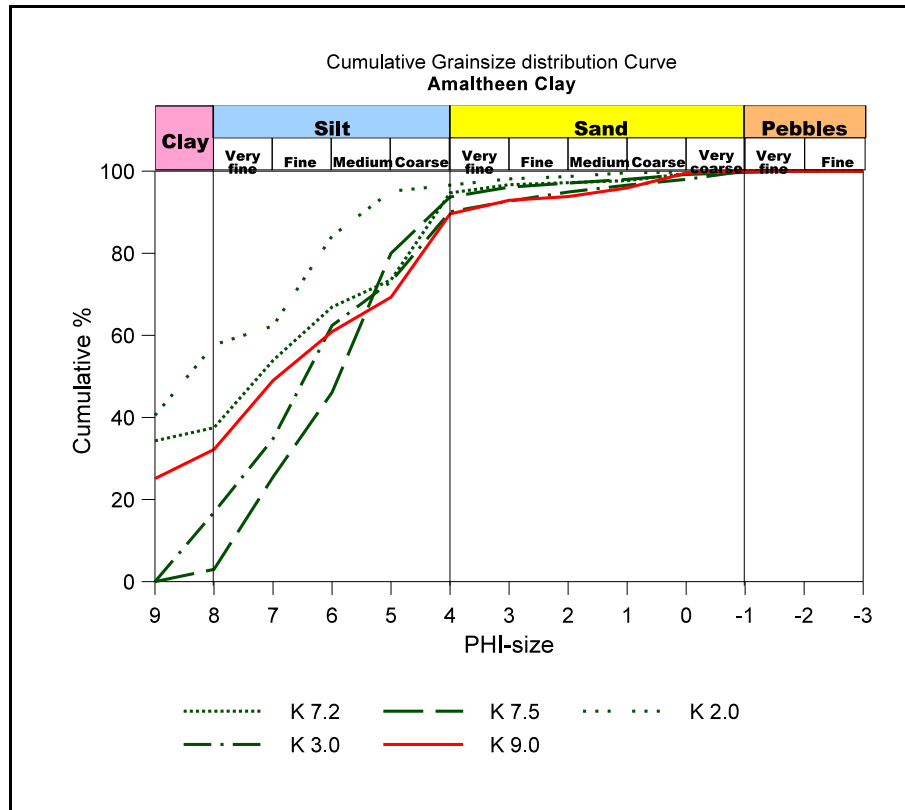
Lower Röttone		%		
Phi	mm	M 2.4	M 6.0	M 11.0
Gravel fine	-3	8	0.0	0.0
Gravel very fine	-2	4	0.0	0.0
Sand very coarse	-1	2	0.0	0.0
Sand coarse	0	1	0.0	0.2
Sand medium	1	0.5	0.4	0.1
Sand fine	2	0.25	3.2	0.6
Sand very fine	3	0.125	9.5	3.3
Silt coarse	4	0.062	9.6	6.0
Silt medium	5	0.031	3.9	7.2
Silt fine	6	0.016	13.4	10.8
Silt very fine	7	0.008	2.0	14.3
Clay	8	0.004	58.0	57.5

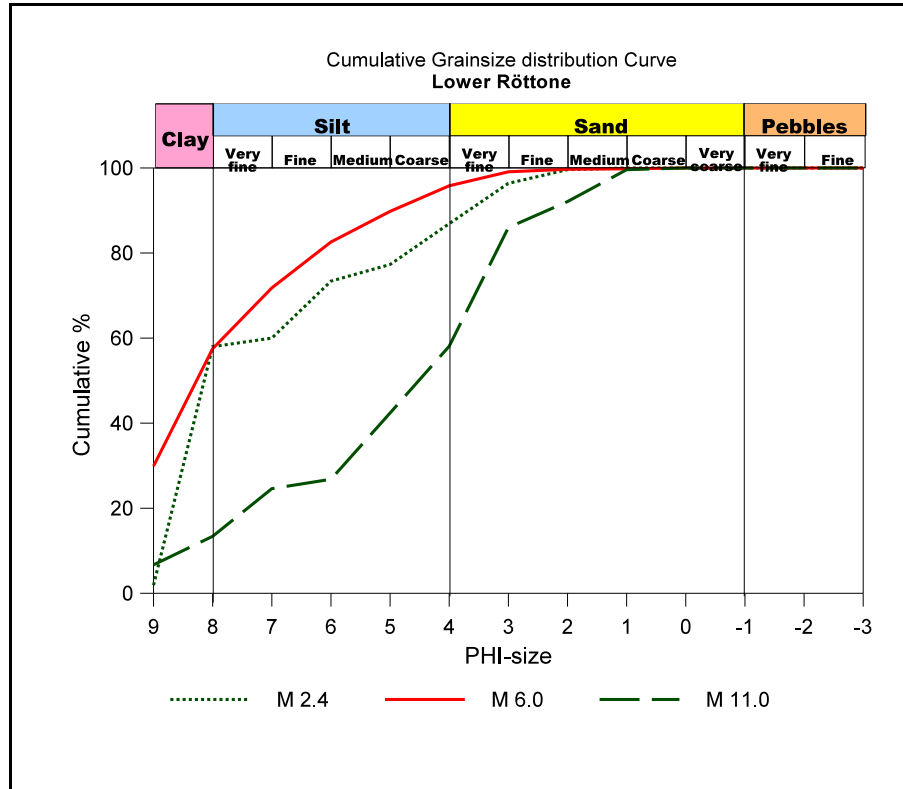
Statistical Analysis	L 12.0	L 11.0	L 0.0	L 3.0	L 6.0
Mode	9.00	6.59	9.00	9.00	7.47
Mean	5.91	6.10	6.33	7.00	5.83
Sorting (Std)	2.76	2.38	2.50	2.23	2.56
Skewness	-1.01	-1.88	-1.16	-1.75	-1.88
Kurtosis	2.16	5.33	2.32	4.62	5.86

Statistical Analysis	M 2.4	M 6.0	M 11.0
Mode	9.00	9.00	4.32
Mean	7.31	7.75	5.00
Sorting (Std)	2.21	1.73	2.23
Skewness	-1.61	-2.18	-0.44
Kurtosis	3.24	5.57	1.74

in red.







Appendix E.3 - Results of water absorption, moisture content, grain density. B = Feuerletten, K = Amaltheen Clay, L = Lehrberg Layers, M = Lower Röttone. Samples used in Diffusion research indicated in red.

Sample	Water Absorption $w_b$ (%)	Moisture content $w$ (%) <sub>105°C</sub>	Grain Density $\rho_s$ (g/cm <sup>3</sup> )
B 0.0	63.4		2.67
B2.7	52.0	23.1	2.55
B2.8	52.0	23.3	
B3.0	49.7	20.5	
<b>B6.0</b>	<b>50.2</b>	<b>20.0</b>	<b>2.53</b>
B8.5	50.7	18.7	
B10.0	42.4	14.4	2.55
Avg:	51.5	20.0	2.58
K2.0	49.7		2.69
K2.8	49.5	14.4	2.63
K3.5	44.7	7.9	2.65
K4.3	49.0	25.2	2.68
K5.2	50.7		
K6.2	48.7		
K7.7	43.7	10.7	2.68
<b>K9.0</b>	<b>48.3</b>	<b>17.4</b>	<b>2.67</b>
Avg:	48.0	15.1	2.67
L3.0	42.5	18.5	2.79
<b>L6.0</b>	<b>47.5</b>	<b>8.4</b>	<b>2.79</b>
<b>L11.0</b>	<b>42.6</b>	<b>13.9</b>	<b>2.78</b>
L12.0	68.0	16.2	2.75
Avg:	50.2	14.3	2.78
M3.3	53.5	20.8	2.63
M4.6	46.2	12.3	
M4.8	39.2	13.5	
<b>M6.0</b>	<b>48.5</b>	<b>16.6</b>	<b>2.66</b>
M8.5	34.2	18.1	
M10.0	38.5		
M11.0	40.5		2.67
Avg:	42.9	16.3	2.65

Appendix E.4 - Hydraulic Data for B = Feuerletten, K = Amaltheen Clay, L = Lehrberg Layers, M = Lower Rötton samples showing hydraulic conductivity ( $k_f$ ), gradient, discharge velocity ( $v_f$ ), effective porosity ( $n_e$ ), and seepage velocity ( $v_s$ ); after PÖTZL (1998). Data applied to diffusion research marked in red.

Feuerletten	$k_f$ (m/s)	gradient	$v_f$ (m/s)	$n_e$ (%)	$v_s$ (m/s)	$v_a$ (m/s)
B1.7	5.8E-10	20	1.2E-08	8	1.4E-07	1.6E-07
B2.3	2.8E-09	20	5.6E-08	29	1.9E-07	2.7E-07
B2.7	1.2E-09	20	2.4E-08	13	1.8E-07	1.8E-07
B3.0	2.1E-10	88	1.8E-08	13	1.4E-07	
<b>B6.0</b>	<b>3.4E-10</b>	<b>69</b>	<b>2.3E-08</b>	<b>20</b>	<b>1.2E-07</b>	
B7.0	2.4E-10	70	1.7E-08	12	1.4E-07	1.3E-07
B8.5	1.6E-09	20	3.2E-08	18	1.8E-07	2.0E-07
Average:	1.0E-09	44	2.6E-08	16	1.6E-07	1.9E-07
Amaltheen	$k_f$ (m/s)	gradient	$v_f$ (m/s)	$n_e$ (%)	$v_s$ (m/s)	$v_a$ (m/s)
K1.0	1.0E-09	88	8.8E-08	26	3.4E-07	2.5E-07
K2.5	4.4E-10	52	2.3E-08	16	1.4E-07	1.5E-07
K2.8	1.7E-09	60	1.0E-07	23	4.4E-07	5.0E-07
K3.0	2.0E-09	140	2.8E-07	9	3.2E-06	
K3.6	3.1E-11	600	1.9E-08	13	1.4E-07	
K4.0	4.5E-10	140	6.3E-08	29	2.2E-07	3.0E-07
K7.2	2.6E-10	80	2.1E-08	15	1.4E-07	9.4E-08
K7.7	1.9E-10	40	7.6E-09	5	1.5E-07	
<b>K9.0</b>	<b>2.6E-10</b>	<b>80</b>	<b>2.1E-08</b>	<b>31</b>	<b>6.7E-08</b>	
Average:	7.0E-10	142	6.9E-08	19	5.4E-07	2.6E-07
Lehrberg	$k_f$ (m/s)	gradient	$v_f$ (m/s)	$n_e$ (%)	$v_s$ (m/s)	$v_a$ (m/s)
L3.0	5.8E-10	20	1.2E-08	8	1.4E-07	1.6E-07
L5.2	1.4E-09	20	2.8E-08	20	1.4E-07	
<b>L6.0</b>	<b>4.1E-09</b>	<b>20</b>	<b>8.2E-08</b>	<b>27</b>	<b>3.1E-07</b>	
L7.5	6.7E-09	20	1.3E-07	19	7.2E-07	
L7.6	7.6E-10	20	1.5E-08	11	1.4E-07	
<b>L11.0</b>	<b>2.8E-09</b>	<b>20</b>	<b>5.6E-08</b>	<b>29</b>	<b>1.9E-07</b>	2.7E-07
Average:	2.7E-09	20	5.4E-08	19	2.8E-07	2.2E-07
Lower Röt.	$k_f$ (m/s)	gradient	$v_f$ (m/s)	$n_e$ (%)	$v_s$ (m/s)	$v_a$ (m/s)
M3.3	9.9E-12	620	6.1E-09	4	1.5E-07	
M4.7	2.4E-10	60	1.4E-08	10	1.4E-07	8.6E-08
M4.8	2.1E-10	70	1.5E-08	10	1.5E-07	1.9E-07
M5.8	2.1E-10	166	3.5E-08	24	1.5E-07	5.7E-08
M5.9	1.0E-10	58	5.8E-09	4	1.5E-07	
<b>M6.0</b>	<b>3.3E-10</b>	<b>131</b>	<b>4.3E-08</b>	<b>31</b>	<b>1.4E-07</b>	
M6.1	3.7E-10	66	2.4E-08	18	1.4E-07	8.8E-08
M6.2	4.0E-10	160	6.4E-08	53	1.2E-07	1.3E-07
Average:	2.3E-10	166	2.6E-08	19	1.4E-07	1.1E-07

Appendix E.5 - Equations for calculating hydraulic conductivity from permanent and falling head experimental set up as seen in figure 5.7.

Hydraulic conductivity calculated according to permanent head experiment:

$k_f$  = hydraulic conductivity in m/s,  $Q$  = discharge volume in  $m^3$ ,  $l$  = length or height of sample in m,  $A_s$  = cross-sectional area of sample in  $m^2$ ,  $h$  = height of water column in m.

$$k_f = \frac{Q * l}{t * A_s * h}$$

Hydraulic conductivity calculated according to falling head experiment:

$k_f$  = hydraulic conductivity in m/s,  $Q$  = discharge volume in  $m^3$ ,  $l$  = length or height of sample in m,  $A_s$  = cross-sectional area of sample in  $m^2$ ,  $A_c$  = cross-sectional area of water column above sample in  $m^2$ ,  $h$  = height of water column in m,  $r_s$  = cross-sectional radius of sample in m.

$$k_f = \frac{A_c * l}{t * A_s} * \ln \frac{h}{h - (\frac{Q}{\pi * r_s^2})}$$

## Appendix F

Appendix F.1 - Results of chemical characteristic computations using SRC (2000) software developed by the U.S. EPA. The SRC (2000) package is a collection of individually developed software programs tied together to give a summarized results page for a variety of chemical parameters of various contaminants and their modeled environmental interactions. The table below shows the individual programs and their computational purpose.

Software in SRC (2000) package	Computational Purpose as quoted in SRC (2000) help files.	Reference
EPI Suite v. 3.10	Input Interface using SMILES notation or CAS number	
AOPWIN v. 1.9	Atmospheric Oxidation Program - estimates the rate constant for the atmospheric, gas-phase reaction between photochemically produced hydroxyl radicals and organic chemicals.	MEYLAN and HOWARD (1993)
BCFWIN v. 2.14	Estimates the bioconcentration factor (BCF) of an organic compound using the compound's log octanol-water partition coefficient ( $K_{ow}$ ).	MEYLAN <i>et al.</i> (1997)
BIOWIN v. 4.0	Biodegradation Probability Program estimates the probability for the rapid aerobic biodegradation of an organic chemical in the presence of mixed populations of environmental microorganisms.	HOWARD <i>et al.</i> (1992)
ECOSAR v. 0.99g	Structure-activity relationships (SARs) program - predicts the aquatic toxicity of chemicals based on their similarity of structure to chemicals for which the aquatic toxicity has been previously measured, using predominantly $K_{ow}$ based calculations.	ECOSAR Program Risk Assessment Division (7403) U.S. Environmental Protection Agency 401 M St., SW Washington, DC 20460
HENRYWIN v. 3.10	Estimates the Henry's Law Constant at 25°C	MEYLAN and HOWARD (1991)
HYDROWIN v. 1.67	Aqueous Hydrolysis Rate Program - estimates aqueous hydrolysis rate constants for the following chemical classes: esters, carbamates, epoxides, halomethanes and selected alkyl halides.	MILL <i>et al.</i> (1987)
KOWWIN v. 1.66	Log Octanol-Water Partition Coefficient Program estimates the logarithmic octanol-water partition coefficient ( $\log P$ ) of organic compounds and, to an extent, inorganic compounds.	MEYLAN and HOWARD (1995)
MPBPWIN v. 1.40	Estimates the boiling point (at 760 mm Hg), melting point and vapor pressure of compounds from chemical structures.	STEIN and BROWN (1994); JOBACK (1982)
PCKOCWIN v. 1.66	Soil Adsorption Coefficient Program estimates the soil adsorption coefficient ( $K_{oc}$ ) of compounds.	LYMAN (1990)
WSKOWWIN v. 1.40	Estimates the water solubility ( $W_{sol}$ ) of a compound using the compounds log octanol-water partition coefficient ( $K_{ow}$ ).	MEYLAN and HOWARD (1994a, 1994b)

Computational results for individual contaminants in artificial leachate:

SMILES : NH(H)(H)(H)Cl  
 CHEM : Ammonium chloride  
 MOL FOR: CL1 K1  
 MOL WT : 53.49  
 ----- EPI SUMMARY (v3.10) -----  
 Log Octanol-Water Partition Coef (SRC):  
 Log Kow (KOWWIN v1.66 estimate) = -4.37  
 Boiling Pt, Melting Pt, Vapor Pressure Estimations (MPBPWIN v1.40):  
 Boiling Pt (deg C): 619.08 (Adapted Stein & Brown method)  
 Melting Pt (deg C): 268.22 (Mean or Weighted MP)  
 VP (mm Hg, 25 deg C): 2.37E-012 (Modified Grain method)  
 MP (exp database): 5.38 (deg C)  
 BP (exp database): 520 (deg C)  
 Water Solubility Estimate from Log Kow (WSKOW v1.40):  
 Water Solubility at 25 deg C (mg/L): 1e+006  
 non-melting pt equation used  
 Water Sol (Exper. database match) = 3.72e+005 mg/L (20 deg C)  
 Exper. Ref: DEANJA (1983)  
 ECOSAR Class Program (ECOSAR v0.99g):  
 Classes found:  
 Neutral Organics  
 Henrys Law Constant (25 deg C) [HENRYWIN v3.10]:  
 Bond Method: Incomplete  
 Group Method: Incomplete  
 Henrys LC [VP:WSol estimate using EPI values]: 1.668E-019 atm-m3/mole  
 Henrys LC [VP:WSol estimate using EPI values]: 1.668E-019 atm-m3/mole  
 Probability of Rapid Biodegradation (BIOWIN v4.00):  
 Linear Model : 0.7221  
 Non-Linear Model : 0.9046  
 Expert Survey Biodegradation Results:  
 Ultimate Survey Model : 3.0810 (weeks)  
 Primary Survey Model : 3.7706 (days)  
 Readily Biodegradable Probability (MITT Model):  
 Linear Model : 0.5437  
 Non-Linear Model : 0.7749  
 Atmospheric Oxidation (25 deg C) [AopWin v1.90]:  
 Hydroxyl Radicals Reaction:  
 OVERALL OH Rate Constant = 0.0000 E-12 cm3/molecule-sec  
 Half-Life (hr) : -----  
 Ozone Reaction:  
 No Ozone Reaction Estimation  
 Soil Adsorption Coefficient (PCKOCWIN v1.66):  
 Koc : 14.3  
 Log Koc: 1.155  
 Aqueous Base/Acid-Catalyzed Hydrolysis (25 deg C) [HYDROWIN v1.67]:  
 Rate constants can NOT be estimated for this structure:  
 BCF Estimate from Log Kow (BCFWIN v2.14):  
 Log BCF = 0.500 (BCF = 3.162)  
 log Kow used: -4.37 (estimated)  
 Volatilization from Water:  
 Henry LC: 3.88E-013 atm-m3/mole (estimated by Bond SAR Method)  
 Half-Life from Model River: 1.304E+007 days  
 Half-Life from Model Lake: 1.204E+010 hours (5.016E+006 days)  
 Removal In Wastewater Treatment:  
 Total removal: 1.85 percent  
 Total biodegradation: 0.09 percent  
 Total sludge adsorption: 1.75 percent  
 Total to Air: 0.00 percent  
 Level III Fugacity Model:  
 Mass Amount Half-Life Emissions  
 (percent) (hr) (kg/yr)  
 Air 1.51e-008 1e+005 1000  
 Water 45.2 360 1000  
 Soil 54.7 360 1000  
 Sediment 0.0755 1.44e+003 0  
 Persistence Time: 420 hr

SMILES : KCl  
 CHEM : Potassium Chloride  
 MOL FOR: CL1 K1  
 MOL WT : 74.55  
 ----- EPI SUMMARY (v3.10) -----  
 Log Octanol-Water Partition Coef (SRC):  
 Log Kow (KOWWIN v1.66 estimate) = -0.46  
 Boiling Pt, Melting Pt, Vapor Pressure Estimations (MPBPWIN v1.40):  
 Boiling Pt (deg C): 695.74 (Adapted Stein & Brown method)  
 Melting Pt (deg C): 304.03 (Mean or Weighted MP)  
 VP (mm Hg, 25 deg C): 1.65E-016 (Modified Grain method)  
 Water Solubility Estimate from Log Kow (WSKOW v1.40):  
 Water Solubility at 25 deg C (mg/L): 3.50E+005  
 non-melting pt equation used  
 ECOSAR Class Program (ECOSAR v0.99g):  
 Classes found:  
 Neutral Organics  
 Henrys Law Constant (25 deg C) [HENRYWIN v3.10]:  
 Bond Method: Incomplete  
 Group Method: Incomplete  
 Henrys LC [VP:WSol estimate using EPI values]: 4.896E-023 atm-m3/mole  
 Henrys LC [VP:WSol estimate using EPI values]: 4.896E-023 atm-m3/mole  
 Probability of Rapid Biodegradation (BIOWIN v4.00):  
 Linear Model : 0.7121  
 Non-Linear Model : 0.8755  
 Expert Survey Biodegradation Results:  
 Ultimate Survey Model : 3.7402 (days/weeks)  
 Primary Survey Model : 3.7402 (days/weeks)  
 Readily Biodegradable Probability (MITT Model):  
 Linear Model : 0.4902  
 Non-Linear Model : 0.5923  
 Atmospheric Oxidation (25 deg C) [AopWin v1.90]:  
 Hydroxyl Radicals Reaction:  
 OVERALL OH Rate Constant = 0.0000 E-12 cm3/molecule-sec  
 Half-Life (hr) : -----  
 Ozone Reaction:  
 No Ozone Reaction Estimation  
 Soil Adsorption Coefficient (PCKOCWIN v1.66):  
 Koc : 14.3  
 Log Koc: 1.155  
 Aqueous Base/Acid-Catalyzed Hydrolysis (25 deg C) [HYDROWIN v1.67]:  
 Rate constants can NOT be estimated for this structure:  
 BCF Estimate from Log Kow (BCFWIN v2.14):  
 Log BCF = 0.500 (BCF = 3.162)  
 log Kow used: -0.54 (estimated)  
 Volatilization from Water:  
 Henry LC: 4.9E-023 atm-m3/mole (calculated from VP/WS)  
 Half-Life from Model River: 1.033E+019 hours (4.302E+017 days)  
 Half-Life from Model Lake: 1.126E+020 hours (4.694E+018 days)  
 Removal In Wastewater Treatment:  
 Total removal: 1.85 percent  
 Total biodegradation: 0.09 percent  
 Total sludge adsorption: 1.76 percent  
 Total to Air: 0.00 percent  
 Level III Fugacity Model:  
 Mass Amount Half-Life Emissions  
 (percent) (hr) (kg/yr)  
 Air 1.51e-008 1e+005 1000  
 Water 45.2 360 1000  
 Soil 54.7 360 1000  
 Sediment 0.0755 1.44e+003 0  
 Persistence Time: 421 hr

SMILES : [Na]Cl  
 CHEM : Sodium Chloride  
 MOL FOR: CL1 Na1  
 MOL WT : 58.44  
 ----- EPI SUMMARY (v3.10) -----  
 Log Octanol-Water Partition Coef (SRC):  
 Log Kow (KOWWIN v1.66 estimate) = -0.46  
 Boiling Pt, Melting Pt, Vapor Pressure Estimations (MPBPWIN v1.40):  
 Boiling Pt (deg C): 605.5 (Adapted Stein & Brown method)  
 Melting Pt (deg C): 304.03 (Mean or Weighted MP)  
 VP (mm Hg, 25 deg C): 1.56E-023 (Modified Grain method)  
 MP (exp database): 804 (deg C)  
 Water Solubility Estimate from Log Kow (WSKOW v1.40):  
 Water Solubility at 25 deg C (mg/L): 3.59E+005  
 non-melting pt equation used  
 Water Sol (Exper. database match) = 3.57E+005 mg/L (25 deg C)  
 Exper. Ref: MERCK INDEX (1989)  
 ECOSAR Class Program (ECOSAR v0.99g):  
 Classes found:  
 Neutral Organics  
 Henrys Law Constant (25 deg C) [HENRYWIN v3.10]:  
 Bond Method: Incomplete  
 Group Method: Incomplete  
 Henrys LC [VP:WSol estimate using EPI values]: 3.533E-030 atm-m3/mole  
 Henrys LC [VP:WSol estimate using EPI values]: 3.533E-030 atm-m3/mole  
 Probability of Rapid Biodegradation (BIOWIN v4.00):  
 Linear Model : 0.7197  
 Non-Linear Model : 0.8983  
 Expert Survey Biodegradation Results:  
 Ultimate Survey Model : 3.0700 (weeks)  
 Primary Survey Model : 3.7634 (days)  
 Readily Biodegradable Probability (MITT Model):  
 Linear Model : 0.6681  
 Non-Linear Model : 0.6981  
 Atmospheric Oxidation (25 deg C) [AopWin v1.90]:  
 Hydroxyl Radicals Reaction:  
 OVERALL OH Rate Constant = 0.0000 E-12 cm3/molecule-sec  
 Half-Life (hr) : -----  
 Ozone Reaction:  
 No Ozone Reaction Estimation  
 Soil Adsorption Coefficient (PCKOCWIN v1.66):  
 Koc : 14.3  
 Log Koc: 1.155  
 Aqueous Base/Acid-Catalyzed Hydrolysis (25 deg C) [HYDROWIN v1.67]:  
 Rate constants can NOT be estimated for this structure:  
 BCF Estimate from Log Kow (BCFWIN v2.14):  
 Log BCF = 0.500 (BCF = 3.162)  
 log Kow used: 0.54 (estimated)  
 Volatilization from Water:  
 Henry LC: 3.53E-030 atm-m3/mole (calculated from VP/WS)  
 Half-Life from Model River: 1.267E+026 hours (5.278E+024 days)  
 Half-Life from Model Lake: 1.382E+027 hours (5.758E+025 days)  
 Removal In Wastewater Treatment:  
 Total removal: 1.85 percent  
 Total biodegradation: 0.09 percent  
 Total sludge adsorption: 1.76 percent  
 Total to Air: 0.00 percent  
 Level III Fugacity Model:  
 Mass Amount Half-Life Emissions  
 (percent) (hr) (kg/yr)  
 Air 1.51e-008 1e+005 1000  
 Water 45.2 360 1000  
 Soil 54.7 360 1000  
 Sediment 0.0755 1.44e+003 0  
 Persistence Time: 421 hr



SMILES : [Na]O[ONa](=O)=O  
 CHEM : Sodium nitrate  
 CAS NUM: 00763-1-99-4  
 MOL WT : 69.00 g/mol  
 MOL WT : 84.99

----- EPI SUMMARY (v3.10) -----

Log Octanol-Water Partition Coef (SRC):  
 Log Kow (KOWWIN v1.66 estimate) = -0.79

Boiling Pt, Melting Pt, Vapor Pressure Estimations (MPBPWIN v1.40):  
 Boiling Pt (deg C): 723.11 (Adapted Grain Method)  
 Melting Pt (deg C): 321.02 (Mean or Weighted MP)  
 VP (mm Hg,25 deg C): 1.6E-017 (Modified Grain method)  
 MP (exp database): 306.8 deg C

Water Solubility Estimate from Log Kow (WSKOW v1.40):  
 Water Solubility at 25 deg C (mg/L): 6.055E+005  
 log Kow used: 0.05 (estimated)  
 no-melting pt equation used

ECOSAR Class Program (ECOSAR v0.99g):  
 Class(es) found:  
 Neutral Organics

Henrys Law Constant (25 deg C) [HENRYWIN v3.10]:  
 Bond Method : Incomplete  
 Group Method : Incomplete  
 Henrys LC [VP/W/Sol estimate using EPI values]: 2.955E-024 atm-m3/mole

Probability of Rapid Biodegradation (BIOWIN v4.00):  
 Linear Model : 0.7071  
 Non-Linear Model : 0.8584  
 Expert Survey Biodegradation Results:  
 Ultimate Survey Model : 3.0113 (weeks)  
 Primary Survey Model : 3.7251 (days-weeks)  
 Readily Biodegradable Probability (MITI Model):  
 Linear Model : 0.4593  
 Non-Linear Model : 0.5180

Atmospheric Oxidation (25 deg C) [AopWin v1.90]:  
 Hydroxyl Radicals Reaction:  
 OVERALL OH Rate Constant = 0.3600E-12 cm3/molecule-sec  
 Half-Life = 29.711 Days (12-hr day; 1.5E6 OH/cm3)  
 Ozone Reaction:  
 No Ozone Reaction Estimation

Soil Adsorption Coefficient (PCKOCWIN v1.66):  
 Koc : 4.3  
 Log Koc: 1.155

Aqueous Base/Acid-Catalyzed Hydrolysis (25 deg C) [HYDROWIN v1.67]:  
 Rate constants can NOT be estimated for this structure!

BCF Estimate from Log Kow (BCFWIN v2.14):  
 Log BCF = 0.500 (BCF = 3.162)  
 log Kow used: 0.21 (estimated)

Volatilization from Water:  
 Henry LC: 2.96E-024 atm-m3/mole (calculated from VP/WS)  
 Half-Life from Model River: 1.827E+020 hours (7.611E+018 days)  
 Half-Life from Model Lake: 1.993E+021 hours (8.303E+019 days)

Removal In Wastewater Treatment:  
 Total removal: 0.05 percent  
 Total biodegradation: 0.09 percent  
 Total sludge adsorption: 1.76 percent  
 Total to Air: 0.00 percent

Level III Fugacity Model:		
Mass Amount (kg)	Half-Life (hr)	Emissions (kg/yr)
Air	717	1000
Water	360	1000
Soil	360	1000
Sediment	1.44E+003	0
Persistence Time: 421 hr		

SMILES : [Na]O[S(O)(=O)](=O)=O  
 CHEM : Disodium sulfate  
 CAS NUM: 00775-7-82-6  
 MOL WT : 142.04 g/mol  
 MOL WT : 142.04

----- EPI SUMMARY (v3.10) -----

Log Octanol-Water Partition Coef (SRC):  
 Log Kow (KOWWIN v1.66 estimate) = -4.38

Boiling Pt, Melting Pt, Vapor Pressure Estimations (MPBPWIN v1.40):  
 Boiling Pt (deg C): 346.06 (Adapted Grain Method)  
 Melting Pt (deg C): 346.06 (Adapted Grain Method)  
 VP (mm Hg,25 deg C): 1.75E-019 (Modified Grain method)

Water Solubility Estimate from Log Kow (WSKOW v1.40):  
 Water Solubility at 25 deg C (mg/L): 1E+006  
 log Kow used: -4.38 (estimated)  
 no-melting pt equation used

ECOSAR Class Program (ECOSAR v0.99g):  
 Class(es) found:  
 Neutral Organics

Henrys Law Constant (25 deg C) [HENRYWIN v3.10]:  
 Bond Method : Incomplete  
 Group Method : Incomplete  
 Henrys LC [VP/W/Sol estimate using EPI values]: 3.271E-026 atm-m3/mole

Probability of Rapid Biodegradation (BIOWIN v4.00):  
 Linear Model : 0.6799  
 Non-Linear Model : 0.7294  
 Expert Survey Biodegradation Results:  
 Ultimate Survey Model : 2.8853 (weeks)  
 Primary Survey Model : 3.6428 (days-weeks)  
 Readily Biodegradable Probability (MITI Model):  
 Linear Model : 0.1749  
 Non-Linear Model : 0.1715

Atmospheric Oxidation (25 deg C) [AopWin v1.90]:  
 Hydroxyl Radicals Reaction:  
 OVERALL OH Rate Constant = 0.0000E-12 cm3/molecule-sec  
 Half-Life = -----  
 Ozone Reaction:  
 No Ozone Reaction Estimation

Soil Adsorption Coefficient (PCKOCWIN v1.66):  
 Koc : 6.124  
 Log Koc: 0.787

Aqueous Base/Acid-Catalyzed Hydrolysis (25 deg C) [HYDROWIN v1.67]:  
 Rate constants can NOT be estimated for this structure!

BCF Estimate from Log Kow (BCFWIN v2.14):  
 Log BCF = 0.500 (BCF = 3.162)  
 log Kow used: -2.20 (estimated)

Volatilization from Water:  
 Henry LC: 2.56E-011 atm-m3/mole (estimated by Bond SAR Method)  
 Half-Life from Model River: 2.726E+007 hours (1.136E+006 days)  
 Half-Life from Model Lake: 2.973E+008 hours (1.239E+007 days)

Removal In Wastewater Treatment:  
 Total removal: 1.85 percent  
 Total biodegradation: 0.09 percent  
 Total sludge adsorption: 1.75 percent  
 Total to Air: 0.00 percent

Level III Fugacity Model:		
Mass Amount (kg)	Half-Life (hr)	Emissions (kg/yr)
Air	213	1000
Water	46	1000
Soil	51.7	1000
Sediment	0.0767	0
Persistence Time: 391 hr		

SMILES : Cl[Ca]Cl  
 CHEM : Calcium chloride (CaCl2)  
 CAS NUM: 010043-52-4  
 MOL WT : 110.98 g/mol  
 MOL WT : 110.98

----- EPI SUMMARY (v3.10) -----

Log Octanol-Water Partition Coef (SRC):  
 Log Kow (KOWWIN v1.66 estimate) = 0.05

Boiling Pt, Melting Pt, Vapor Pressure Estimations (MPBPWIN v1.40):  
 Boiling Pt (deg C): 1935.22 (Adapted Grain Method)  
 Melting Pt (deg C): 205.22 (Adapted Grain Method)  
 VP (mm Hg,25 deg C): 4.42E-010 (Modified Grain method)

Water Solubility Estimate from Log Kow (WSKOW v1.40):  
 Water Solubility at 25 deg C (mg/L): 9.797E+004  
 log Kow used: 0.05 (estimated)  
 no-melting pt equation used

ECOSAR Class Program (ECOSAR v0.99g):  
 Class(es) found:  
 Neutral Organics

Henrys Law Constant (25 deg C) [HENRYWIN v3.10]:  
 Bond Method : Incomplete  
 Group Method : Incomplete  
 Henrys LC [VP/W/Sol estimate using EPI values]: 6.588E-016 atm-m3/mole

Probability of Rapid Biodegradation (BIOWIN v4.00):  
 Linear Model : 0.6947  
 Non-Linear Model : 0.8073  
 Expert Survey Biodegradation Results:  
 Ultimate Survey Model : 2.9539 (weeks)  
 Primary Survey Model : 3.6876 (days-weeks)  
 Readily Biodegradable Probability (MITI Model):  
 Linear Model : 0.1749  
 Non-Linear Model : 0.3366

Atmospheric Oxidation (25 deg C) [AopWin v1.90]:  
 Hydroxyl Radicals Reaction:  
 OVERALL OH Rate Constant = 0.0000E-12 cm3/molecule-sec  
 Half-Life = -----  
 Ozone Reaction:  
 No Ozone Reaction Estimation

Soil Adsorption Coefficient (PCKOCWIN v1.66):  
 Koc : 23.74  
 Log Koc: 1.376

Aqueous Base/Acid-Catalyzed Hydrolysis (25 deg C) [HYDROWIN v1.67]:  
 Rate constants can NOT be estimated for this structure!

BCF Estimate from Log Kow (BCFWIN v2.14):  
 Log BCF = 0.500 (BCF = 3.162)  
 log Kow used: 0.05 (estimated)

Volatilization from Water:  
 Henry LC: 6.59E-016 atm-m3/mole (calculated from VP/WS)  
 Half-Life from Model River: 9.302E+011 hours (3.901E+010 days)  
 Half-Life from Model Lake: 1.021E+013 hours (4.256E+011 days)

Removal In Wastewater Treatment:  
 Total removal: 1.85 percent  
 Total biodegradation: 0.09 percent  
 Total sludge adsorption: 1.76 percent  
 Total to Air: 0.00 percent

Level III Fugacity Model:		
Mass Amount (kg)	Half-Life (hr)	Emissions (kg/yr)
Air	738E+007	1000
Water	44.9	1000
Soil	55.1	1000
Sediment	0.0755	0
Persistence Time: 421 hr		

----- EPI SUMMARY (v3.10) -----

<p>SMILES : O=C(O)=O[Cu](ON)(=O)=O            CHEM : NITRIC ACID, COPPER (2+) SALT            CAS NUM: 003251-23-8            ORG : 06            MOL WT : 187.56</p> <p>----- EPI SUMMARY (v3.10) -----            Physical Property Inputs:</p> <p>Log Octanol-Water Partition Coef (SRC):            Log Kow (KOWWIN v1.66 estimate) = -0.61            Exper. Ref: Hansch et al. (1995)</p> <p>Boiling Pt, Melting Pt, Vapor Pressure Estimations (MPBPWIN v1.40):            Boiling Pt (deg C): 283.88 (Adapted Stein &amp; Brown method)            Melting Pt (deg C): 283.88 (Open VP or assigned MP)            VP (mm Hg, 25 deg C): 4.75E-013 (Modified Grain method)            VP (mm Hg, 25 deg C): 4.75E-013 (Modified Grain method)</p> <p>Water Solubility Estimate from Log Kow (WSKOW v1.40):            log Kow used: -0.61 (estimated)            no-melting pt equation used</p> <p>ECOSAR Class Program (ECOSAR v0.99g):            Classes found:            Neutral Organics</p> <p>Henrys Law Constant (25 deg C) [HENRYWIN v3.10]:            Group Method: Incomplete</p> <p>Henrys LC [VPW] Soil estimate using EPI values]: 6.974E-019 atm-m<sup>3</sup>/mole</p> <p>Probability of Rapid Biodegradation (BIOWIN v4.00):            Linear Model : 0.6583            Non-Linear Model : 0.5853</p> <p>Expert Survey Biodegradation Results:            Ultimate Survey Model : 2.7847 (weeks )            Primary Survey Model : 3.5771 (days-weeks )            Readily Biodegradable Probability (MITI Model):            Linear Model : 0.1142            Non-Linear Model : 0.0327</p> <p>Atmospheric Oxidation (25 deg C) [AopWin v1.90]:            Hydroxyl Radicals Reaction:            OVERALL OH Rate Constant = 0.7200 E-12 cm<sup>3</sup>/molecule-sec            Half-Life = 14.856 Days (12-hr day; 1.5E6 OH/cm<sup>3</sup>)</p> <p>Ozone Reaction:            No Ozone Reaction Estimation</p> <p>Soil Adsorption Coefficient (PCKOCWIN v1.66):            Koc : 23.74            Log Koc : 1.376</p> <p>Aqueous Base/Acid-Catalyzed Hydrolysis (25 deg C) [HYDROWIN v1.67]:            Rate constants can NOT be estimated for this structure!</p> <p>BCE Estimate from Log Kow (BCEWIN v2.14):            Log BCE = 0.500 (BCE = 3.16)            log Kow used: -0.61 (estimated)</p> <p>Volatilization from Water:            Henry LC: 6.97E-019 atm-m<sup>3</sup>/mole (calculated from VP/WS)            Half-Life from Model River: 1.15E+015 hours (4.791E+013 days)            Half-Life from Model Lake: 1.254E+016 hours (5.226E+014 days)</p> <p>Removal In Wastewater Treatment:            Total removal: 1.85 percent            Total biodegradation: 0.09 percent            Total sludge adsorption: 1.76 percent            Total to Air: 0.00 percent</p> <p>Level III Fugacity Model:            Mass Amount Half-Life Emissions            (kg/m<sup>3</sup>) (days) (kg/m<sup>3</sup>/day)            Air 2.33E+007 357 1000            Water 45.2 360 1000            Soil 54.7 360 1000            Sediment 0.0755 1.44E+003 0            Persistence Time: 42.1 hr</p>	<p>SMILES : Oc(ccc)Clc1ccccc1            CHEM : 1,2-DICHLOROETHANE            CAS NUM: 000095-57-6            ORG : 06            MOL FOR: C6 H15 Cl1 O1            MOL WT : 128.56</p> <p>----- EPI SUMMARY (v3.10) -----            Physical Property Inputs:</p> <p>Log Octanol-Water Partition Coef (SRC):            Log Kow (KOWWIN v1.66 estimate) = 2.16            Exper. Ref: Hansch et al. (1995)</p> <p>Boiling Pt, Melting Pt, Vapor Pressure Estimations (MPBPWIN v1.40):            Boiling Pt (deg C): 203.06 (Adapted Stein &amp; Brown method)            Melting Pt (deg C): 8.99 (Open VP or assigned MP)            VP (mm Hg, 25 deg C): 0.716 (Open VP or Antoine &amp; Grain methods)            MP (exp database): 9.8 deg C            BP (exp database): 174.9 deg C            VP (exp database): 2.53E+00 mm Hg at 25 deg C</p> <p>Water Solubility Estimate from Log Kow (WSKOW v1.40):            Water Solubility at 25 deg C (mg/L): 5165            log Kow used: 2.15 (expkow database)            no-melting pt equation used</p> <p>ECOSAR Class Program (ECOSAR v0.99g):            Classes found:            Phenols</p> <p>Henrys Law Constant (25 deg C) [HENRYWIN v3.10]:            Bond Method: 4.15E-007 atm-m<sup>3</sup>/mole            Group Method: 5.60E-007 atm-m<sup>3</sup>/mole            Exper. Ref: BANERJEE, S ET AL. (1980)</p> <p>Henrys LC [VPW] Soil estimate using EPI values]: 2.345E-005 atm-m<sup>3</sup>/mole</p> <p>Probability of Rapid Biodegradation (BIOWIN v4.00):            Linear Model : 0.6197            Non-Linear Model : 0.5191</p> <p>Expert Survey Biodegradation Results:            Ultimate Survey Model : 2.7649 (weeks )            Primary Survey Model : 3.5366 (days-weeks )            Readily Biodegradable Probability (MITI Model):            Linear Model : 0.3327            Non-Linear Model : 0.3927</p> <p>Atmospheric Oxidation (25 deg C) [AopWin v1.90]:            Hydroxyl Radicals Reaction:            OVERALL OH Rate Constant = 9.8706 E-12 cm<sup>3</sup>/molecule-sec            Half-Life = 1.084 Days (12-hr day; 1.5E6 OH/cm<sup>3</sup>)</p> <p>Ozone Reaction:            No Ozone Reaction Estimation</p> <p>Reaction With Nitrate Radicals May Be Important:            Soil Adsorption Coefficient (PCKOCWIN v1.66):            Koc : 443.1            Log Koc : 2.646</p> <p>Aqueous Base/Acid-Catalyzed Hydrolysis (25 deg C) [HYDROWIN v1.67]:            Rate constants can NOT be estimated for this structure!</p> <p>BCE Estimate from Log Kow (BCEWIN v2.14):            Log BCE = 0.956 (BCE = 9.026)            log Kow used: 2.15 (expkow database)</p> <p>Volatilization from Water:            Henry LC: 1.12E-005 atm-m<sup>3</sup>/mole (Henry experimental database)            Half-Life from Model River: 60.43 hours (2.518 days)            Half-Life from Model Lake : 754.3 hours (31.43 days)</p> <p>Removal In Wastewater Treatment:            Total removal: 3.02 percent            Total biodegradation: 0.10 percent            Total sludge adsorption: 2.30 percent            Total to Air: 0.62 percent</p> <p>Level III Fugacity Model:            Mass Amount Half-Life Emissions            (kg/m<sup>3</sup>) (days) (kg/m<sup>3</sup>/day)            Air 41.5 360 1000            Water 55 360 1000            Soil 1.14E+003 1.44E+003 0            Sediment 0.145 1.44E+003 0            Persistence Time: 287 hr</p>
---	--

Appendix F.2 - Summary of results of activity coefficient calculations for SLL at varying temperatures using PHREEQC<sub>i</sub> (2002).

### Input data

SOLUTION 30  
 temp 30  
 pH 6.16  
 pe 4  
 redox pe  
 units mmol/kgw  
 density 1  
 Na 4327.35208750987 mg/kgw  
 K 629.36623968882 mg/kgw  
 Ca 409.018545983971 mg/kgw  
 N(-3) 709.738198386615 mg/kgw  
 Cu(2) 10.5180229757978 mg/kgw  
 Cl 7052.21189869296 mg/kgw  
 S(6) 2502.25377577142 mg/kgw  
 N(5) 823.221880317739 mg/kgw  
 water 1 # kg

-----  
Initial solution calculations  
-----

Initial solution 30.

## -----Solution composition-----

Elements	Molality	Moles
Ca	1.021e-002	1.021e-002
Cl	1.989e-001	1.989e-001
Cu(2)	1.655e-004	1.655e-004
K	1.610e-002	1.610e-002
N(-3)	5.067e-002	5.067e-002
N(5)	5.877e-002	5.877e-002
Na	1.882e-001	1.882e-001
S(6)	2.605e-002	2.605e-002

## -----Description of solution-----

pH = 6.160  
 pe = 4.000  
 Activity of water = 0.991  
 Ionic strength = 3.075e-001  
 Mass of water (kg) = 1.000e+000  
 Total alkalinity (eq/kg) = 3.332e-004  
 Total carbon (mol/kg) = 0.000e+000  
 Total CO2 (mol/kg) = 0.000e+000  
 Temperature (deg C) = 30.000  
 Electrical balance (eq) = -3.438e-002  
 Percent error, 100\*(Cat-|An|)/(Cat+|An|) = -6.10  
 Iterations = 5  
 Total H = 1.112150e+002  
 Total O = 5.578683e+001

## -----Redox couples-----

Redox couple	pe	Eh (volts)
N(-3)/N(5)	5.8657	0.3528

## -----Distribution of species-----

Species	Molality	Activity	Log Molality	Log Activity	Log Gamma
OH-	2.140e-007	1.434e-007	-6.670	-6.843	-0.174
H+	1.282e-007	1.000e-007	-6.892	-7.000	-0.108
H2O	5.551e+001	9.908e-001	-0.004	-0.004	0.000
Ca	1.021e-002				
Ca+2	8.253e-003	2.352e-003	-2.083	-2.628	-0.545
CaSO4	1.952e-003	2.095e-003	-2.710	-2.679	0.031
CaOH+	5.289e-009	3.868e-009	-8.277	-8.412	-0.136
CaHSO4+	1.791e-009	1.310e-009	-8.747	-8.883	-0.136
Cl	1.989e-001				
Cl-	1.989e-001	1.347e-001	-0.701	-0.871	-0.169
Cu(2)	1.655e-004				
Cu+2	9.059e-005	2.589e-005	-4.043	-4.587	-0.544
Cu(OH)2	4.947e-005	5.310e-005	-4.306	-4.275	0.031
CuSO4	2.172e-005	2.331e-005	-4.663	-4.632	0.031
CuOH+	3.748e-006	2.565e-006	-5.426	-5.591	-0.165
Cu(OH)3-	4.335e-011	3.170e-011	-10.363	-10.499	-0.136
Cu(OH)4-2	2.191e-016	6.267e-017	-15.659	-16.203	-0.544
H(0)	1.256e-025				
H2	6.280e-026	6.741e-026	-25.202	-25.171	0.031
K	1.610e-002				
K+	1.562e-002	1.058e-002	-1.806	-1.975	-0.169
KSO4-	4.722e-004	3.453e-004	-3.326	-3.462	-0.136
KOH	3.387e-010	3.635e-010	-9.470	-9.439	0.031
N(-3)	5.067e-002				
NH4+	4.814e-002	3.068e-002	-1.318	-1.513	-0.196
NH4SO4-	2.304e-003	1.685e-003	-2.638	-2.773	-0.136
NH3	2.305e-004	2.474e-004	-3.637	-3.607	0.031
N(5)	5.877e-002				
NO3-	5.877e-002	3.847e-002	-1.231	-1.415	-0.184
Na	1.882e-001				
Na+	1.842e-001	1.330e-001	-0.735	-0.876	-0.142
NaSO4-	4.007e-003	2.930e-003	-2.397	-2.533	-0.136
NaOH	8.109e-009	8.704e-009	-8.091	-8.060	0.031
O(0)	0.000e+000				
O2	0.000e+000	0.000e+000	-40.489	-40.458	0.031
S(6)	2.605e-002				
SO4-2	1.729e-002	4.263e-003	-1.762	-2.370	-0.608
NaSO4-	4.007e-003	2.930e-003	-2.397	-2.533	-0.136
NH4SO4-	2.304e-003	1.685e-003	-2.638	-2.773	-0.136
CaSO4	1.952e-003	2.095e-003	-2.710	-2.679	0.031
KSO4-	4.722e-004	3.453e-004	-3.326	-3.462	-0.136
CuSO4	2.172e-005	2.331e-005	-4.663	-4.632	0.031
HSO4-	6.334e-008	4.632e-008	-7.198	-7.334	-0.136
CaHSO4+	1.791e-009	1.310e-009	-8.747	-8.883	-0.136

## -----Saturation indices-----

Phase	SI	log IAP	log KT	
Anhydrite	-0.61	-5.00	-4.39	CaSO4
Gypsum	-0.42	-5.01	-4.58	CaSO4:2H2O
H2(g)	-22.00	-22.00	0.00	H2
H2O(g)	-1.39	-0.00	1.38	H2O
Halite	-3.34	-1.75	1.59	NaCl
NH3(g)	-5.28	5.49	10.76	NH3
O2(g)	-37.48	43.99	81.47	O2

## Input data.

```

SOLUTION 10
temp 10
pH 6.16
pe 4
redox pe
units mmol/kgw
density 1
Na 4327.35208750987 mg/kgw
K 629.36623968882 mg/kgw
Ca 409.018545983971 mg/kgw
N(-3) 709.738198386615 mg/kgw
Cu(2) 10.5180229757978 mg/kgw
Cl 7052.21189869296 mg/kgw
S(6) 2502.25377577142 mg/kgw
N(5) 823.221880317739 mg/kgw
water 1 # kg

```

## -----Initial solution calculations.-----

## Initial solution 10.

## -----Solution composition-----

Elements	Molality	Moles
Ca	1.021e-002	1.021e-002
Cl	1.989e-001	1.989e-001
Cu(2)	1.655e-004	1.655e-004
K	1.610e-002	1.610e-002
N(-3)	5.067e-002	5.067e-002
N(5)	5.877e-002	5.877e-002
Na	1.882e-001	1.882e-001
S(6)	2.605e-002	2.605e-002

## -----Description of solution-----

```

pH = 6.160
pe = 4.000
Activity of water = 0.991
Ionic strength = 3.087e-001
Mass of water (kg) = 1.000e+000
Total alkalinity (eq/kg) = 1.595e-004
Total carbon (mol/kg) = 0.000e+000
Total CO2 (mol/kg) = 0.000e+000
Temperature (deg C) = 10.000
Electrical balance (eq) = -3.421e-002
Percent error, 100*(Cat-|An|)/(Cat+|An|) = -6.05
Iterations = 5
Total H = 1.112152e+002
Total O = 5.578683e+001

```

## -----Redox couples-----

Redox couple	pe	Eh (volts)
N(-3)/N(5)	7.0563	0.3964

## -----Distribution of species-----

Species	Molality	Activity	Molality	Log Activity	Log Gamma	Log
H+	1.274e-007	1.000e-007		-6.895	-7.000	-0.105
OH-	4.279e-008	2.898e-008		-7.369	-7.538	-0.169
H2O	5.551e+001	9.908e-001		-0.004	-0.004	0.000
Ca	1.021e-002					
Ca+2	8.404e-003	2.484e-003		-2.076	-2.605	-0.529
CaSO4	1.801e-003	1.933e-003		-2.745	-2.714	0.031
CaOH+	5.531e-009	4.085e-009		-8.257	-8.389	-0.132
CaHSO4+	1.309e-009	9.668e-010		-8.883	-9.015	-0.132
Cl	1.989e-001					
Cl-	1.989e-001	1.362e-001		-0.701	-0.866	-0.165
Cu(2)	1.655e-004					
Cu+2	9.026e-005	2.665e-005		-4.045	-4.574	-0.530
Cu(OH)2	5.090e-005	5.465e-005		-4.293	-4.262	0.031

	CuSO4	2.054e-005	2.205e-005	-4.687	-4.657	0.031
	CuOH+	3.819e-006	2.640e-006	-5.418	-5.578	-0.160
	Cu(OH)3-	4.418e-011	3.263e-011	-10.355	-10.486	-0.132
	Cu(OH)4-2	2.168e-016	6.451e-017	-15.664	-16.190	-0.526
H(0)		1.543e-025				
	H2	7.717e-026	8.285e-026	-25.113	-25.082	0.031
K		1.610e-002				
	K+	1.574e-002	1.078e-002	-1.803	-1.967	-0.165
	KSO4-	3.519e-004	2.599e-004	-3.454	-3.585	-0.132
	KOH	3.449e-010	3.703e-010	-9.462	-9.431	0.031
N(-3)		5.067e-002				
	NH4+	4.817e-002	3.108e-002	-1.317	-1.508	-0.190
	NH4SO4-	2.451e-003	1.810e-003	-2.611	-2.742	-0.132
	NH3	5.394e-005	5.791e-005	-4.268	-4.237	0.031
N(5)		5.877e-002				
	NO3-	5.877e-002	3.891e-002	-1.231	-1.410	-0.179
Na		1.882e-001				
	Na+	1.845e-001	1.345e-001	-0.734	-0.871	-0.137
	NaSO4-	3.734e-003	2.758e-003	-2.428	-2.559	-0.132
	NaOH	8.203e-009	8.807e-009	-8.086	-8.055	0.031
O(0)		0.000e+000				
	O2	0.000e+000	0.000e+000	-47.353	-47.322	0.031
S(6)		2.605e-002				
	SO4-2	1.769e-002	4.520e-003	-1.752	-2.345	-0.593
	NaSO4-	3.734e-003	2.758e-003	-2.428	-2.559	-0.132
	NH4SO4-	2.451e-003	1.810e-003	-2.611	-2.742	-0.132
	CaSO4	1.801e-003	1.933e-003	-2.745	-2.714	0.031
	KSO4-	3.519e-004	2.599e-004	-3.454	-3.585	-0.132
	CuSO4	2.054e-005	2.205e-005	-4.687	-4.657	0.031
	HSO4-	4.383e-008	3.237e-008	-7.358	-7.490	-0.132
	CaHSO4+	1.309e-009	9.668e-010	-8.883	-9.015	-0.132

## -----Saturation indices-----

Phase	SI	log IAP	log KT	
Anhydrite	-0.61	-4.95	-4.34	CaSO4
Gypsum	-0.37	-4.96	-4.59	CaSO4:2H2O
H2(g)	-22.00	-22.00	0.00	H2
H2O(g)	-1.92	-0.00	1.92	H2O
Halite	-3.28	-1.74	1.55	NaCl
NH3(g)	-6.32	5.49	11.82	NH3
O2(g)	-44.43	43.99	88.43	O2

## Appendix G

### Appendix G.1 - Diffusion Experiment Data with Lithium Bromide (LiBr)

Diffusion research was conducted in especially designed diffusion cells at fixed temperatures as in-diffusion or transient diffusion experiments. Leachate chambers were filled with 1L of LiBr solution (concentration strength 1000 mg/L). Collection chambers contained 1L of distilled water.

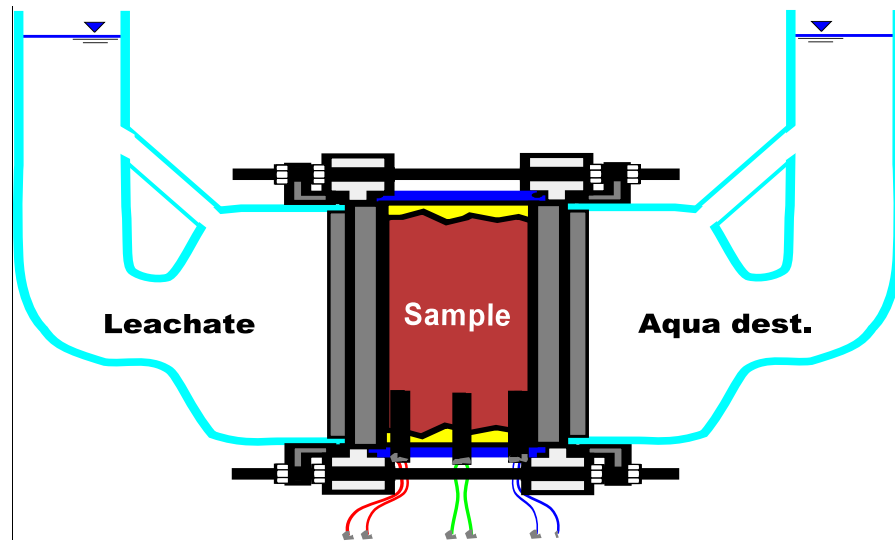
#### Conductivity measurements

Conductivity changes were approximated within the sample chamber using mounted gold electrodes with an electrode spacing of 0.54mm. Data for in-sample measurements was referenced to arbitrary 100  $\mu\text{S}/\text{cm}$  (*italics*) and should be considered qualitative in nature, because measurements could not be calibrated.

Conductivity was also evaluated in the leachate & collection chambers at time interval  $t$  using conventional instruments as well as gold electrodes. Conventional direct measurements were corrected to standard 25°C and are shown in **bold**. Conductivity data from intermediate electrode measurements is shown in regular print and was recalculated using a straight line correlation assumption.

#### Chemical concentrations

Samples (10mL) were taken from the leachate & collection chamber at time interval  $t$ . Collected samples were analyzed for Li and Br by UV/Vis spectrometer. Concentrations are recorded in mg/L.



Sample L 6.0  
LiBr 1000mg/L  
Temp.: 10°C

Time days	Li mg/L	Br mg/L	Distance from leachate source in cm					Li mg/L	Br mg/L
			0	0.2	0.9	2.4	2.7		
0	79.2	993.7	<b>1267</b>	100	100	100	<b>2.43</b>	0.02	<0.1
0.5	79.9	984.1	1152	97.87	98.21	97.06	2.91	0.02	0.26
1	78.2	963.7	1022	95.74	93.45	92.35	4.10	0.01	0.17
2	77.5	970.3	1008	98.94	95.24	92.35	4.97	<0.01	<0.1
4	77.5	965.9	1005	106.38	95.24	92.35	6.13	<0.01	<0.1
7	77.3	965.9	1094	111.70	98.21	92.35	9.10	<0.01	<0.1
28	75.1	965.6	1166	121.28	98.81	94.12	26.28	<0.01	1.04
47	72.9	962.4	1224	122.34	98.81	96.47	56.24	0.05	8.07
<b>62</b>			<b>1215</b>	<b>121.28</b>	<b>97.62</b>	<b>95.29</b>	<b>65.00</b>		

Sample L 11.5  
LiBr 1000mg/L

Time days	Li mg/L	Br mg/L	Distance from leachate source in cm					Li mg/L	Br mg/L
			0	1.3	2.4	3.3	4		
<b>0</b>			<b>1629</b>	<b>100</b>	<b>100</b>	<b>100</b>	<b>2.86</b>		
0.5	80.3	975.3	1601	96.10	96.82	98.11	7.16		
1	79.2	976.2	1494	91.56	93.63	94.34	7.16	0.02	<0.1
2	79.2	977.5	1455	92.21	92.99	94.34	7.96	<0.01	<0.1
4	77.2	990.3	1427	94.16	92.99	94.34	8.87	<0.01	<0.1
7	80.2	989.9	1382	96.10	95.54	94.34	10.56	<0.01	<0.1
28	79.2	976.8	1208	111.69	103.82	99.06	28.33	<0.01	3.6
47	77.8	984.2	1214	114.29	104.46	99.06	65.83	0.09	17.3
<b>62</b>			<b>1236</b>	<b>112.99</b>	<b>101.91</b>	<b>99.06</b>	<b>83.00</b>		

## Appendix G.2 - Diffusion Experiment Data with SLL

Diffusion research was conducted in especially designed diffusion cells at fixed temperatures as in-diffusion or transient diffusion experiments. Leachate chambers were filled with 1L of artificial leachate (concentration strength 16504 mg/L). Collection chambers contained 1L of distilled water.

### Conductivity measurements

Conductivity changes were approximated within the sample chamber using mounted gold electrodes with an electrode spacing of 0.54mm. Data for in-sample measurements was referenced to arbitrary 100  $\mu\text{S}/\text{cm}$  (*italics*) and should be considered qualitative in nature, because measurements could not be calibrated.

Conductivity was also evaluated in the leachate & collection chambers at time interval  $t$  using conventional instruments as well as gold electrodes. Conventional direct measurements were corrected to standard 25°C and are shown in **bold**. Conductivity data from intermediate electrode measurements is shown in regular print and was recalculated through curve fitting processes using nominal conductivity measurements as reference.

### Chemical concentrations

Samples (10mL) were taken from the leachate & collection chamber at time interval  $t$ . Collected samples were analyzed for

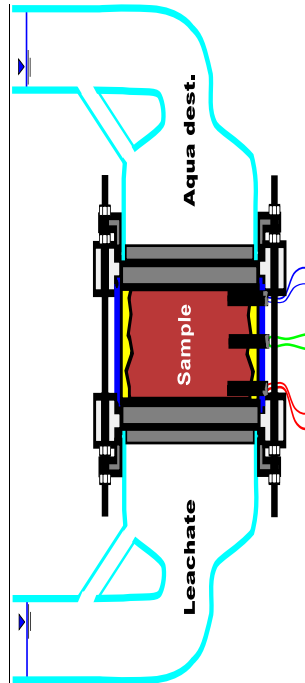
Cl, SO<sub>4</sub>, NO<sub>3</sub>, NH<sub>4</sub>, CPL (Chlorphenol) by UV/Vis spectrometer  
Anion concentration also occasional confirmed by HPLC  
Na, K, Ca by flame photometer  
Cu by AAS

Concentrations are recorded in mg/L.



Diffusion data:

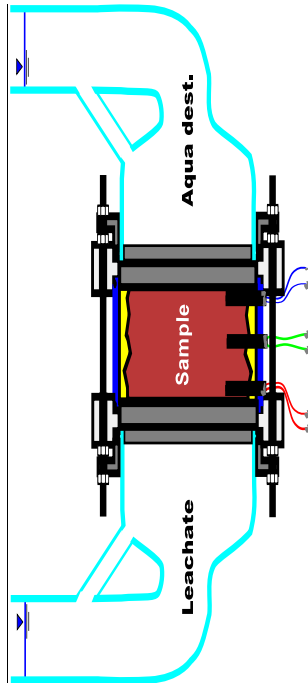
Sample Core K 9.0  
 Sampling depth: 9 m  
 Stratigraphic unit: Amaltheen Clay (J1δ)



C	m /	0.24	20.2	220.5
C	mg/L			
N	mg/L	0	< 1	3.3
	m /	0.9	69	66.4
K	mg/L	0.12	33	26.8
N	mg/L	0.35	62	85136
N	mg /	0	< 0.1	
SO	mg/L	<	.	
C	mg	0	< 0.1	
C	mg/cm	18	29.95	1356.00
C	mg/cm	2943	2436	667.11
C	μS	100		
C	mg/cm	1752	1122	7.35.79
D	cm	15	2340	2400
C	mg	327	27.26	32.8
C	mg/L	10	0.50	872.18
N	mg /	69	71	746
	mg/L	709	570	5657.861
K	mg/L			
N	mg /	482	3629	8383.830
N	mg/L			
SO	mg	2662		2250
	m /L			
Sample	Concentration	765	944	g/L

Diffusion data:

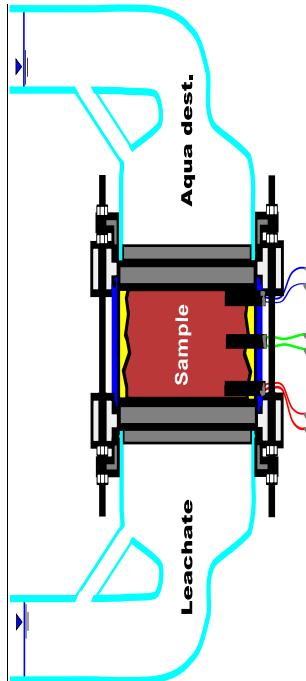
Sample Core B 6.0  
 Sampling depth: 6 m  
 Sample Core B 7.0  
 Sampling depth: 7 m  
 Stratigraphic unit: Feuerletten (Trkmf)



Parameter	Value	Parameter	Value
CPmg/L	0.17.37.482.4	C <sub>m</sub> /	0.36 0.762.3
Gmg/L	0.0.5 5 51.2	Gmg/L	<0.50.50.5 5
NC <sub>n</sub> /	2.4	NC <sub>n</sub> /L	0<0.40.<0.40.
mg/L	0 81.523 3 39	m /	3 341 019 2 51
Kmg/L	0:05	Kmg/L	0 19 008 6
N m /	0 06.20.935.8	Nmg/L	0 00 1 27.1
NC <sub>g</sub> /L	0.1	N <sub>n</sub> /	0<0.<0. 7
SO <sub>n</sub> /	0< 116.2	SO <sub>n</sub> /L	<08*031 0.1
Cmg/L	0<0.1	Cmg	0<0.40.1 91.6
C <sub>2</sub> 88/cm	7.05.30.90570.00	C <sub>2</sub> 88/cm	6 4.52.56185.00
C <sub>2</sub> 88/cm	129126135288.29	C <sub>2</sub> 88/cm	
Cl <sub>μ</sub> S	1002 2 5	Cl <sub>μ</sub> S	100
C <sub>2</sub> 88/cm	100122129.41.41	C <sub>2</sub> 88/cm	100159257588.24
C <sub>2</sub> 88/cm	22560.24304200	C <sub>2</sub> 88/cm	24500.25800200
Distance	22560.24304200 source in cm	Distance	24500.25800200 source in cm
CRmg	351.48.28.3025	CRmg	320.21.2675 12
Gmg/L	10.30.6999.5	Gmg/L	10 1 4 3.02
NC <sub>n</sub> /	62 68 679	NC <sub>n</sub> /	61962 66
mg/L	709665753609	mg/L	70942048626639
Kmg/L		Kmg/L	
N m /	48236307680896	N m /	48236307680896
NC <sub>g</sub> /L		NC <sub>g</sub> /L	
SO <sub>n</sub> /	2662 2392	SO <sub>n</sub> /	266232829
m /L		m /L	
Sample Concentration	16594mg/L	Sample Concentration	16594mg/L

Diffusion data:

Sample Core L 11.0  
 Sampling depth: 11 m  
 Stratigraphic unit: Lehrberg  
 Layers (Trkmg)

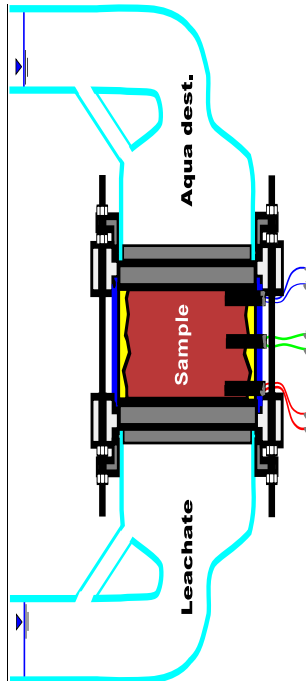


C m /	0.26	0.26	0.26	0.44	0.50	0.82	0.70	0.83	0.99	C m /	0.99	5.3
Crng/L	<0.5	<0.5	<0.5	<0.5	<0.5	<0.5	<0.5	<0.5	<0.5	Crng/L	<0.5	
Crng/L	0.5	0.1	0.1	0.1	0.1	0.1	0.1	0.1	0.3	Crng/L	0.3	0.3
m /	0.37	0.63	1.83	5.53	9.53	16.5				m /	16.5	12
Kmg/L	0.02	0.02	0.02	0.02	0.02	0.02	0.02	0.02	0.02	Kmg/L	0.02	0.02
Nmg/L	0.0	0.0	0.19	1.32						Nmg/L	0.19	1.32
N % /	<0.1	<0.1	0.28	5	1	9				N % /	5.92	14.2
SO4g/L	<0.5	<0.5	0.1	<0.1	<0.1	0.1				SO4g/L	<0.1	0.1
Cmg	<0.1	<0.1	2.9	17.3	36.2	60.3				Cmg	60.3	67.928
Co/cm	0.86	2.0	0.5	5.0	21.5	79.1	102.3	110.7	238.0	Co/cm	238.0	254.5
Co/cm	105.1	131.3	139.1	166.1	178.1	191.3	207.2	229.5	239.5	Co/cm	217.8	239.5
Cl μS	1001	1	1	1	1	1	1	1	2	Cl μS	2	2
Co/cm	100.1	55.6	178.9	183.9	197.2	226.6	253.3	301.0		Co/cm	20.1	20.1877
CpSi	25.4	29.0	20.8	22.3	23.0	23.5	24.0	23.2	23.0	CpSi	23.2	23.0
CRng	32.6	26.3	26.6	26.2	24.5	24.3	22.5	24.1		CRng	24.1	33.2
Gmg/L	10.3	69.7	109.0	99.8	88.9	79.8	88.8	55.6		Gmg/L	5.6	7.8
NC # /	67	5	8							NC # /		
mg/L	709	386	411	63	47	147	237	174	176	mg/L	560	406
Kmg/L										Kmg/L		
N m /	482	306	406	606	625	736	736	693	606	N m /	306	306
NGg/L										NGg/L		
SO4g	262	129	504	207	226	283	353	326	276	SO4g	276	226
m /L										m /L		
Sample ID	Sample ID 11006									Sample ID	Sample ID 11006	
Concentration	Concentration approx. 14750mg/L									Concentration	Concentration approx. 14750mg/L	

Diffusion data:

Sample Core L 6.0  
 Sampling depth: 6.0 m  
 Stratigraphic unit: Lehrberg  
 Layers (Trkmg)

Sample used in previous  
 LiBr diffusion experiments  
 (see Appendix E.1)

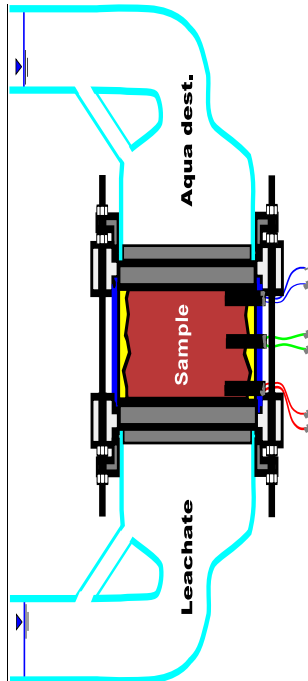


Parameter	Sample 1 (Left)	Sample 2 (Right)
C m /	0 30.32 45.47 60.60 861.1 213 2	C m / 20 236.5
Gmg/L	<0.5 <0.5 <0.5 <0.5 <0.5 <0.5	Gmg/L <.5 8
Nmg/L	0.0 <0.1 <0.1 0.9 0.40 40.6	Nmg/L 0.6 0.2 4
m /	0.82 11 2 25. 5 26 1 20 24 7 .	m / 4 . 4 . 80
Kmg/L	0 .10.0 10.22 30.60 2637.99 991.7	Kmg/L 1.7 260.2
Nmg/L	0 10.10 2 . 1.1. 3.1 8 15 . .	Nmg/L . . 128
N g /	0<0. <0.1 1 3 30 25.6	N g / 35.6 48 34.3
SO4mg/L	<081 <091 <0.1 <0.1 <0.1 . .	SO4mg/L . . 25 9
Cmg	0<0.1 1.4 13.4 25.6 71.33 56.3	Cmg 158.3 194382
Cp / cm	0.96 34.24 0.75 155.14 27639740 6592.00	Cp / cm 59 260732492.00
Cp / cm	95.89 26100 107 17 10 19 22 125 130 0.02	Cp / cm 100 135 100 69
Ω μS	9 10 10 1 1 1 1 1 1 1 1	Ω μS 1 1 1 1
Ω / cm	135.28 183.66 187.98 154.92 7.19 272.54 80	Ω / cm 380 325.58 71
Cp Dis	8570 500 24800 24300 24700 24300 23900	Cp Dis 899 29500 22800
CRmg	23 24.34 24.34 27.27 26.28 29.3	CRmg 29.3 26 23.2
Gmg/L	10 7.2 7.3 7.2 7.8 7.9 7.26 3.6 2.5 0.5 5	Gmg/L 5.5 5.3 2.3
NC 4 /	mg/L 409 683 732 275 87 107 327 159 72 86 360 650	mg/L 650 624 605
Kmg/L		Kmg/L
N m /	482 362 648 565 537 506 506 506 506 506	N m / 366 362 366
LiBr pres	LiBr pres from previous diffusion experiment	LiBr pres from earlier diffusion experiment
SO4mg	76 25 22 22 70 62 29 13 7 6 2 5 4 9 2 3 30	SO4mg 2532 233 360
m / l		m / l
Sample concentration	Sample concentration approx. 14982mg/L	



Diffusion data:

Sample Core M 6.0  
 Sampling depth: 6 m  
 Stratigraphic unit:  
 Lower Röttone (Tsu3T)



C m /	0.20	0.26	0.38	0.42	0.44	0.26	0.36	0.64	3
C mg/L	<0.5	<0.5	<0.5	<0.5	<0.5	<0.5	<0.5	<0.5	<0.5
N mg/L	0.5	<0.5	1.0	1.1	1.0	1.0	1.0	1.0	1.0
m /	0.33	1.72	33	95	5	91	48	8	7
K mg/L	0.06	0.22	1.0	1.0	1.0	1.0	1.0	1.0	1.0
N mg/L	0.1	1.3	4	1	24	1	115		
N g /	0	2	0.8	7.2	3.9	6.6	1	2.7	
SO mg/L	<0.1	<0.1					8.2	55.6	
C mg	0	0.1	3.3	10.5	19.1	36	57	70	43
Con cm	0.9	3.5	19	42	55	68	113	130	170
Cl gS	100	198	212	238	135	142	153	157	155
Con cm	100	100	100	100	100	100	100	100	100
C n Dis	2560	100	25700	26200	23200	23100	23100	22600	
CR mg	323.9	222	27.8	27	275	26	24	25	25.3
G mg/L	108	88	88	8	8	7	8	7	2
N g /	409	807	626	761	59	752	46	96	70
K mg/L	70	86	76	76	159	752	46	96	70
N m /	482	752	269	293	285	305	305	305	305
N g/L	26	36	23	28	51	23	23	25	24
SO mg	76	23	23	23	51	23	23	25	24
m /L									

C m /	1.3	1.23
C mg/L	<0.5	8
N mg/L	5.8	19.4
m /	7	100
K mg/L	5.8	21.2
N mg/L	115	1288
N g /	32.7	60.6
SO mg/L	55.6	142
C mg	321	338
Con cm	1.2	1.3
Con cm	188	248
Con cm	100	100
C n Dis	2560	20700
CR mg	25.3	23
G mg/L	5.8	5.2
N g /	418	589
K mg/L		
N m /	300	365
N g/L		
SO mg	20.95	20.25
m /L		

Sample M 6.0 Contention 115420/30 40 50 60 70 80 92 Sample M 6.0 Contention approx. 13722mg/L

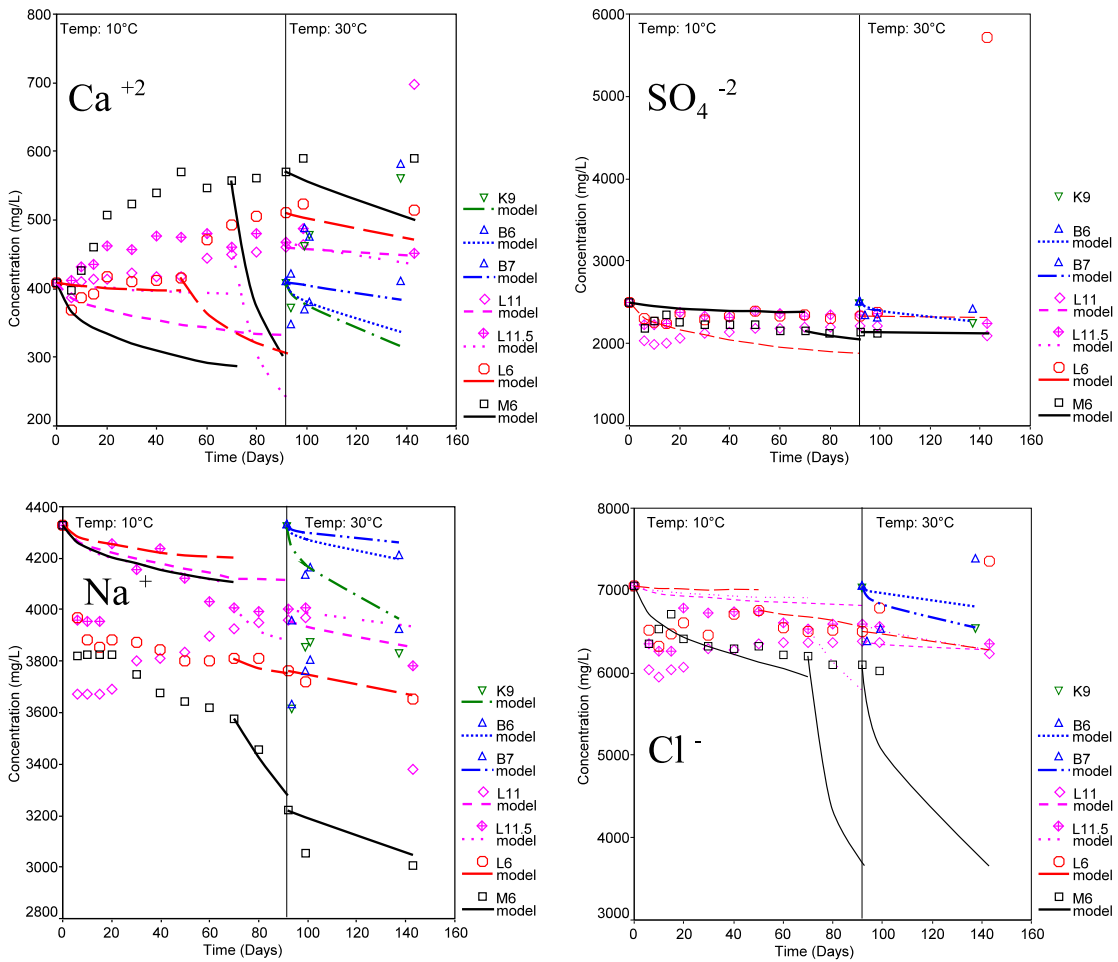
Appendix G.3 - Diffusion Coefficients calculated with Pollute6.3 according to receptor reservoir.

Totals in italics indicate weighted averages (according to source concentration) of diffusion coefficients for individual chemical species. F - Freundlich sorption exponent; L - Langmuir sorption max. sorption value

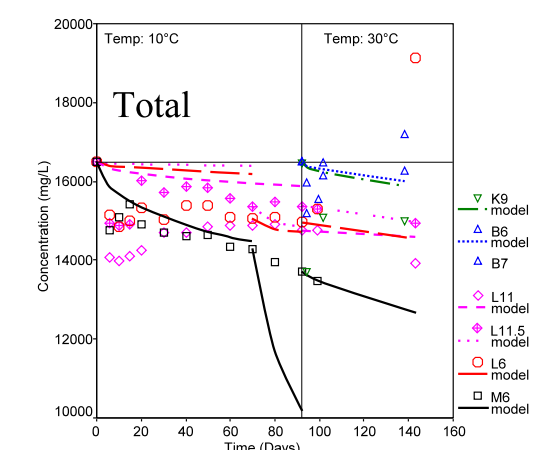
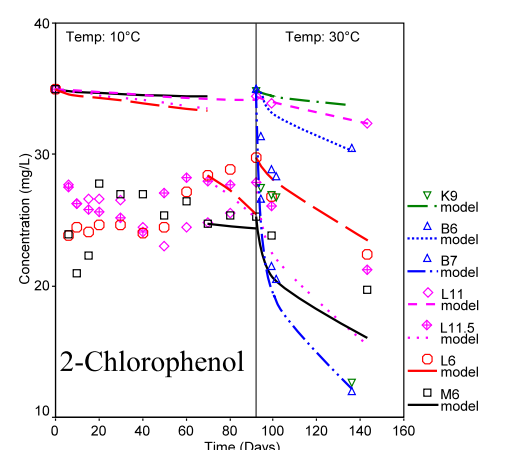
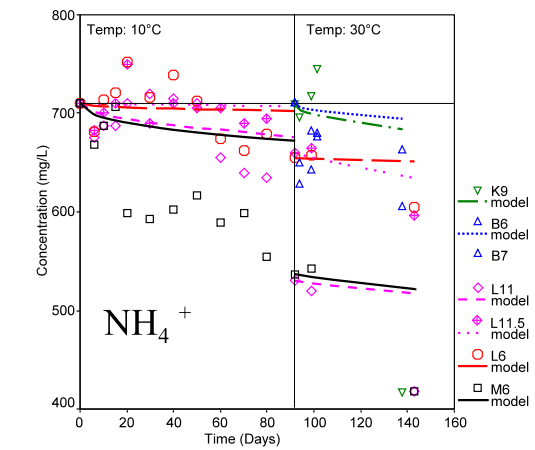
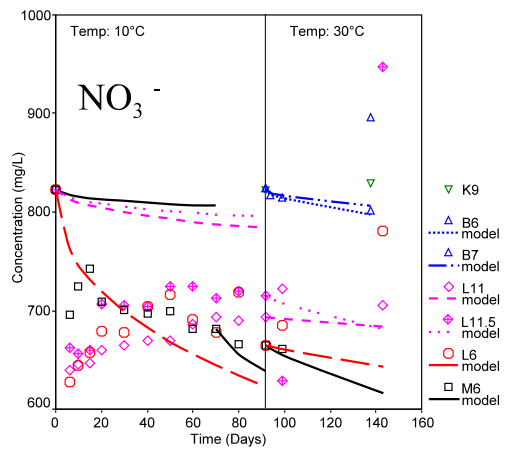
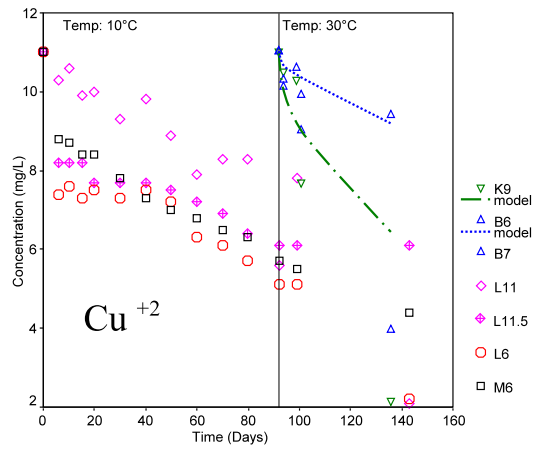
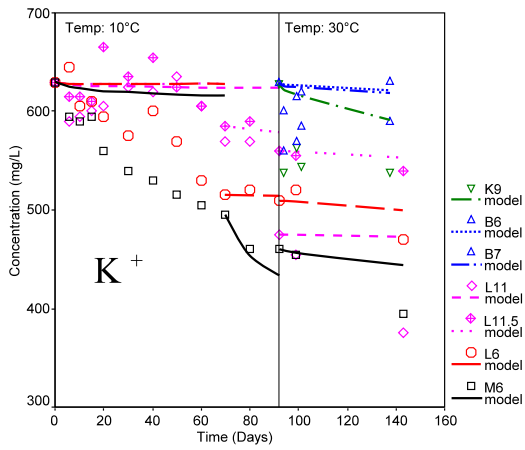
Appendix G.4 - Graphical representation of diffusion modeling outcome for source reservoir.

Sample	Species	$D_e$ (cm <sup>2</sup> /s)	$K_d$ (cm <sup>3</sup> /g)	$K_d$ F or L values	Sample	Species	$D_e$ (cm <sup>2</sup> /s)	$K_d$ (cm <sup>3</sup> /g)	$K_d$ F or L values	Sample	Species	$D_e$ (cm <sup>2</sup> /s)	$K_d$ (cm <sup>3</sup> /g)	$K_d$ F or L values
										K9@30°C	Na	3.41E-06	0.50	
											K	3.17E-06	0.05	
											Ca	1.57E-05	10.00	0.5F
											NH4	9.53E-07	211.14	0.282L
											Cu	3.84E-05	8.00	0.01F
											Cl	n/a		
											NO3	n/a		
											SO4	n/a		
											CPL	1.41E-06	77.27	0.09L
											<i>1.47E-06</i> TOTAL	1.90E-06	0.00	
										B6@30°C	Na	1.85E-06	0.15	
											K	1.11E-06	-0.09	1F
											Ca	1.69E-05	14.00	0.5F
											NH4	1.09E-06	2.14	0.52F
											Cu	1.78E-05	3.00	0.01F
											Cl	3.03E-06	1.19	0.2F
											NO3	2.63E-06	-52.74	0.036L
											SO4	4.05E-06	1.28	
											CPL	1.20E-05	3	0.5F
											<i>3.07E-06</i> TOTAL	2.40E-06	3	0.5F
										B7@30°C	Na	1.08E-06	0.00	
											K	1.53E-06	-0.07	1F
											Ca	1.10E-05	-0.80	1F
											NH4	0		
											Cu	no data match		
											Cl	4.58E-06	0.50	
											NO3	1.87E-06	0.00	
											SO4	0		
											CPL	8E-05	5	1.5F
											<i>2.84E-06</i> TOTAL	2.80E-06	-1.1	1F
L6@10°C	Na	6.50E-07	12.00	0.5F	L6@10°C	Na	2.28E-06	30	0.5F	L6@30°C	Na	1.80E-06	-0.1	1F
	K	8.00E-08	-0.13	1F	70 to 92 days	K	5.80E-07	5	0.5F		K	1.30E-06	0	
	Ca	1.80E-06	0.00			Ca	3.36E-05	450	0.5F		Ca	6.10E-06	-0.13	1F
	NH4	1.50E-07	0.00								NH4	2.90E-07	0	
	Cu	0				Cl	1.90E-06	200	0.1F		Cu	no data match		
	Cl	3.40E-07	-0.10	1F							Cl	2.60E-06	-0.13	1F
	NO3	4.10E-06	3.80			CPL	2.60E-05	200	0.2F		NO3	2.20E-06	0	
	SO4	4.20E-06	160.00	0.5F							SO4	6.30E-07	-0.14	1F
	CPL	2.06E-06	0.00								CPL	1.83E-05	10	0.5F
	<i>1.22E-06</i> TOTAL	4.43E-06	-4.50	1F		<i>2.32E-06</i> TOTAL	4.81E-06	82	0.7F		<i>2.04E-06</i> TOTAL	2.01E-06	-0.14	1F
L11@10°C	Na	8.60E-07	0.40							L11@30°C	Na	1.43E-06	0.7	
	K	1.98E-07	-0.07	1F							K	5.80E-07	0	
	Ca	5.30E-06	1.50								Ca	2.40E-06	-0.12	1F
	NH4	5.80E-07	52.28	0.517L							NH4	1.34E-06	52.28	0.517L
	Cu	0									Cu	no data match		
	Cl	8.50E-07	0.08								Cl	1.15E-06	0.08	
	NO3	1.02E-06	0.25								NO3	1.15E-06	0.25	
	SO4	0									SO4	0		
	CPL	1.43E-06	-0.15	1F							CPL	5.60E-06	-0.15	1F
	<i>8.07E-07</i> TOTAL	7.98E-07	3.00	0.2L							<i>1.08E-06</i> TOTAL	9.40E-07	1	0.5F
L11.5@10°C	Na	9.90E-07	0.5		L11.5@10°C	Na	4.87E-06	30	0.5F	L11.5@30°C	Na	1.60E-06	-0.15	1F
	K	1.13E-07	-0.15	1F	70 to 92 days	K	2.14E-06	20	0.5F		K	1.33E-06	-0.15	1F
	Ca	2E-06	0			Ca	3.50E-04	>5000	0.3F		Ca	7.50E-06	-0.15	1F
	NH4	9.11E-08	-0.41	1F		NH4					NH4	3.18E-06	52.28	0.517F
	Cu	0				Cu					Cu	no data match		
	Cl	6.20E-07	0			Cl	2.03E-05	285	0.6F		Cl	4.18E-06	0.1	
	NO3	8.50E-07	0.1			NO3	5.90E-06	0			NO3	3.70E-06	1.25	
	SO4	4.30E-06	150	0.4F							SO4	error		
	CPL	3.00E-06	-0.15	1F							CPL	1.90E-04	-0.15	1F
	<i>1.28E-06</i> TOTAL	2.80E-07	-0.02	1.2F		<i>1.91E-05</i> TOTAL	9.50E-06	100	0.7F		<i>3.17E-06</i> TOTAL	2.66E-06	-0.152	1F
M6@10°C	Na	1.17E-06	20.00	0.5F	M6@10°C	Na	1.23E-05	700.00	0.3F	M6@30°C	Na	4.10E-06	-0.15	1F
	K	4.22E-07	2.00	0.5F	70 to 92 days	K	5.14E-06	70.00	0.3F		K	2.49E-06	-0.1	1F
	Ca	9.84E-06	50.00	0.5F		Ca	8.80E-05	1000.00	0.2F		Ca	1.14E-05	-0.17	1F
	NH4	7.30E-07	94.28	0.517L		NH4	2.69E-06	0.00			NH4	1.90E-06	-0.175	1F
	Cu	0									Cu	no data match		
	Cl	3.40E-06	50.00	0.6F							Cl	3.12E-05	800	0.5F
	NO3	5.80E-07	0.00								NO3	5.24E-06	0.29	
	SO4	1.05E-06	10.00	0.6F							SO4	3.50E-06	10	0.5F
	CPL	7.10E-07	-0.10	1F							CPL	1.30E-04	1000	0.3F
	<i>2.24E-06</i> TOTAL	2.60E-06	23.00	0.7F		<i>6.66E-04</i> TOTAL	5.32E-05	600.00	0.7F		<i>1.59E-05</i> TOTAL	5.56E-06	0.1	

Because of changing diffusion coefficient as interpreted in the receptor, samples L6, L11.5, and M6 shown with three varying diffusion models for specific chemical species.



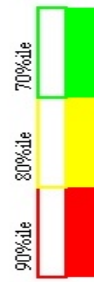




Appendix H

Appendix H.1 - Significant correlations of Soil pH, Mineralogy, Kd and D<sub>e</sub> values vs. D<sub>e</sub>

	Soil pH	Illite	Kaolinite	Gypsum	Apatite	Albite	Carbon	MnO	Ka NH4	Kd Cl		Kd CFL	N <sub>a</sub> -D <sub>e</sub>	K-D <sub>e</sub>	C <sub>a</sub> -D <sub>e</sub>	Cl-D <sub>e</sub>	CFL-D <sub>e</sub>
										linear	K <sub>d</sub> NO3						
Na-D <sub>e</sub> @30°C	Pearson Cor	-0.872	0.384	0.427	-0.164	0.681	-0.789	-0.576	0.687	0.325	-0.127	0.744					
	Sig. (2-tailed)	0.054	0.523	0.473	0.793	0.206	0.113	0.309	0.2	0.594	0.839	0.149					
	N	5	5	5	5	5	5	5	5	5	5	5					
K-D <sub>e</sub> @30°C	Pearson Cor	-0.581	0.056	0.755	-0.524	0.862	-0.605	-0.539	0.847	0.365	0.151	0.384	0.897				
	Sig. (2-tailed)	0.305	0.929	0.14	0.365	0.06	0.28	0.349	0.07	0.321	0.808	0.523	0.039				
	N	5	5	5	5	5	5	5	5	5	5	5	5				
Cu-D <sub>e</sub> @30°C	Pearson Cor	0.199	-0.493	0.907	-0.935	0.733	0.091	-0.569	0.718	0.96	0.269	-0.39	0.286	0.614			
	Sig. (2-tailed)	0.748	0.399	0.034	0.002	0.159	0.884	0.316	0.172	0.009	0.662	0.516	0.641	0.27			
	N	5	5	5	5	5	5	5	5	5	5	5	5	5			
Ca-D <sub>e</sub> @30°C	Pearson Cor	-0.216	0.228	0.469	-0.395	0.366	-0.438	-0.926	0.338	0.765	-0.45	0.085	0.476	0.583			
	Sig. (2-tailed)	0.728	0.713	0.426	0.29	0.544	0.461	0.024	0.554	0.131	0.447	0.891	0.418	0.302			
	N	5	5	5	5	5	5	5	5	5	5	5	5	5			
NH4-D <sub>e</sub> @30°C	Pearson Cor	-0.667	0.377	-0.156	0.228	0.189	-0.309	-0.465	0.251	0.091	-0.402	0.715	0.533	0.188	0.103		
	Sig. (2-tailed)	0.219	0.532	0.802	0.713	0.76	0.613	0.43	0.684	0.884	0.503	0.174	0.355	0.762	0.869		
	N	5	5	5	5	5	5	5	5	5	5	5	5	5	5		
Cl-D <sub>e</sub> @30°C	Pearson Cor	-0.997	0.806	-0.886	0.646	0.849	-0.846	-0.475	0.814	-0.058	-0.438	1	0.993	0.943	0.277		
	Sig. (2-tailed)	0.003	0.194	0.114	0.354	0.151	0.154	0.525	0.186	0.942	0.562	0	0.005	0.057	0.723		
	N	4	4	4	4	4	4	4	4	4	4	4	4	4	4		
NO3-D <sub>e</sub> @30°C	Pearson Cor	-0.823	0.423	-0.993	0.566	0.978	-0.458	-0.329	0.989	0.013	-0.19	0.857	0.808	0.643	-0.008	0.861	
	Sig. (2-tailed)	0.177	0.577	0.002	0.434	0.022	0.542	0.671	0.011	0.987	0.81	0.143	0.192	0.357	0.992	0.139	
	N	4	4	4	4	4	4	4	4	4	4	4	4	4	4	4	
SO4-D <sub>e</sub> @30°C	Pearson Cor	-0.51	0.802	-0.32	-0.273	0.107	-0.645	-0.979	0.126	0.705	-0.996	0.494	0.568	0.576	0.961	0.516	
	Sig. (2-tailed)	0.49	0.198	0.68	0.727	0.893	0.355	0.021	0.874	0.295	0.004	0.506	0.432	0.424	0.039	0.484	
	N	4	4	4	4	4	4	4	4	4	4	4	4	4	4	4	
CFL-D <sub>e</sub> @30°C	Pearson Cor	-0.963	0.814	-0.33	0.562	0.02	-0.827	-0.282	0.044	-0.329	-0.505	0.993	0.708	0.341	0.056	0.993	
	Sig. (2-tailed)	0.008	0.093	0.588	0.401	0.974	0.084	0.645	0.944	0.589	0.385	0	0.18	0.574	0.929	0.002	
	N	5	5	5	5	5	5	5	5	5	5	5	5	5	5	5	
TOTAL-D <sub>e</sub> @30°C	Pearson Cor	-0.965	0.863	-0.21	-0.338	0.4	0.079	-0.488	0.094	-0.148	-0.609	0.963	0.782	0.47	0.316	0.966	0.961
	Sig. (2-tailed)	0.008	0.06	0.734	0.555	0.304	0.899	0.404	0.88	0.812	0.275	0.003	0.118	0.424	0.605	0.034	0.009
	N	5	5	5	5	5	5	5	5	5	5	5	5	5	5	5	5



Correlation is significant at the 0.05 level (2-tailed).  
Correlation is significant at the 0.01 level (2-tailed).

Appendix H.2 - Significant correlations of barrier physical properties vs.  $D_e$

	Porosity	$K_g \cdot 10^{-9}$	Grain density	dry density	Absorption	Water	Grainsize mean	Grainsize sorting	Grainsize skewness	Grainsize Kurtosis
Na- $D_e$ @30°C	Pearson Correlation	-0.292	-0.259	0.162	0.435	0.694	0.405	-0.183	-0.205	
	Sig. (2-tailed)	0.633	0.228	0.795	0.464	0.194	0.498	0.769	0.741	
	N	5	5	5	5	5	5	5	5	5
K- $D_e$ @30°C	Pearson Correlation	-0.65	-0.219	0.526	0.48	0.439	0.739	0.246	-0.521	
	Sig. (2-tailed)	0.235	0.283	0.363	0.413	0.46	0.153	0.689	0.368	
	N	5	5	5	5	5	5	5	5	5
Cu- $D_e$ @30°C	Pearson Correlation	-0.964	-0.441	0.719	0.387	0.016	0.91	0.855	-0.932	
	Sig. (2-tailed)	0.008	0.297	0.171	0.52	0.979	0.032	0.065	0.021	
	N	5	5	5	5	5	5	5	5	5
Ca- $D_e$ @30°C	Pearson Correlation	-0.533	-0.884	0.083	0.872	0.641	0.463	0.352	-0.856	
	Sig. (2-tailed)	0.355	0.078	0.894	0.054	0.244	0.432	0.562	0.064	
	N	5	5	5	5	5	5	5	5	5
NH4- $D_e$ @30°C	Pearson Correlation	0.216	-0.316	-0.355	-0.077	0.622	-0.171	-0.538	0.278	
	Sig. (2-tailed)	0.727	0.277	0.605	0.902	0.262	0.784	0.35	0.65	
	N	5	5	5	5	5	5	5	5	5
Cl- $D_e$ @30°C	Pearson Correlation	0.714	-0.199	-0.561	0.318	0.798	-0.986	-0.971	0.255	
	Sig. (2-tailed)	0.286	0.428	0.439	0.682	0.202	0.014	0.029	0.745	
	N	4	4	4	4	4	4	4	4	4
NO3- $D_e$ @30°C	Pearson Correlation	0.649	-0.532	-0.346	-0.125	0.557	-0.783	-0.889	0.505	
	Sig. (2-tailed)	0.351	0.468	0.95	0.875	0.443	0.217	0.111	0.495	
	N	4	4	4	4	4	4	4	4	4
SO4- $D_e$ @30°C	Pearson Correlation	-0.202	-0.931	-0.996	0.851	0.928	-0.472	-0.295	-0.679	
	Sig. (2-tailed)	0.798	0.091	0.004	0.149	0.072	0.528	0.705	0.321	
	N	4	4	4	4	4	4	4	4	4
CPL- $D_e$ @30°C	Pearson Correlation	0.466	-0.123	-0.508	0.24	0.77	-0.553	-0.822	0.418	
	Sig. (2-tailed)	0.429	0.599	0.382	0.698	0.128	0.561	0.088	0.484	
	N	5	5	5	5	5	5	5	5	5
TOTAL- $D_e$ @30°C	Pearson Correlation	0.323	-0.482	-0.476	0.494	0.896	-0.233	-0.694	0.169	
	Sig. (2-tailed)	0.596	0.411	0.578	0.397	0.04	0.705	0.193	0.786	
	N	5	5	5	5	5	5	5	5	5



Correlation is significant at the 0.05 level (2-tailed).  
Correlation is significant at the 0.01 level (2-tailed).

Appendix H.3 - Significant correlations of Geochemistry and CEC vs.  $D_e$ 

	SiO2	Fe2O3	MgO	K2O	TiO2	MnO	C-Total	Ba	Y	Cu	CEC Na	CEC K
Na-D <sub>e</sub>												
Pearson Correlation	0.724	0.793	-0.83	0.548	0.585	-0.573	-0.789	0.787	-0.488	0.536	0.833	0.057
Sig. (2-tailed)	0.167	0.11	0.082	0.339	0.301	0.312	0.113	0.115	0.405	0.352	0.08	0.928
N	5	5	5	5	5	5	5	5	5	5	5	5
K-D <sub>e</sub>												
Pearson Correlation	0.54	0.809	-0.846	0.154	0.723	-0.458	-0.605	0.45	-0.301	0.792	0.514	0.451
Sig. (2-tailed)	0.348	0.097	0.071	0.805	0.168	0.438	0.28	0.447	0.623	0.11	0.376	0.445
N	5	5	5	5	5	5	5	5	5	5	5	5
Cu-D <sub>e</sub>												
Pearson Correlation	0.199	0.595	-0.626	-0.626	0.81	-0.407	0.091	-0.299	-0.244	0.848	-0.232	0.871
Sig. (2-tailed)	0.748	0.29	0.259	0.259	0.097	0.496	0.884	0.626	0.692	0.069	0.707	0.055
N	5	5	5	5	5	5	5	5	5	5	5	5
Ca-D <sub>e</sub>												
Pearson Correlation	0.767	0.911	-0.883	-0.127	0.976	-0.868	-0.438	0.001	-0.764	0.42	0.24	0.288
Sig. (2-tailed)	0.13	0.032	0.047	0.839	0.005	0.056	0.461	0.998	0.133	0.482	0.697	0.638
N	5	5	5	5	5	5	5	5	5	5	5	5
NH4-D <sub>e</sub>												
Pearson Correlation	0.555	0.309	-0.373	0.616	0.136	-0.549	-0.309	0.808	-0.638	0.052	0.712	-0.355
Sig. (2-tailed)	0.331	0.613	0.557	0.268	0.828	0.338	0.613	0.098	0.247	0.934	0.177	0.558
N	5	5	5	5	5	5	5	5	5	5	5	5
Cl-D <sub>e</sub>												
Pearson Correlation	0.741	0.687	-0.745	0.984	0.387	-0.532	-0.846	0.966	-0.525	0.664	0.997	-0.964
Sig. (2-tailed)	0.259	0.313	0.255	0.016	0.613	0.468	0.154	0.034	0.475	0.336	0.003	0.036
N	4	4	4	4	4	4	4	4	4	4	4	4
NO3-D <sub>e</sub>												
Pearson Correlation	0.487	0.373	-0.479	0.83	0.113	-0.383	-0.458	0.933	-0.422	0.952	0.829	-0.698
Sig. (2-tailed)	0.513	0.627	0.521	0.17	0.887	0.617	0.542	0.047	0.578	0.048	0.171	0.302
N	4	4	4	4	4	4	4	4	4	4	4	4
SO4-D <sub>e</sub>												
Pearson Correlation	0.957	0.962	-0.953	0.381	0.987	-0.98	-0.645	0.336	-0.957	0.076	0.578	-0.626
Sig. (2-tailed)	0.043	0.038	0.047	0.619	0.013	0.02	0.355	0.664	0.043	0.924	0.422	0.374
N	4	4	4	4	4	4	4	4	4	4	4	4
CPL-D <sub>e</sub>												
Pearson Correlation	0.667	0.394	-0.396	0.975	0.056	-0.411	-0.827	0.941	-0.466	-0.186	0.976	-0.653
Sig. (2-tailed)	0.219	0.512	0.309	0.005	0.929	0.492	0.084	0.017	0.429	0.764	0.004	0.233
N	5	5	5	5	5	5	5	5	5	5	5	5
TOTAL-D <sub>e</sub>												
Pearson Correlation	0.83	0.61	-0.595	0.897	0.301	-0.596	-0.929	0.867	-0.618	-0.101	0.981	-0.565
Sig. (2-tailed)	0.082	0.275	0.29	0.039	0.623	0.288	0.023	0.057	0.267	0.871	0.003	0.321
N	5	5	5	5	5	5	5	5	5	5	5	5



Correlation is significant at the 0.05 level (2-tailed).  
Correlation is significant at the 0.01 level (2-tailed).